Copyright 2022. De Gruyter. All rights reserved. May not be reproduced in any form without permission from the publisher, except fair uses permitted under U.S. or applicable copyright law.

DE GRUYTER

DRINKING WATER TREATMENT

NEW MEMBRANE TECHNOLOGY

Editors in Chief:
Bingzhi Dong, Tian Li

Editors:
Huaqiang Chu, Huan He,
Shumin Zhu, and Junxia Liu

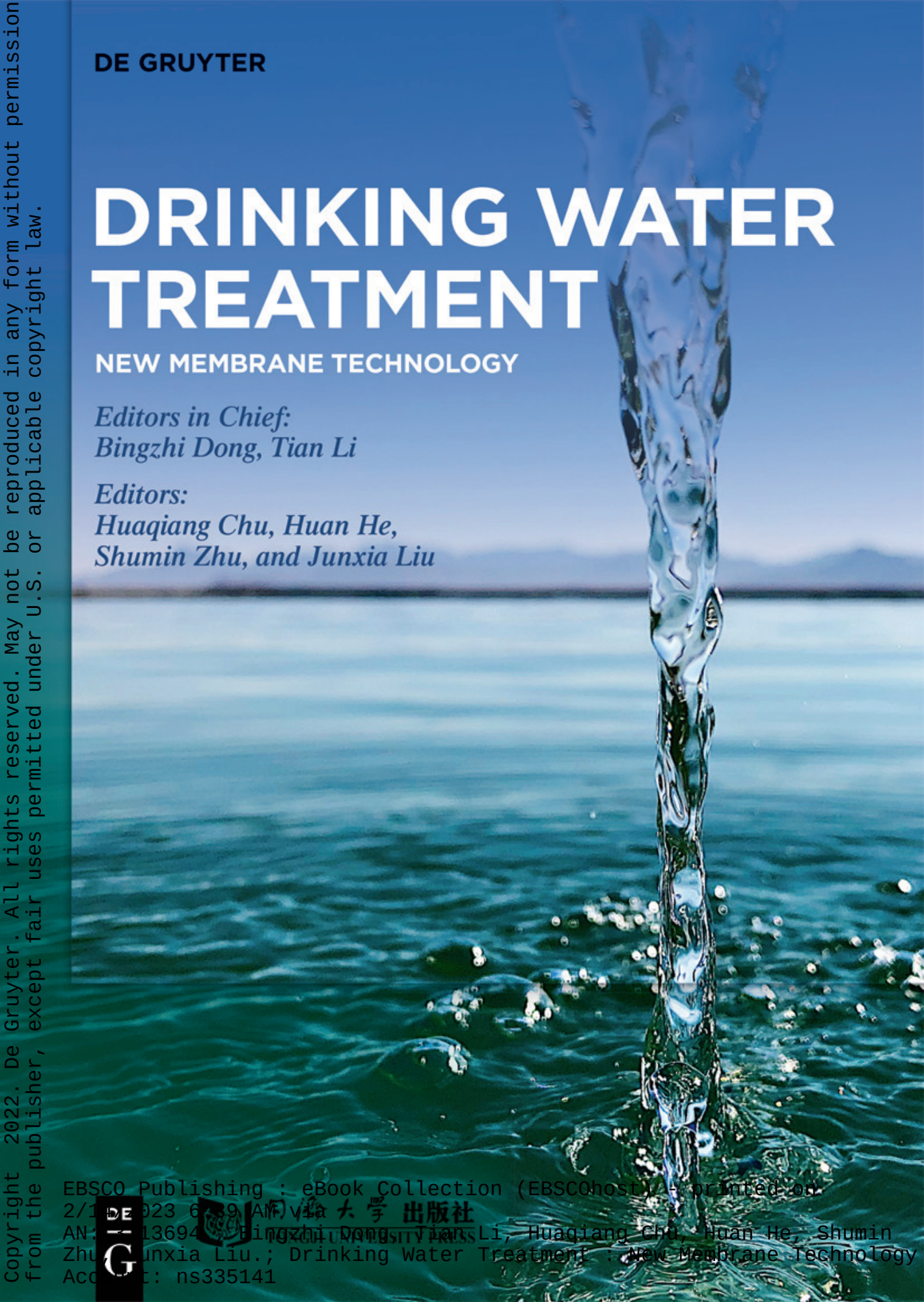

EBSCO Publishing : eBook Collection (EBSCOhost) - printed on 2/1[illegible]023 6:39 AM via [illegible] 出版社
AN: [illegible]13694 ; Bingzhi Dong, Tian Li, Huaqiang Chu, Huan He, Shumin Zhu, Junxia Liu.; Drinking Water Treatment : New Membrane Technology
Account: ns335141

Bingzhi Dong, Tian Li (Eds.)
Drinking Water Treatment

EBSCOhost - printed on 2/14/2023 6:39 AM via . All use subject to https://www.ebsco.com/terms-of-use

Also of Interest

Drinking Water Treatment.
An Introduction
Eckhard Worch, 2019
ISBN 978-3-11-055154-9, e-ISBN 978-3-11-055155-6

Adsorption Technology in Water Treatment.
Fundamentals, Processes, and Modeling
Eckhard Worch, 2021
ISBN 978-3-11-071542-2, e-ISBN 978-3-11-071550-7

Wastewater Treatment.
Application of New Functional Materials
Jianyu Chen, Jun Luo, Qijin Luo et al., 2018
Civil and Environmental Engineering Reports
ISBN 978-3-11-054278-3, e-ISBN 978-3-11-054438-1

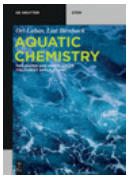

Aquatic Chemistry.
Applications and Non-traditional Alternatives
Ori Lahav, Liat Birnhack, 2019
ISBN 978-3-11-060392-7, e-ISBN 978-3-11-060395-8

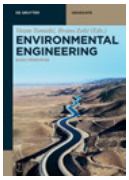

Environmental Engineering.
Basic Principles
Vesna Tomašić, Bruno Zelić (Eds.), 2018
ISBN 978-3-11-046801-4, e-ISBN 978-3-11-046803-8

EBSCOhost - printed on 2/14/2023 6:39 AM via . All use subject to https://www.ebsco.com/terms-of-use

Drinking Water Treatment

New Membrane Technology

Edited by
Bingzhi Dong, Tian Li

DE GRUYTER 同济大学出版社 TONGJI UNIVERSITY PRESS

EBSCOhost - printed on 2/14/2023 6:39 AM via . All use subject to https://www.ebsco.com/terms-of-use

Editors
Bingzhi Dong
College of Environmental Science and Engineering
Tongji University
Shanghai
P.R. China
dbz77@tongji.edu.cn

Tian Li
College of Environmental Science and Engineering
Tongji University
Shanghai
P. R. China
litian001@tongji.edu.cn

Huaqiang Chu
College of Environmental Science and Engineering
Tongji University
Shanghai
P. R. China

Huan He
College of Environmental Science and Engineering
Tongji University
Shanghai
P. R. China

Shumin Zhu
College of Civil Engineering
Hunan University
Changsha, Hunan
P. R. China

Junxia Liu
School of Civil and Transportation Engineering
Guangdong University of Technology
Guangzhou, Guangdong
P. R. China

ISBN 978-3-11-059559-8
e-ISBN (PDF) 978-3-11-059684-7
e-ISBN (EPUB) 978-3-11-059315-0

Library of Congress Control Number: 2021941505

Bibliographic information published by the Deutsche Nationalbibliothek
The Deutsche Nationalbibliothek lists this publication in the Deutsche Nationalbibliografie; detailed bibliographic data are available on the Internet at http://dnb.dnb.de.

© 2022 Tongji University Press Co., Ltd, Shanghai, Walter de Gruyter GmbH, Berlin/Boston
Cover image: Getty Images
Typesetting: Integra Software Services Pvt. Ltd.
Printing and binding: CPI books GmbH, Leck

www.degruyter.com

EBSCOhost - printed on 2/14/2023 6:39 AM via . All use subject to https://www.ebsco.com/terms-of-use

Contents

List of authors —— VII

Huan He, Shumin Zhu, Zheng Liu
Chapter 1 Classification and Characteristics of Organic Matter in Surface Water —— 1

Huaqiang Chu, Fangchao Zhao
Chapter 2 Vibration Membrane for Algae Separation —— 61

Weiwei Huang, Lin Wang, Bingzhi Dong
Chapter 3 The Membrane Fouling —— 73

Pingyun Zhang, Yong Wei, Tian Li
Chapter 4 Fabrication and Anti-fouling Evaluation of PVDF Membranes via Surface Modification —— 109

Tian Li, Junxia Liu, Bingzhi Dong
Chapter 5 The Influence of Pretreatment on Low-pressure Membrane Filtration Performance —— 143

Tian Li, Junxia Liu, Nianping Chi
Chapter 6 Nanofiltration in Water Treatment —— 211

Lin Wang, Wanzhu Zhang, Bingzhi Dong
Chapter 7 Forward Osmosis Membrane Separation Technology —— 267

Huaqiang Chu, Zhenxun Yu, Wen Sun
Chapter 8 Dynamic Membrane Reactor for Micro-polluted Surface Water/Municipal Wastewater Treatment —— 325

Qingqing Zhao, Yong Wei, Kuo Gao
Chapter 9 Pollution Removal by TiO_2/UV Photocatalysis Coupled with Membrane Filtration —— 353

Index —— 393

EBSCOhost - printed on 2/14/2023 6:39 AM via . All use subject to https://www.ebsco.com/terms-of-use

EBSCOhost - printed on 2/14/2023 6:39 AM via . All use subject to https://www.ebsco.com/terms-of-use

List of authors

Huan He
College of Environmental Science and Engineering
Tongji University
Shanghai
P. R. China

Shumin Zhu
College of Civil Engineering
Hunan University
Changsha, Hunan
P. R. China

Zheng Liu
The Institute of Seawater Desalination and Multipurpose Utilization, MNR
Tianjin
P. R. China

Huaqiang Chu
College of Environmental Science and Engineering
Tongji University
Shanghai
P. R. China

Fangchao Zhao
School of Environmental and Municipal Engineering
Qingdao University of Technology
Qingdao, Shandong
P. R. China

Weiwei Huang
Eco-Environment Protection Research Institute
Shanghai Academy of Agricultural Sciences
Shanghai
P. R. China

Lin Wang
School of Municipal and Environmental Engineering
Shandong Jianzhu University
Jinan, Shandong
P. R. China

Bingzhi Dong
College of Environmental Science and Engineering
Tongji University
Shanghai
P. R. China

Pingyun Zhang
National Engineering Research Center of Urban Water Resources
Shanghai
P. R. China

Yong Wei
School of Environmental and Safety Engineering & School of Urban Construction
Changzhou University
Changzhou, Jiangsu
P. R. China

Tian Li
College of Environmental Science and Engineering
Tongji University
Shanghai
P. R. China

https://doi.org/10.1515/9783110596847-203

EBSCOhost - printed on 2/14/2023 6:39 AM via . All use subject to https://www.ebsco.com/terms-of-use

Junxia Liu
School of Civil and Transportation Engineering
Guangdong University of Technology
Guangzhou, Guangdong
P. R. China

Nianping Chi
School of Municipal and Geomatics Engineering
Hunan City University
Yiyang, Hunan
P. R. China

Wanzhu Zhang
Beijing General Municipal Engineering Design & Research Institute Co., Ltd.
Beijing
P. R. China

Zhenxun Yu
School of Civil and Environmental Engineering
Ningbo University
Ningbo, Zhejiang
P. R. China

Qingqing Zhao
College of Environmental Science and Engineering
Tongji University
Shanghai
P. R. China

Kuo Gao
College of Environmental Science and Engineering
Tongji University
Shanghai
P. R. China

Wen Sun
College of Environmental Science and Engineering
Suzhou University of Science and Technology
Suzhou, Jiangsu
P. R. China

EBSCOhost - printed on 2/14/2023 6:39 AM via . All use subject to https://www.ebsco.com/terms-of-use

Huan He, Shumin Zhu, Zheng Liu

Chapter 1
Classification and Characteristics of Organic Matter in Surface Water

Organic matter has a great influence on water treatment processes, especially the membrane process. There are many kinds of organic substances in natural water with different properties. They are usually categorized based on their properties, i.e. the molecular weight, hydrophobicity/hydrophilicity and fluorescence spectrum of organic matter. Organic matters with large size can be intercepted by membranes. The molecular weight of the organic matter can be used to determine the size of the organic matter and their distribution range, thereby providing a basis for the selection of the membrane and the corresponding process. Therefore, understanding the molecular weight of organic matter is an indispensable task in the membrane study. Membrane entrapment of organic matter not only depends on the size of the pores, but also its interaction with organic matter. The intensity of this interaction is closely related to the hydrophilicity and fluorescence characteristics of organic matter.

1.1 Principles and methods for determination of molecular weight of organic matter

1.1.1 Ultrafiltration membrane filtration method and gel chromatography

1.1.1.1 Principle and method of measurement

There are two main methods for determining the molecular weight distribution of organic matter, which are Gel Permeation Chromatography (GPC) and Ultrafiltration (UF) membrane filtration. In GPC method, a column is filled with a porous gel with a certain pore size distribution as a solid phase. When water flows through the gel, the organic matter with larger molecular weight in the water enters the effluent fast through the gel column because it cannot enter the gel, and the organic matter with smaller molecular weight enters the porous gel. The longer the molecular weight of

Huan He, College of Environmental Science and Engineering, Tongji University, Shanghai, P. R. China
Shumin Zhu, College of Civil Engineering, Hunan University, Changsha, Hunan, P. R. China
Zheng Liu, The Institute of Seawater Desalination and Multipurpose Utilization, MNR, Tianjin, P. R. China

https://doi.org/10.1515/9783110596847-001

EBSCOhost - printed on 2/14/2023 6:39 AM via . All use subject to https://www.ebsco.com/terms-of-use

the organic substance moves in the gel, the longer it takes to pass through the column. In this way, organic substances of different molecular weights pass through the gel at different time, appear in the effluent with different retention time, and achieve the purpose of separating organic substances of different molecular weights.

In the ultrafiltration membrane filtration method, an ultrafiltration membrane with known molecular weight cut-off is placed in a stirred cell with agitation and provided with the driving force from pure nitrogen for separation. The organic matter with molecular weight smaller than the molecular weight cut-off by the membrane in the water can pass through the membrane and appear in the effluent, and the organic matter with molecular weight larger than the molecular weight cut-off can be trapped by the membrane. The molecular weight distribution of organic matter can be obtained by separating the water sample with a series of different ultrafiltration membranes with known molecular weight cut-off (Figure 1.1).

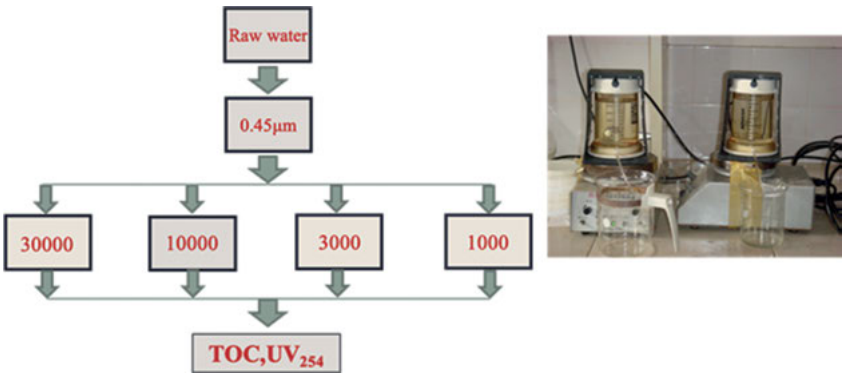

Figure 1.1: Determination of molecular weight distribution by ultrafiltration membrane filtration method.

In the GPC method, some organic matter in the water can repel the ions with the gel, and pass through the gel column faster, resulting in a higher molecular weight measured; and some organic substances can adsorb the gel or induce the electrostatic interaction with the gel to hinder the movement, resulting in a smaller molecular weight measured. Moreover, pretreatment of the water sample by evaporation or freezing is required before the GPC measurement, which may change the size of the dissolved organic matter in the water, thereby affecting the analysis results. One of the advantages of GPC method is that the molecular weight distribution obtained is continuous (Figure 1.2). The UF membrane filtration method results are affected by the pore size distribution of the selected membranes, applied pressure, temperature of the water sample, pH, ionic strength, size and shape of the dissolved organic matter, and the properties of the membranes. The advantage of the UF membrane filtration method is that the analytical equipment and method adopted are simple, and a large amount of

EBSCOhost - printed on 2/14/2023 6:39 AM via . All use subject to https://www.ebsco.com/terms-of-use

separated water samples can be obtained for further analysis. The molecular weight distribution obtained by the UF membrane filtration method is discontinuous.

Amy compared the GPC method with the UF membrane filtration method. The results showed that for the same water sample, different molecular weight distributions were exhibited in the two methods [1]. The molecular weight distribution measured with the GPC method was higher than that with the UF membrane filtration method. Since both methods are carried out using substances of given molecular weight, the molecular weight obtained is only Apparent Molecular Weight.

In recent years, in order to obtain the accurate relative molecular weight distribution of organic matter with the gel chromatography method, a variety of detectors are used to connect online. For example, Kawasaki et al. adopted a new high-performance gel chromatograph coupled with a UV detector and an NDIR total organic carbon analyzer to obtain a linear correlation between UV absorbance and NDIR total organic carbon concentration for relative molecular weight ($R^2 > 0.99$) [2]. In addition, to better detect the ultraviolet response of humus in water and prevent the interference such as nitrate, the UV wavelength is set at 260 nm. The improved HPLC-UV-TOC system can well determine the molecular weight distribution of organic matter in natural raw water such as natural lake water, river water, groundwater, etc. And it can be also used to quantitatively study the UV and DOC results obtained by UV detector and NDIR total organic carbon analyzer and to learn more about the physicochemical properties of DOM.

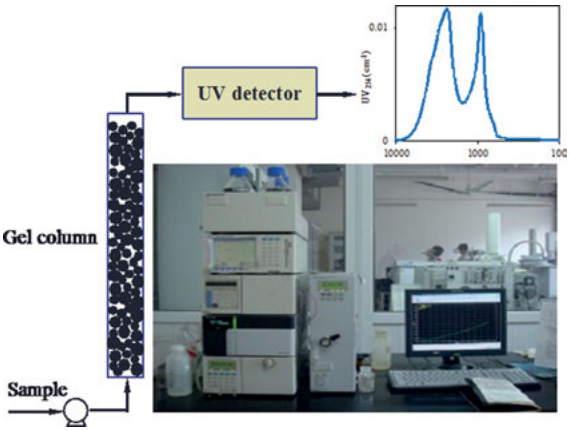

Figure 1.2: Determination of molecular weight distribution by gel chromatography.

1.1.1.2 Molecular weight distribution of organic matter in natural raw water

1 Molecular weight distribution of organic matter

Humic acid (HA), tannic acid (TA) and sodium alginate (SA) were selected and their molecular weight distributions were determined with the ultrafiltration membrane

EBSCOhost - printed on 2/14/2023 6:39 AM via . All use subject to https://www.ebsco.com/terms-of-use

filtration method, as shown in Figure 1.3. The molecular weights of HA and SA are mainly concentrated above 30,000, while the molecular weight of TA is mainly at less than 1,000. This indicates that HA and SA are typical macromolecular organics, while TA is a typical small molecule organic substance.

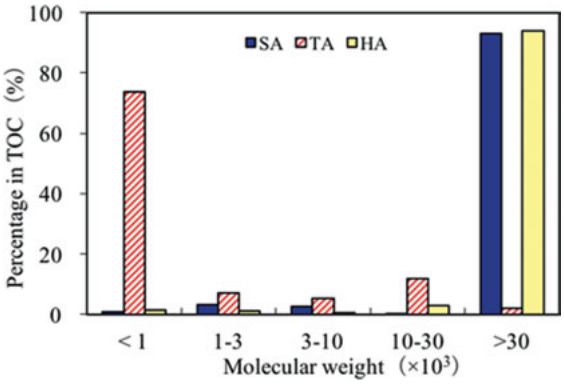

Figure 1.3: Molecular weight distribution of organic matter.

2 Molecular weight distribution of natural raw water

The molecular weight distributions of some typical domestic surface water sources have been reported, as shown in Figure 1.4. Different raw water have different molecular weight distributions of organic matter. However, most organic matters are small molecules with molecular weight less than 1,000. Organic matter having molecular weight of less than 1,000 accounts for 45%, molecular weight of 1,000–10,000 accounts for 34%, and molecular weight greater than 10,000 only 17%. Some of the organic matters in the natural water are contaminants from various sources, and some from the decay of plants or animals. The main representative of natural organic substance is humic acid. However, as can be seen from Figure 1.3, the molecular weight of humic acid is mostly greater than 30,000. Therefore, the proportion of humic acid in natural water is very low, and most of the organic matters come from domestic or industrial wastewater.

The molecular weight distributions of some other water bodies were also measured, as shown in Figures 1.5 and 1.6. The results are similar as those in Figure 1.3 that small molecules of organic matters are dominated.

Moreover, the molecular weights of organics from Huangpu River, Sanhaowu and Kunshan Water are also measured and the result is shown in Figure 1.7. They all have three distinct molecular weight ranges located at 6,000–2,000 Da, 2,000–1,000 Da and 100–20 Da, respectively. At 100–6,000 Da, Kunshan water has the strongest response, followed by Sanhaowu, while the Huangpu River has the least response. In addition, Sanhaowu water and Kunshan water have response at the molecular weight of 10,000–100,000, while the Huangpu River water doesn't.

EBSCOhost - printed on 2/14/2023 6:39 AM via . All use subject to https://www.ebsco.com/terms-of-use

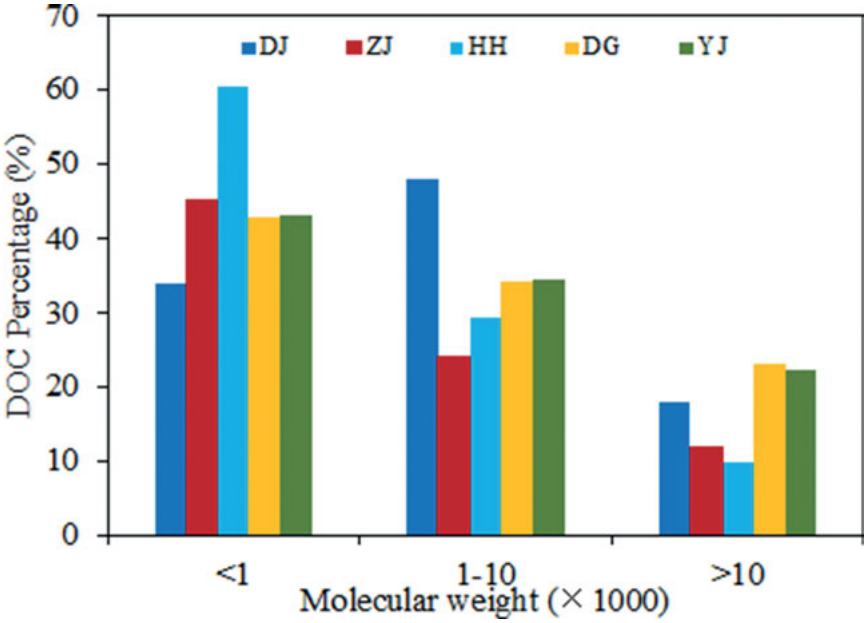

Figure 1.4: Comparison of molecular weight distributions of different water sources.

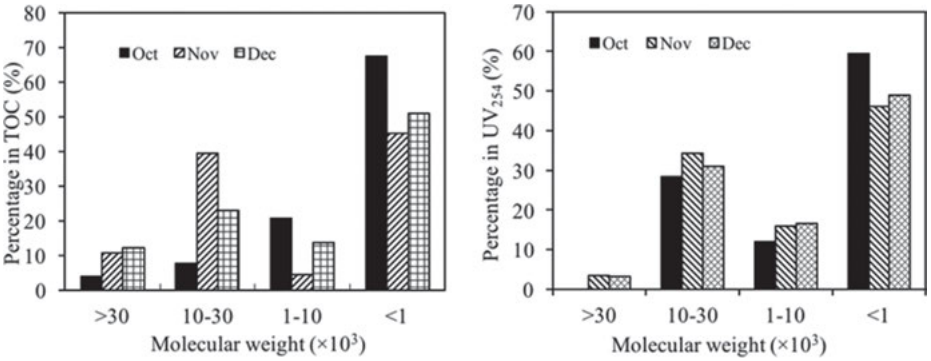

Figure 1.5: Molecular weight distribution of Huaihe River water.

3 Comparison of ultrafiltration membrane filtration method and gel chromatography in determining molecular weight distribution

A comparison study between the ultrafiltration membrane filtration method and the gel chromatography method was conducted to characterize the molecular weight distribution of Sanhaowu water, Yellow River water, Huangpu River water, Kunshan Miaojing River water and Gaoyou reservoir water, and to further analyze their similarities and differences in the characteristics of dissolved organic matter.

EBSCOhost - printed on 2/14/2023 6:39 AM via . All use subject to https://www.ebsco.com/terms-of-use

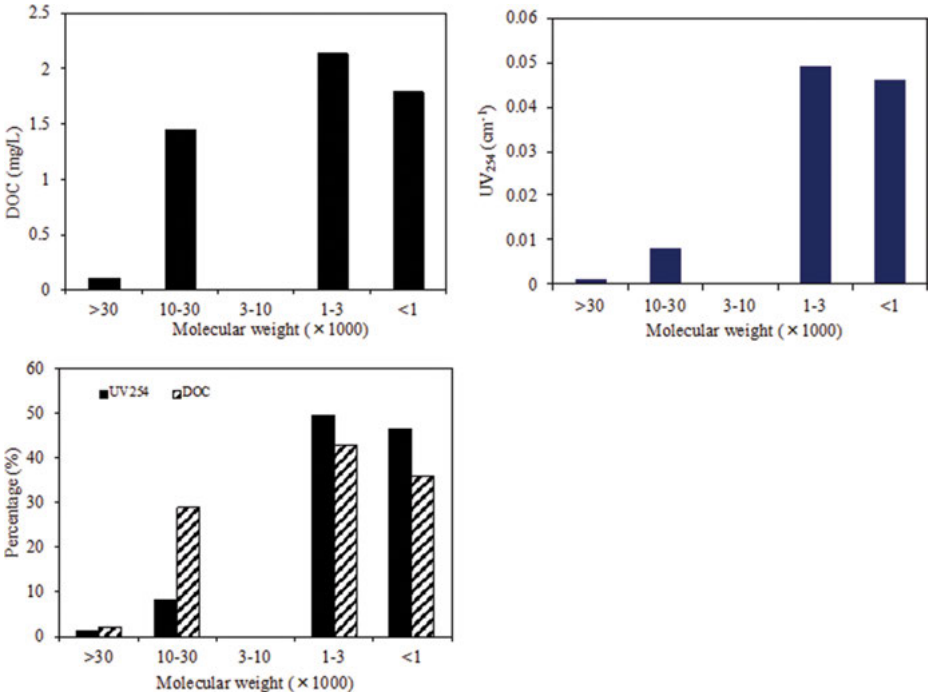

Figure 1.6: Molecular Weight Distribution of Yanlingjiaotang water in Zhenjiang China.

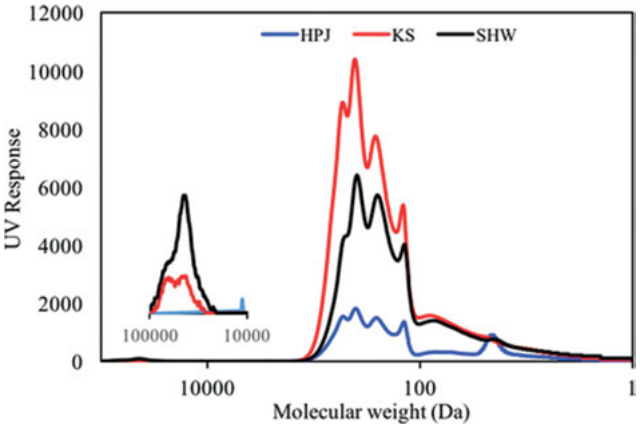

Figure 1.7: Molecular weight distribution of organic matter from different water sources (Gel Chromatography).

EBSCOhost - printed on 2/14/2023 6:39 AM via . All use subject to https://www.ebsco.com/terms-of-use

Table 1.1 shows the basic conditions of water qualities of five types of water sources. According to the provisions of environmental quality standard for surface water in China (GB3838-2002), the pHs of the above five water sources are within a reasonable range. Among the collected source water, the organic matter concentration index of the Yellow River water belongs to Class I, while the other four source water are in the standard range of Class II and III, which are typical micro-polluted water sources. Among them, the organic matter pollution of Kunshan and Huangpu River water sources is the most serious. Of all the five water sources, the UV absorption intensity (SUVA) value of the Huangpu River is the highest, followed by the Yellow River, Gaoyou, Kunshan and Sanhaowu water.

Table 1.1: Basic water quality of five water sources.

Water source	Sanhaowu	Yellow River Water	Huangpu River Water	Kunshan Water	Gaoyou Water
Sampling location	Tongji University	Gansu Lanzhou	Shanghai Yangshupu Water Treatment Plant	Kunshan Water Treatment Plant	Jiangsu Gaoyou
Water source type	lake water	river water	river water	lake water	lake water
Turbidity (NTU)	23.9	5.83	24.3	15.2	50.3
pH	8.4	8.63	8.22	8.3	8.2
DOC (mg/L)	4.75	1.48	5.42	5.86	4.24
UV_{254} (cm^{-1})	0.076	0.034	0.177	0.114	0.087
SUVA (L/(mg · m))	1.61	2.27	3.27	1.95	2.06

Figure 1.8 shows the molecular weight distribution of four raw water by the ultrafiltration membrane filtration method. There are the most organic matters with the molecular weight less than 1 kDa, followed by the organics with the molecular weight in the range of 1 k–3 kDa, 10 k–30 kDa, and 3 k–10 kDa, while there are the least organic substances with the molecular weight greater than 30 kDa. There are 60%–70% small molecule organic matters (molecular weight < 3 kDa), 5%–10% medium molecular organic matters (molecular weight between 3 k–10 kDa) and 20%–35% macromolecular organic matters (molecular weight > 10 kDa). It can be observed that the organic matters in the raw water are mainly composed of small molecules, which represents typical surface water qualities. Kunshan water and Sanhaowu water have the highest proportion of macromolecular organic matters, i.e. 12.5% and 8.8%, respectively. The other two kinds of raw water have rare macromolecular organic matters with molecular weight greater than 30 kDa. This phenomenon can be due to that more macromolecular organic matter are in closed water than in flowing water bodies since Sanhaowu and Kunshan are closed water bodies, while the Huangpu River and the Yellow River are flowing water bodies.

EBSCOhost - printed on 2/14/2023 6:39 AM via . All use subject to https://www.ebsco.com/terms-of-use

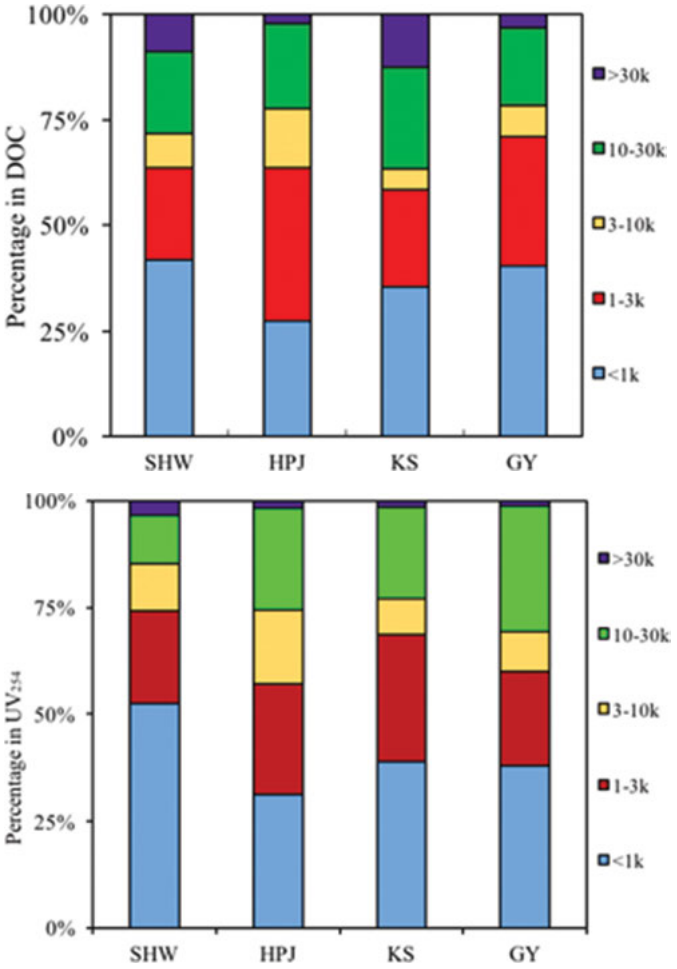

Figure 1.8: Molecular weight distribution of four kinds of raw water (Ultrafiltration membrane filtration method).

While in the molecular weight distribution of UV_{254} measurement, the proportion of macromolecules with molecular weight larger than 30 kDa significantly reduced, below 3% for all the four raw water (Figure 1.9). It can be regarded that this part of organic matter is mainly colloid, polysaccharide or protein organic matters. The proportion of the organics with the molecular weight in the range of 10–30 kDa in Sanhaowu and Kunshan decreased obviously, while that in Huangpu River and Gaoyou increased. This indicates that the UV absorption of polysaccharides and proteins is still low in the 10 k–30 kDa macromolecules in Sanhaowu and Kunshan, and the Huangpu River and Gaoyou water may contain humic macromolecular polymers that greatly absorb UV.

EBSCOhost - printed on 2/14/2023 6:39 AM via . All use subject to https://www.ebsco.com/terms-of-use

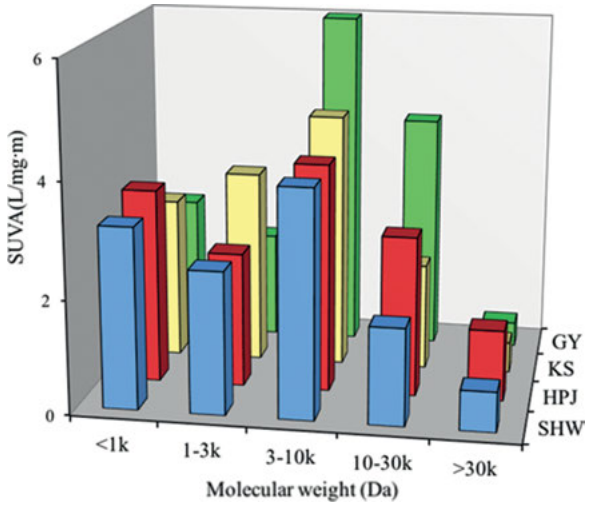

Figure 1.9: SUVA molecular weight distribution of different raw water.

From the SUVA distribution of the molecular weight interval for each raw water, it can be clearly seen that the SUVA value of organics with molecular weight over 30 kDa is significantly low, except for the Huangpu River water, which is below 1.0. The SUVA value of the macromolecules with molecular weight over 30 kDa for Huangpu River water is 1.24, indicating that the macromolecular organic matter in this interval may contain benzene ring structure, such as aromatic protein or humic acid. For the molecular weight range of 10–30 kDa, the SUVA value of Sanhaowu and Kunshan raw water is between 1.0–2.0, while that of Huangpu River and Gaoyou Water is over 2.0. This shows that Huangpu River water and Gaoyou water contain more humic macromolecular organic matter with the molecular weight of 10 k–30 kDa. The macromolecules in Sanhaowu and Kunshan water are still mainly macromolecular polysaccharides and proteins with low UV response.

Of all the raw water, the medium molecular organics with the molecular weight in the range of 3 k–10 kDa have the largest SUVA values, all above 4.0. Especially Gaoyou water has a SUVA value as high as 6.0.

The macromolecular organic matter is characterized by hydrophilicity, low UV response and small SUVA value. While the medium molecular organic substances mainly have high UV-responsive organic substances, such as humic acids, and have large SUVA values. The small molecular organic substances can be both hydrophilic and hydrophobic, and their SUVA value is between 2.0 and 4.0.

Figure 1.10 is a molecular weight distribution diagram of five raw water determined by gel chromatography. It can be seen that the water in SHW has the lowest response peak, followed by Kunshan Water, while Huangpu River and Yellow River have the highest response peak. Due to the use of UV detectors, the difference in peak height on the gel chromatogram is derived from the effect of organic matter in the

EBSCOhost - printed on 2/14/2023 6:39 AM via . All use subject to https://www.ebsco.com/terms-of-use

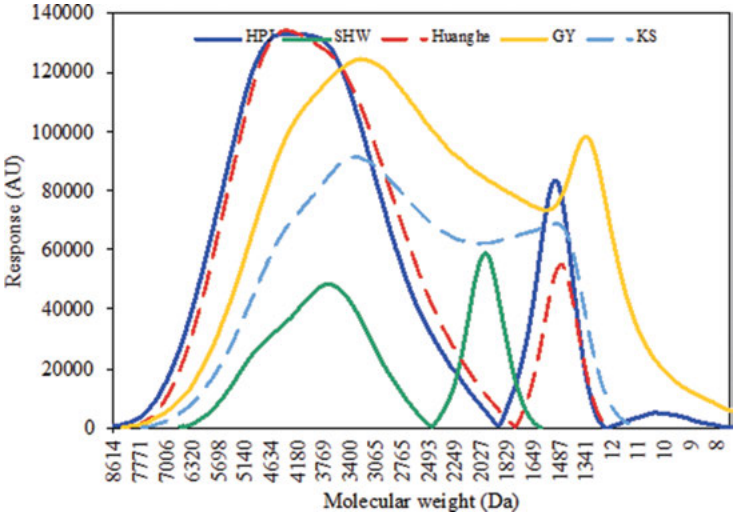

Figure 1.10: Molecular weight distribution of five raw water determined by gel chromatography.

raw water on the UV response. That is, the peak height of each raw water molecular weight is related to the SUVA value in Table 1.1. Figure 1.10 shows that medium organic compounds of 3 k–10 kDa have the highest UV response in organics larger than 3 kDa.

It is noted that SHW Water and KS Water are closed water bodies, so their response peaks are significantly smaller than other kinds of raw water, due to more hydrophilic organic matter. The UV responses of the Huangpu River and the Yellow River are the strongest, indicating that they have more hydrophobic organic matter.

1.1.2 OCD (organic carbon detectors) method

Although the ultrafiltration membrane filtration method and the GPC method have their respective advantages in determining the molecular weight of organic matter, there are still some defects in use. For example, although the ultrafiltration membrane filtration method is simple, the obtained organic matter has a discontinuous molecular mass distribution. Conventional gel chromatography uses a UV detector that responds only to compounds containing conjugated double bonds and aromatic structures. Certain organic components, such as hydrophilic molecules and benzene-free compounds containing carbon single bonds, cannot be detected, which may cause deviations in molecular weight determination.

The advantage of the OCD method is that the TOC detector can detect all organic compounds (Figure 1.11). The two different concentration characterization values of UV and TOC can also provide some important information, such as SUVA, which can reflect the structural characteristics and physical/chemical properties of organic matter more accurately.

EBSCOhost - printed on 2/14/2023 6:39 AM via . All use subject to https://www.ebsco.com/terms-of-use

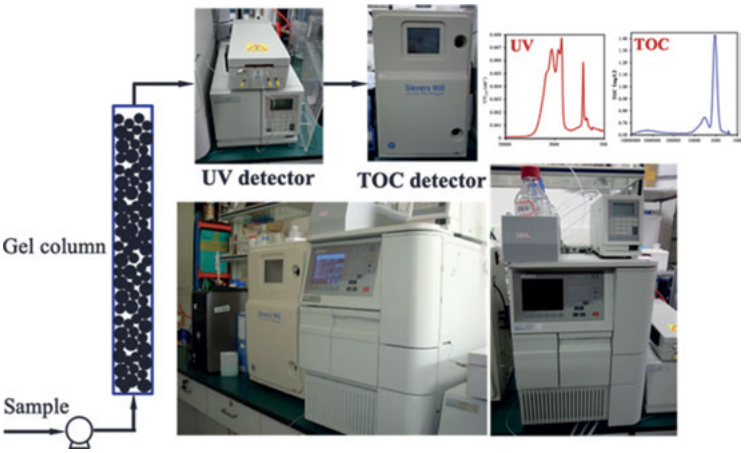

Figure 1.11: Schematic diagram of the OCD method.

1.1.2.1 Organic matter

The OCD system tested four different physicochemical properties including tannic acid (TA), humic acid (HA), sodium alginate (SA), and sucrose (SUC) to study the difference in molecular weight between UV and TOC results. SA is a typical macromolecular hydrophilic organic substance, SUC is a hydrophilic small molecule organic substance, HA is a typical hydrophobic organic substance, and TA has hydrophilic and hydrophobic properties. The concentration of the four organic substances was 30 mg/L. Figure 1.12 is a plot of TOC and UV as a function of relative molecular weight for four organics. It can be seen from the TOC chart that the main response peak of SA exhibits a typical macromolecule at a relative molecular weight of 8.25×10^5–3.57×10^4. The response peak of HA is at a molecular weight of 1,000–10,000, which is a medium molecule. The response peak of TA is about 300–3,000, which is basically a small molecule organic matter. The response peak of sucrose is concentrated at 1,000.

For the UV gel map, it can be seen that only TA and HA respond, while SA and SUC are completely unresponsive, indicating that SA and SUC are hydrophilic organics that do not respond to UV.

Low molecular weight organics, such as acetic acid, oxalic acid, etc., are regarded to be precursors of assimilable organic carbon (AOC) and are hydrophilic. Their OCD gel diagrams are shown in Figure 1.13. The molecular weights of formaldehyde and acetone are very low, the main response peaks are 400 and 300 respectively, the molecular weight of oxalic acid is relatively large, the main response is 2,100, and the molecular weights of acetic acid and formic acid are both 1,500.

EBSCOhost - printed on 2/14/2023 6:39 AM via . All use subject to https://www.ebsco.com/terms-of-use

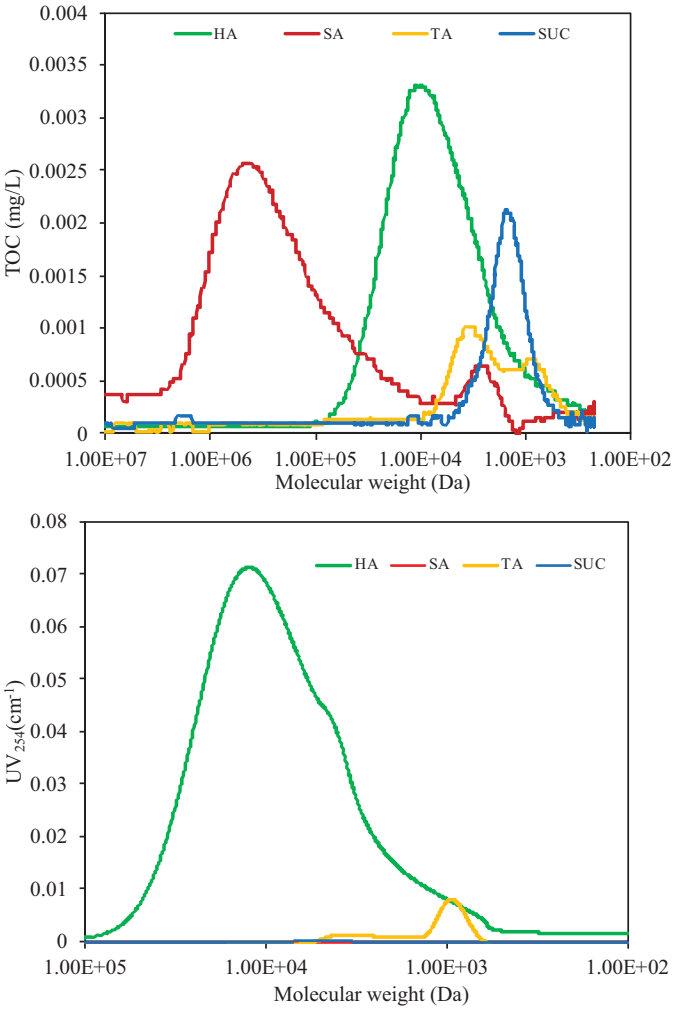

Figure 1.12: Molecular weight distribution of four organic compositions.

1.1.2.2 Natural raw water

The relative molecular weight distribution of organic matter in the raw water of Xiangjiang River and Taihu Lake was determined by HPSEC-UV-TOC combined technique, as shown in Figure 1.14. Before the measurement, the concentration of the water sample was adjusted to about 5 mg/L, the pH was adjusted to neutral, and the conductivity was adjusted to be consistent with the concentration of Ca^{2+}.

In the molecular weight distribution of the two raw water of Taihu Lake and Xiangjiang River, there are three response peaks, which can be divided to three distribution intervals. The first interval is the macromolecular organic matter. Organics in

EBSCOhost - printed on 2/14/2023 6:39 AM via . All use subject to https://www.ebsco.com/terms-of-use

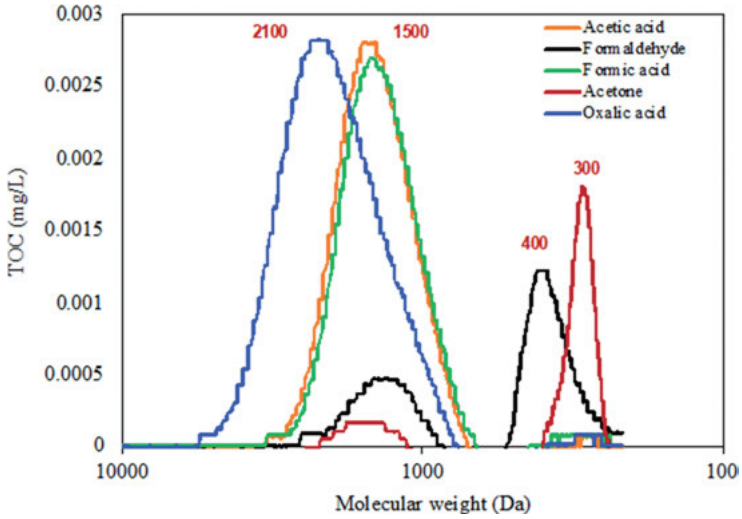

Figure 1.13: Molecular weight distribution of small molecular organic matter.

different raw water have different molecular weight ranges. The distribution of macromolecules in Taihu Lake is 1.0×10^7–1.0×10^5 Da, while that in Xiangjiang River is 1.18×10^6–6.04×10^4 Da. It can be seen that the molecular weight of macromolecule in Taihu Lake is larger than that of the Xiangjiang River and the content is higher. It can be seen from the UV map that this part of organic matter does not respond to ultraviolet light, indicating that this part is polysaccharide, colloid, or high molecular protein with very low UV absorption. The second interval is the medium molecular organic matter interval. The molecular weight range of Taihu Lake is from 1.03×10^4 to 1.78×10^3 Da, and that of Xiangjiang River water is 3.95×10^3–9.78×10^2 Da. Compared with the UV map, this part of organic matter responds strongly to UV_{254}, which is inferred to be humic organic matter that exhibits extremely strong UV absorption. The third interval is the small molecule organic matter. The molecular weight of Taihu lake water is 1.78×10^3–3.29×10^2 Da, and the Xiangjiang River water is 9.78×10^2–3.94×10^2 Da. Although the TOC response of small molecule organic matter is the largest in contrast to the UV result, the response to UV is small, indicating that this part of organic matter is mainly composed of single carbon bond and hydrophilic organic substance with less aromatic structure.

The molecular weight distribution of Qingcaosha and Wuhu water is shown in Figure 1.15. The molecular weight distribution of organic matter is similar to that of Taihu Lake and Xiangjiang River, and is mainly distributed in three intervals. The molecular weight of the first interval is mainly distributed between 5,000 kDa and 50 kDa. This part of the organic matter has a high molecular weight and is non-responsive to ultraviolet light, and accounts for a small proportion of total organic matter in the water, indicating that it is mainly composed of a hydrophilic organic substance such as polysaccharide or high molecular protein. The content of macromole-

EBSCOhost - printed on 2/14/2023 6:39 AM via . All use subject to https://www.ebsco.com/terms-of-use

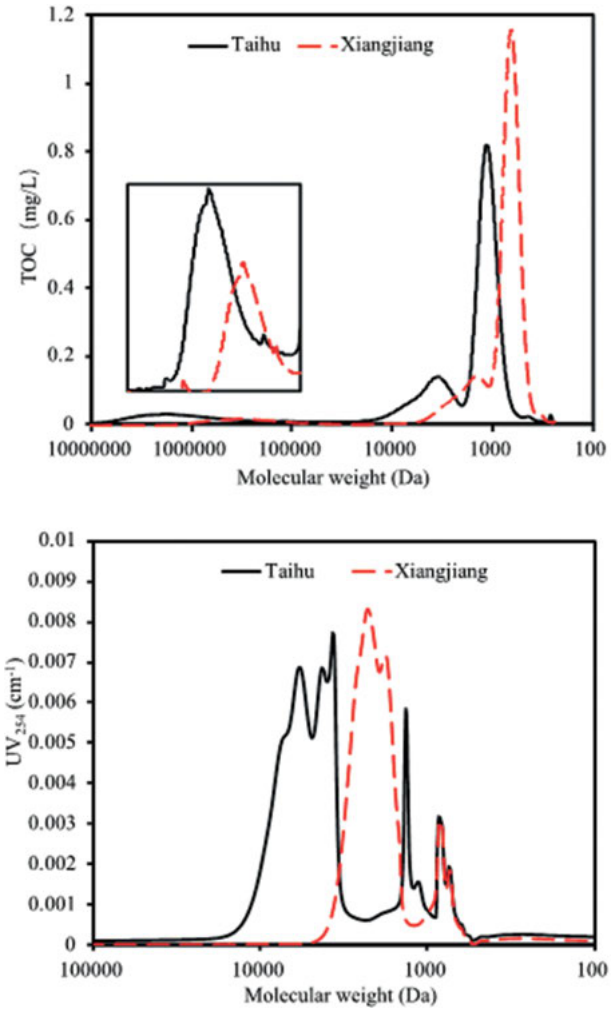

Figure 1.14: Molecular weight distribution of Taihu Lake and Xiangjiang River.

cules in Wuhu is higher than that in Qingcaosha. The molecular weight of the second interval ranges from 10 kDa to 2 kDa. Similar to Taihu Lake and Xiangjiang River, this part of organic matter has a strong response to ultraviolet light, which also indicates that it is mainly composed of humic acid and other hydrophobic organic substances with high UV response. The raw water in Wuhu contains more medium-molecular hydrophobic organic matter. The third interval has a molecular weight distribution ranging from 2 kDa to 200 Da and a peak at around 1 kDa. This part of organic matter has the largest response to TOC, but the response to UV is lower, indicating that this part of organic matter mainly includes some single carbon bonds and small hydrophilic molecular organic compounds with lower aromatic structure. The content of

EBSCOhost - printed on 2/14/2023 6:39 AM via . All use subject to https://www.ebsco.com/terms-of-use

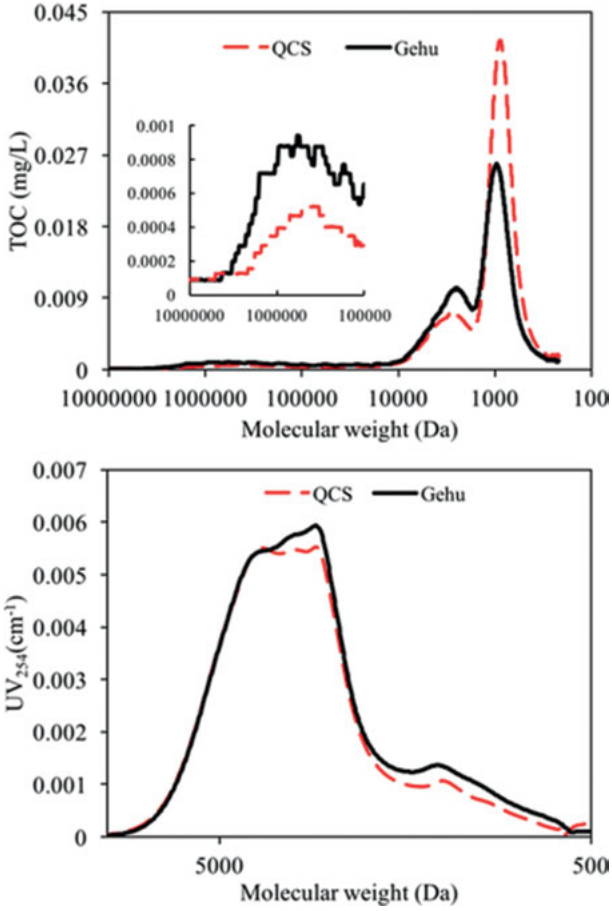

Figure 1.15: Molecular weight distribution of Qingcaosha and Wuhu water.

small molecular organic matter in Qingcaosha water is obviously higher than that of Wuhu.

Figure 1.16 shows the molecular weight distribution of Taihu Lake, Huangpu River, Yellow River and Qingcaosha. It indicates that the molecular weight response range is in three intervals, similar as the previous raw water. The distribution of macromolecules in Taihu Lake and Huangpu River is larger than that in the Yellow River and Qingcaosha, and the response intensity is also stronger. For medium molecules, the Huangpu River has the highest response intensity, followed by the Yellow River, Qingcaosha and Taihu Lake with the lowest response intensity. The small molecule response of the Huangpu River is the lowest, and the rest are similar.

EBSCOhost - printed on 2/14/2023 6:39 AM via . All use subject to https://www.ebsco.com/terms-of-use

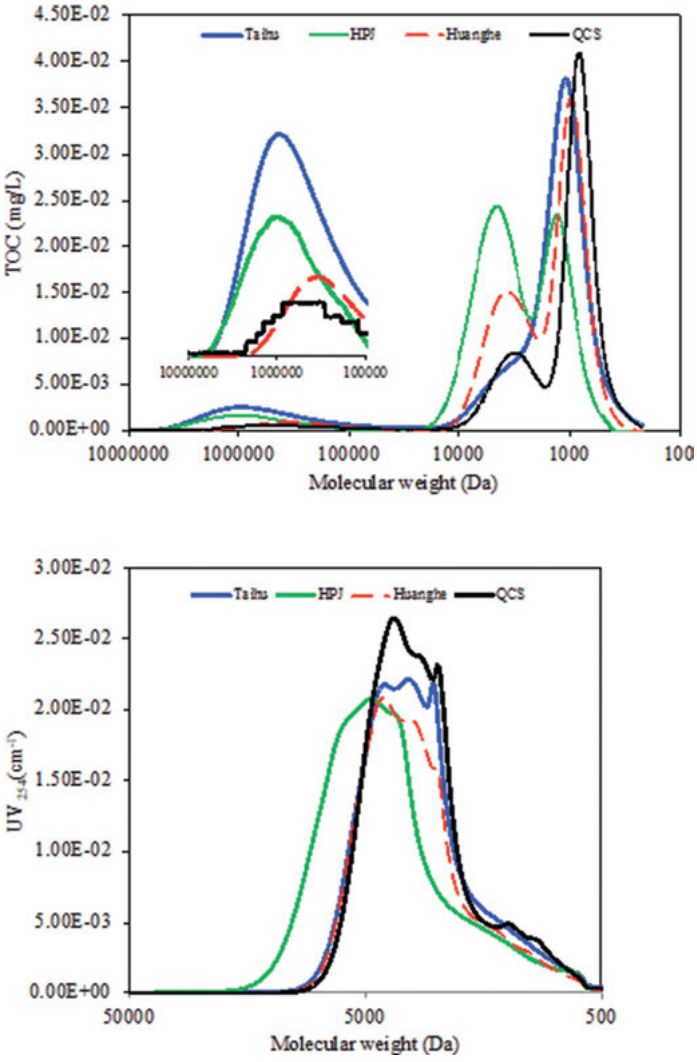

Figure 1.16: Molecular weight distribution of different raw water.

1.1.2.3 Algal organic matter

Algal organic matter (AOM) is a metabolic product secreted by algae growth process. Algae can easily grow in many closed water bodies, such as lakes and reservoirs, so the organic matter in such water bodies is composed of large number of algal organic matters. Therefore, analysis of the molecular weight distribution of algal organics helps for the understanding of the water quality affected by algae and the selection of proper water treatment processes.

EBSCOhost - printed on 2/14/2023 6:39 AM via . All use subject to https://www.ebsco.com/terms-of-use

Figures 1.17 and 1.18 show the molecular weight distribution of six algal organics. Similar to natural raw water, they are also apparently composed of three response intervals. However, some algal organics have higher large-MW content than natural raw water. Among them, ANF is the highest, followed by APF and MA, while Cy is the lowest. In some lakes, such as Taihu Lake, there are high large-MW organics, which is mainly affected by algae. In addition, it is also found there is macromolecular response range in Taihu Lake water and the basic overlap of some algae such as patina, since the Microcystis is the dominant algae in Taihu Lake.

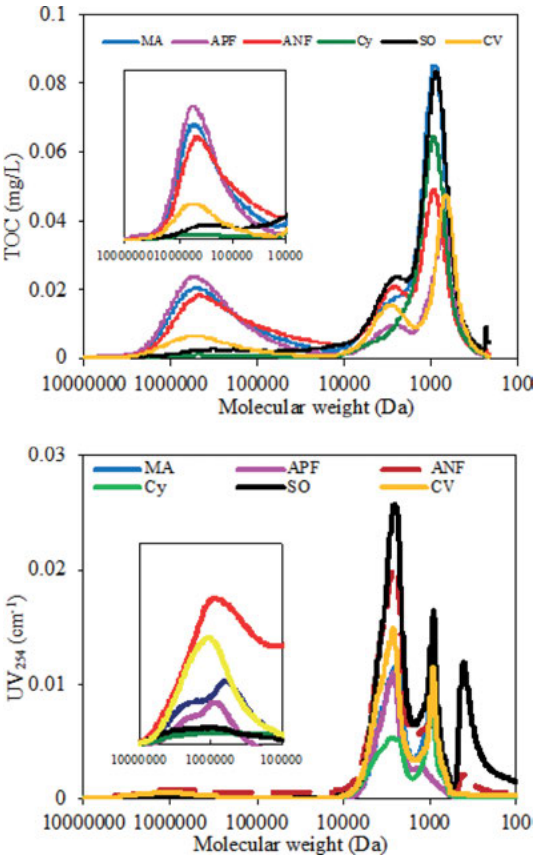

Figure 1.17: Molecular weight distribution of algal organic matter.

By analyzing the molecular weight distribution of various raw water and algal organic matter, the characteristics of molecular weight distribution can be summarized, as shown in Figure 1.19. The molecular weight distribution can be divided into three intervals, the large-MW interval, with the molecular weight distribution ranging from tens of thousands to millions, mainly composed of polysaccharides and protein

EBSCOhost - printed on 2/14/2023 6:39 AM via . All use subject to https://www.ebsco.com/terms-of-use

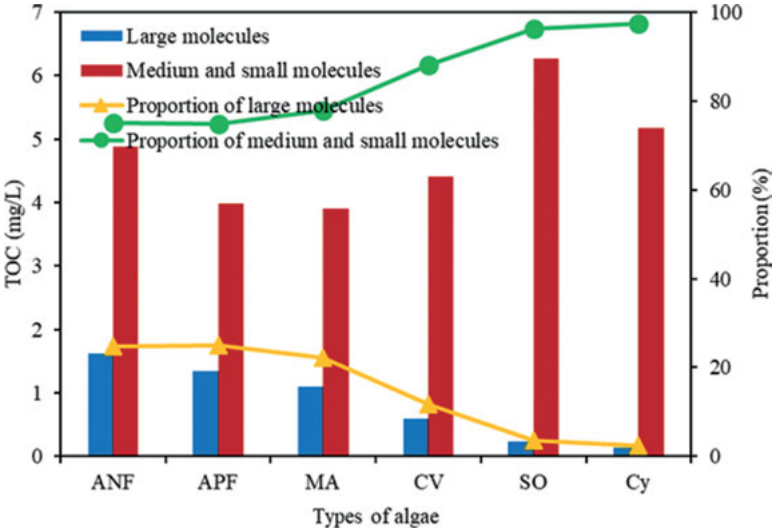

Figure 1.18: Molecular weight distribution of algal organic matter.

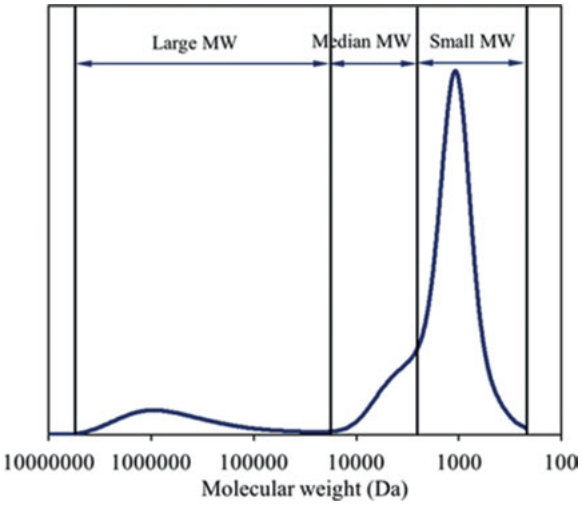

Figure 1.19: Molecular weight distribution of natural organic matter in natural water.

organic substances, with the UV_{254} response being weak or even non-responsive; the medium molecular range, with the molecular weight range being several thousand to 10,000, mainly composed of hydrophobic organic matter such as humic acid, which is strongly absorbed by UV_{254}; small molecular interval, with molecular weight from 2,000 to several hundred, mostly hydrophilic organic matter.

EBSCOhost - printed on 2/14/2023 6:39 AM via . All use subject to https://www.ebsco.com/terms-of-use

1.1.3 Comparison of OCD method and ultrafiltration membrane filtration method

Ultrafiltration membranes with different molecular weight cut-offs were used for the filtration of Taihu Lake water, and the filtrate was measured by OCD system. The results are shown in Figure 1.20. With the membrane filtration with molecular weight cut-off of 100 k, the response peak of the permeate decreased, but the peak of the organic matter with 100 k still existed. However, with the membrane filtration with the molecular weight cut-off of 30 k, the peak of the organic matter with 100 k completely disappeared. With the membrane filtration with the molecular weight cut-off

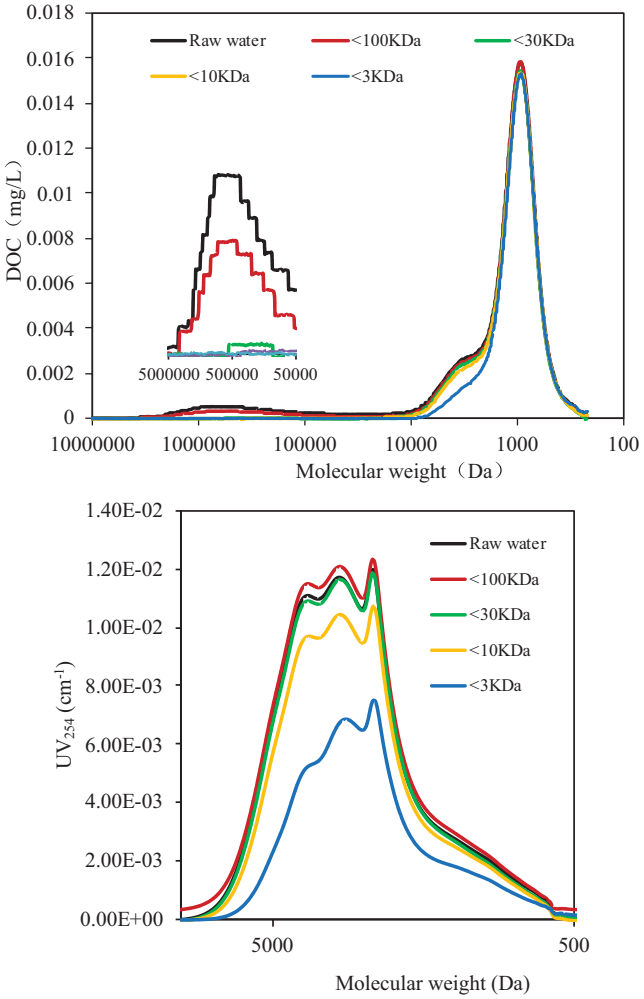

Figure 1.20: Comparison between OCD method and ultrafiltration membrane filtration method.

EBSCOhost - printed on 2/14/2023 6:39 AM via . All use subject to https://www.ebsco.com/terms-of-use

of 3 k, the organic matters with molecular weight of 3 k are still present in a large amount. It can be observed that the molecular weight cut-off of the ultrafiltration membrane is not the same as that of the OCD system, and they are not equivalent.

1.2 Organic components

Organic matter in natural water is a mixture of many organic substances. Although with different properties, they have some common physicochemical properties. These properties greatly affect the effect of water treatment and thus become a concern. Hydrophilic and hydrophobic properties are important parameters for characterizing organic matter. Current study indicates that pro-hydrophobicity is closely related to the production of disinfection by-products. In addition, the effect of drinking water to remove organic matter is also closely related to their hydrophobicity.

1.2.1 Separation method

The hydrophilicity and hydrophobicity of the organic substance can be obtained by adsorption of resin [3]. The water sample is first filtered with 0.45 μm to remove the suspended solids. Then the water sample is adjusted to pH 2 with HCl and passes through a column packed with DAX-8 resin. DAX-8 resin adsorbs strong hydrophobic organic substances such as humic acid. The aqueous organics then pass through the adsorption column. The organic substance adsorbed on the DAX-8 resin can be eluted with NaOH of pH 13, and the eluate is separated into a strong hydrophobic and weakly hydrophobic organic substance by an adsorption column packed with IRC-120 resin. The permeate of the DAX-8 resin adsorption column enters the XAD-4 adsorption column, and the XAD-4 resin adsorbs weakly hydrophobic organic matter, and the organic matter in the permeate is recognized to be a hydrophilic organic substance. The permeate passes through an IRA-958 resin adsorption column to separate the hydrophilic organics into neutral and non-neutral hydrophilic organics. The separation processes are shown in Figure 1.21.

It has been found in a large number of studies that the organic components with the same compositions have some similar compositions, and there are large differences in functional group types, element contents and chemical bond saturation between different components. Table 1.2 summarizes the compositions of the materials in the hydrophilic and hydrophobic components of natural organic matter.

EBSCOhost - printed on 2/14/2023 6:39 AM via . All use subject to https://www.ebsco.com/terms-of-use

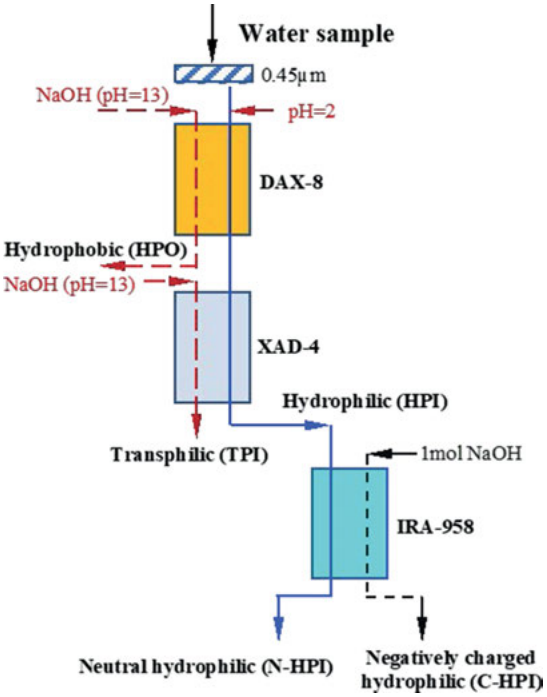

Figure 1.21: Separation process of organic components.

Table 1.2: Composition of organic and hydrophilic components.

Organic component	Main compound composition
Strong hydrophobic component	humic acid, phenolic compounds (such as lignin), aromatic compounds
Weakly hydrophobic component	aliphatic, aromatic compounds, amino compounds, unsaturated carbon, and increased C-O and C-H bond ratios
Charged hydrophilic component	esters, amides, carboxylic acid functional groups, proteins, small amounts of unsaturated aromatic compounds
Neutral hydrophilic component	polysaccharides, amino sugars, small molecular organics

1.2.2 Organic components of natural raw water

1.2.2.1 Components of organic matter

Humic acid, tannic acid and sodium alginate were selected and their components were determined. The results are shown in Figure 1.22. The proportion of strong components of humic acid exceeds 70%, while the hydrophilic component is only 10%,

EBSCOhost - printed on 2/14/2023 6:39 AM via . All use subject to https://www.ebsco.com/terms-of-use

indicating that humic acid is a typical hydrophobic organic matter. The proportion of the hydrophilic component of sodium alginate exceeds 80%, indicating that it is a typical hydrophilic organic substance. The proportions of the hydrophilic and hydrophobic components of tannic acid are relatively the same.

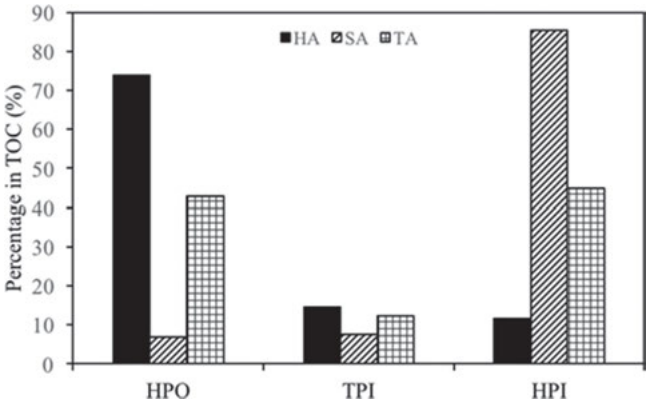

Figure 1.22: Components of organic matter.

1.2.2.2 Organic components of natural raw water

The organic compositions of Sanhaowu, Yellow River, Huangpu River, Kunshan Miaohe River and Gaoyou Reservoir are shown in Figure 1.23. The distribution of organic components in different raw water varies widely. From the total proportion of hydrophilic and hydrophobic organic matter, more than 60% of the organic matters of the five raw water are hydrophilic components (including the transphilic), and the proportion of the hydrophilic components of Sanhaowu and Kunshan water is more than 70%. Among the five kinds of raw water, the proportion of hydrophobic organic matter is 30%–40%, and the largest proportion of hydrophobic components is the raw water of Huangpu River, followed by the Yellow River. For hydrophobic component, the content of the strong component is higher than that of the weak one, and the order of the content of each strong component is basically the same as the order of the SUVA value of the raw water, indicating that the SUVA value has a good correlation with the hydrophobic component. Figure 1.24 show the SUVA values of the components. It can be seen that the response order of each component to the SUVA value is: strong hydrophobic > weakly hydrophobic > charged hydrophilic > neutral hydrophilic, indicating that the UV absorption intensity by four components is reduced along with the reducing molecular structure of the benzene ring.

The proportion of pro-hydrophobicity of natural raw water varies with the source of water, but what they have in common is the high proportion of hydrophilic com-

EBSCOhost - printed on 2/14/2023 6:39 AM via . All use subject to https://www.ebsco.com/terms-of-use

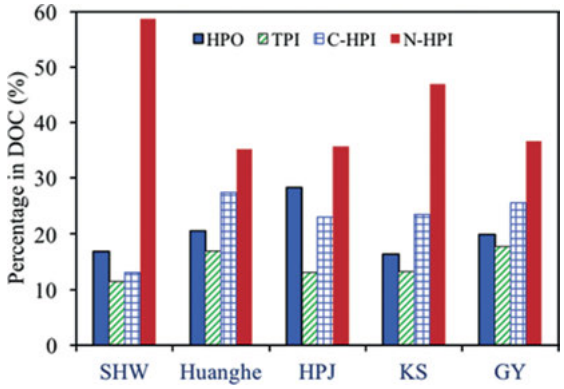

Figure 1.23: Organic components of different raw water.

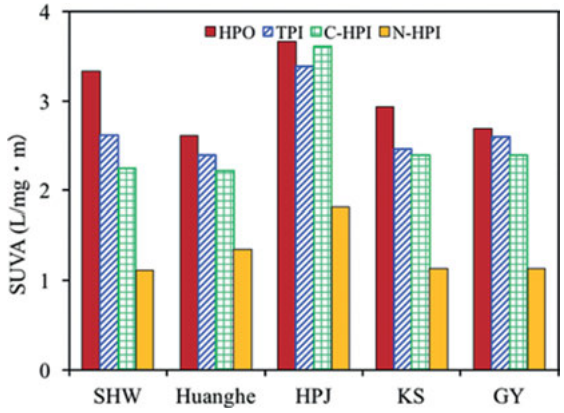

Figure 1.24: SUVA of different raw water components.

ponents. For water sources that are not contaminated, the organic matter should be dominated by humic acid and should be strong hydrophobic. The hydrophilicity of natural raw water comes from contaminants in the water body.

Figure 1.25 shows the organic components of Taihu Lake and Xiangjiang River. It can be seen that the proportion of the neutral hydrophilic component is the highest, followed by the strong hydrophobic component, and the ratio of transphilic and negatively charged hydrophilic component is the lowest. The composition of Shanghai Qingcaosha and Changzhou Wuhu is shown in Figure 1.26. Unlike the component distribution in other water sources, the proportion of strong hydrophobic components is the highest, followed by the neutral hydrophilic, while the proportion of the transphilic and negatively charged hydrophilic components is still the least.

By comparing the organic components of various raw water, it can be seen that the neutral hydrophilic and strong hydrophobic compositions are the most impor-

EBSCOhost - printed on 2/14/2023 6:39 AM via . All use subject to https://www.ebsco.com/terms-of-use

tant organic components in natural raw water. In most cases, the lakes and reservoirs contain the highest transphilic components.

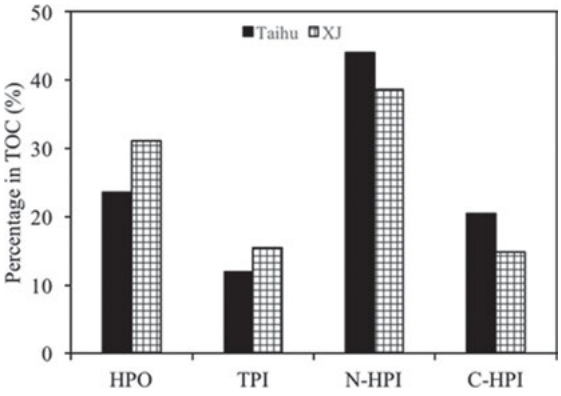

Figure 1.25: Organic components of Taihu Lake and Xiangjiang River.

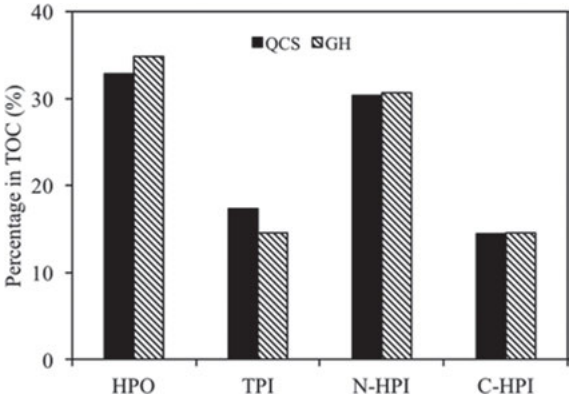

Figure 1.26: Organic components of Qingcaosha and Wuhu.

1.2.3 Algal organic matter

The composition of algal organics is shown in Figure 1.27. Unlike natural raw water, the proportion of the neutral hydrophilic components of algal organic matter is very high, over 50% for all the six algae species. Thus, algal organics are typically hydrophilic. And algae can easily grow in lakes and reservoirs due to the closed system. The organic substances in these water bodies are mostly composed of algal organic matters, with high degree of hydrophilicity. The water bodies mentioned above, such as Sanhaowu,

EBSCOhost - printed on 2/14/2023 6:39 AM via . All use subject to https://www.ebsco.com/terms-of-use

Kunshan and Taihu Lake, are hydrophilic, so the proportion of neutral hydrophilic is significantly higher than other flowing water bodies, such as the Yellow River.

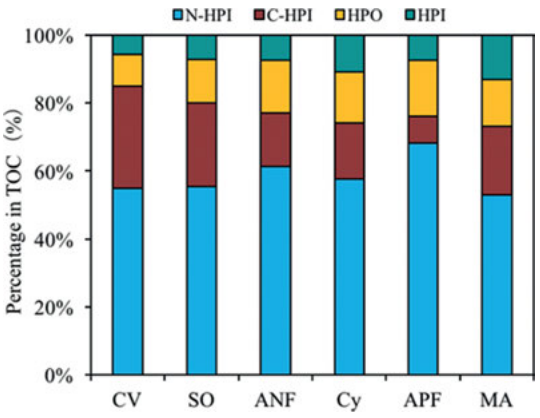

Figure 1.27: Components of algal organic matter.

1.3 Three-dimensional fluorescence spectra of organic matter

Fluorescence spectroscopy has been used in water related studies for more than 50 years. In the 1990s, researchers began to analyze the source and composition of water samples using three-dimensional fluorescence spectroscopy. Since water treatment technology and its effects are greatly affected by water quality sources and components, three-dimensional fluorescence spectroscopy is widely used in the analysis of water treatment technology. The intensity of fluorescence is directly related to the molecular structure of the organic matter. Molecular structures, such as aromatic compound containing a π bond, unsaturated carbon bond (C = C), characteristic functional group including hydroxyl group, amino group or alkoxy group, all cause fluorescence easily.

With the wide application of three-dimensional fluorescence spectroscopy in the field of water treatment, such detection methods with high sensitivity, good selectivity, high information volume, and no damage to water-like structures have received increasing attention. Three-dimensional fluorescence spectroscopy allows spectral identification and characterization of complex multi-component systems and is ideal for the understanding of dissolved organic matter in natural water. Related studies have shown that three-dimensional fluorescence spectrum provides a wealth of material information for the study of dissolved organic matter. For different sources of dissolved organic pollutants, the position, intensity and regional distribution of fluorescence peaks are different, thus forming fluorescence spectral information representative of various water

EBSCOhost - printed on 2/14/2023 6:39 AM via . All use subject to https://www.ebsco.com/terms-of-use

source characteristics. Table 1.3 provides the results obtained by some researchers in recent years using three-dimensional fluorescence spectroscopy for the analysis of water quality component information. It can be seen from the table that the three-dimensional fluorescence spectrum can be used to determine the source and composition of organic matter in the water sample. It can provide at least two kinds of spectral information of fluorophores, i.e. humic acids and proteins, and two kinds of organic substances. Both are important components of membrane fouling.

In addition, many researchers have conducted in-depth study on three-dimensional fluorescence spectroscopy, and found that three-dimensional fluorescence spectroscopy can not only characterize the composition and source information of organic matter, but also have certain correlation with the molecular weight and hydrophobicity of DOM. When studying the fluorescence properties of amino acid organics in natural water, Wu and Tanoue found that the protein fluorescence peak is mainly composed of large molecular weight tryptophan, while the humic acid fluorescence peak contains many small molecules of neutral and aromatic amino acids [4]. Yue et al. analyzed DOM fluorescence peaks in natural water sources using HPSEC, and found humic fluorescence peak is mainly in the organics with molecular weight range of 1–3 kDa, whereas proteins fluorescence peak is mainly in the organics with molecular weight greater than 2 kDa [5]. According to a study by Marhaba et al., various hydrophilic and hydrophobic organic components separated by a large pore size adsorption resin have different characteristic regions in the three-dimensional fluorescence spectrum [6]. The more hydrophobic component is in the longer wavelength region of the spectrum (the humic acid fluorescent region), while the more hydrophilic component is in the short wavelength region (protein fluorescent region). In a test by Lee et al., in addition to the characteristic fluorescence peak of hydrophobic organic matter located outside the humic-like fluorescing region, algal organic matter also showed significant fluorescence peaks in this region [7].

Table 1.3: Water quality characteristics by three-dimensional fluorescence spectroscopy measurement.

Source	Name	Type	Region	Source
Coble [8]	Peak A	Ultraviolet humic acid	250–260/380–480	Fresh water, coastal and marine environment such as purple river water
	Peak C	Visible area humic acids	330–350/420–480	Terrestrial organic matter, freshwater, deep seawater, deeply degraded humic organic matter
	Peak M	Marine humic acid	310–320/380–420	Marine sample
	Peak B	Tyrosine, Protein	270–280/300–320	Marine samples, biologically active, biodegradable organic matter

EBSCOhost - printed on 2/14/2023 6:39 AM via . All use subject to https://www.ebsco.com/terms-of-use

Table 1.3 (continued)

Source	Name	Type	Region	Source
	Peak T	Tryptophan, Protein, or phenols	270–280/320–350	Biologically active ingredient
Baker et al. [9]	Peak A	Fulvic acid	220–250/400–460	Fulvic acid
	Peak C	Humic acid	300–340/400–460	Humic acid
	Peak T	Tryptophan	220–235/330–370	Microbial and algal metabolites in rivers and lakes
Fu et al. [10]	Peak A	Ultraviolet fulvic acid	235–255/320–350	The unpolluted rivers are dominated by terrestrial humic acid fluorescence peaks. The lake-like water contaminated by industrial and domestic sewage has strong fluorescence peaks. Peak C and DOC have good correlations in DOM from different sources.
	Peak C	Visible fulvic acid	310–330/410–450	
	Peak B	Protein Tryptophan	270–290/320–350	
	Peak D	Protein Tyrosine	220–250/300–320	
Chen et al. [11]	Region I	Aromatic protein	200–250/280–330	Tyrosine
	Region II	Aromatic protein	200–250/330–380	BOD_5
	Region III	Fulvic acid	200–250/380–480	Hydrophobic acid
	Region IV	Soluble microbial byproduct	250–280/280–380	Tryptophan
	Region V	Humic acid	280–340/380–480	Humic acid, Hydrophobic acid

1.3.1 Three-dimensional fluorescence spectrum

The three-dimensional fluorescence spectroscopy matrix (EEM) data was taken from the Hitachi F-4500 fluorescence spectrometer. The excitation source was a xenon lamp. The wavelength scanning range was Ex/Em = 200–400 / 275–575 nm, and the excitation and emission slit widths were both 5 nm. The speed is 12,000 nm · min^{-1}, and the multiplying tube voltage (PMT) is 400 V. According to the test, the three-dimensional fluorescence spectrum is greatly affected by the pH of the water sample, but is less affected by the ionic strength of the water sample. Therefore, before the test, the water sample should be adjusted to pH ~ 7.0, and the temperature should be kept at 20–25 °C. The test was carried out using a 1 cm fluorescent cuvette. Before each sample is scanned, a blank measurement is performed with Milli-Q ultrapure water to exclude Rayleigh scattering and Raman scattering peaks due to pure water, and thereby control the stability of the fluorometer. The test data was processed using Matlab 7.0.

The three-dimensional fluorescence spectrum is exhibited in the form of contour maps and three-dimensional projections, as shown in Figure 1.28. In comparison, the

EBSCOhost - printed on 2/14/2023 6:39 AM via . All use subject to https://www.ebsco.com/terms-of-use

3D projection map can present more intuitive visual effects, while the contour map can more accurately represent the fluorescence information and also exhibit the relationship with the traditional two-dimensional fluorescence spectrum.

For discontinuous fluorescence matrix data, the fluorescence region intensity (φ_i) is calculated from:

$$\varphi_{\mathrm{i}} = \sum_{ex}\sum_{em} I(\lambda_{ex}\lambda_{em})\Delta\lambda_{ex}\Delta\lambda_{em} \tag{1.1}$$

where $\Delta\lambda_{\mathrm{ex}}$ and $\Delta\lambda_{\mathrm{em}}$ are the excitation and emission wavelength spacing (5 nm), which is the fluorescence intensity corresponding to each pair of excitation and emission wavelengths. The total fluorescence intensity is: $\varphi_{\mathrm{T}} = \sum \varphi_{\mathrm{i}}$. The percentage of fluorescence intensity in a region is:

$$P_i = \varphi_{\mathrm{i}} / \varphi_{\mathrm{T}} \times 100\% \tag{1.2}$$

When the water quality components are hydrophilic, the three-dimensional fluorescence spectrum intensity has a certain linear correlation with them. However, when characterizing the water quality from different water sources, it is not possible to directly correlate the fluorescence intensity with the components. Then further normalized treatment is required, and the fluorescence intensity of the DOC is adjusted to eliminate the difference in fluorescence intensity by water concentration. The ultraviolet absorption intensity at the referenced unit DOC concentration is expressed by SUVA, and the fluorescence intensity at the unit DOC concentration after treatment is indicated by the symbol FLU.

The spectrum is divided into five regions as shown in Figure 1.29. The boundary division of the five regions and the main characteristics are shown in Table 1.4.

Zone 1 and Zone 2 can be also combined to form 4 response zones, i.e.

- Fluorescence peak A: Ex/Em = 230–250/400–460 nm;
- Fluorescence peak C: Ex/Em = 280–350/400–470 nm;
- Fluorescence peak B: Ex/Em = 220–250/300–350 nm;
- Fluorescence peak T: Ex/Em = 250–310/300–360 nm.

As shown in Figure 1.30, fluorescence peaks A and C refer to humic acid fluorescence, and the region where the fluorescence peak A is located is called the fulvic acid fluorescence in the ultraviolet region, and the region where the fluorescence peak C is located is called the visible region humic acid fluorescence. The fluorescence peaks B and T belong to protein fluorescence, the fluorescence peak B can be called tyrosine fluorescence, and the fluorescence peak T is called tryptophan fluorescence.

EBSCOhost - printed on 2/14/2023 6:39 AM via . All use subject to https://www.ebsco.com/terms-of-use

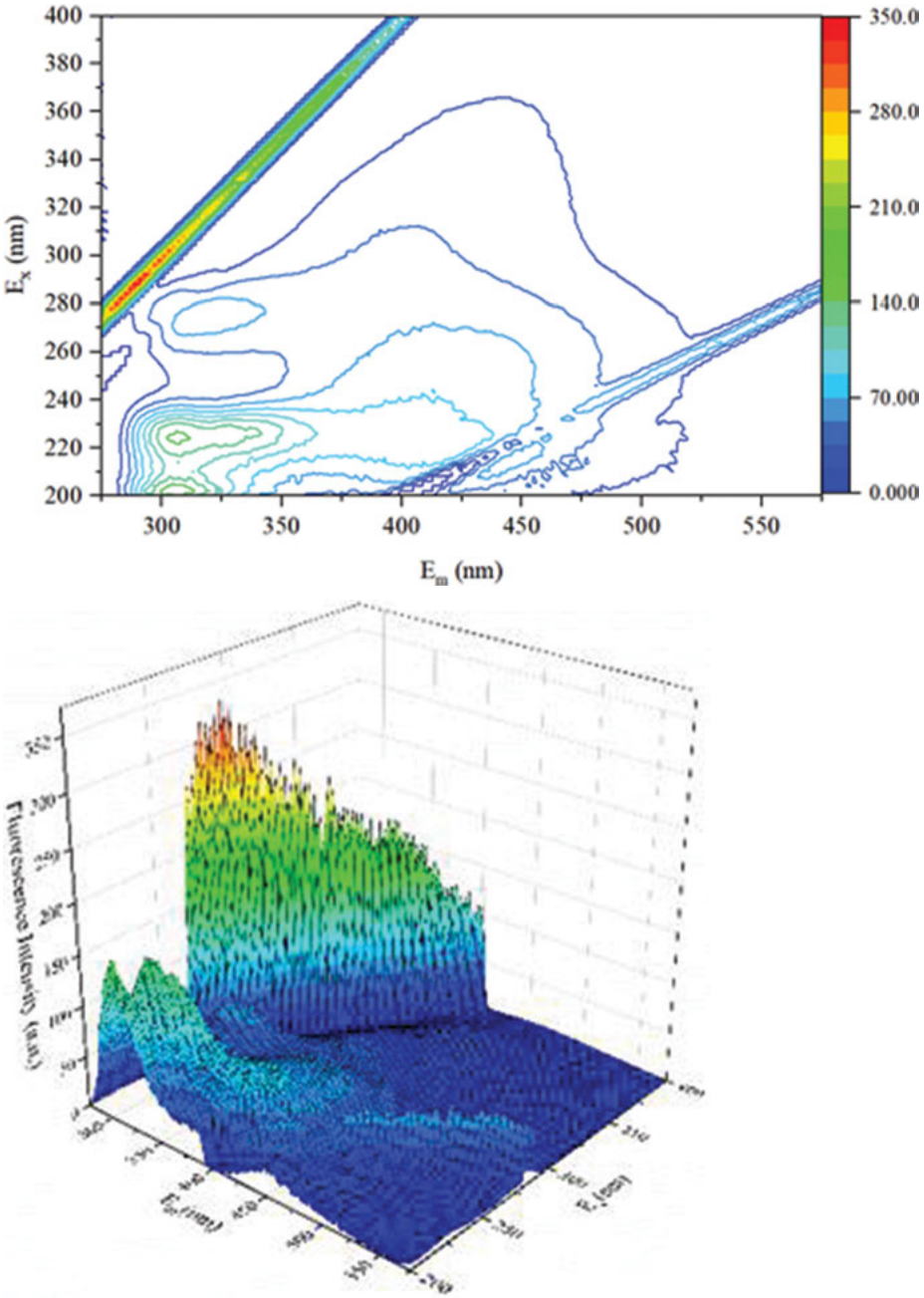

Figure 1.28: Representation of three-dimensional fluorescence spectrum.

EBSCOhost - printed on 2/14/2023 6:39 AM via . All use subject to https://www.ebsco.com/terms-of-use

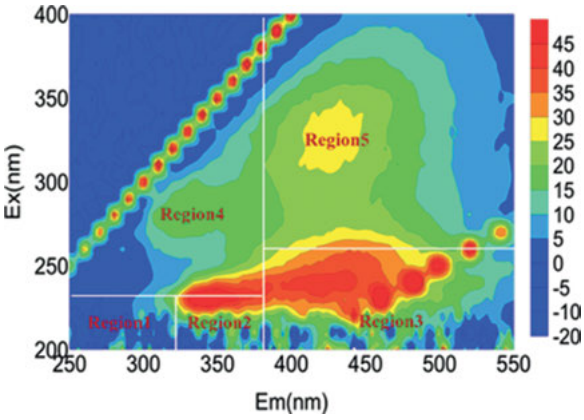

Figure 1.29: Three-dimensional fluorescence spectral response area.

Table 1.4: Divided regions in FEEM and characteristic organic substances.

Region	Excitation wavelength (Ex/nm)	Emission wavelength (Em/nm)	Characteristic organic matter
Region 1	200–255	280–330	Aromatic Protein
Region 2	200–255	335–380	Aromatic Protein
Region 3	200–280	385–500	Fulvic acid
Region 4	260–320	280–380	Soluble Microbial Products
Region 5	285–350	385–500	Humic acid

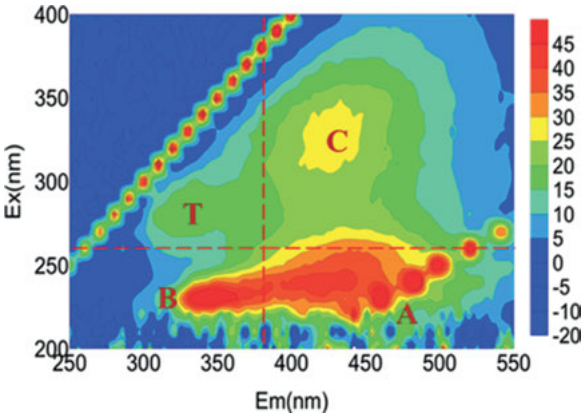

Figure 1.30: Fluorescence spectral response area division diagram.

EBSCOhost - printed on 2/14/2023 6:39 AM via . All use subject to https://www.ebsco.com/terms-of-use

1.3.2 The EEM of natural raw water

1.3.2.1 Natural raw water

Figure 1.31 presents the excitation-emission matrix (EEM) of water from Sanhaowu, Yellow River, Huangpu River, Kunshan Miaojing River and Gaoyou reservoir. All of the five raw water samples appeared fluorescence peaks in four regions as specified below.

As shown in the distribution of fluorescence peaks, water samples from Sanhaowu, Yellow River, Huangpu River and Kunshan, presented strong protein fluorescence peaks. Protein fluorescence mainly originates from the organic matter produced by metabolism of aquatic organisms such as algae and sewage coming from human activity. It is reported that tryptophan fluorescence peak T consists of two parts: (1) macromolecular protein organic matter (Ex/Em = 280/325 nm) as generally believed, and (2) phenolic substances (Ex/Em = 275/306 nm) with relatively small molecular weight, mainly coming from the plant degradation, which is a precursor of humus. Therefore, there may exist a certain amount of macromolecular protein organic matter in the water of Sanhaowu, Yellow River, Huangpu River and Kunshan, considering the four kinds of raw water with stronger T peak.

As seen from the fluorescence intensity, different sources of soluble organic matter exhibited various responses in fluorescence intensity, indicating the different source and composition of dissolving organic matter in different water. According to Table 1.5, the total fluorescence intensity of the five water declines in the order of Huangpu River > Kunshan > Sanhaowu > Yellow River > Gaoyou. For different types of fluorescence peaks, the fluorescence intensity follows the order of FLU T > FLU B > FLU A > FLU C, showing that the aromatic protein organic matter has higher response in fluorescence intensity than humic organic matter. Humic fluorescence peaks are often masked by high intensity protein fluorescence.

The fluorescent area integration method as described by Chen et al. was used to further quantify the fluorescence intensity [11]. The EEM was divided into five regions, and then the fluorescence intensity was integrated over the area to calculate the total fluorescence intensity for each region and the proportion of the fluorescence intensity in each region relative to the whole intensity of the five regions. The fluorescence area integration method can help to avoid inaccurate location of the fluorescence peak when multiple peaks are present in the same region (such as water from Yellow River, Figure 1.31), and also to analyze organic matter compositions of water samples by comparing the proportions of total fluorescence intensities integrated for different regions.

According to the fluorescence area integration method, the proportions of total fluorescence intensities for each fluorescence region is calculated and shown in Figure 1.32. Sanhaowu water had the strongest response in region 2; Yellow River responded most strongly in regions 1 and 2; both Huangpu River and Kunshan water

EBSCOhost - printed on 2/14/2023 6:39 AM via . All use subject to https://www.ebsco.com/terms-of-use

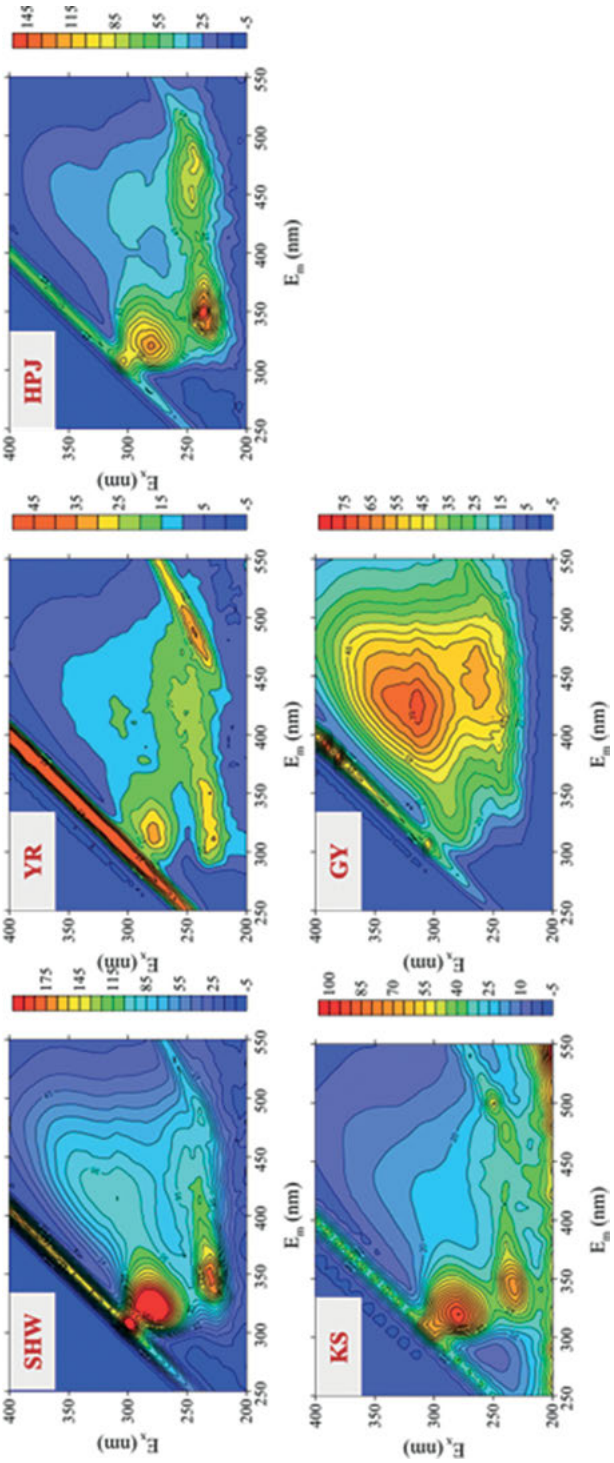

Figure 1.31: The EEM of natural water samples.

EBSCOhost - printed on 2/14/2023 6:39 AM via . All use subject to https://www.ebsco.com/terms-of-use

Table 1.5: The corresponding fluorescence intensity of raw water.

Source of water		Sanhaowu	Yellow River	Huangpu River	Kunshan	Gaoyou
A peak	Ex/Em	245/415	240/435	245/445	240/420	255/430
	FLU	4.45	5.55	18.06	7.29	3.9
C peak	Ex/Em	315/415	300/420	305/435	310/420	325/420
	FLU	3.85	3.75	7.87	4.6	3.09
T peak	Ex/Em	285/320	280/310	280/320	280/320	285/320
	FLU	8.79	7.01	25.67	18.97	2.15
B peak	Ex/Em	235/350	225/310	235/350	230/340	–
	FLU	6.63	6.60	34.26	14.64	–
The total fluorescence peak		23.72	22.91	85.86	45.5	9.14
$f_{450/500}$a		1.44	1.32	1.43	1.34	1.3
$r(a, c)$		1.16	1.48	2.29	1.58	1.26
$r(t, b)$		1.33	1.06	0.75	1.30	–

had strong response in region 2, followed by region 1; while Gaoyou water had the strongest response in region 3, followed by region 5. Water samples from Sanhaowu, Huangpu River and Kunshan had higher response fraction in region 2 than the other two water samples, while Gaoyou had higher response proportions in regions 3 and 5 than the others. In summary, different raw water exhibited various fluorescence responses, which is largely due to various sources of organic matters in these water bodies. Further, observations in Figure 1.32 reveals that closed water bodies, such as lakes and reservoirs, (e.g., Sanhaowu and Kunshan) had common characteristic of fluorescence response that region 2 responds most strongly. Although Huangpu River is a flowing water body, its characteristics of organic matter are largely similar to that of its primary source, Taihu lake.

Water samples originated from different sources exhibited significantly different fluorescence intensity proportions. The raw water of Gaoyou was obviously different from other water sources, with high proportion (65%) of humus fluorescent regions (regions 3 and 5), while small proportion of protein fluorescence (regions 1 and 2). The fluorescence of other sources of water was mainly protein fluorescence, accounting for 65%–75% of the total fluorescence intensity, indicating these water bodies are contaminated by protein-like organic matters with high fluorescence responses.

Two fluorescence parameters could be utilized to determine the source of organic compounds in humus fluorescence region. The fluorescence index $f_{450/500}$ represents the corresponding fluorescence intensity ratio at the emission wavelength of 450 nm and 500 nm when the excitation wavelength is 370 nm. The fluorescence index $f_{450/500}$

EBSCOhost - printed on 2/14/2023 6:39 AM via . All use subject to https://www.ebsco.com/terms-of-use

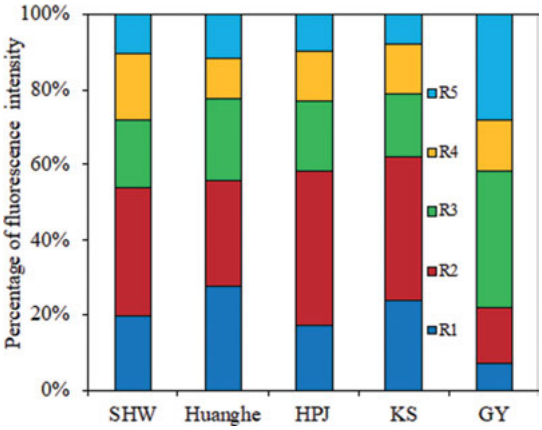

Figure 1.32: Fluorescence area intensity.

is typically about 1.4 for water contaminated by biological sources, while generally around 1.9 for water contaminated by terrestrial sources containing humus organisms. The fluorescence indices of the five kinds of raw water turned out to be all around 1.4 (as summarized in Table 1.6), indicating that all of these water sources exist dissolved organic substances from aquatic organisms, algae and phytoplankton sources.

The other fluorescence parameter is $r(a, c)$, which is the ratio of fluorescence peak A to C, and can be used to judge the degree of humification of water source. A smaller $r(a, c)$ indicates a higher degree of humification and a larger molecular weight of organic matters in water. In addition, the change of $r(a, c)$ reflects the difference sources of humic organics imported to the water body. Coble's results showed that $r(a, c)$ of groundwater was 0.77, $r(a, c)$ of river water was 1.08, and $r(a, c)$ of CuiCui lake was 1.26 [8]. The $r(a, c)$ of plateau lake measured by Fu et al. is influenced by the pollution of urban production and living pollution, which is up to 2.09 [10]. Values of $r(a, c)$ were compared amongst the five kinds of raw water in Table 1.5, indicating a wide variation in their sources of humic substances. Among them, the $r(a, c)$ of raw water in Huangpu River reached as high as 2.29, which is higher than that of the contaminated plateau lakes measured by Fu et al. [10]. This shows that the raw water from Huangpu River has been severely affected by domestic pollution and industrial wastewater discharge. The $r(a, c)$ values of other raw water were generally within the range of normal surface water conditions, though their sources of humic substances vary greatly.

There is a third fluorescence parameter $r(t, b)$ that can be used to determine the source of organic matter in the protein fluorescence region, which is calculated as the intensity ratio of the fluorescence peak T to B. The water with larger $r(t, b)$ (1.4) had more macromolecules from algae and biodegradation, while the water with small $r(t, b)$ (0.6) contains a large number of protein fluorescence peaks, usually due to wastewater discharged from human production. By comparing $r(t, b)$ of five kinds

EBSCOhost - printed on 2/14/2023 6:39 AM via . All use subject to https://www.ebsco.com/terms-of-use

of raw water, we found that $r(t, b)$ of raw water from Sanhaowu and Kunshan are the largest with values close to 1.4 (1.3–1.33), indicating that there were more organic matters in these two water bodies. Although the fluorescence intensity of the raw water from Huangpu River was very high, the $r(t, b)$ is only 0.75, indicating that the molecular weight of protein-based organic matter in Huangpu River was relatively small, typically due to serious pollution of human production and domestic sewage. The protein fluorescence peak of raw water from Gaoyou was very low, and no $r(t, b)$ exists, indicating that the raw water from Gaoyou contained little organic protein.

In summary, through the analysis of two fluorescence parameters $r(a, c)$ and $r(t, b)$, it is found that the fluorescence parameters of protein and humic acids are basically consistent with the origin of organic matter. To simplify the analysis, the fluorescence intensities of the protein fluorescence peak T and the humic fluorescence peak A were compared as $r(t, a)$ (the ratio of fluorescence peaks T and A), which can determine the results of these two fluorescence parameters. The significance of $r(t, a)$ includes: (1) firstly, it reflects the ratio of macromolecular organic compounds to small ones; according to the above, the fluorescence peak T is related to the presence of protein-like macro-molecule organic matter, while the fluorescence peak A reflects the small-molecule humic organics, thus the value of $r(t, a)$ is proportional to the molecular weight; (2) secondly, it reflects the source of organic matter; fluorescence peak T mainly comes from protein-based organisms, and these organisms mainly exist in sewage discharge by human or other organisms, while fluorescence peak A represents terrestrial small-molecule organic matters, thus the ratio between the two is closely related to the source of organic matters.

The following table shows the $r(t, a)$ of the five raw water and their hydrophilic and hydrophobic components. It can be seen that the wide range of $r(t, a)$ (from 2.0 (or above) to less than 1.0) reflects various degrees of pollution and sources of organic pollutants. Raw water with higher $r(t, a)$ (2.0 or above) is most seriously polluted, and raw water with lower $r(t, a)$ (less than 1.0) is less polluted, which mainly contains terrestrial organic pollutants from land, especially humic substances. Raw water with $r(t, a)$ between 1.0 and 2.0, is greatly affected by the discharge of human production and living sewage, containing pollutants with smaller molecular weight.

Table 1.6: The $r(t, a)$ of raw water and its components.

r(t, a)	Sanhaowu	Yellow River	Huangpu River	Kunshan	Gaoyou
Raw water	1.98	1.26	1.42	2.60	0.55
Strong hydrophobic	0.00	0.41	0.72	0.63	0.00
Weakly hydrophobic	1.20	0.64	1.30	1.67	0.42
Charged hydrophilic	5.43	1.16	2.09	3.32	0.84
Neutral hydrophilic	0.66	0.00	0.47	0.43	0.56

EBSCOhost - printed on 2/14/2023 6:39 AM via . All use subject to https://www.ebsco.com/terms-of-use

The fluorescence spectra of other four kinds of raw water are shown in Figure 1.33. The fluorescence response areas of Xiangjiang River and Taihu Lake are similar, with the strong response of region T and B. The difference is that Xiangjiang River water has additional response in region A and C, with more intense response in region A. The fluorescence response of Taihu Lake water is mainly concentrated in region T and B. Qingcaosha water has all 4 response regions, with stronger response in regions B and A. In contrast, the fluorescence response of Ge lake is mainly concentrated in the C and A regions.

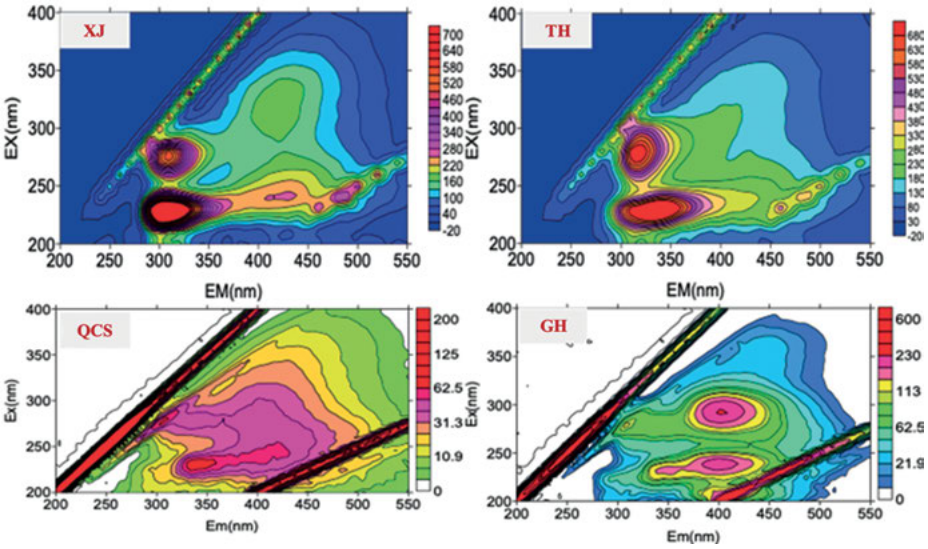

Figure 1.33: The Three-dimensional Fluorescence Spectroscopy of different raw water.

1.3.2.2 Algal organic matter

The fluorescence spectra of the six algae organisms are shown in Figure 1.34. Scenedesmus has a strong fluorescence response at Ex/Em = 350/425 nm and Ex/Em = 270/450 nm, indicating that Scenedesmus has a lot of humic substances. Humic acids (region A and region C) are mainly derived from the catabolism of dead algal cells and macromolecules such as polysaccharides and proteins. Studies have shown that in the metabolic process of green algae, the intensity of the humic acid fluorescence region increases with the weakening of the protein fluorescence region, indicating that the humic acids may be mainly derived from macromolecular proteins and other organic substances. For Anabaena, Microcystis aeruginosa, Chlorella, Cyclotella, and Aphanizomenon, in addition to humic acid peak A and fulvic acid peak C, the response intensity of protein fluorescence peak T is also strong, indicating

EBSCOhost - printed on 2/14/2023 6:39 AM via . All use subject to https://www.ebsco.com/terms-of-use

that Anabaena, Microcystis aeruginosa, Chlorella, Cyclotella, and Aphanizomenon have a large number of protein-based organic matters.

The ratio of fluorescence intensity for six algal organic matters are shown in Figure 1.35.

1.4 The hydrophilicity/hydrophobicity and fluorescence spectra of organic matter

The position of fluorescence peak and the hydrophilicity/hydrophobicity of organic matter has a certain correlation. Marhaba et al. [6] and Wang et al. [12] used positions of three-dimensional fluorescence peak to rapidly characterize various hydrophilic and hydrophobic components. Hydrophobic acid-base components are generally found in the longer excitation-emission wavelength range, while hydrophilic acid-base components appear in the shorter wavelength region. Previous studies also found that in the humus-like fluorescence region, the fluorescence intensity in the longer emission wavelength (Em) is often related to the hydrophobic organic species.

Figures 1.36 and 1.37 show the fluorescence spectra of different components of water in Xiangjiang River and Taihu Lake. The predominant component of Xiangjiang River is mainly composed of fulvic acid in region A and humus in region C, with a few protein-rich organic matters. In contrast, there are more protein-rich organic matter in Taihu Lake with a few humic acids. The weakly-hydrophobic organic matter in raw water from Xiangjiang River mainly consists of humic acids in region C and fulvic acids in region A, and its response strength is less than that of strong-hydrophobic components. In Taihu Lake weakly-hydrophobic fractions are dominated by some protein-based organic compounds, with some small molecules of phenols, tryptophan and humus-like. Peaks exist in four regions for strong-hydrophilic components of Xiangjiang River and Taihu Lake, indicating that the strong-hydrophilic components contain many types of substances, such as protein-based and humus-based organic matters. The response of neutral-hydrophilic components mainly occurs in the fluorescence range of humic acid and fulvic acid, which is beyond our expectations. The neutral-hydrophilic components are mainly composed of polysaccharides and protein-based organic matters. Polysaccharides have very weak fluorescence response or even do not have any, thus the neutral-hydrophilic substances with fluorescence response usually represent protein-based organic matters.

Figures 1.38 and 1.39 show the fluorescence spectra of different components of water in Qingcaosha and Ge Lake. The strong hydrophobic organic matter in raw water from Qingcaosha consists of fulvic acids, humic acids and protein organic substances, while the strong hydrophobic organic matter in raw water from Ge Lake includes mainly fulvic acids and humic acids. Peaks exist in four regions for the weakly hydrophobic components of both Qingcaosha and Ge Lake, suggesting that the raw water of both feeds contain many types of organics, such as protein-based and humus-based

EBSCOhost - printed on 2/14/2023 6:39 AM via . All use subject to https://www.ebsco.com/terms-of-use

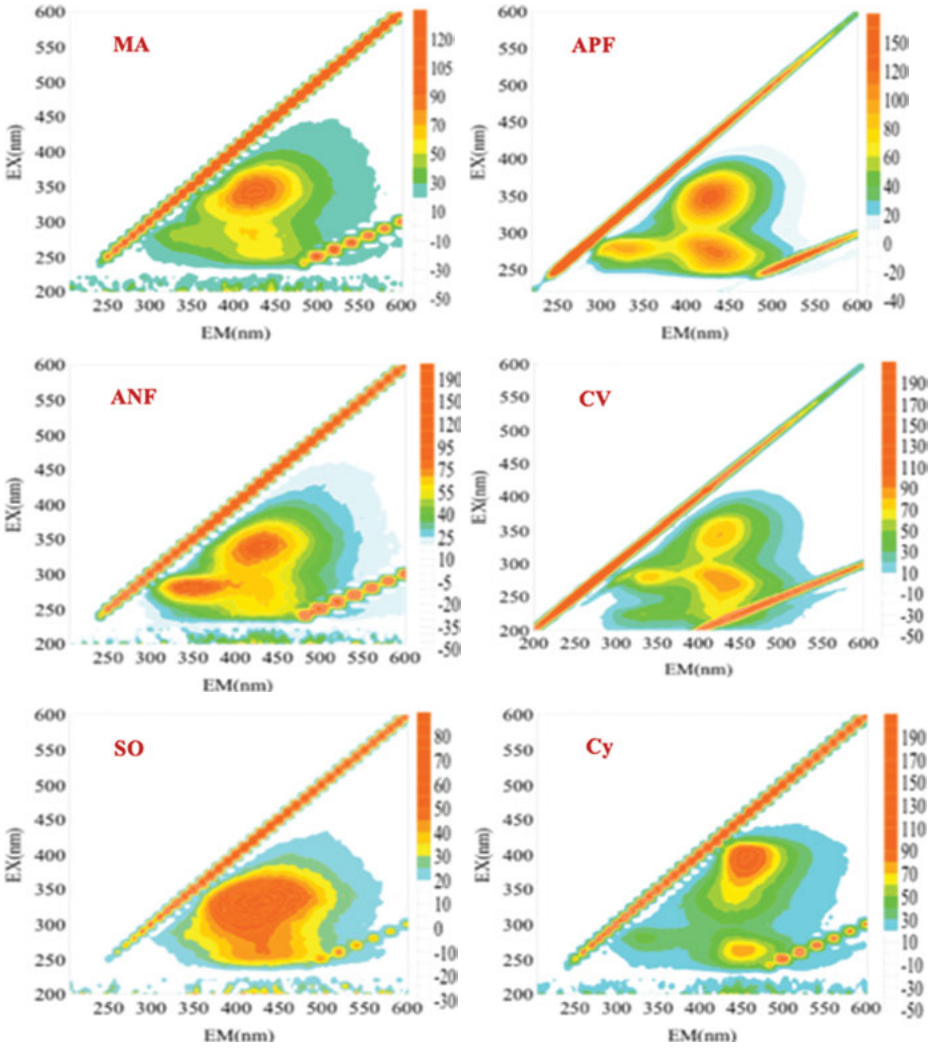

Figure 1.34: Three-dimensional Fluorescence Spectroscopy of organisms in algal organic matter.

organic substances. There are also four peaks for the charged hydrophilic components of both Qingcaosha and Ge Lake, thus proteins exist in the hydrophilic fractions.

Fluorescence spectrum analysis of different water components of Sanhaowu, Yellow River, Huangpu River, Kunshan River and Gaoyou reservoir (Figures 1.40–1.43) shows that strong hydrophobic components have strong humus fluorescence peaks A and C, while protein fluorescence peaks T and B are relatively weak. This indicated that the fluorescent groups of strong hydrophobic organic compounds mainly appear in the long wavelength region. The tryptophan fluorescence peak T was the weakest among the strong hydrophobic components, indicating that the fluorescence peak T had the

EBSCOhost - printed on 2/14/2023 6:39 AM via . All use subject to https://www.ebsco.com/terms-of-use

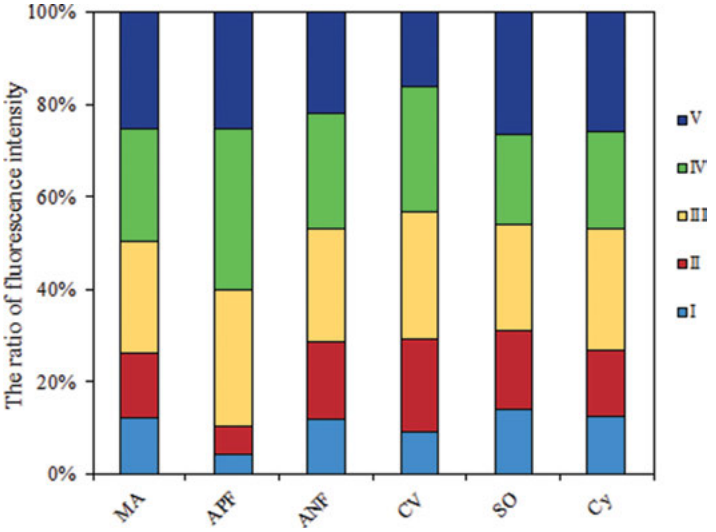

Figure 1.35: The ratio of fluorescence intensity for different algal organic matter.

least correlation with humic organics. Among the strong hydrophobic components of the five kinds of raw water, the Em wavelength of humic fluorescence peaks appeared in the range of 420 nm. Among them, the water with the longest Em wavelength of A was from Gaoyou (440 nm), followed by the Yellow River (435 nm) and Huangpu River (420 nm). The water of Kunshan (420 nm) and Sanhaowu (420 nm) have the shortest Em wavelength of A. Therefore, it can be concluded that the strong hydrophobic organic matter in Gaoyou water has the highest degree of aromatic structure and the highest number of aromatic compounds, while the strong hydrophobic organic matter in Kunshan water and Sanhaowu water have the highest degree of aromatic structure. Among the weakly-hydrophobic components, the intensity of tryptophan fluorescence peak was significantly higher than that of the strong hydrophobic components. The peak of humic acid fluorescence in the weakly-hydrophobic components still appears in Em > 420 nm, while the weakly-hydrophobic components in some water sources tend to shift to the short Em, indicating that the aromatic groups of organic compounds in weakly-hydrophobic components decreased. Charged hydrophilic components have protein fluorescence peaks, especially the fluorescence peak T which responses strongly. Compared with other components, it can be found that the fluorescence peak T in raw water mainly comes from charged hydrophilic components. The main fluorescence peaks of neutral hydrophilic components are not in the protein fluorescent region with short wavelength, but in the humic acid and fulvic acid regions.

Figures 1.44–1.46 show the fluorescence response of organic components of different raw water. The components respond in all of the fluorescence regions. Differences in the proportion of their response intensities indicated that the different components have their fluorescence response characteristics. Further investigation of the fluores-

EBSCOhost - printed on 2/14/2023 6:39 AM via . All use subject to https://www.ebsco.com/terms-of-use

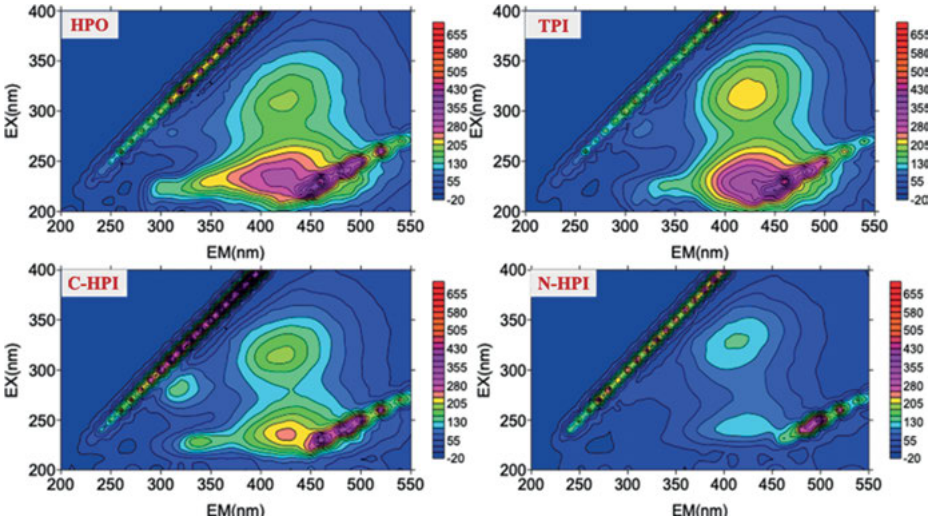

Figure 1.36: The fluorescence spectra of organic components in Xiangjiang River.

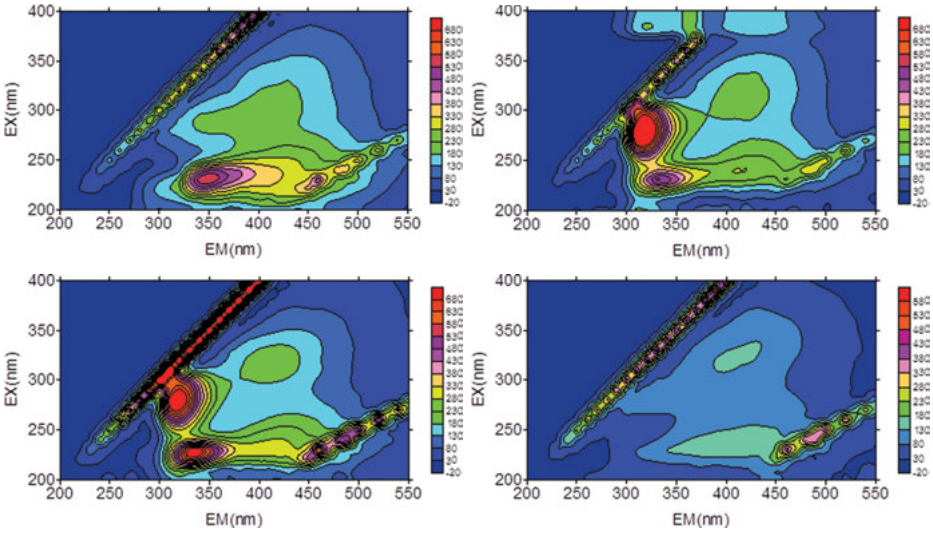

Figure 1.37: The fluorescence spectra of organic components in West Taihu Lake (strong hydrophobic, weakly hydrophobic, charged hydrophilic, neutral hydrophilic).

cence response of different components of the region, for strong hydrophobic components, Sanhaowu was in regions 2, 3, 5, Huangpu River was in regions 2, 3, Yellow River was in regions 3, 2 and 5, Gaoyou was in regions 3 and 5, and Kunshan was in regions 1 and 2. For weakly hydrophobic components, Sanhaowu was in regions 3, 2 and 5, Huangpu River was in regions 2 and 3, Gaoyou was in regions 3 and 5, and Kunshan was in regions 1 and 2. For charged hydrophilic components, Sanhaowu was

EBSCOhost - printed on 2/14/2023 6:39 AM via . All use subject to https://www.ebsco.com/terms-of-use

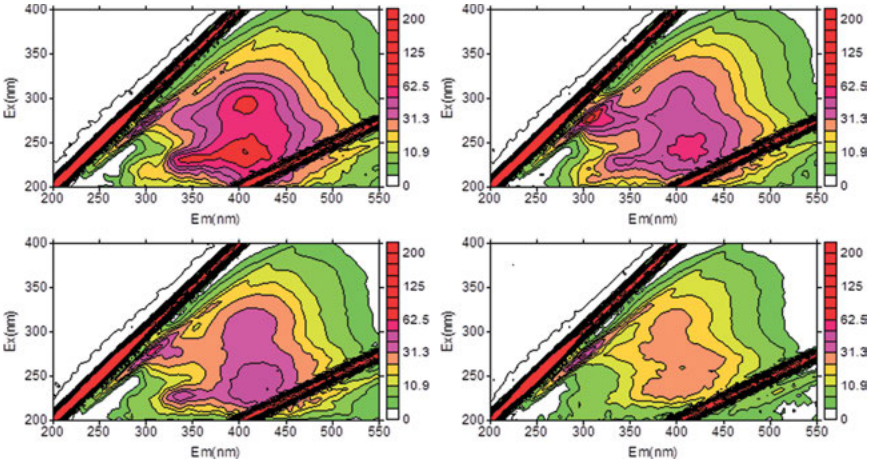

Figure 1.38: The fluorescence spectra of organic components in Qingcaosha (strong hydrophobic, weakly hydrophobic, charged hydrophilic, neutral hydrophilic).

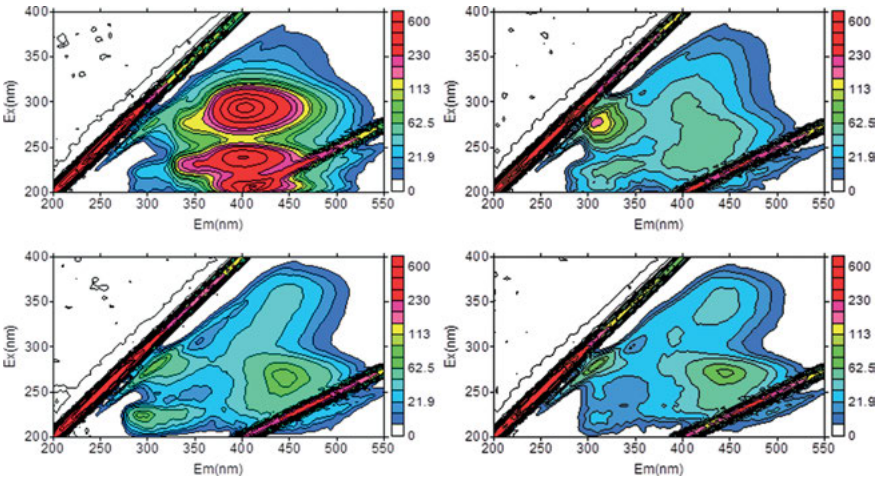

Figure 1.39: The fluorescence spectra of organic components in Ge Lake (strong hydrophobic, weakly hydrophobic, charged hydrophilic, neutral hydrophilic).

in regions 1 and 2, Huangpu River was in regions 1 and 2, Yellow River was in regions 3, 2 and 5, Gaoyou was in regions 3 and 5, and Kunshan was in regions 1 and 2. For neutral hydrophobic components, Sanhaowu was in regions 2 and 3, Huangpu River was in regions 2 and 3, Yellow River was in regions 3, 2 and 5, Gaoyou was in regions 2, 3 and 5, and Kunshan was in regions 1 and 2. Thus, the fluorescence response of different components is closely related to organic matter. For example, Sanhaowu, Huangpu River and Kunshan water responded strongly in regions 1 and 2, and thus their different components basically also have strong response in these regions.

EBSCOhost - printed on 2/14/2023 6:39 AM via . All use subject to https://www.ebsco.com/terms-of-use

While the response of organic matter in Gaoyou water is mainly in regions 3 and 5, the fluorescence response of its components should be also in these regions.

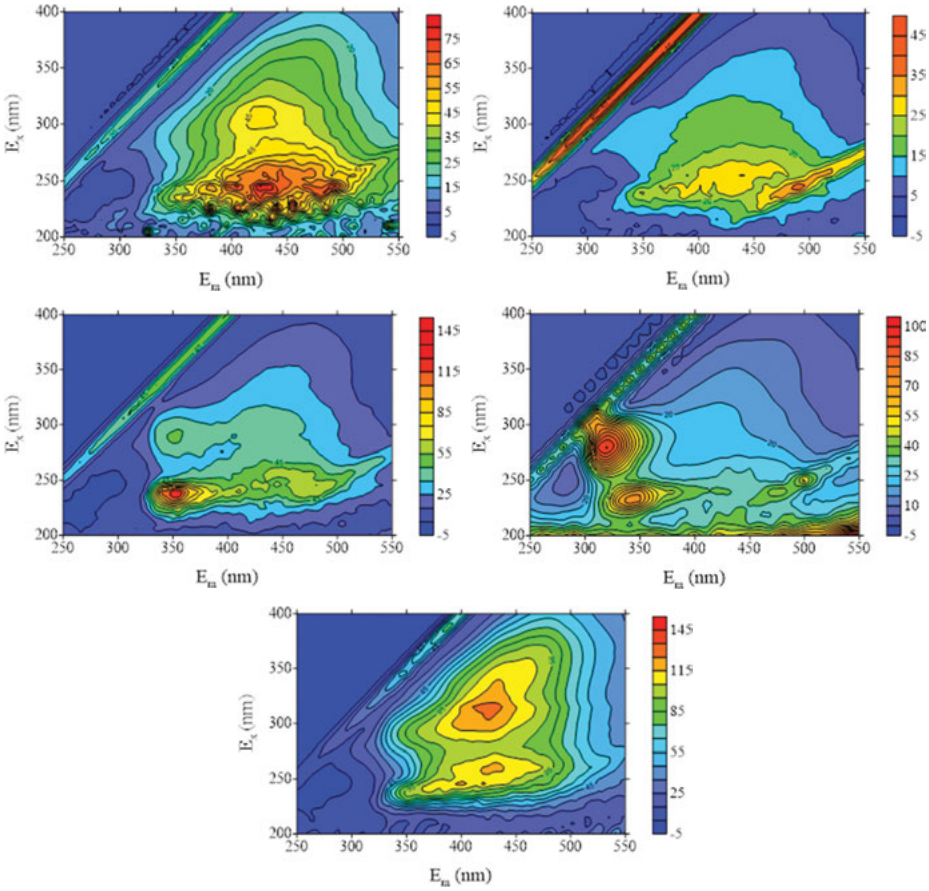

Figure 1.40: The three-dimensional fluorescence spectra of strong hydrophobic components from different raw water (Gaoyou, Yellow River, Huangpu River, Kunshan, Sanhaowu).

Thus, there is no necessary relationship between organic components and the regions of fluorescence response. However, organic components strongly reflect the organic characteristics of different water sources.

The fluorescence response of different algal organic components is shown in Figures 1.47–1.51. It can be seen that no component has a significant strength advantage in a particular area. Therefore, there is no evidence that the components have specific response areas. Some studies suggest that there is a correspondence between the organic components and the response regions, while this can only be adapted to a particular water source and cannot extend to other water sources.

EBSCOhost - printed on 2/14/2023 6:39 AM via . All use subject to https://www.ebsco.com/terms-of-use

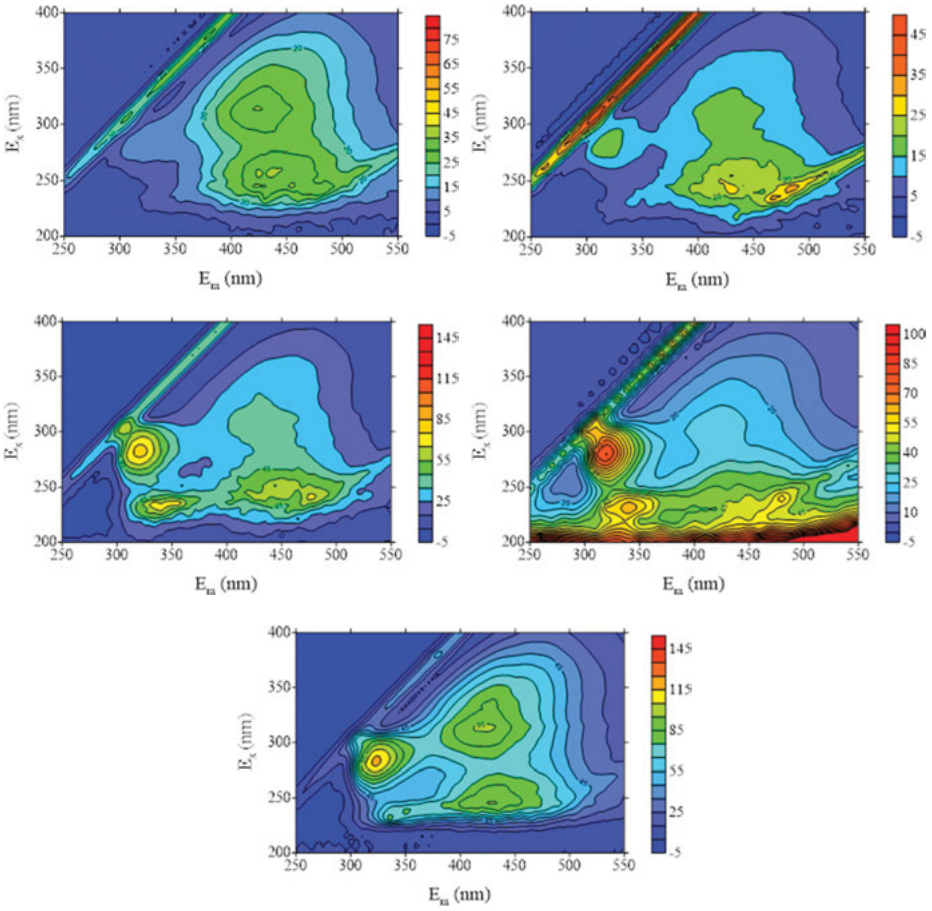

Figure 1.41: The three-dimensional fluorescence spectra of weekly-hydrophobic components from different raw water (Gaoyou, Yellow River, Huangpu River, Kunshan, Sanhaowu).

1.5 The relationship between hydrophilicity/hydrophobicity for organic matters and its molecular weight

Figure 1.52 shows the relationship between the hydrophilicity/hydrophobicity and the molecular weight distribution in Sanhaowu, Yellow River, Huangpu River, Kunshan and Gaoyou reservoirs. Among the four components in Sanhaowu, the content of organic matters with the molecular weight more than 30 kDa in the neutral hydrophilic components were the highest, while the ones in the other components were lower, which indicated that the macromolecules larger than 30 kDa in the raw water of Sanhaowu were mainly neutral hydrophilic organic matter. As the main organic matter of the neutral

EBSCOhost - printed on 2/14/2023 6:39 AM via . All use subject to https://www.ebsco.com/terms-of-use

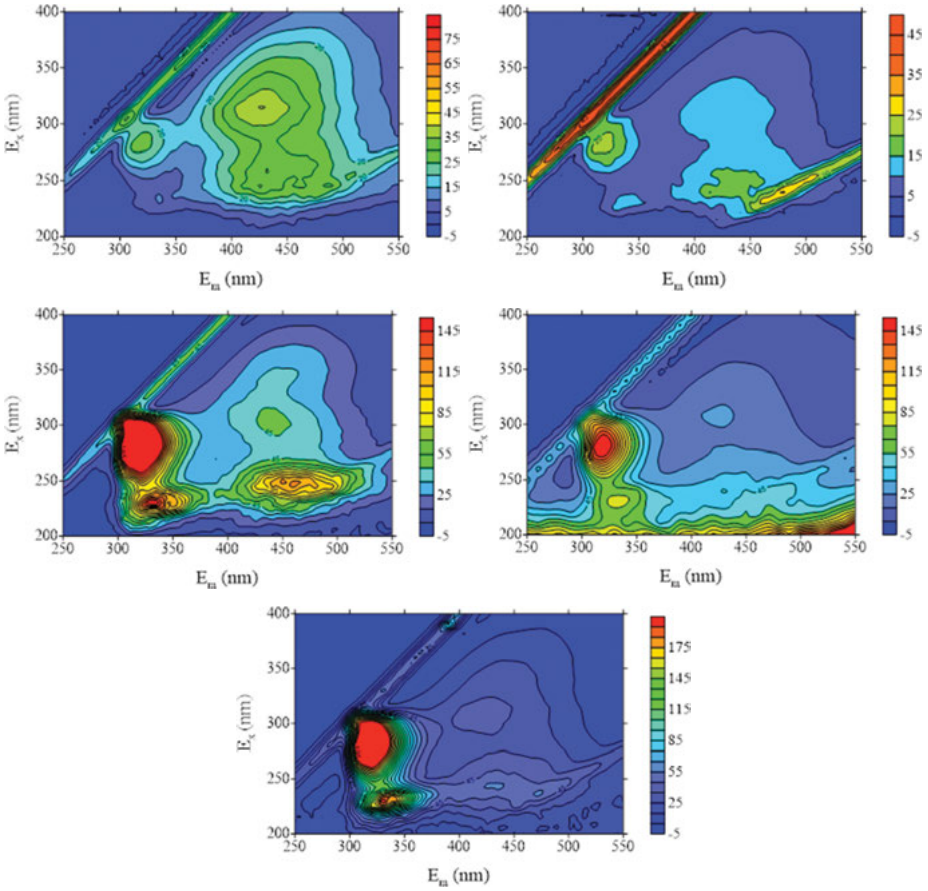

Figure 1.42: The three-dimensional fluorescence spectra of polar components from different raw water (Gaoyou, Yellow River, Huangpu River, Kunshan, Sanhaowu).

hydrophilic components is polysaccharide, it can be regarded that macromolecular organic substances which are larger than 30 kDa in Kunshan water are mainly polysaccharides. However, since the strong hydrophobic, weakly hydrophobic and charged hydrophilic components of Kushan water also contain small amounts of macromolecular organic compounds larger than 30 kDa, the molecular composition of Kunshan raw water larger than 30 kDa is more complicated than that in Sanhaowu. The organic matter larger than 30 kDa in the strong hydrophobic, weakly hydrophobic and charged hydrophilic components of Huangpu River is significantly more than that in Sanhaowu. Therefore, the macrophages larger than 30 kDa in Huangpu River mainly consist of humic substances and protein-based organic compounds. The content of organics of more than 30 kDa for each component of Gaoyou Water is very low (less than 2.0%), while the content of neutral hydrophilic components is slightly more.

EBSCOhost - printed on 2/14/2023 6:39 AM via . All use subject to https://www.ebsco.com/terms-of-use

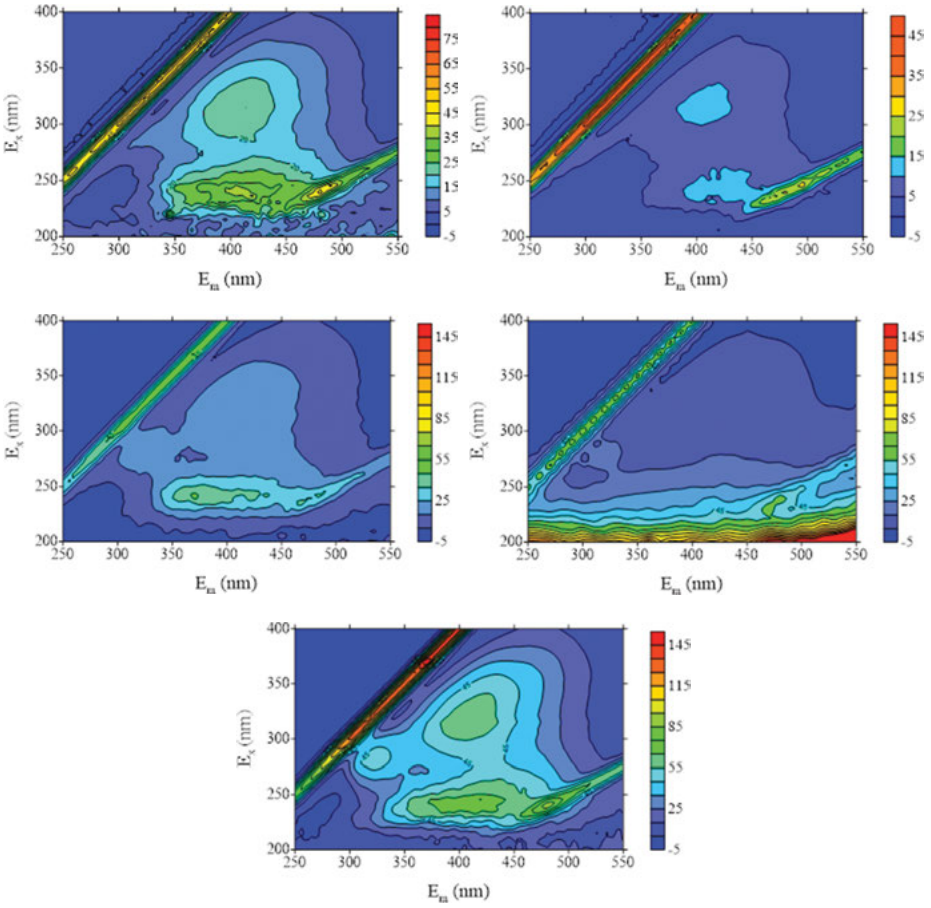

Figure 1.43: The three-dimensional fluorescence spectra of neutral-hydrophilic components from different raw water (Gaoyou, Yellow River, Huangpu River, Kunshan, Sanhaowu).

For organic matter of 10–30 kDa, the hydrophobic components of Sanhaowu and Kunshan water are lower than the neutral hydrophilic components, indicating that there is less humic organism in the 10–30 kDa macromolecules of these two kinds of raw water, while the majorities are polysaccharides or protein-based organic matter. There is a strong proportion of hydrophobic components in the raw water of Huangpu River and Gaoyou. So, 10–30 kDa macromolecules of the two raw water contain more humus organisms.

For organic matter of 3–10 kDa, there are a lot of medium-molecular organic compounds in Sanhaowu and Kunshan water, and they mainly appear in the neutral hydrophilic components, rather than in other components. There is a relatively low content of medium-molecular organic matter in the raw water of Huangpu River, and the proportion of each component is consistent. Therefore, it can be considered that there are various

EBSCOhost - printed on 2/14/2023 6:39 AM via . All use subject to https://www.ebsco.com/terms-of-use

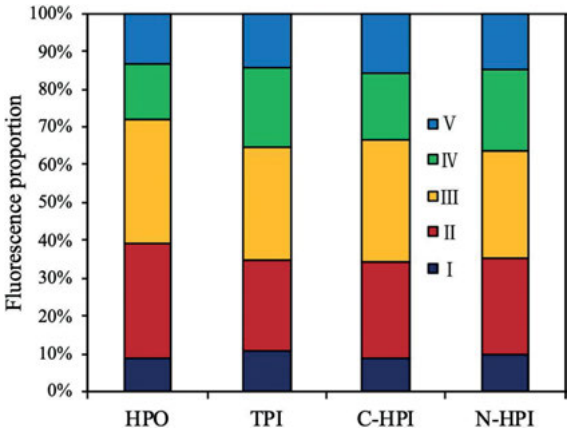

Figure 1.44: The fluorescence proportion of organic components from Qingcaosha.

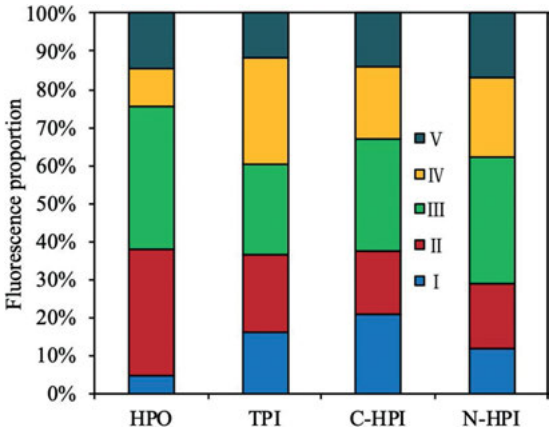

Figure 1.45: The fluorescence proportion of organic components from Ge Lake.

medium-molecular organic substances in Huangpu River water, including humus organics, protein organics and less amino sugar. The medium-molecular organic substances in Gaoyou water mainly appear in the hydrophobic and charged hydrophilic components, while there is almost no 3–10 kDa organic compounds in neutral hydrophilic components. It may be concluded that the medium-molecular organic matters of Gaoyou water are mainly humus and aromatic protein organic matter.

The different molecular weights and corresponding organic compounds of the above five kinds of raw water were summarized in Table 1.7. Figure 1.53 shows the relationship between molecular weights and composition of organic matters in Taihu Lake. Small molecules accounted the most, followed by medium molecules, while

EBSCOhost - printed on 2/14/2023 6:39 AM via . All use subject to https://www.ebsco.com/terms-of-use

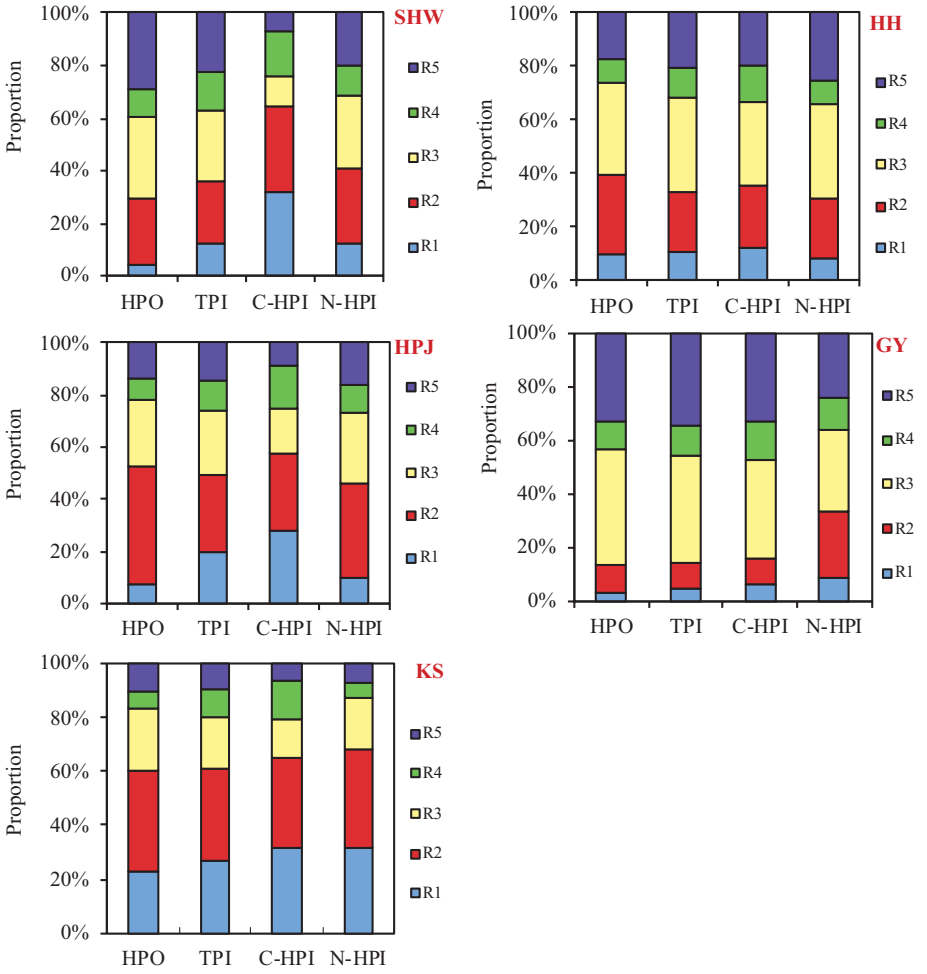

Figure 1.46: The proportion of fluorescence intensity for organic components.

macromolecules the least. For the strong hydrophobic components, medium molecules accounted the largest proportion, followed by small molecules, and macromolecules also occupied a certain proportion. The proportion of small molecules in weakly hydrophobic components further expanded, the proportion of medium molecules reduced, and macromolecules disappeared. Small molecules in hydrophilic component accounted the largest proportion. While the medium molecules made up the lowest proportion and the macromolecules accounted the largest, compared with the remaining components.

EBSCOhost - printed on 2/14/2023 6:39 AM via . All use subject to https://www.ebsco.com/terms-of-use

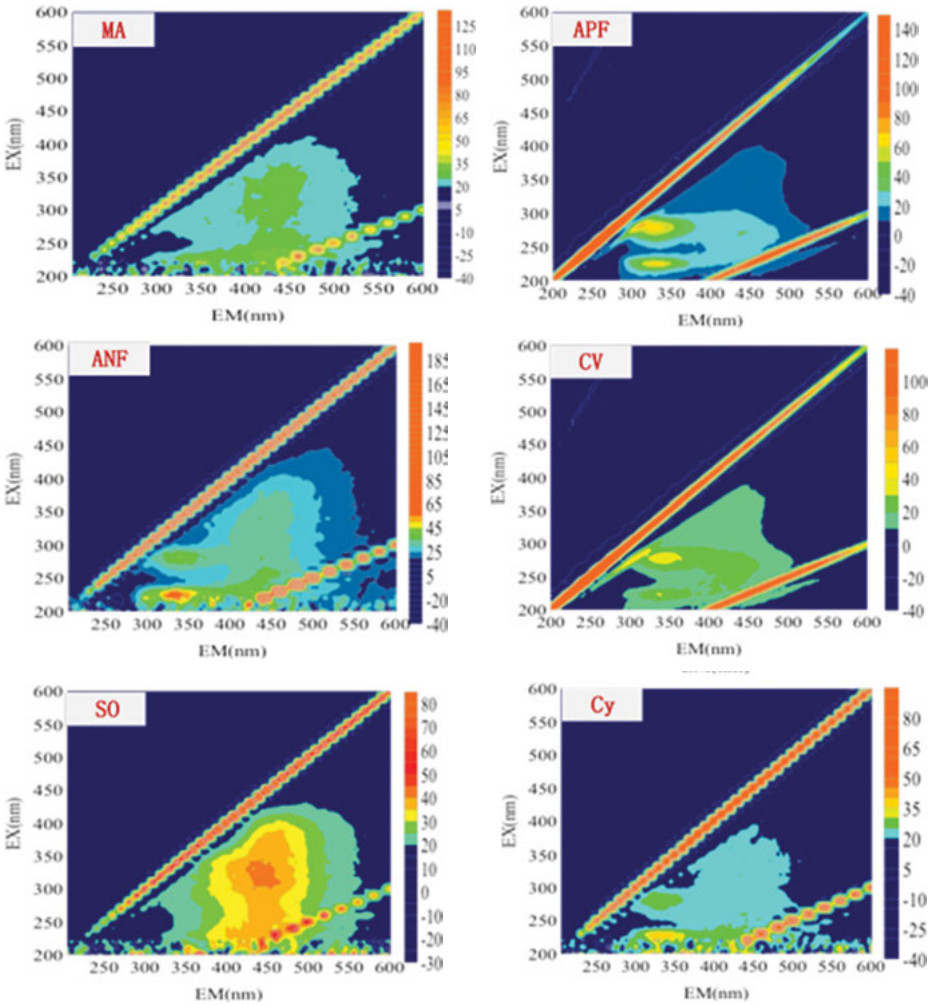

Figure 1.47: Three-dimensional fluorescence of HPO components of algae organisms.

Figure 1.54 shows the molecular weight distribution of different components of the six algae organisms. Unlike natural raw water, certain components of some algal organisms have many macromolecules such as Anabaena, Aphanizomenon and Microcystis aeruginosa. Further observation shows that macromolecules are mainly from the neutral hydrophilic components, followed by strong hydrophobic components. This result is similar to that of the natural raw water described above and similarly showed that macromolecules consist mainly of neutral hydrophilic and strong hydrophobic components. Neutral hydrophilic components also have a strong response to the medium molecules of certain algae such as Anabaena, Microcystis

EBSCOhost - printed on 2/14/2023 6:39 AM via . All use subject to https://www.ebsco.com/terms-of-use

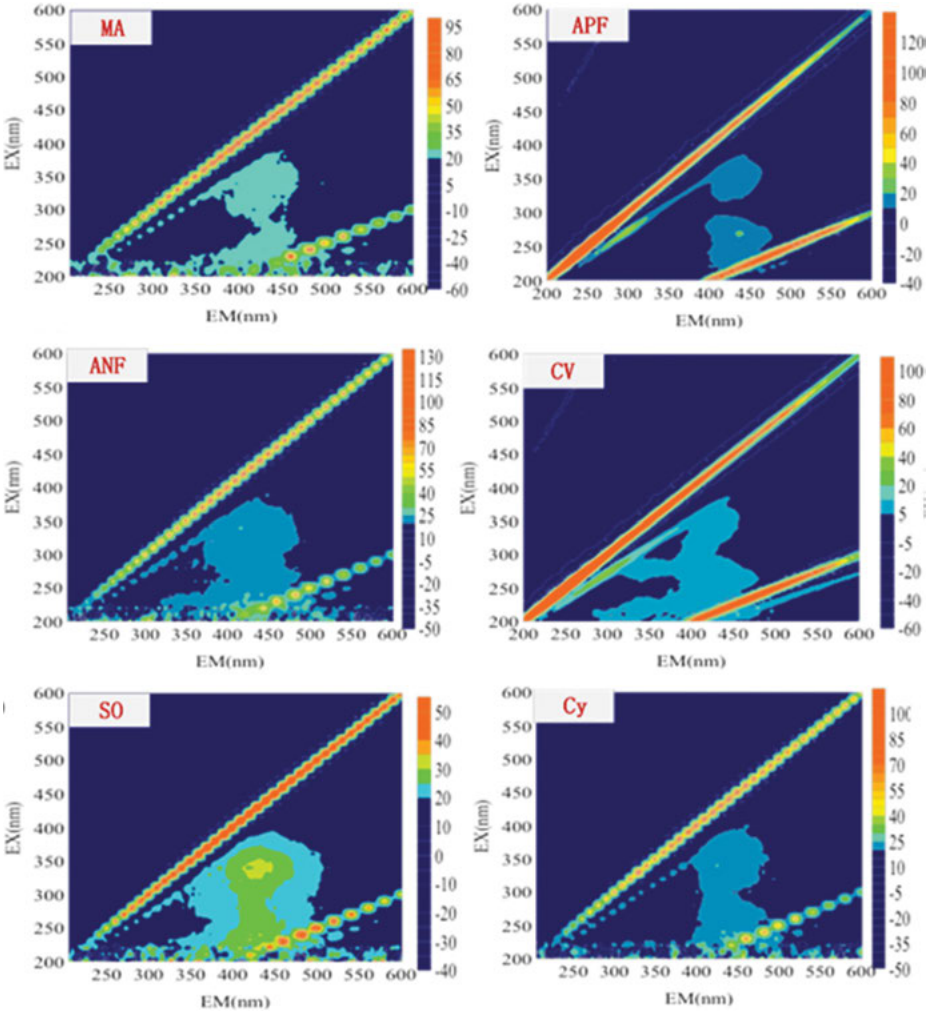

Figure 1.48: Three-dimensional fluorescence of TPI components of algae organisms.

aeruginosa and Scenedesmus, indicating that the medium molecules of these algae are composed of neutral and hydrophilic components. For the medium molecules, the strong hydrophobic components have a strong response to the six tested algal organisms, indicating that strong hydrophobic components are the predominant components of the medium molecules. As for small molecules, neutral hydrophilic components have a strong response in addition to Anabaena. Weakly hydrophobic and charged hydrophilic components are mainly distributed in small and medium molecules, and vary with the algae species.

EBSCOhost - printed on 2/14/2023 6:39 AM via . All use subject to https://www.ebsco.com/terms-of-use

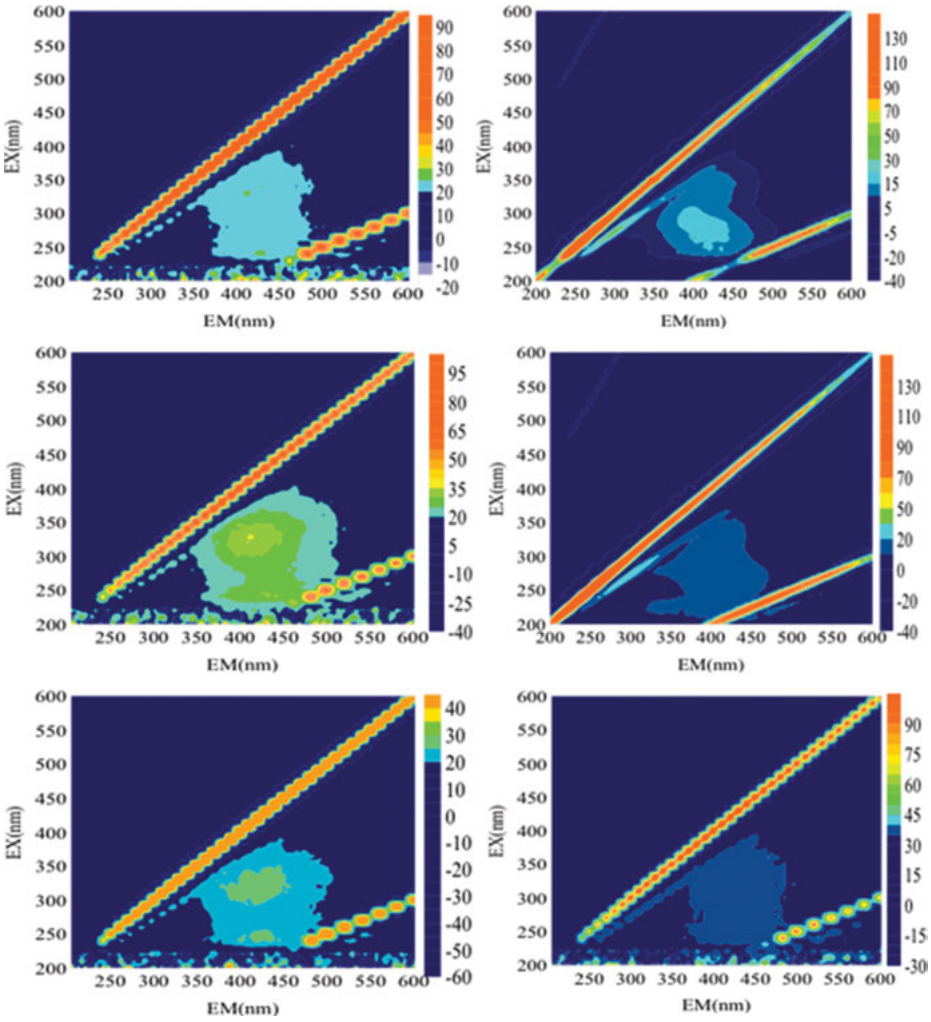

Figure 1.49: Three-dimensional fluorescence of strong hydrophilic components of algae organisms (Microcystis aeruginosa, Aphanizomenon, Anabaena, Chlorella, Scenedesmus and Cyclotella).

1.6 Fluorescence spectra and molecular weights of organics

The intensity of fluorescence peak is also related to the molecular weight of organic matter. Some studies also agreed with this. Most studies suggested that the peak T was related to macromolecular organics or colloidal particles, while peak B represented small molecules of organic matters. In the humic fluorescence region, the fulvic acid

EBSCOhost - printed on 2/14/2023 6:39 AM via . All use subject to https://www.ebsco.com/terms-of-use

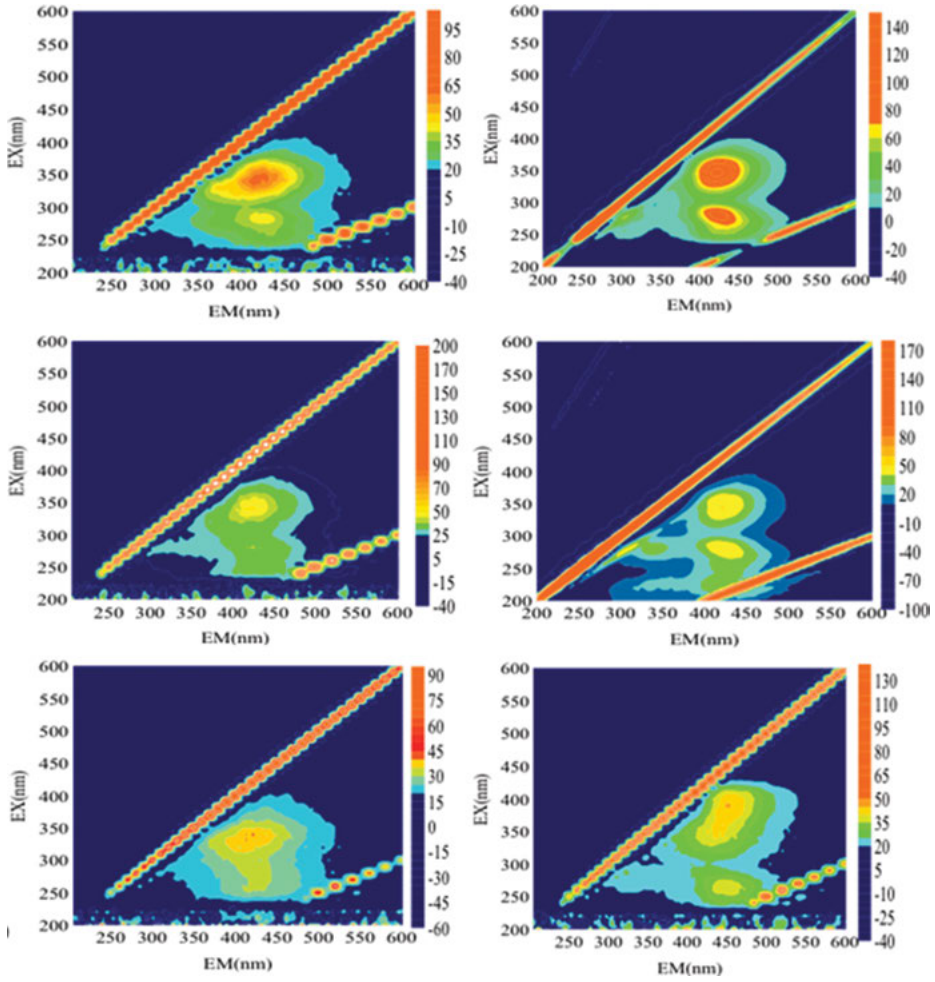

Figure 1.50: Three-dimensional fluorescence of neutral hydrophilic components of algae organisms (Microcystis aeruginosa, Aphanizomenon, Anabaena, Chlorella, Scenedesmus and Cyclotella).

fluorescence peak A with a smaller molecular weight tended to have a higher intensity than the humic fluorescence peak C.

The three-dimensional fluorescence spectroscopy of different molecular weights of Gaoyou raw water separated by UF membrane were tested. By comparing the organic fluorescence spectroscopy with different molecular weights, the relationship between the fluorescence spectroscopy and organic molecular weights was investigated. The results are shown in Figure 1.55.

With UF membrane the molecular weights of the organics in raw water could be divided into five segments. In each segment it was the dissolved organic matter which

EBSCOhost - printed on 2/14/2023 6:39 AM via . All use subject to https://www.ebsco.com/terms-of-use

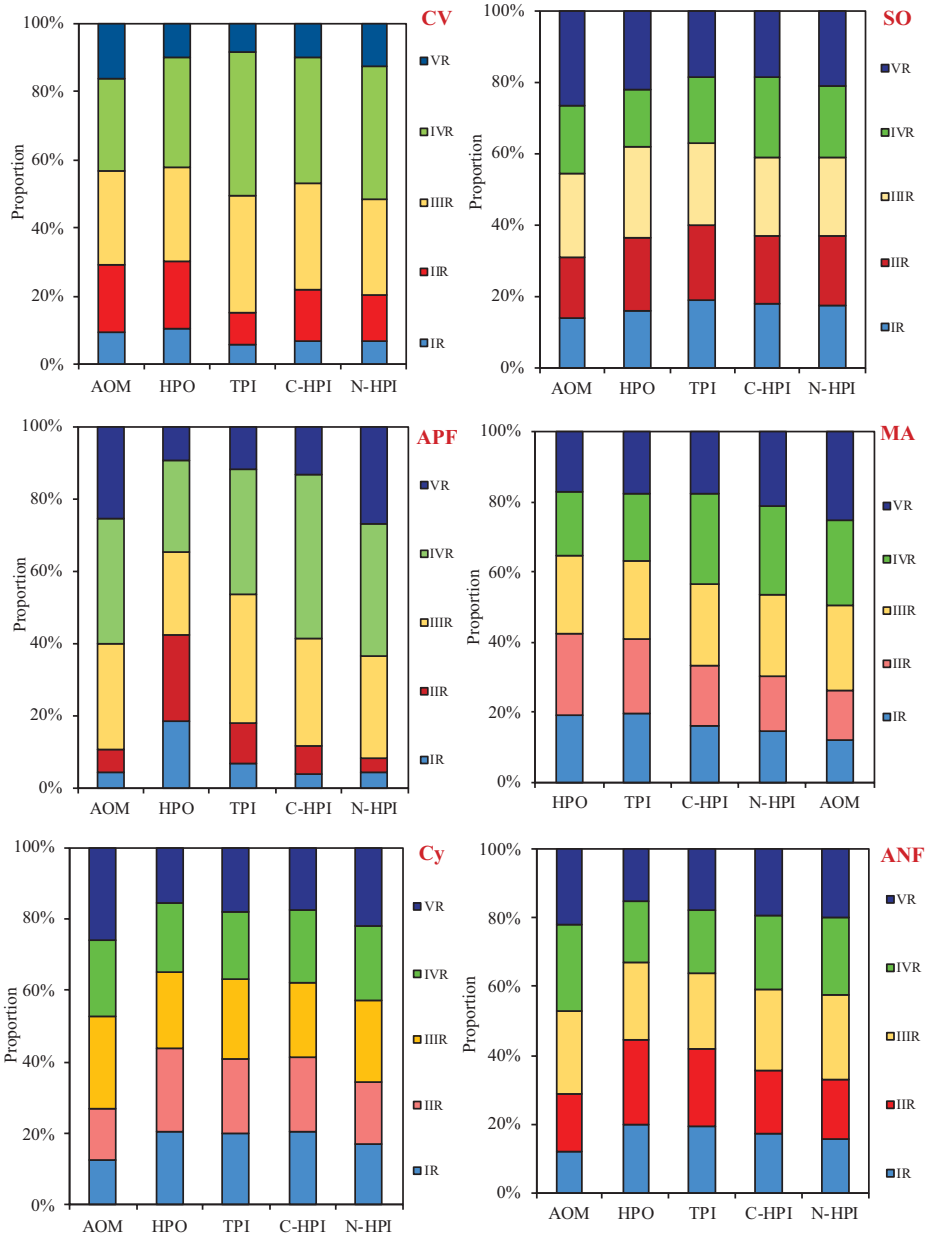

Figure 1.51: The fluorescence ratio of different algal organic components.

EBSCOhost - printed on 2/14/2023 6:39 AM via . All use subject to https://www.ebsco.com/terms-of-use

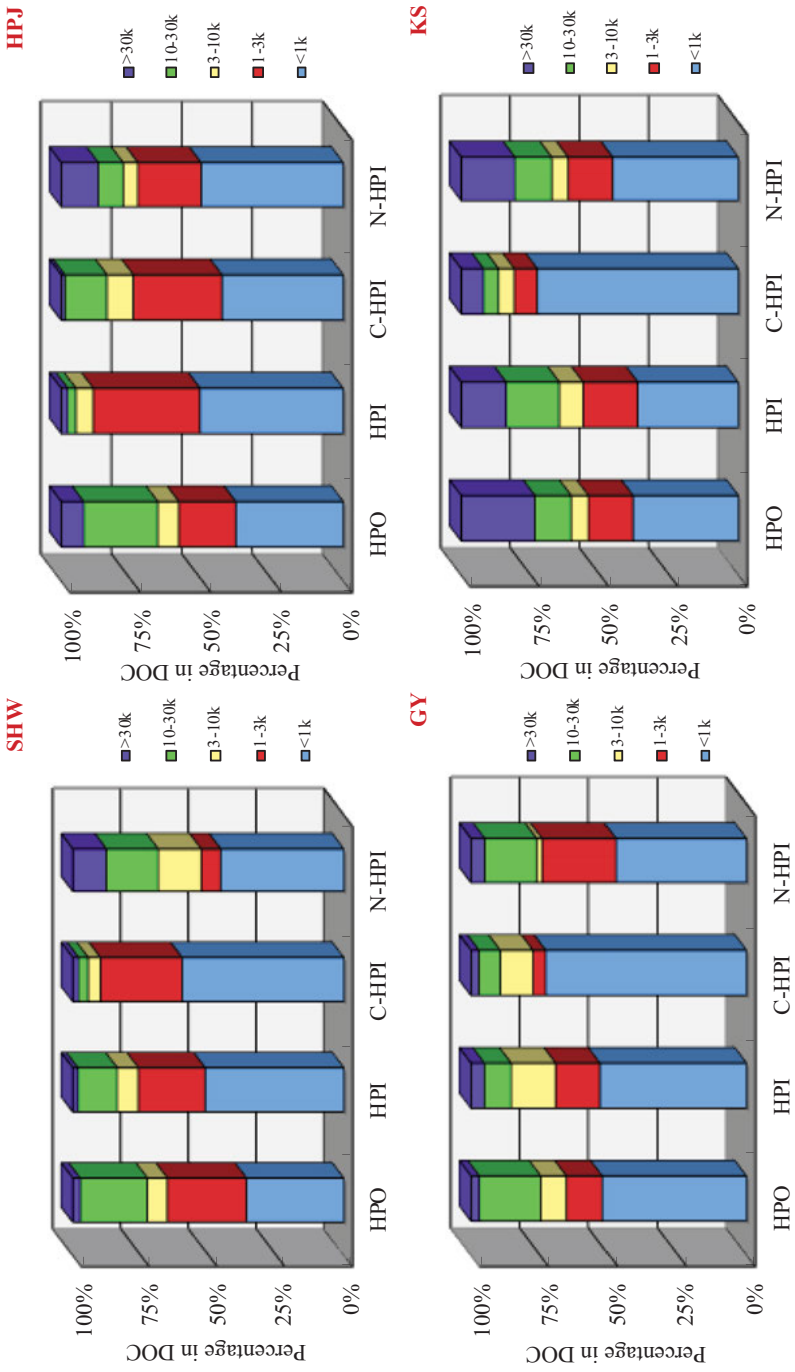

Figure 1.52: The relationship between organic components and molecular weights in raw water.

EBSCOhost - printed on 2/14/2023 6:39 AM via . All use subject to https://www.ebsco.com/terms-of-use

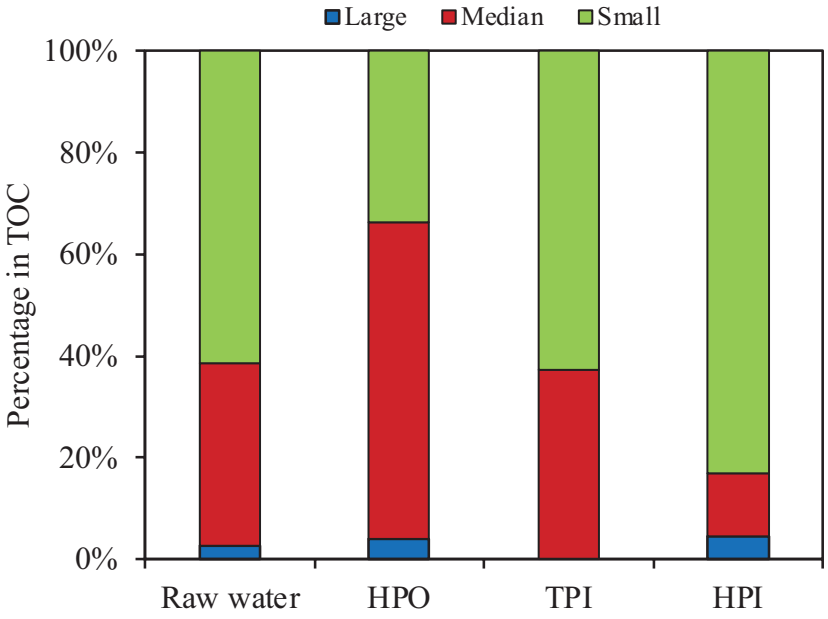

Figure 1.53: The relationship between organic components and molecular weights of Taihu Lake water.

Table 1.7: The different molecular weights and the corresponding organic composition.

Source of water	>30 kDa	10–30 kDa	3–10 kDa	<3 kDa
Sanhaowu	Colloid, polysaccharide	Mainly polysaccharide, a few humus species	Peptides, amino sugars, etc.	The decomposition product of the above substance.
Huangpu River	Polysaccharide, Aromatic proteins, Humus macromolecular polymer	Mainly humus, a few polysaccharide or protein	Humus and aromatic proteins with benzene ring structure	The decomposition product of the above substance.
Kunshan	Colloid, polysaccharide, protein	Polysaccharide, mainly protein, a few humus	Humus and aromatic proteins with benzene ring structure, Peptide polysaccharides, amino sugars	The decomposition product of the above substance.
Gaoyou	Extremely low or no macromolecular organic matter	Mainly humus organic matter, a few polysaccharide and protein	Humus and aromatic proteins with benzene ring structure	The decomposition product of the above substance.

EBSCOhost - printed on 2/14/2023 6:39 AM via . All use subject to https://www.ebsco.com/terms-of-use

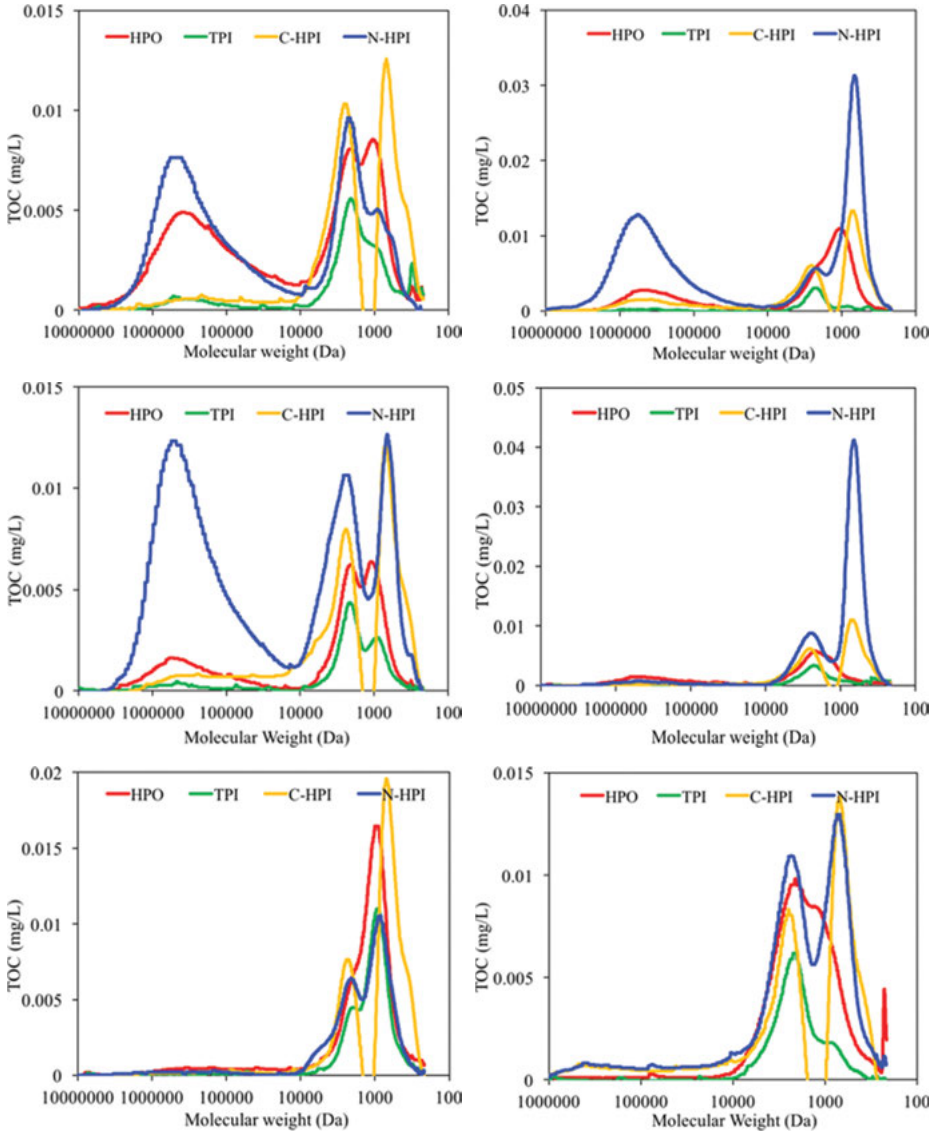

Figure 1.54: Molecular weights distribution of various algal organic groups (Anabaena, Aphanizomenon, Microcystis aeruginosa, Chlorella, Cyclotella and Scenedesmus).

has been filtered by UF membrane. Using fluorescence regional integration method, it was found that there was a certain correlation between the different fluorescence regions and the molecular weights of organic matter. The most obvious phenomenon was the fluorescence intensity of two water samples (<0.45 μm and <30 kDa). After the removal of macromolecular organics larger than 30 kDa, the intensities of all the fluorescence regions increased, which meant that organic compounds larger than 30

EBSCOhost - printed on 2/14/2023 6:39 AM via . All use subject to https://www.ebsco.com/terms-of-use

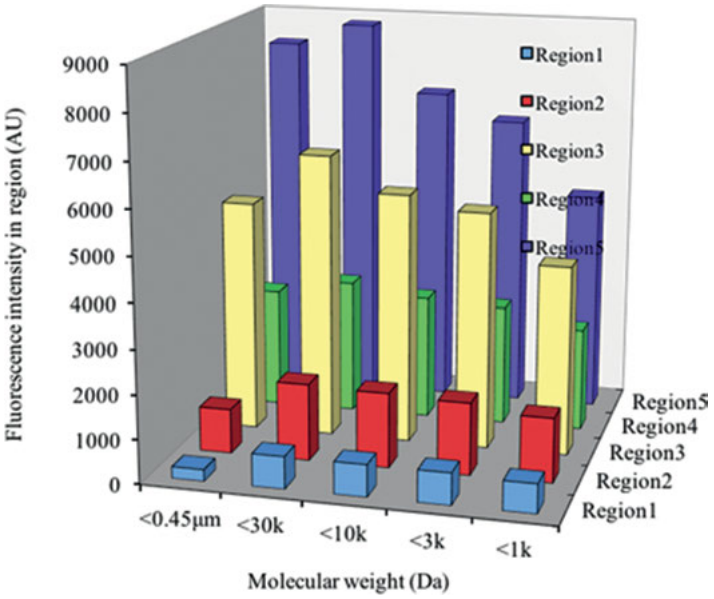

Figure 1.55: Relationship between molecular weights and fluorescence response of organic matter in Gaoyou water.

kDa could not induce any fluorescence, and their existence may even reduce the fluorescence intensity of water samples.

When the organic matter with molecular weight less than 30 kDa continued to be trapped by the membrane, the fluorescence intensity of the entire area gradually decreased. Among them, the reduction of humic fluorescence region 3 and 5 were the most obvious, while that of protein fluorescence regions was less, which indicated that the humic organism in each molecular weight range contributed to the fluorescence intensity, while the fluorescence intensity of protein mainly came from small molecule organics. At the same time, it was noteworthy that small molecule organic compounds smaller than 1 kDa had high fluorescence intensity, and their intensity value accounted for more than 60% of the total fluorescence intensity, indicating that the small molecule organic matter mainly contributed to the fluorescence intensity.

The same test was also carried out for the Taihu Lake water (Figure 1.56). According to the subtraction method, the molecular weight range of fluorescence spectra was obtained, and shown in Figure 1.57. Fluorescence spectra between different molecular weights were quite different. The raw water responded in four regions of B, T, A and C, and the most intense response was in regions B and T. The response of less than 3 kDa in regions B and T were comparable to that of raw water, but the responses of regions A and C were significantly lower than that of raw water. Most of the aromatic proteins and soluble microbial products in regions B and T had a molecular weight of less than 3,000 Da, while some of the humic acids in regions A and C had a molecular weight

EBSCOhost - printed on 2/14/2023 6:39 AM via . All use subject to https://www.ebsco.com/terms-of-use

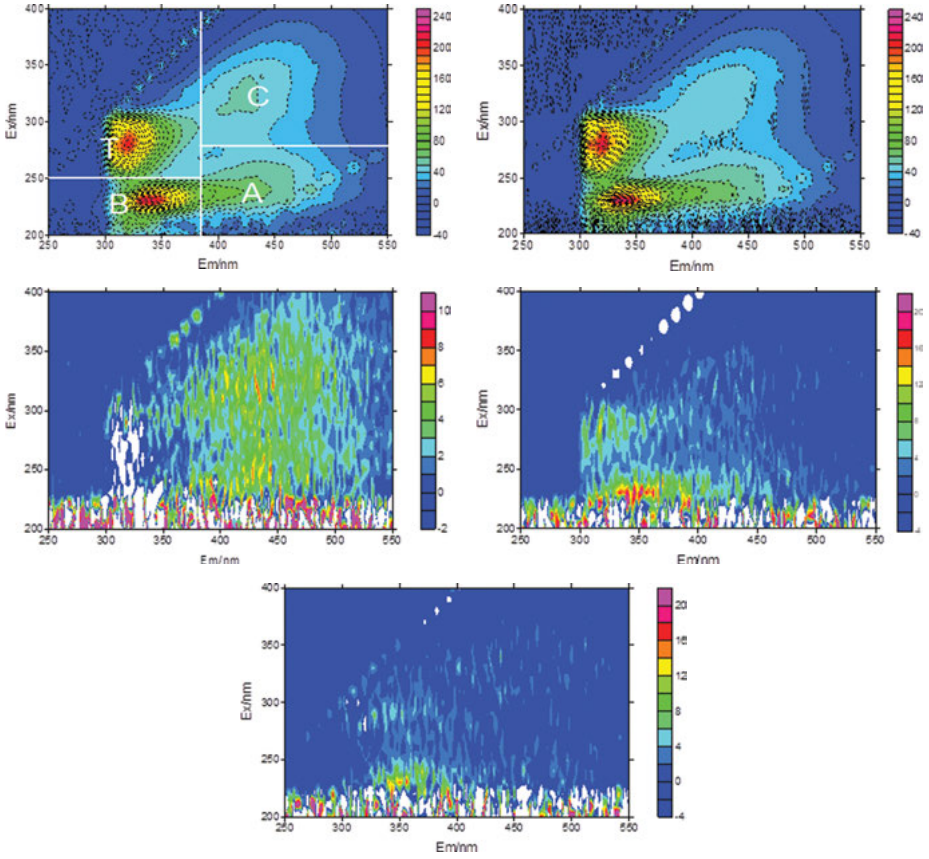

Figure 1.56: Three-dimensional fluorescence of organics in Taihu Lake water.

greater than 3,000 Da. According to the subtractive fluorescence analysis of 3–10 kDa, 10–100 kDa and >100 kDa, the organic matter occupied less. The organic matter of 3–10 kDa was dominated by humic acid organic compounds in regions A and C. The 100 kDa organic matter was mainly dominated by protein organic compounds in regions B and T. And both showed a greater response in region B than in region T.

As shown in Figure 1.56, fluorescence intensity of raw water was about the same as that of components less than 3,000 Da. However, when the molecular weight was more than 3,000 Da, the fluorescence intensity dropped sharply, only 40% of that of raw water, indicating that the majority of fluorescence response was contributed by organic matter less than 3,000 Da. It can be also seen that when the molecular weight was less than 3,000 Da, the proportion of the fluorescence intensity in regions B and T slightly increased compared to the raw water. In the range of molecular weight of 3–10 k, most of the fluorescence intensity was contributed by regions A and C, indicating that most of the organic matters with the molecular weights of 3–10 k were humic acid organic compounds. When the molecular weights were more than 10 k, most of the fluorescence

EBSCOhost - printed on 2/14/2023 6:39 AM via . All use subject to https://www.ebsco.com/terms-of-use

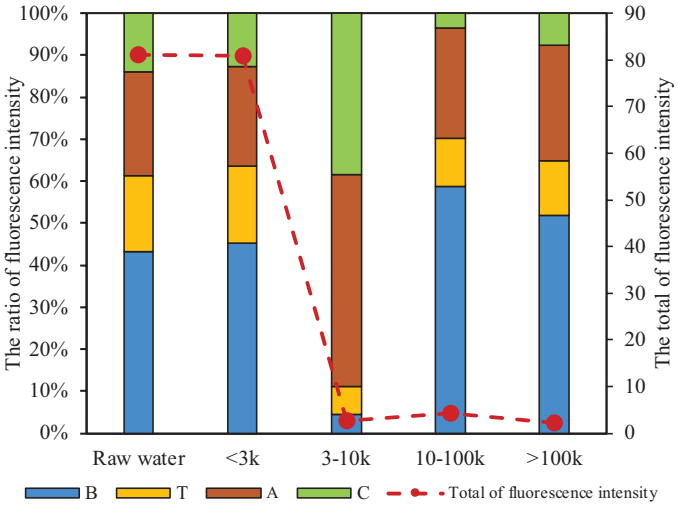

Figure 1.57: Relationship between molecular weight and fluorescence response of Taihu Lake.

intensity was contributed by region B, which indicated that the protein macromolecules were mainly expressed by the fluorescence response of region B. Thus, the fluorescence response of regions B and T mainly represented small molecules and macromolecular organic matter, while regions A and C mainly medium organic matter.

1.7 Summary

The molecular weight distribution of natural organic matter can be divided into three intervals. The molecular weight distribution of macromolecules ranges from tens of thousands to one million, while the response to ultraviolet light is weak or there is even no response. The macromolecules are mainly composed of hydrophilic organic matters, and strong hydrophobic components also appear in macromolecules. The molecular weight of the medium-molecular range is between one to ten thousand, mainly made up of hydrophobic organic substances with the strong-UV absorption such as humic acid. The molecular weights of the small molecules range from a few hundred to two thousand, which are mostly hydrophilic organic matter. Weakly hydrophobic components and charged hydrophilic components cannot appear in the macromolecules, and they mainly appear in the distribution of small and medium molecules, and vary when the raw water is changed. The number of small molecules is the largest in the raw water, followed by that of medium molecules, and macromolecules the least.

Strong hydrophobic components account the largest proportion in medium molecules, followed by small molecules, while macromolecules also occupy a certain

EBSCOhost - printed on 2/14/2023 6:39 AM via . All use subject to https://www.ebsco.com/terms-of-use

percentage. Weakly hydrophobic components account a larger proportion of small molecules, the proportion of medium molecules is less, and there is no macromolecule. Hydrophilic components of small molecules account the largest proportion. And compared to the rest of the components, the proportion of medium molecules is less, while that of macromolecules is the largest.

Organic components are not necessarily related to the region of fluorescence response, but they can strongly reflect the organic characteristics of different sources.

The fluorescence response in regions B and T mainly represent small molecules and macromolecular organic matters, while regions A and C mainly medium molecular organic matters.

References

[1] Amy, G., Fundamental understanding of organic matter fouling of membranes. Desalination, 2008. 231(1–3): p. 44–51.
[2] Kawasaki, N., et al., Fast and precise method for HPLC-size exclusion chromatography with UV and TOC (NDIR) detection: Importance of multiple detectors to evaluate the characteristics of dissolved organic matter. Water Research, 2011. 45(18): p. 6240–6248.
[3] Leenheer, J.A., Comprehensive approach to preparative isolation and fractionation of dissolved organic-carbon from natural-waters and wastewaters. Environmental Science & Technology, 1981. 15(5): p. 578–587.
[4] Wu, F.C. and Tanoue, E., Isolation and partial characterization of dissolved copper-complexing ligands in streamwaters. Environmental Science & Technology, 2001. 35(18): p. 3646–3652.
[5] Yue, L.X., et al., Relationship between fluorescence characteristics and molecular weight distribution of natural dissolved organic matter in Lake Hongfeng and Lake Baihua, <i>China. Chinese Science Bulletin, 2006. 51(1): p. 89–96.
[6] Marhaba, T.F., Van, D., and Lippincott, L., Rapid identification of dissolved organic matter fractions in water by spectral fluorescent signatures. Water Research, 2000. 34(14): p. 3543–3550.
[7] Lee, N., Amy, G., and Croue, J.P., Low-pressure membrane (MF/UF) fouling associated with allochthonous versus autochthonous natural organic matter. Water Research, 2006. 40(12): p. 2357–2368.
[8] Coble, P.G., Characterization of marine and terrestrial DOM in seawater using excitation emission matrix spectroscopy. Marine Chemistry, 1996. 51(4): p. 325–346.
[9] Baker, A., et al., To what extent can portable fluorescence spectroscopy be used in the real-time assessment of microbial water quality? Science of the Total Environment, 2015. 532: p. 14–19.
[10] Fu, P.Q., et al., Spectroscopic characterization and molecular weight distribution of dissolved organic matter in sediment porewaters from Lake Erhai, <i>Southwest China. Biogeochemistry, 2006. 81(2): p. 179–189.
[11] Chen, W., et al., Fluorescence excitation – Emission matrix regional integration to quantify spectra for dissolved organic matter. Environmental Science & Technology, 2003. 37(24): p. 5701–5710.
[12] Wang, L.Y., et al., Characterization of dissolved organic matter fractions from Lake Hongfeng, Southwestern China Plateau. Journal of Environmental Sciences, 2009. 21(5): p. 581–588.

EBSCOhost - printed on 2/14/2023 6:39 AM via . All use subject to https://www.ebsco.com/terms-of-use

EBSCOhost - printed on 2/14/2023 6:39 AM via . All use subject to https://www.ebsco.com/terms-of-use

Huaqiang Chu, Fangchao Zhao

Chapter 2
Vibration Membrane for Algae Separation

Membrane fouling is one of the key points during the membrane filtration utilization, which can result in flux decline and operation cost increase. It was reported to be a useful method to reduce membrane fouling by increasing the shear rate at the membrane surface under the high vibration frequencies or amplitudes, and various vibration membranes have been confirmed to increase the filtration flux [1–4].

Microalgae containing the high crude oil in its body is considered as the most promising material to resolve the energy crisis [5–7]. But, the harvest of microalgae is a crucial obstacle to limit its commercial use because of the small size of the microalgae particles [8–10]. Among the various harvesting methods, the membrane filtration can separate the microalgae cells effectively [11–14], which attracted more and more attention to improve the applicability of membrane technology in algae harvesting [15–17].

Among these, the vibration membrane could control membrane fouling at a small amplitude or frequency [18–20], whose shear action near the membrane surface can alleviate the shear damage on algae cells [21]. The irreversible membrane fouling caused by EOM deposition on the membrane surface or in the pores cannot be avoided by the LVM mode, but the reversible membrane fouling of algae cells deposition can be alleviated [2, 17, 22, 23]. Reversible membrane fouling and irreversible membrane fouling are caused by different substances, such as the loosely bound fouling layer and gel layer, should be removed by physical methods [24, 25] and chemical methods [26, 27], respectively. EOM of the algae broth containing high concentration of proteins and polysaccharides could lead to severe irreversible membrane fouling [28, 29], and the alleviation mechanism of membrane fouling under the vibration membrane operation mode should be further investigated.

2.1 Materials and methods

2.1.1 Experimental materials

Chlorella pyrenoidosa (*C.pyrenoidosa*, FACHB-9) was cultured with a sterile Basal medium in a 25 L glass box inside of an incubator under cultivation temperature of 30 ± 0.5 °C, light intensity of 127 μmol/(m^2·s) and light/dark sequence of 12 h/12 h.

Huaqiang Chu, College of Environmental Science and Engineering, Tongji University, Shanghai, P. R. China
Fangchao Zhao, School of Environmental and Municipal Engineering, Qingdao University of Technology, Qingdao, Shandong, P. R. China

https://doi.org/10.1515/9783110596847-002

EBSCOhost - printed on 2/14/2023 6:39 AM via . All use subject to https://www.ebsco.com/terms-of-use

An axial vibratory membrane (AVM) system was built to investigate the membrane fouling mechanism of the microalgae harvesting under different various variation frequencies, whose schematic diagram is shown in Figure 2.1. The setup includes a 50-L filtration tank, a servo-motor (60FSM-04030, USA) for the membrane vibration, a digital servo-drive (FDS15A-400X, USA) for the frequency adjustment and a peristaltic pump (BT100-LJ, Kejian, China) for the effluent suction. A hydrophilic PVDF membrane (Minglie, China) was adopted with nominal pore size of 0.1 μm and total effective membrane area of 0.02 m^2. The experimental parameters were set at the algae concentration of 0.4 g/L, the filtration flux of 30 $L/(m^2 \cdot h)$ and the vibration frequencies of 0, 5 and 10 Hz with a same amplitude of 1 cm.

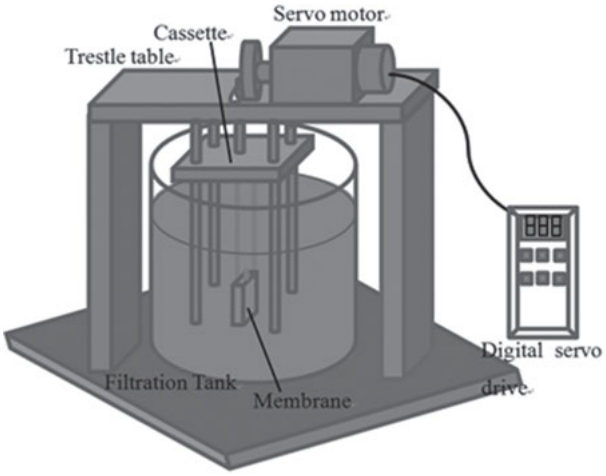

Figure 2.1: Schematic diagram of the AVM system.

2.1.2 Experimental methods

A sharp knife was used to cut the fouled membrane when the filtration process finished. The first fouled membrane was directly filtrated through a cup-type filtration vessel driven by nitrogen gas at 0.05 MPa for the total membrane fouling evaluation [30], then the scanning electron microscopy (SEM) analysis was conducted to examine fouled membrane after the pressurized water cleaning. While algae on the second fouled membrane was sloughed by water to a beaker for the algae and reversible EOM analysis. And then, the filtration of irreversible membrane fouling test was carried out under different frequencies. At the end, the irreversible membrane fouling caused by the irreversible EOM was separated by soaking in a solution (0.5 g/L NaOH) and shaking at 100 rpm for 2 h [31].

EBSCOhost - printed on 2/14/2023 6:39 AM via . All use subject to https://www.ebsco.com/terms-of-use

Three kinds of membrane fouling, reversible, irreversible and total membrane fouling are clarified. The water filtration flux of new membrane is defined as J_0, the fouled membrane flux is J_1, and the rinsed membrane flux is J_2. The total fouling rate (TF), irreversible fouling rate (IF) and reversible fouling rate (RF) can be defined as follows [29, 32]:

$$TF = 1 - J_1/J_0 \tag{2.1}$$

$$IF = 1 - J_2/J_0 \tag{2.2}$$

$$RF = TF - IF \tag{2.3}$$

where the total fouling rate refers to the flux decline rate of the fouled membrane without rinsing; the irreversible fouling rate refers to the flux decline rate of the fouled membrane after rinse; and the reversible fouling rate refers to the flux decline rate induced by the reversible foulants.

2.2 Results and discussion

2.2.1 The performance of long-term filtration

2.2.1.1 Filtration characteristics

The filtration performance of the AVM was carried out under various frequencies, as shown in Figure 2.2. Without the vibration (the vibration frequency of 0 Hz), the filtration process could only last only 2 h because of the severe membrane fouling. The AVM can last 12 h under the vibration frequency of 5 Hz. On the contrary, the TMP of the AVM remained stable under the vibration frequency of 10 Hz after the long filtration period of 24 h.

The pictures of the fouled membrane and SEM of the rinsed membrane under different frequencies are shown in Figure 2.3. It can be seen that the algae particles deposited on the membrane surface reduced remarkably as the vibration frequency increased. The membrane surface was covered completely by algae particles after the 2 h filtration at 0 Hz. However, there were almost no algae particles deposited at 10 Hz with the long filtration period of 24 h. Enhancing the frequency reduced the deposition of algae on the membrane, thus the AVM can be operated for a long filtration period under the higher vibration frequency coupled with less deposited algae particles and lower TMP, which was consistent with the previous results [23]. The shear force on the membrane surface was improved under the increased vibration frequency, which can control the deposition of algae particles on the membrane surface [23]. At the end of the filtration periods, the content of the deposited

EBSCOhost - printed on 2/14/2023 6:39 AM via . All use subject to https://www.ebsco.com/terms-of-use

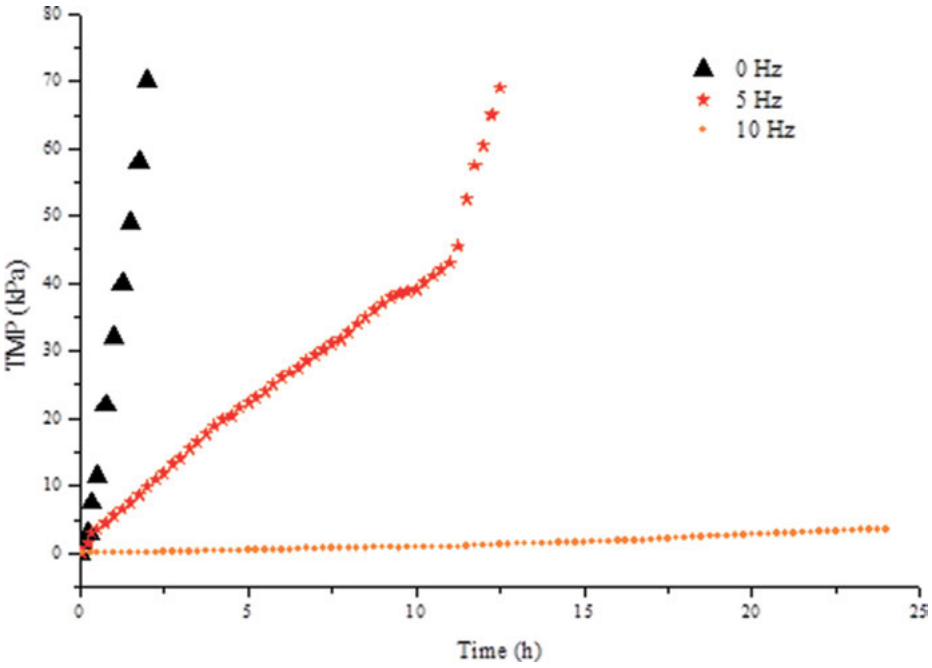

Figure 2.2: The TMP variations at the different frequencies.

algae particles on the membrane was 8.64 g/m^2, 0.97 g/m^2 and 0.28 g/m^2 under the vibration frequencies 0 Hz, 5 Hz and 10 Hz, respectively, which also agreed with the aforementioned results.

2.2.1.2 Membrane fouling analysis

As shown in Figure 2.3, there are also abundant EOM covered on the membrane surface even under the vibration frequency of 10 Hz, which can be identified as the irreversible foulants. It was reported that the vibration membrane system could control the deposition of large particles on the membrane surface, but small particles or macromolecular substances could still be deposited [2, 17]. It was interesting that the content of EOM also increased at the high vibration frequency, which was contrary on the algae particle's deposition. Under a high vibration frequency, the filtration process was prolonged, which provided more opportunity for the EOM adhesion to the membrane [33].

Under a certain pressure of 0.05 MPa, the fluxes of the new membrane and fouled membrane before and after rinse with various vibration frequencies are present in Figure 2.4. The filtration flux of fouled membranes without rinse improved from 24.2 to 221.3 L/(m$^2 \cdot$ h) when the vibration frequency increased from 0 to 10 Hz. However,

EBSCOhost - printed on 2/14/2023 6:39 AM via . All use subject to https://www.ebsco.com/terms-of-use

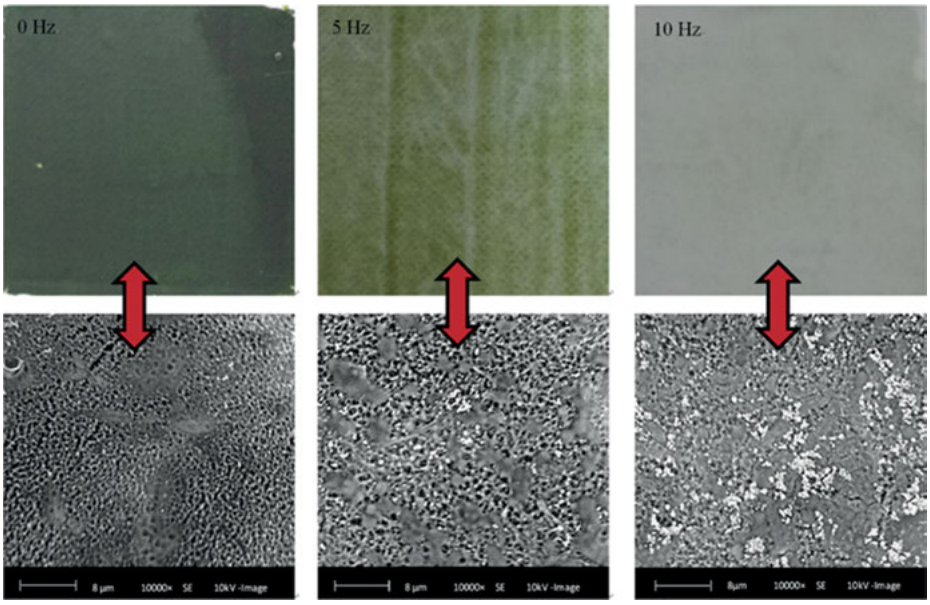

Figure 2.3: The pictures of the fouled membrane and SEM of the rinsed membrane under different frequencies.

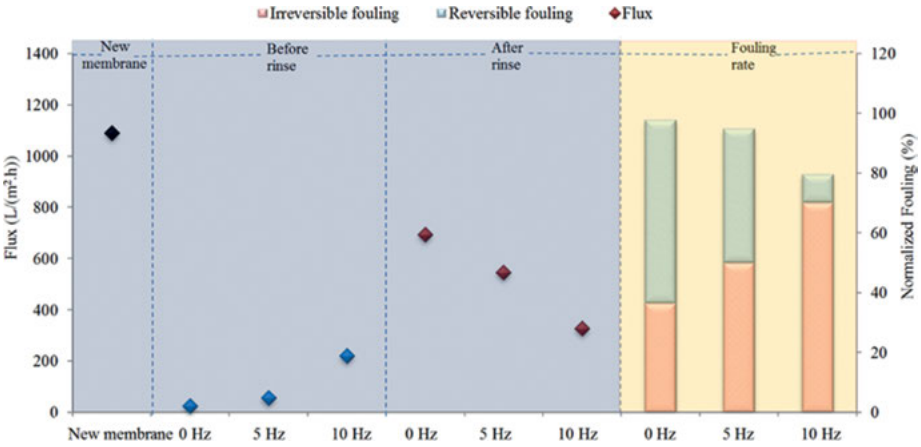

Figure 2.4: The fluxes, the reversible and irreversible fouling of the new membrane and fouled membrane before and after rinse with various vibration frequencies.

the filtration flux declined with increased vibration frequency when the rinse process was adopted. With the increased vibration frequency, the total membrane fouling declined, together with the reversible fouling part decreasing and the irreversible fouling part increasing. The increased vibration frequency can reduce the deposition of algae cells. Therefore, the reversible membrane fouling reduced. While more EOM

EBSCOhost - printed on 2/14/2023 6:39 AM via . All use subject to https://www.ebsco.com/terms-of-use

deposited on the membrane during the long filtration time under the high frequency, resulting in severe irreversible fouling. Combined with the TMP variations in Figure 2.2, the membrane reversible fouling caused by algal deposition plays the major role in the flux decline and TMP increase during algae filtration process.

2.2.2 The performance of short-term filtration

2.2.2.1 Filtration characteristics

The TMP changes under different vibration frequencies with short filtration time are shown in Figure 2.5. The filtration process was set for 2 h. After reaching the predetermined filtration time, the TMP exhibited slightly increase at 10 Hz, with almost no algae covered on the membrane surface (Figure 2.6); while the TMP increased to 8.9 kPa at 5 Hz, with the algae deposition of 0.39 g/m^2 (Figure 2.6), which was much lower than that of 0.97 g/m^2 in long duration filtration in Figure 2.2. It can be seen from Figure 2.7 that the water flux of the fouled membrane increased obviously as compared with that in the long duration filtration under all the vibration frequencies. However, there was no obvious trend of the membrane water flux after rinse at different vibration frequencies. But the flux of the rinsed membrane at 5 and 10 Hz increased obviously compared with those in long-time filtration with less EOM and reducing irreversible membrane fouling. It also can be seen from Figure 2.7 that the proportion of irreversible membrane fouling and reversible fouling sharply decreased and increased, respectively, compared with those in the long-time filtration at 10 Hz. At a high frequency, the AVM can effectively reduce algal deposition, but cannot effectively control EOM adherence to the membranes, which caused more severe irreversible fouling in the long-term filtration experiment.

2.2.2.2 Membrane fouling analysis

The judgment standard of reversible foulants and irreversible foulants is whether the EOM and the algae layer can be washed away by water rinse, with the analysis results shown in Table 2.1. It can be seen that the reversible foulants, such as TOC, PN and PS, exhibited obvious decline trends with the increased vibration frequencies in the short filtration periods. The AVM could effectively remove the reversible EOM at the higher vibration frequency, except the irreversible EOM foulants. The increased frequency could reduce the EOM concentration near the membrane, which might be the reason that there was less EOM on the membranes at a higher frequency [34]. Meanwhile, the deposited algae particles could form a thick algal layer on the membrane surface at a low vibration frequency, which could retain more EOM in the algae layer

EBSCOhost - printed on 2/14/2023 6:39 AM via . All use subject to https://www.ebsco.com/terms-of-use

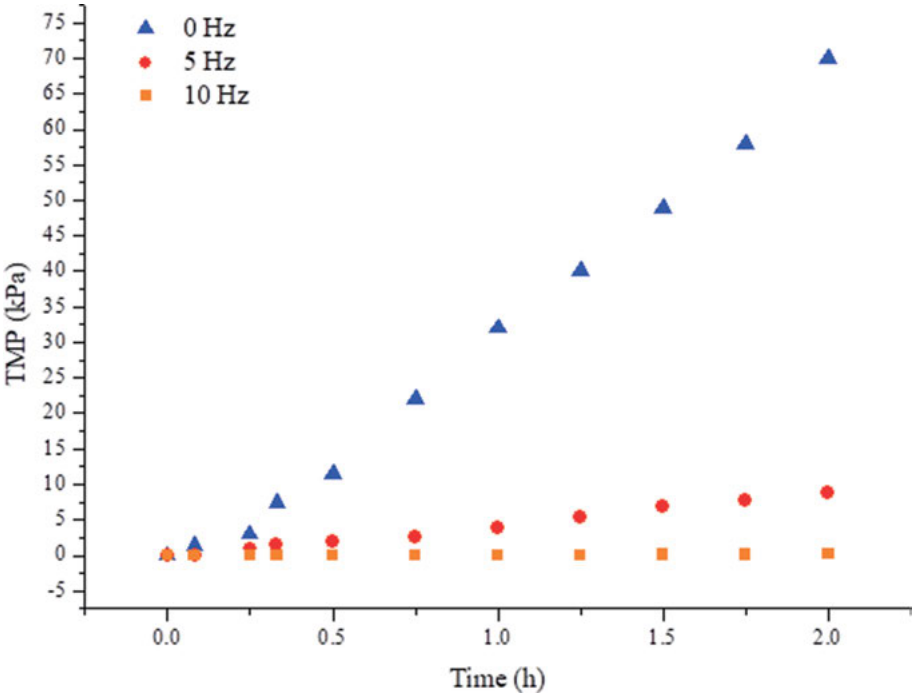

Figure 2.5: The TMP changes under different vibration frequencies with short filtration time.

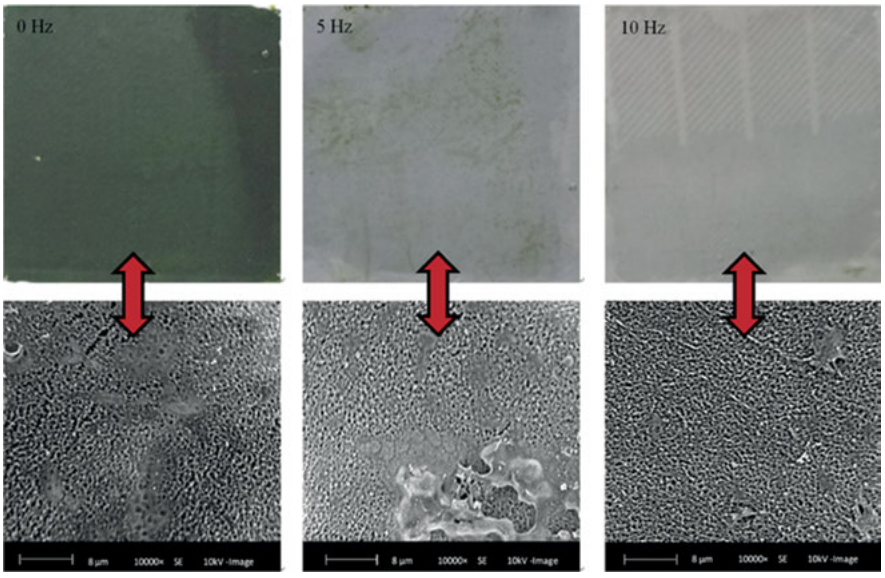

Figure 2.6: The pictures of the fouled membrane and SEM of the rinsed membrane under different vibration frequencies in short filtration time.

EBSCOhost - printed on 2/14/2023 6:39 AM via . All use subject to https://www.ebsco.com/terms-of-use

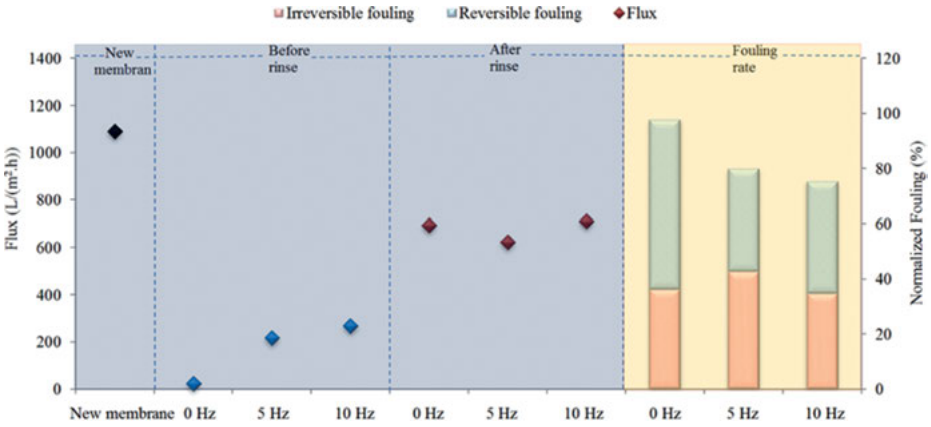

Figure 2.7: The fluxes, the reversible and irreversible fouling of the new membrane and fouled membrane before and after rinse with various vibration frequencies in short filtration time.

[35, 36]. Based on the foulants quantities analysis, the reversible foulants, such as TOC, protein and polysaccharide, had coverage rotios of 269.1, 181.8 and 90.9 mg/m^2, respectively, which were all much higher than those of the deposited algae particles of 30.0 mg/m^2 on the membrane at 10 Hz. Therefore, it could be inferred that the reversible membrane fouling was mainly caused by EOM adhesion rather than the algae particles deposition in the short filtration with the high vibration frequency of 10 Hz. On the contrary, the situation of membrane fouling controlled by the low vibration frequency was opposite.

Table 2.1: Analysis of TOC, protein (PN) and polysaccharide (PS) under different circumstances.

Sample		TOC (mg/m^2)	PN (mg/m^2)	PS (mg/m^2)
0 Hz	Reversible	529.1 ± 20.1	305.5 ± 14.3	254.5 ± 11.2
	Irreversible	68.2 ± 3.5	45.0 ± 2.2	16.5 ± 0.6
5 Hz	Reversible	380.0 ± 16.4	278.2 ± 12.1	112.7 ± 4.4
	Irreversible	78.4 ± 3.5	55.6 ± 2.3	19.2 ± 0.8
10 Hz	Reversible	269.1 ± 10.8	181.8 ± 9.7	90.9 ± 3.8
	Irreversible	59.5 ± 3.3	28.5 ± 1.0	17.4 ± 0.9

2.2.2.3 Molecular weight (MW) distribution of membrane foulants

Figure 2.8 presents the MW distributions of reversible and irreversible EOM at different frequencies. There were many EOM peaks in the raw algae solution, with ranges mainly above 10 kDa. It can be seen from Figure 2.9 that the reversible EOM foulants were mainly in the range of low-MW (<1 kDa) and high-MW (>100 kDa) regions.

EBSCOhost - printed on 2/14/2023 6:39 AM via . All use subject to https://www.ebsco.com/terms-of-use

From Figure 2.8, as the vibration frequencies increased from 0 Hz to 5 Hz and 10 Hz, the obvious MW peak of the irreversible EOM was at approximately 3.5, 4 and 5 kDa, respectively, which indicated that a right shift tendency of the MW peak of irreversible EOM when the frequency increased, as well as the peak intensities of the irreversible EOM decreased. There were considerable irreversible EOM on the membrane identified in the MW distribution of 1 to 10 kDa during the filtration, which was very low intensity in the raw EOM solution (Figure 2.9). From Figure 2.9, it also can be seen that the low-MW parts in the irreversible EOM declined as the vibration frequency increased from 0 Hz to 5 Hz and 10 Hz, whereas the high-MW parts increased slightly.

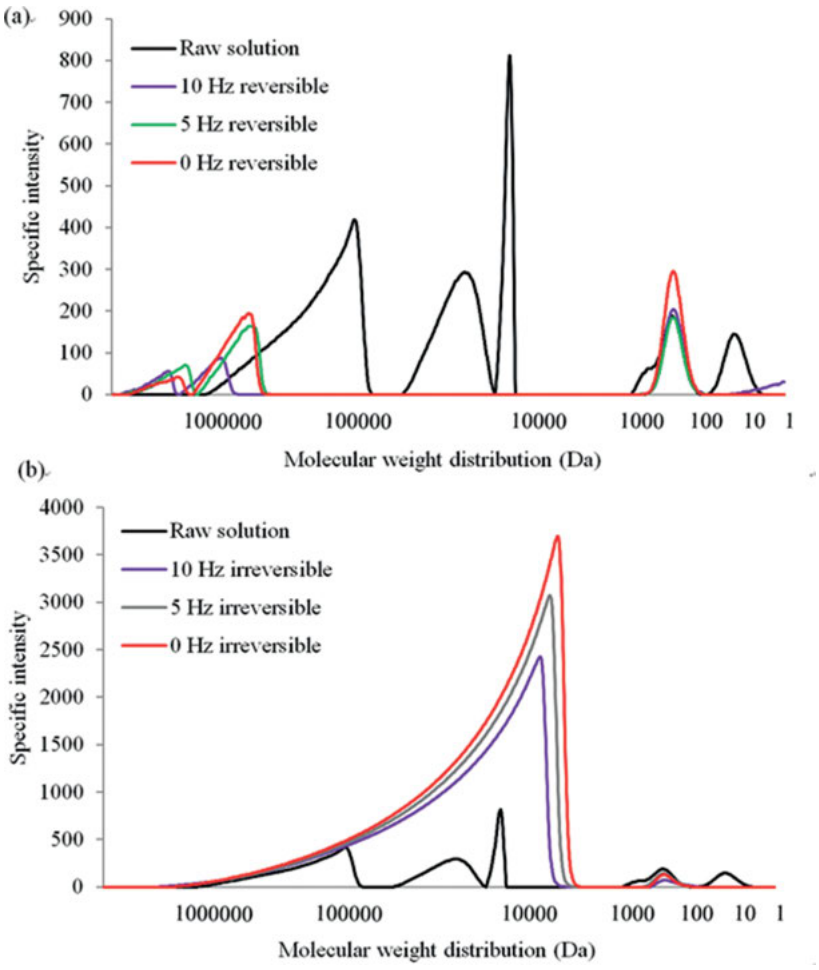

Figure 2.8: MW distributions of EOM: (a) reversible EOM and (b) irreversible EOM.

EBSCOhost - printed on 2/14/2023 6:39 AM via . All use subject to https://www.ebsco.com/terms-of-use

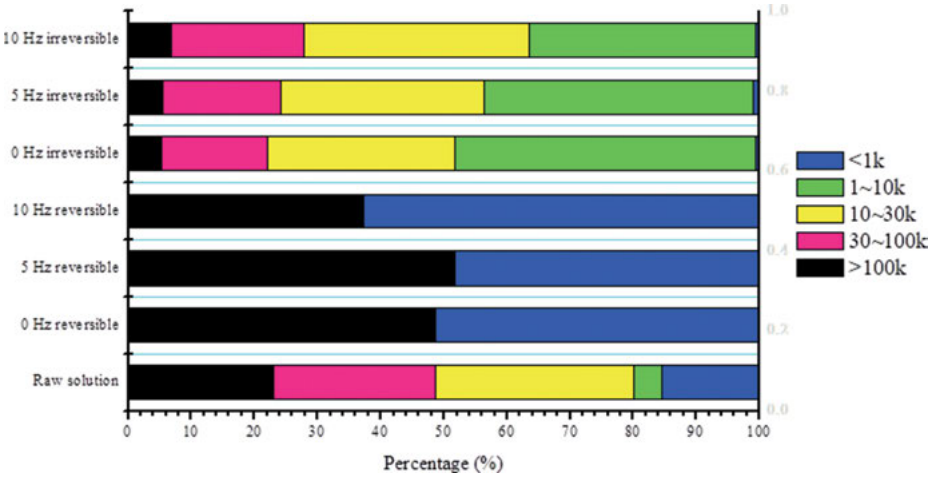

Figure 2.9: The percentage of MW distribution of reversible and irreversible EOM.

2.3 Summary

Combined with the AVM operation mode, the reversible membrane fouling can be controlled effectively as the vibration frequency increased, while the irreversible membrane fouling is not. The AVM could maintain a long filtration period of the algae filtration process with a smaller TMP change under a constant flux with the high vibration frequency of 10 Hz. With a low vibration frequency, the deposited algae layer could retain more high-MW EOM without contacting the membrane surface; but with a high vibration frequency, more high-MW EOM could adhere onto the membrane surface without forming the algae layer obviously.

References

[1] Li, Y., Bilad, M.R., and Vankelecom, I.F.J., Application of a magnetically induced membrane vibration (MMV) system for lignocelluloses hydrolysate filtration. Journal of Membrane Science, 2014. 452: p. 165–170.

[2] Anusha., K., et al., Transverse vibrationas nove lmembrane fouling mitigation strategy in anaerobic membrane bioreactor applications. Journal of Membrane Science, 2014. 455: p. 320–329.

[3] Subramani, A., et al., Vibratory shear enhanced process (VSEP) for treating brackish water reverse osmosis concentrate with high silica content. Desalination, 2012. 291: p. 15–22.

[4] Bilad, M.R., et al., Novel magnetically induced membrane vibration (MMV) for fouling control in membrane bioreactors. Water Research, 2012. 46(1): p. 63–72.

EBSCOhost - printed on 2/14/2023 6:39 AM via . All use subject to https://www.ebsco.com/terms-of-use

[5] Gerardo, M.L., et al., Harvesting of microalgae within a biorefinery approach: A review of the developments and case studies from pilot-plants. Algal Research, 2015. 11: p. 248–262.
[6] Ahmad, A.L., et al., Comparison of harvesting methods for microalgae Chlorella sp. and its potential use as a biodiesel feedstock. Environmental Technolnology, 2014. 35(17–20): p. 2244–2253.
[7] Show, K.Y., Lee, D.J., and Chang, J.S., Algal biomass dehydration. Bioresource Technology, 2013. 135: p. 720–729.
[8] Pragya, N., Pandey, K.K., and Sahoo, P.K., A review on harvesting, oil extraction and biofuels production technologies from microalgae. Renewable and Sustainable Energy Reviews, 2013. 24: p. 159–171.
[9] Milledge, J.J. and Heaven, S., A review of the harvesting of micro-algae for biofuel production. Reviews in Environmental Science and Bio/ Technology, 2012. 12(2): p. 165–178.
[10] Ahmad, A.L., et al., Optimization of microalgae coagulation process using chitosan. Chemical Engineering Journal, 2011. 173(3): p. 879–882.
[11] Zhang, X., et al., Harvesting algal biomass for biofuels using ultrafiltration membranes. Bioresource Technology, 2010. 101(14): p. 5297–5304.
[12] Bilad, M.R., et al., Harvesting microalgal biomass using submerged microfiltration membranes. Bioresource Technology, 2012. 111: p. 343–352.
[13] Sun, X., et al., A comparative study of microfiltration and ultrafiltration for algae harvesting. Algal Research, 2013. 2(4): p. 437–444.
[14] Hwang, T., et al., Microalgae recovery by ultrafiltration using novel fouling-resistant PVDF membranes with in situ PEGylated polyethyleneimine particles. Water Research, 2015. 73: p. 181–192.
[15] Rickman, M., Pellegrino, J., and Davis, R., Fouling phenomena during membrane filtration of microalgae. Journal of Membrane Science, 2012. 423–424: p. 33–42.
[16] Ahmad, A.L., et al., Harvesting of microalgal biomass using MF membrane: Kinetic model, CDE model and extended DLVO theory. Journal of Membrane Science, 2013. 446: p. 341–349.
[17] Anusha., K., et al., Application of low frequency transverse vibration on fouling limitation in submerged hollow fibre membranes. Journal of Membrane Science, 2012. 409–410: p. 54–65.
[18] Li, T., et al., Fouling control of submerged hollow fibre membranes by vibrations. Journal of Membrane Science, 2013. 427: p. 230–239.
[19] Li, T., Law, A.W.-K., and Fane, A.G., Submerged hollow fibre membrane filtration with transverse and longitudinal vibrations. Journal of Membrane Science, 2014. 455: p. 83–91.
[20] Pourbozorg, M., Li, T., and Law, A.W., Effect of turbulence on fouling control of submerged hollow fibre membrane filtration. Water Research, 2016. 99: p. 101–111.
[21] Zhao, F., et al., Using axial vibration membrane process to mitigate membrane fouling and reject extracellular organic matter in microalgae harvesting. Journal of Membrane Science, 2016. 517: p. 30–38.
[22] Bilad, M.R., et al., Harvesting microalgal biomass using a magnetically induced membrane vibration (MMV) system: Filtration performance and energy consumption. Bioresource Technology, 2013. 138: p. 329–338.
[23] Zhao, F., et al., Microalgae harvesting by an axial vibration membrane: The mechanism of mitigating membrane fouling. Journal of Membrane Science, 2016. 508: p. 127–135.
[24] Huyskens, C., et al., A new method for the evaluation of the reversible and irreversible fouling propensity of MBR mixed liquor. Journal of Membrane Science, 2008. 323(1): p. 185–192.
[25] Wu, G., Cui, L., and Xu, Y., A novel submerged rotating membrane bioreactor and reversible membrane fouling control. Desalination, 2008. 228(1–3): p. 255–262.

EBSCOhost - printed on 2/14/2023 6:39 AM via . All use subject to https://www.ebsco.com/terms-of-use

[26] Kimura, K., et al., Irreversible membrane fouling during ultrafiltration of surface water. Water Research, 2004. 38(14–15): p. 3431–3441.
[27] Hamad, J.Z., et al., Irreversible membrane fouling abatement through pre-deposited layer of hierarchical porous carbons. Water Research, 2014. 65: p. 245–256.
[28] Qu, F., et al., Characterization of dissolved extracellular organic matter (dEOM) and bound extracellular organic matter (bEOM) of Microcystis aeruginosa and their impacts on UF membrane fouling. Water Research, 2012. 46(9): p. 2881–2890.
[29] Qu, F., et al., Ultrafiltration membrane fouling by extracellular organic matters (EOM) of Microcystis aeruginosa in stationary phase: Influences of interfacial characteristics of foulants and fouling mechanisms. Water Research, 2012. 46(5): p. 1490–1500.
[30] Zhao, F., et al., Comparison of axial vibration membrane and submerged aeration membrane in microalgae harvesting. Bioresource Technology, 2016. 208: p. 178–183.
[31] Zhang, Y., et al., Chemical cleaning of fouled PVC membrane during ultrafiltration of algal-rich water. Journal of Environmental Sciences, 2011. 23(4): p. 529–536.
[32] Qu, F., et al., Ultrafiltration membrane fouling caused by extracellular organic matter (EOM) from Microcystis aeruginosa: Effects of membrane pore size and surface hydrophobicity. Journal of Membrane Science, 2014. 449: p. 58–66.
[33] Zhao, F., et al., Effect of temperature on extracellular organic matter (EOM) of Chlorella pyrenoidosa and effect of EOM on irreversible membrane fouling. Colloids Surf B Biointerfaces, 2015. 136: p. 431–439.
[34] Omar, A., et al., Treatment of dairy process waters using a vibrating filtration system and NF and RO membranes. Journal of Membrane Science, 2004. 235: p. 111–122.
[35] Wu, Q., et al., Temperature-responsive membrane for hydrophobic interaction based chromatographic separation of proteins in bind-and-elute mode. Journal of Membrane Science, 2014. 471: p. 56–64.
[36] Chu, H., et al., Dewatering of Chlorella pyrenoidosa using a diatomite dynamic membrane: Characteristics of a long-term operation. Journal of Membrane Science, 2015. 492: p. 340–347.

EBSCOhost - printed on 2/14/2023 6:39 AM via . All use subject to https://www.ebsco.com/terms-of-use

Weiwei Huang, Lin Wang, Bingzhi Dong

Chapter 3
The Membrane Fouling

Low pressure membrane has been increasingly used in water and wastewater treatment, but some drawbacks are still limitations to its widespread application, such as membrane fouling and insufficient removal of relatively smaller organic foulants. Extensive study has been conducted on the principle foulants and fouling mechanisms involved in this problem and it is found that there were generally four kinds of membrane foulants, including colloidal and suspended solids, inorganic matters, natural organic matter (NOM), and microorganisms. Each kind of organic might induce unique fouling mechanism [1–3]. NOM is a complex mixture of organic materials, which generally includes humic substances, polysaccharides, proteins, peptides, amino acids, fatty acids, lipids, phenols, alcohols and small hydrophilic acids [4]. Previous study indicated that many factors affecting the membrane fouling by NOM, including the nature of the NOM (size, hydrophobicity, charge), the membrane (hydrophobicity, charge, surface roughness), the solution (pH, ionic strength, hardness ion concentration), as well as the hydrodynamics of the membrane system (solution flux, surface shear) [5]. The membrane foulants and their fouling mechanism can be found in Table 3.1. In this chapter, better analysis of the membrane fouling mechanism was discussed systematically.

Table 3.1: Different types of membrane foulants and their fouling mechanism.

Types	Substances	Fouling mechanisms
Colloid and suspended solids	Clay minerals, oxide of silica gel, iron, aluminum or manganese, organic colloids and suspensions	Pore blockage and cake layer formation
Inorganic matter	Inorganic salts such as calcium, magnesium, barium, iron, silicic acid and metal hydroxides	Accumulation on the membrane surface or deposition into the membrane pores
NOM	Protein, polysaccharide, amino sugar, nucleic acid, humic acid, fulvic acid, biological cell components	Cake layer formation or adsorption into membrane pore

Weiwei Huang, Eco-Environment Protection Research Institute, Shanghai Academy of Agricultural Sciences, Shanghai, P. R. China
Lin Wang, School of Municipal and Environmental Engineering, Shandong Jianzhu University, Jinan, Shandong, P. R. China
Bingzhi Dong, College of Environmental Science and Engineering, Tongji University, Shanghai, P. R. China

https://doi.org/10.1515/9783110596847-003

EBSCOhost - printed on 2/14/2023 6:39 AM via . All use subject to https://www.ebsco.com/terms-of-use

Table 3.1 (continued)

Types	Substances	Fouling mechanisms
Micro-organism	Extracellular polymers (EPS) and soluble microbial products (SMP)	Microorganisms attachment to the membrane surface, multiplication and production of extracellular polymers to form a viscous hydrated gel

3.1 Influence of membrane characteristics on membrane fouling

Membrane characteristics had significant effects on membrane fouling. It was widely considered that the contamination of hydrophobic membrane was significantly higher than that of hydrophilic membrane, while the hydrophilic membrane is not prone to be polluted by NOM [6, 7]. The hydrogen bonding between hydrophilic membrane surface and water molecules might make the water more adsorbed, while when the hydrophobic material close to the membrane surface, the ordered structure of water might be further destroyed and the energy consumed.

The surface charge of the membrane also played significant effects on membrane fouling. When the surface of the membrane was positively charged, the colloidal impurities tended to deposit on the membrane surface, causing the membrane fouling and deteriorating the membrane performance. While when the surface of membrane was negatively charged, the colloid could adhere to the membrane surface, weaken the electrostatic repulsion, and inhibit the membrane fouling. The interaction between the protein and membrane in the initial filtration phase can also be affected by the membranes surface charge, which afterwards affect the filtration flux and protein penetration.

Elimelech et al. found that membrane with higher roughness and porosity was more susceptible to membrane fouling [8]. Ho et al. suggested that membrane with interconnected membrane pores tend to be fouled slowly [9]. The above result thus suggested that the possibility of adsorbing foulants on the membrane surface could be affected by the increased membrane surface roughness, which might be due to that water can bypass the clogged membrane pores and flow through the membrane with interconnected pore structures. The disturbance of the membrane surface would also be increased by the membrane surface roughness, which hindered the formation of foulants on the membrane surface.

EBSCOhost - printed on 2/14/2023 6:39 AM via . All use subject to https://www.ebsco.com/terms-of-use

3.2 Influence of organic hydrophobicity on membrane fouling

Natural organic matter (NOM) is a very complex mixture. The extent of MF fouling is highly variable when the characteristics of feed water are different. Therefore, characterizing foulants are critical to understand the membrane fouling in natural water filtration.

Generally, organic molecular size distribution and hydrophobicity are the most useful characteristics in describing membrane foulants [10]. Some studies suggested that dissolved organic matter (DOM) with molecular weight ranging from a few hundreds to over 100 kDa caused significant fouling in the membrane filtration. The others found that only a small proportion of organic matter in the colloidal contributed to membrane fouling [3, 11]. The use of NOM fraction to test the types of compounds that are responsible for MF membrane fouling revealed that for a polypropylene (PP) hollow fibre system, the neutral hydrophilic fraction was the most strongly implicated [12]. There was a 40% decrease in flux after a throughput that caused only a 20% decrease for the other fractions of the strong and weakly hydrophobic acids (WHAs) and charged hydrophilic material. Gray et al. investigated the fouling of microfiltration (MF) membrane by NOM and found that MF of the hydrophilic fractions lead to rapid flux decline and the formation of cake or gel layer, while the hydrophobic fractions show a steady flux decline with no obvious formation of gel or cake layer [13]. In order to better understand the characteristics of which fraction lead to more serious membrane fouling, further studies are still needed to be conducted.

In this work, organic hydrophobicity and molecular weight distribution were analyzed as the major characteristics for MF membrane fouling.

3.2.1 Organic fractions on membrane fouling

3.2.1.1 Materials and methods

Tap water, Yangcheng, Xiangjiang River, Taihu Lake, Qingcaosha and Ge Lake and their associated organic components were used to investigate their contributions of different organic fractions on membrane fouling.

XAD-4, DAX-8 and IRA-958 resins were employed to separate the organics into the hydrophobic fraction (HPO), the transphilic fraction (TPI), the negatively charged hydrophilic fraction (C-HPI) and the neutral hydrophilic fraction (N-HPI). AOM fractionation was conducted by SUPELCO VISIPREPTM DL (USA).

EBSCOhost - printed on 2/14/2023 6:39 AM via . All use subject to https://www.ebsco.com/terms-of-use

3.2.1.2 Membrane filtration

Membrane filtration was performed on a flat filtration unit of a dead-end filtration mode. Two types of membranes including PVDF 150K membrane and a commercially available flat sheet microfiltration membrane (MF-Millipore™) were used in this study, which consisted of 80–100% nitrocellulose (Cas No. 9004-70-0) and 0–20% cellulose acetate (Cas No. 9004-35-7). Prior to filtration, all virgin membranes were presoaked and stored in ultrapure (Milli-Q) water for 24 h at 4 °C to remove impurities. High purity N_2 gas at transmembrane pressure (TMP) of 0.1 MPa was used for filtration. The permeate flux was recorded using an electronic balance (Shimadzu, VW2200H, accuracy ± 0.1 g) connected with a computer at a fixed interval. Before filtration, prefiltration was conducted using ultrapure water until a constant permeate flux was achieved.

All experiments were conducted at room temperature (20–25 °C). For each test, 800 mL of permeate volumes were measured. The relative flux (J/J_0) was calculated by the ratio of the permeate flux (J) to the initial flux (J_0) for comparing the effect of membrane fouling potential.

3.2.1.3 Results and Discussion

Figures 3.1 and 3.2 show the filtration flux by various NOM fractions. As can be seen, the filtration flux decline caused by both N-HPI fractions in tap and Yangcheng water were the most serious, with 69% and 89% decrease as compared to the initial flux, whereas the HPO, TPI, and C-HPI in tap water had less effects on the filtration flux decline, and the filtration flux caused by TPI, HPO and C-HPI were 33%, 59%, and 60% respectively, in the tap water. Whereas, the filtration flux caused by HPO and C-HPI were only 17% and 21% of the initial flux in Yangcheng-Lake water filtration, suggesting that neutral hydrophilic organics has great effects on membrane fouling.

Similar results can also be observed by Xiangjiang River and Taihu Lake (Figures 3.3 and 3.4) water filtration, which can be found that both N-HPI fractions in Xiangjiang River and Taihu Lake water caused more serious membrane fouling than the other fractions, and the filtration flux had the order of N-HPI > HPO > C-HPI > TPI for Xiangjiang River, and N-HPI > HPO > TPI > C-HPI for Taihu Lake. This result was consistent with previous studies that N-HPI formed a dense gel layer on the membrane surface, causing a rapid decrease in membrane flux.

However, in regard to the four fractions, it was found that there were some differences between the two water, for example, TPI in Xiangjiang River caused the least filtration flux, while the membrane fouling caused by C-HPI of Taihu Lake was the least. The filtration flux of both water at the end of filtration was in Table 3.2.

EBSCOhost - printed on 2/14/2023 6:39 AM via . All use subject to https://www.ebsco.com/terms-of-use

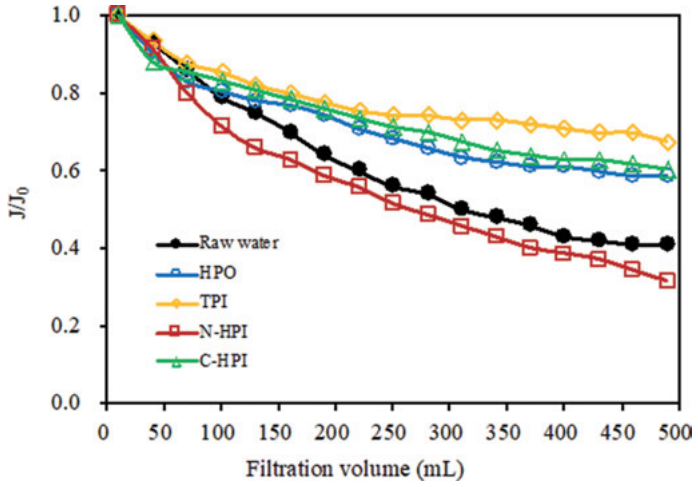

Figure 3.1: Influence of organic fractions of tap water on filtration flux of PVDF 150K membrane.

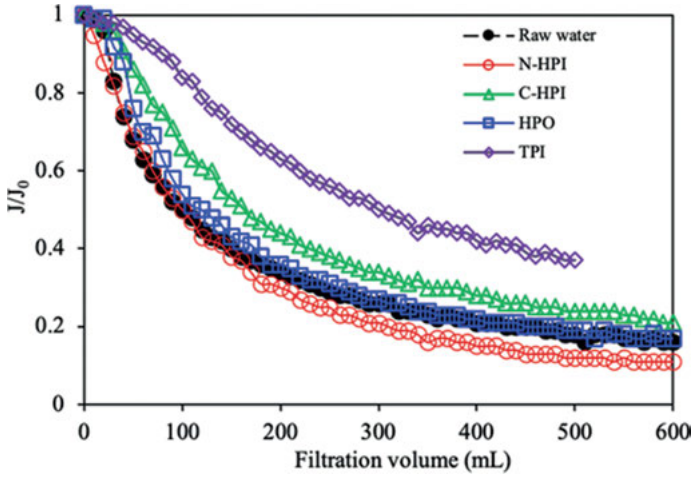

Figure 3.2: Influence of organic fractions of Yangcheng water on filtration flux of PVDF 150K membrane.

Similar phenomenon can also be observed in Qingcaosha and Ge lake that N-HPI caused the most serious membrane fouling (Figures 3.5 and 3.6), followed by HPO. However, it was very different between C-HPI and HPO fractions, which might be due to their different organic characteristics. The hydrophobic components had little effects on filtration flux, and the flux at the end of filtration was 90% of that in the initial flux, indicating hydrophobic organics contributed little to hydrophilic microfiltration membrane fouling during this study.

EBSCOhost - printed on 2/14/2023 6:39 AM via . All use subject to https://www.ebsco.com/terms-of-use

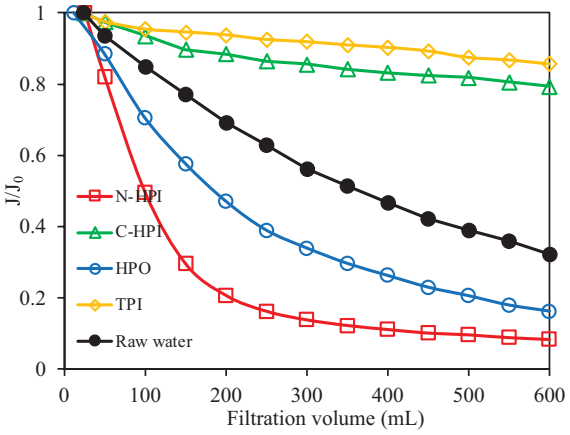

Figure 3.3: Influence of organic fractions of Xiangjiang River water on filtration flux of 0.1 μm CA membrane.

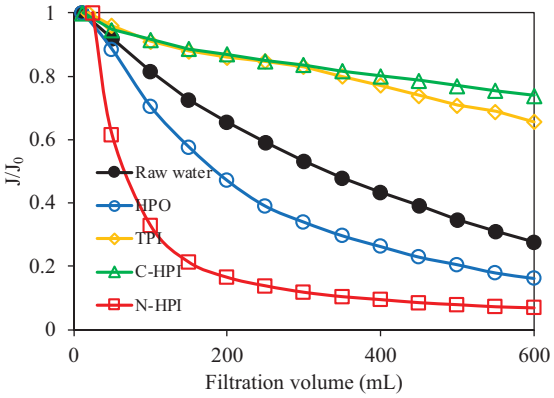

Figure 3.4: Influence of organic fractions of Taihu Lake water on filtration flux of 0.1 μm CA membrane.

3.2.2 Effect of various hydrophilic fractions on membrane fouling

3.2.2.1 Preparation of water samples

This study was conducted by using five natural water, which included the Sanhaowu Lake (SHW) water in Tongji University in April, representing the surface water polluted by allochthonous NOM; Yellow River, Huangpu River (HPJ) in Shanghai City, in July, representing the heavy polluted river by waste of industry and human beings; the Gaoyou (GY) in Jiangsu province, presenting the lower polluted reservoir water and Kunshan water (KS).

EBSCOhost - printed on 2/14/2023 6:39 AM via . All use subject to https://www.ebsco.com/terms-of-use

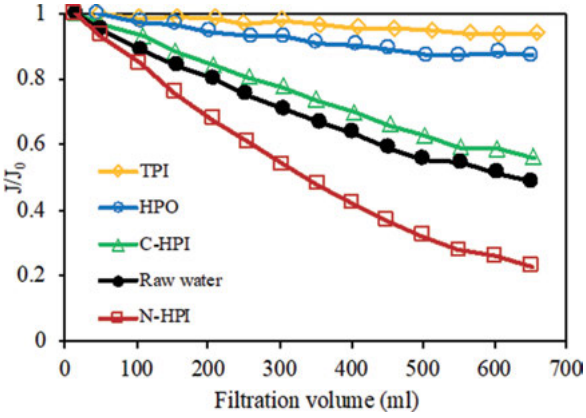

Figure 3.5: Influence of organic fractions of Qingcaosha water on filtration flux of 0.1 μm CA membrane.

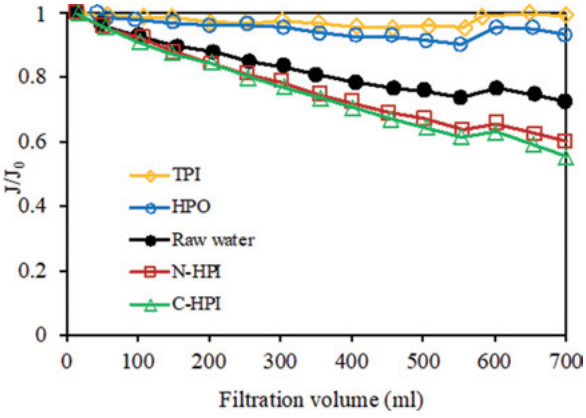

Figure 3.6: Influence of organic fractions of Gehu water on filtration flux of 0.1 μm CA membrane.

Table 3.2: Filtration flux (J/J_0) of Xiangjiang River and Taihu Lake at the end of filtration.

Fraction	Raw	HPO	TPI	C-HPI	N-HPI
Xiangjiang River	0.322	0.165	0.857	0.794	0.084
Taihu Lake	0.276	0.162	0.657	0.739	0.072

Reverse osmosis (RO) with a fiber pre-filter was utilized to concentrate the source water into 20–25 mg/L (as dissolved organic carbon). Then, the water samples were filtered through a 0.45 μm membrane (regenerated cellulose) and stored at 4 °C in a refrigerator.

A commercially available flat sheet microfiltration membrane (MF-Millipore™) was used in this study, which consisted of 80–100% nitrocellulose (Cas No. 9004-70-

EBSCOhost - printed on 2/14/2023 6:39 AM via . All use subject to https://www.ebsco.com/terms-of-use

0) and 0–20% cellulose acetate (Cas No. 9004-35-7). Membrane filtration was consistent with that described in Section 3.1.1.

3.2.2.2 Results and discussion

Figure 3.7 shows the hydrophilic and hydrophobic properties of different NOMs water. The hydrophilic fraction accounted over 60% for all the examined NOM water, and over 70% in SHW water. The N-HPI fraction was the largest portion of the DOC among the four isolated fractions in all the NOMs. However, there were large fluctuations among different NOMs, and the N-HPI fraction in SHW water accounted for 60% in DOC, followed by KS, GY, and HP, Yellow River water.

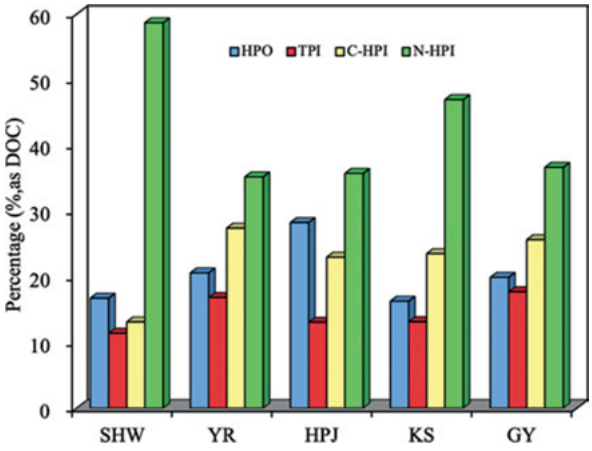

Figure 3.7: Hydrophilic and hydrophobic properties of different NOMs water.

From the flux decline of different source water, it can be found that there were significant differences in the filtration flux behaviors of various NOMs. SHW water declined the most rapidly, followed by KS and HPJ water, while the Yellow River and GY displayed slow downward trend, and the filtration flux at the end of filtration was 30% of that in the initial filtration flux. SHW water with low SUVA value and higher N-HPI fraction proportion had the most serious membrane fouling, which implies that N-HPI fraction is responsible for flux decline. Previous study suggested that macromolecular organics in N-HPI could form a dense cake layer on the membrane surface, leading to a rapid decline of filtration flux. Carroll et al. suggested that small molecules in N-HPI fractions lead to serious membrane fouling [12]. The results thus indicated that macro MW organics in N-HPI had an important effect on membrane fouling, especially for those organics with MW > 30 KDa.

EBSCOhost - printed on 2/14/2023 6:39 AM via . All use subject to https://www.ebsco.com/terms-of-use

Nevertheless, the N-HPI might not be the only factor that caused membrane fouling. HPO might also have certain relations with the membrane fouling. N-HPI fraction was consistent for HP and GY River, however, HPO in HP was higher than in GY, which might be one of the reasons that HP had serious membrane fouling than GY water. In addition, macro MW took a higher account of over 10% in HPO in HP than those in other water, which might also be one of the reasons of fast filtration flux decline.

Figure 3.8 shows the flux decline of different DOM fractions. For all the water sources, it was found that the filtration flux with N-HPI declined the most rapidly, followed by HPO and TPI, while C-HPI showed the least. Note that, for the same fraction, different water sources showed different filtration flux declines. For all the fractions, SHW exhibited the greatest flux decline, followed by HPJ, and GY, which implies that water source is also important to the membrane fouling than the DOM hydrophobicity. This can be due to that as a complex mixture of various organic matters, the concentration, chemistry and composition of DOM are highly dependent on the source water. Although DOM with similar functional groups or structures can be characterized as the same hydrophobicity fraction, they are still different in many other characteristics.

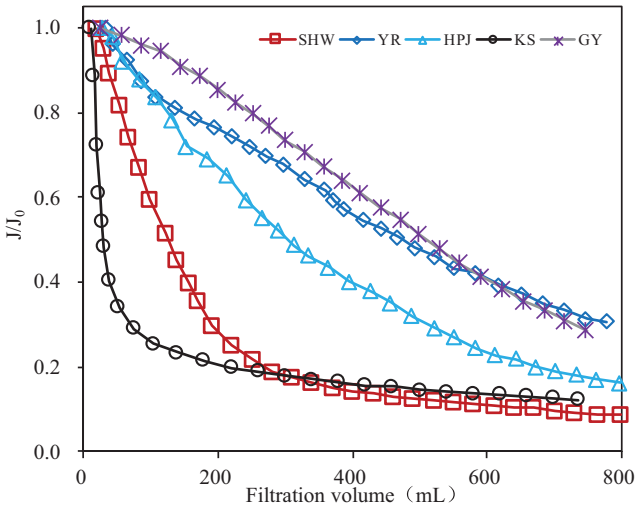

Figure 3.8: Filtration flux of the raw water.

3.3 Effect of molecular weight on membrane fouling

The determination of the molecular weight of organic matter in water has important significance for the understanding of water pollution and evaluation of various treatment methods. Generally, the organic matter with larger MW is more likely to

EBSCOhost - printed on 2/14/2023 6:39 AM via . All use subject to https://www.ebsco.com/terms-of-use

be trapped by the membrane, depositing on the membrane surface or into the membrane pore, causing a rapid decrease in filtration flux. While the organics with small MW could pass through the membrane pores, which had less effects on membrane fouling. This part mainly investigated the NOM MW on the membrane fouling.

Algal organic matter is produced by algae in natural environment, which represents a considerable proportion of the organic carbon source in surface water during algal blooms. Compared with the focused studies that have been performed on the membrane fouling by inorganic particles and NOM, the knowledge of algal fouling on MF membrane is inadequate. Qu et al. investigated ultrafiltration (UF) membrane fouling by *Microcystis aeruginosa* EOM and found that pore clogging and cake layer formation were the key factors in membrane fouling [14]. A macro molecular biopolymer was demonstrated to be the major component in membrane fouling. Moreover, the irreversible fouling by EOM was found to be mainly caused by polysaccharides under ambient solution chemistry, and fouling by tryptophan-like substances turned out to be more irreversible with the presence of calcium.

Despite these studies, membrane fouling caused by AOM was complicated due to that the AOMs characteristics on the MF membrane fouling might be caused by various algae species, cultivation time, as well as other environmental factors. This study investigated the MF fouling by various algae. Five algae were selected in this study because they represent three classical seasonal algal blooms, i.e., cyanobacteria, green algae and diatoms.

3.3.1 Experimental procedures and methods

Freshwater algae of *Microcystis aeruginosa*, *Aphanizomenon flos-aquae*, *Anabaena flos-aquae*, *Scenedesmus obliquus* and *Cyclotella* were purchased from the Institute of Hydrobiology, Chinese Academy of Sciences, China. *M. aeruginosa*, *Aphanizomenon flos-aquae* and *Anabaena flos-aquae* were cultivated at 20 °C using BG-11 medium under the control ambient conditions of 12 h fluorescent light: 12 h dark and an irradiance of about 90 μmol/($m^2 \cdot s$) provided by cool-white fluorescent light. *S. obliquus* was cultivated using SE medium at 25 °C and a 12–12 h light-dark cycle with an irradiance of about 120 μmol/($m^2 \cdot s$). *Cyclotella* was cultivated using D1 medium at 20 °C and a 12–12 h light-dark cycle with an irradiance of about 90 μmol/($m^2 \cdot s$).

AOM was extracted from algal solutions of stationary growth phase by centrifuging at 10,000 g for 15 min and filtering through a Millipore 0.45 μm filter subsequently. AOM extracted from *M. aeruginosa*, *Aphanizomenon flos-aquae*, *Anabaena flos-aquae*, *S. obliquus* and *Cyclotella* were denoted as MA-AOM, APF-AOM, ANF-AOM, SO-AOM and Cy-AOM, respectively.

EBSCOhost - printed on 2/14/2023 6:39 AM via . All use subject to https://www.ebsco.com/terms-of-use

3.3.2 Membrane and filtration unit

The MF membrane used was a 0.1 μm Millipore hydrophilic mixed cellulose flat sheet membrane (VCWP, 80%–100% of nitrate cellulose and 0%–20% of acetate cellulose) (Millipore Corporation, US). A dead-end filtration unit was used for the MF experiment, which was consistent with the filtration vessel described in Section 3.2.2.2.

3.3.3 Analytical methods

Dissolved organic carbon (DOC) and ultraviolet absorbance at a wavelength of 254 nm (UV_{254}) were measured by a total organic carbon analyzer (TOC-VCPH, Shimadzu) and a UV spectrophotometer (Hach-5000), respectively. Specific ultraviolet absorbance (SUVA) was calculated using the ratio of UV_{254} to DOC.

The molecular weight (MW) distribution of the dissolved organic matter (DOM) was determined using an HPSEC (Waters e2695, USA) system with a TSKgelG3000P-WXL column (0.78 cm × 30 cm).

3.3.4 Results of the MF experiments

Figure 3.9 shows the normalized flux as a function of specific volume for the five AOMs using the MF membrane. The Cy-AOM solution caused slightly less flux decline during the filtration process than the other four AOMs did; the final normalized flux (J/J_0) for Cy-AOM was approximately 31%; in comparison, the flux for APF-AOM, ANF-AOM and MA-AOM dropped rapidly, and the flux at the end of the filtration were 9%, 10% and 12%, respectively, of the initial flux. To identify the diverse fouling behavior of various AOMs, AOM characteristics, including AOM MW distribution, hydrophobicity, were investigated.

Table 3.3 shows the hydrophilic and hydrophobic properties of different AOMs. The hydrophilic fraction was over 60% for all the examined AOMs, and over 80% in ANF- and Cy-AOMs. N-HPI fraction was the largest portion of the DOC among the four isolated fractions in all the AOMs. However, among the different AOMs, C-HPI had the largest fluctuations of 8.19–21.36%. APF-, ANF-, and MA-AOMs, which had higher proportions of N-HPI, causing more substantial filtration flux decline at the end of filtration, which was consistent with previous studies that membrane flux decline is often associated with neutral hydrophilic fractions [12]. Although Cy-AOM had an N-HPI fraction that was comparable to that of MA-AOM (Table 3.3), the filtration flux change was small, indicating that N-HPI was not the sole reason for the flux decline. In this case, MW distribution and chemical compositions should also be considered.

EBSCOhost - printed on 2/14/2023 6:39 AM via . All use subject to https://www.ebsco.com/terms-of-use

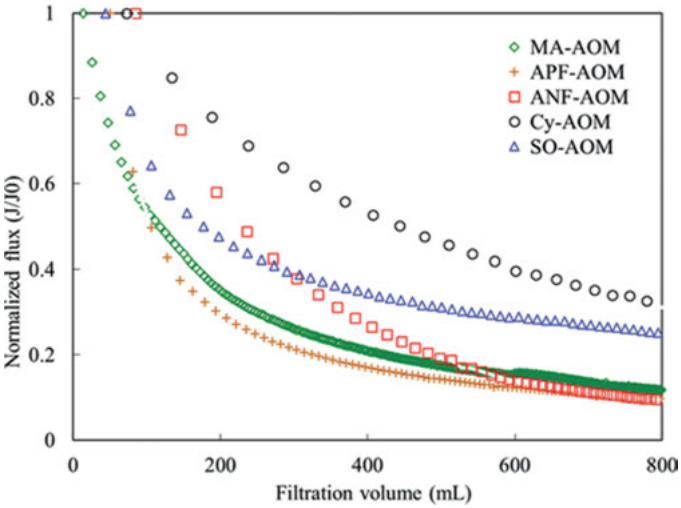

Figure 3.9: Normalized flux vs. specific volume for the MF of the AOMs solutions.

Table 3.3: Hydrophilic properties of AOMs.

	N-HPI (%)	C-HPI (%)	HPO (%)	TPI (%)
PF-AOM	70.56 ± 0.025	8.19 ± 0.0949	16.98 ± 0.038	7.67 ± 0.053
ANF-AOM	68.1 ± 0.082	17.22 ± 0.120	17.22 ± 0.016	8.25 ± 0.007
MA-AOM	65 ± 0.00428	13 ± 0.04714	16 ± 0.0816	5 ± 0.102
SO-AOM	48.07 ± 0.098	21.36 ± 0.071	11.29 ± 0.29	6.08 ± 0.049
Cy-AOM	64.85 ± 0.085	18.52 ± 0.196	17.12 ± 0.046	12.07 ± 0.07

Values are given as mean value ± standard deviation (n = 3).

Figure 3.10 shows the MW distributions of the AOMs. The TOC chromatograms of AOMs were almost identical in the total MW distribution, and there were two different molecular size fractions identified for each AOM. However, they were distinctly different in the TOC peak heights and/or areas. The apparent MW of fraction 1, which was typically attributed to proteins, polysaccharides or macromolecules of humic acid organics, was > 100,000 Da for all the AOM samples.

AOM at fraction 1 showed different characteristics. APF-, MA-, and ANF-AOMs had higher TOC peak heights of 0.00371, 0.0037 and 0.0034 mg/L in macro MW, whereas the TOC peak heights of SO- and Cy-AOMs were 0.00085 and 0.00038 mg/L, respectively, indicating that APF-, MA-, and ANF-AOMs contained significantly more high MW organic components. Differences of peak heights and areas at fraction 2 were also detected among the AOMs at medium and small MW distributions. The TOC peak height was highest for Cy-AOM in fraction 2, indicating that Cy-AOM contains more medium and small organic components.

EBSCOhost - printed on 2/14/2023 6:39 AM via . All use subject to https://www.ebsco.com/terms-of-use

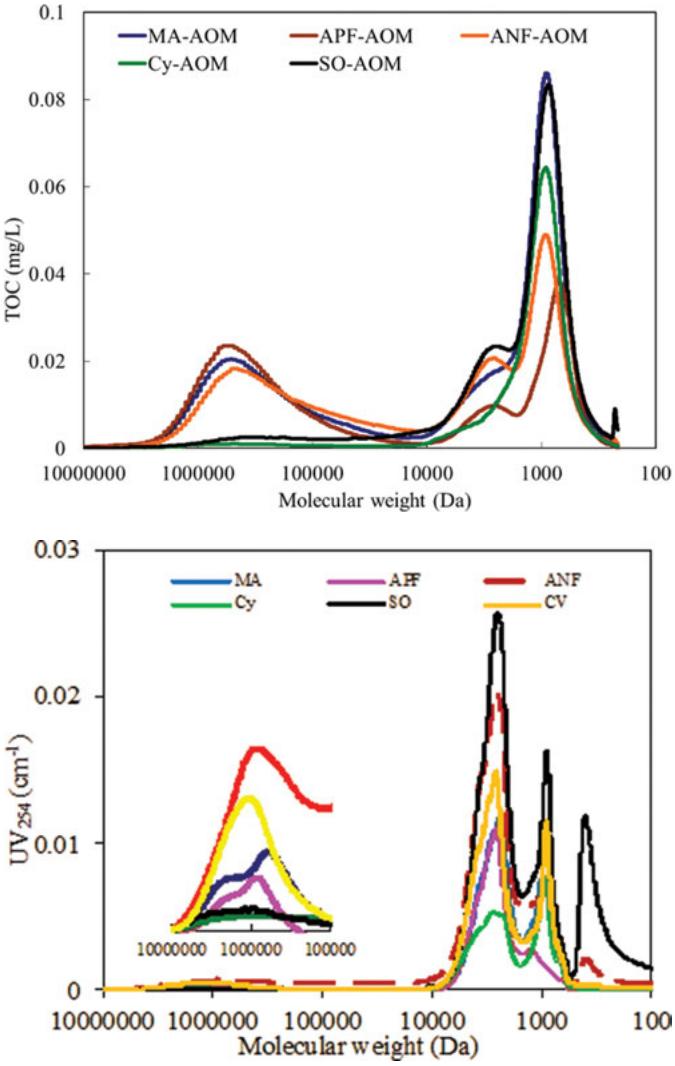

Figure 3.10: MW distribution of AOM detected by HPSEC-UV-TOC.

After MF (Figure 3.11), it was found that the TOC peak intensity in the macromolecular fraction was greatly reduced, which means that macromolecular organics were successfully intercepted by the MF that exerted the most effect on membrane flux decline. The TOC peak intensities in the macro MW of ANF-, APF, and MA-AOMs were significantly higher than those of SO- and Cy-AOMs; which was consistent with their filtration fluxes. Huang et al. found that macromolecular organics is mainly composed of polysaccharides, proteins and humic acid colloidal organic matters. The above result thus indicated that polysaccharides, proteins and macromolecular humic acids were the main organics that caused membrane fouling [15]. Gray et al.

EBSCOhost - printed on 2/14/2023 6:39 AM via . All use subject to https://www.ebsco.com/terms-of-use

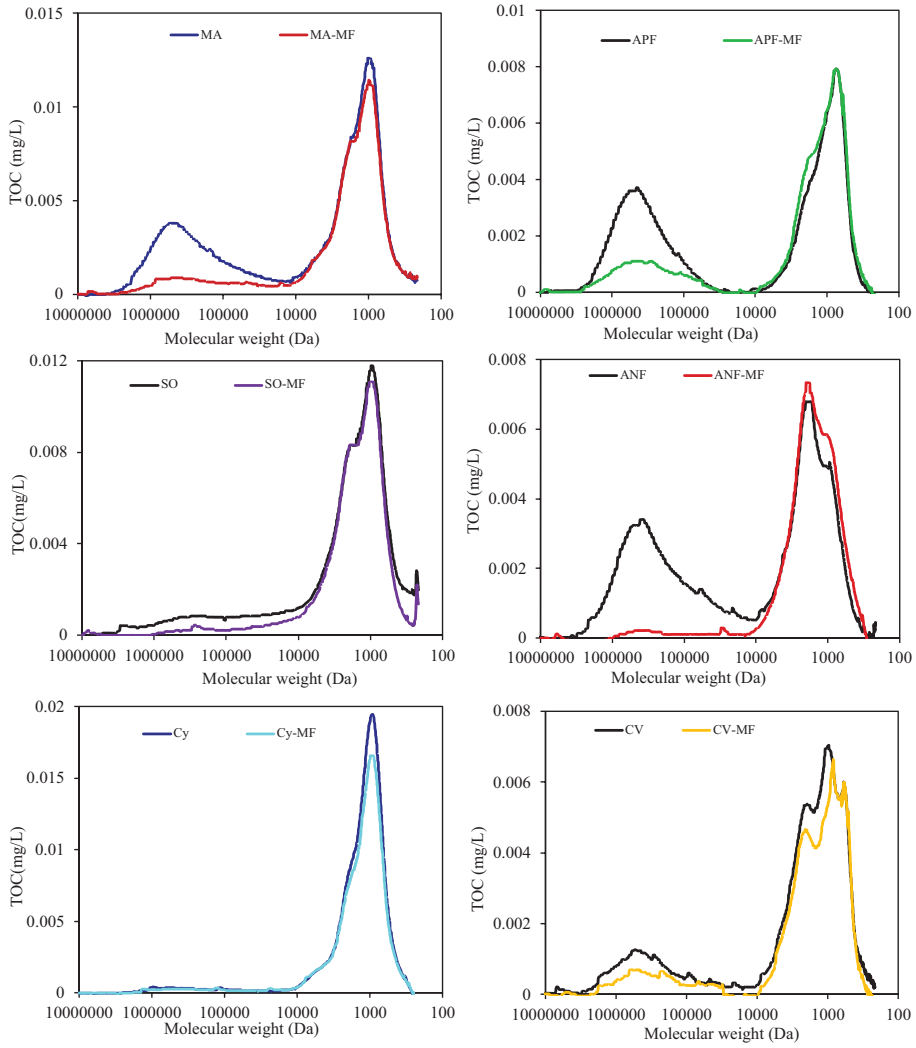

Figure 3.11: MW distribution of AOMs before and after MF.

found that macromolecular organics could form a gel layer on the membrane surface, or enter membrane pores, make membrane pores clogged, causing serious filtration flux decline [13]. It should be noted that although the TOC response of macromolecular organics after MF was significantly reduced, as the TOC response of SO- and Cy-AOMs was lower, the filtration flux caused by SO- and Cy-AOMs was less serious than the other three AOMs.

To analysis the MW on membrane fouling, the relationships between MW organics and filtration flux was analyzed.

EBSCOhost - printed on 2/14/2023 6:39 AM via . All use subject to https://www.ebsco.com/terms-of-use

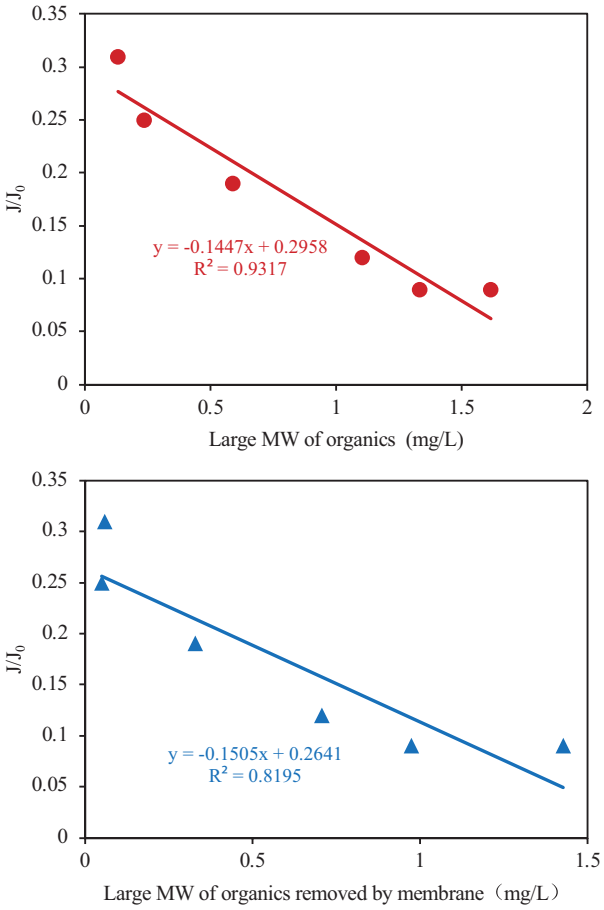

Figure 3.12: The relationship between the macromolecules and the filtration flux.

From the relationship between the macromolecules and the filtration flux at the end of the filtration, it can be found that macromolecular organics have a close relationship with the filtration (Figure 3.12) flux. The R^2 was 0.93 and 0.81 for J/J_0 of macro and large MW organics. This result indicated that the more macromolecular organics in natural water, the more it is easily intercepted by membrane, and the more serious membrane fouling may be caused.

The MW changes of Xiangjiang River and Taihu lake organic fractions before and after UF can also be found in Figures 3.13 and 3.14. For Xiangjiang River, it can be found that macro MW organics was greatly reduced after UF, while there were little fluctuations in the other areas. HPO also had high peaks at macromolecular areas, however, the response is much lower than that in N-HPI. Besides, there were three peaks in medium and small MW areas in HPO, which was consistent with that in N-HPI. Macro MW organics in HPO was also rejected by MF, as well as some medium and small MW organics.

EBSCOhost - printed on 2/14/2023 6:39 AM via . All use subject to https://www.ebsco.com/terms-of-use

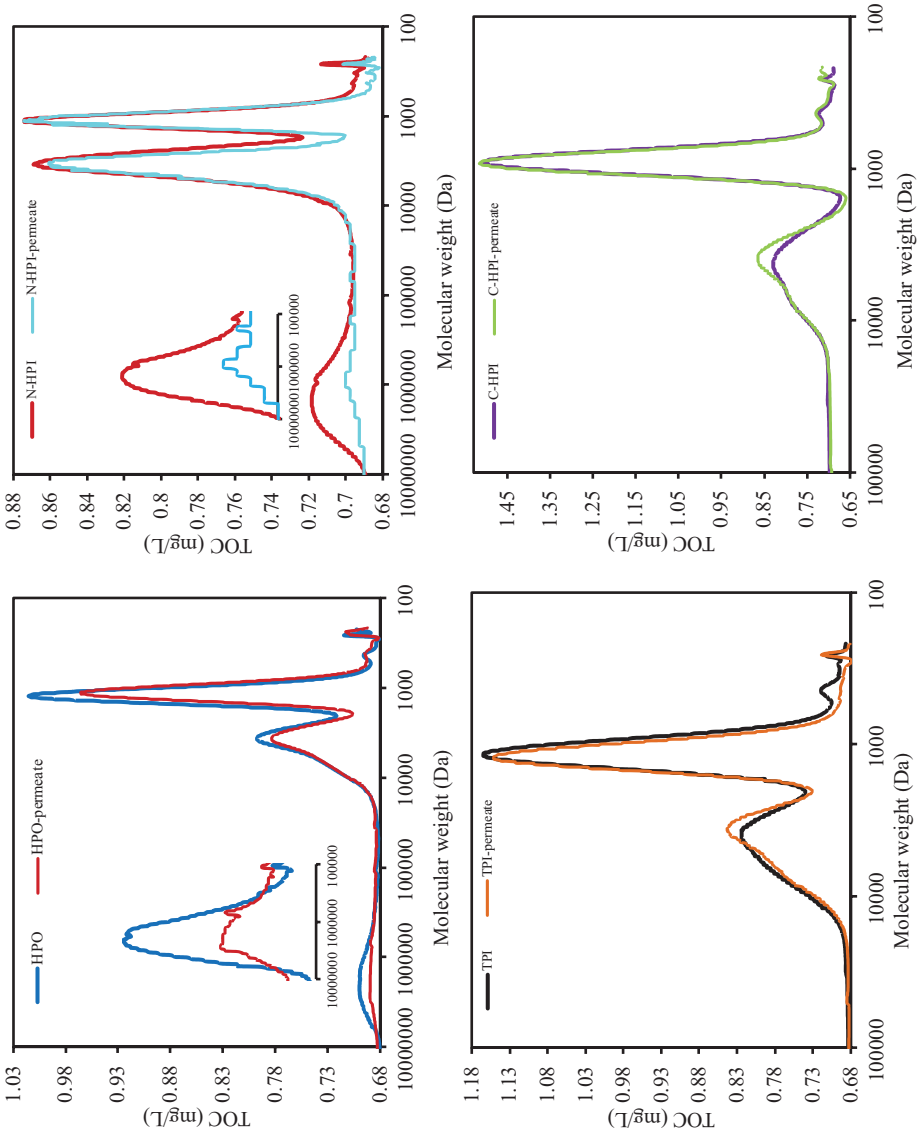

Figure 3.13: Changes in MW distribution of organic fractions of Xiangjiang River before and after MF.

For TPI and C-HPI, it can be found that there was little removal efficiency of TPI and C-HPI. Combined with the filtration flux, it can be inferred that the organic removal of MF was mainly by pore size screening, and due to the higher removal of macro MW organics in N-HPI and HPO, the filtration flux drop was more serious, while there were little declines in TPI and C-HPI.

EBSCOhost - printed on 2/14/2023 6:39 AM via . All use subject to https://www.ebsco.com/terms-of-use

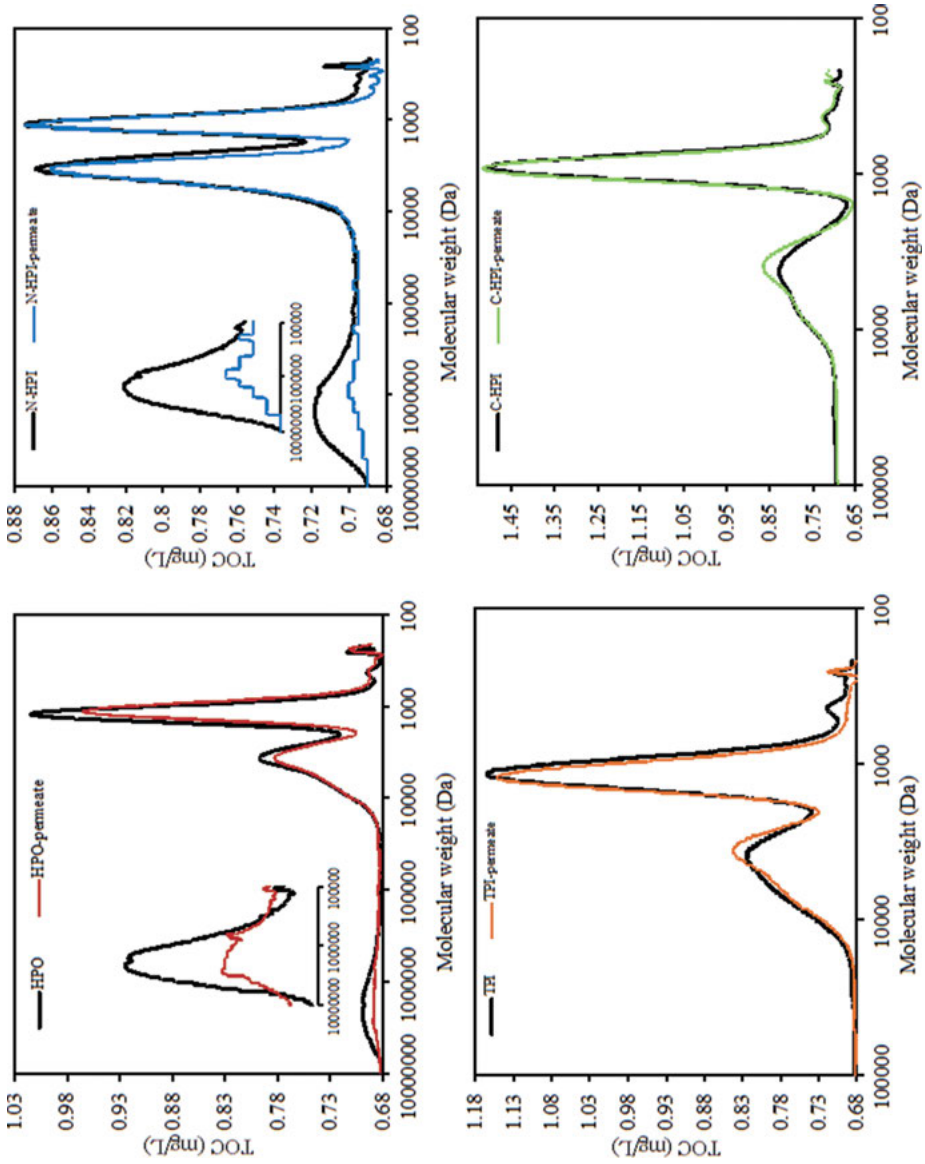

Figure 3.14: Changes of MW distribution of organic fraction of Taihu lake before and after MF.

Similar with Xiangjiang River, MF membrane could also mainly reject macro MW organics in N-HPI of Taihu lake which was distributed at 6.60×10^6–1.72×10^5 Da, while there were little fluctuations of organic removals in TPI and C-HPI. Besides, it was found that the TOC peak height was lower in HPO than that in N-HPI, MF also rejected this part of organics, consistent with that in Xiangjiang River.

EBSCOhost - printed on 2/14/2023 6:39 AM via . All use subject to https://www.ebsco.com/terms-of-use

Compared with MW distribution of both Xiangjiang River and Taihu lake, it was found that for the same fraction, Taihu Lake had high TOC of MW than that in Xiangjiang River, which might be one of the explanations of the low filtration flux. The discrepancies of these two water samples might be caused by the interaction of these components. TPI and C-HPI had similar MW, however, their filtration flux was different, which might be due to their difference in the structural properties.

3.4 Effect of fluorescence spectra on membrane fouling

Recently, the fluorescence excitation-emission matrix (EEM) spectroscopy has been widely used in analyzing the relationships of membrane foulants. Kimura et al. investigated the irreversible fouling of UF membrane and revealed that different NOM fractions could have different EEM locations [16]. Peiris et al. reported that the most problematic foulants were in the lower range of excitation and emission wavelengths [17]. Despite these studies, as there are still few universal conclusions drawn by analyzing membrane foulants from fluorescence EEM spectra, the usage of fluorescence EEM spectroscopy to identify foulants needs further discussion.

3.4.1 Materials and methods

The water samples were consistent with that in Section 3.3.2.1 including the Sanhaowu Lake (SHW) water, Huangpu River (HPJ) and the Gaoyou (GY) in Jiangsu province. The filtration vessel and membrane were consistent with that described in Section 3.2.2.2.

3.4.2 Result and discussion

Table 3.4 shows the fluorescence spectral parameters of fluorescence area volumes (expressed by FLU) and different peak intensity ratios, i.e. $r(a, c)$, $r(t, b)$, $r(t, a)$ of DOM fractions. NOM samples showed extremely different fluorescence area volumes, which may imply the differences of compound structures and concentrations. FLU followed the order of HP > KS > H > KS > GY. FLU mainly comes from the protein-like fluorescent region, but it is weak to humic-like fluoresce response, which indicated that the water polluted by domestic sewage might have high FLUz values, while the water polluted by terrestrial organic matter might have a very low FLUz value.

EBSCOhost - printed on 2/14/2023 6:39 AM via . All use subject to https://www.ebsco.com/terms-of-use

From the analysis of total fluorescence area volumes and filtration flux, it can be found that raw water with high FLU showed serious membrane fouling, while NOM with low FLU demonstrated less membrane fouling. It should be noted that as FLU cannot exhibit the total trend of membrane filtration flux, for example, when the total fluorescence area volumes of HP was higher, the filtration flux was the least, which can be due to that NOM fluorescence area volumes did not only consist in protein-like organics but also humic-like substances and their influences on filtration flux were significantly different.

The peak intensity ratios could also be used to provide additional information about the chemical nature of biological macromolecules and further implements of the structural differences [18]. HP showed a higher $r(a, c)$, while SHW exhibited an opposite trend, revealing that the humification of SHW was lower. $r(t, b)$ in NOM was also calculated for the macromolecular protein-like organics of algal metabolites. $r(t, b)$ in SHW was the highest, followed by KS and HPJ, indicating that SHW contained higher content of macromolecular organics.

Table 3.4: Fluorescence spectral parameters and filtration flux.

Parameter	FLU	$f450/500$[a]	$r(a, c)$	$r(t, b)$	J/J_0
SHW	23.72	1.44	1.16	1.33	10%
Yellow	22.91	1.32	1.48	1.06	30%
HPJ	85.86	1.43	2.29	0.75	20%
KS	45.5	1.34	1.58	1.30	9%
GY	9.14	1.3	1.26	–	31%

By viewing $r(t, b)$ of NOMs (Table 3.5), it was found that SHW with higher $r(t, b)$ caused more serious flux decline, which might indicate that $r(t, b)$ have good correlations with membrane fouling. The fluorescence peak position of $r(t, a)$ were meanwhile investigated. It should be noted that NOM $r(t, a)$ had a positive correlation with the filtration flux, and the higher $r(t, a)$, the more serious filtration flux. This is not surprising, as $r(t, a)$ in dissolved organic matter was not only related with organic resources, but also the molecular weight of organic matters, and both of these factors have important influence on membrane fouling.

Liu et al. reported that the fluorescence peak position of NOM (i.e., Em wavelength of peaks A and C) also has certain relations with membrane fouling [19]. It was obvious that SHW induced the serious filtration flux decline and its organics had short emission wavelength of peak A than the other NOMs (Table 3.4). Besides, the fulvic-like fluorophore (peak A) has shifted from Em > 450 nm to Em < 425 nm. The blue shift of fluorophores is associated with a decomposition of condensed aromatic moieties and the break-up of the large molecules into smaller fragments [18, 20]. This result suggested that Em wavelength of fluorescence A was also an effective method for filtration flux assessment.

EBSCOhost - printed on 2/14/2023 6:39 AM via . All use subject to https://www.ebsco.com/terms-of-use

Table 3.6: Fluorescence spectral parameters of AOM and filtration flux.

	MA-AOM	APF -AOM	ANF -AOM	CV-AOM	SO-AOM	Cy-AOM
$\Phi_{T,n}$ ($\times 10^{-5}$) (AU · nm^2 ·(mg/L)$^{-1}$)	3.2	3.25	3.55	3.76	2.63	3.7
$r(t, a)$	1.01	1.18	1.02	0.97	0.82	0.816
$r(t, b)$	1.71	5.56	1.52	1.36	1.11	1.51
Em (peak A) (nm)	<425	<430	<420	<425	<430	>450
J/J_0	12%	8.9%	9.1%	19%	25.2%	31%

From the subtraction of EEM fluorescence spectra (Figure 3.15) of raw water. It can be found that the retentions of all the raw water have fluorophores in the special region. But there are still some differences, SHW subtraction is closer to the tyrosine-like fluorophore, which implies that the foulants of SHW water come from microbial origins while GY water is closer to the fulvic-like fluorophore, implying that the source of GY water foulants tend to be terrestrial substances. Comparatively, the HPJ foulants may come from the sources because of the intermediate fluorophore range of retentions.

AOM fluorescence characteristics could also be correlated with the properties of membrane foulants. Table 3.6 shows the total fluorescence area volumes. Combined with the filtration flux in Figure 3.9, it can be found that the total fluorescence area volumes cannot be well related with the membrane filtration flux, for example, the total fluorescence area volumes of Cy-AOM was higher, while the filtration flux was the least. This might be due to that AOM fluorescence area volumes did not only consist in protein-like organics but also humic-like substances and their influences on filtration flux were significantly different. By viewing AOMs $r(t, b)$, it was found that AOM (ANF-AOM 5.56, APF-AOM 1.52, MA-AOM 1.71) with higher $r(t, b)$ caused more serious flux decline, which might suggest that $r(t, b)$ in fluorescence had good correlations with membrane fouling. However, the $r(t, b)$ in Cy-AOM was higher, but with the smallest filtration flux, indicating that AOM fluorescence parameters, $r(t, b)$, can only be considered as primary judgment for filtration flux, and other factors also need to be considered. The fluorescence peak position, $r(t, a)$, was meanwhile investigated. It should be noted that the AOM $r(t, a)$ was positively correlated with their filtration flux, and the higher $r(t, a)$, the more serious filtration flux. This is reasonable since $r(t, a)$ in dissolved organic matter was not only related with organic resources, but also molecular weight of organic matters, and both of these factors have important influence on membrane fouling.

EBSCOhost - printed on 2/14/2023 6:39 AM via . All use subject to https://www.ebsco.com/terms-of-use

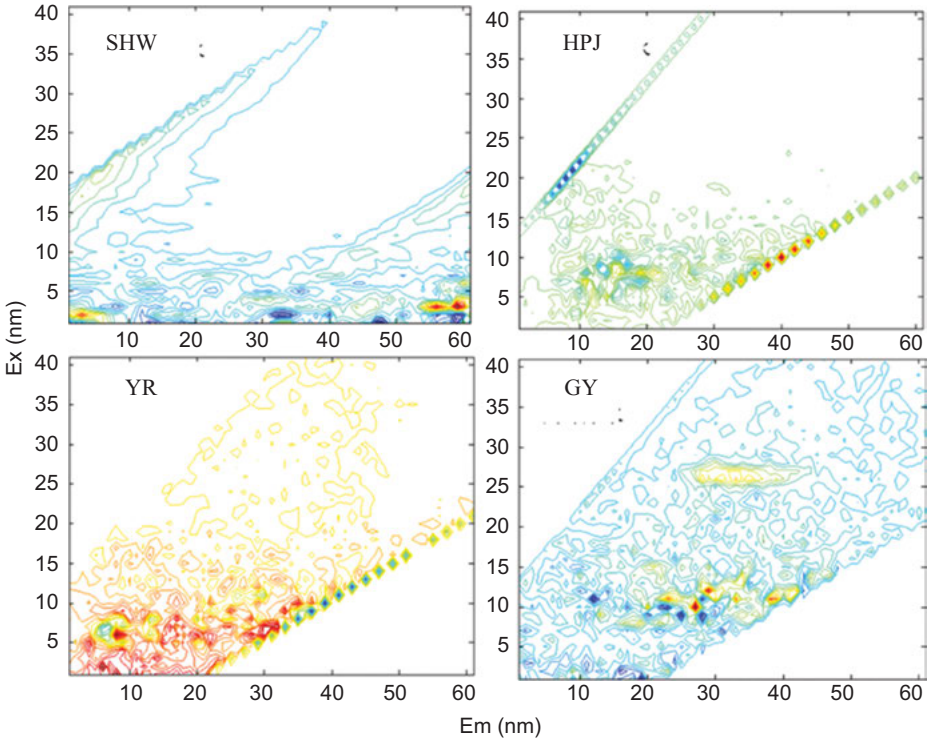

Figure 3.15: Subtraction EEM fluorescence spectra of raw water (DOC 5.0 mg/L, pH 7.0).

Table 3.5: Fluorescence spectral parameters and filtration flux.

index	SHW	Yellow	HP	KS	GY
$r(t, a)$	>2.0	1.0–1.5	1.0–1.5	>2.0	<1.0
Em (peak A)	<420 nm	>420 nm	>420 nm	420 nm	>420 nm
J/J0	10%	30%	20%	9%	31%

3.5 Effect of operating pressure, composition of the solution and membrane material on membrane fouling

Solution compositions such as ionic strength, hardness, and hydraulic conditions had significant effects on membrane fouling. This section investigated the effects of operating pressure, solution concentration and membrane pore size on membrane flux decline based on the analysis of dissolved organic matter on the filtration flux.

The feed water used in this study was collected from Taihu Lake, Wuxi, China. Before UF, the raw water was pre-filtered by 0.45 μm, and the DOC was adjusted to

EBSCOhost - printed on 2/14/2023 6:39 AM via . All use subject to https://www.ebsco.com/terms-of-use

5 mg/L. Reservoir water was algae-rich, and the main algae categories were *Microcystis* and *Chlorella*.

The membrane flux was tested using a flat microfiltration unit in the dead-end filtration mode which was consistent with Section 3.3.1. Constant pressure was maintained at 0.1 MPa and 0.15 MPa. The flat Millipore hydrophilic, mixed cellulose, VCWP membranes (with pore size of 0.1 μm, 80–100% nitrate cellulose; 0–20% acetate cellulose) with MWCO of 100 KDa and 30 KDa were used in this experiment (Millipore Corporation, US).

3.5.1 Effect of operating conditions on filtration flux of CA microfiltration membrane

Figure 3.16 shows the normalized flux changes of NOM under various pressures. Normalized flux with NOM declined dramatically in first stage before filtration volume of 400 mL, and decreased slowly and stabilized at the end of filtration. The initial filtration flux was 1.75×10^4 g/m$^2 \cdot$ min and 3.38×10^4 g/m$^2 \cdot$ min for pressure at 0.1 MPa and 0.15 MPa, respectively, while decreased to 88.2% and 91.4% at the end of filtration. This result indicated that higher operating pressure would lead to more severe membrane fouling, which might be due to that under higher operating pressure, the initial filtration flux was high, thus more effluent was produced and more foulant was brought on the membrane surface. In addition, high permeate flux would cause severe concentration polarization and increase the adsorption of organic matters on the membrane surface, which resulted in severe membrane fouling. It was noted that although the initial flux under the two driving pressures were extremely different, the steady fluxes were almost the same at the end of filtration, indicating that there might exist a limit flux for the MF membrane, and the increased operating pressure could no longer result in higher limiting flux. Previous studies suggested that there existed extreme fluxes in reverse osmosis and nanofiltration membranes [16]. The forces acting on organic matter mainly included the hydraulic drag force toward the membrane surface and the resistance to the membrane surface. Hydraulic drag could promote the deposition of membrane foulants on the membrane surface, whereas the resistance could reduce the membrane fouling, while their interaction determined the total membrane fouling. However, the membrane flux can no longer decrease until the hydraulic drag and resistance were balanced. And the increased operating pressure could have no effect on the membrane flux.

Table 3.7 shows the organic removals of MF under both pressures. The TOC and UV removal were 4.02% and 6.38% for pressure at 0.15 MPa, respectively, while they were 3.52 and 5.32% at 0.1 MPa, suggesting that the increased operating pressure had little effects on organic removals.

EBSCOhost - printed on 2/14/2023 6:39 AM via . All use subject to https://www.ebsco.com/terms-of-use

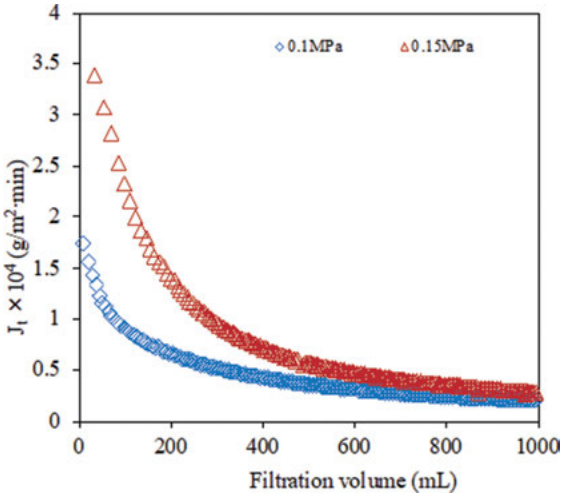

Figure 3.16: Normalized flux changes of NOM under various pressures.

Table 3.7: Organic removals of MF under both pressures.

Pressure (MPa)	TOC			UV_{254}		
	Feed (mg/L)	Permeate (mg/L)	Removal (%)	Feed (cm^{-1})	Permeate (cm^{-1})	Removal (%)
0.10	4.147	4.001	3.52	0.094	0.089	5.32
0.15	4.147	3.98	4.02	0.094	0088	6.38

Figure 3.17 shows the MW distributions of organic matter by MF under both pressures, as can be seen, MF mainly rejected macro MW organic matters, while there were little discrepancies for the reductions of TOC peaks of macro MW organics, indicating that the operating pressure has little effects on the distribution of MW of dissolved organic matter. Of course, it is also possible that the pressure gradient points set in this experiment was little, which was not enough to show the trend of regularity. And it is recommended that more pressure gradient points were recommended for the further exploration of the effect of operating pressure on membrane fouling.

Figure 3.18 shows the subtraction of EEM fluorescence spectra of raw water. There were mainly two fluorescence peaks intercepted in the raw water sample (EX = 235 nm, EM = 335 nm; EX = 280 nm and EM = 335 nm), which belong to soluble microbial product fluorescent region (region 4) and the aromatic protein fluorescent region, respectively. This result indicated that the substances that cause the rapid decline of membrane flux of Taihu Lake are mainly composed of macromolecular protein-like organics. Comparing the fluorescence under the two operating pressures, it was also found that humic-like organic was also rejected under high operating pressure of 0.15 MPa, suggesting that more organics can be intercepted by MF under high pressure.

EBSCOhost - printed on 2/14/2023 6:39 AM via . All use subject to https://www.ebsco.com/terms-of-use

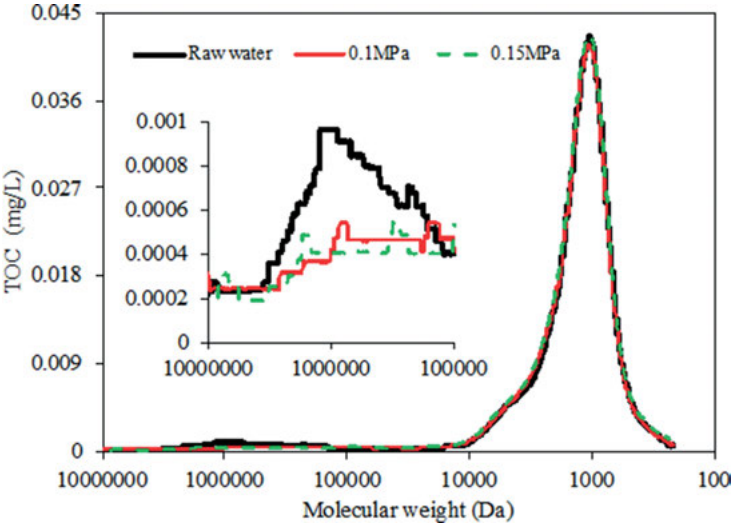

Figure 3.17: Changes of MW distributions of organic matter by MF under various pressures.

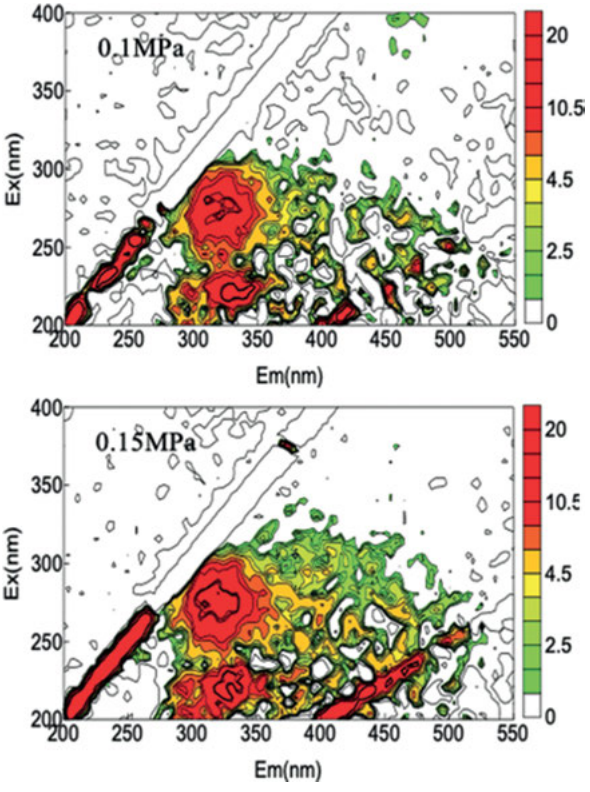

Figure 3.18: Subtraction EEM fluorescence spectra of raw water under various pressures.

EBSCOhost - printed on 2/14/2023 6:39 AM via . All use subject to https://www.ebsco.com/terms-of-use

3.5.2 Effect of solution composition on filtration flux of CA microfiltration membrane

Figure 3.19 shows the variation of the filtration flux under different solution compositions. As can be seen, in the initial filtration flux, both water showed rapid decline, however, the membrane flux of raw water decreased faster than that of the concentrated water, which was extremely different from predication. It is generally believed that the higher TOC of raw water, the higher organic matter reached on the membrane surface, and the faster membrane flux decayed. Raw water had serious filtration flux than concentrated water, which might be due to that high organic matter in concentrated water might form a thick cake layer, making the organic matter further retained by the cake layer. It is noted that as the filtration flux at the end of filtration was consistent for both water, the concentration of organic matter in the influent might have little effects on the filtration flux. Tang et al. investigated the filtration flux of humic acid, and found that the stable flux is related to the interactions between foulants and also foulants and membranes, but not for the concentration of raw water.

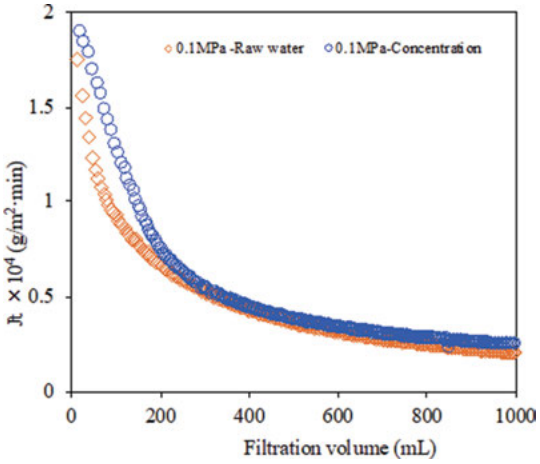

Figure 3.19: Filtration flux under different solution compositions.

Table 3.8 show the organic removals of TOC by MF. MF has little effects on the organic removal of both water. The TOC and UV removal were 3.52 and 5.32% for raw water, and 3.51 and 0.44% for concentrated water respectively. MF had little effects on UV removal for the concentrated water, which can be due to that MF membrane mainly removes hydrophilic organic substances of weak ultraviolet absorbance.

Figure 3.20 show the MW distribution of raw water and permeate after MF. It was found that macro MW organics remain the mainly organics that were rejected by MF.

EBSCOhost - printed on 2/14/2023 6:39 AM via . All use subject to https://www.ebsco.com/terms-of-use

Table 3.8: Organic removals of MF.

Parameters	TOC			UV_{254}		
	Feed (mg/L)	Permeate (mg/L)	Removal (%)	Feed(cm^{-1})	Permeate(cm^{-1})	Removal(%)
Raw	4.147	4.001	3.52	0.094	0.089	5.32
Concentrated	10.204	9.846	3.51	0.227	0.226	0.44

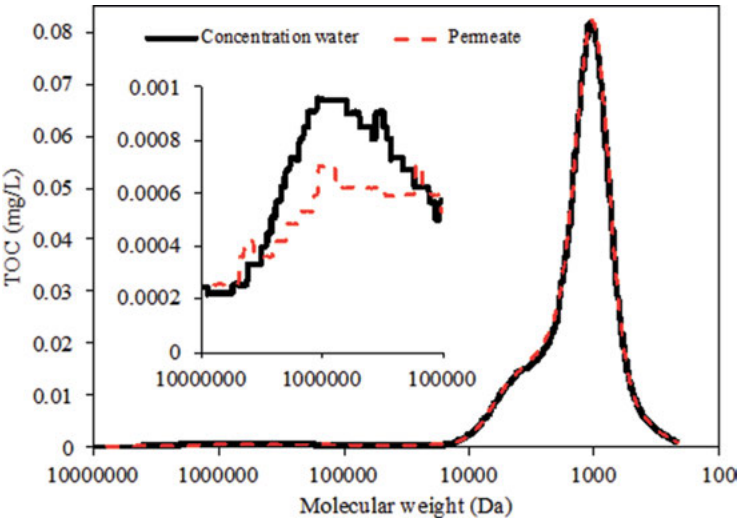

Figure 3.20: MW distribution of raw and concentrated water.

While there were little discrepancy among the removal efficiencies between raw water and concentrated water. The TOC peaks decreased from 0.00097 mg/L to 0.00046 mg/L for raw water while decreased from 0.00085 mg/L to 0.00052 mg/L for concentrated water. And in the primary filtration time, a lot of macro MW organics were rejected, thus, the filtration flux decreased faster for raw water than concentrated water.

Figure 3.21 shows the subtraction EEM fluorescence spectra of raw water. There were two fluorescence perks intersected in the raw water sample, i.e. soluble microbial product fluorescent region (region 4) and the aromatic protein fluorescent region. The response was wider and stronger for the concentrated water, indicating that more fluorescence organics were rejected in the concentrated water. It was noted that not all the NOM in water show fluorescence. For instance, polysaccharides, which are known to contribute greatly to membrane fouling, do not exhibit fluorescence. EEMs might be invalid as an indicator of membrane fouling by polysaccharides or protein-enriched water.

EBSCOhost - printed on 2/14/2023 6:39 AM via . All use subject to https://www.ebsco.com/terms-of-use

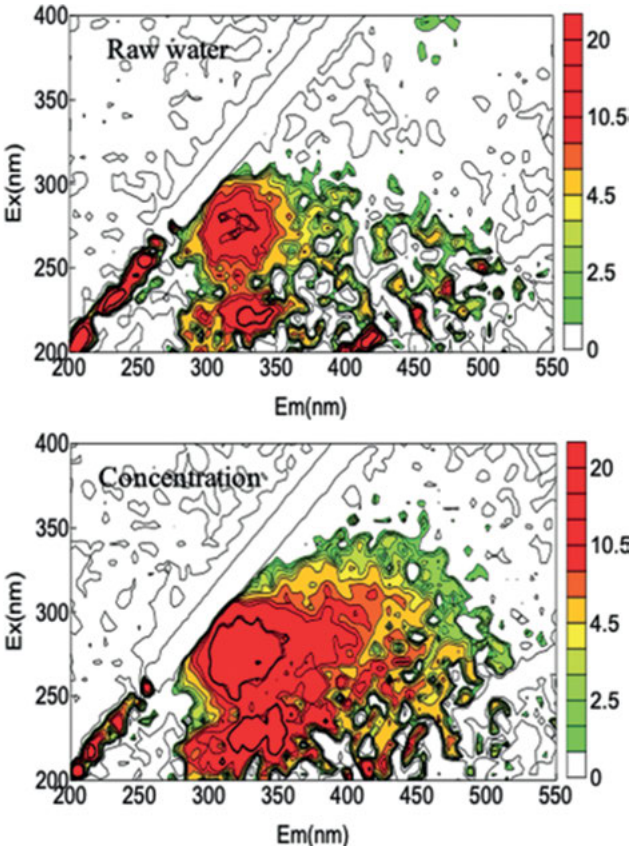

Figure 3.21: Subtraction EEM fluorescence spectra of raw and concentrated water.

3.5.3 Effect of membrane materials on filtration flux of microfiltration

The feed water used in this study was collected from Taihu Lake, Wuxi, China. Before UF, the raw water was filtered by 0.45 μm, and the DOC was adjusted to 5 mg/L.

The membrane used included PVDF 150K, PES 100K, PES 30K and CA 0.1 μm, the characteristics of the membranes can be found in Table 3.9.

Figures 3.22–3.25 show the filtration flux of fractions of tap water under the same conditions, as can be seen, N-HPI caused the most serious flux decline for the four membranes, with the end of filtration fluxes 69%, 75%, 41% and 30% for PVDF 150K, PES 100K, CA 0.1 μm, and PES 30K respectively. Raw water also caused serious rapid filtration flux decline, and the flux at the end of filtration were 59%, 66%, 19%, 15% for PVDF 150K, PES 100K, CA 0.1 μm and PES 30K, respectively. While for HPO, TPI and C-HPI, they had little effects on membrane fouling. The filtration flux caused

EBSCOhost - printed on 2/14/2023 6:39 AM via . All use subject to https://www.ebsco.com/terms-of-use

Table 3.9: Characteristics of the membrane used.

Membrane	MW (Da)	Contact angel (°)	Filtration flux of pure water (kg/m² · h)	Production
PVDF	15×10^4	49.5	722.89	Membrane Technology Research and Development Center, Shanghai
PES	10×10^4	78.5	650.60	Chinese Academy of Sciences Ecological Environment
	3×10^4	54.5	72.29	
	1×10^4	71.5	31.63	
CA	0.1 μm	43	867.47	Millipore, US

by HPO were 59%, 78%, 93%, and 108% for PVDF 150K, PES 100K, CA 0.1 μm and PES 30K, respectively, while they were 61%, 76%, 94% and 104% for TPI, and 60%, 72%, 94%, and 103% for C-HPI, respectively. This result indicated that N-HPI were the main components that caused the membrane fouling.

For the four membranes, it was also found that there were great discrepancies for the four membranes on the filtration flux. Although the raw water and N-HPI had great influence on membrane fouling, the filtration flux had the order that PES 100K > PVDF 150K > CA 0.1 μm > PES 30K. For HPO, TPI, and C-HPI, the filtration flux had the order that PVDF 150K > PES 100K > CA 0.1 μm > PES 30K, indicating that membrane materials was also one of the factors influencing membrane fouling.

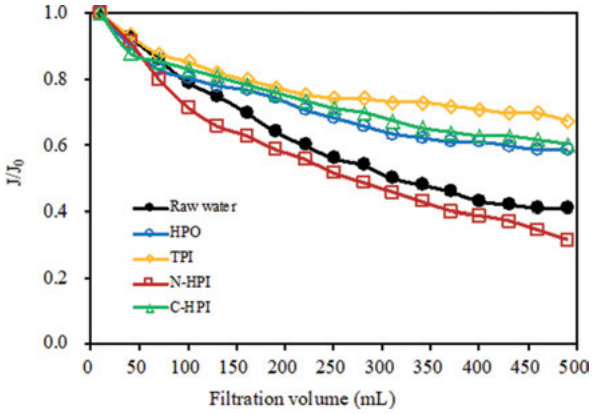

Figure 3.22: Filtration flux of tap water fractions by PVDF 15 membrane.

Previous studies suggested that hydrophobic membrane was more prone to be polluted by NOM than hydrophilic membrane [6, 7]. The contact angels of the four membranes were 78.5°, 49.5°, 43° and 54.5° for PES 100K, PVDF 150K, CA 0.1 μm and PES 30K, respectively. High contact angels indicated more hydrophobicity. PES 100K,

EBSCOhost - printed on 2/14/2023 6:39 AM via . All use subject to https://www.ebsco.com/terms-of-use

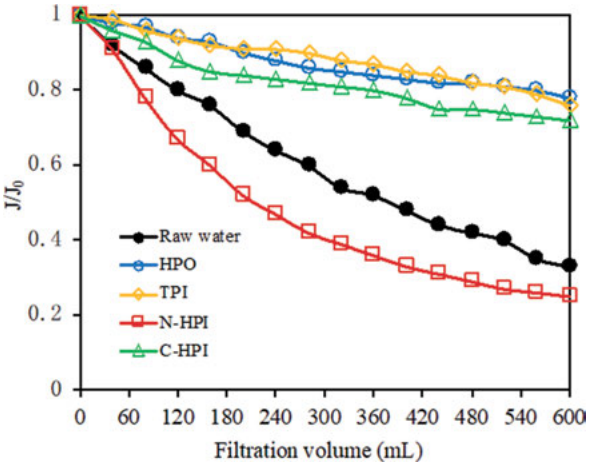

Figure 3.23: Filtration flux of tap water fractions by PES 100K membrane.

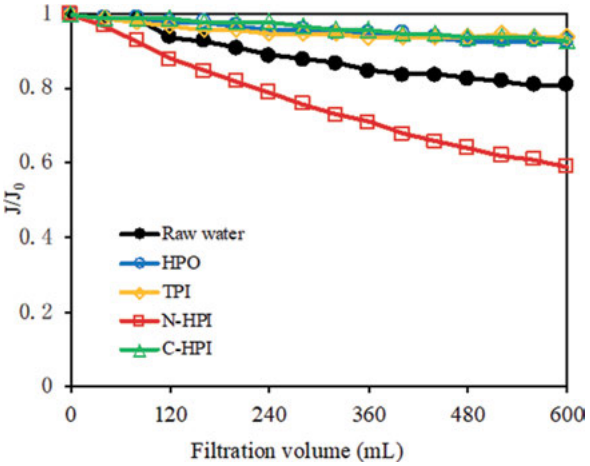

Figure 3.24: Filtration flux of tap water fractions by 0.1 μm CA membrane.

PVDF 150K caused more serious membrane fouling than CA 0.1 μm membrane, indicating that hydrophobic membrane was more prone to be contaminated by NOM. Sun et al. suggested that membrane with high MWCO was easily polluted by NOM [21]. The contact angel result was consistent among PES 30K, PVDF 150K and CA 0.1 μm, while the MW was smaller for PES 30K, thus, the filtration flux caused for PES 30K might be the least.

In addition, the water temperature, pH, as well Ca^{2+} also had certain influence on membrane fouling.

EBSCOhost - printed on 2/14/2023 6:39 AM via . All use subject to https://www.ebsco.com/terms-of-use

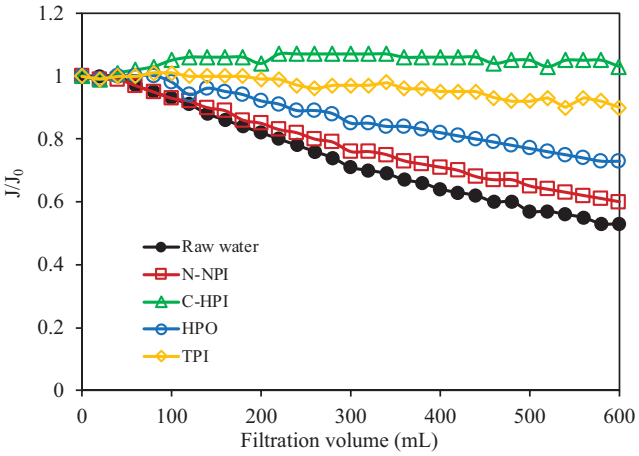

Figure 3.25: Filtration flux of tap water fractions by PES 30K membrane.

3.6 Identification of membrane foulants

Conventional NOM fouling characterization techniques include protein or polysaccharide determination, molecular weight distribution, fluorescence excitation emission matrices. Recent studies have also proposed physical and chemical cleaning to remove membrane fouling and to recover membrane flux as a relatively simple methodology [22–24]. To identify membrane foulants, attenuated total reflection-Fourier infrared spectroscopy (ATR-FTIR), and scanning electron microscopy (SEM) were utilized to analyze the fouled membrane. In this section, the membrane foulants was identified by various methods.

3.6.1 Identification of membrane foulants from tap water and Yangcheng water

The water used was Tap water, Yangcheng water and their fractions. The membrane used was PVDF 150K.

The surface properties of clean and fouled membranes were examined on the basis of Omnic Fourier Transform Infrared Analyzer (USA). The spectra were ranged from 400 to 4,000 cm^{-1}, with a resolution of 4 cm^{-1}, and a signal-to-noise ratio of 50,000:1.

From the FTIR spectra of fouled membranes of Tap water, and Yangcheng water (Figures 3.26 and 3.27), it can be found that there were three absorption peaks of 1716.3 cm^{-1}, 1250.3 cm^{-1}, and 1100.3 cm^{-1} in the fouled membranes for all the fractions. The peak at 1716.3 cm^{-1} is attributed to absorption of C = O and C(=O)OH [25]. All the

EBSCOhost - printed on 2/14/2023 6:39 AM via . All use subject to https://www.ebsco.com/terms-of-use

membranes have strong absorption peaks at 1716.3 cm^{-1}, while the intensity followed the order of C-HPI > Tap water > TPI > HPO > N-HPI of Yangcheng water, for Tap water, the intensity was N-HPI ≈ TPI ≈ C-HPI > HPO ≈ Raw water. Moreover, the absorption peak intensity of each component in Yangcheng is stronger than that in tap water, indicating that the carboxylic acid organic matter containing C = O, C(=O)OH was the major organic that caused membrane fouling, and the higher the content of this kind of organic matter, the more serious it might cause membrane fouling.

1,100 cm^{-1} is an absorption peak of C-O in diethyl ether, esters, and polysaccharides, which is a component of hydrophilic group in organic matter. All the membranes also have strong absorption peaks at 1,100 cm^{-1}, however, there were still discrepancy for the fractions, such that the intensity had the order of Tap water > C-HPI > TPI > H PO > N-HPI, and for Yangcheng water, the order was TPI > C-HPI > N-HPI > HPO > Raw water. In addition, the absorption peak intensity of each component in Yangcheng were stronger than that in tap water, which indicated that the membrane foulants was also consistent at 1,100 cm^{-1}, however, there were some discrepancies in the membrane fouling intensities. In all, organic compounds containing C = O, C(=O)OH, C-H, carboxylic acids of O-H, ethers with C-O, esters, and polysaccharides were the major organics that caused the membrane fouling.

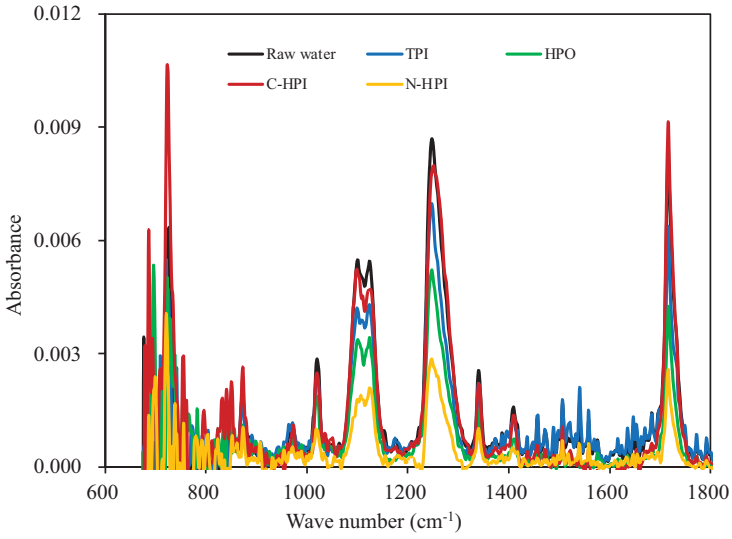

Figure 3.26: FTIR spectra of fouled membranes under various tap water solutions.

EBSCOhost - printed on 2/14/2023 6:39 AM via . All use subject to https://www.ebsco.com/terms-of-use

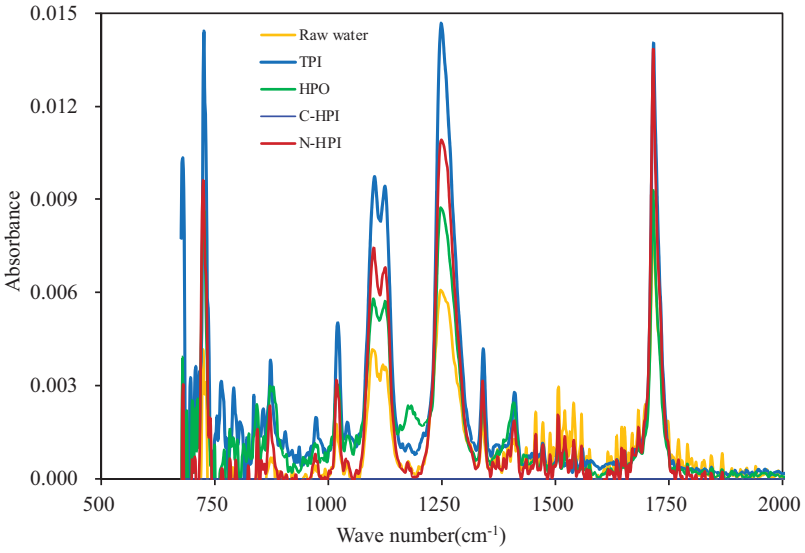

Figure 3.27: FTIR spectra of fouled membranes under various Yangcheng solutions.

3.6.2 Identification of membrane foulants from SHW, Yellow, HPJ, KS and GY water

The FTIR spectra of clean and fouled membranes under various solutions are compared in Figure 3.28. There were four peaks detected at the clean membrane of 840 cm^{-1}, 1,080 cm^{-1}, 1,280 cm^{-1} and 1,650 cm^{-1}, which has been demonstrated to be C-H stretching vibration, C-O bonding vibration, -OH bonding vibration and C = O stretching vibration [10]. These saturated structures might come from polysaccharides, amino sugars-like organics, humic acid -like organics and amino acids.

Comparing the fractional groups of fouled membranes and clean ones, it was observed that the peaks were consistent among new and fouled membranes, however, there were some discrepancies about the peak intensities, suggesting that membrane foulant was consistent with MF interception. The membrane foulant mainly come from saturated bond areas, which indicated that polysaccharides, amino sugars-like organics were the main organics that were rejected by MF, while humic-like organics were the least rejected. Since the pore size of MF was large, the effect of humic organic matter on membrane fouling may be due to pore shrinkage, while the effect of polysaccharides and protein-like organic matter on membrane fouling may contribute to cake layer formation.

Figure 3.29 presents SEM surface images of clean and fouled membranes. A large number of membrane pores are distributed on the membrane surface of new ones,

EBSCOhost - printed on 2/14/2023 6:39 AM via . All use subject to https://www.ebsco.com/terms-of-use

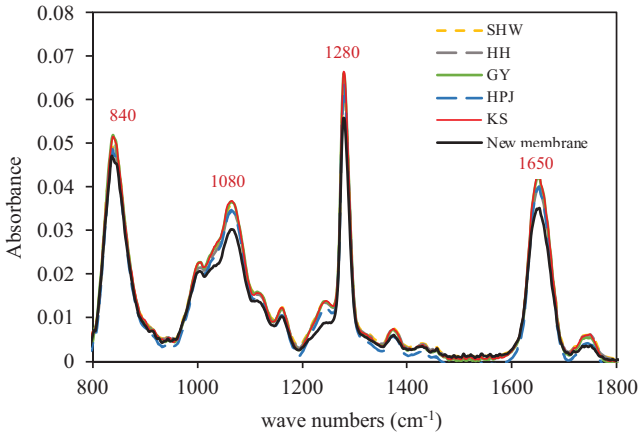

Figure 3.28: The FTIR spectra of clean and fouled membranes under various solutions.

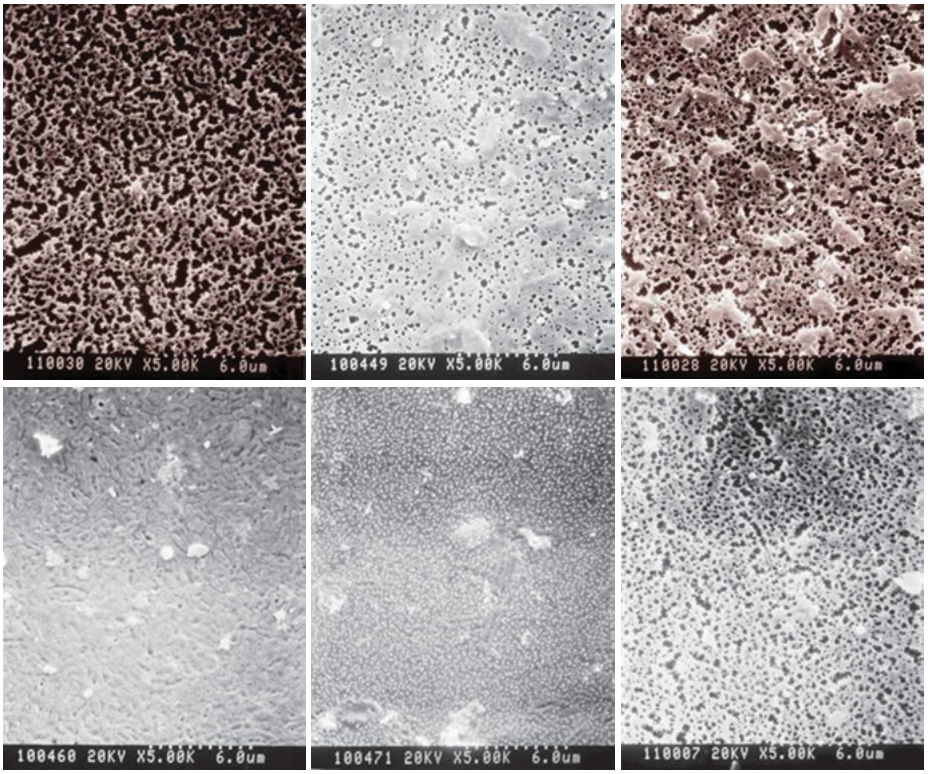

Figure 3.29: SEM of water after MF (a. new membrane; b. SHW; c. Yellow River; d. HPJ; e. KS; f. GY).

EBSCOhost - printed on 2/14/2023 6:39 AM via . All use subject to https://www.ebsco.com/terms-of-use

while the membrane pores are differently covered when different influent was filtered. Besides, it was found that a dense cake layer formed on the membrane surface when filtering HPJ water, however, for the KS water, it was found that in addition to the cake layer, the membrane pores were completely covered, while there were only a few membrane pores covered for Yellow River and GY water, which was consistent with their filtration fluxes.

3.7 Summary

(1) Factors affecting membrane fouling were mainly related to organics type, the physical and chemical properties of natural water, as well as the membrane properties. Organic characteristics such as organic hydrophobicity, molecular weight distribution and fluorescence spectrum had great relations with membrane fouling.
(2) Most of N-HPI in natural water in this study caused rapid decrease of filtration flux, followed by HPO, comparatively, the membrane fouling caused by TPI and C-HPI was relatively lower.
(3) Molecular weight distribution indicated that macromolecular organics in N-HPI and HPO were the main components that caused the membrane fouling.
(4) EEMs characteristics demonstrated that $r(t, a)$ and the Em wavelength of peak A have certain relations with membrane fouling. However, as some organics cannot be determined by EEM, such as polysaccharides, the determination of membrane fouling cannot be fully used by fluorescence spectrum index, and other factors are still needed to be investigated.
(5) Operating pressure and solution conditions also have certain effects on membrane fouling. Membrane fouling experiment with different membrane materials suggested that the higher hydrophobicity of membrane, the more susceptible to membrane fouling.

References

[1] Aoustin, E., et al., Ultrafiltration of natural organic matter. Separation and Purification Technology, 2001. 22–3(1–3): p. 63–78.
[2] Fan, L.H., et al., Influence of the characteristics of natural organic matter on the fouling of microfiltration membranes. Water Research, 2001. 35(18): p. 4455–4463.
[3] Lee, N., Amy, G., and Croue, J.P., Low-pressure membrane (MF/UF) fouling associated with allochthonous versus autochthonous natural organic matter. Water Research, 2006. 40(12): p. 2357–2368.
[4] Van Geluwe, S., et al., Ozone oxidation of nanofiltration concentrates alleviates membrane fouling in drinking water industry. Journal of Membrane Science, 2011. 378(1–2): p. 128–137.

EBSCOhost - printed on 2/14/2023 6:39 AM via . All use subject to https://www.ebsco.com/terms-of-use

[5] Taniguchi, M., et al., Distorted odor maps in the olfactory bulb of semaphorin 3A-deficient mice. Journal of Neuroscience, 2003. 23(4): p. 1390–1397.
[6] Bartels, C.R., et al., Design considerations for wastewater treatment by reverse osmosis. Water Science and Technology, 2005. 51(6–7): p. 473–482.
[7] Yoon, Y.M., et al., Effects of retained natural organic matter (NOM) on NOM rejection and membrane flux decline with nanofiltration and ultrafiltration. Desalination, 2005. 173(3): p. 209–221.
[8] Elimelech, M., et al., Role of membrane surface morphology in colloidal fouling of cellulose acetate and composite aromatic polyamide reverse osmosis membranes. Journal of Membrane Science, 1997. 127(1): p. 101–109.
[9] Ho, C.C. and Zydney, A.L., Effect of membrane morphology on the initial rate of protein fouling during microfiltration. Journal of Membrane Science, 1999. 155(2): p. 261–275.
[10] Zularisam, A.W., Ismail, A.F., and Salim, R., Behaviours of natural organic matter in membrane filtration for surface water treatment – a review. Desalination, 2006. 194(1–3): p. 211–231.
[11] Howe, K.J. and Clark, M.M., Fouling of microfiltration and ultrafiltration membranes by natural waters. Environmental Science & Technology, 2002. 36(16): p. 3571–3576.
[12] carroll, T., et al., The fouling of microfiltration membranes by NOM after coagulation treatment Water Research, 2000. 34(11): p. 2861–2868.
[13] Gray, S.R., et al., Effect of NOM characteristics and membrane type on microfiltration performance. Water Research, 2007. 41(17): p. 3833–3841.
[14] Qu, F.S., et al., Ultrafiltration membrane fouling by extracellular organic matters (EOM) of Microcystis aeruginosa in stationary phase: Influences of interfacial characteristics of foulants and fouling mechanisms. Water Research, 2012. 46(5): p. 1490–1500.
[15] Huang, H., et al., Natural organic matter fouling of low-pressure, hollow-fiber membranes: Effects of NOM source and hydrodynamic conditions. Water Research, 2007. 41(17): p. 3823–3832.
[16] Kimura, K., et al., Irreversible membrane fouling during ultrafiltration of surface water. Water Research, 2004. 38(14–15): p. 3431–3441.
[17] Peiris, R.H., et al., Understanding fouling behaviour of ultrafiltration membrane processes and natural water using principal component analysis of fluorescence excitation-emission matrices. Journal of Membrane Science, 2010. 357(1–2): p. 62–72.
[18] Coble, P.G., Characterization of marine and terrestrial DOM in seawater using excitation emission matrix spectroscopy. Marine Chemistry, 1996. 51(4): p. 325–346.
[19] Liu, Z., et al., Characterization of natural organic foulants removed by microfiltration. Desalination, 2011. 277(1–3): p. 370–376.
[20] Korshin, G.V., Benjamin, M.M., and Sletten, R.S., Adsorption of natural organic matter (NOM) on iron oxide: Effects on nom composition and formation of organo-halide compounds during chlorination. Water Research, 1997. 31(7): p. 1643–1650.
[21] Sun, W.G., et al., Influence and mechanism of different molecular weight organic molecules in natural water on ultrafiltration membrane fouling reversibility. RSC Advances, 2016. 6(86): p. 83456–83465.
[22] Cho, J., et al., Effects of molecular weight cutoff, f/k ratio (a hydrodynamic condition), and hydrophobic interactions on natural organic matter rejection and fouling in membranes. Journal of Water Supply Research and Technology-Aqua, 2002. 51(2): p. 109–123.
[23] Henderson, R.K., et al., Fluorescence as a potential monitoring tool for recycled water systems: A review. Water Research, 2009. 43(4): p. 863–881.
[24] Metzger, U., et al., Characterisation of polymeric fouling in membrane bioreactors and the effect of different filtration modes. Journal of Membrane Science, 2007. 301(1–2): p. 180–189.
[25] Chang, E.E., et al., Assessing the fouling mechanisms of high-pressure nanofiltration membrane using the modified Hermia model and the resistance-in-series model. Separation and Purification Technology, 2011. 79(3): p. 329–336.

EBSCOhost - printed on 2/14/2023 6:39 AM via . All use subject to https://www.ebsco.com/terms-of-use

EBSCOhost - printed on 2/14/2023 6:39 AM via . All use subject to https://www.ebsco.com/terms-of-use

Pingyun Zhang, Yong Wei, Tian Li

Chapter 4
Fabrication and Anti-fouling Evaluation of PVDF Membranes via Surface Modification

Among the technologies for reclamation and reuse of water, membrane technology is a competitive candidate. Membrane could be used to capture water from the non-traditional waste-water sources, such as pharmaceutical, food industries, hydrocarbon processing, metallurgy and so on [1]. As one of the membrane materials with outstanding properties, PVDF has been paid great attentions because of its high hydrophobicity, good thermal stability, strong mechanical properties and good chemical resistance. Up to now, many applications extensively rely on PVDF membranes, such as membrane contactor, membrane distillation and membrane separation process [2].

PVDF membranes are mainly prepared via NIPS process. It is realized via immersing the casting solutions into a non-solvent coagulation bath to produce phase separation. Firstly, liquid-liquid demixing process is induced by the diffusive exchange between solvent and non-solvent. Secondly, a porous structure is induced by the successive liquid-solid phase separation [3, 4]. According to the formation mechanism of bimodal demixing membrane, the nucleation and growth of PVDF starts from the lean phase. Subsequently, the crystallization of PVDF phases, or solidification of PVDF rich phase fix the membrane morphology. Usually the precipitation process is controlled by both kinetic and thermodynamic factors, and the casting solution temperature could affect the precipitation process. The reason is that the high temperature produces diffusion process of polymer and solvent, tending to form a thinner skin layer [5].

However, due to the low surface energy of PVDF membranes, there is still a challenge for them to treat aqueous solution containing natural organic matters. To solve the problem, great importance in terms of good permeability and improved fouling detachment has been explored on PVDF membrane performance improvement. In addition, in order to expand the membrane application field, significant effort has been devoted to develop the suitable techniques for hydrophilic PVDF membrane fabrication.

Pingyun Zhang, National Engineering Research Center of Urban Water Resources, Shanghai, P. R. China
Yong Wei, School of Environmental and Safety Engineering & School of Urban Construction, Changzhou University, Changzhou, Jiangsu, P. R. China
Tian Li, College of Environmental Science and Engineering, Tongji University, Shanghai, P. R. China

https://doi.org/10.1515/9783110596847-004

EBSCOhost - printed on 2/14/2023 6:39 AM via . All use subject to https://www.ebsco.com/terms-of-use

Good mechanical property and high permeability of PVDF membranes are always highly pursued. Those membranes with reduced fouling resistance, high PWF, and improved rejection, narrow pore size distribution, as well as reasonable mechanical strength have been successfully fabricated [6, 7]. Besides, membranes with interconnected bi-continuous structure seem to be more prevailing than those with finger-like structure [8], for their good mechanical property. The appreciation methods and technologies are thus created to improve the mechanical property without filtration property loss.

To establish the antifouling modification and diverse hydrophilic properties, two straightforward approaches are usually used. They are primarily classified into surface modification and blending modification [2]. The former is usually achieved by grafting or coating, i.e., a functional layer on the prepared membrane surface is immobilized with most of the modified sites at the bottom and/or on top surface of the membrane [9–14]. Usually, additional steps and increased costs are required by surface grafting, due to the involvement of plasma or electron beam. Moreover, the modification layer has limitations on its long-term stability. For example, the layer could be removed during long-term operation or cleaning. The preparation and modification process of the latter one can be accomplished in a single step. Therefore, the blending modification is usually used to achieve the desired functional properties via membrane preparation [15–19]. Compared with surface modification, the blending route is the better method for the fabrication of large-scale hydrophilic porous membranes.

During the preparation process of PVDF membrane, additives play an important role. There are several kinds of widely used additives, such as inorganic salt like lithium chloride (LiCl) [20–22], Al_2O_3 [23], ferrous chloride [24], TiO_2 [25] and polymeric additives, like poly(ethylene glycol) (PEG) [26], polyvinylpyrrolidone (PVP) [27], as well as weak solvent like glycerol [28].

In recent years, blending with inorganic materials, like nanoparticles, has attracted great attention. Reason for that is the convenient operation and mild conditions of phase inversion method [29, 30]. The nanoparticles introduced to polymer membranes might be polymeric nanoparticles, i.e. SiO_2, ZnO, Fe_3O_4, TiO_2, ZrO_2, CdS, and Al_2O_3 [29]. TiO_2 has gained special interest, for its good characteristics like high hydrophilicity, good chemical stability, avirulent and antibacterial property [31]. Besides, anatase TiO_2 could be utilized as a photocatalyst during water purification process [32].

Besides, self-synthesized amphiphilic copolymers have been blended as pore-forming additives, tunable membrane morphology and antifouling surface modifiers. It has received significant attention in the PVDF membrane surface modification. Amphiphilic copolymers are special molecules including both hydrophilic

EBSCOhost - printed on 2/14/2023 6:39 AM via . All use subject to https://www.ebsco.com/terms-of-use

chains (polar head groups) and hydrophobic hydrocarbon chains. In polar solutions, they tend to form various micelle structures. The micelle structures contribute to the formation of porous structures. It is believed that PVDF matrix has good compatibility with the amphiphilic copolymer. This contributes to the engineered surface properties of the membranes.

The anatase TiO_2 nanowires and amphiphilic copolymers were used to modify the surface of PVDF membranes via blending method. The influences of TiO_2 nanowires and amphiphilic copolymers on membranes properties were studied via examining mechanical properties, hydrophilicity, thermal stability and membrane microstructures. Besides, the anti-fouling evaluation of PVDF membrane surface modification was investigated. Main results are as follows:

(1) A new PVDF-TiO_2 nanowire hybrid ultrafiltration membrane was prepared via phase inversion using TiO_2 nanowire as additive. The characteristics of the hybrid membranes, i.e., hydrophilicity, permeation performance, crystal structure, morphology, mechanical properties, and thermal stability, were studied.

(2) Tween 80 and H_2O work as mixture additive to improve the performances of PVDF membranes. Those membranes were prepared by non-solvent induced phase separation (NIPS) process from both 60 °C and room-temperature (RT) casting solution, adding water into the PVDF-DMAc-Tween 80 system. And pure water flux (PWF), mechanical properties, Bovine serum albumin (BSA) and Dextran rejection were investigated. Besides, the effect of coagulants on interconnected bi-continuous structures, mechanical properties and hydrophilicity improvement were studied.

(3) Simplified blend method was utilized to fabricate Polyvinylidene fluoride (PVDF)-P(PEGMA-r-MMA) blend membranes from water and ethanol coagulants. The method was realized via directly blending amphiphilic copolymer solution of P(PEGMA-r-MMA) (including the reaction mixture) to PVDF so as to form casting solution. The influences of the variations in coagulant compositions and dopant contents on those blend membrane performances were studied. To obtain small-size supramolecular aggregates, in-situ free radical polymerization is proposed. Reason for that is the formation of large size nanoparticulate aggregates caused by amphiphilic copolymer, which limited the function in term of modulation morphology and pore-forming of resultant membranes. On one hand, in-situ polymerization increased the recovery water flux after filtration experiments of bovine serum albumin (BSA). On the other hand, it improved the PVDF membrane hydrophilicity of both top surface and bottom surface.

EBSCOhost - printed on 2/14/2023 6:39 AM via . All use subject to https://www.ebsco.com/terms-of-use

4.1 Effect of TiO_2 nanowire addition on PVDF ultrafiltration membrane performance

4.1.1 Introduction

TiO_2 nanoparticles have been widely explored on the surface modification of PVDF blending membranes in terms of improving the thermal stability, antibacterial hydrophilicity, photocatalytic performance, antifouling, and mechanical strength [33–36]. However, the TiO_2 nanoparticles-organic hybrid membrane possesses significant drawbacks and some inherence. High TiO_2 concentration could induce nanoparticles to aggregate when TiO_2 was dispersed to casting solutions, which results in permeability, hydrophilicity decline and defective pore structure [30]. Besides, TiO_2 could be leached out easily from hybrid membranes, resulting in lower elongation ratio. Mechanical tests indicated that the hybrid membranes had higher strength, but were cheaper than the neat membrane [19]. In addition, TiO_2 nanoparticles leached out from hybrid membrane could significantly decrease the membrane thermal stability, antifouling, hydrophilicity, mechanical strength, but higher breaking strength. Hence, as an inorganic addition material, to redesign TiO_2 structure is very important. Recently, chemical or physical methods were used to synthesize one dimensional (1D) nanostructured TiO_2 of various morphologies, including nanotubes nanowires, nanorods and nanofibers [37–42]. For the easy operation of hydrothermal method, the 1D nanostructured TiO_2 is widely used. With TiO_2 nanoparticles, these 1D nanomaterials had new properties.

Phase inversion method was utilized to prepare a new organic-inorganic PVDF-TiO_2 nanowire hybrid UF membrane, using the anatase TiO_2 nanowires via hydrothermal method. Finely dispersed TiO_2 nanowires in the polymer matrix of PVDF-TiO_2 nanowire hybrid membranes was discussed. The influences of organic framework and TiO_2 nanowires existence on membrane properties were investigated by examining membrane hydrophilicity, mechanical properties, microstructures, and thermal stability, as well as performances.

4.1.2 Performance of hybrid UF membrane by organic-inorganic PVDF-TiO_2 nanowire

4.1.2.1 TiO_2 nanowire

The XRD pattern of the synthesized TiO_2 nanowires (shown in Figure 4.1(I)) agreed well with the former reported results [39, 43]. The product had high purity. Anatase TiO_2 has better photocatalytic activity than other phases of TiO_2. The nanocomposite membrane with anatase TiO_2 has been successfully used to remove Indigo Carmine

EBSCOhost - printed on 2/14/2023 6:39 AM via . All use subject to https://www.ebsco.com/terms-of-use

dyes and photo-degradation Brilliant Green [44]. Two typical SEM (a) and FESEM (b) images of the prepared TiO_2 nanowires are shown in Figure 4.1(II). Figure 4.1(II) indicated that the quantity of nanowires was very copious and no contaminants were attached to their surface.

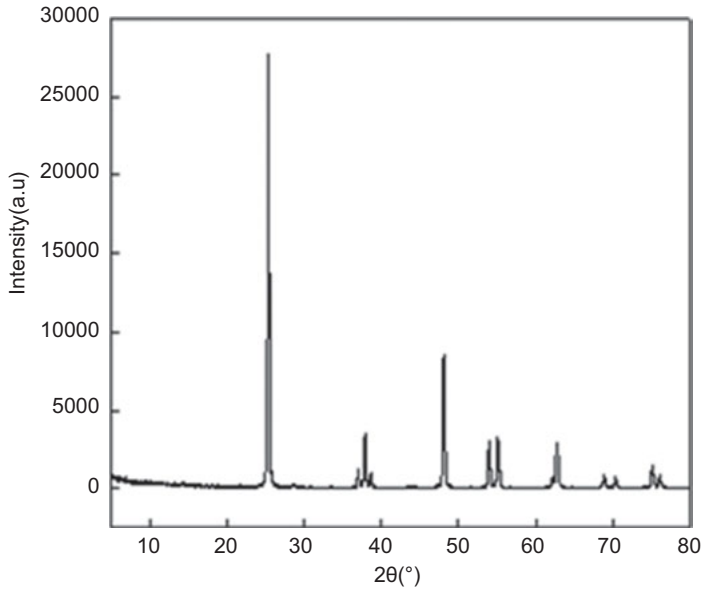

(I)

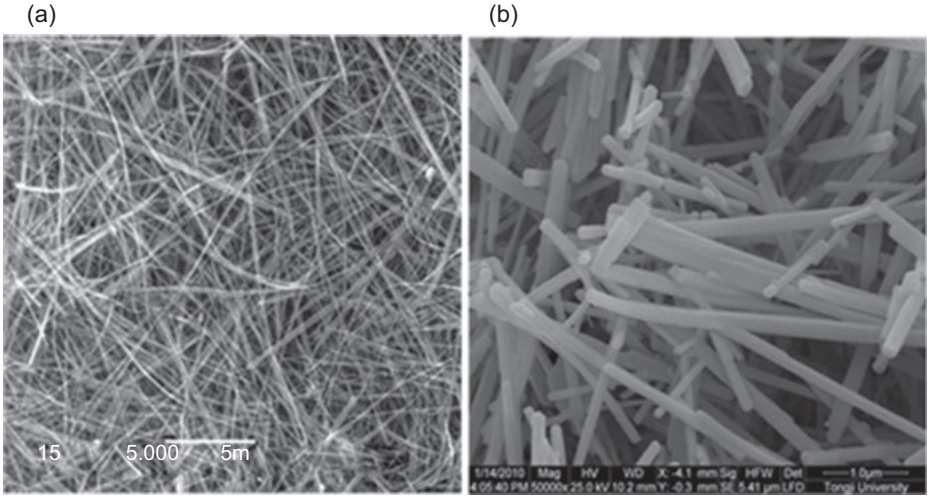

(II)

Figure 4.1: XRD pattern of the as-prepared anatase nanowires.

EBSCOhost - printed on 2/14/2023 6:39 AM via . All use subject to https://www.ebsco.com/terms-of-use

4.1.2.2 Morphologies of membranes

Figure 4.2(a–g) showed SEM pictures of the surface, cross-section and inner porous structures of hybrid UF membranes. Those images revealed that TiO_2 nanowires

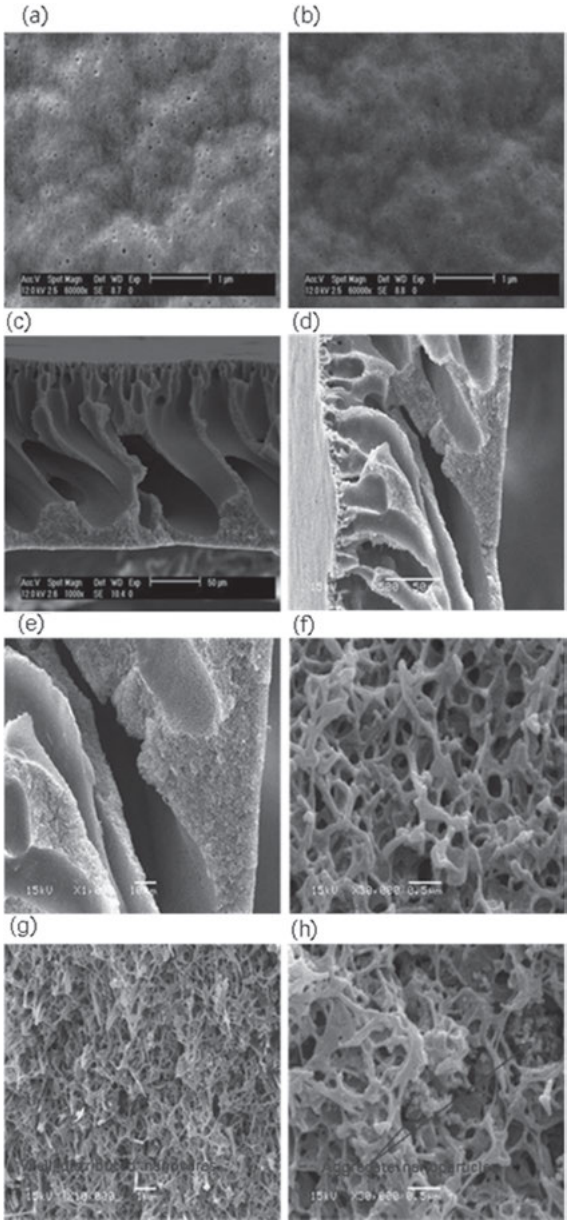

Figure 4.2: Surface morphologies of hybrid UF membrane by organic-inorganic PVDF-TiO_2 nanowire.

EBSCOhost - printed on 2/14/2023 6:39 AM via . All use subject to https://www.ebsco.com/terms-of-use

were well-distributed in micro-pores, which contributed to the enhancement of membrane mechanical strength. It was believed that TiO_2 nanoparticles would aggregate and be leached out partly from the modified membrane [29]. Moreover, TiO_2 nanowires were firmly restricted into micro-pores, which were not easy to leach out in the permeation process. TiO_2 nanoparticle is easy to aggregate for the nano-size effect [45]. In contrast, the ultralong lengths of TiO_2 nanowires are up to a few millimeters. This resulted in that (1) the TiO_2 nanowires had better dispersity in casting solution compared to TiO_2 nano-particle; (2) they were finely dispersed in the polymer matrix; and (3) the ultralong TiO_2 nanowires were firmly restricted into the micro-pores in membrane.

Besides, the hybrid membrane porosity (ε) was not significantly changed, whereas the mean pore size (d) decreased with the increase of TiO_2 nanowires in the membrane. Reason for that was the increased stress between TiO_2 nanowires of organic phase and polymer shrinkage during the precipitation process.

Contact angle was used to characterize the membrane hydrophilicity. The hybrid membrane hydrophilicity enhanced as the increase of TiO_2 nanowire amount in the membrane bulk. It is believed that the existence of TiO_2 nanowires generated hydrolysis with hydroxyl groups, resulting in hydrophilicity improvement.

TiO_2 nanowire also contributed to the mechanical strength enhancement of membranes. The tensile strength increased from 1.67 MPa to 2.23 MPa as the concentration of TiO_2 nanowires increased from 0 wt.% to 5 wt.%. However, the elongation ratio enlarged from 36.91% to 59.01%. The introduction of TiO_2 nanowire contributed to link the polymeric chains, increasing the rigidity and elasticity of polymeric chains. Moreover, Figure 4.3(I) showed that PVDF-TiO_2 nanowire hybrid membrane possessed higher thermal decomposition temperature T_d (defined as the temperature at 3% weight loss) when compared with the pure PVDF membrane. The TiO_2 nanowires could strongly hinder the volatility of the decomposed products with limitation of the continuous decomposition of PVDF content and pyrolysis [36]. For good dispersion and good thermal transmission properties, TiO_2 nanowires could strongly hinder the volatility of the decomposed products with limitation of the continuous decomposition of PVDF content and pyrolysis [36]. This enhanced thermal decomposition temperature (T_d).

Figure 4.3(II) show the XRD diffraction patterns of TiO_2 nanowires, PVDF membrane and PVDF-TiO_2 nanowire hybrid membrane. The pattern of TiO_2 crystal nanowire has three crystalline characteristic peaks in the order of $2\theta = 25.38°$, 37.88° and 48.12° [39, 40, 43]. For PVDF-TiO_2 nanowire hybrid membrane, when a new peak at $2\theta = 25.34°$ appeared, the characteristic peak of TiO_2 nanowires crystal could be observed. This is different from the neat PVDF membrane. From Figure 4.3(III), confirmation of the crystalline structures measured by XRD, and the increase in formed -OH groups with the TiO_2 nanowire content were observed.

EBSCOhost - printed on 2/14/2023 6:39 AM via . All use subject to https://www.ebsco.com/terms-of-use

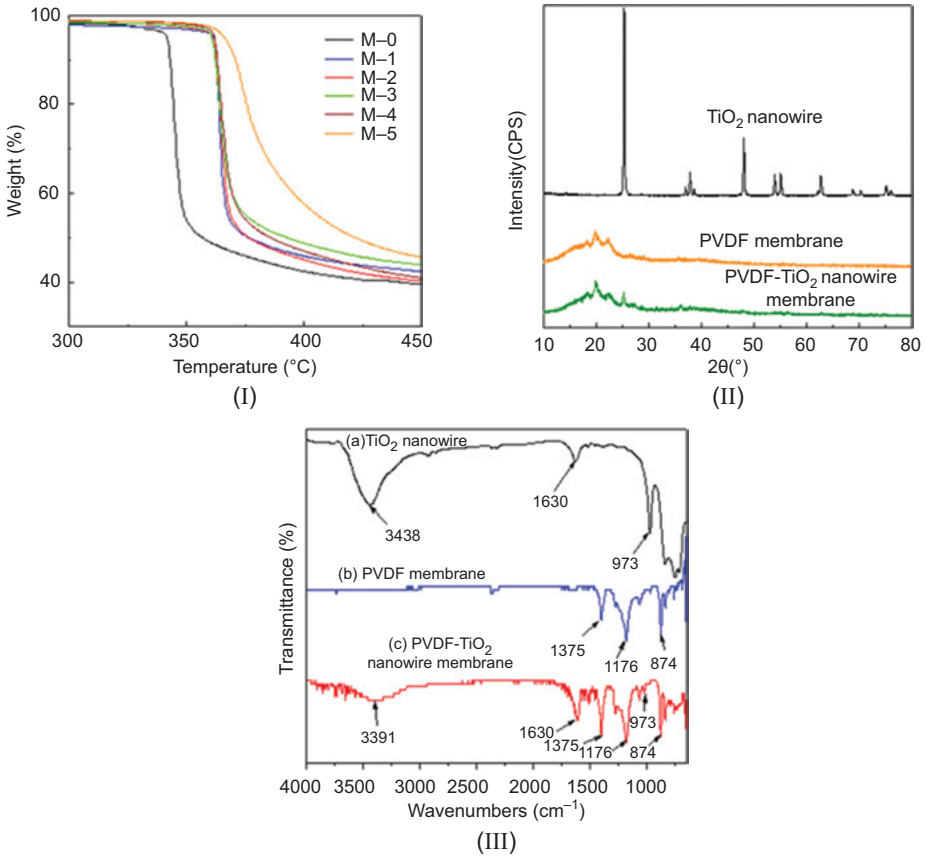

Figure 4.3: TG curves (I), X-ray diffraction patterns (II), and FTIR spectra (III) of PVDF-TiO_2 nanowire hybrid membranes.

UF experiments were utilized to investigate the effect of TiO_2 nanowire on permeability and rejection capacity of PVDF-TiO_2 nanowire hybrid membranes (shown in Figure 4.4(I)). The flux of PVDF-TiO_2 nanowires hybrid membrane increased as the increase of TiO_2 nanowire concentration. However, BSA rejection increased slightly as the increase of TiO_2 nanowires content.

The ratio of BSA solution flux (J_{BSA}) and pure water flux (J_w) was used to evaluate the antifouling properties of PVDF-TiO_2 nanowire hybrid UF membranes. Higher antifouling UF membrane always showed less flux loss and the higher ratio (J_{BSA}/J_w) with the addition of BSA in the feed solution [46]. As shown in Figure 4.4(I), the ratio (J_{BSA}/J_w) increased slightly for PVDF-TiO_2 nanowire hybrid membrane. This could be ascribed to its higher hydrophilicity, which is the main factor affecting the membrane surface-adsorption properties [47].

Figure 4.4(II) shows the three-dimensional AFM surface images of PVDF-TiO_2 nanowire hybrid membrane. Roughness parameters of these membranes could also be

EBSCOhost - printed on 2/14/2023 6:39 AM via . All use subject to https://www.ebsco.com/terms-of-use

obtained through the AFM analysis software. Results indicated that roughness parameters for neat PVDF membranes were larger than that of hybrid membrane. It revealed that the modified membrane possessed smoother surface, as well as denser skins. It is believed that the membrane roughness was the most effective factor on membrane antifouling capability if the operating conditions were not taken into account [29].

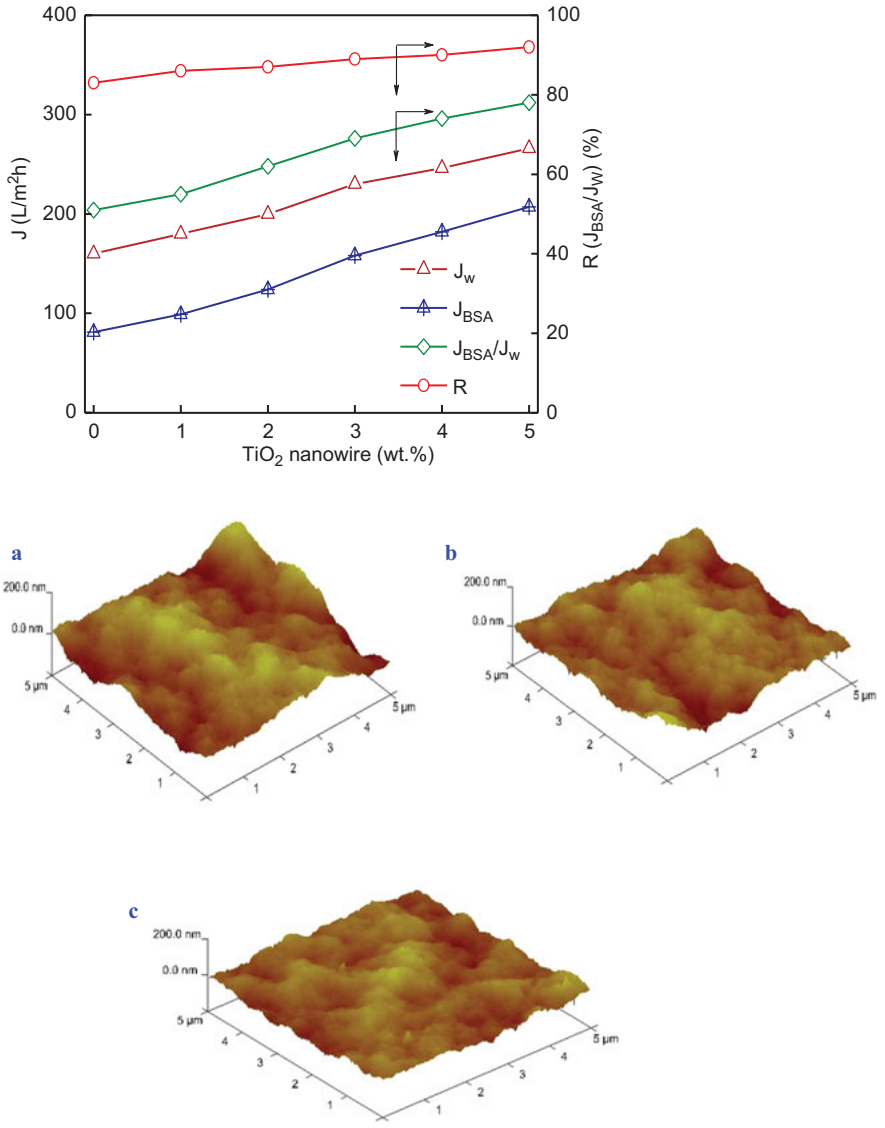

Figure 4.4: Permeation properties of J_w, J_{BSA}, rejection (R) and the ratio (J_{BSA}/J_w) (I), and three-dimensional AFM surface images (II) of PVDF-TiO_2 nanowire hybrid membrane.

EBSCOhost - printed on 2/14/2023 6:39 AM via . All use subject to https://www.ebsco.com/terms-of-use

4.2 Surface modification of polyvinylidene fluoride (PVDF) membranes via NIPS process using Tween 80-H_2O mixture as dope additive

4.2.1 Introduction

In several reports of the membrane preparation process, surfactants like Tween 20 and Tween 80 have been chosen as additives [48–50]. Surfactants are special molecules with both hydrophobic hydrocarbon chains and hydrophilic chains (polar head groups). In polarity solution, which tends to form reverse micelle structure. And such structure could contribute to the formation of porous structure. However, the reported membrane fabricated with surfactant as single additive was not obvious, due to the micelles structure.

Tween 80 is a non-ionic surfactant with a strong affinity with water. When water is added into the mixing medium of DMAc- Tween 80, H_2O molecules can be solubilized by reverse micelle. Figure 4.5(I) indicates that the water pool of polar head groups of Tween 80 reverse micelle is formed.

When casting solution was immersed into various coagulants, H_2O was diffused out from Tween 80 reverse micelle. This broke the equilibrium of the interaction between polar head of surfactant and water, and the interconnection between surfactant's hydrophobic chains and PVDF. X-ray photoelectron spectroscopy (XPS) analysis in papers indicated the surface segregation of the amphiphilic component [51, 52]. It is speculated that in casting solution, the confined diffused path of H_2O by reverse micelle favor surface segregation of surfactant's polar head groups (hydrophilic groups). This resulted in the hydrophilicity improvement of PVDF. Figure 4.5(II) showed the possible surface segregation process of Tween 80 polar head groups.

In this work, the effect of various contents non-solvent H_2O on membrane morphology and PVDF-Tween 80 solution were investigated. DLS results were utilized to provide more direct information of solution property. The influence of two kinds of casting solutions temperatures on membranes properties, i.e. mechanical property, crystallization, filtration, hydrophilicity and morphology, etc. was also investigated.

4.2.2 Results and discussion

4.2.2.1 Basic physical-chemical property of casting solution

Surface tension, viscosity and light transmittance experiment were carried out to obtain the basic physical-chemical property of casting solution. Figure 4.6(I) showed that with increasing concentration of H_2O, the surface tension slowly decreased. The decreasing surfaces tension could be related to solubilization of high polarity water

EBSCOhost - printed on 2/14/2023 6:39 AM via . All use subject to https://www.ebsco.com/terms-of-use

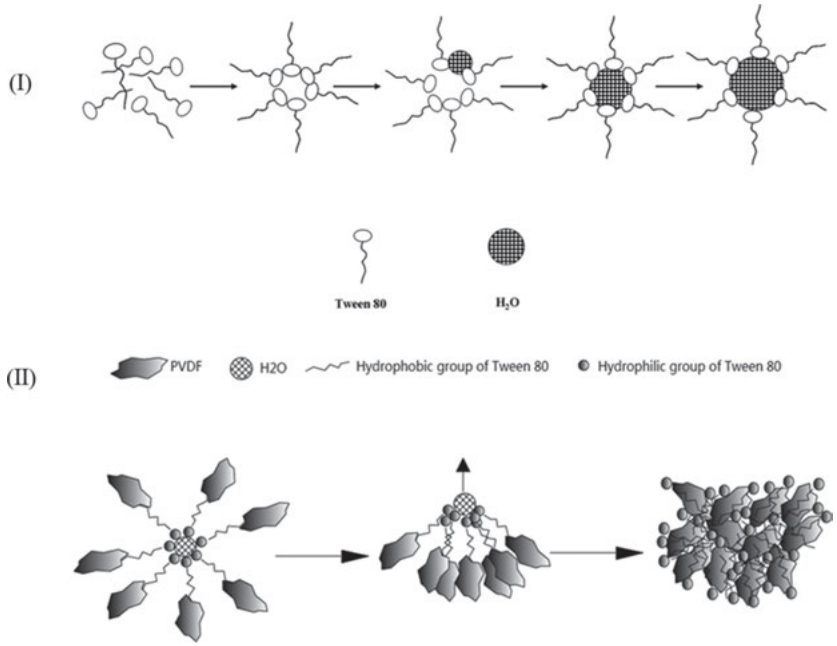

Figure 4.5: (I) H_2O solubilization process of Tween 80 reverse micelles in DMAc medium; (II) Schematic diagram of the surface segregation process of Tween 80's polar head groups during de-mixing process.

molecules of Tween 80 reverse micelle in DMAc medium, considering the relationship between surface tension and surface arrangement of molecules on the interface between liquid and air. This contributed to the micrograph structure adjustment of the molecules in casting solution.

The viscosity variation with H_2O concentration in Figure 4.6(II) revealed that the viscosity increased as H_2O content increased in solution both at 60 °C and at RT. The higher viscosity indicated a stronger interconnection between molecules [53]. Tween 80 micelles with solubilization water played an important role in the improvement of interconnection between the molecules. The interconnection between polymer and hydrocarbon chains of reverse micelle could enhance the chain entanglement degree of PVDF, which was also the reason for the increase of viscosity.

Light transmission experiment was used to investigate precipitation kinetics of the casting solutions as shown in Figure 4.6(III). The curves showed that the precipitation rate speeded up when H_2O content increased.

To provide more information, the dynamic light scattering (DLS, Zatasizer Nano ZS, Malvern Instruments Ltd., UK) measurement was carried out in the PVDF-DMAc-Tween 80-H_2O system for low PVDF solution. Figure 4.7(I) showed the intensity-weighted micelle size distribution of DMAc-Tween 80 system at RT and 60 °C, respectively. With the increase of H_2O content, the harmonic intensity weighted average hydrodynamic

EBSCOhost - printed on 2/14/2023 6:39 AM via . All use subject to https://www.ebsco.com/terms-of-use

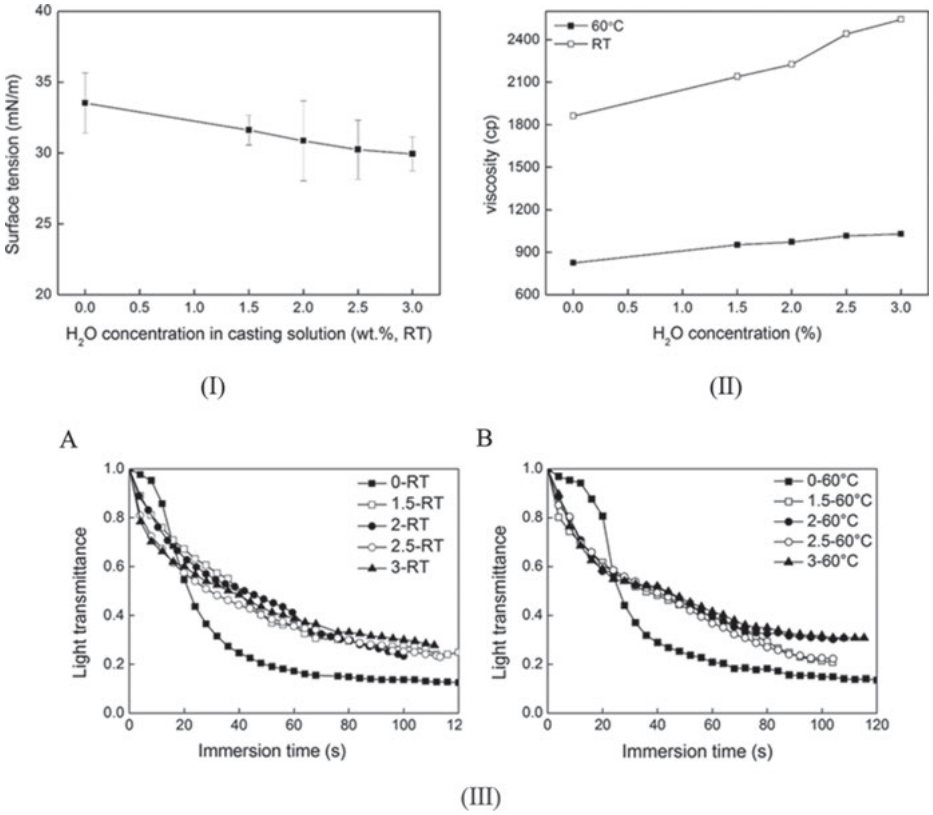

Figure 4.6: Surface tension (I) viscosity (II) and light transmittance (III) of PVDF-DMAc-Tween 80-H_2O system.

diameter (D_h) of the micelle first decreased and then increased [54] at room temperature. As shown in Figure 4.7(I)(A), Tween 80 was tightly bound to H_2O molecules with addition of small amount of H_2O. This explained the decreasing of micelle hydrodynamic diameter. As the increase of H_2O amount, the size of the inner core of the micelle composed by water increased, so the D_h of micelle increased [55]. At 60 °C as showed in Figure 4.7(I)(B), the micelle hydrodynamic diameter increased with the addition of water, which was due to that the bounding between surfactant and water became less tight [56].

The DLS data of 1.0 wt.% PVDF solution at RT (A) and 60 °C (B) were shown in Figure 4.7(II). PVDF chains were in a lowly coiled state and tended to extend, then to be entangled with neighboring chains in pure DMAc solvent [53], and its corresponding D_h at RT was 248.5 nm.

However, because of the formation of large aggregates (incipient precipitation), Figure 4.7(II) showed that when H_2O was taken as single additive, the D_h of micelles significantly increased [57]. While when Tween 80 was chosen as single additive, the D_h of micelles decreased. This contributed to the better entanglement with neigh-

EBSCOhost - printed on 2/14/2023 6:39 AM via . All use subject to https://www.ebsco.com/terms-of-use

boring chains of PVDF and further enhancement of lowly coiled state caused by the interconnection between polymer and reverse micelle. Besides, the D_h of micelles increased when further addition of water as mixture additive with Tween 80. The slow increased D_h of micelles of 76:3:3:1 system at 60 °C revealed the improved thermodynamic stability when compared with other samples [58]. It was the interaction between water and surfactant polar head that provided a balance resistance to the interconnection between hydrophobic chains of surfactant and PVDF.

Comparing the micelles size to intensity signal in Figure 4.7(I), polymer-surfactant solution possessed very complex micelle structures, with both micelle structure and polymer aggregate. Mainly two peaks could be observed in Figure 4.7(II). The micelle structure corresponded to narrower intensity signal of a few hundred nm scale. While the other corresponded to the aggregated structure of PVDF themselves or mixed with separated surfactant molecules.

Above data about the morphology solution of different composition revealed that the micro-structure adjustment of the solution was attributed to the interaction between surfactant and water as well as the interconnection between polymer and hydrocarbon chains of reverse micelle. Such change surely would be embodied in the membrane formation process.

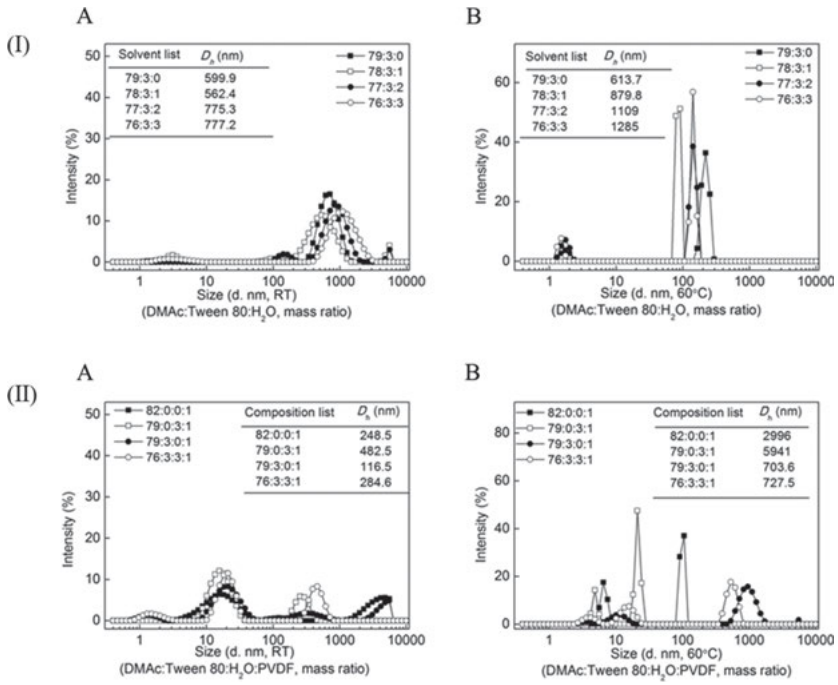

Figure 4.7: Intensity-weighted micelle size distribution of solution systems (I: DMAc-Tween80-H_2O; II: DMAc-Tween80-H_2O-PVDF) at RT (A) and 60 °C (B).

EBSCOhost - printed on 2/14/2023 6:39 AM via . All use subject to https://www.ebsco.com/terms-of-use

4.2.2.2 Membrane performance

Figure 4.8 indicated the top surface and cross-section of resultant PVDF membranes. Differences of membrane morphology with existence of H_2O could be observed when examined in detail. The macrovoids were irregular, less confined and larger without addition of H_2O. While the wall structure between macrovoids increased, the finger-like structure became slim and confined in the case of H_2O addition. Membranes prepared with RT casting temperature showed more random macrovoids as compared with those prepared at higher.

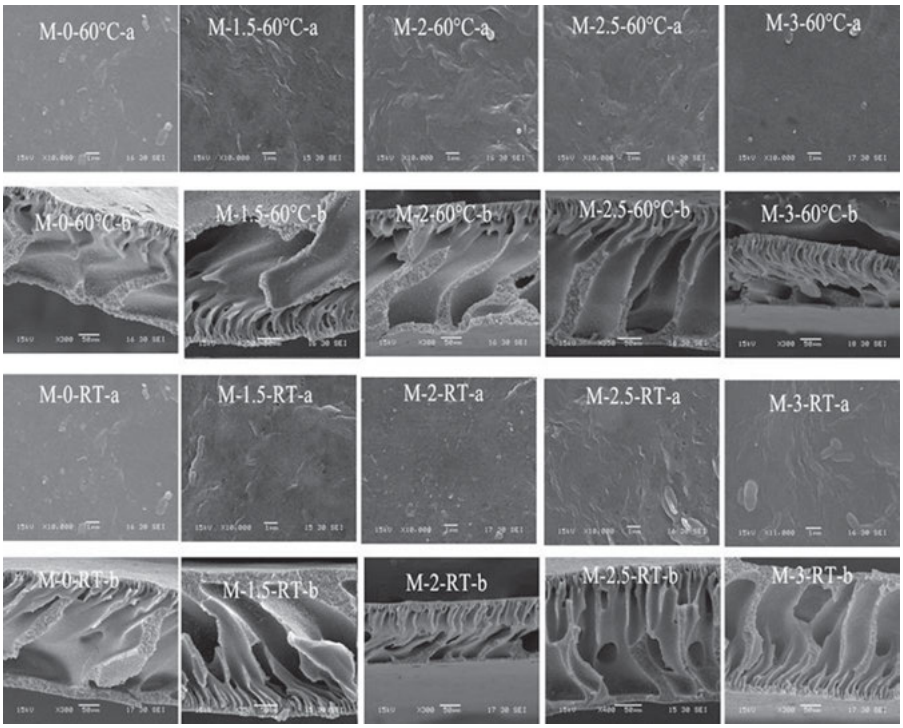

Figure 4.8: SEM images of PVDF membrane prepared from DMAc-Tween80-H_2O-PVDF at 60 °C and RT.

The filtration properties of resultant membranes showed that the PWF increased with the increase of H_2O content. Besides, the membranes prepared with RT casting temperatures had higher PWF. And finger-like macrovoids of membranes always resulted in higher porosity. The overall resulted membrane porosity was in the range of 78–88%. PVDF membranes had stability and well rejection property of BSA and Dextran.

Dynamic contact angles of membranes were shown in Figure 4.9(I). The results revealed that the H_2O existence enhanced both the membrane initial contact angle (s)

EBSCOhost - printed on 2/14/2023 6:39 AM via . All use subject to https://www.ebsco.com/terms-of-use

and equilibrium contact angle (θ_E). The larger of H_2O concentration, the larger the θs was. However, the difference between θs and θ_E was small with various H_2O contents. Contact angle decreased with time and trended to θ_E in finite time.

XRD spectra of PVDF membranes with various fabrication conditions were illustrated in Figure 4.9(II). The results indicated that the characteristic peak such as α and β could not be identified clearly, and the range of a very strong intensity peak was wide [8]. The crystal formation of PVDF was a mixture of α and β crystallites, or an undeveloped α or β crystalline phase [59].

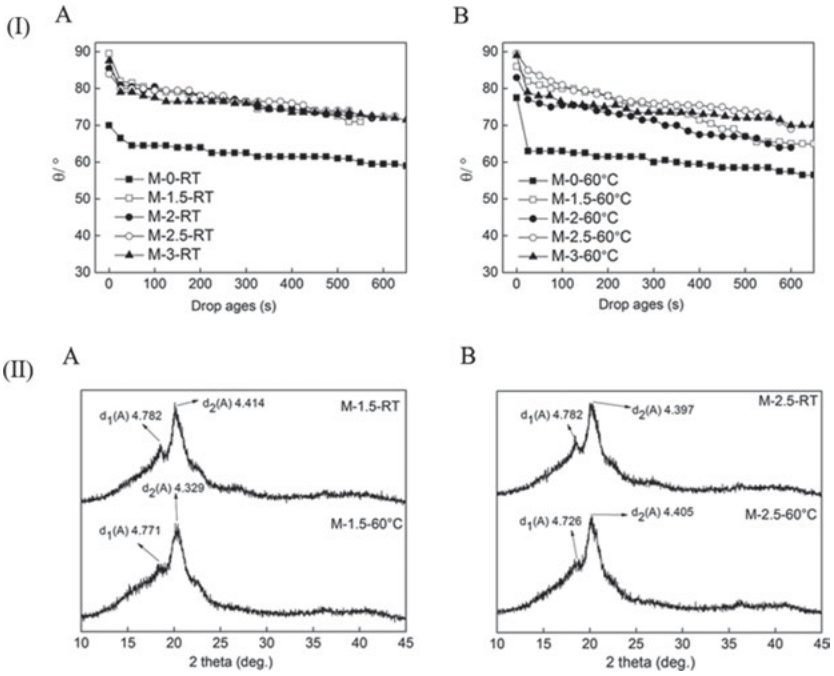

Figure 4.9: Dynamic contact angles (I) and X-ray diffraction scans (II) of PVDF membrane prepared from DMAc-Tween80-H_2**O-PVDF at 60** °C and RT.

Figure 4.10 showed membrane mechanical properties. PVDF membrane possessed higher break strength, enlarged elongation at break and improved Yong's modulus as the increase of H_2O concentration. Non-solvent in solution always led to mechanical properties deterioration. However, the results in Figure 4.10 were contrary to the normal hypothesis. The increased wall structure between macrovoids contributed to the improvement of mechanical properties. High temperature improved polymer chain mobility, leading to better arrangement.

EBSCOhost - printed on 2/14/2023 6:39 AM via . All use subject to https://www.ebsco.com/terms-of-use

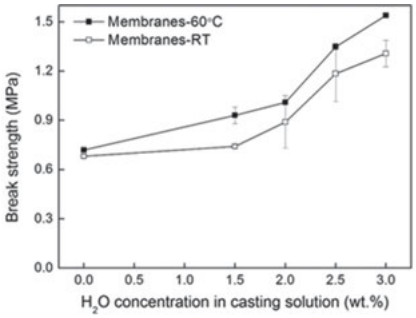

Membrane	Elongation at break (%)		Yong's modulus(MPa)	
No	60°C	RT	60°C	RT
M-0	12.8±1.5	10.8±0.1	14.0±1.8	15.7±0.2
M-1.5	18.0±0.9	32.7±0.7	20.2±0.1	16.9±0.5
M-2	32.5±1.1	32.3±2.1	22.2±1.4	22.2±1.5
M-2.5	35.2±3.1	38.9±1.1	25.3±2.1	35.2±3.5
M-3	39.1±3.3	42.2±2.4	25.7±0.3	32.2±1.1

Figure 4.10: Mechanical properties in terms of break strength, elongation ratio at break and Yong's modulus of PVDF membrane prepared from DMAc-Tween80-H_2**O-PVDF at 60** °C and RT.

4.3 Surface modification of PVDF membranes via in-situ free radical polymerization method

4.3.1 Introduction

The blending modification route is the most convenient method in terms of practical and large-scale application when compared with graft surface modification on preparation of porous and hydrophilic polymer membranes.

In recent years, for surface modification of PVDF membranes, the blending of self-synthesized amphiphilic copolymers as tune membrane morphology, antifouling surface modifiers and pore-forming additives has received much attention. The reason is that the amphiphilic copolymer has good compatibility with the PVDF matrix. This provides PVDF membrane engineered surface properties. It was believed that configuration of membranes was confined by the existence of amphiphilic copolymer supramolecular aggregates with various morphologies [19, 60].

Recently, the easier and more economical method of simplified atom transfer radical polymerization (ATRP) method was used for the synthesization of amphiphilic copolymers blending with PVDF as a hydrophobic backbone [19, 61, 62]. In principle, in order to improve the micellization of amphiphilic copolymer and to

EBSCOhost - printed on 2/14/2023 6:39 AM via . All use subject to https://www.ebsco.com/terms-of-use

avoid the isolation of the synthesized copolymer, the simplified polymerization steps are performed.

The simplified method has been utilized to form PVDF casting solution via directly adding the P (PEGMA-r-MMA) copolymer solution (including the reaction mixture) into DMAc and TEP (30:70, mass ratio) co-solvent (Figure 4.11) [63]. The copolymer nanosphere with size of 100–200 nm was formed in the co-solvent. After addition of 1.0% PVDF (Figure 4.12), its morphology transferred to nanosphere (size: 100–200 nm) and reverse micelle (size: 10–100 nm) [63].

The function of amphiphilic copolymer on modulation morphology and pore-forming of resultant membranes was limited by those large size nanoparticulate aggregates. Generally, in selective solvents, the supramolecular aggregates morphologies are in the range from micelle of simple spherical star-like to self-associate of polymerases micelles [61]. On one hand, the morphologies could be tailored by changing the composition, nature, architecture of the amphiphilic copolymers or lengths. On the other hand, for tuning the aggregates behavior of the copolymers, external parameters, i.e., addition of additives or change in solvent, such as co-solvents and electrolytes provided extra degrees of freedom [64, 65]. In amphiphilic copolymer self-assembly, it is an important issue to modulate the polymer aggregates distinctive geometry at nanometer size [66]. So, membranes configuration could be utilized to modulate the amphiphilic copolymer tune aggregates behavior by self-assembly so as to meet special requirements.

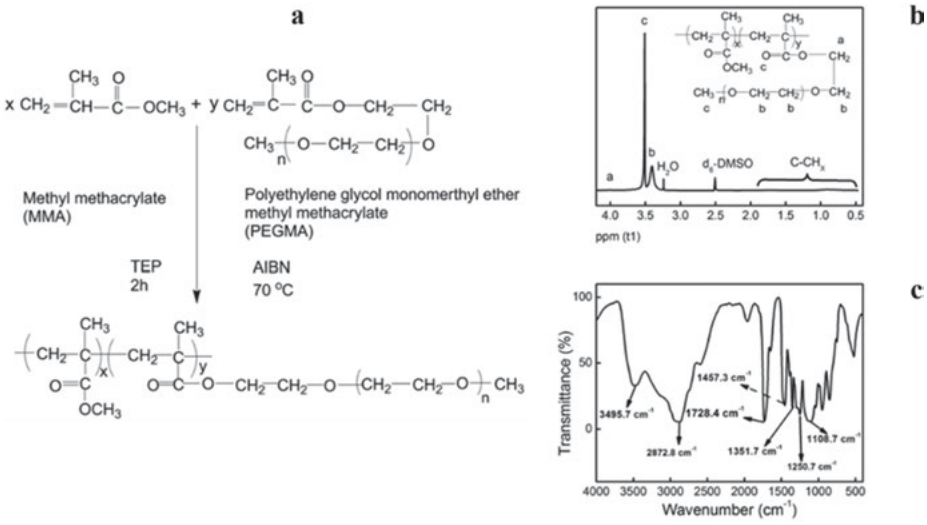

Figure 4.11: P(PEGMA-r-MMA) amphiphilic copolymer fabricated by simplified blend method [63]. (a: the synthesis route; b: ^{1}H NMP spectrum (solvent: d_6**-DMSO); c: FT-IR spectra)**

EBSCOhost - printed on 2/14/2023 6:39 AM via . All use subject to https://www.ebsco.com/terms-of-use

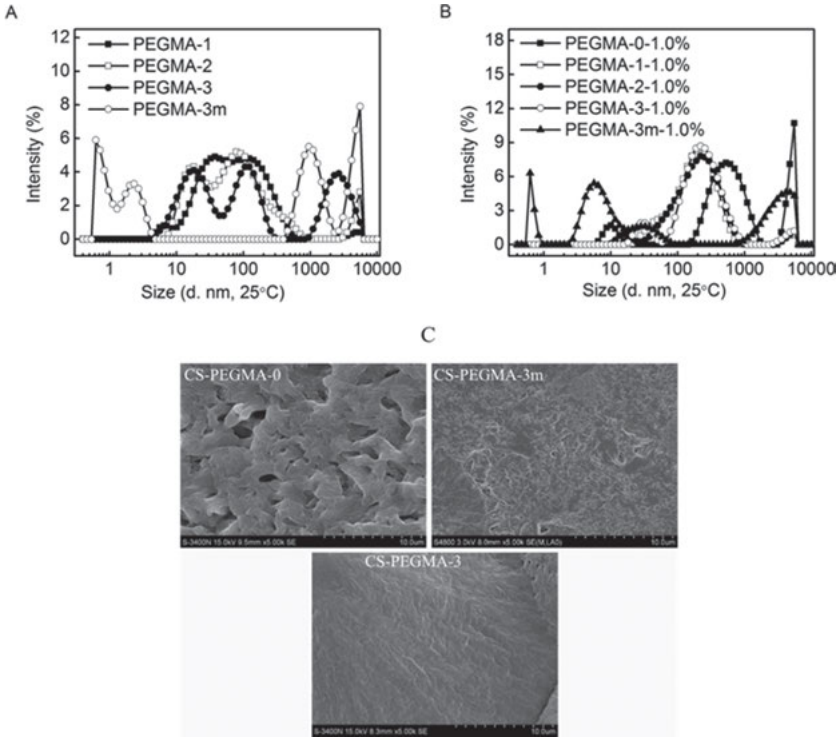

Figure 4.12: Conformation of various solutions [63].

(A: Intensity-weighted micelle size distribution of P (PEGMA-r-MMA) in TEP-DMAc co-solvent; B: Intensity-weighted particle size distribution of 1.0 wt.% PVDF in TEP-DMAc co-solvent containing P (PEGMA-r-MMA); C: Influence of P (PEGMA-r-MMA) on morphology tune of PVDF casting solutions (CS: casting solution))

In this study, small-size supramolecular aggregates were obtained via in-situ free radical polymerization (IFRP). The specific amount of azobisisobutyronitrile (AIBN) required is directly added into PVDF-TEP-DMAc-PEGMA-MMA system. Then polymerization is initiated as shown in Figure 4.13. Considering the time required for drying, purification and even sampling of the copolymer solution (including the reaction mixture) with high viscosity, IFRP method appears to be more economical and easier. Additionally, during IFRP process, some unreacted AIBN is expected to be easily decomposed as nitrogen. Finally, the excess or unreacted PEGMA and MMA could work as pore-forming agent during NIPS process. This is expected to be washed out [67]. Thus, through tuning the micro-structure adjustment of polymer solution, IFRP is expected to provide modulation morphology of PVDF membranes in the selective co-solvent. Furthermore, during membranes fabrication process, compared with ATRP, IFRP is environment-friendly, as it can avoid the pollution from heavy metals.

EBSCOhost - printed on 2/14/2023 6:39 AM via . All use subject to https://www.ebsco.com/terms-of-use

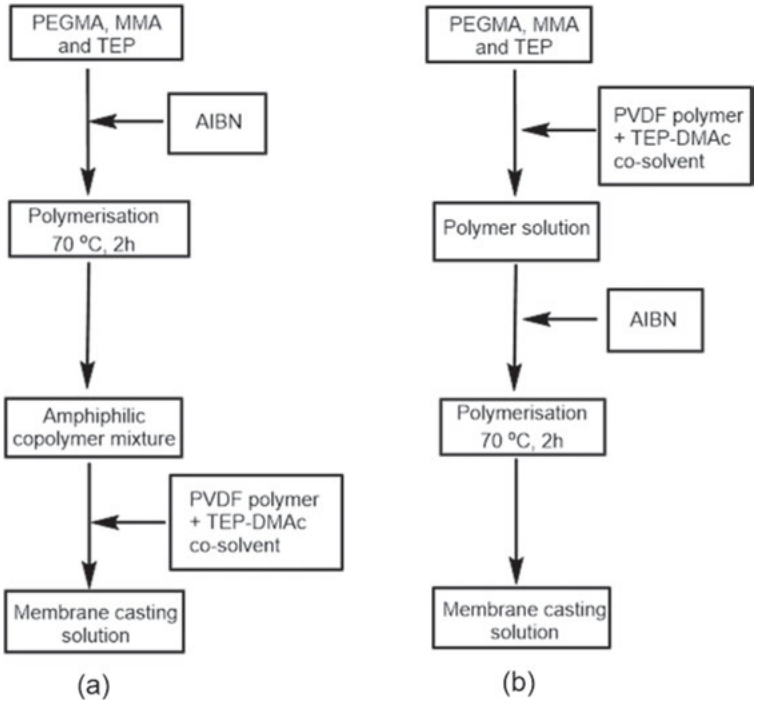

Figure 4.13: Preparation methods of PVDF casting solution: (a) simplified blend and (b) IFRP.

4.3.2 Results and discussion

4.3.2.1 Micro-structure modulation of the solution via IFRP

DLS is widely used to probe the size distribution and size of reverse micelles, submicron-sized particles, and proteins [68]. DLS could struggle to show the correct particle size distributions in various IFRP solutions, containing polydisperse particles or droplets with sizes range over several orders of magnitude. Figure 4.14(a) indicates that the structures are very complex with both monomers aggregate and monomers existing in solution. Figure 4.14(b) illustrates that the dominating population is the aggregate of the monomers themselves and polymer-monomers. Besides, Figure 4.14(b) shows that the population of polymer-monomers aggregates decreases as the increase of the monomers content.

After IFRP, the intensity-weighted aggregates reveal novel results as shown in Figure 4.14(c, d). The distribution of supramolecular aggregates of monomers system is obviously narrow after IFRP. This evidence is that IFRP contributes to the copolymer formation. While Figure 4.14(d) indicates that the size of dominating and narrow distribution population aggregates enlarged as the existence of PVDF. The supramo-

EBSCOhost - printed on 2/14/2023 6:39 AM via . All use subject to https://www.ebsco.com/terms-of-use

lecular aggregates between the copolymer and PVDF resulted in the enlarged size. This suggests the conformation of PVDF and micro-structure adjustment of polymer solution. It is reported that the hydrophobic group of the copolymer leads to the consequence of the formation of mixed adsorption layers or polymer adsorption over copolymer layer [69]. And the formation of narrow distribution supramolecular aggregates between the copolymer and PVDF indicated the existence of the hydrophobic group of the copolymer.

The DLS data exhibits that 1.0 wt.% pure PVDF chains tend to extend in a coiled state, then to be entangled with neighboring chains in the selective co-solvent [59]. Its corresponding D_h was 609.7 nm. The further enhancement of lowly coiled state and better entanglement with neighboring chains of PVDF contributes to the sharply decreased D_h of supramolecular aggregates of PVDF-monomers. IFRP is attributed to the formation of supramolecular aggregates between PVDF and the copolymer.

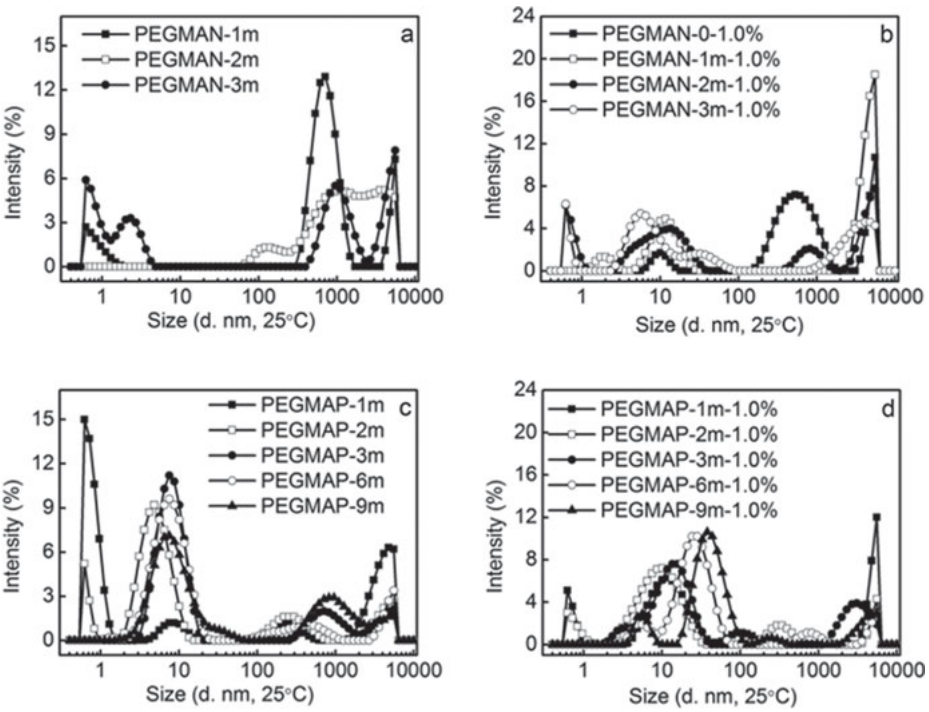

Figure 4.14: Intensity-weighted aggregate size distribution of various IFRP solutions.

EBSCOhost - printed on 2/14/2023 6:39 AM via . All use subject to https://www.ebsco.com/terms-of-use

Figure 4.15 further indicates the conformation of PVDF in the co-solvent after IFRP. Pure PVDF shows the characteristic morphology of lobed-structure. And the characteristic lobed-structure of polymer domains is replaced by irregular mesh-like network of continuous domains. As addition of monomers, the change from lobed-structure to mesh-like is consistent with the existence of the monomers themselves and aggregating with polymer-monomers. Besides, it is consistent with the decreasing D_h. On one hand, IFRP results in a series of discontinuous circular interstice in the total area occupied by the mesh-like domains. On the other hand, IFRP results in the case of a decrease in separation of the highly continuous domains. With the increase of the concentration of monomers, morphologies continue to change. Dramatic morphological changes could be obtained, i.e. regularly discrete globules agglomerates (with one of the globules bearing on the surface of another). The formation of supramolecular aggregates between copolymer and polymer after IFRP is confirmed when combined with the DLS results. Additionally, with increasing concentration of monomers of IFRP, the distribution of the supramolecular aggregates become narrow and regular.

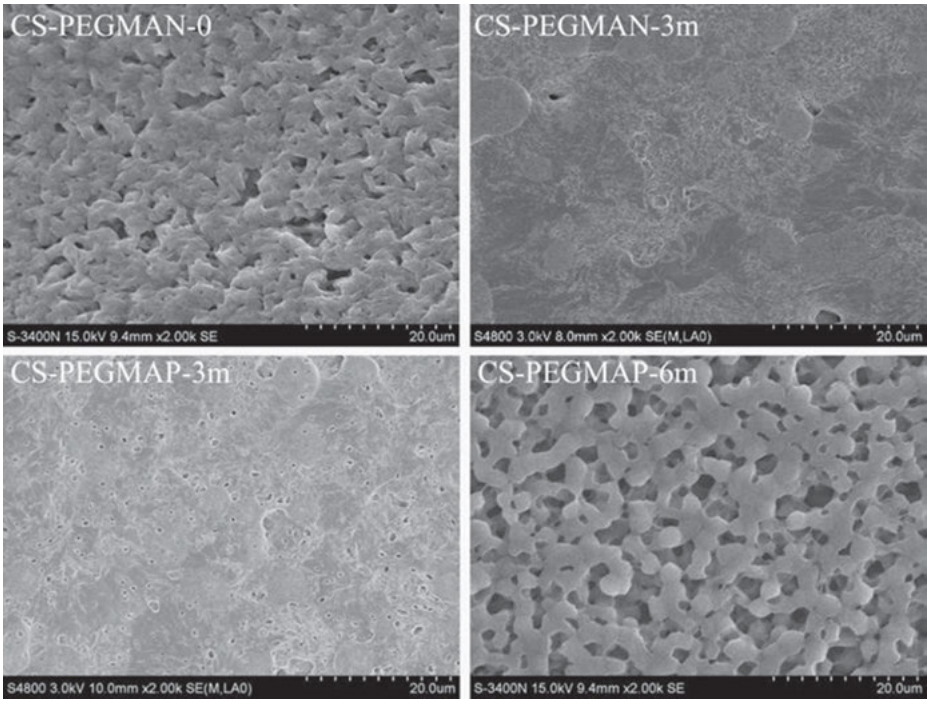

Figure 4.15: Morphologies of various IFRP solutions.

EBSCOhost - printed on 2/14/2023 6:39 AM via . All use subject to https://www.ebsco.com/terms-of-use

4.3.2.2 Determination of basic physical-chemical properties of casting solution

Figure 4.16(I) lists the precipitation kinetics of various casting solutions, it could be obtained that the precipitation rate decreases as the addition of monomers. While after IFRP, the precipitation rate accelerated. The miscibility between the coagulant and casting solution increases for the formation of narrow distribution supramolecular aggregates between the copolymer and PVDF. This facilitates the demixing process [70].

Figure 4.16(II) gives the surface tension of various PVDF solutions. The curves indicate that the surface tension increases as the monomers exist. The increasing surface tension is attributed to impartation of hydrophilic functional group of the monomers. This increases the miscibility between casting solution and coagulant, and leads to the decreasing precipitation rate. However, the surface tension decreases via IFRP. For the molecule micrograph structure adjustment caused by hydrocarbon functional group of copolymer that covered the surface of casting solution, as well as the formation of supramolecular aggregates between the copolymer and PVDF, the larger concentration of monomers, the lower surface tension is.

Figure 4.16(III) reveals the shear viscosity with a shear-thinning behavior. The results exhibit that the shear viscosities increase as the increase of the monomers concentration. After IFRP, the casting solution shows larger viscosity. The larger viscosity illustrates a stronger interconnection of molecules (supramolecular aggregates between PVDF and the copolymer) [59]. Larger viscosities are attributed to the chain entanglement degree of PVDF enhanced by the aggregates strong interconnection [69]. The novel result is that after IFRP, all polymer solution has trivial strain thinning behavior. It is the strong molecular interconnection that dominates the sliding under shear and chain stretching in these solution systems [59].

4.3.2.3 Performance of various PVDF membranes

Figures 4.17 and 4.18 show the PVDF membranes top surface and cross section morphologies prepared without /via IFRP, respectively. Top-surface of pure PVDF membranes in Figure 4.17 reveals cauliflower type morphology. After addition of monomers, the cauliflower becomes wizened and dense. Under high magnification, the pure membrane interior bulk is constructed by the cauliflower grainy nanograins. However, the size of the cauliflower become similar grainy nanograins and thin with PEGMA and MMA monomers added. After AFRP, the morphologies of PVDF membranes exhibit significant difference.

Firstly, as monomers content increasing, the wizened top-surface transfers to dense-packing lotus-shape type configuration with enlarging size. Secondly, below the sponge-like cross-structures are confined regular macrovoids of finger-like struc-

EBSCOhost - printed on 2/14/2023 6:39 AM via . All use subject to https://www.ebsco.com/terms-of-use

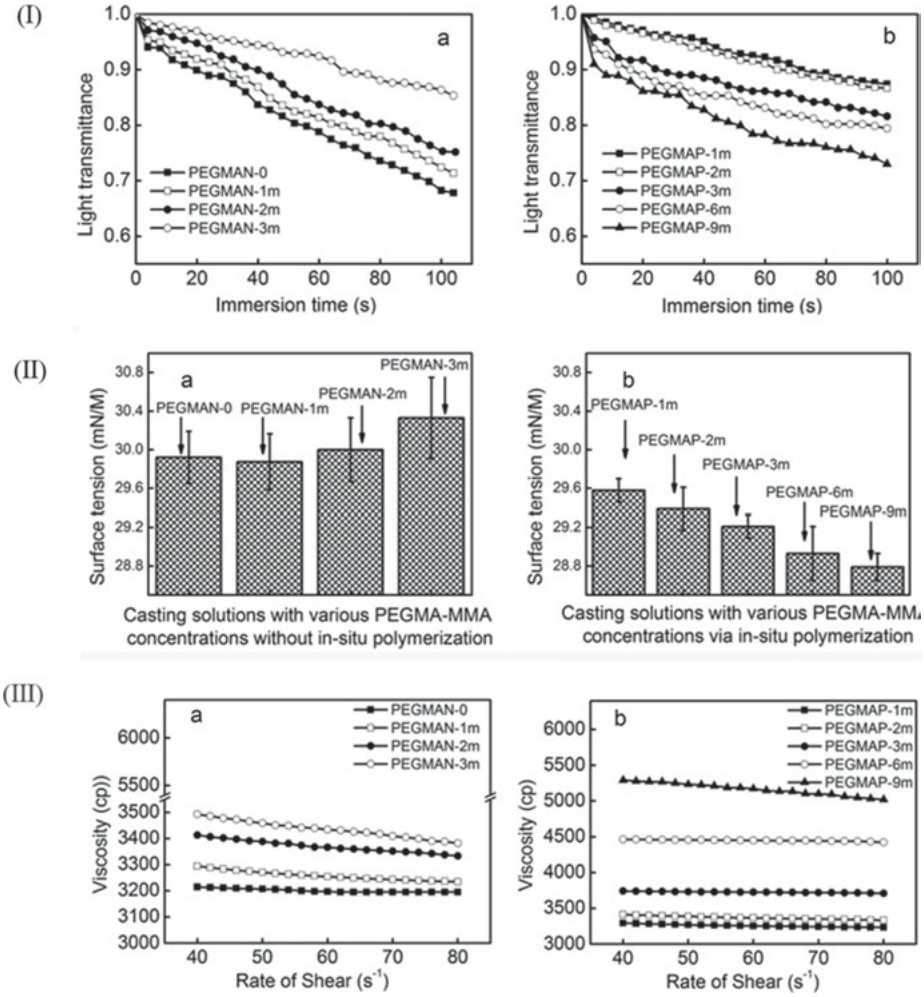

Figure 4.16: Basic physical-chemical properties (I: precipitation rates; II: surface tensions; III: shear viscosities) of various PVDF casting solutions.

tures. The supramolecular aggregates of copolymer and PVDF confine the macrovoids structures, whereas, casting solution high precipitation rate is favorable to the macrovoids formation of finger-like structures. Detail information on the influence of the in-situ polymerization on tune configuration of PVDF membrane is provided under high magnification. It reveals that the nanograins morphology of PVDF from stripe-shape grains to globules agglomerates (with one of the globules bearing on the surface of another) is attributed to the modulation of supramolecular aggregates between the copolymer and polymer [71].

XRD spectra is used to elucidate the crystal structure alternation of various PVDF membranes fabricated via IFRP. Results are shown in Figure 4.19. Obviously, mem-

EBSCOhost - printed on 2/14/2023 6:39 AM via . All use subject to https://www.ebsco.com/terms-of-use

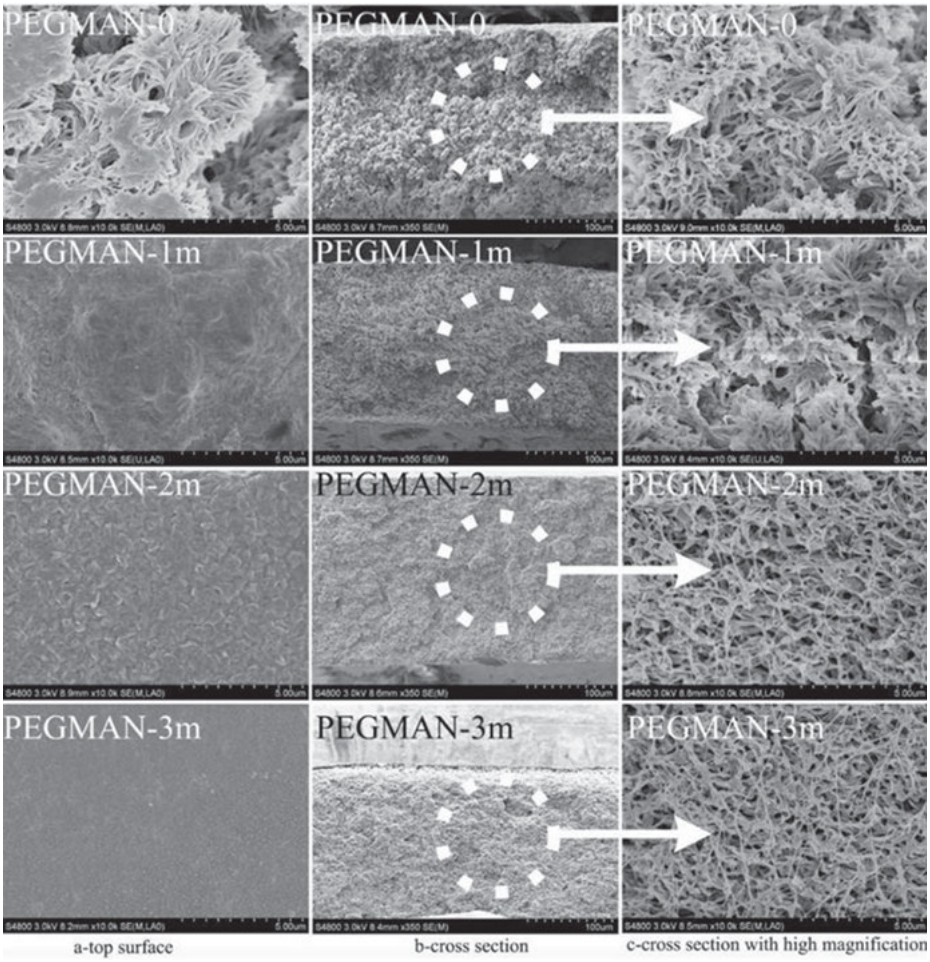

Figure 4.17: FESEM results of various PVDF membranes fabricated without IFRP.

branes fabricated via IFRP have wider diffraction peaks of 18.4–26.6°, and less identifiable peaks could be obtained. The characteristic α phase for PVDF is at $2\theta = 18.4°$ and 26.6°. While the simultaneous presence of α and β (largely in β-phase form) is corresponded to the peak at some overlap around $2\theta = 20°$ [72, 73]. Especially, the crystallinity of unresolved hybridized α and β phase is significant enhanced by IFRP.

J_W, J_B, FRR and porosity are utilized to characterize the filtration properties of resultant PVDF membranes. The J_W, J_B and FRR decrease with addition of monomers. Significant improvement of FRR suggests that these membranes have better protein-resistance. The copolymer prepared via IFRP works as pore-forming additive. This contributes to the flux increase which was due to the dense-packing lotus-shape morphology.

EBSCOhost - printed on 2/14/2023 6:39 AM via . All use subject to https://www.ebsco.com/terms-of-use

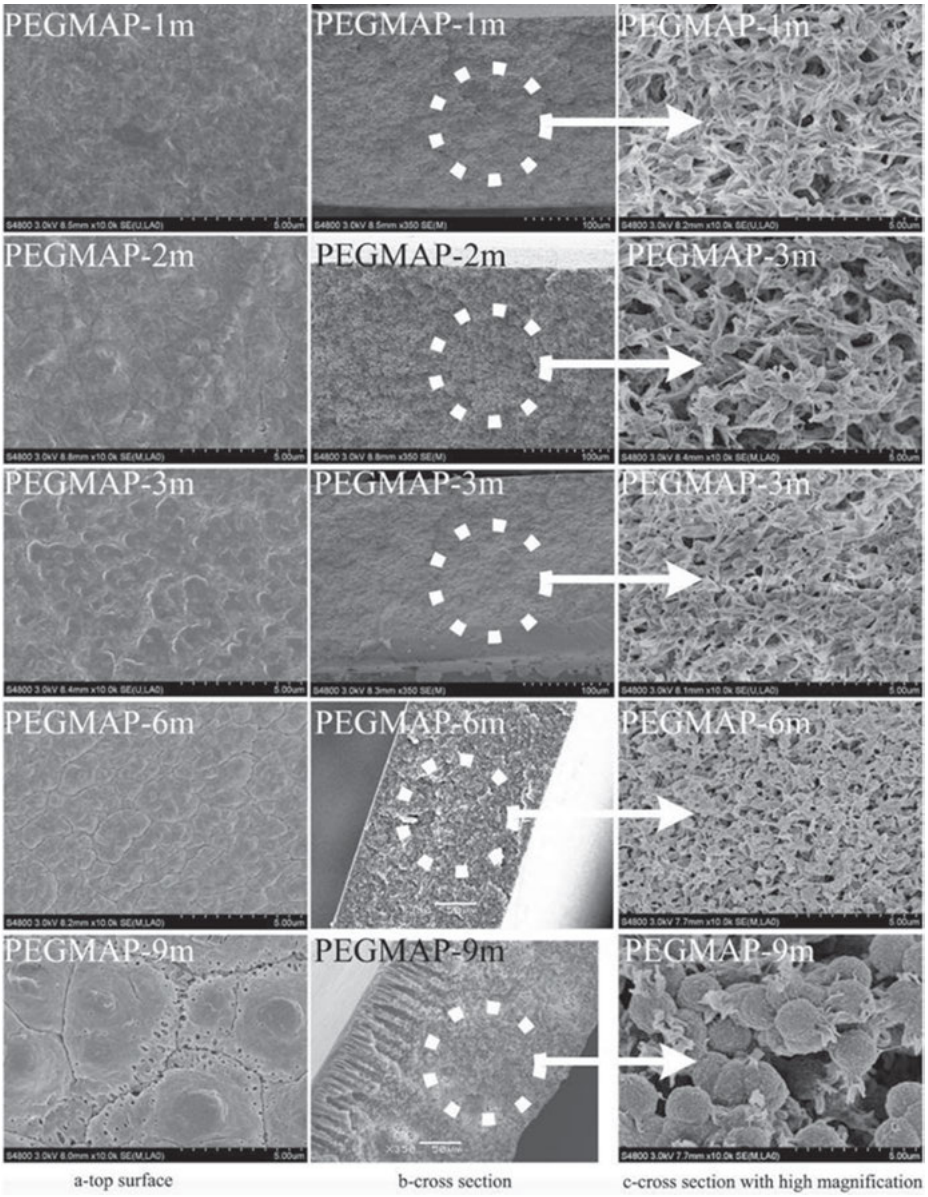

Figure 4.18: FESEM results of various PVDF membranes fabricated via IFRP.

Figure 4.20 shows the curves of cumulative pore size distribution and probability density function of PVDF membranes in terms of μ, σ and MWCO. Results indicate that after IFRP, the MWCO and μ increase, whereas, their corresponding distribution of pore size is narrow. Apparently, after IFRP, μ and MWCO decrease with the increase

EBSCOhost - printed on 2/14/2023 6:39 AM via . All use subject to https://www.ebsco.com/terms-of-use

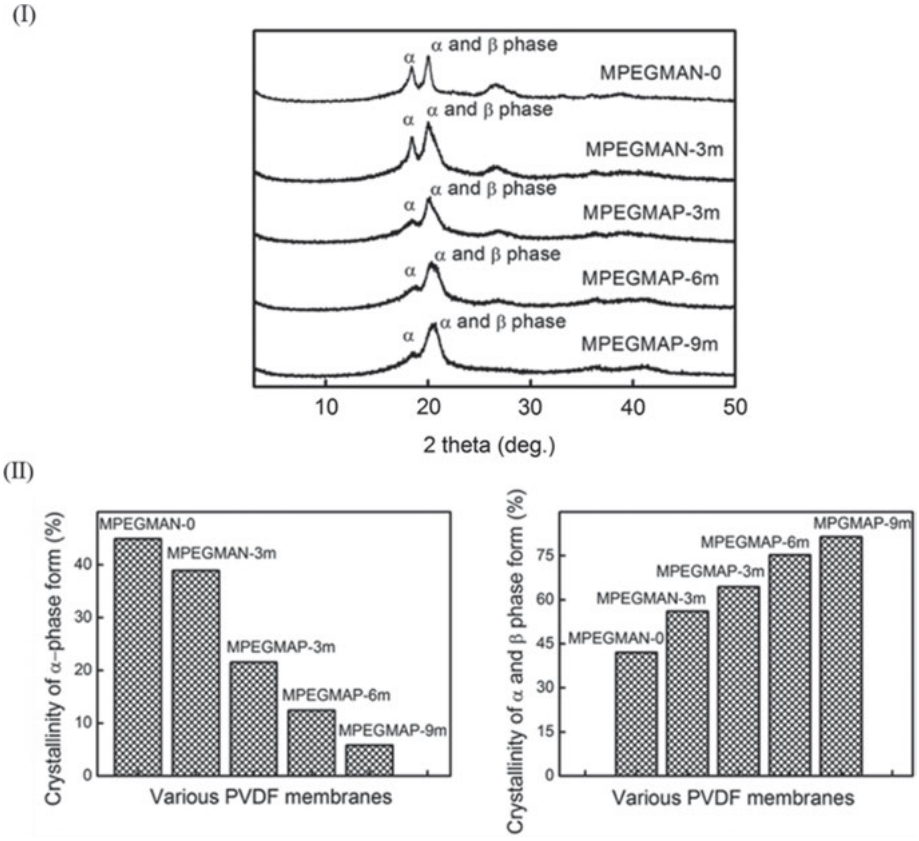

Figure 4.19: XRD analysis (I) and crystallinities (II) of various PVDF membranes fabricated via IFRP.

of monomers content. The reason is that dense-packing lotus-shape type configuration originally occupies those porous structure as the FESEM images shown.

The dynamic contact angle curves reveal that both the top-surface and bottom-surface of PVDF membranes prepared without in-situ polymerization show excellent hydrophobic property. Previous studies illustrated that the configuration of lotus-shape type was beneficial to the hydrophobic improvement [74, 75]. However, lotus-shape type configuration has its hydrophilicity improvement in our current study. Besides, combining with the above filtration properties results, those membranes contact angle doesn't originate in porosity [76]. Nevertheless, it is speculated that the decreasing θs and θ_E is attributed to that the polar head groups of the copolymer have been self-segregated on both surfaces of the membranes [51, 77–79].

EBSCOhost - printed on 2/14/2023 6:39 AM via . All use subject to https://www.ebsco.com/terms-of-use

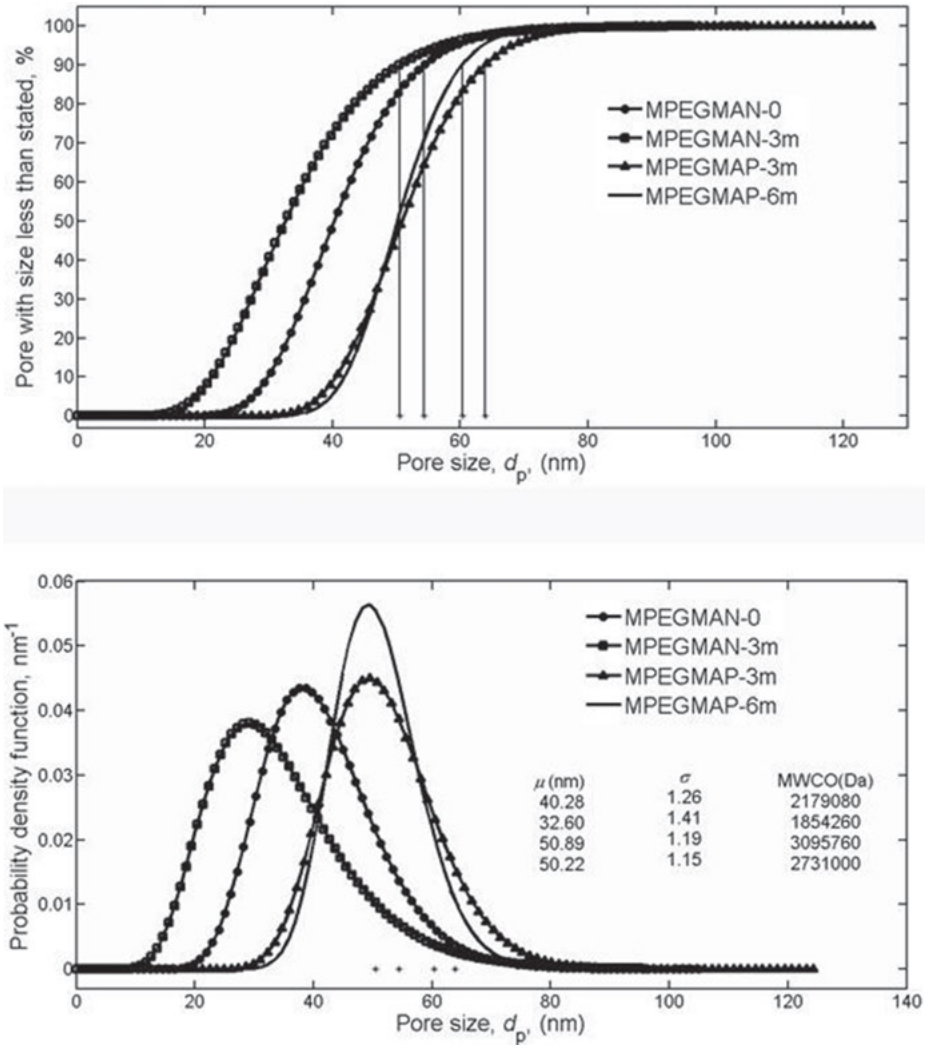

Figure 4.20: Curves of cumulative pore size distribution and probability density function of various PVDF membranes fabricated via IFRP.

4.4 Summary

(1) TiO_2 nanowires were firmly restricted into micro-pores, and difficult to leak out during the permeation process. The existence of interactions between polymers and TiO_2 nanowires was confirmed by thermal stability, mechanical property and XRD analyses. At 5 wt.% TiO_2 nanowire, the hybrid membranes possessed

EBSCOhost - printed on 2/14/2023 6:39 AM via . All use subject to https://www.ebsco.com/terms-of-use

extraordinary elongation ratio, excellent thermal properties and mechanical strength. Because of the presence of hydroxyl groups, hydrophilicity, antifouling performance and permeability of the hybrid membrane improved as the increase of TiO_2 nanowires concentration.

(2) PVDF membranes with good rejection of Dextran and BSA, enhanced mechanical properties and improved PWF could be obtained from PVDF-DMAc-Tween 80-H_2O system. The key parameters of physical-chemical and precipitation kinetics of casting solution, as well as the resultant morphology and mechanical properties of PVDF membranes were influenced by polymer casting compositions (i.e. surfactant, various H_2O concentration) and casting temperatures (i.e. 60 °C and RT). H_2O changed the PVDF-DMAc-Tween 80 system precipitation kinetics and physical-chemical property. H_2O favored the molecules micro-structure adjustment, resulting in the increase of viscosity and decrease of surface tension. The interaction between H_2O and surfactant polar head supplied a balance resistance to interconnection between hydrophobic chains of surfactant and PVDF. This improved the casting solution's thermodynamics stability. Besides, the reverse micelle structure favored the diffusion of H_2O in the solution. This resulted in the precipitation rate increase and insufficient crystallization process of PVDF, especially at 60 °C. All membranes showed finger-like structure with wall structure between macrovoids. Besides, Tween 80 reverse micelles confined the macrovoid structure.

(3) Novel in-situ free radical polymerization (IFRP) method was utilized to fabricate PVDF membranes with superior mechanical properties. DLS and SEM results confirmed the narrow distribution supramolecular aggregates formation between copolymer and PVDF, causing the change of casting solution basic physical-chemical properties in terms of increasing viscosity, accelerating precipitation rate and decreasing surface tension. The micro-structure adjustment of molecules resulted in the formation of dense-packing lotus-shape configuration in top-surface with tune micro-morphology, i.e. PVDF membrane bulk transfers from stripe-shape grains to globules agglomerates. Besides, those membranes with modulate configuration possessed enhanced recovery water flux after filtration experiments with hydrophilicity improvement, bovine serum albumin (BSA) and fine tune filtration properties (MWCO, flux, pore size with narrow distribution and porosity). In addition, the superior mechanical properties were interpreted by the progressive enhanced crystallinity of α and β phase (largely in β-phase form), combining with the globules agglomerates between copolymer and PVDF.

EBSCOhost - printed on 2/14/2023 6:39 AM via . All use subject to https://www.ebsco.com/terms-of-use

References

[1] Chen, W., et al., Efficient wastewater treatment by membranes through constructing tunable antifouling membrane surfaces. Environmental Science and Technology, 2011. 45(15): p. 6545–6552.

[2] Liu, F., et al., Progress in the production and modification of PVDF membranes. Journalof Membrane Science, 2011. 375(1–2): p. 1–27.

[3] Kim, J.H., et al., Phase behavior and mechanism of membrane formation for polyimide/DMSO/water system. Journalof Membrane Science, 2001. 187: p. 47–55.

[4] Machado, P.S.T., Habert, A.C., and Borges, C.P., Membrane formation mechanism based on precipitation kinetics and membrane morphology: flat and hollow fiber polysulfone membranes. Journalof Membrane Science, 1999. 155: p. 171–183.

[5] Buonomenna, M.G., et al., Poly(vinylidene fluoride) membranes by phase inversion: the role the casting and coagulation conditions play in their morphology, crystalline structure and properties. European Polymer Journal, 2007. 43(4): p. 1557–1572.

[6] Loh, C.H., et al., Fabrication of high performance polyethersulfone UF hollow fiber membranes using amphiphilic Pluronic block copolymers as pore-forming additives. Journalof Membrane Science, 2011. 380(1–2): p. 114–123.

[7] Bonyadi, S. and Chung, T.S., Highly porous and macrovoid-free PVDF hollow fiber membranes for membrane distillation by a solvent-dope solution co-extrusion approach. Journalof Membrane Science, 2009. 331(1–2): p. 66–74.

[8] Liu, F., et al., Progress in the production and modification of PVDF membranes. Journalof Membrane Science, 2011. 375(1–2): p. 1–27.

[9] Wang, P., et al., Plasma-induced immobilization of poly(ethylene glycol) onto poly(vinylidene fluoride) microporous membrane. Journalof Membrane Science, 2002. 195: p. 103–114.

[10] Chen, Y., et al., Poly(vinylidene fluoride) with grafted poly(ethylene glycol) side chains via the RAFT-mediated process and pore size control of the copolymer membranes. Macromolecules, 2003. 36(9451–9457).

[11] Akthakul, A., Salinaro, R.F., and Mayes, A.M., Antifouling polymer membranes with subnanometer size selectivity. Macromolecules, 2004. 37: p. 7663–7668.

[12] Liu, X., Peng, Y., and Ji, S., A new method to prepare organic–inorganic hybrid membranes. Desalination, 2008. 221(1–3): p. 376–382.

[13] Meng, J.Q., et al., Surface modification of PVDF membrane via AGET ATRP directly from the membrane surface. Applied Surface Science, 2011. 257: p. 6282–6290.

[14] Sui, Y., et al., Antifouling PVDF ultrafiltration membranes incorporating PVDF-g-PHEMA additive via atom transfer radical graft polymerizations. Journalof Membrane Science, 2012. 413–414: p. 38–47.

[15] Dong, C., et al., Antifouling enhancement of poly(vinylidene fluoride) microfiltration membrane by adding $Mg(OH)_2$ nanoparticles. Journalof Membrane Science, 2012. 387–388: p. 40–47.

[16] Song, H., et al., Natural organic matter removal and flux decline with PEG–TiO_2-doped PVDF membranes by integration of ultrafiltration with photocatalysis. Journalof Membrane Science, 2012. 405–406: p. 48–56.

[17] Zhao, Y.H., et al., Modification of porous poly(vinylidene fluoride) membrane using amphiphilic polymers with different structures in phase inversion process. Journalof Membrane Science, 2008. 310(1–2): p. 567–576.

[18] Zhao, Y.H., et al., Improving hydrophilicity and protein resistance of poly(vinylidene fluoride) membranes by blending with amphiphilic hyperbranched-star polymer. Langmuir, 2007. 23: p. 5779–5786.

EBSCOhost - printed on 2/14/2023 6:39 AM via . All use subject to https://www.ebsco.com/terms-of-use

[19] Hashim, N.A., Liu, F., and Li, K., A simplified method for preparation of hydrophilic PVDF membranes from an amphiphilic graft copolymer. Journalof Membrane Science, 2009. 345(1–2): p. 134–141.
[20] Mansourizadeh, A. and Ismail, A.F., Effect of LiCl concentration in the polymer dope on the structure and performance of hydrophobic PVDF hollow fiber membranes for CO_2 absorption. Chemical Engineering Journal., 2010. 165(3): p. 980–988.
[21] Elashmawi, I.S., Effect of LiCl filler on the structure and morphology of PVDF films. Materials Chemistry and Physics, 2008. 107(1): p. 96–100.
[22] Fontananova, E., et al., Effect of additives in the casting solution on the formation of PVDF membranes. Desalination, 2006. 192(1–3): p. 190–197.
[23] Yan, L., Li, Y.S., and Xiang, C.B., Preparation of poly(vinylidene fluoride)(pvdf) ultrafiltration membrane modified by nano-sized alumina (Al2O3) and its antifouling research. Polymer, 2005. 46(18): p. 7701–7706.
[24] Ma, J., et al., A study on the multifunction of ferrous chloride in the formation of poly(vinylidene fluoride) ultrafiltration membranes. Journalof Membrane Science, 2009. 341(1–2): p. 214–224.
[25] Yuliwati, E. and Ismail, A.F., Effect of additives concentration on the surface properties and performance of PVDF ultrafiltration membranes for refinery produced wastewater treatment. Desalination, 2011. 273(1): p. 226–234.
[26] Hou, D., et al., Fabrication and characterization of hydrophobic PVDF hollow fiber membranes for desalination through direct contact membrane distillation. Separation and Purification Technology, 2009. 69(1): p. 78–86.
[27] Yoo, S.H., et al., Influence of the addition of PVP on the morphology of asymmetric polyimide phase inversion membranes: Effect of PVP molecular weight. Journalof Membrane Science, 2004. 236(1–2): p. 203–207.
[28] Mansourizadeh, A. and Ismail, A.F., Preparation and characterization of porous PVDF hollow fiber membranes for CO_2 absorption: Effect of different non-solvent additives in the polymer dope. International Journal of Greenhouse Gas Control, 2011. 5(4): p. 640–648.
[29] Cao, X., et al., Effect of TiO_2 nanoparticle size on the performance of PVDF membrane. Applied Surface Science, 2006. 253(4): p. 2003–2010.
[30] Yang, Y. and Wang, P., Preparation and characterizations of a new PS/TiO_2 hybrid membranes by sol–gel process. Polymer, 2006. 47(8): p. 2683–2688.
[31] Diebold, U., The surface science of titanium dioxide. Surface Science Reports, 2003. 48: p. 53–229.
[32] Zhong, S.-H., Li, C.-F., and Xiao, X.-F., Preparation and characterization of polyimide–silica hybrid membranes on kieselguhr–mullite supports. Journal of Membrane Science, 2002. 199: p. 53–58.
[33] Damodar, R.A., You, S.J., and Chou, H.H., Study the self cleaning, antibacterial and photocatalytic properties of TiO2 entrapped PVDF membranes. Journal of Hazardous Material, 2009. 172(2–3): p. 1321–1328.
[34] Li, J.-H., et al., Fabrication and characterization of a novel TiO2 nanoparticle self-assembly membrane with improved fouling resistance. Journal of Membrane Science, 2009. 326(2): p. 659–666.
[35] Oh, S.J., Kim, N., and Lee, Y.T., Preparation and characterization of PVDF/TiO2 organic–inorganic composite membranes for fouling resistance improvement. Journal of Membrane Science, 2009. 345(1–2): p. 13–20.
[36] Yu, L.-Y., Shen, H.-M., and Xu, Z.-L., PVDF-TiO2composite hollow fiber ultrafiltration membranes prepared by TiO_2 sol-gel method and blending method. Journal of Applied Polymer Science, 2009. 113(3): p. 1763–1772.

EBSCOhost - printed on 2/14/2023 6:39 AM via . All use subject to https://www.ebsco.com/terms-of-use

[37] Jung, J.H., et al., Creation of novel helical ribbon and double-layered nanotube TiO_2 structures using an organogel template. Chemistry of Materials, 2002. 14: p. 1445–1447.
[38] Kasuga, T., et al., Formation of titanium oxide nanotube. Langmuir, 1998. 14: p. 3160–3163.
[39] Yoshida, R., Suzuki, Y., and Yoshikawa, S., Syntheses of TiO_2(B) nanowires and TiO_2 anatase nanowires by hydrothermal and post-heat treatments. Journal of Solid State Chemistry, 2005. 178(7): p. 2179–2185.
[40] Yuan, Z.-Y. and Su, B.-L., Titanium oxide nanotubes, nanofibers and nanowires. Colloids and Surfaces A: Physicochemical and Engineering Aspects, 2004. 241(1–3): p. 173–183.
[41] Chen, Y., et al., Preparation of a novel TiO_2-based p-n junction nanotube photocatalyst. Environmental Science & Technology, 2005. 39: p. 1201–1208.
[42] Yao, B.D., et al., Formation mechanism of TiO2 nanotubes. Applied Physics Letters, 2003. 82(2): p. 281–283.
[43] Zhang, Y.X., et al., Hydrothermal synthesis and photoluminescence of TiO_2 nanowires. Chemical Physics Letters, 2002. 365: p. 300–304.
[44] Alaoui, O.T., et al., Elaboration and study of poly(vinylidene fluoride)–anatase TiO_2 composite membranes in photocatalytic degradation of dyes. Applied Catalysis A: General, 2009. 358: p. 13–20.
[45] Ji, Z., et al., Dispersion and stability optimization of TiO_2 nanoparticles in cell culture media. Environmental Science & Technology, 2010. 44: p. 7309–7314.
[46] Yu, L.-Y., et al., Preparation and characterization of PVDF–SiO2 composite hollow fiber UF membrane by sol–gel method. Journal of Membrane Science, 2009. 337(1–2): p. 257–265.
[47] Yan, L., et al., Effect of nano-sized Al2O3-particle addition on PVDF ultrafiltration membrane performance. Journal of Membrane Science, 2006. 276(1–2): p. 162–167.
[48] Amirilargani, M., Saljoughi, E., and Mohammadi, T., Improvement of permeation performance of polyethersulfone (PES) ultrafiltration membranes via addition of Tween-20. Journal of Applied Polymer Science, 2010. 115(1): p. 504–513.
[49] Amirilargani, M., Saljoughi, E., and Mohammadi, T., Effects of Tween 80 concentration as a surfactant additive on morphology and permeability of flat sheet polyethersulfone (PES) membranes. Desalination, 2009. 249(2): p. 837–842.
[50] Field, R., Hang, S., and Arnot, T., The influence of surfactant on water flux through microfiltration membranes. Journal of Membrane Science, 1994. 86(3): p. 291–304.
[51] Hester, J.F., Banerjee, P., and Mayes, A.M., Preparation of protein-resistant surfaces on poly(vinylidene fluoride) membranes via surface segregation. Macromolecules, 1999. 32: p. 1643–1650.
[52] Hester, J.F., Olugebefola, S.C., and Mayes, A.M., Preparation of pH-responsive polymer membranes by self-organization. Journalof Membrane Science, 2002. 208: p. 375–388.
[53] Panu, S. and Chung, T.-S., Molecular elucidation of morphology and mechanical properties of PVDF hollow fiber membranes from aspects of phase inversion, crystallization and rheology. Journalof Membrane Science, 2009. 340(1–2): p. 192–205.
[54] Santiago, P.S., et al., Dynamic light scattering and optical absorption spectroscopy study of pH and temperature stabilities of the extracellular hemoglobin of glossoscolex paulistus. Biophysical Journal. 2008. 94(6): p. 2228–2240.
[55] Falcone, R.D., Correa, N.M., and Silber, J.J., On the formation of new reverse micelles: A comparative study of benzene/surfactants/ionic liquids systems using UV–visible absorption spectroscopy and dynamic light scattering. Langmuir, 2009. 25(18): p. 10426–10429.
[56] Ghosh, S., Comparative studies on brij reverse micelles prepared in benzene/surfactant/ethylammonium nitrate systems: Effect of head group size and polarity of the hydrocarbon chain. Journal of Colloid Interface Science, 2011. 360(2): p. 672–680.

EBSCOhost - printed on 2/14/2023 6:39 AM via . All use subject to https://www.ebsco.com/terms-of-use

[57] Cheng, L.P., et al., PVDF membrane formation by diffusion-induced phase separation-morphology prediction based on phase behavior and mass transfer modeling. *Journal of Polymer Science Part B*: *Polymer Physics*, 1999. 37: p. 2079–2092.
[58] Loos, K., et al., Micellar aggregates of amylose-block-polystyrene rod-coil block copolymers in water and THF. Macromolecules, 2005. 38: p. 873–879.
[59] Sukitpaneenit, P. and Chung, T.S., Molecular elucidation of morphology and mechanical properties of PVDF hollow fiber membranes from aspects of phase inversion, crystallization and rheology. Journalof Membrane Science, 2009. 340(1–2): p. 192–205.
[60] Zhang, P.Y., Yang, H., and Xu, Z.L., Preparation of Polyvinylidene Fluoride (PVDF) membranes via nonsolvent induced phase separation process using a tween 80 and H_2O mixture as an additive. Industrial and Engineering Chemical Research, 2012. 51(11): p. 4388–4396.
[61] Hussain, H., et al., Micelle formation of amphiphilic polystyrene-b-poly(N-vinylpyrrolidone) diblock copolymer in methanol and water–methanol binary mixtures. Langmuir, 2009. 25(10): p. 5557–5564.
[62] Shi, F., et al., Preparation and characterization of PVDF/TiO_2 hybrid membranes with ionic liquid modified nano-TiO_2 particles. Journal of Membrane Science, 2013. 427: p. 259–269.
[63] Zhang, P.Y., et al., Preparation and characterization of PVDF-P(PEGMA-r-MMA) ultrafiltration blend membranes via simplified blend method. Desalination, 2013. 319: p. 47–59.
[64] Letchford, K. and Burt, H., A review of the formation and classification of amphiphilic block copolymer nanoparticulate structures: micelles, nanospheres, nanocapsules and polymersomes. European Journal of Pharmacuetics and Biopharmacuetics, 2007. 65(3): p. 259–269.
[65] Zhang, W., et al., A convenient method of tuning amphiphilic block copolymer micellar morphology. Macromolecules, 2004. 37: p. 2551–2555.
[66] Jia, L., et al., Self-assembly of amphiphilic liquid crystal block copolymers containing a cholesteryl mesogen: Effects of block ratio and solvent. Polymer, 2011. 52(12): p. 2565–2575.
[67] Neugebauer, D., Graft copolymers with poly(ethylene oxide) segments. Polymer International, 2007. 56(12): p. 1469–1498.
[68] Law, S.J. and Britton, M.M., Sizing of reverse micelles in microemulsions using NMR measurements of diffusion. Langmuir, 2012: p. 120714104229000.
[69] Petkova, R., Tcholakova, S., and Denkov, N.D., Foaming and foam stability for mixed polymer–surfactant solutions: Effects of surfactant type and polymer charge. Langmuir, 2012. 28(11): p. 4996–5009.
[70] Amirilargani, M., Saljoughi, E., and Mohammadi, T., Improvement of permeation performance of polyethersulfone (PES) ultrafiltration membranes via addition of Tween-20. Journal of Applied Polymer Science, 2010. 115(1): p. 504–513.
[71] Lin, D.J., et al., Fine Structure and formation mechanism of particulate phase-inversion poly (vinylidene fluoride) membranes. *Journal of Polymer Science Part B*: *Polymer Physics*, 2003: p. 1578–1588.
[72] Buonomenna, M.G., et al., Poly(vinylidene fluoride) membranes by phase inversion: the role the casting and coagulation conditions play in their morphology, crystalline structure and properties. European Polymer Journal, 2007. 43(4): p. 1557–1572.
[73] Lund, A., et al., Enhancement of β phase crystals formation with the use of nanofillers in PVDF films and fibres. Composites Science and Technology., 2011. 71(2): p. 222–229.
[74] Teshima, K., et al., Ultra-Water-Repellent Poly(ethylene terephthalate) Substrates. Langmuir, 2003. 19: p. 10624–10627.
[75] Li, Q., Xu, Z.L., and Liu, M., Preparation and characterization of PVDF microporous membrane with highly hydrophobic surface. Polymers of Advanced Technologies, 2009. 22(5): p. 520–531.
[76] Yang, Q., et al., Surface Modification of polypropylene microporous membranes with a novel glycopolymer. Chemistry of Materials, 2005. 17: p. 3050–3058.

EBSCOhost - printed on 2/14/2023 6:39 AM via . All use subject to https://www.ebsco.com/terms-of-use

[77] Hester, J.F., et al., ATRP of Amphiphilic graft copolymers based on PVDF and their use as membrane additives. Macromolecules, 2002. 35(20): p. 7652–7661.
[78] Hester, J.F. and Mayes, A.M., Design and performance of foul-resistant poly(vinylidene fluoride) membranes prepared in a single-step by surface segregation. Journal of Membrane Science, 2002. 202: p. 119–135.
[79] Hester, J.F., Olugebefola, S.C., and Mayes, A.M., Preparation of pH-responsive polymer membranes by self-organization. Journal of Membrane Science, 2002. 208: p. 375–388.

EBSCOhost - printed on 2/14/2023 6:39 AM via . All use subject to https://www.ebsco.com/terms-of-use

EBSCOhost - printed on 2/14/2023 6:39 AM via . All use subject to https://www.ebsco.com/terms-of-use

Tian Li, Junxia Liu, Bingzhi Dong

Chapter 5
The Influence of Pretreatment on Low-pressure Membrane Filtration Performance

The membrane separation technology with different pore sizes for contaminant removal in water treatment started in the 1970s and developed rapidly in the 1990s. Membrane fouling is the deposition of foulants on the membrane surface or in the pores which can decrease the permeate flux or increase the trans-membrane pressure. Thus membrane fouling is the "bottleneck" for its application expansion. The methods to control membrane fouling have attracted great attention in the area of water treatment [1, 2]. Generally, the membrane fouling mechanisms include pore clogging, contaminant adsorption, gel layer formation, concentration polarization and cake layer deposition [3, 4]. The membrane fouling can also be categorized to organic fouling, inorganic fouling and microbial contamination according to the fouling substances [5]. In surface water treatment, natural organic matter (NOM) is regarded as the main membrane fouling, which is a complex of organic substance consisting of colloidal polysaccharide, humic acid, fatty acids, proteins, etc. [6–8]. Membrane fouling induced by NOM cannot be completely eliminated through only physical scrub such as air/water cleaning, and normally chemical cleaning or pretreatment process is demanded to maintain a long-term stable operation for the membranes.

Many researchers studied the different components of organics, and found that the hydrophilicity/hydrophobicity of organic matters played a key role in membrane filtration performance [9, 10]. Lim et al. summarized organic compounds assigned to a particular fraction according to their chain length and functional groups [11] (adopted from Buchanan et al. [12]). Carroll et al. found that the neutral hydrophilic organics from surface water mainly induced the microfiltration fouling [13]. Fan et al. studied three types of surface water in Australia, and found that the hydrophilicity/hydrophobicity affected the membrane fouling significantly, with the order of neutral hydrophilic fraction > strong hydrophobic fraction > weakly hydrophobic fraction > charged hydrophilic fraction [14]. Differently, Gray et al. found that the neutral hydrophilic organics and charged hydrophilic organics in a lake in Australia could form a gel layer on the surface of microfiltration membrane and induced rapid flux decline, while the hydrophobic component could only cause a slow flux decline [15]. Chen et al. found the hydrophilic

Tian Li, Bingzhi Dong, College of Environmental Science and Engineering, Tongji University, Shanghai, P. R. China
Junxia Liu, School of Civil and Transportation Engineering, Guangdong University of Technology, Guangzhou, Guangdong, P. R. China

https://doi.org/10.1515/9783110596847-005

EBSCOhost - printed on 2/14/2023 6:39 AM via . All use subject to https://www.ebsco.com/terms-of-use

organics from river water only caused a slow flux decrease of ultrafiltration membrane, while the hydrophobic organics of macromolecules caused sharp flux decline [16]. The membrane surface parameters, such as hydrophobicity, charge, morphology, roughness, etc. can be critical to the membrane fouling mechanism, which, in turn, could affect the permeate quality and performance [17, 18]. In addition, it was also indicated that the membrane surface charge could be influenced significantly by the types of cleaning agents and membranes. Studies of both zeta potential and flux behavior suggested that for very rough membranes the impact of surface charge became negligible, thereby not playing any effect in subsequent membrane filtration performance [19].

The molecular size of organics had a significant effect on membrane filtration performance. In accordance with the mechanical sieving principle of membrane filtration, organics with relative molecular weight larger than the membrane pore size could block the membrane pores, leading to the membrane flux drop; while organics with relative molecular weight lower than the membrane pore size can enter the membrane pores, which also affected the membrane filtration behavior. Therefore, the molecular weight of organics is an important factor in membrane fouling studies. Lankes et al. discovered that organics with relative large molecular weight, e.g. polysaccharides or long-chain aliphatic substances, can be retained by the membranes easily, while aromatic organics with relative medium molecular weight, e.g. lignin or tannic acid, can pass the membranes easily [20]. It was observed that colloidal and hydrophilic organic macromolecules with molecular weight larger than 10 kDa from algae metabolism induced the most severe low-pressure membrane fouling among different hydrophilic and hydrophobic materials [18, 21]. Fan et al. also found that organics with macromolecules with molecular weight higher than 30 kDa produced rapid membrane flux drop [14]. However, some researchers reported that small organic molecules with molecular weight lower than 3 kDa could also induce severe membrane fouling phenomenon [22]. The influence of micro-molecules on the membrane flux behavior was usually subjected to their chemical properties. The effect of neutral hydrophilic organics with micro-molecules on membrane fouling was often greater than other small hydrophobic molecules [13] with the removal due to the interaction force with small organic molecules rather than the physical sieving principle [23]. With the pore size of the low-pressure membrane at the micron level, the molecular sizes of dissolved organic matter were much smaller than the membrane pore size, thus the fouling performance of low pressure membranes induced from the synthesis effect of macro and small organic molecules was significantly affected by the interactions between the molecules and the membrane pores [24]. Studies of effect of MW distribution on the reversible and irreversible fouling of submerged ultrafiltration membranes of natural water also showed that the hydrophilic fractions with lower MW were preferentially transmitted through the membrane pores, due to the hydrophilic fractions of the NOM being smaller than the hydrophobic ones [25], and different MW components exhibited different fouling tendencies. Thus, molecular size was the most fundamental parameter in membrane fouling studies.

EBSCOhost - printed on 2/14/2023 6:39 AM via . All use subject to https://www.ebsco.com/terms-of-use

The low-pressure membranes normally have relatively large pores, leading to undesirable removal efficiencies of NOM and disqualified effluent. Meanwhile, pollutants in influent can cause severe membrane flux decline. Frequent membrane cleaning increased operation costs. Thus, a suitable pre-treatment process before membrane filtration can not only improve the operation efficiencies of the whole system, but also reduce membrane fouling and cleaning frequencies, as well as prolong membrane life time. The conventional pretreatment methods include coagulation, activated carbon adsorption, ozonation, etc. These methods can avoid the fast accumulation of contaminants on the membrane surface through changing their interactions.

The coagulation-sedimentation process is a traditional and useful pre-treatment technology, widely applied in the area of water treatment owing to its low cost and easy operation. With this technology, the turbidity can be greatly reduced, but the organic matter removal is limited. In addition, the hydrophobic macromolecules have high removal efficiencies, while the micro organics with large solubility cannot be removed effectively with this process. There are mainly two types of pre-coagulation methods, i.e. standard coagulation and online coagulation. The online coagulation refers to the operation that coagulants are directly dosed in the influent before membrane filtration without sedimentation. The coagulation is widely used in water treatment as a pre-treatment method. Liang et al. studied three pretreatment methods using coagulation, coagulation-sedimentation, and coagulation-sedimentation-ultrafiltration for algae-abundant reservoir water treatment, and they found that the coagulation-sedimentation had the highest treatment efficiency [26]. Chen et al. suggested that online coagulation could generate a cake layer on the membrane surface, which was effective for the natural organics removal and effluent quality improvement [16]. Li et al. obtained that the removal efficiencies of DOC and UV_{254} by ultrafiltration could be greatly improved with online coagulation as pretreatment [10]. The studies from Kimura et al. indicated that the pre-coagulation/sedimentation could not remove the irreversible membrane fouling induced by the macromolecular organics, such as polysaccharides and proteins [27]. Moreover, Gao et al. suggested that the types of coagulants and the dosing conditions shall be properly chosen based on the influent quality to obtain a suitable removal efficiency [5].

The combination of powdered activated carbon (PAC) and low pressure membrane filtration has been regarded as the “crystal technology” in water treatment. The main function of PAC is to improve pollutant removals in the influent through its adsorption. Similar as the pretreatment of coagulation, the cake layer formed with PAC on the membrane surface can also facilitate the filtration efficiency. It is suggested that PAC could alter the structure of cake layer rather than eliminate the pollutants to reduce membrane fouling [28, 29]. However, the PAC absorption was able to just slightly reduce the membrane filtration resistance due to that only a small part of soluble organic substances with low molecular weight could be removed, while the macromolecular organic matter that affected the filtration flux was seldom eliminated [30, 31]. Suzuki et al. examined the performance of the composite MF system with

EBSCOhost - printed on 2/14/2023 6:39 AM via . All use subject to https://www.ebsco.com/terms-of-use

different sizes and concentrations of PAC. They found that PAC could help improve the filtration behavior and they attributed to that PAC could adsorb both macromolecular and low molecular weight compounds [32]. Gai et al. investigated the long term operation of microfiltration for around 50 days. They discovered that the addition of PAC could reduce the trans-membrane pressure significantly as compared without PAC dosing [33]. In addition, Ma et al. found that chemical irreversible membrane fouling in a membrane bioreactor (MBR) was reduced when the dosage of PAC was increased [34]. However, some opposite results were also obtained from the studies with PAC as pretreatment. Lin et al. examined the effect of humus on ultrafiltration and found that the effluent volume was reduced with PAC as the pre-treatment due to severe membrane fouling induced [35]. Li et al. drew the similar conclusion that PAC could mainly adsorb non-pollutants for the membrane, so that the rest would bring more severe fouling [22]. Da Silva et al. used the obtained fluxes, filtrating water artificially contaminated with E. coli as the influent, and found that the coupling of granular activated carbon (GAC) treatment with membrane filtration could obtain a higher initial flux with GAC pretreatment working with a clean membrane and the addition of GAC could also decrease the membrane fouling [36]. Park et al. [37] and Milovic et al. [38] employed the gram-positive bacterium Staphylococcus aureus to investigate the bactericidal effect of the coatings and chose the microbicidal surface coatings based on immobilized hydrophobic polycations. In addition, they proved that the S. aureus organism had been suitable for demonstrating the damage of cell membranes and the killing of cells (loss of culturability) upon contact with bactericidal surfaces [37, 38].

The molecular weight distribution of organic substances in the influent has a significant influence on membrane filtration performance. Ozone is a strong oxidant that can preferentially oxidize electron rich moieties with double carbon bonds and aromatic alcohols [39]. It could revise the molecular weight distributions of organics in the feed [40]. With ozone oxidation, macromolecular organics could be oxidized to small molecules or even to inorganic molecules, which could further reduce the membrane fouling. You et al. studied the combination of ozonation and membrane filtration, and they observed that the substances adhered to the membrane surface could be oxidized by the ozone, thus the membrane fouling could be relieved [41]. Oh et al. found that after ozone oxidation, the degree of fouling reduction was much higher than the concentration difference of organic substances [42]. Thus, they suggested that the organic matter reduction by ozonation might not be the only factor for membrane fouling alleviation, while the mechanisms of organic fouling degradation and membrane flux enhancement by ozonation were still not clear, since the oxidization of ozone was so strong that the membrane module could be corroded as well. However, it was undoubtedly that ozonation played a positive character in lowering the organic substance and membrane fouling [42]. The studies from De Velasquez et al. using ozonation for the dissolved organic matter (DOM) removal from a secondary effluent also confirmed that ozonation could effectively reduce ultrafiltration membrane fouling and improve effluent quality [39].

EBSCOhost - printed on 2/14/2023 6:39 AM via . All use subject to https://www.ebsco.com/terms-of-use

Inclusive the pre-treatment methods mentioned above, there are some other methods, such as MIEX resin exchange, biological treatment, and integrated pre-treatment processes to reduce fouling and enhance membrane filtration performance. MIEX resins can remove the ions in the influent through ion exchange, and they also reduce the low molecular organic substances, which was more effective than coagulation for fouling control [43]. Studies indicated that the MIEX resin pre-treatment was effective for DOC removal, but less effective to reduce short-term membrane fouling or to remove viruses or biological fouling [43], where the extracellular polymeric substances (EPS) had been regarded as the major formation [44] and an optimal concentration of bio-carrier could effectively control irreversible membrane fouling [34]. Khan et al. had quantified and demonstrated the hybrid PAC-MF MBR as a sustainable technology for treating river water [45]. Moreover, Jeong et al. employed a submerged membrane adsorption bioreactor (SMABR) as a pretreatment in seawater reverse osmosis (RO) desalination for biofouling control, and they discovered that the SMABR was a sustainable biological pretreatment for RO even with only a small amount of PAC [46]. In addition, integrated pretreatments were designed and implemented in different types of industries to treat diverse sources of water to take the advantage of each process, e.g. the combination processes of UF and RO [47], MBR-RO process [48], integrated UF-NF [10], the hybrid MF-NF-RO system [49] and MBR-RO-AOP [50] etc. Furthermore, the combined advanced oxidation and coagulation could also be a useful method for UF pre-treatment, which had been confirmed in the study from Tian et al. applying low dosage of $FeCl_3$ coagulation and $KMnO_4$ for UF membrane fouling control [51].

Although these pretreatment methods have been applied in potable water treatment and their implementations have made an effect, the fact of membrane fouling and flux drop in long-term operation still exists and constrains the development of membrane technology for large-scale applications. Based on the characteristics and abilities of the pretreatment methods and the related chemicals used, it should be highlighted that proper pretreatment methods can be considered before their real applications, which shall be described in the following. (1) The coagulation pretreatment can remarkably improve the permeate flux, reduce reversible fouling, lower the contents of colloids and NOM, however, no obvious removal of small molecule organics could occur and the dosage of coagulants need to be tested before using. (2) The adsorption pretreatment could enhance the filtration flux and remove the majority of small molecules, while the absorbents, i.e. PAC, might also aggravate membrane fouling. They exist in the influent and are difficult to be eliminated, moreover, they have a poor removal efficiency for macromolecular substances. However, the PAC adsorption is still active and popular in the water treatment industry at present. (3) The oxidation pretreatment could strengthen the permeate flux, lower the concentration of organic matters in the influent and reduce the possibility of biological contamination, nevertheless, the byproducts (such as halide acetate and trihalomethanes) might be formed and the membranes could be oxidized as well in the oxidation.

EBSCOhost - printed on 2/14/2023 6:39 AM via . All use subject to https://www.ebsco.com/terms-of-use

The combination of membrane technology and pretreatment processes are still immature. Research on novel technologies to control membrane fouling, to realize real-time monitoring, and to optimize operation shall be the key direction for water treatment in a period of time. In addition, the high operation cost of the membrane separation technology is a main constraint for its application, which should be given full consideration when appropriate pretreatment method is utilized. And finally, the membrane life time span and the frequency of membrane cleaning and replacement need to be taken into consideration before proper pretreatment applications are implemented, since multiple novel hybrid pretreatment processes have been emerged for water purification technologies in drinking water, municipal wastewater, recycled water, and sea-water treatment.

5.1 Coagulation pretreatment

5.1.1 The effect of coagulant dosages and types on membrane fouling control

5.1.1.1 Experimental setup and methodology

The influent used in the experiment was taken from Taihu Lake, with the quality shown in Table 5.1.

Table 5.1: The influent quality in the experiment.

Parameters	Values	Average value
Turbidity (NTU)	4.21–15.4	7.96
DOC (mg/L)	2.763–4.25	3.3
UV_{254} (cm^{-1})	0.063–0.072	0.065
pH	7.5–8.19	7.79

The experimental setup is shown in Figure 5.1. Microfiltration hollow fiber membranes, made of polyvinylidene fluoride (PVDF) from DOW company was used in this study. The membranes had a pore size of 0.03 μm and an outer diameter of 1.30 mm. The membrane module consisted of 16 fibres, with a length of 40 cm and a total surface area of 0.003 m^2. The outside-inside operation was adopted, with a flux of 60 $L/(h \cdot m^2)$ and a total filtration duration of 180 min in each experiment. The transmembrane pressure (TMP) was monitored with a pressure gauge and was recorded automatedly every 30 s.

EBSCOhost - printed on 2/14/2023 6:39 AM via . All use subject to https://www.ebsco.com/terms-of-use

The coagulants of AC (with an effective content more than 28%) and $FeCl_3$ (with an effective content more than 97%) were dosed in the influent. The mixture was first mixed at a fast rotation speed of 300 r/min for 1 min, then at a medium rotation speed of 100 r/min for also 1 min, and finally at a slow rotation speed of 50 r/min for 10 min. After the mixing, the mixture was put aside for 10 min, then the supernatant was collected for analysis.

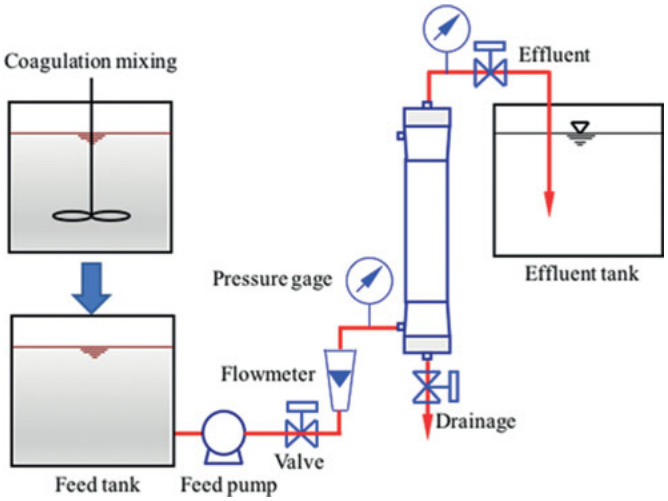

Figure 5.1: Schematic diagram of the experimental setup.

5.1.1.2 Results and discussion

1 Organics removal

The result of organics removal of DOC and UV_{254} is presented in Figure 5.2. With only the MF membranes, the DOC and UV_{254} removal rates were 25.5% and 7.8%, respectively. With the additional alum and ferric salt, the organics removal efficiencies were higher, suggesting that coagulation enhanced the organics removal. With the increase of dosages of coagulants, the DOC removal decreased first then increased, while the UV_{254} removal increased all the time. In addition, the ferric salt had a higher DOC removal, e.g. when the dosage was 100 mg/L, the removal efficiencies were around 57% and 44% by the ferric salt and by the alum, respectively. The ferric salt had a higher UV_{254} removal rate than the alum when the dosage concentration was over 30 mg/L. And with the increase of the coagulant concentration, the increase of UV_{254} removal rate was much faster than the alum, e.g. when the dosage concentration was at 30 mg/L, the removal rate was similar around 30%, and when the dosage concentration increased to 100 mg/L, the UV_{254} removal efficiencies were around 55% and 38% by the ferric salt and by the alum, respectively.

EBSCOhost - printed on 2/14/2023 6:39 AM via . All use subject to https://www.ebsco.com/terms-of-use

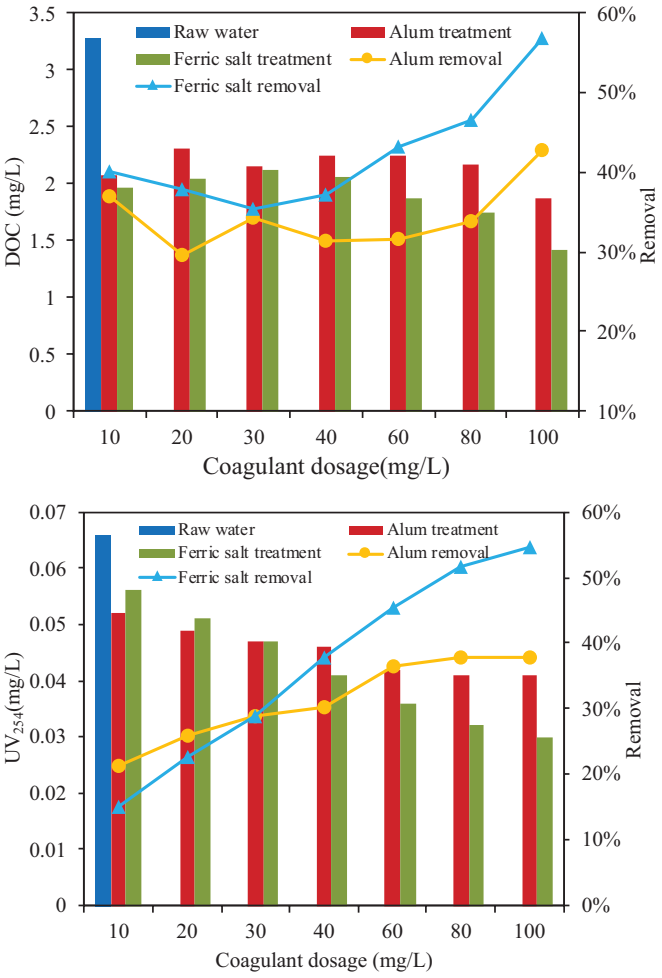

Figure 5.2: The effect of organics removal by coagulation with alum and ferric salt.

2 Membrane filtration performance

The TMP values for the membrane filtration with different dosages of coagulants of alum and ferric salt are exhibited in Figures 5.3 and 5.4, respectively. Without coagulation, the TMP increased fast to above 80 kPa for 180 min filtration. With coagulation, the TMP increased slowly, e.g. with 10 mg/L alum and ferric salt, the TMP values were 27 and 40 kPa, respectively, at the end of the filtration. In addition, it could be observed that with the increase of alum concentration from 10 to 100 mg/L, the final TMP reduced significantly at the end of the filtration, while it first reduced when the ferric salt concentration increased from 10 to 80 mg/L, then increased slightly when the ferric salt dosage further increased to 100 mg/L. For a same dosage, the TMP value was lower induced by alum than by ferric salt, indicating that the alum coagulation

EBSCOhost - printed on 2/14/2023 6:39 AM via . All use subject to https://www.ebsco.com/terms-of-use

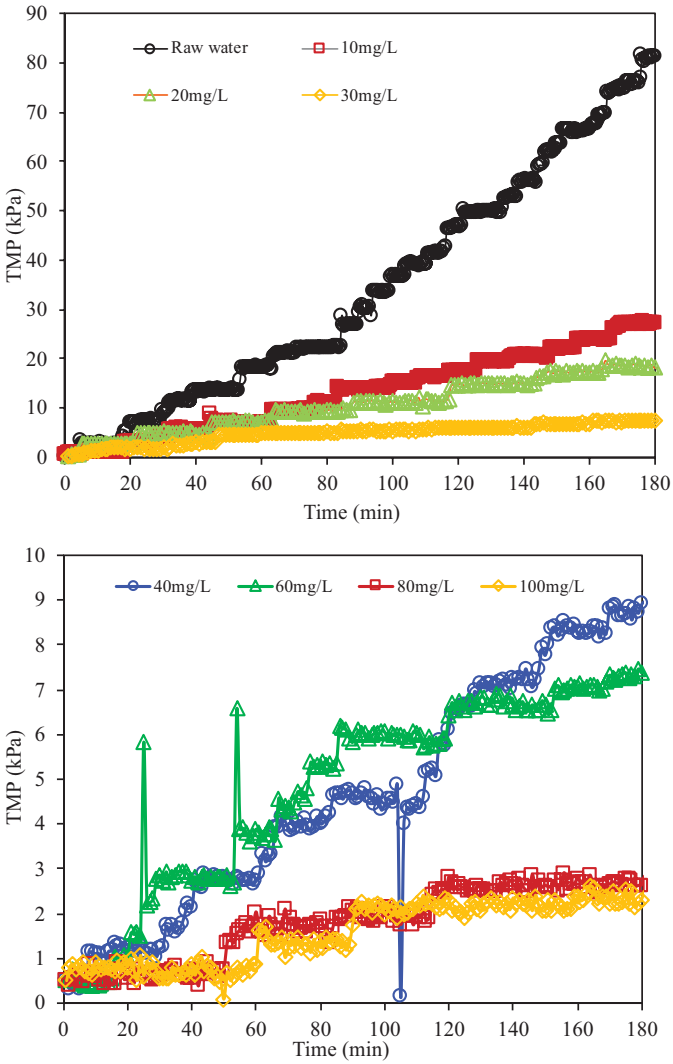

Figure 5.3: The effect of alum dosages on TMP performance.

was more efficient than the ferric salt in terms of membrane fouling control of Taihu Lake water. Furthermore, when the dosage was over 40 mg/L, the final TMP was all below 10 kPa for both coagulants, suggesting that the dosage of 40 mg/L was effective to maintain a relative clean membrane.

3 Molecular weight distribution

The MW distribution of organics in Taihu Lake before and after the MF filtration with both DOC and UV_{254} detection is shown in Figure 5.5. There were three response peaks

EBSCOhost - printed on 2/14/2023 6:39 AM via . All use subject to https://www.ebsco.com/terms-of-use

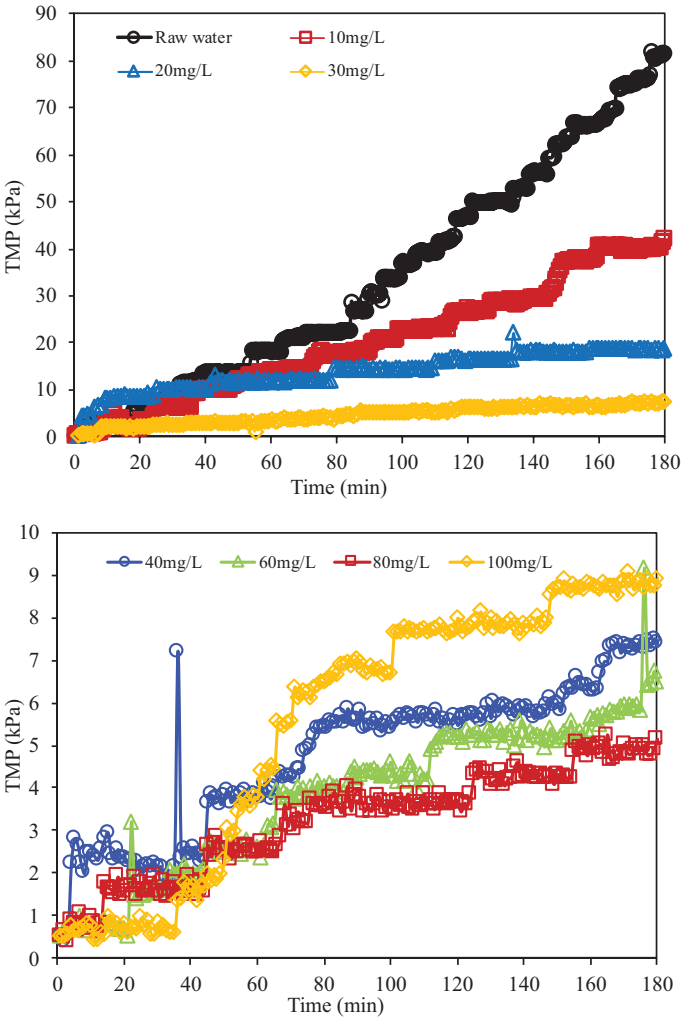

Figure 5.4: The effect of ferric salt dosages on TMP performance.

for the DOC detection, i.e. 100,000 Da, 2,300 Da and 1,000 Da, representing large, medium and small organic molecules, respectively. While there were two response peaks for the UV_{254} detection, representing MW of 3,000 Da and 1,000 Da, respectively. The peak at 1,000 Da with UV_{254} detection showed weaker response than that of DOC detection, while the 3,000 Da showed stronger response, suggesting that large and small organics in Taihu Lake were composed of hydrophilic substances, and medium organics were hydrophobic.

After UF, the response of 100,000 Da in DOC detection disappeared, while the one of 1,000 Da was slightly reduced, indicating that all large organic substances and part of small organic molecules were removed. However, in the UV_{254} detection, the

EBSCOhost - printed on 2/14/2023 6:39 AM via . All use subject to https://www.ebsco.com/terms-of-use

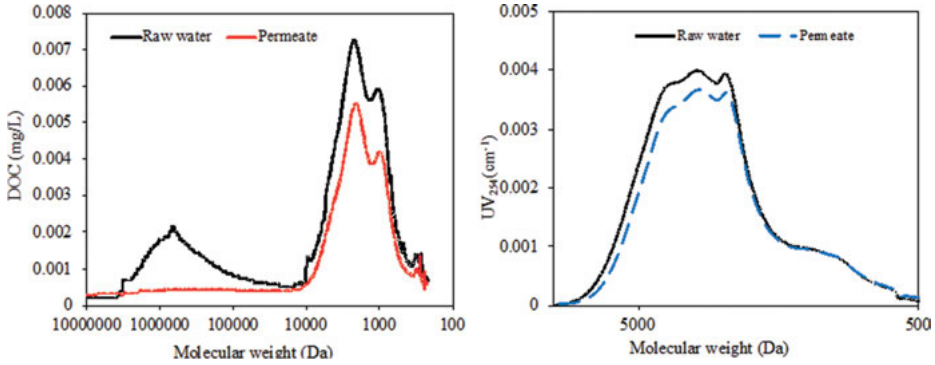

Figure 5.5: The molecular weight distribution before and after membrane filtration.

response in the permeate dropped only slightly, which might be due to that the influent was mainly composed of the medium organics, with the size much smaller than the membrane pore size to pass the membranes. While the large organics had size greater than the membrane pores, thus they were retained by the membranes. It could be also found that the peak response of the medium and small molecules in the permeate in both detection methods was comparable to that in the influent, indicating that the MF had a poor removal of these organic substances.

The MW distribution results of the organics after different dosages of alum and ferric salt with DOC and UV_{254} detections are shown in Figures 5.6 and 5.7. With 10 mg/L coagulant, the response peak of large organics almost disappeared, suggesting that just a little dosage was effective to remove large organics. With the reduction of large molecules, the TMP could decrease significantly. When the dosage was increased, the response peaks of small organics dropped further, with the ones induced by the ferric salt lower than that by alum. This phenomenon demonstrated that the ferric salt was more effective than the alum for small organics removal. In addition, it could be also observed that the response peaks for the medium organics remained similar as that in the influent, suggesting that coagulation removed medium organic substances poorly regardless the types of coagulants and dosages.

The MW distribution results of the Taihu Lake in the influent, after coagulation and in the membrane permeate with 5 and 10 mg/L alum and ferric salt are further plotted in Figures 5.8–5.10. These results demonstrated that when the concentrations of coagulants were low, the coagulation had a poorer organic removal than the MF membrane filtration, with the dosages of the coagulants increased, it had a comparable performance on the organic removal as the MF membranes.

EBSCOhost - printed on 2/14/2023 6:39 AM via . All use subject to https://www.ebsco.com/terms-of-use

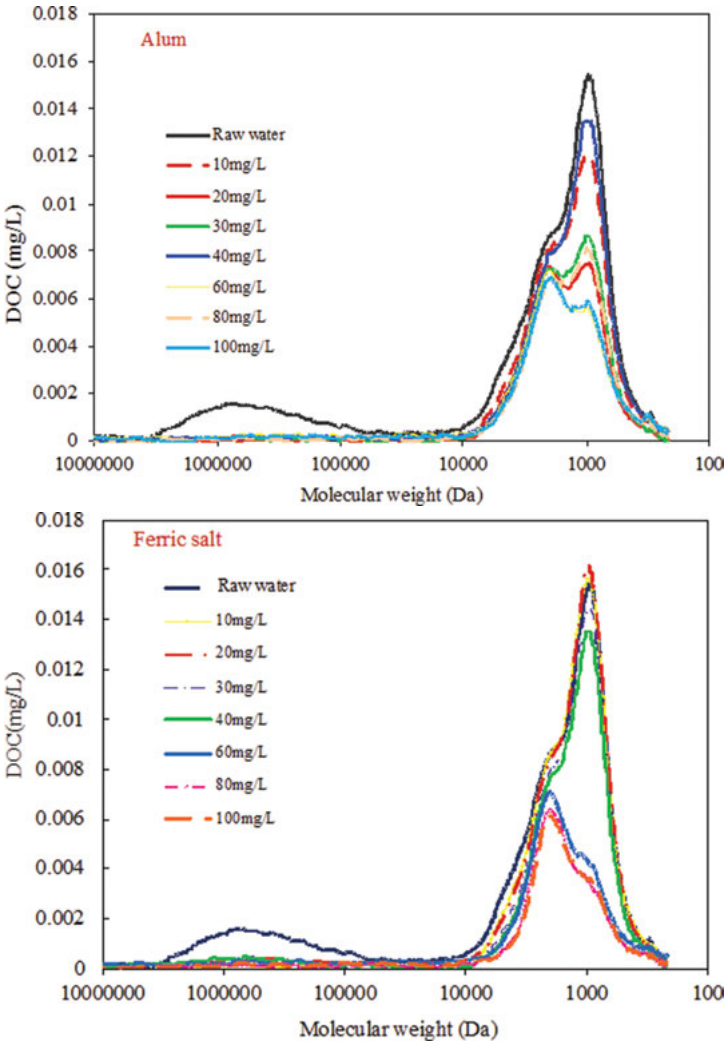

Figure 5.6: The effect of alum and ferric salt dosages on molecular weight distribution with DOC detection.

5.1.2 Foulant analysis in the coagulation-microfiltration process

A pilot scale of coagulation-microfiltration was operated for Taihu Lake water treatment. The main purpose is to understand the reversible and irreversible fouling in the hybrid process. A lot of analyisis methods were used, such as molecular weight distribution, HPSEC and fluorescence excitation-emission matrix (EEM) spectroscopy, etc.

EBSCOhost - printed on 2/14/2023 6:39 AM via . All use subject to https://www.ebsco.com/terms-of-use

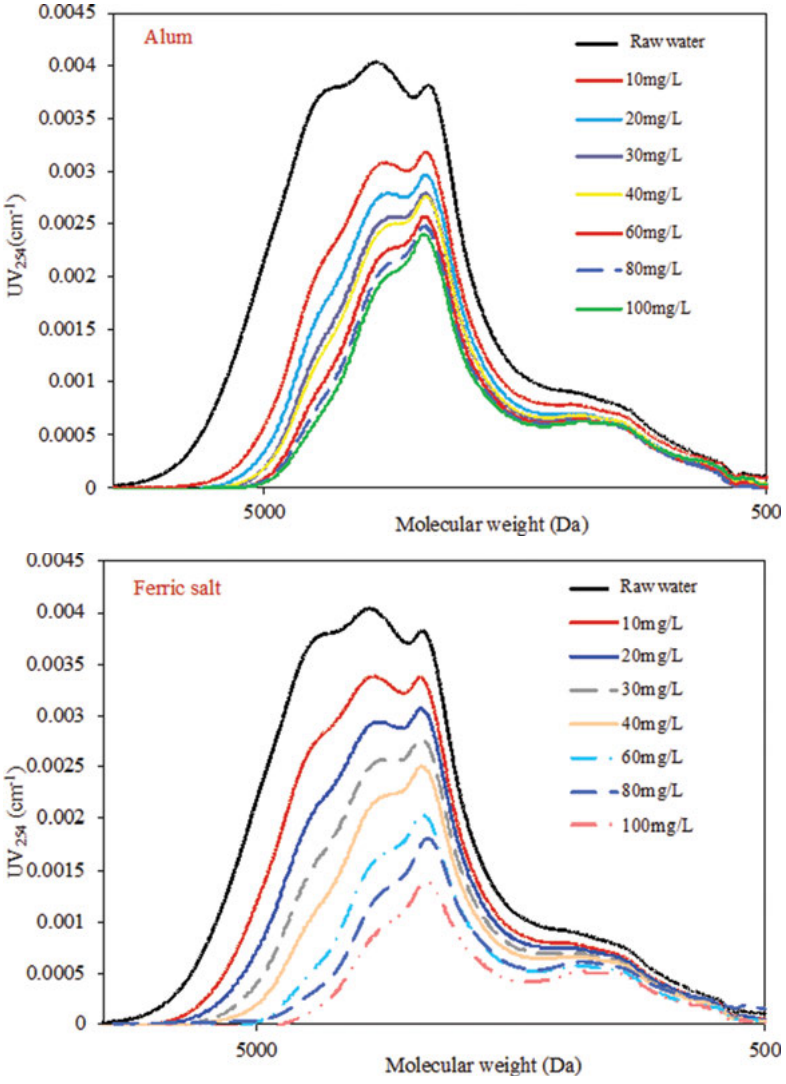

Figure 5.7: The effect of alum and ferric salt dosages on molecular weight distribution with UV_{254} detection.

5.1.2.1 Materials and methodology

1 Feed water

The feed water for the pilot test was from Taihu Lake with the influent quality shown in Table 5.2.

EBSCOhost - printed on 2/14/2023 6:39 AM via . All use subject to https://www.ebsco.com/terms-of-use

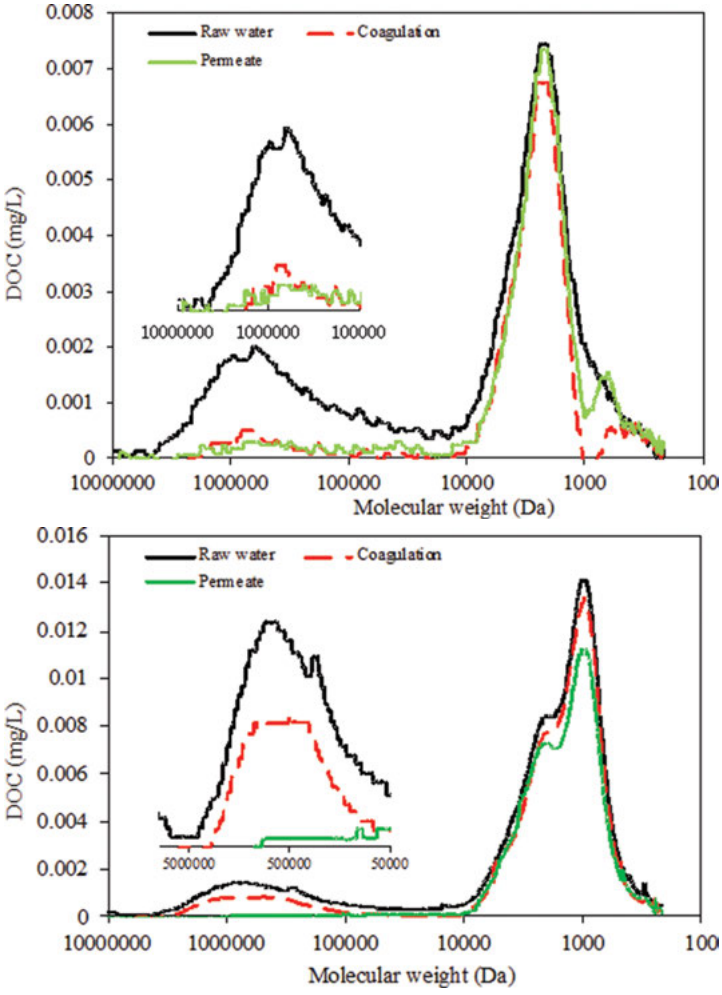

Figure 5.8: The influence of 5 mg/L alum and ferric salt on MW distribution.

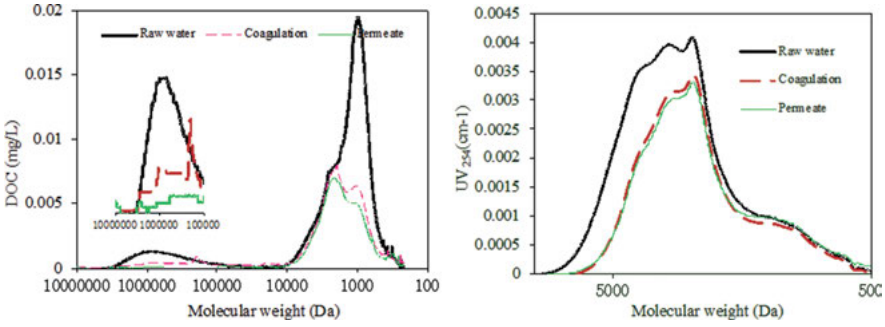

Figure 5.9: The influence of 10 mg/L alum on MW distribution.

EBSCOhost - printed on 2/14/2023 6:39 AM via . All use subject to https://www.ebsco.com/terms-of-use

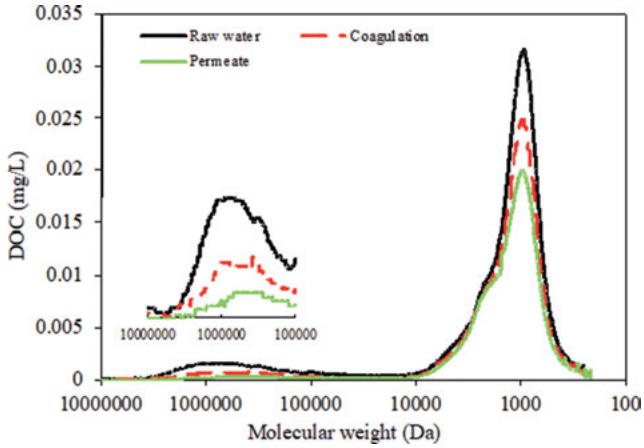

Figure 5.10: The influence of 10 mg/L ferric salt on MW distribution.

Table 5.2: The influent quality in the pilot test.

Parameters	Values	Average value
Temperature (°C)	12.1–33.4	22
Turbidity (NTU)	29.3–84.2	48.7
COD_{Mn} (mg/L)	4.56–8.82	5.86
UV_{254} (cm^{-1})	0.074–0.089	0.082
Algae count (cell/mL)	922–52,713	5,631

To speed up the membrane fouling performance, the influent was concentrated with a reverse osmosis membrane with a fiber filter, and then filtrated with a 0.45 μm membrane to remove suspended particles. The permeate was thus collected for subsequent use, with the characteristics shown in Table 5.3.

Table 5.3: Characteristics of concentrated water.

Parameter	Turbidity (NTU)	pH	DOC (mg/L)	UV_{254} (cm^{-1})	SUVA (L/(mg · m))
Value	26	8.1	9.88	0.118	1.19

2 Pilot scale experimental setup

The pilot scale experimental setup was located at Chongshan Waterworks, Wuxi City, Jiangsu Province, with the schematic diagram shown in Figure 5.11. Detail descriptions of the pilot setup can be found in the study of Dong et al., thus it is not repeated here.

EBSCOhost - printed on 2/14/2023 6:39 AM via . All use subject to https://www.ebsco.com/terms-of-use

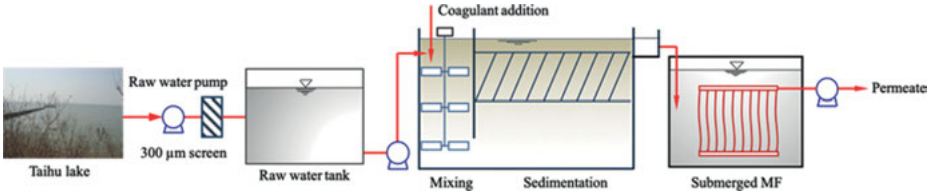

Figure 5.11: Schematic diagram of the pilot-scale membrane system.

5.1.2.2 Results and discussion

1 The effect of coagulant dosage on TMP performance in the pilot test

The TMP behavior of the pilot setup with different dosages of coagulants for long term operation is exhibited in Figure 5.12. It can be observed when the concentration of the coagulant increased from 10 to 30 mg/L, the initial TMP decreased from 0.028 to 0.010 MPa, and the cycle duration increased from 6 to 12 days. When the dosage was further increased to 40 mg/L, the initial TMP maintained the similar, and the cycle duration decreased to 10 days. This suggested that the optimum coagulation dosage for the Taihu Lake water treatment was 30 mg/L.

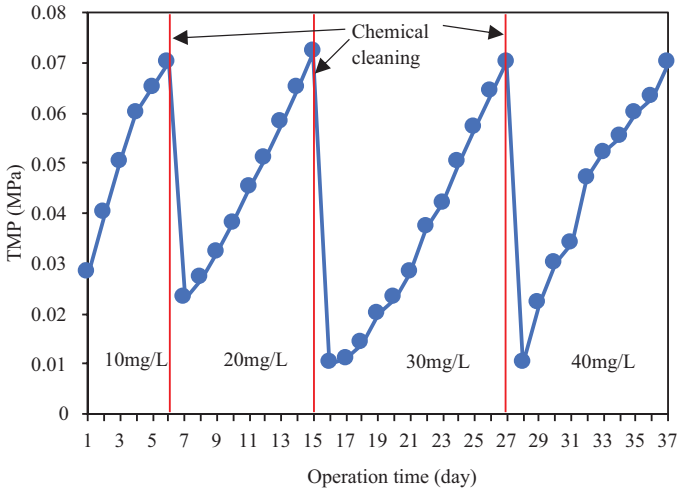

Figure 5.12: TMP variation in the pilot test for long term operation.

2 The effect of coagulant dosage on organic removal in the pilot test

The effect of direct coagulation and the combined coagulation and membrane filtration on the organic removal in the pilot test is shown in Figure 5.13. It can be found when the dosage was increased from 10 to 30 mg/L, the organic removal of COD_{Mn} and UV_{254} also increased. When the dosage was further increased to 40 mg/L, no addi-

EBSCOhost - printed on 2/14/2023 6:39 AM via . All use subject to https://www.ebsco.com/terms-of-use

tional organic removal efficiency was obtained. This result implied that the coagulation could mitigate the membrane fouling, and the best dosage for the Taihu Lake water treatment was 30 mg/L.

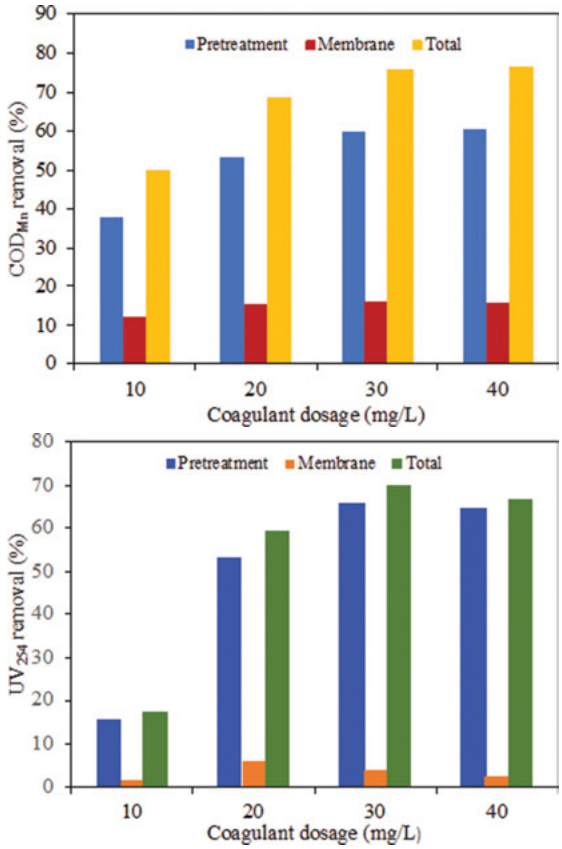

Figure 5.13: Organics removal with different dosages of coagulant in the pilot test.

3 MW distribution of the Taihu Lake water in the pilot test

The MW distribution results with the SEC-UV-TOC measurement of a sample from the Taihu Lake water, the supernatant after the coagulation and the permeate from the MF filtration are shown in Figure 5.14. For the Taihu Lake feed water, there were four peaks, around 300, 2, 0.6 and 0.35 kDa for the TOC detection, while there were two peaks, 2.5 and 0.9 kDa for the UV detection, with the former one with much higher intensity. The difference between these two detection measurements was due to that the high MW region could be weakly or scarcely detected by the UV detector. It also suggested that the high MW organics in Taihu Lake water were mainly hydrophilic.

EBSCOhost - printed on 2/14/2023 6:39 AM via . All use subject to https://www.ebsco.com/terms-of-use

Moreover, it can be found that the organic substances with MW greater than 10 kDa were almost completely removed, the organics with MW lower than 1 kDa were also eliminated significantly, however, only a small portion of organics with MW of 2 kDa were reduced after the coagulation pre-treatment in the TOC detection. This indicated that the coagulation pretreatment could remove humic substances more effectively than the non-humic ones. It is reported that coagulation can have a great removal efficiency of NOMs with high MW which are believed to induce the most severe membrane fouling. Since this part of NOMs were eliminated almost completely by the coagulation, they may not contribute significantly to the flux drop in the subsequent membrane filtration. Thus the NOMs with high MW could lead to the reversible fouling only.

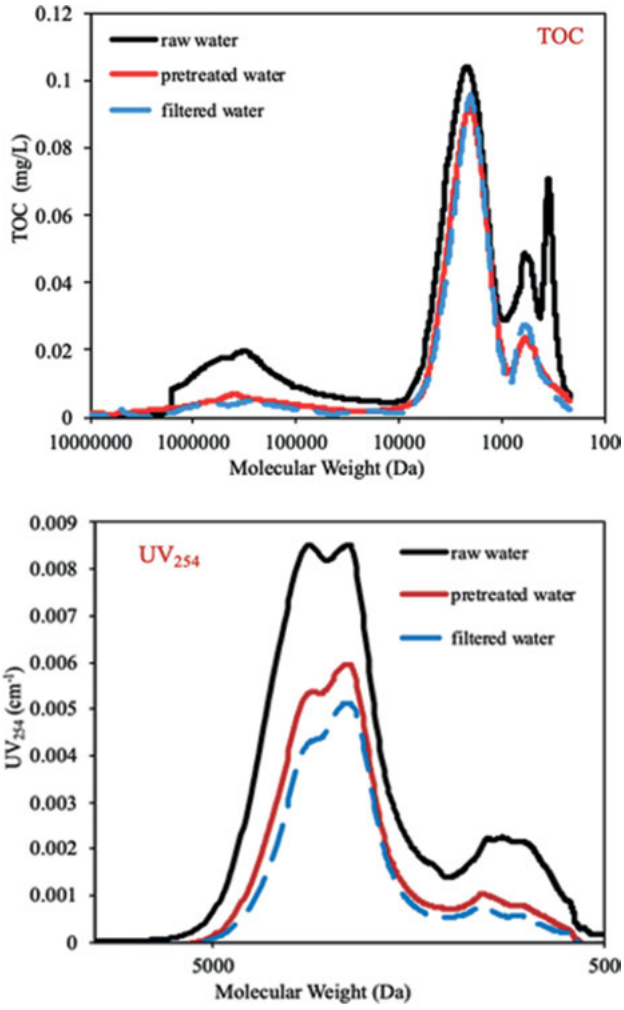

Figure 5.14: MW distribution of Taihu Lake water with different processes in the pilot test.

EBSCOhost - printed on 2/14/2023 6:39 AM via . All use subject to https://www.ebsco.com/terms-of-use

To further understand the interactions between the membrane and the organic molecules, the feed water, the supernatant after coagulation and the filtrated water were separated into four fractions (HPO, TPI, N-HPI and C-HPI) with their MW distributions examined by HPSEC-UV-TOC detections, and the results are shown in Figure 5.15. There were three peaks, i.e. around 300, 2 and 0.66 kDa for the N-HPI fraction with the SEC-TOC detection, while the HPO fraction with the SEC-UV detection showed a similar result but much higher intensity at the peak of 2 kDa. This was due to that the NOMs with medium MW were mainly hydrophobic. It can be also found that the Neut fraction with small MW had a higher intensity than the feed water, which demonstrated that the NOMs with low MW were mainly hydrophilic. It should be noted that both the SHA fraction and the Neut fraction with high MW were almost completely removed, and the HPO fraction with medium and small MW was eliminated better than the N-HPI fraction.

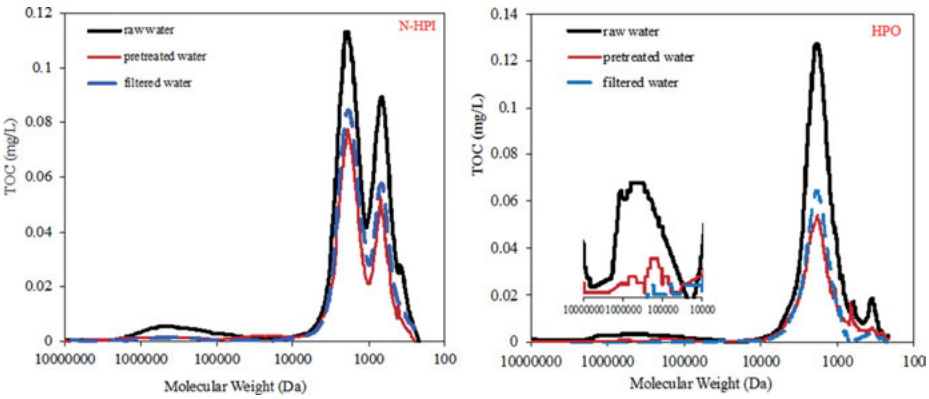

Figure 5.15: MW distribution of N-HPI and HPO fraction with different processes in the pilot test.

4 Chemical cleaning

To further understand the ability of pretreatment, chemical cleaning of the fouled membranes was carried out. In this study, when the TMP went to 0.07 MP, the chemical cleaning was initiated. Both alkaline and acid cleanings were involved in the procedures, with each one for 2 h. In the alkaline cleaning, NaOH and NaClO were used, while in the acid cleaning, HCl was adopted, with the former one to remove organic foulants and the latter one inorganic ions and part of organic matters. The organics from the chemical cleaning were fractionated and the results are shown in Figure 5.16. It can be found that more organic substances were obtained from the alkaline cleaning than the acid cleaning. As for each fraction, the organics in both N-HPI and HPO were much higher than TPI and C-HPI fractions, which exhibited that the neutral hydrophilic and strong hydrophobic compounds were key irreversible mem-

EBSCOhost - printed on 2/14/2023 6:39 AM via . All use subject to https://www.ebsco.com/terms-of-use

brane fouling contributors. In addition, it can be also discovered that the organics from N-HPI fraction in the alkaline cleaning were comparable from the acid cleaning, but much more organics from HPO fraction were achieved, which indicated that acid cleaning could remove some part of dominated hydrophilic organic foulants, since acid cleaning was effective in removing inorganic substances, but less effective in reducing organics.

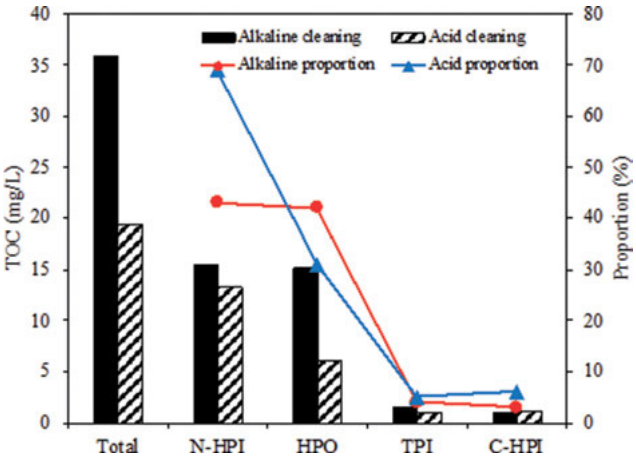

Figure 5.16: Effect of chemical cleaning on organic fractions.

The MW distribution of the organics from chemical cleaning with SEC-TOC-UV detections were measured and the result is shown in Figure 5.17. The MW of the foulants from cleaning was around 2 and 0.6 kDa for both UV and TOC detections, which indicated that the medium and small molecules were main irreversible foulants. This is consistent with the result in Figure 5.14 since high MW organics were removed completely with coagulation. In addition, it can be also observed that the UV intensity from the alkaline cleaning was much stronger than the acid cleaning, which also indicated that the alkaline cleaning was more effective for organics removal.

The MW distribution for the organic fractions were examined and the results are shown in Figure 5.18. The HPO fraction was mainly composed of medium MW organic substances with MW around 2 kDa, while N-HPI fraction contained medium and small MW molecules with the TOC intensity for small MW organics higher than medium MW substances no matter what kind of chemical cleaning was applied. These findings confirmed that medium and small MW molecules rather than high MW substances contributed severe irreversible membrane fouling.

It was reported that the hydrophobic substances with high MW usually led to dramatic flux decline, while the neutral hydrophilic organics with relatively low MW contributed less seriously to the membrane flux drop. Similar results were also obtained in this study. Such performance was due to that, the HPO fraction with medium

EBSCOhost - printed on 2/14/2023 6:39 AM via . All use subject to https://www.ebsco.com/terms-of-use

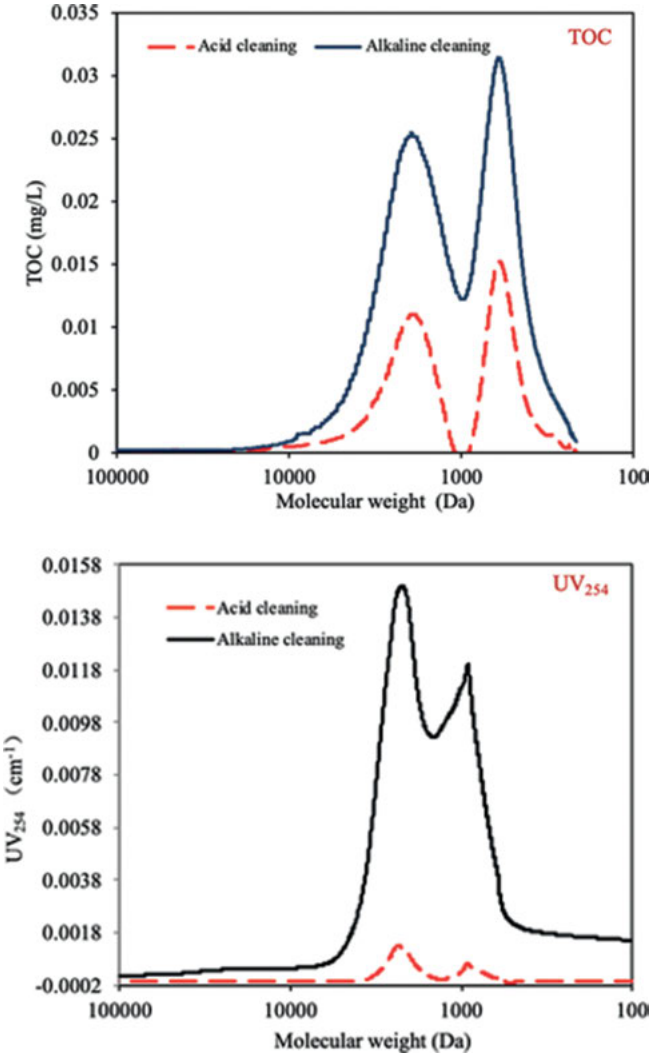

Figure 5.17: MW distribution of organics in chemical cleaning solution.

MW organics (10–1 kDa) could block the membrane pores and induced a rapid flux decline, while some of the N-HPI fraction with low MW substances (<1 kDa) passed the membrane pores, resulting in a slow membrane flux drop. Thus the existence of HPO and N-HPI fractions determined the membrane performance.

5 EEM fluorescence

To further qualify the types of substances removed in the coagulation and membrane filtration processes, the 3D fluorescence EEM spectrum of the Tiahu Lake feed

EBSCOhost - printed on 2/14/2023 6:39 AM via . All use subject to https://www.ebsco.com/terms-of-use

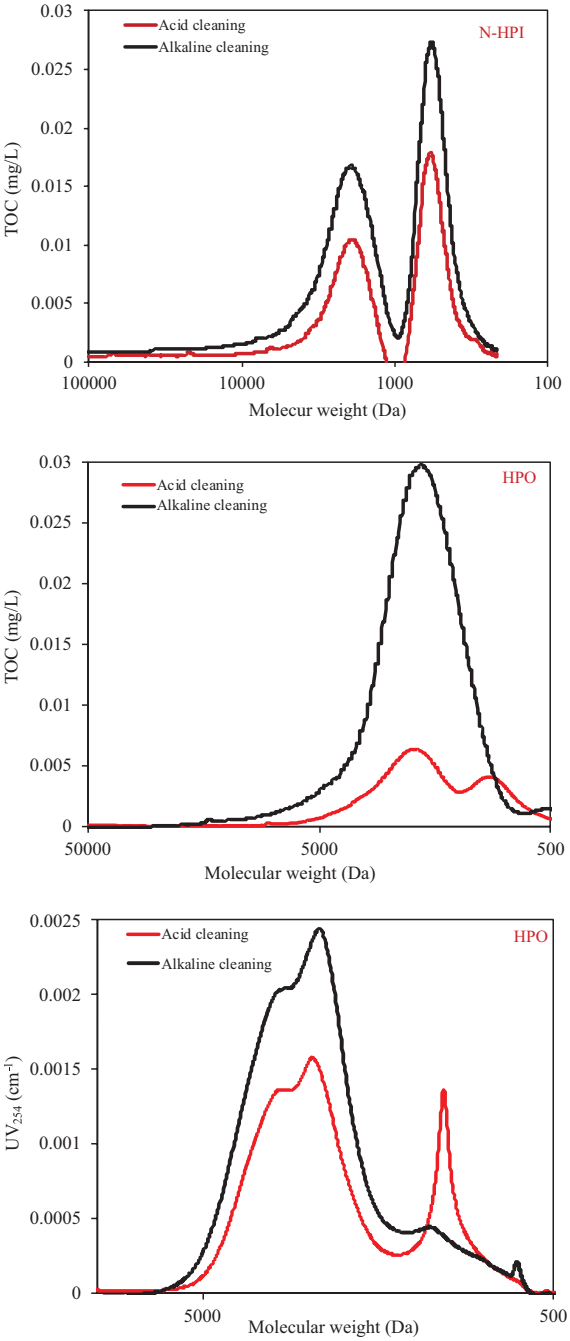

Figure 5.18: MW distribution of N-HPI and HPO fractions in chemical cleaning solutions.

EBSCOhost - printed on 2/14/2023 6:39 AM via . All use subject to https://www.ebsco.com/terms-of-use

water, feed fractions, the foulants rejected by the membrane, and the foulants from the chemical cleaning were measured and the results are shown in Figures 5.19–5.22, respectively. In the fluorescence EEM spectrum of the feed water (Figure 5.19), four peaks were obtained, two peaks with strong intensity at Ex/Em = 280/315 nm and Ex/Em = 230/340 nm labeled as peaks I and II, and another two peaks with weak intensity at Ex/Em = 340/420 nm and Ex/Em = 240/430 nm labeled as peaks III and IV, respectively. It has been reported that peaks I and II represent protein-like substances such as tryptophan and tyrosine, whereas peaks III and IV humic-like substances such as humic acid and fulvic acid. The Taihu Lake water is suffered frequently from algae bloom, thus it contains a lot of aromatic proteins and SMPs due to algae metabolism. The fluorescence intensity in peak II was highest, followed by peak III and peak IV. These findings suggested that proteins and SMPs dominated in organics in Taihu Lake.

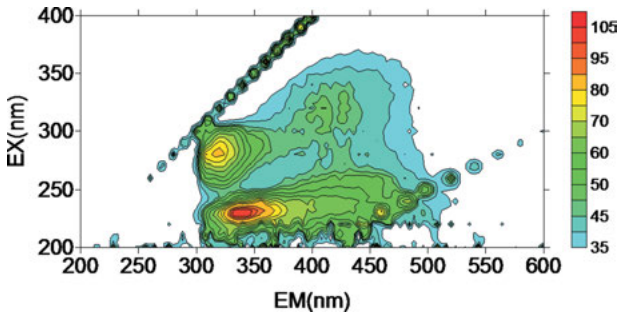

Figure 5.19: EEM fluorescence spectra of the Taihu Lake raw water.

In the EEM fluorescence spectra of the four different fractions (Figure 5.20), varied intensities and locations of peaks were exhibited. The HPO and C-HPI had peaks at the locations of III and IV, while N-HPI had nearly no peaks. The EEM fluorescence spectra of the foulants rejected by the membrane (Figure 5.21) was achieved by the subtraction of intensity values between the supernatant after the coagulation and the permeate after the coagulation and membrane filtration, and it had peaks at the protein-like regions (peaks I and II). In the EEM fluorescence spectra of the foulants from the chemical cleaning (Figure 5.22), there were peaks at protein-like regions. Moreover, the EEM fluorescent spectra of acid cleaning had only peak at location I, while for the alkaline cleaning, two peaks I and II were observed, indicating more removal of SMPs. Such behavior agrees with the previous studies. Therefore, it can be further suggested that aromatic proteins and soluble microbial products induced greater irreversible membrane fouling, which were composed primarily of HPO and N-HPI fractions.

EBSCOhost - printed on 2/14/2023 6:39 AM via . All use subject to https://www.ebsco.com/terms-of-use

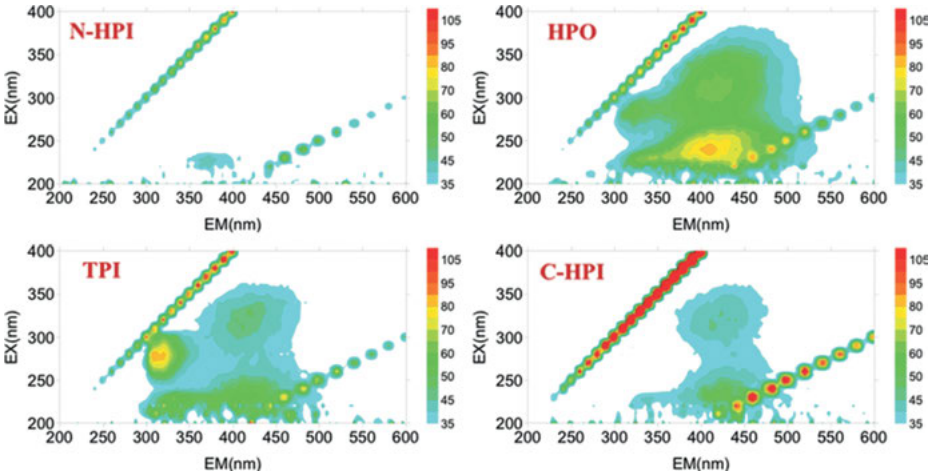

Figure 5.20: EEM fluorescence spectra of four fractions of Taihu Lake water.

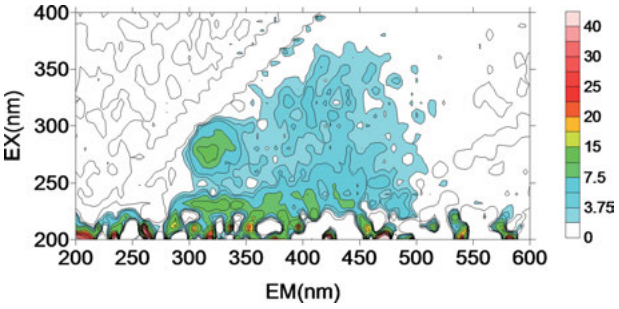

Figure 5.21: EEM fluorescence spectra of foulants rejected by MF.

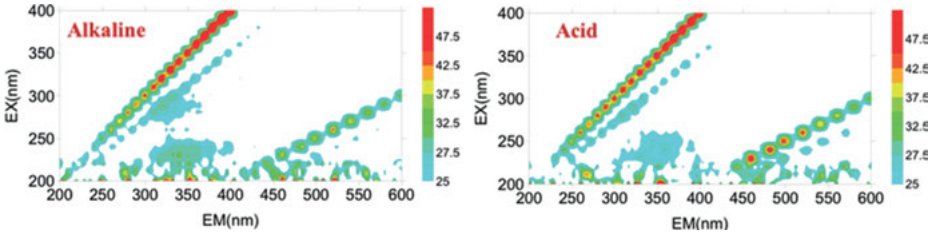

Figure 5.22: EEM fluorescence spectra of foulants from chemical cleaning.

6 Mechanism of coagulation pretreatment on controlling membrane fouling

To further understand the mechanism of coagulation on the membrane fouling control, a schematic diagram is drawn and exhibited in Figure 5.23. In the direct membrane filtration, large and part of medium organics deposit on membrane surface to

EBSCOhost - printed on 2/14/2023 6:39 AM via . All use subject to https://www.ebsco.com/terms-of-use

form gel and cake layer resulting in reversible membrane fouling, and most of small organic molecules enter the membrane pores and shrink, producing irreversible fouling. With coagulation, not only large organic substances, but also medium and small organic molecules were aggregated to become large particles, which could be removed in subsequent sedimentation process. Thus coagulation could reduce some irreversible fouling to purify the membranes.

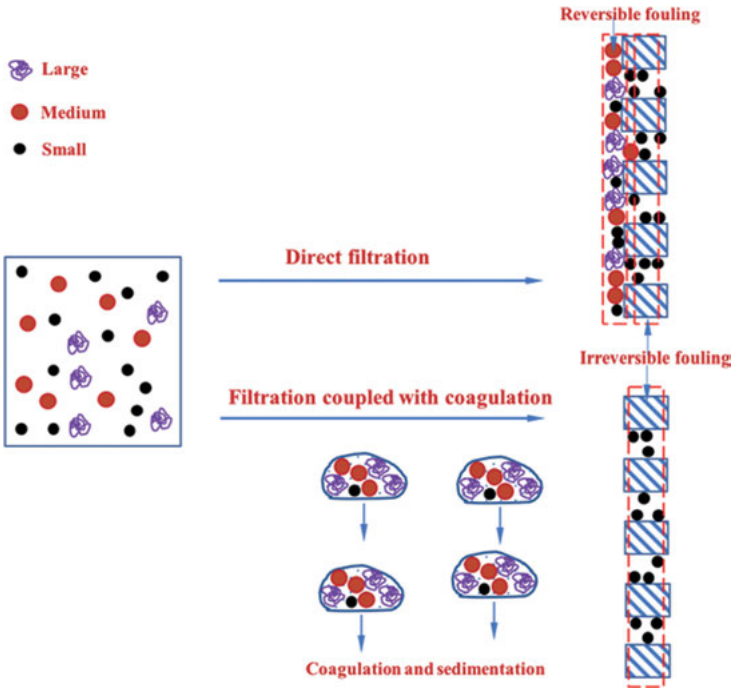

Figure 5.23: Schematic diagram of membrane fouling control mechanism by coagulation pretreatmen.

5.2 Adsorption pretreatment

5.2.1 The effect of PAC adsorption on membrane fouling control

5.2.1.1 Experimental setup and methodology

In this study, PAC adsorption was adopted as a pretreatment method for UF membrane fouling control. The experimental setup was adopted from our previous study, with the schematic diagram shown in Figure 5.24. Two surface feed sources were used, i.e. Sanhaowu lake water (SLW) and Huangpu river water (HRW).

EBSCOhost - printed on 2/14/2023 6:39 AM via . All use subject to https://www.ebsco.com/terms-of-use

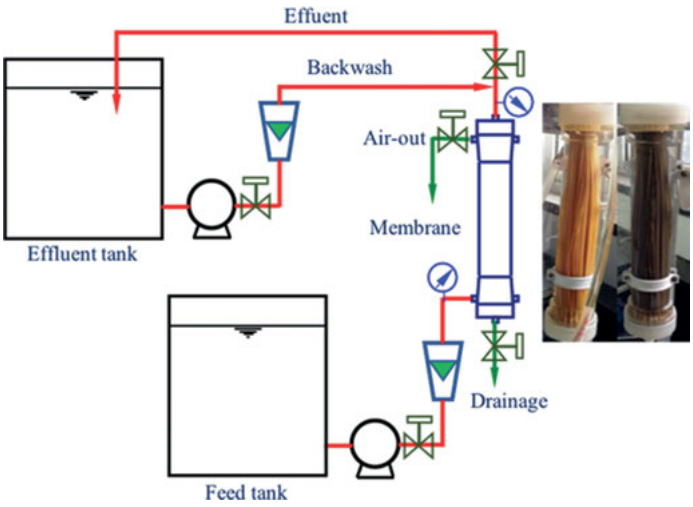

Figure 5.24: Schematic diagram of the experimental setup for PAC adsorption.

5.2.1.2 TMP performance

The TMP values of the direct UF filtration of SLW and HRW water were measured and the results are shown in Figure 5.25. There were six stages in total for the whole filtration, and each stage lasted 90 min. At the initial stage, no obvious TMP differences were found between the direct UF of the influent and PAC-treated water. While for the later stages, the TMP gap between them became larger, demonstrating that PAC played a significant role in reducing membrane fouling.

Based on the filtration, the reversibility of the membranes with and without PAC were calculated adopting the method from our previous published work, in the manner of reversible fouling resistance (R_{re}) and irreversible fouling resistance (R_{ir}), with the results shown in Figure 5.26. R_{re} increased and decreased alternately due to the periodic backwash, while R_{ir} continued to rise in the six stages. At the end of the operation, R_{ir} values were much higher than R_{re}. It should be noted that low fouling resistances were obtained with PAC-treated influent. These observations showed that the addition of PAC could reduce the foulants thus to decrease both R_{re} and R_{ir}.

5.2.1.3 Molecular weight distribution

To understand the effect of PAC on UF membrane fouling control, the molecular weight (MW) distribution of both the SLW and HRW influent and the PAC-treated water was examined with the liquid chromatograph (LC) coupled with TOC detection. Figure 5.27 shows the analysis of an influent sample of this method. The MW

EBSCOhost - printed on 2/14/2023 6:39 AM via . All use subject to https://www.ebsco.com/terms-of-use

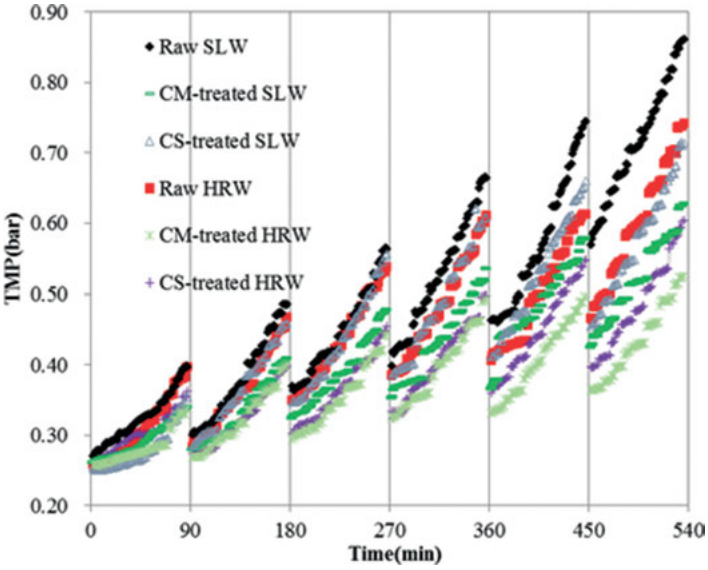

Figure 5.25: TMP performance of direct UF and PAC-UF for surface water filtration.

distribution of the resolved peak (black curve) was divided into 500 Da (Peak 1), 1,420 Da (Peak 2), 5,250 Da (Peak 3) and 1,000 kDa (Peak 4) via Peak-fitting software, which could be regarded as low molecular weight neutrals (LMWN), low molecular weight acids and building blocks (LMWA and BB), humic substances (HS), and biopolymers (BP) such as colloids, proteins (PN) and polysaccharides (PS) in the sample, respectively. Then the MW distribution based on the areas of each peak was calculated, with the results of both feeds, PAC-treated water and UF permeate shown in Figure 5.28.

It can be seen that the UF had very low rejection rates for LMW fractions, such as BB and LMWA and LMWN. On the contrary, PAC had relatively high removal efficiencies for LMW (14.3%–46.4%) and HS fractions (18.4% to 42.8%). The PAC had lots of pores in its surface or inside the structures, which could adsorb the molecules thus to remove them. The absorbability of PAC was greatly related to its pore size and also the size of the absorbent, i.e. the molecules in the influent. In this study, the PAC used was mainly composed of micro- and mesopores (approximately < 16 nm), thus only small molecules were adsorbed, and the high MW fractions (such as BP) were unable to enter these pores, resulting in a poor removal efficiency. Therefore, the mechanism of PAC to mitigate membrane fouling was its removal of LWM and HS fractions of NOM, which reduced the blockage of membrane pores.

EBSCOhost - printed on 2/14/2023 6:39 AM via . All use subject to https://www.ebsco.com/terms-of-use

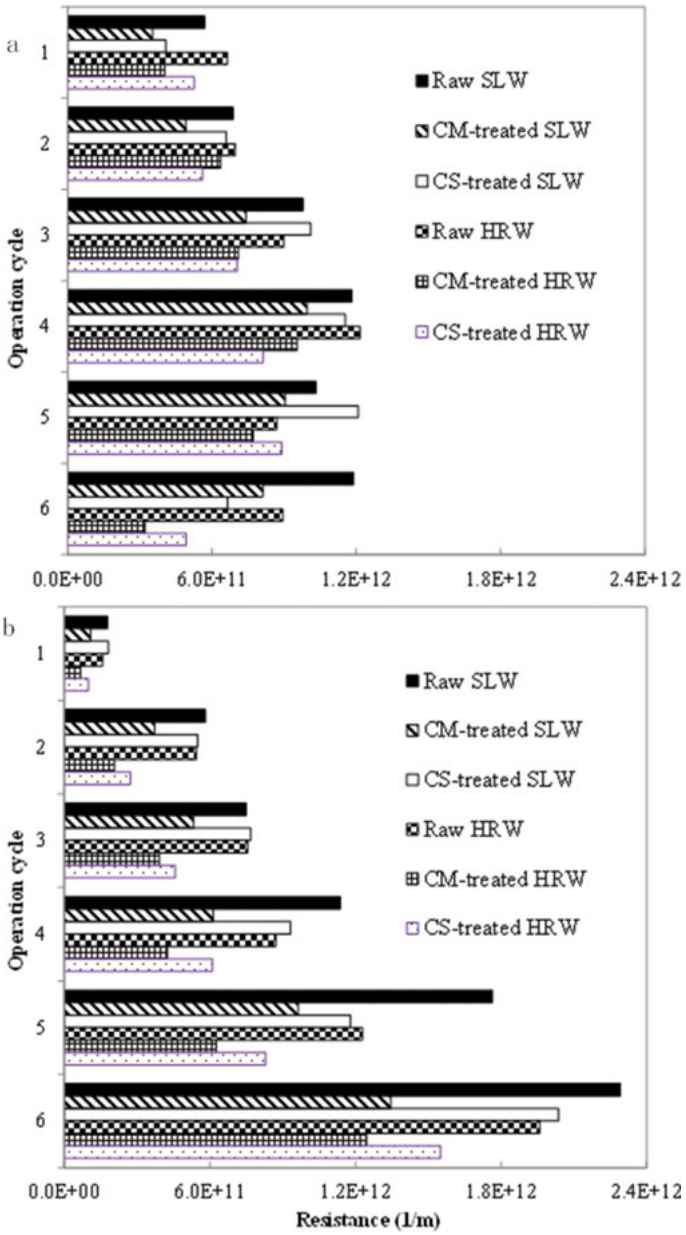

Figure 5.26: Effect of PAC on R_{re} (a) and R_{ir} (b) during the UF of surface water.

EBSCOhost - printed on 2/14/2023 6:39 AM via . All use subject to https://www.ebsco.com/terms-of-use

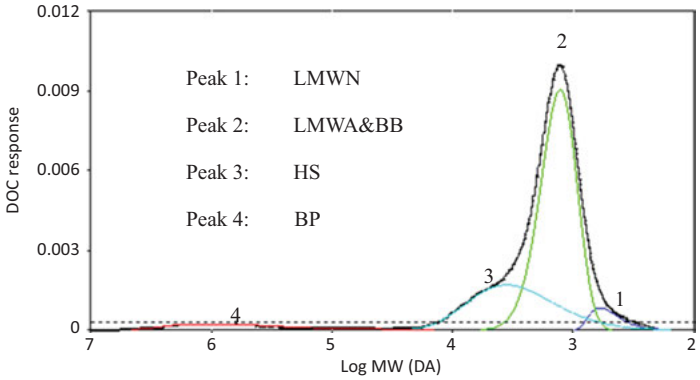

Figure 5.27: LC-OCD-Peakfit analysis of surface water.

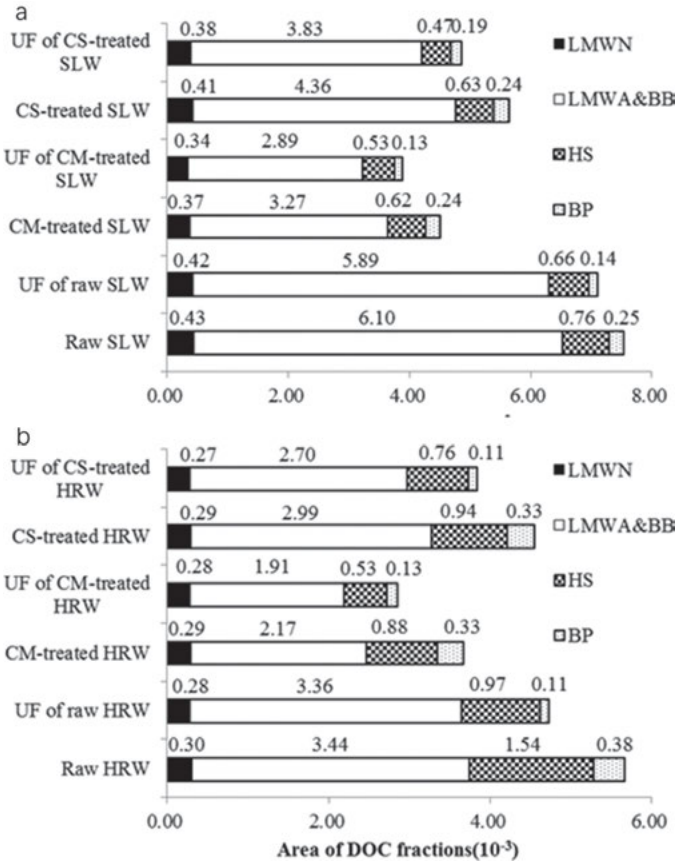

Figure 5.28: MW components of water samples: (a) SLW and (b) HRW.

EBSCOhost - printed on 2/14/2023 6:39 AM via . All use subject to https://www.ebsco.com/terms-of-use

5.2.1.4 Correlation of membrane fouling resistances and influent characteristics

Principal component analysis (PCA) was performed to correlate membrane fouling resistances with the influent characteristics and the result is shown in Figure 5.29.

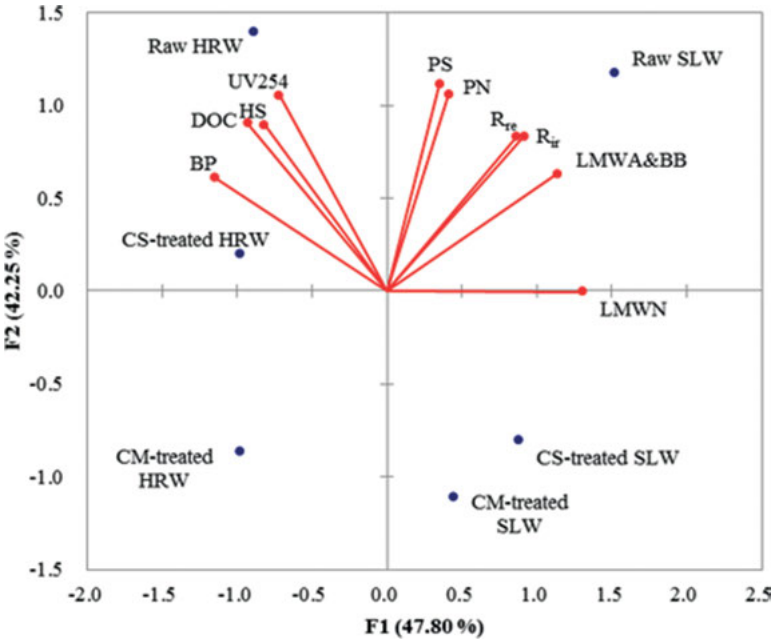

Figure 5.29: PCA of membrane fouling resistances and feed qualities.

In the PCA method, samples with high fouling potentials were clustered together with R_{re} and R_{irr} while low fouling potentials, such as CM-treated HRW and CS-treated SLW etc. were placed far away from R_{re} and R_{ir}. It was observed there was no obvious correlation between fouling resistance and DOC ($r^2 < 0.02$), or UV_{254} ($r^2 < 0.03$). This is due to that DOC is only a parameter of the total amount of NOM without being able to distinguish the main fouling constituents. More importantly, there were no strong correlations between polysaccharides (PS) / proteins (PN) and fouling resistances ($0.3 < r^2 < 0.4$), and biopolymers (BP) and FR ($r^2 < 0.1$). These findings were different from most observations in the literature. However, such minor results were also reported, e.g. the study from Kimura et al. suggested that the influent characteristics rather than the quantities of macro-MW substances have a key influence on membrane fouling performance. It should be noted that LMWA and BB was placed next to fouling resistances with a high correlation value ($r^2 = 0.8430$, $p = 0.0098$). This is due to that the low-MW fractions, especially LMWA and BB were the most significant fouling contributors.

EBSCOhost - printed on 2/14/2023 6:39 AM via . All use subject to https://www.ebsco.com/terms-of-use

5.2.2 Effect of mesoporous and microporous carbons on membrane fouling control

5.2.2.1 Experimental methodology

Two types of carbons, one microporous carbon and one mesoporous carbon were adopted in this study to investigate the effect of PAC characteristics on membrane fouling control. The microporous carbon (CPAC) was commercially purchased from Shanghai Company, and the mesoporous carbon (SOMC) was synthesized using the method from Nanjing University. The surface area of CPAC and SOMC were 580.13 and 988 m^2/g, and the pore size 1.86 and 3.7 nm, respectively, while the mesoporous volume of SOMC was 1.29 cm^3/g. Details of the characteristics of these two carbons are listed in Table 5.4.

Table 5.4: The Characteristics of the two carbons used in the experiment.

	Mesoporous carbon	Microporous carbon
carbon (%)	95.57	98.4
Surface area (m^2/g)	988	580.13
Pore size (nm)	3.7	1.86
Microporous volume (cm^3)	0.04	0.2015
Mesoporous volume (20–500 Å) (cm^3/g)	1.29	–

Before the MF filtration experiment, the PAC adsorption ability was investigated with the equilibrium measurement. In the PAC adsorption combined with MF filtration experiment, different concentrations of 20, 50 and 100 mg/L of PAC were dosed in three same feed samples. After that, the mixtures were first stirred at 100 r/min for 30 min, and then at 50 r/min for 2 h. Subsequently for a 45 min rest, they were separated into the supernatant and the solid part. Then the supernatant was collected and filtrated with a Millipore 0.45 μm filter. After that, the permeate were used for subsequent analysis including filtration flux measurement, organic removal efficiency and foulant detection and detail results were reported in the following sections.

5.2.2.2 Results and discussions

1 The effect of two carbons on membrane filtration performance

The membrane filtration flux of the permeate after the 0.45 μm Millipore filter were examined and results are shown in Figure 5.30. With the addition of SOMC, the filtration flux was greatly increased, especially with the dosage of 100 mg/L, the flux increased by 60%. When the concentration of SOMC was increased, the permeate

EBSCOhost - printed on 2/14/2023 6:39 AM via . All use subject to https://www.ebsco.com/terms-of-use

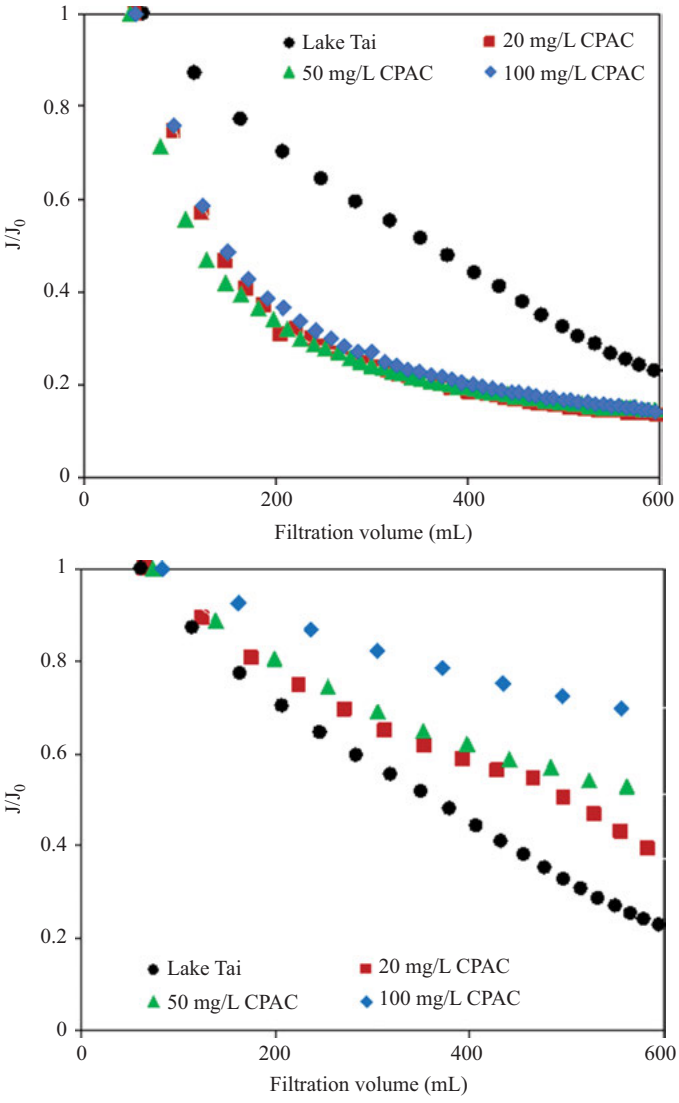

Figure 5.30: The effect of CPAC and SOMC pretreatment on membrane filtration performance.

flux also enhanced. Thus the SOMC could reduce the membrane fouling due to the organics adsorbed. On the contrary, with the addition of CPAC, the flux decreased significantly. And the concentration of CPAC didn't make any difference on the permeate flux. Similar flux drop trends were obtained with different dosages of CPAC. Such phenomenon may be attributed to the small sizes of CPAC that could stay on the MF surface and block the passage of the permeate.

EBSCOhost - printed on 2/14/2023 6:39 AM via . All use subject to https://www.ebsco.com/terms-of-use

2 The effect of two carbons on organics removal

The organic removal efficiencies of the permeate after the 0.45 μm Millipore filter and the permeate after MF with different dosages of CPAC and SOMC were examined and the results are presented in Figure 5.31. With the addition of the two carbons, the organics removal efficiencies of both TOC and UV_{254} increased significantly. It could be observed that with combined SOMC and MF, the UV_{254} removal efficiency could be achieved as high as 80%, and TOC 28%. With combined CPAC and MF, the

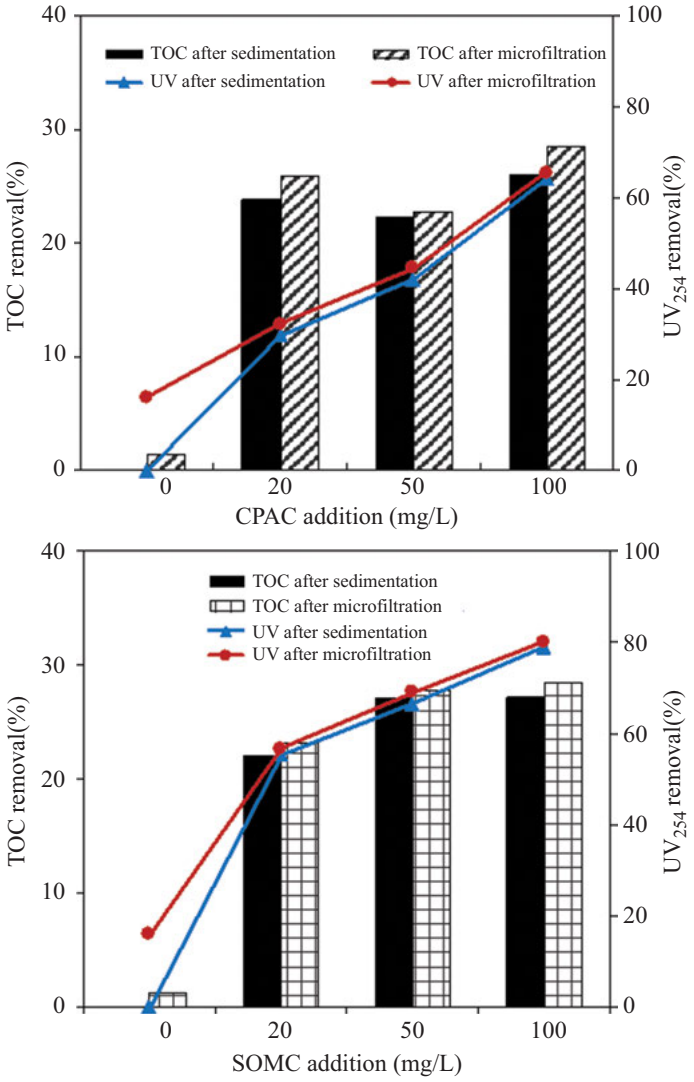

Figure 5.31: The effect of CPAC and SOMC pretreatment on organic removal.

EBSCOhost - printed on 2/14/2023 6:39 AM via . All use subject to https://www.ebsco.com/terms-of-use

organic removal efficiencies were comparable to that with SOMC, indicating that both carbons could adsorb organic substances in Taihu Lake.

3 The effect of two carbons on MW distribution

The relative MW distribution of organic substance in terms of TOC and UV_{254} measurement with the combined carbon adsorption and MF filtration was measured and the results are presented in Figures 5.32 and 5.33. It can be found that all the peak intensities of the macromolecular organics almost disappeared after MF filtration with the adsorption of both carbons as pretreatment, indicating that the macromolecular substances were main membrane fouling contributors. In addition, the effects of the two carbons on MW distribution were slightly different. The SOMC had a good absorption efficiency for macromolecular organic substances, with the removal efficiency increased as the dosage amount increased. While the CPAC had little effect on the macromolecular organics removal no matter what concentration was dosed. However, both carbons could remove small molecules with the MW < 1 kDa especially those with the MW < 100 Da.

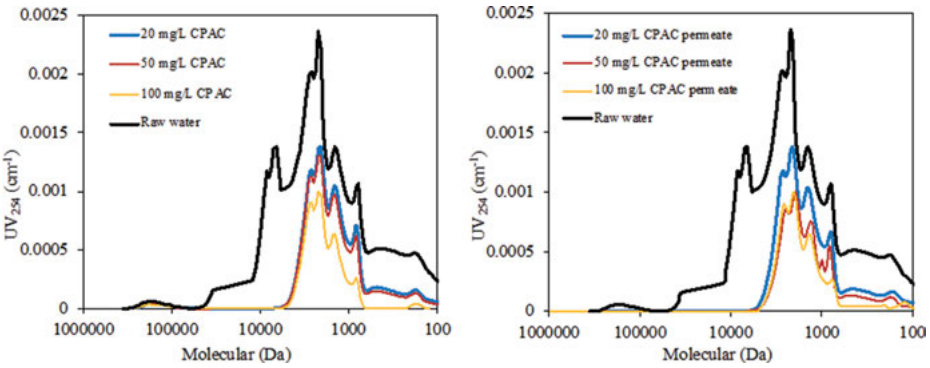

Figure 5.32: The influence of CPAC pretreatment on MW distribution.

4 The effect of two carbons on EEM performance

The fluorescence spectrum of EEM measurement of the Taihu Lake influent with the combined carbon adsorption and MF filtration was examined and the result is shown in Figure 5.34. The fluorescence peak of the protein and tyrosine regions disappeared after the direct membrane filtration, suggesting that these organics can be key membrane fouling contributors. While the fluorescence peak of the protein tyrosine and humic substances was greatly reduced after the SOMC carbon pretreatment, indicating that SOMC could remove these organics (Figure 5.34(b, d)). With SOMC treatment, most of the peaks disappeared suggesting that SOMC treatment could delete most of organics thus to reduce the subsequent membrane fouling (Figure 5.34(c, e)). In contrast, CPAC removed lower amount of protein and tyrosine like substances than SOMC did.

EBSCOhost - printed on 2/14/2023 6:39 AM via . All use subject to https://www.ebsco.com/terms-of-use

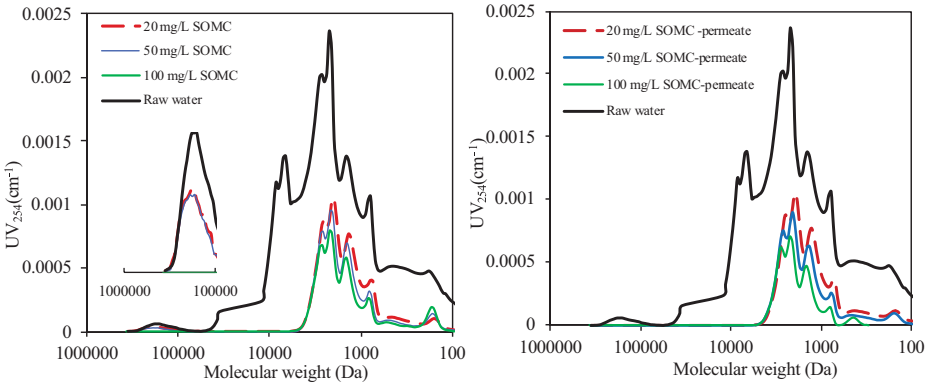

Figure 5.33: The influence of SOMC pretreatment on MW distribution.

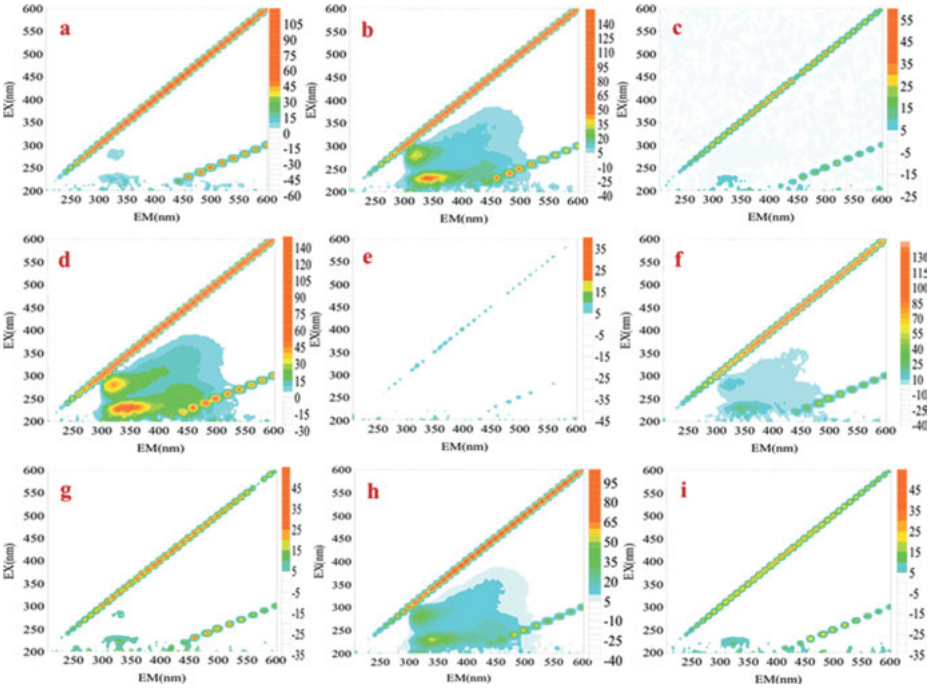

Figure 5.34: Subtracted EEMs of Taihu Lake water with PAC pretreatment and MF filtration. (a. permeate of direct filtration, b. supernatant after 20 mg/L SOMC adsorption, c. permeate of MF filtration with 20 mg/L SOMC adsorption, d. supernatant after 100 mg/L SOMC adsorption, e. permeate of MF filtration with 100 mg/L SOMC adsorption, f. supernatant after 20 mg/L CPAC adsorption, g. permeate of MF filtration with 20 mg/L CPAC adsorption, h. supernatant after 100 mg/L CPAC adsorption, i. permeate of MF filtration with 100 mg/L CPAC adsorption)

EBSCOhost - printed on 2/14/2023 6:39 AM via . All use subject to https://www.ebsco.com/terms-of-use

The scanning electron microscope of membrane surface with direct filtration and the adsorption of 100 mg/L of the two carbons is shown in Figure 5.35. It can be seen that after direct filtration of Taihu Lake water, a thick fouling layer was formed on the membrane surface and the pore was covered completely. Thus the fouling can be composed of large organic molecules. With 100 mg/L SPAC, similar performance was observed that the membrane surface was covered with very thick fouling. In contrast, with 100 mg/L SOMC, the surface of the membrane was very clean and no fouling was found on it. Thus the SOMC could effectively remove the large organic substances.

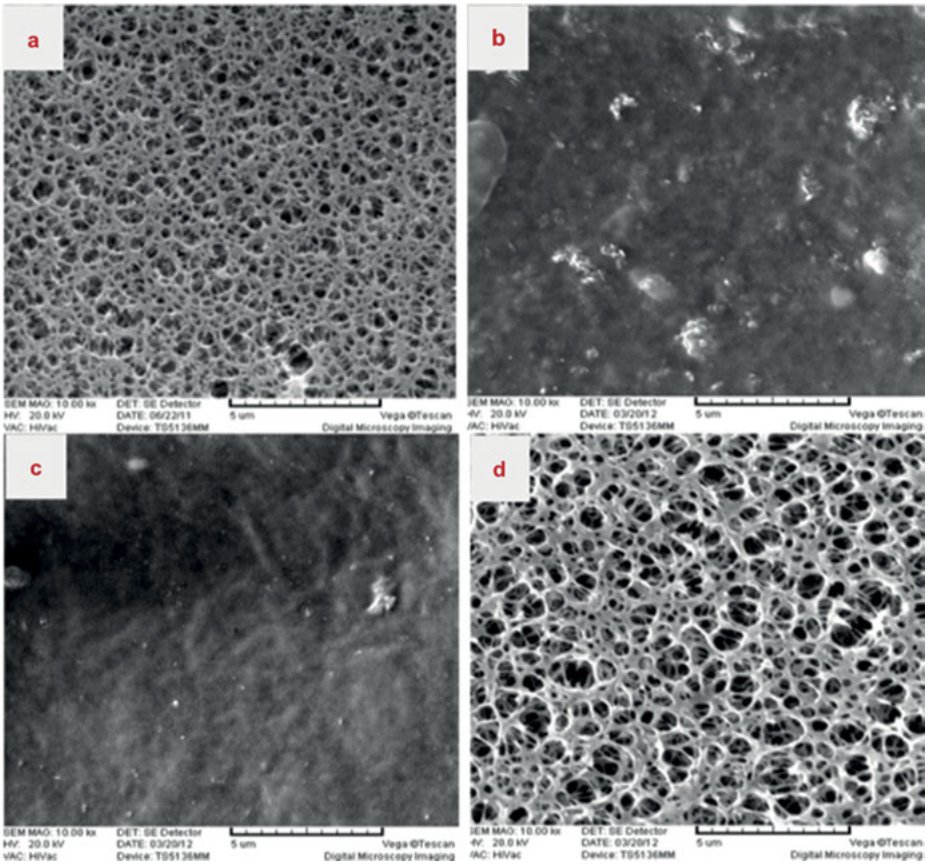

Figure 5.35: SEMs of micromembrane filtrated by Taihu Lake after PAC treatment.
(a. New membrane, b. direct filtration, c. 100 mg/L CPAC adsorption, d. 100 mg/L SOMC adsorption)

The infra-red spectrogram of Taihu Lake water with direct filtration and carbon treatment is in Figure 5.36. It can be seen that the response of the membrane surface with direct filtration appeared at the wavelengths of 1,550, 2,950 and 3,350 cm^{-1} reflecting protein, polysaccharide and humic acid with large MW in comparison with the new

EBSCOhost - printed on 2/14/2023 6:39 AM via . All use subject to https://www.ebsco.com/terms-of-use

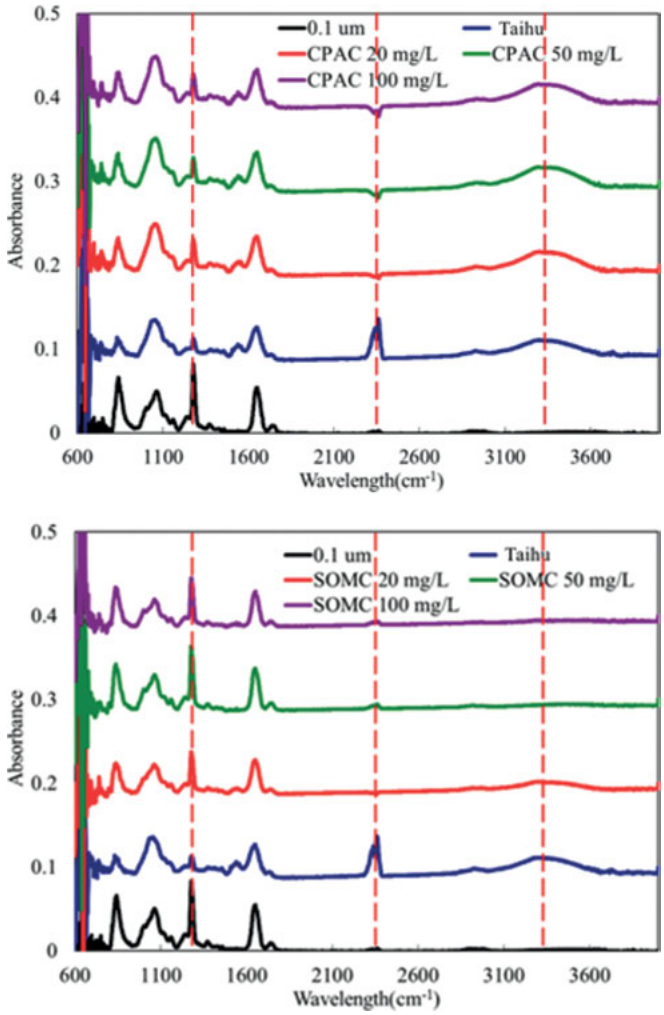

Figure 5.36: FTIR spectra of micromembrane fouled by Taihu Lake water after PAC treatment.

membrane. With the treatment of 20 mg/L SOMC, the intensity of the three responses reduced slightly. While with the dosages of 50 mg/L and 100 mg/L, no additional reduction of the response was observed, suggesting that the fouling substances with the infra-red response at the wavelengths of 1,550, 2,950 and 3,350 cm^{-1} were removed by SOMC completely. With SPAC treatment, the response on the membrane surface was as the same as that with direct filtration and no reduction of infra-red intensity was observed. It can be suggested that protein like, polysaccharide like and humic acid with large MW can be the main foulants, and they could be removed by the direct membrane filtration resulting in the fast flux decline.

EBSCOhost - printed on 2/14/2023 6:39 AM via . All use subject to https://www.ebsco.com/terms-of-use

5.2.3 Mechanism of membrane fouling reduction by PAC pre-treatment

When the surface water was treated with PAC adsorption and membrane filtration, the membrane fouling performance was determined by the organics remained on the membrane surface. Large-MW substances were usually retained by UF membrane, causing reversible fouling that can be removed by backwashing. PAC has little ability to remove such large-MW organics, as a result, it played a poor effect on the mitigation of reversible fouling. As shown in Figure 5.37, small-MW organics could block the membrane pores or be adsorbed to the inner pore wall, inducing irreversible fouling. PAC has a good ability to adsorb small organics, thus less small organics can be deposited in the membrane pore, resulting in the reduction of irreversible fouling.

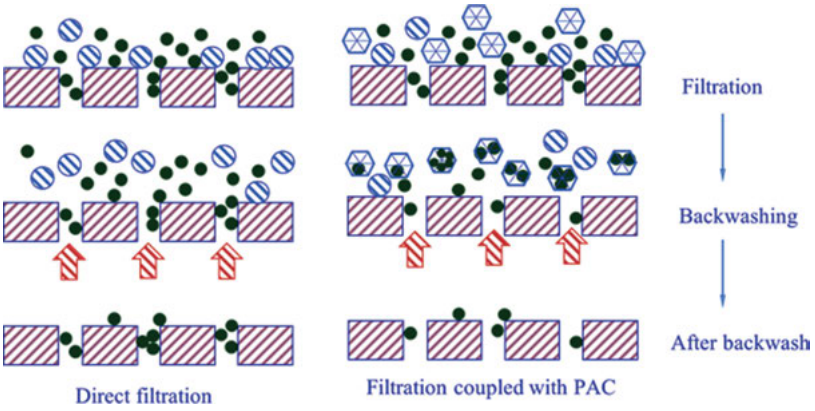

Figure 5.37: Mechanism of membrane fouling reduction by PAC adsorption for surface water.

5.3 The effect of granular macro-porous anion exchange resin pre-treatment on membrane fouling control

5.3.1 Experimental device and methodology

5.3.1.1 Characteristics of the granular macro-porous anion exchange resins

The resins used in this study were commercially available from Dow Company, US. Two types of resins, AMBERLITE™ PW16 (PW16) and AMBERLITE™ PWA9 (PWA9), were

EBSCOhost - printed on 2/14/2023 6:39 AM via . All use subject to https://www.ebsco.com/terms-of-use

adopted because both are styrene macroporous resins, with the functional groups of quaternary ammonium. The characteristics of the resins are shown in Table 5.5. PWA9 are white and opaque beads with sizes and water content lower than PW16; however, the total exchange capacity and shipping weight of PWA9 are comparatively higher.

Table 5.5: Characteristics of the resins used.

Resin	PW16	PWA9
Type	macroporous	
Skeleton structure	Styrene – divinylbenzene cross linked copolymer	
Functional groups	Quaternary ammonium groups	
Ionic form	Cl^-, OH^-	
Physical form	White opaque beads	
Wetting pore size	100–500 nm	
Total exchange capacity (eq/L)	≥0.7	≥0.8
Water content (%)	70–82	66–72
Particle size (mm)	0.42–1.2	0.3–1.18
Screen grading	(below 0.42 < 5%;	(below 0.355 < 1%)
Fines content	Above 1.2 < 3%)	
Shipping weight (kg/m^3)	689	700
Maximum operation temperature (°C)	60 (OH^-), 100 (Cl^-)	40
Swelling index	17%	25%
Void volume	25%	29%
maximum adsorbing capacity (mg/mL)	DOC 1.0328	0.9363
(cm^{-1}/mL)	UV 0.0124	0.0112

5.3.1.2 Experimental setup

The dynamic adsorption of the resins was conducted with the filtration columns. A schematic diagram of the experimental setup is shown in Figure 5.38.

In order to examine the resin adsorption behaviors, quasi-one and quasi-two adsorption kinetic equations were investigated, which can be presented as follows

$$\log(Q_e - Q_t) = \log Q_e - k_1 \times \frac{t}{2.303} \tag{5.1}$$

$$\frac{t}{Q_t} = \frac{1}{k_2 Q_e^2} + \frac{1}{Q_e} \tag{5.2}$$

where Q_e is the equilibrium adsorption capacity (mg/mL or cm^{-1}/mL), Q_t is the instantaneous adsorption capacity, k_1 and k_2 represent the adsorption rate constants of the quasi-one and quasi-two adsorption kinetics equations, respectively.

EBSCOhost - printed on 2/14/2023 6:39 AM via . All use subject to https://www.ebsco.com/terms-of-use

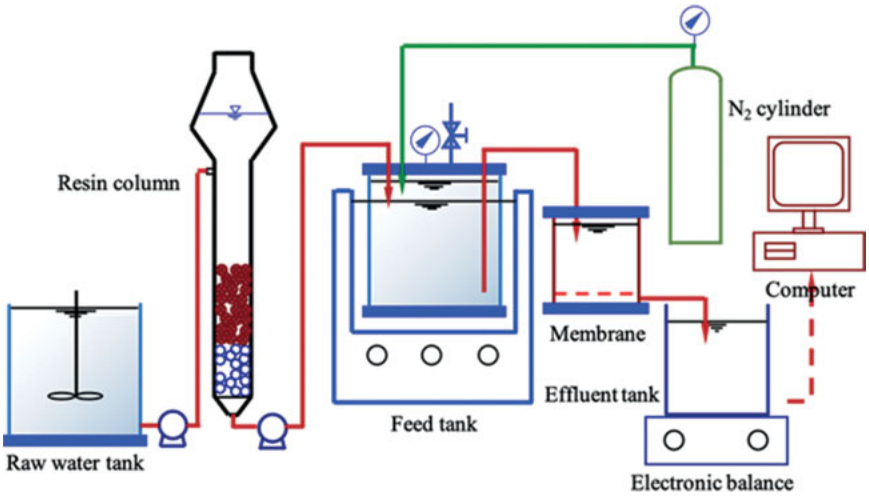

Figure 5.38: Schematic diagram of the experimental setup.

The adsorption curve with DOC and UV quasi-one and quasi-two fitting is shown in Figure 5.39. Both resins had poor linear correlations with DOC adsorption in quasi-one curves. However, in quasi-two fitting curves, both resins exhibited good correlation with DOC and UV_{254} adsorptions, with the R^2 of 0.9974 and 0.9919 for DOC, and 0.9964 and 0.9939 for UV_{254} for PW16 and PWA9, respectively. The measured Q_e was close to the calculated value by the quasi-two kinetic equation, while it was quite different from that by the quasi-one kinetic equation. In addition, it was found no matter in quasi-one or quasi- two kinetic equations, both resins had higher UV_{254} adsorption rate constants than DOC adsorption rate constants, with 39 and 37 times higher of UV_{254} adsorption rate constants than DOC adsorption rate constants for resins PW16 and PWA9, respectively. Thus, the UV_{254} organics could be much easier to be eliminated than the DOC organics by both resins.

In this study, the 0.1 μm Millipore flat sheet of hydrophilic mixed cellulose membrane (VCWP, Millipore Corporation, US), composed of 80–100% nitrate cellulose and 0–20% acetate cellulose was adopted. In each test, a new membrane was used.

Two types of natural surface water, Sanhaowu water (SHW) and Taihu Lake water (LT), were collected for the feed. SHW is a typical river, containing allochthonous natural organic matter (NOM), while LT is a typical lake, comprising lots of algal organics. The characteristics of the water samples are presented in Table 5.6. It can be seen that both feeds have high UV_{254} values, and SHW water has a high amount of DOC and a low turbidity and COD_{Mn}; while LT water has a low DOC content and a high turbidity and COD_{Mn}. SHW water was mainly used in the experiment for resin pretreatment to reduce membrane fouling, while LT water was to investigate the effect of the combination of coagulation and resin pretreatment on membrane fouling control.

EBSCOhost - printed on 2/14/2023 6:39 AM via . All use subject to https://www.ebsco.com/terms-of-use

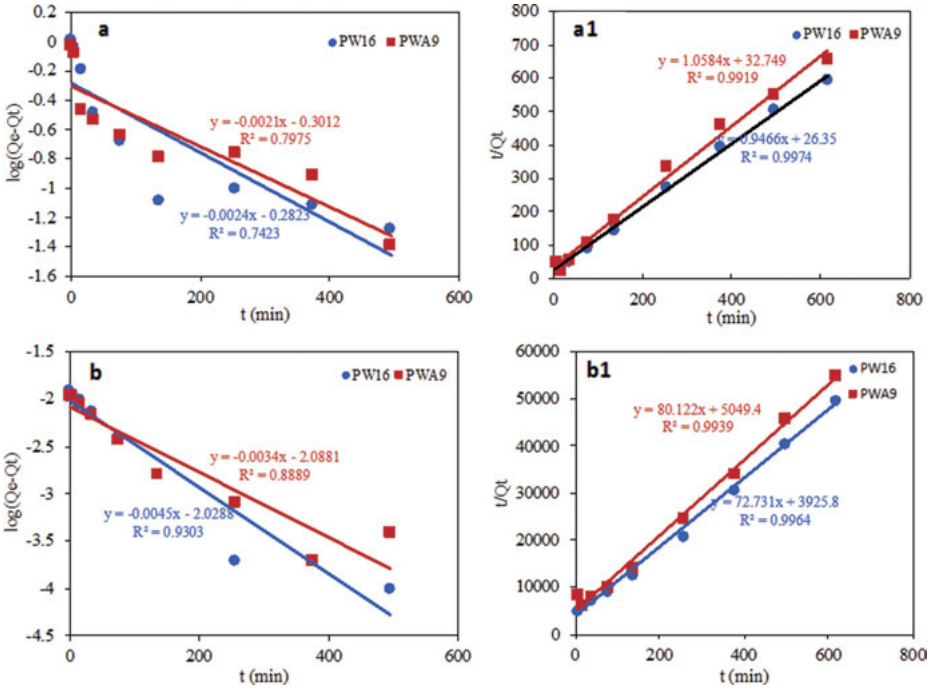

Figure 5.39: DOC and UV quasi-one and quasi-two fitting curves. a, DOC (quasi-one); b, UV_{254} (quasi-one); a1, DOC (quasi-two); b1, UV_{254} (quasi-two).

Table 5.6: Characteristics of water samples.

Parameter	LT	SHW
Turbidity (NTU)	38.8	5.3
COD_{Mn} (mg/L)	3.91	3.23
pH	8.56	8.40
DOC (mg/L)	4.134	6.005
UV_{254} (cm^{-1})	0.099	0.080

5.3.2 Results and discussion

5.3.2.1 The effect of resin pretreatment on fouling mitigation

The effect of the resins on MF filtration performance is shown in Figure 5.40. The final normalized flux (J/J_0) at the end of the filtration for the feed was about 17%; with the resin as pre-adsorption, the flux increased to 21%. The results showed that the pre-

EBSCOhost - printed on 2/14/2023 6:39 AM via . All use subject to https://www.ebsco.com/terms-of-use

treatment of PW16 and PWA9 could reduce the membrane fouling slightly and both MIEX had the similar effect on permeate flux improvement.

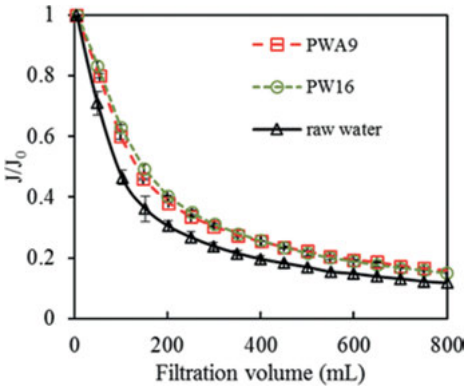

Figure 5.40: Effect of resin on MF performance.

The membrane filtration performance by the PWA9 resin with different adsorption time is exhibited in Figure 5.41. With the first 10 h adsorption, the PWA9 resin improved the filtration flux significantly (PWA9-10). However, the ability of the resin to control membrane fouling could gradually reduce with the relative long pretreatment process (PWA9-20 and PWA9-30).

5.3.2.2 The effect of resin pretreatment on organic removal

The water qualities with and without the resins adsorption and MF filtration are listed in Table 5.7. The resins adsorption had a higher UV_{254} removal rate than the DOC. This is due to that the UV_{254} organics consist of benzene-ring or double ring structures, which can be removed by the ion exchange with Cl^- or OH^- from the resins. With additional MF filtration, the organics could be further removed, with the total DOC removal rate of 69.57% and 68.99% and total UV_{254} removal rate of 89.04% and 84.93% for the PW16 and PWA9 resins, respectively.

5.3.2.3 Effect of resin adsorption on organics molecular weight distribution

The molecular weight (MW) distribution of the SHW water before and after the resin adsorption and MF filtration is shown in Figure 5.42. The MW distribution of the feed can be divided into three types of organics, i.e. type I: large-MW organics (5.0×10^6–5.0×10^4 Da), type II: medium MW organics (1.10×10^4–2.64×10^3 Da), and

EBSCOhost - printed on 2/14/2023 6:39 AM via . All use subject to https://www.ebsco.com/terms-of-use

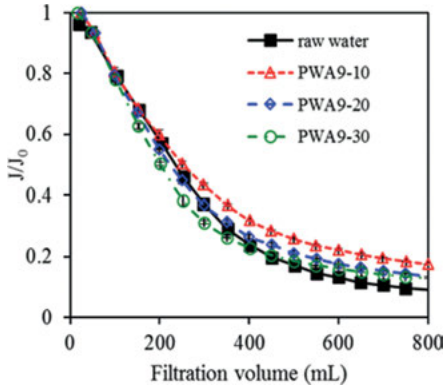

Figure 5.41: Effect of pre-adsorption time on MF performance. The legend "10, 20 and 30" represents the adsorption time is 0–10 h, 10–20 h and 20–30 h, respectively.

Table 5.7: DOC and UV Removal efficiencies in SHW water.

Samples	DOC (mg/L)			UV_{254} (cm^{-1})		
	PW16	PWA9	Raw water	PW16	PWA9	Raw water
Before membrane	1.925	2.084	5.334	0.012	0.016	0.073
After membrane	1.623	1.654	4.807	0.008	0.011	0.067
Resin removal efficiency (%)	63.92	60.93	–	83.56	78.08	–
Membrane removal efficiency (%)	5.65	8.06	9.89	5.48	6.85	8.22
Total removal efficiency (%)	69.57	68.99	–	89.04	84.93	–

type III: micro-MW organics (2.64×10^3–1.6×10^2 Da), corresponding to biopolymers (PN and PS), humic-like organics, and low MW hydrophilic organics, respectively.

The large-MW organics were slightly reduced after 10 h resin adsorption pre-treatment, indicating that PWA9 resin was not able to effectively remove the macro-molecules. On the contrary, the medium and small MW organics were significantly removed in the initial 10 h treatment. This is due to that the PWA9 has a pore size range from 100–500 nm and plays a limited effect on the removal of macro-MW organics (particle size at 0.1–1.0 μm). LC-UV result showed that PWA9 could preferentially remove the UV-absorbing compounds. At the initial absorption period (0–10 h), there may be enough exchange sites for both UV and non-UV-absorbance organics to be adsorbed. Nevertheless, available exchange sites are gradually decreased in the following stage and those non-UV absorbance matters could be replaced or swapped out to the permeate. Therefore, removal efficiency of DOC by the resin adsorption decreased with the extension of filtration time. It is worth noting that MW of the water with 10 h resin pre-treatment and that with further membrane filtration nearly coincide (except for large-MW organics), indicating the poor effect of MF membrane on medium and micro MW organics removal but preference on the retention of the

EBSCOhost - printed on 2/14/2023 6:39 AM via . All use subject to https://www.ebsco.com/terms-of-use

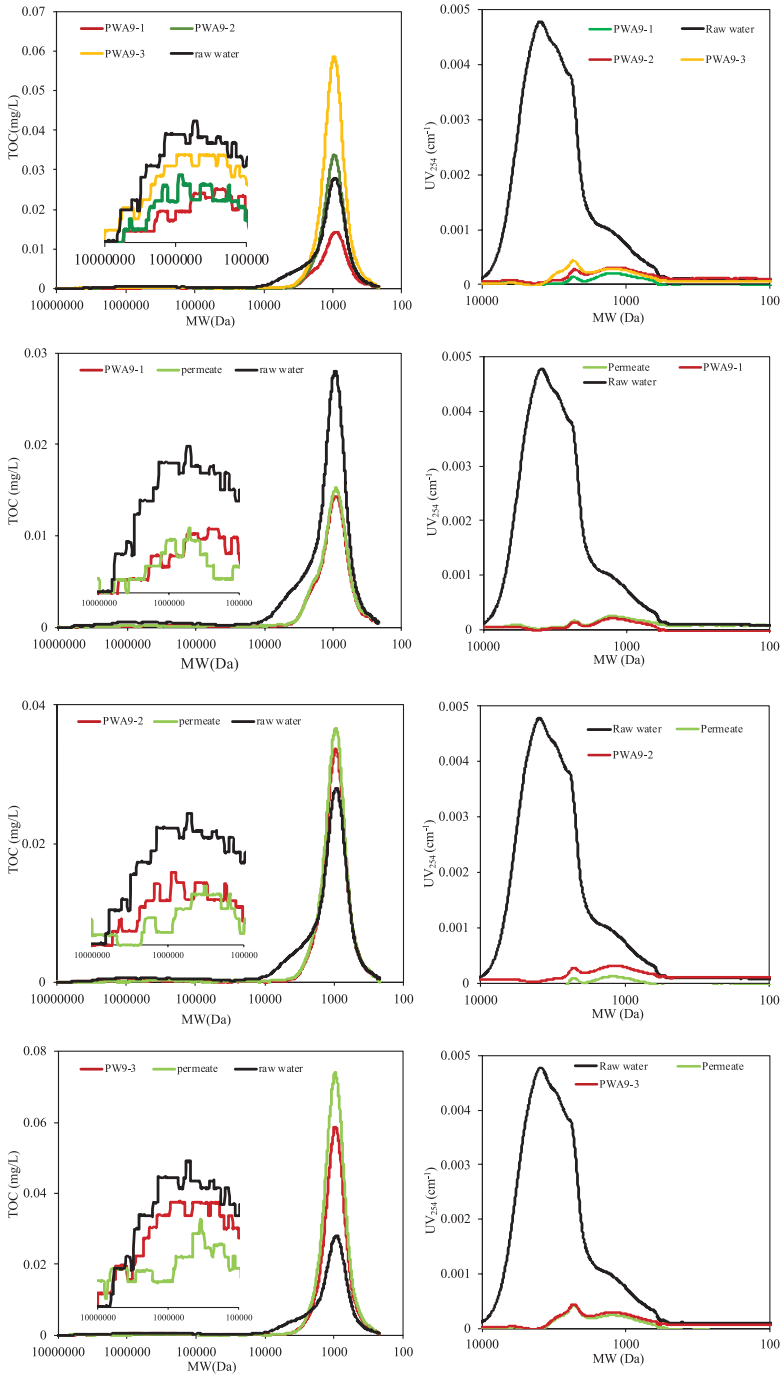

Figure 5.42: MW distribution of SHW water with/without resin adsorption followed by membrane filtration. The legend "1, 2 and 3" represent pre-adsorption time is 10, 20 and 30 h, respectively.

EBSCOhost - printed on 2/14/2023 6:39 AM via . All use subject to https://www.ebsco.com/terms-of-use

macro-MW substances. The concentration of the latter increased after MF filtration probably due to the continuous exchange effects on the small organics by the resin.

5.3.2.4 Effect of resin on fluorescence EEM of NOM

The fluorescence EEM spectra of the SHW water and the effluent after the MF filtration and resin adsorption is shown in Figure 5.43. There are four fluorescence peaks (Figure 5.43(a)) representing humic-like (Peak A), fulvic-like (peak C), protein-like (peak T), and tryptophan-like (peak B) substances. The substances at peak B and peak T were mainly retained by the MF filtration, thus they are important membrane fouling contributors (Figure 5.43(b)). However, with the resin 10 h absorption pretreatment, almost all the EEM organics could be removed (Figure 5.43(c)), indicating the higher removal efficiencies of the fluorescence organics by resin adsorption than by MF filtration. In addition, it can be observed from Figure 5.43(d) that despite the resin adsorption pretreatment, some of the organics at peak T and peak B were still retained in the MF filtration, thus the resin adsorption could only remove part of protein-like organics.

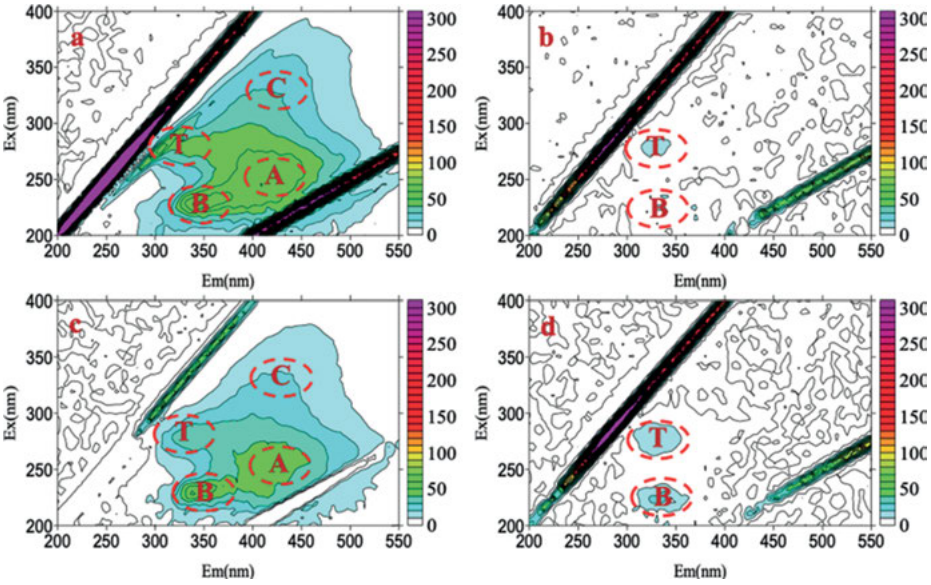

Figure 5.43: EEM of (a) SHW feed water; (b) subtracted fluorescence by MF; (c) subtracted fluorescence by resin (10 h); (d) subtracted fluorescence between resin (10 h) and MF.

EBSCOhost - printed on 2/14/2023 6:39 AM via . All use subject to https://www.ebsco.com/terms-of-use

5.3.2.5 Effect of the combination of coagulation and resin adsorption on fouling mitigation

As mentioned above, the resin adsorption can remove medium and large-MW organics, however, it plays very limited effect on large-MW organics removals. While the coagulation could effectively remove macro MW organics, the combination of coagulation and resin adsorption was proposed as a pretreatment to reduce membrane fouling.

The filtration flux of LT water with and without the pretreatment of coagulation and the PW16 resin adsorption is shown in Figure 5.44. Without any pretreatment, the final flux gets to only 5.3% of its initial flux for around 800 mL volume of water filtration. With coagulation as the pretreatment, the final water flux increased to 33%. With both resin 10 h and coagulation as pretreatment, slight improvement in the filtration flux was observed. After 20 h of resin adsorption, the trend of flux curve was extremely different from that of coagulation alone. This may be due to that the coagulation pretreatment could remove most of the macro-MW organics which can be adsorbed by resin pretreatment prior to the filtration process.

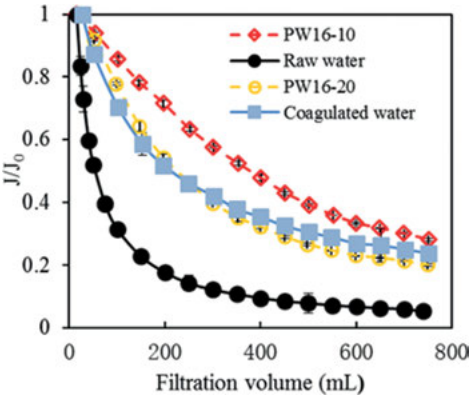

Figure 5.44: Role of coagulation and resin adsorption on MF performance for LT water treatment.

The MW distribution of the LT water before and after the coagulation and the PW16 resin adsorption is presented in Figure 5.45. With coagulation, the peak of the macro MW almost disappeared and the intensity of the medium MW peak (at 2,500 Da) was reduced with the TOC detection, indicating that coagulation was able to reduce the macro MW organics and some medium MW molecules. With the combination of resin pretreatment and coagulation, the TOC absorbance at 2,500 Da was further decreased with 0–10 h resin adsorption. In addition, the peak at 1–10 kDa with the resin adsorption with the UV_{254} detection almost disappeared, demonstrating that the subsequent resin treatment (0–10 h) played an important effect in further reducing the organics.

The MW distribution result of the UV detection was similar with the TOC detection. With UV detection, it was observed that the organics with MW of 2,500 Da was greatly

EBSCOhost - printed on 2/14/2023 6:39 AM via . All use subject to https://www.ebsco.com/terms-of-use

reduced with coagulation pretreatment, and they disappeared with resin adsorption. Thus the resin PWA9 was very effective to remove the molecules with UV_{254} absorbance.

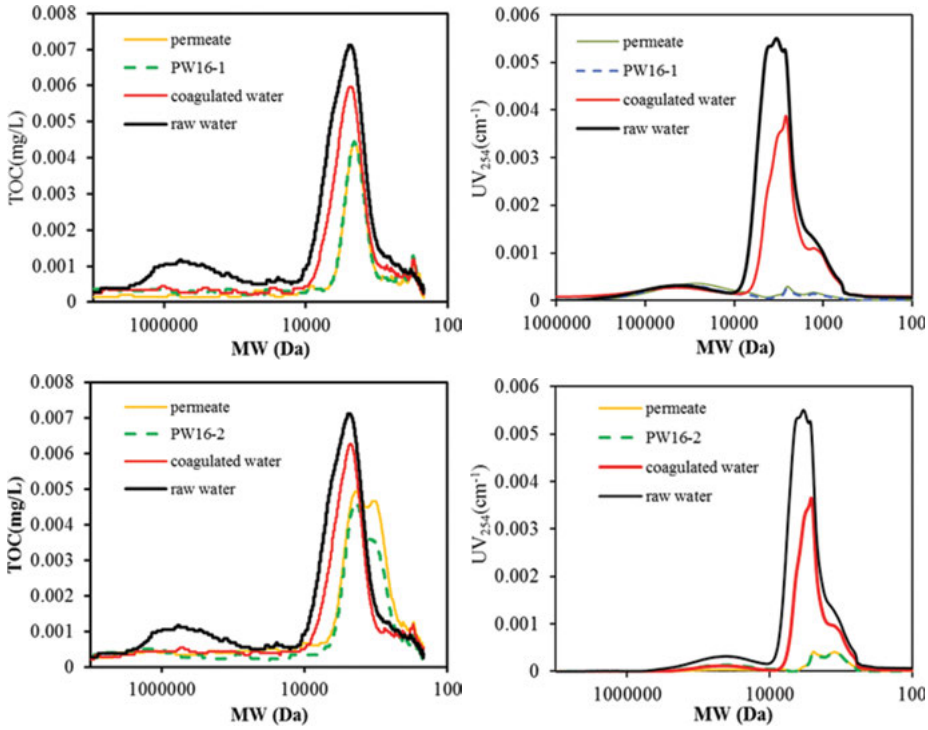

Figure 5.45: MW distribution of LT water with/without coagulation, resin 16 and MF treatment. The legend "1 and 2" represent pre-adsorption time is 10 h and 20 h, respectively.

The SEM images of membrane surface with/without coagulation/resin treatment are presented in Figure 5.46. For the SHW water, the SEM result of the direct filtration exhibited a thick gel layer deposition on the membrane surface. With resin PWA9 0–10 h adsorption, a lot of visible membrane pores and some large MW molecules foulant could be observed, which suggested that the resin adsorption could remove most contaminants in SHW water. With PWA9 10–20 h and 20–30 h treatments, membrane pores were further obstructed and gel layer emerged, which might be due to more macromolecules adsorption by the resin exchange. Compared with SHW water, in addition to a gel layer, some large organics accumulation was observed in the SEM image of the LT water filtration, which were probably protein-like or polysaccharides-like large-MW organics. After the coagulation pretreatment, membrane pores were partially visible, indicating the removal of large molecules. After PW16 adsorption, membrane pores were even more visible with 0–10 h treatment, and partly gel layer deposition were obtained in 10–20 h treatment.

EBSCOhost - printed on 2/14/2023 6:39 AM via . All use subject to https://www.ebsco.com/terms-of-use

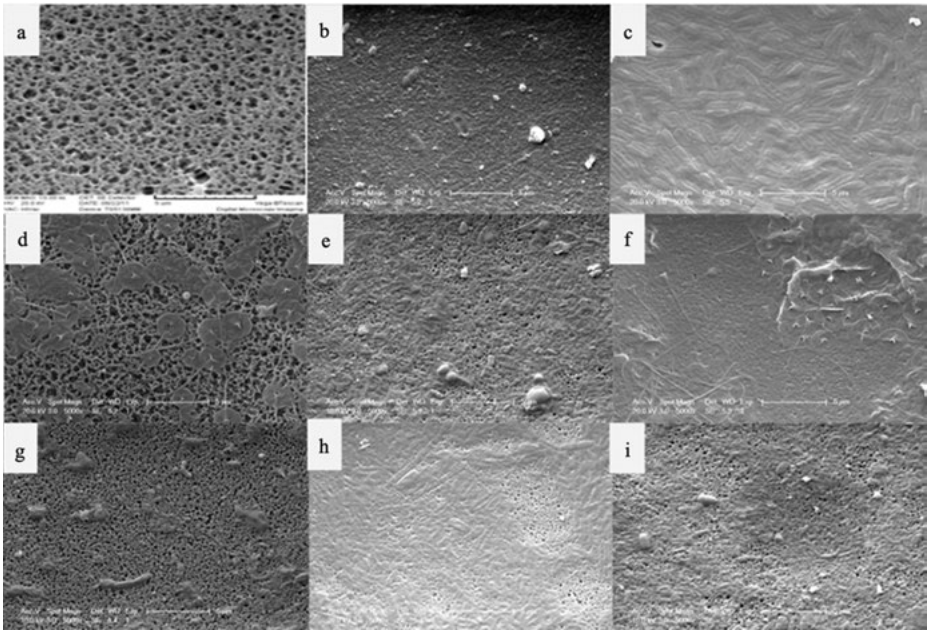

Figure 5.46: SEM micrograph a, clean membrane; b, SHW water; c, PWA9 0–10 h; d, PWA9 10–20 h; e, PWA9 20–30 h; f, LT water; g, after coagulation; h, coagulation + PW16 0–10 h; i, coagulation + PW16 10–20 h.

It has been reported that particles preferentially accumulate on rough surfaces, causing more severe flux decline than on smooth surfaces in membrane filtration. Thus the surface topological properties of membranes have strong implications for membrane behaviors and fouling propensities. The AFM images of clean and fouled membranes were examined with the results shown in Figure 5.47. The AFM measurements of the membrane fouled by SHW water, SHW water with resin PWA9 0–10 h, 10–20 h, and 20–30 h treatment were conducted at 59.1, 49.1, 60.9, and 57.5 nm, respectively, while the AFM detections of the membrane contaminated by LT water, LT water with coagulation, LT water with coagulation and 0–10 h PW16 resin adsorption, and LT water with coagulation and 10–20 h PW16 resin adsorption were carried out at 50.0, 26.2, 23.8, and 33.5 nm, respectively, as compared with the new membrane measured at 25.9 nm. It was found that some protuberances were exhibited on the membrane fouled by SHW water, while many uniform asperities by the LT water. The discrepancy can be due to that more macromolecular organics were in LT water than in SHW water such that a thicker cake layer was formed on the membrane fouled by the LT water. However, with the 0–10 h PWA9 resin treatment, less roughness was observed with the membrane fouled by SHW water, and some higher protrusions were even emerged after the 10–20 h and 20–30 h resin adsorption. Such phenomenon might be due to that the macromolecules could be replaced or swapped out by the resin exchange.

EBSCOhost - printed on 2/14/2023 6:39 AM via . All use subject to https://www.ebsco.com/terms-of-use

The surface morphologies of the membrane fouled by LT water after coagulation and resin PW16 treatment were significantly different, and a lot of valleys were exhibited, which were extremely similar to the clean membrane surface. In addition, higher protrusions appeared with the membrane fouled by the LT water with coagulation and 0–10 h and 10–20 h PW16 resin treatment, which was similar as that of the membrane fouled by the SHW water with resin adsorption. Furthermore, it was found that the roughness of the membranes caused by both types of feed after coagulation and/or resin adsorption coincided with those observed during the membrane filtration measurement.

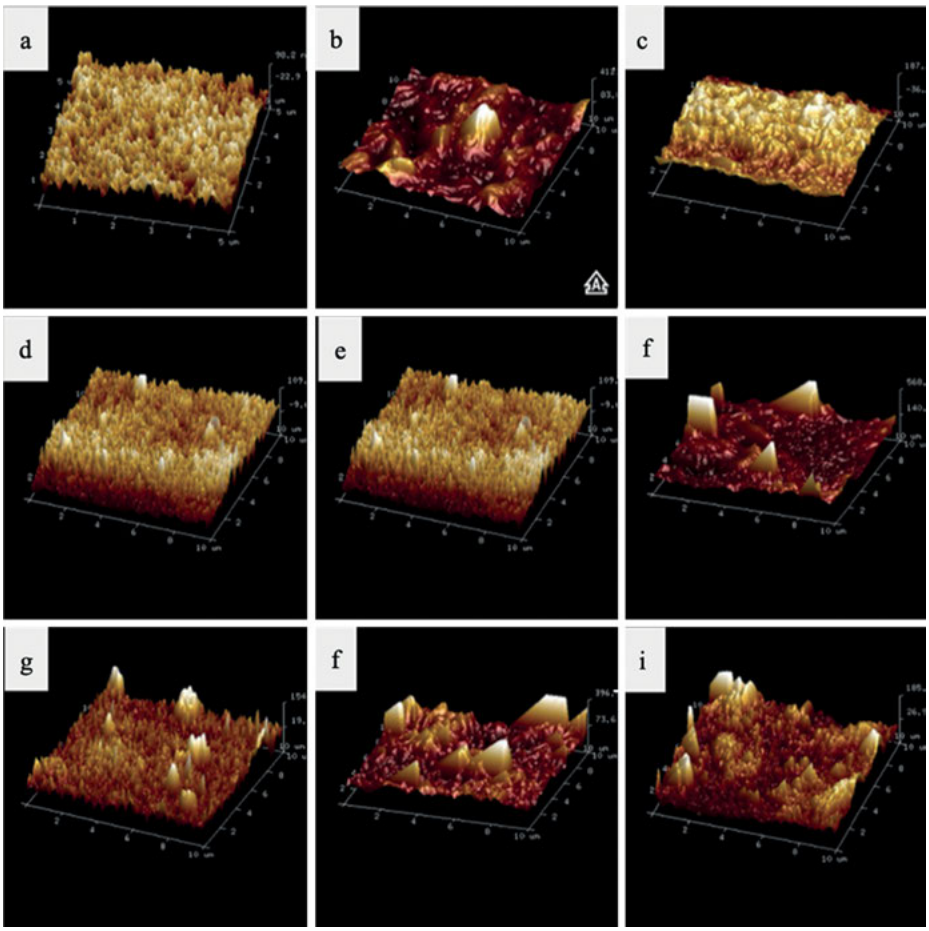

Figure 5.47: AFM images of the membranes filtrated with SHW/LT water with/without coagulation and/or resin adsorption. (a) clean membrane; (b) SHW water; (c) PWA9 0–10 h; (d) PWA9 10–20 h; (e) PWA9 20–30 h; (f) LT water; (g) after coagulation; (h) coagulation + PW16 0–10 h; (i) coagulation + PW16 10–20 h.

EBSCOhost - printed on 2/14/2023 6:39 AM via . All use subject to https://www.ebsco.com/terms-of-use

The fouling mitigation mechanism of the combination of resin adsorption and coagulation is illustrated in Figure 5.48. The resins could effectively reduce the medium and small MW organics, especially moderate molecules with UV absorbance, but were ineffective in removing organics with large MW. The sole use of resin adsorption can improve the filtration flux in the first 10 h adsorption, however, the ability to enhance the filtration flux gradually dropped for the long time adsorption. The integration of coagulation, resin adsorption and membrane filtration could significantly remove the organics thus to reduce membrane fouling. The SEM and AFM measurement of membrane surface morphologies and the membrane filtration performance as well as the MW distribution of the organics indicated that biopolymers played a key role in membrane fouling composition, while the coagulation could effectively remove them. The combination of coagulation and resin adsorption with filtration columns is thus suggested for surface water pretreatment prior to membrane filtration.

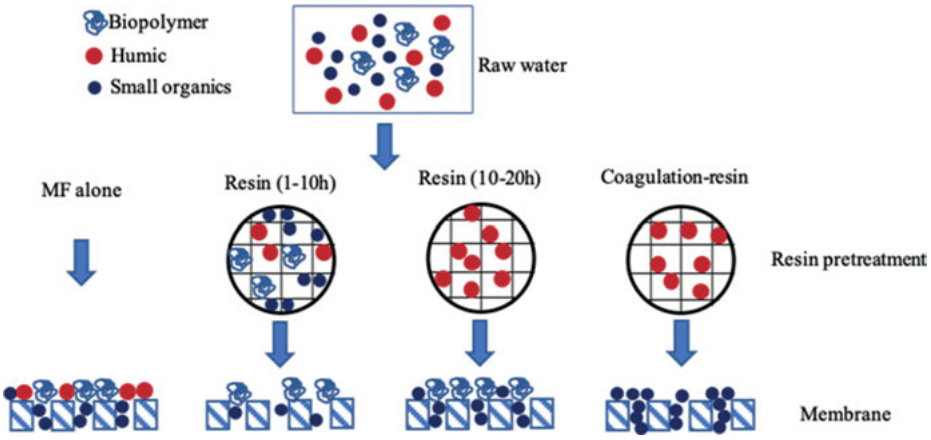

Figure 5.48: Fouling mitigation mechanism of resin adsorption and coagulation pretreatment.

5.4 Oxidation pretreatment

5.4.1 The effect of combination of pre-ozonation and microfiltration process

5.4.1.1 Materials and methods

1 Source water

Raw water was taken from Huangpu River, with the qualities presented in Table 5.8.

EBSCOhost - printed on 2/14/2023 6:39 AM via . All use subject to https://www.ebsco.com/terms-of-use

Table 5.8: Characteristics of Huangpu River raw water.

Parameters	Values
pH	7.2–7.6
Turbidity (NTU)	13.7–75
COD_{Mn} (mg/L)	5.2–6.9
UV_{254} (cm^{-1})	0.128–0.157
DOC (mg/L)	5.1–6.6

2 Bench scale experiment

The pure oxygen was used to produce ozone with the ozone generator (SKCFG-1, JiNan SanKang). The generated ozone was dosed into a static tank for a contact time of 10 min each. Different doses of 0.5, 1.0, 1.5, 2.0, 2.5, and 3.0 mg/L were performed in this study. After the ozonation, the residual ozone was aerated by pure N_2 in order to prevent the ozone from destroying the membrane. Then the ozonated water was transferred for subsequent filtration test.

The microfiltration experimental setup is shown in Figure 5.49, which consists of a N_2 pressure cylinder, feed water tank and a hollow fiber MF membrane module from Toray Japan, with the characteristics shown in Table 5.9. The N_2 gas cylinder was used to provide a constant pressure for the ozonated water in the feed tank for the microfiltration. A magnetic stirrer was located at the bottom of the feed tank for completely mixing the feed water. In each filtration test, a volume of 800 mL ozonated water was filtrated and then the chemical cleaning was carried out. Two steps of chemical cleaning were included, i.e. oxalic acid and sodium hypochlorite cleaning for 2 h each.

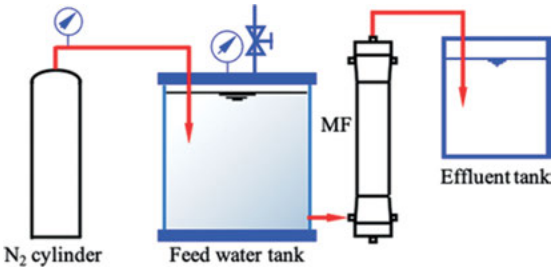

Figure 5.49: Schematic diagram of the bench scale membrane system.

5.4.1.2 Results and discussion

1 Effect of ozone dosage on organics removal

Figure 5.50 shows the DOC concentration with different ozone dosage. The efficiency of DOC removal increased with the increase of ozone dosages, e.g. 1.6% and 3.8%

EBSCOhost - printed on 2/14/2023 6:39 AM via . All use subject to https://www.ebsco.com/terms-of-use

Table 5.9: Characteristics of membrane.

Material	PVDF
Type	Hollow fiber
Pore size (μm)	0.1
Membrane surface area (cm^2)	0.128–0.157
Type of filtration	Dead-end
Type of pressure	Out-in

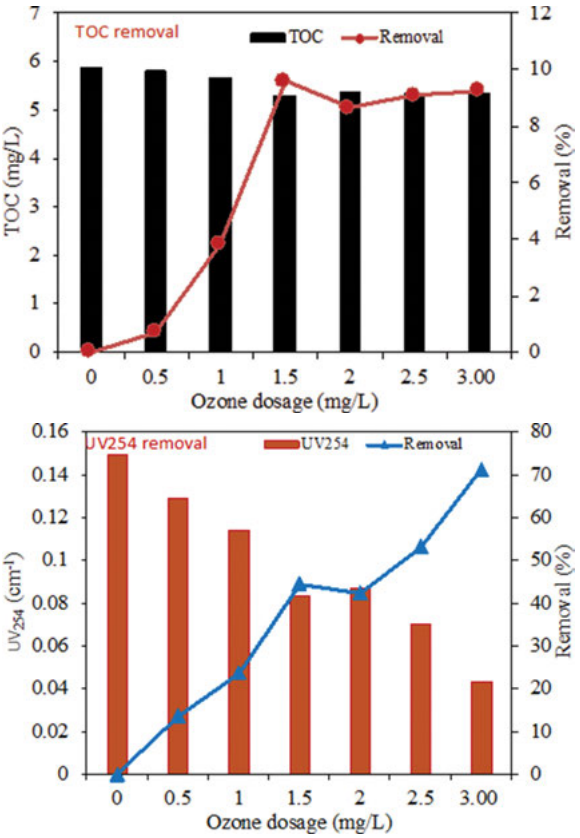

Figure 5.50: The effect of ozone dosage on organics removal.

DOC removals were obtained with 0.5 mg/L and 1.0 mg/L ozone concentrations, respectively. In addition, it was found there was an optimized ozone dosage for DOC removal. When the ozone dosage was 1.5 mg/L, the DOC removal efficiency rose to 9.6%. When more ozone was added, no additional DOC removal was obtained. It may be due to that the organic matter in Huangpu River was not easily degraded by ozonation. The ozone could probably broke the macromolecules to small molecules only.

EBSCOhost - printed on 2/14/2023 6:39 AM via . All use subject to https://www.ebsco.com/terms-of-use

However, the UV_{254} removal increased from 13% to 71% with the increment of ozone dosage from 0.5 mg/L to 3.0 mg/L. Obviously higher UV_{254} removal rate was obtained than DOC removal, which suggests that ozone could effectively degrade the hydrophobic matter since most UV organics are humic substances with aromatic structures, while DOC organics contain both humic and non-humic organic materials.

2 Effect of ozone dosage on molecular weight distribution

Figure 5.51 shows the molecular weight distribution of the organic matter with different ozone dosages. The molecular weight of the organic substances in Huangpu River water is mainly between 2–7 kDa, and partly around 0.2 kDa. Significant differences of the molecular weight distribution can be observed with varied ozone dosages. When low ozone concentration of 0.5 mg/L or 1.0 mg/L was injected, the concentration of organic matter, with the molecular weight between 2 kDa and 7 kDa decreased a little as compared with the raw water, whereas the concentration of organic matter with molecular weight smaller than 0.2 kDa increased. It could be probably due to that the ozone degraded the macromolecular organic matter to small molecular matter. But when the ozone dosage is up to 1.5 mg/L, the reduction of organics with molecular weight about 2–7 kDa is obvious. And with more ozone dosed, less organic matter with molecular weight between 2 kDa and 7 kDa were exhibited.

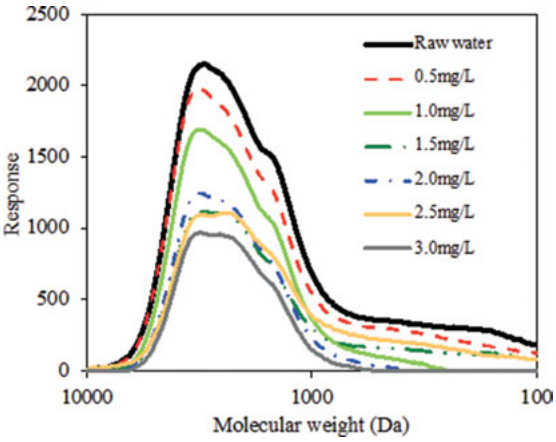

Figure 5.51: Effect of ozone dosages on molecular weight distribution of organics.

EBSCOhost - printed on 2/14/2023 6:39 AM via . All use subject to https://www.ebsco.com/terms-of-use

3 Effect of ozone dosage on organic hydrophilicity

Figure 5.52 shows the effect of ozonation on different hydrophilic/hydrophobic fractions. With ozone addition, the concentration of HPO fraction reduced and the HPI increased, while the TPI maintained nearly the same. These results indicated that the ozone could convert the hydrophobic substances to hydrophilic ones. In addition, with high concentration of ozone dosages, the concentration of the hydrophilic organics reduced, which was probably due to that ozonation could partially mineralize the organic matter. With high intensities of ozonation, both the hydrophobic and hydrophilic substances in terms of UV_{254} dropped, which revealed that ozone could oxidize the aromatic hydrocarbon, double bond or carbonyl organic substances, which usually represent UV_{254} organics.

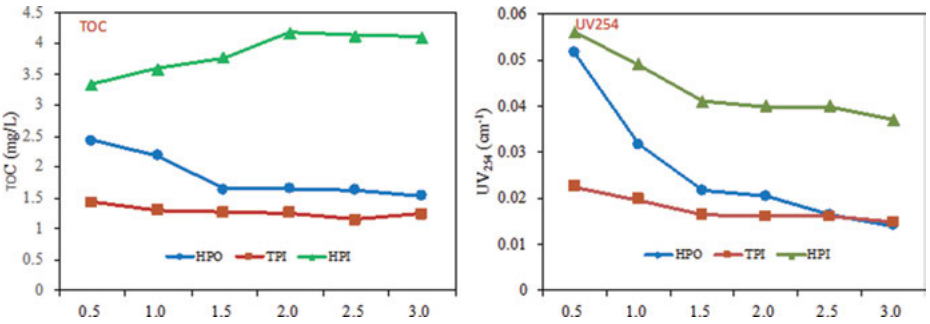

Figure 5.52: The effect of ozone dosage on organic hydrophilicity.

4 Effect of membrane filtration on molecular weight distribution of hydrophilic/hydrophobic fractions

The molecular weight distribution of hydrophilic/hydrophobic fractions with/without membrane filtration is shown in Figure 5.53. The raw water had a weak response at the molecular weight between 10,000–100,000, while the HPI fraction also exhibited less weak response in the same region, indicating that large molecules are mainly HPI fractions. After the membrane filtration, the large molecular weight response for both raw water and HPI disappeared, thus the membrane could effectively remove macromolecules. It can be also found that the content of the medium and small molecules in both HPI and HPO fractions decreased after the membrane filtration, thus the membrane filtration could only partially remove these organics.

5 Effect of ozonation on membrane permeability

Figure 5.54 shows the effect of ozonation on membrane permeability. The addition of ozone mitigates the membrane flux decline. When the Huangpu River water is filtrated directly without ozonation pretreatment, the J/J_0 decreased to 21% after 800 mL filtration. With low ozone concentration of 0.5 mg/L and 1.0 mg/L as pretreatment,

EBSCOhost - printed on 2/14/2023 6:39 AM via . All use subject to https://www.ebsco.com/terms-of-use

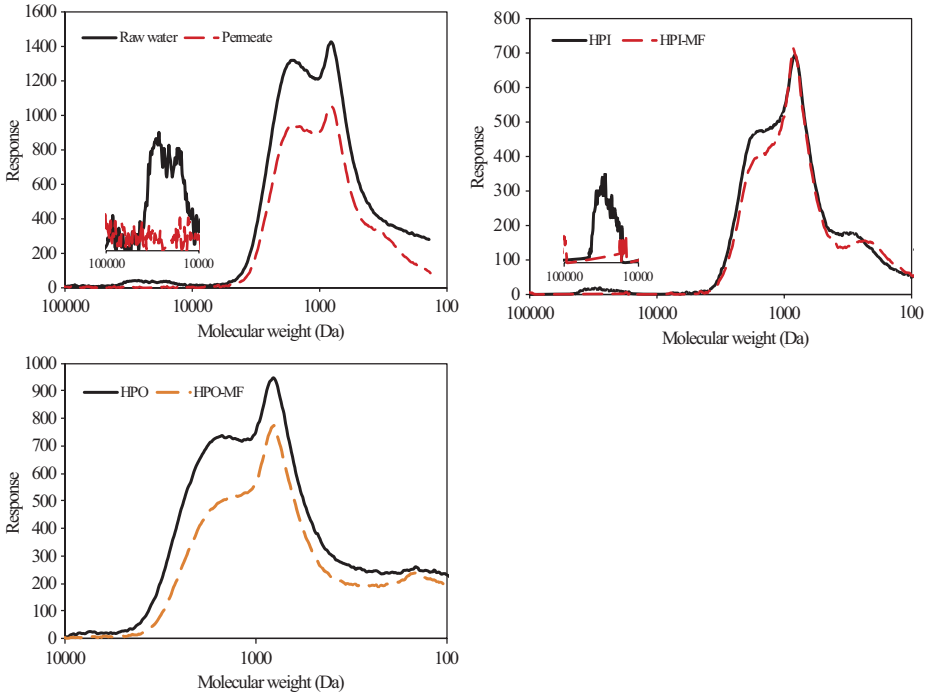

Figure 5.53: The effect of membrane filtration on molecular weight distribution of hydrophilic/hydrophobic fractions.

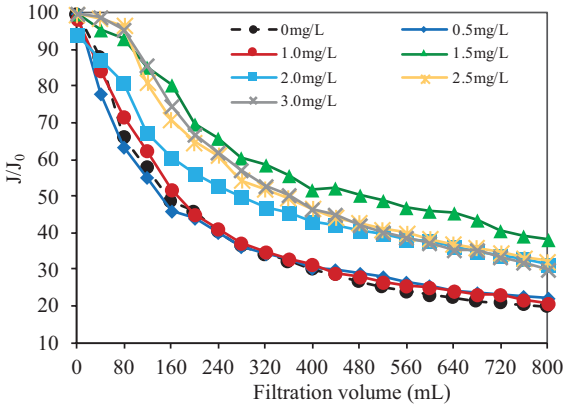

Figure 5.54: The effect of ozone dosage on membrane permeate flux.

there is no improvement on the permeate flux. When the ozone dosage increased to 1.5 mg/L, the flux increased dramatically. However, with the further increase of the ozone dosage, no additional flux improvement was observed but the flux even dropped slightly. Thus the optimal ozone dosage for Huangpu River water is 1.5 mg/L.

EBSCOhost - printed on 2/14/2023 6:39 AM via . All use subject to https://www.ebsco.com/terms-of-use

The ozonation could change the molecular weight distribution and hydrophilicity of organic matter in the raw water, producing smaller and more hydrophilic substances, thereby affecting the membrane filtration performance.

5.4.2 The effect of the combination of oxidation and coagulation on membrane fouling control of Huangpu River water

5.4.2.1 Materials and methods

In this study, the feed was collected from Huangpu River, with the characteristics listed in Table 5.10. The PVDF UF membrane was adopted, with a pore size of 0.03 μm and effective surface area of 0.003 m^2. In the filtration experiment, the flux was controlled at 60 $L/(h \cdot m^2)$ with a duration of 65 min.

In the oxidation process, the feed was oxidized with different oxidants of ozone, sodium hypochlorite and potassium permanganate, then filtrated with the PVDF hollow fiber membrane at a flow rate of 1.6 L/h. After 65 min filtration, the permeate was collected and the organic molecular weight distribution, dissolved organic carbon, UV_{254}, EEM, etc. were measured. After the filtration, the chemical cleaning of the membrane was conducted.

Table 5.10: Raw water quality.

Parameters	Variety range	Average
Water temperature	15.2–27.6	22.3
pH	7.50–8.19	7.79
Turbidity (NTU)	4.21–15.47	7.96
DOC (mg/L)	2.763–4.250	3.3
UV_{254} (cm^{-1})	0.063–0.072	0.065

The experimental setup diagram for the combination of oxidation and coagulation is shown in Figure 5.55. In the combination of ozonation and coagulation process, ozone with given concentration was injected to the feed. After 10 min ozonation, the residual ozone was purged by the pure nitrogen. Then the refined coagulant of aluminum sulfate was added to the ozonated water. Two dosages of 10 and 30 mg/L were carried out. In the coagulation process, the ozonated water was first stirred rapidly at 1,000 r/min for 1 min then slowly at 200 r/min for 30 min. After the coagulation, the treated water was filtrated by the UF to investigate the effect of the hybrid process on fouling reduction and organics removal.

EBSCOhost - printed on 2/14/2023 6:39 AM via . All use subject to https://www.ebsco.com/terms-of-use

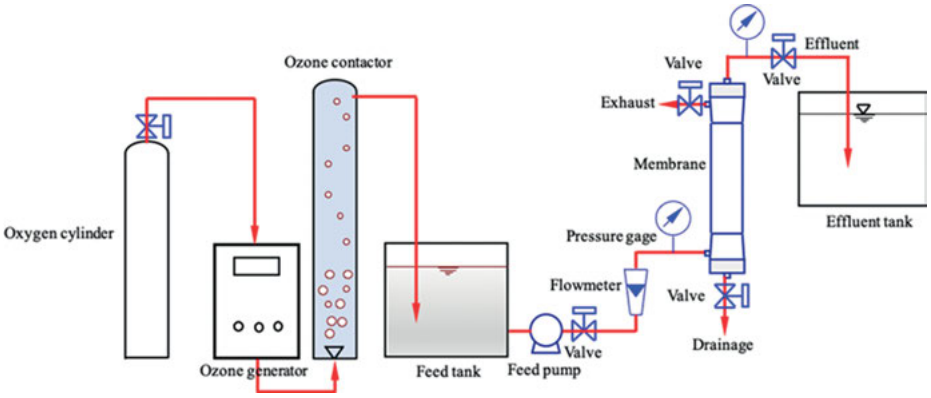

Figure 5.55: Schematic diagram of bench scale experiment system.

5.4.2.2 Results and discussion

1 The effect of pre-oxidation with different oxidants on TMP reduction

The effect of different oxidants on TMP reduction were examined and the results are shown in Figure 5.56. Without any oxidants, the TMP/TMP_0 of the raw water increased dramatically. With 1 mg/L chlorine, the TMP/TMP_0 remained unchanged as compared with raw water filtration. When the chlorine concentration was increased to 2 mg/L, no obvious reduction of TMP/TMP_0 was observed. With additional dosage of coagulant, the reduction of TMP/TMP_0 was remarkable, e.g. with 1 mg/L chlorine and 10 mg/L aluminum sulfate, the TMP/TMP_0 arrived to 1.4 at the end of the filtration, with a 36% reduction rate, and with a higher coagulant concentration of 30 mg/L, TMP/TMP_0 rose to a lower value of 1.2.

With 0.5 mg/L potassium permanganate, the TMP/TMP_0 reached 1.33 at the end of filtration, but it rose to a higher value of 1.9 with a higher dosage of 1 mg/L potassium permanganate. With additional dosage of aluminum sulfate, the TMP/TMP_0 dropped at the end of the filtration no matter a higher or lower concentration of potassium permanganate was added, suggesting that the pretreatment of potassium permanganate could be enhanced with the coagulation.

The effect of ozone on TMP/TMP_0 reduction was also examined. With 1 mg/L zone, the TMP/TMP_0 arrived to 1.72 at the end of the filtration. With additional dosage of 10 mg/L aluminum sulfate, the TMP/TMP_0 reached 1.28, however, it remained unchanged when the coagulant concentration increased to 30 mg/L.

Thus the effect of pre-oxidation on membrane fouling control depends on the types of the oxidants and also on the dosages.

EBSCOhost - printed on 2/14/2023 6:39 AM via . All use subject to https://www.ebsco.com/terms-of-use

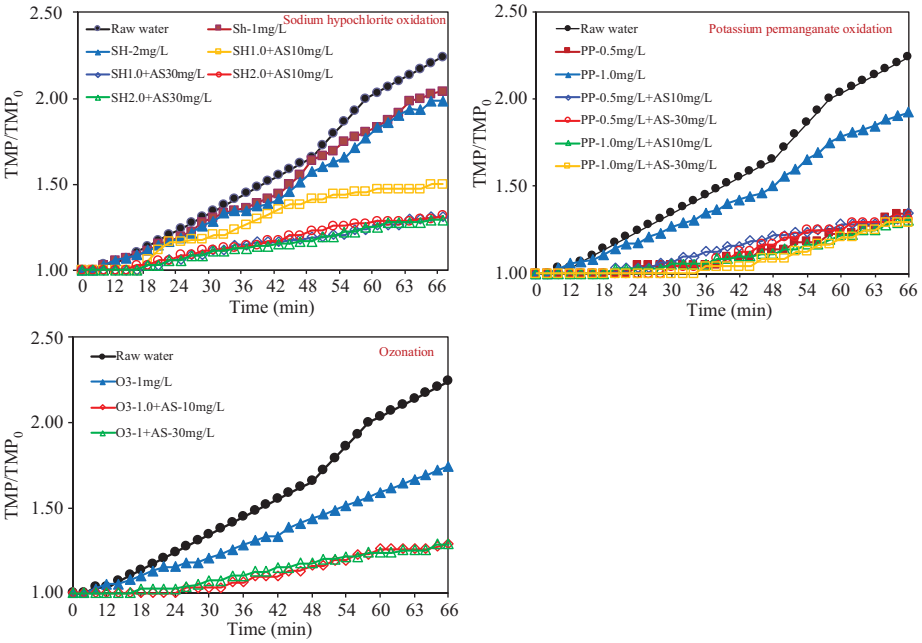

Figure 5.56: The effect of different oxidants pretreatment on TMP reduction.

2 The effect of pre-oxidation by different oxidants on organics removal

The organics removal efficiency by sodium hypochlorite oxidation and membrane filtration were examined and the results are shown in Figure 5.57. With direct membrane filtration, the TOC and UV_{254} had removal efficiencies of 52% and 35.5%, respectively. With 1 mg/L chlorine, the TOC removal efficiency was only 24%, while it dropped to 17% when the chlorine concentration increased to 2 mg/L. With the combination of 1 mg/L chlorine and 10 mg/L aluminum sulfate, the organics removal efficiency could be greatly increased.

Figure 5.58 showed that the potassium permanganate oxidation had a higher organic removal efficiency as compared with the chlorine oxidation. In addition, it was found that with the increasing dosage, the removal efficiency was also enhanced. However, with additional coagulation, the organic removal efficiency increased only slightly.

Figure 5.59 demonstrated that the pre-ozonation had the highest organics removal efficiency among the three oxidants. However, with the combination of coagulation, the organic removal efficiency increased very slightly.

3 The influence of pre-oxidation by different oxidants on organic MW distribution

As shown in Figure 5.60, in the MW distribution with TOC detection, there were two response peaks, i.e. one peak reflected large organics with the MW region in 10,000–100,000 with weak response, and the other reflected small organics with MW region

EBSCOhost - printed on 2/14/2023 6:39 AM via . All use subject to https://www.ebsco.com/terms-of-use

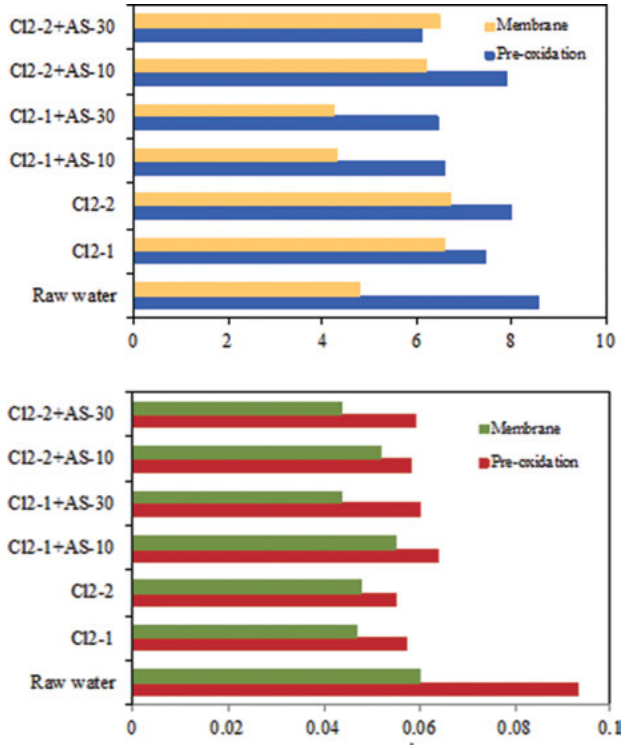

Figure 5.57: The effect of combination of sodium hypochlorite pre-oxidation and coagulation on organics removal.

around 1,000 with strong response. With chlorine oxidation, the response peak for large organics reduced slightly, while it dropped further when the dosage increased. However, the chlorine oxidation had almost no effect on the removal of the small organics. With the additional coagulation, the response peak for the large molecules were further reduced as compared with the chlorination only.

Figure 5.61 showed that with 0.5 mg/L potassium permanganate, the response peak for the large organics reduced significantly. When the concentration increased to 1 mg/L, the response peak for the large organics remained the same, while the one for the small organics dropped significantly. With the combination of potassium permanganate oxidation and coagulation, the removal efficiencies for both large and small organics were enhanced.

Ozonation could effectively oxidize the large organics but it had very limited effect for the small organics, as shown in Figure 5.62. As compared with the chlorination and potassium permanganate oxidation, the ozonation had better removal efficiencies for the large organics. With the combination of ozonation and coagulation, the removal efficiencies for both the large and small organics remained nearly the same.

EBSCOhost - printed on 2/14/2023 6:39 AM via . All use subject to https://www.ebsco.com/terms-of-use

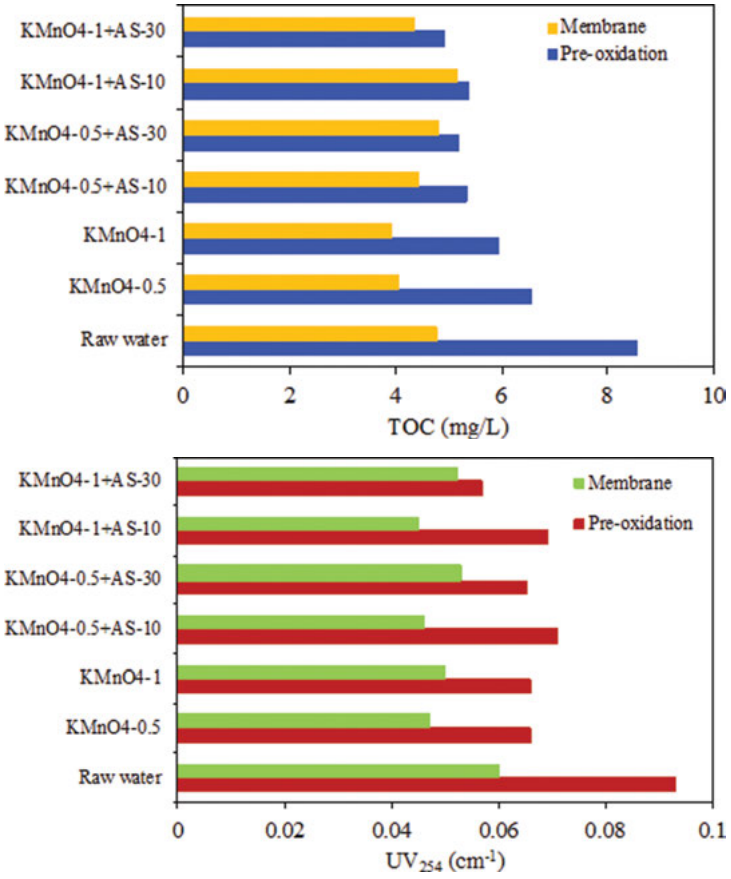

Figure 5.58: The effect of combination of potassium permanganate pre-oxidation and coagulation on organics removal.

It was reported that the large MW organics could be oxidized to small organics by oxidants and they can also be removed by the coagulation effectively. Here the Huangpu River feed water was treated with the combination of pre-oxidation and coagulation, with the result shown in Figure 5.63. The three oxidants could effectively oxidize the large organics, and the ozone exhibited the best performance, which may be due to its strongest oxidation ability. In the combination of pre-oxidation and coagulation, the combined ozonation and coagulation showed very slightly improvement on the large organic removal, while the other two combinations exhibited much higher removal efficiencies for large MW organics. This may be due to that the coagulation could further remove the rest large organics.

There were three regions for the MW of the organics in the feed water, i.e. large MW zone (with MW greater than 10,000), medium MW zone (with MW between 1,000 and 10,000) and small MW zone (with MW smaller than 1,000). The relationship between

EBSCOhost - printed on 2/14/2023 6:39 AM via . All use subject to https://www.ebsco.com/terms-of-use

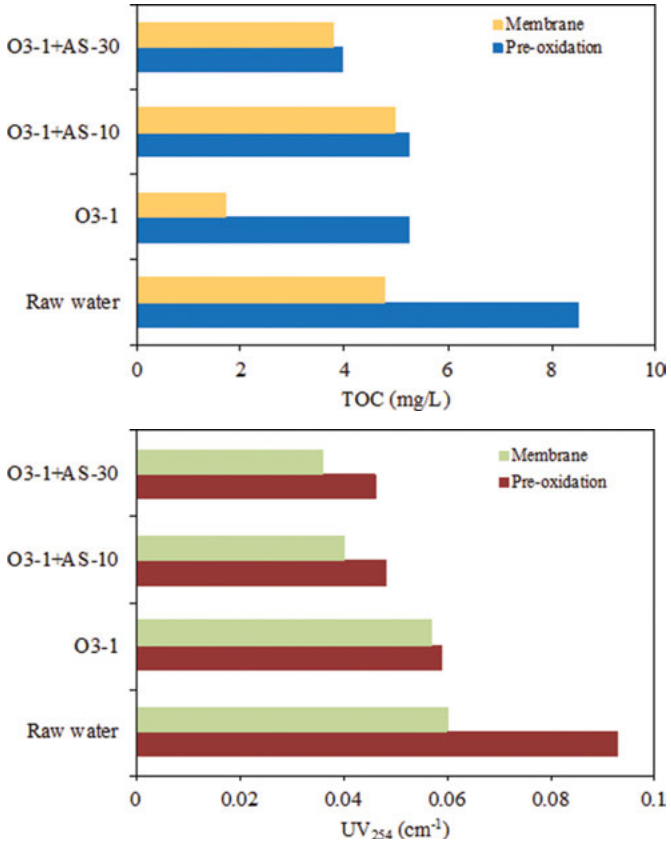

Figure 5.59: The effect of combination of pre-ozonation and coagulation on organics removal.

the organics concentration with the three MW regions and the TMP was investigated, with the result shown in Figure 5.64. It can be found that the TMP was closely correlated to large MW organics concentration and poorly to small and medium ones, indicating that large organics induced severer membrane fouling, while small and medium organics caused less membrane fouling.

5.5 Summary

Coagulation could effectively remove large-MW substances, and partially remove low and medium MW organic compounds. After coagulation, the residual organic matters are mainly HPO and N-HPI fractions. Large MW organics are key reversible fouling contributors, while N-HPI and strong HPO fractions with low and medium MW are primary cause of irreversible fouling.

EBSCOhost - printed on 2/14/2023 6:39 AM via . All use subject to https://www.ebsco.com/terms-of-use

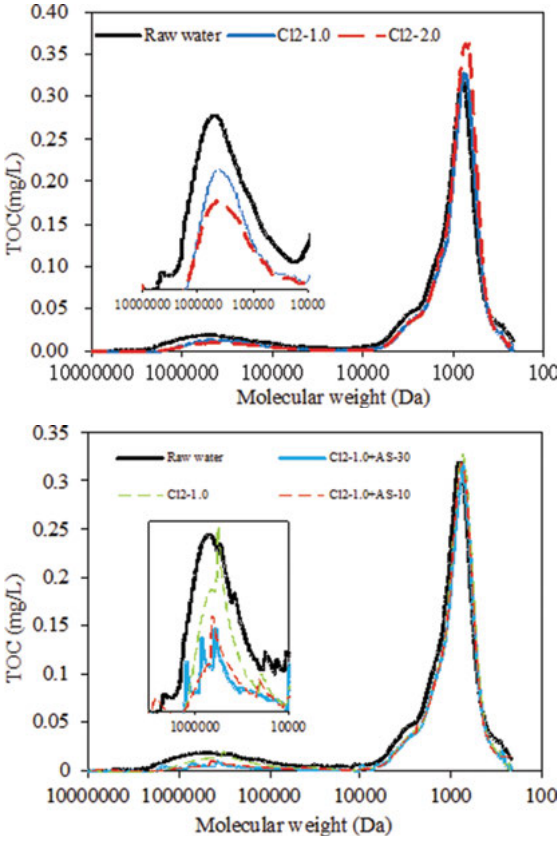

Figure 5.60: The influence of combination of sodium hypochlorite pre-oxidation and coagulation on organic MW distribution.

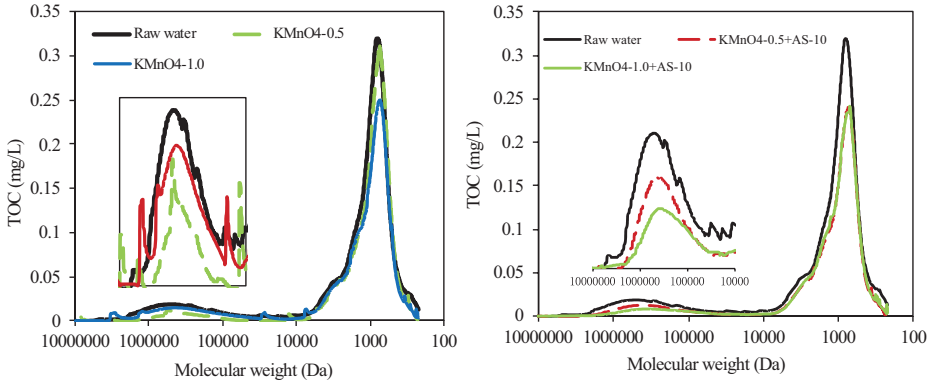

Figure 5.61: The influence of combination of potassium permanganate pre-oxidation and coagulation on organic MW distribution.

EBSCOhost - printed on 2/14/2023 6:39 AM via . All use subject to https://www.ebsco.com/terms-of-use

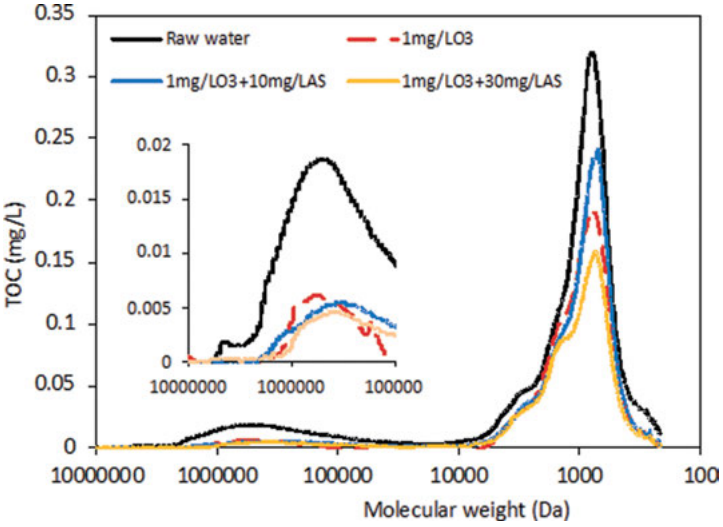

Figure 5.62: The influence of combination of pre-ozonation and coagulation on organic MW distribution.

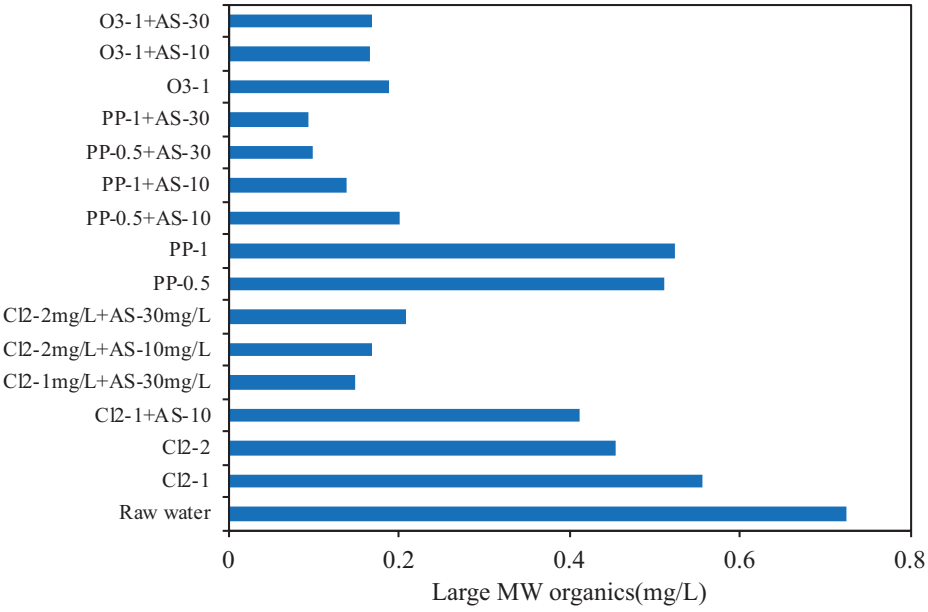

Figure 5.63: The effect of the combination of oxidation and coagulation of large MW organics.

EBSCOhost - printed on 2/14/2023 6:39 AM via . All use subject to https://www.ebsco.com/terms-of-use

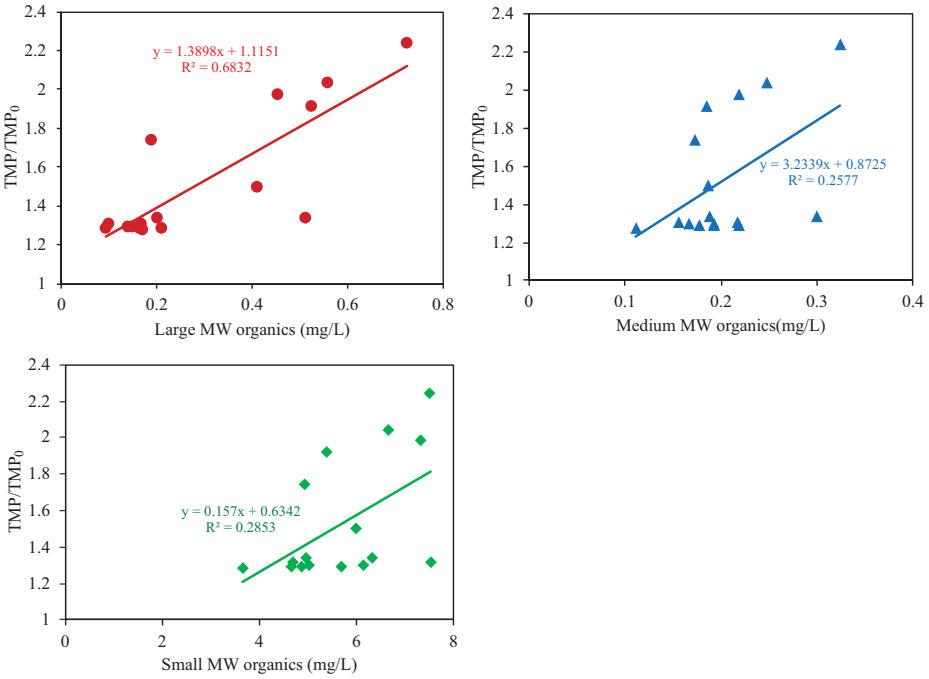

Figure 5.64: The relationship between organics concentration with different MW and TMP.

Both PAC and resin adsorption can alleviate membrane fouling mainly due to the enhanced removal of small and medium MW substances. However, the remaining NOM fractions, e.g. biopolymers, still lead to severe membrane fouling. Therefore, the PAC or resin adsorption alone is limited in membrane fouling control. The integrated coagulation and adsorption pretreatment may be a promising technology to effectively reduce membrane fouling for surface water treatment.

The pre-oxidation of ozone, chlorine and potassium permanganate can be used to control membrane fouling, of which ozone has the best oxidation ability, followed by potassium permanganate and chlorine. The membrane fouling depends on the concentration of large MW organics, while the removal efficiency of the latter in the pre-oxidation process is greatly related to the oxidation abilities of the oxidants. Thus the combination of oxidation and coagulation could further reduce the membrane fouling. And better membrane fouling reduction is achieved in the combination process where oxidants with weaker oxidation ability are used.

EBSCOhost - printed on 2/14/2023 6:39 AM via . All use subject to https://www.ebsco.com/terms-of-use

References

[1] Jiang, Y., et al., Membrane fouling in a powdered activated carbon – membrane bioreactor (PAC-MBR) for micro-polluted water purification: Fouling characteristics and the roles of PAC. Journal of Cleaner Production, 2020. 277.

[2] Liu, X., et al., Application of sodium alginate as a coagulant aid for mitigating membrane fouling induced by humic acid in dead-end ultrafiltration process. Separation and Purification Technology, 2020. 253.

[3] Zhang, M.J., et al., Effect of calcium ions on fouling properties of alginate solution and its mechanisms. Journal of Membrane Science, 2017. 525: p. 320–329.

[4] Long, Y., et al., Filtration behaviors and fouling mechanisms of ultrafiltration process with polyacrylamide flocculation for water treatment. Science of the Total Environment, 2020. 703.

[5] Gao, W., et al., Membrane fouling control in ultrafiltration technology for drinking water production: A review. Desalination, 2011. 272(1–3): p. 1–8.

[6] Kaiya, Y., et al., Study on fouling materials in the membrane treatment process for potable water. Desalination, 1996. 106(1–3): p. 71–77.

[7] Lee, N., et al., Morphological analyses of natural organic matter (NOM) fouling of low-pressure membranes (MF/UF). Journal of Membrane Science, 2005. 261(1–2): p. 7–16.

[8] Amy, G., Fundamental understanding of organic matter fouling of membranes. Desalination, 2008. 231(1–3): p. 44–51.

[9] Gao, K., et al., Ultrafiltration membrane fouling performance by mixtures with micromolecular and macromolecular organics. Environmental Science-Water Research & Technology, 2019. 5(2): p. 277–286.

[10] Li, T., et al., Application of coagulation-ultrafiltration-nanofiltration in a pilot study for Tai Lake water treatment. Water Environment Research, 2020. 92(4): p. 579–587.

[11] Lim, S.M., et al., A study on the removal of humic acid using advanced oxidation processes. Separation Science and Technology, 2007. 42(7): p. 1391–1404.

[12] Buchanan, W., et al., Fractionation of UV and VUV pretreated natural organic matter from drinking water. Environmental Science & Technology, 2005. 39(12): p. 4647–4654.

[13] Carroll, T., et al., The fouling of microfiltration membranes by NOM after coagulation treatment. Water Research, 2000. 34(11): p. 2861–2868.

[14] Fan, L.H., et al., Influence of the characteristics of natural organic matter on the fouling of microfiltration membranes. Water Research, 2001. 35(18): p. 4455–4463.

[15] Gray, S.R., et al., Effect of NOM characteristics and membrane type on microfiltration performance. Water Research, 2007. 41(17): p. 3833–3841.

[16] Chen, Y., et al., Effect of coagulation pretreatment on fouling of an ultrafiltration membrane. Desalination, 2007. 204(1–3): p. 181–188.

[17] Schafer, A.I., et al., Charge effects in the fractionation of natural organics using ultrafiltration. Environmental Science & Technology, 2002. 36(12): p. 2572–2580.

[18] Lee, N., Amy, G., and Lozier, J., Understanding natural organic matter fouling in low-pressure membrane filtration. Desalination, 2005. 178(1–3): p. 85–93.

[19] Weis, A., et al., The influence of morphology, hydrophobicity and charge upon the long-term performance of ultrafiltration membranes fouled with spent sulphite liquor. Desalination, 2005. 175(1): p. 73–85.

[20] Lankes, U., Ludemann, H.D., and Frimmel, F.H., Search for basic relationships between “molecular size” and “chemical structure” of aquatic natural organic matter – Answers from C-13 and N-15 CPMAS NMR spectroscopy. Water Research, 2008. 42(4–5): p. 1051–1060.

[21] Lee, N.H., et al., Identification and understanding of fouling in low-pressure membrane (MF/UF) filtration by natural organic matter (NOM). Water Research, 2004. 38(20): p. 4511–4523.

EBSCOhost - printed on 2/14/2023 6:39 AM via . All use subject to https://www.ebsco.com/terms-of-use

[22] Li, C.W. and Chen, Y.S., Fouling of UF membrane by humic substance: Effects of molecular weight and powder-activated carbon (PAC) pre-treatment. Desalination, 2004. 170(1): p. 59–67.
[23] Yoon, Y.M., et al., Effects of retained natural organic matter (NOM) on NOM rejection and membrane flux decline with nanofiltration and ultrafiltration. Desalination, 2005. 173(3): p. 209–221.
[24] Yamamura, H., Kimura, K., and Watanabe, Y., Mechanism involved in the evolution of physically irreversible fouling in microfiltration and ultrafiltration membranes used for drinking water treatment. Environmental Science & Technology, 2007. 41(19): p. 6789–6794.
[25] Cho, J.W., Amy, G., and Pellegrino, J., Membrane filtration of natural organic matter: Comparison of flux decline, NOM rejection, and foulants during filtration with three UF membranes. Desalination, 2000. 127(3): p. 283–298.
[26] Liang, H., et al., Cleaning of fouled ultrafiltration (UF) membrane by algae during reservoir water treatment. Desalination, 2008. 220(1–3): p. 267–272.
[27] Kimura, K., Hane, Y., and Watanabe, Y., Effect of pre-coagulation on mitigating irreversible fouling during ultrafiltration of a surface water. Water Science and Technology, 2005. 51(6–7): p. 93–100.
[28] Teychene, B., Guigui, C., and Cabassud, C., Engineering of an MBR supernatant fouling layer by fine particles addition: A possible way to control cake compressibility. Water Research, 2011. 45(5): p. 2060–2072.
[29] Lee, W.N., et al., Effect of PAC addition on the physicochemical characteristics of bio-cake in a membrane bioreactor. Separation Science and Technology, 2010. 45(7): p. 896–903.
[30] Huang, W.W., et al., Performance of PAC treatments on MF membrane fouling behavior and mechanism by various algogenic organic matter. Desalination and Water Treatment, 2020. 190: p. 28–43.
[31] Liu, J.X., et al., Mechanism analysis of powdered activated carbon controlling microfiltration membrane fouling in surface water treatment. Colloids and Surfaces a-Physicochemical and Engineering Aspects, 2017. 517: p. 45–51.
[32] Suzuki, T., et al., Removal of soluble organics and manganese by a hybrid MF hollow fiber membrane system. Desalination, 1998. 117(1–3): p. 119–129.
[33] Gai, X.J. and Kim, H.S., The role of powdered activated carbon in enhancing the performance of membrane systems for water treatment. Desalination, 2008. 225(1–3): p. 288–300.
[34] Ma, C., et al., High concentration powdered activated carbon-membrane bioreactor (PAC-MBR) for slightly polluted surface water treatment at low temperature. Bioresource Technology, 2012. 113: p. 136–142.
[35] Lin, C.F., Liu, S.H., and Hao, O.J., Effect of functional groups of humic substances on UF performance. Water Research, 2001. 35(10): p. 2395–2402.
[36] da Silva, F.V., et al., Effects of coconut granular activated carbon pretreatment on membrane filtration in a gravitational driven process to improve drinking water quality. Environmental Technology, 2012. 33(6): p. 711–716.
[37] Park, D., Wang, J., and Klibanov, A.M., One-step, painting-like coating procedures to make surfaces highly and permanently bactericidal. Biotechnology Progress, 2006. 22(2): p. 584–589.
[38] Milovic, N.M., et al., Immobilized N-alkylated polyethylenimine avidly kills bacteria by rupturing cell membranes with no resistance developed. Biotechnology and Bioengineering, 2005. 90(6): p. 715–722.
[39] de Velasquez, M.T.O., Monje-Ramirez, I., and Paredes, J.F.M., Effect of ozone in UF-membrane flux and dissolved organic matter of secondary effluent. Ozone-Science & Engineering, 2013. 35(3): p. 208–216.

EBSCOhost - printed on 2/14/2023 6:39 AM via . All use subject to https://www.ebsco.com/terms-of-use

[40] Wang, X.D., et al., Ozonation pretreatment for ultrafiltration of the secondary effluent. Journal of Membrane Science, 2007. 287(2): p. 187–191.
[41] You, S.H., Tseng, D.H., and Hsu, W.C., Effect and mechanism of ultrafiltration membrane fouling removal by ozonation. Desalination, 2007. 202(1–3): p. 224–230.
[42] Oh, B.S., et al., Role of ozone for reducing fouling due to pharmaceuticals in MF (microfiltration) process. Journal of Membrane Science, 2007. 289(1–2): p. 178–186.
[43] Huang, H.O., et al., Effects of magnetic ion exchange pretreatment on low pressure membrane filtration of natural surface water. Water Research, 2012. 46(17): p. 5483–5490.
[44] Nagaoka, H., Yamanishi, S., and Miya, A., Modeling of biofouling by extracellular polymers in a membrane separation activated sludge system. Water Science and Technology, 1998. 38(4–5): p. 497–504.
[45] Khan, M.M.T., et al., Combined effects of EPS and HRT enhanced biofouling on a submerged and hybrid PAC-MF membrane bioreactor. Water Research, 2013. 47(2): p. 747–757.
[46] Jeong, S., Naidu, G., and Vigneswaran, S., Submerged membrane adsorption bioreactor as a pretreatment in seawater desalination for biofouling control. Bioresource Technology, 2013. 141: p. 57–64.
[47] Song, Y.F., et al., The feasibility of UF-RO integrated membrane system combined with coagulation/flocculation for hairwork dyeing effluent reclamation. Science of the Total Environment, 2019. 691: p. 45–54.
[48] Qin, H.J., et al., New option of MBR-RO process for production of NEWater from domestic sewage. Journal of Membrane Science, 2006. 272(1–2): p. 70–77.
[49] Zou, L., Sanciolo, P., and Leslie, G., Using MF-NF-RO train to produce low salt and high nutrient value recycled water for agricultural irrigation. Water Science and Technology, 2008. 58(9): p. 1837–1840.
[50] Munakata, N., et al., Comparing traditional UF-RO-AOP to MBR-RO-AOP for treatment of recycled water for indirect potable reuse. Abstracts of Papers of the American Chemical Society, 2012. 243.
[51] Tian, J.Y., et al., KMnO4 pre-oxidation combined with FeCl3 coagulation for UF membrane fouling control. Desalination, 2013. 320: p. 40–48.
[52] Kimura, K., Hane, Y., and Watanabe, Y., Effect of pre-coagulation on mitigating irreversible fouling during ultrafiltration of a surface water. Water Science and Technology, 2005. 51(6–7): p. 93–100.
[53] Dong, B., et al., Analysis of organic foulants in the coagulation-microfiltration process for the treatment of Taihu Lake. Environmental Technology, 2019. 40(25): p. 3364–3370.

EBSCOhost - printed on 2/14/2023 6:39 AM via . All use subject to https://www.ebsco.com/terms-of-use

EBSCOhost - printed on 2/14/2023 6:39 AM via . All use subject to https://www.ebsco.com/terms-of-use

Tian Li, Junxia Liu, Nianping Chi

Chapter 6
Nanofiltration in Water Treatment

6.1 Working principle of nanofiltration

6.1.1 Concept of nanofiltration

Nanofiltration is a new type of pressure-driven membrane separation technology between the ultrafiltration and reverse osmosis developed in the mid-1980s [1–4]. It was called the low pressure loose reverse osmosis. As it has a smaller molecular weight cut-off than ultrafiltration, larger transmittance than reverse osmosis and low operating pressure, it has been developed rapidly in the past decade. In nanofiltration, the water flux is proportional to the operating pressure, while the permeability of the inorganic micromolecules is almost independent on the pressure, thus as long as the operating pressure is properly controlled, both the toxic and harmful substances in the feed can be removed. Since some of the trace elements with micromolecules can be retained by nanofiltration, the permeate quality target of maximum removal of toxic and harmful substances and retaining of trace elements and minerals beneficial to human health in the feed can be achieved [5].

6.1.2 Classification and characteristics of nanofiltration

Nanofiltration membranes can be divided into two categories, traditional softening nanofiltration membranes and high-yield water-charged nanofiltration membranes. The former ones are originally intended for water softening rather than organics removal. They have over 90% removal of conductivity, alkalinity and calcium and have molecular weight cut-offs between 200 and 300 Da, which allows them to remove more than 90% of TOC. The latter nanofiltration membranes are specifically for organics removal rather than water softening (only 5–50% for inorganic removal). These membranes are made of materials resistant to organic pollutants (such as sulfonated polyether oxime). They have negatively charged surface and at the same time have a higher water yield than conventional membranes [6].

Tian Li, College of Environmental Science and Engineering, Tongji University, Shanghai, P. R. China
Junxia Liu, School of Civil and Transportation Engineering, Guangdong University of Technology, Guangzhou, Guangdong, P. R. China
Nianping Chi, School of Municipal and Geomatics Engineering, Hunan City University, Yiyang, Hunan, P. R. China

https://doi.org/10.1515/9783110596847-006

EBSCOhost - printed on 2/14/2023 6:39 AM via . All use subject to https://www.ebsco.com/terms-of-use

Nanofiltration membranes have pore size of nanometers and multi-charged surface, thus they have the following characteristics [5, 7]: (1) They are suitable for separating dissolved components with a relative molecular weight between 200 and 1,000 and a size of around 1 nm. Therefore, they can be used for the separation of organic substances with different relative molecular weights; (2) the inter-membrane osmotic pressure difference required for separation is low, generally 0.5–2.0 MPa, which is lower than the pressure difference required to achieve the same permeate flux with RO of 0.5–3.0 MPa; (3) Due to the fact that the nanofiltration membranes often carry a charge group, the Donnan effect existing on ions of different valence states by electrostatic action, they have ion selectivity and are able to separate ions with different valence [8].

6.1.3 Separation mechanism of nanofiltration

It is general that the mass transfer mechanism of nanofiltration is dissolution-diffusion. The separation behavior of inorganic salts is affected not only by chemical potential gradient but also electric potential gradient. Currently there are various separation models for NF membranes, including thermodynamic irreversible models, charge models, electrostatic repulsion and steric hindrance models [9].

6.1.3.1 Thermodynamic irreversible model

As the same as microfiltration, ultrafiltration, and reverse osmosis separation processes, the pressure difference of NF membrane separation is the driving force. The flux can be characterized by the phenomenological equation established by the non-equilibrium thermodynamic model:

$$J_v = L_p(\Delta P - \delta\Delta\pi) \tag{6.1}$$

$$J_s = (1 - \delta)C_s J_v + K_p\Delta C \tag{6.2}$$

where
J_s – solvent migration flux;
J_v – solute migration flux;
L_p – hydraulic permeability coefficient of membranes;
ΔP – trans-membrane pressure;
δ – retention coefficient of solute;
$\Delta\pi$ – osmotic pressure difference between both sides of membrane;
C_s – solute concentration in membranes;
K_p – solute permeability coefficient;

EBSCOhost - printed on 2/14/2023 6:39 AM via . All use subject to https://www.ebsco.com/terms-of-use

6.1.3.2 Charge model

According to different assumptions about the distribution of charge and potential in the membrane, the charge model is divided into the space charge model and the fixed-charge model. The space charge model was first proposed by Gross and Osterle [10], which assumes that the membrane consists of micropores with uniform pore sizes and uniform charge distribution on the wall. The ion concentration and electric field potential distribution, ion transport and fluid flow in the micropores are determined by Poisson-Boltzmann equation, Nernst-Plank equation and Navier-Stokes Stokes equations etc., respectively. The fixed charge mode was first proposed by Teorell, Meyer, Sievers, etc., thus it is also called the TMS model [11–13]. This model assumes that the membrane phase is a gel layer and the microporous structure of the membrane is ignored; the ion concentration and potential are evenly distributed in any direction in the membrane; there is only certain distribution of potential and ion concentration in the vertical direction of the membrane due to the Donnan effect and ion migration.

6.1.3.3 Electrostatic repulsion and steric hindrance model

Later, Wang et al. established an electro-static and steric-hindrance model, which is referred to as an electrostatic steric hindrance model [14]. The model assumes that the membrane separation layer consists of micropores with uniform pore size and uniform surface charge distribution; the structural parameters of membranes include pore size, porosity, membrane separation layer thickness and bulk charge density. According to the above parameters, for known separation systems, the electrostatic steric hindrance model can be used to predict the separation characteristics of various solutes through the membrane. The electrostatic steric hindrance model includes the steric effect of the membrane pores on the size of the neutral solute described in the pore model, and also the electrostatic repulsion of the charged characteristics of the membrane described in the solid charge, so the model can be used to describe the separation mechanism of the NF membrane.

6.2 Application of nanofiltration technology in micro-polluted water treatment

The characteristics of nanofiltration technology determine its unique role in drinking water treatment, mainly in the removal of various harmful and toxic organic substances and inorganic salts, colloids, bacteria and pathogens, and also various trace organic substances, especially those toxic, mutagenic, carcinogenic contaminants.

EBSCOhost - printed on 2/14/2023 6:39 AM via . All use subject to https://www.ebsco.com/terms-of-use

According to the charge effect, nanofiltration can reduce the hardness in the feed and remove inorganic pollutants such as nitrate, arsenic, fluoride and heavy metals which are harmful to human body in drinking water source [15–17]. According to the screening effect, nanofiltration can effectively remove trichloromethane and its intermediate products, environmental hormones, and natural organic matters [18, 19]. Nanofiltration technology has the advantages of high separation efficiency, easy control, simple process, flexible operation, low removal of inorganic substances, light scale and fouling, high permeate flux, and no mineralization for the product in the treatment of micro-polluted drinking water source [8, 20]. When NF technology is used to obtain high-quality drinking water from a water source with low salt content, a safe and stable effluent with high quality can be anticipated with less dosage of disinfectants such as chlorine. When nanofiltration is used to treat micro-polluted water source, it can not only effectively remove harmful substances such as inorganic and organic pollutants in the feed, but also meet the requirements for the removal of toxic, mutagenic and carcinogenic organic substances in the drinking water. In addition, it has a low removal for minerals such as Ca^{2+}, NaCl, to remain some of the minerals needed by the human body. Thus nanofiltration is an effective method for treating micro-polluted water and producing high-quality drinking water, and has broad application prospects in the advanced drinking water treatment [21].

6.3 Factors affecting the removal of PPCPs by nanofiltration

It is general that the separation of trace organic substances (such as PPCPs, endocrine disruptors, insecticides, etc.) by nanofiltration is mainly through particle size exclusion and electrostatic repulsion. When the organic matter is neutrally charged, the separation mechanism is mainly sieving filtration or particle size exclusion; however, when the organic matter is negatively charged, since most nanofiltration membranes are charged, the separation mechanism is mainly steric hindrance effect and electrostatic repulsion [22, 23].

6.3.1 Structural characteristic of nanofiltration membranes and organic molecules

The parameters characterizing the structural characteristics of nanofiltration membranes include molecular weight cut-off (MWCO), salt rejection and porosity. In general, for a neutral organic molecule, if its relative molecular weight (MW) is greater than the relative MWCO of the membrane, the nanofiltration has a high rejection.

EBSCOhost - printed on 2/14/2023 6:39 AM via . All use subject to https://www.ebsco.com/terms-of-use

However, some studies have found that MW cannot be used accurately to predict the removal efficiency of organic matter by membrane [24]. Since the steric hindrance effect is one of the important mechanisms for organic matter removal by membranes [25], the particle size and spatial structure and the membrane pore size of polymers can more accurately reflect the interception effect of nanofiltration on organic matter rather than MWCO, MW or salt rejection [26]. Berg et al. suggests that molecular structure, such as the number of methyl groups, is an important parameter to predict the effect of membranes on the removal of neutral organic matter [27]. They also found that the more methyl groups with neutral compounds, the higher removal rate by the membrane. Kiso et al. showed that when the main removal mechanism of organic matter by membrane is steric hindrance, the molecular width (MWd) is more accurate than the relative molecular weight (MW) to predict the solute rejection [26].

6.3.2 Nanofiltration membrane and charge of organic matter

Electrostatic repulsion is an important mechanism for membrane to remove charged materials. Most nanofiltration membranes are negatively charged to prevent adsorbing a large amount of negatively charged colloids in the water during the actual water treatment process and to avoid membrane clogging. At the same time, the Donnan effect is used to separate ions with different valence states to improve the selectivity and permeate flux of membranes. The negatively charged membrane is typically made of a polymeric material containing a sulfonic acid group (-SO_3H) or a carboxyl group (-COOH) or a negatively charged group introduced on the polymers [28–31].

Studies have found that changing the pH of a water body can change the surface charge of membranes [7, 32]. Increasing the pH can remove protons from the surface functional groups of the membranes, thereby increasing the electronegativity of the membrane surface. When the pH of the water is greater than the pKa of the acid ionization equilibrium constant of the pharmaceuticals and personal care products (PPCPs), the PPCPs are ionized and negatively charged, thereby generating electrostatic repulsion on the surface of the negatively charged nanofiltration membrane, resulting in the increased removal of the organic matter (i.e. the PPCPs) [32–34]. Nghiem et al. found that with the increase of pH, the removal rate of negatively charged sulfamethoxazole and ibuprofen was increased by nanofiltration, while the removal of the non-ionizing molecule carbamazepine (carhamazepine) was not substantially changed [33].

It is reported that the ionic strength of the solution (such as Ca^{2+} concentration) has a great effect on the removal of PPCPs by nanofiltration. Boussahel et al. found that the dosage of Ca^{2+} in the solution neutralized the negative charge on the surface of nanofiltration membranes, which weakened the repulsion between the functional groups on the membrane surface, thereby reducing the membrane pore

EBSCOhost - printed on 2/14/2023 6:39 AM via . All use subject to https://www.ebsco.com/terms-of-use

size and thus improving the removal of organic matter [35]. In summary, the chemical properties in the feed (such as pH, ionic strength) can significantly affect the removal of organic matter in nanofiltration.

6.3.3 Adsorption between nanofiltration membranes and organic compounds (PPCPs)

The adsorption of hydrophobic micro-contaminants by nanofiltration membranes is an important factor affecting the removal rate of organic matter [36]. Most nanofiltration membranes are hydrophobic, and their hydrophilicity or hydrophobicity can be characterized by the contact angle. The larger the contact angle, the more hydrophobic compounds are adsorbed per unit area of the membrane than the nanofiltration membrane with a smaller contact angle. The hydrophilicity or hydrophobicity of the compound can be characterized by the octanol/water partition coefficient (Kow) [37]. Kiso found that the removal rate of most hydrophobic compounds by cellulose acetate (CA) membrane increased with the increase of Kow value [38]. Studies have shown that adsorption only has a positive effect on the removal of PPCPs in the initial stage of filtration [19, 39, 40]. When the membrane reaches saturation, PPCPs adsorbed on the membrane surface can dissolve and diffuse through the membrane, thus reducing the removal rate from the initial stage.

6.3.4 Effect of natural organic matter in the feed on the removal of PPCPs

There are two different opinions on the effect of NOM on the removal of trace organics such as PPCPs, EDCs or pesticides by nanofiltration [41, 42]. (1) NOM in the feed improves the removal rate of trace organics, and its mechanism is that trace organic substances are adsorbed on the organic matter in the feed solution to form macromolecules, which are removed by nanofiltration through the mechanical interception or electrostatic interaction between NOM and the membrane. (2) The presence of NOM reduces the removal of trace organics. Nghiem and Schäfer found that the nanofiltration membranes or reverse osmosis membranes TFCSR2 (UF/NF), AGM-4 (NF), XN-40 (NF), TFC -SR1 (NF), X-20 (NF/RO), TS-80 (NF/RO), TFC-S (NF/RO) and TFC-ULP (ULPRO) could remove up to 95% of cholesterol with pure water as solvent; however, the removal rate was decreased when the cholesterol was added to the secondary effluent of the wastewater treatment plant or humic acid solution [43]. Moreover, the secondary effluent from the wastewater treatment plant has a greater impact on its removal rate. Although the mechanism of the phenomenon is not clear enough, studies have shown that feed quality and composition have a significant impact on the removal of PPCPs [44].

EBSCOhost - printed on 2/14/2023 6:39 AM via . All use subject to https://www.ebsco.com/terms-of-use

6.4 Experimental setup, materials and methodology

6.4.1 Experimental setup and materials

6.4.1.1 Polyamide composite membrane

NF270 and NF90 polyamide composite membranes produced by Dow in the United States were used in the test. The specific parameters are shown in Table 6.1. A new membrane was used in each test and the membrane was stored in Milli-Q ultrapure water at 4 °C, and immersed for at least 48 h before use.

Table 6.1: Main characteristics of the nanofiltration membranes used in the test.

Type	Salt rejection (2000×10^{-6} $MgSO_4$)	Pore size (nm)	Contact angle (°)	pH range (continuous running)	Water flux (10^{-5} $L \cdot M^{-2} \cdot h^{-1} \cdot Pa^{-1}$)
NF270	>97%	0.84	23.4	3–10	16.5 ± 0.5
NF90	>97%	0.68	42.2	3–10	9 ± 0.5

Note:
1 bar = 100,000 Pa

6.4.1.2 Experimental setup and operating conditions

A cross-flow nanofiltration was used in the test. The schematic diagram and the membrane element are shown in Figure 6.1. The effective membrane area is 60 cm^2. A centrifugal pump manufactured by IWAKI Co., Ltd., with model No. MGP-M256B220 was in the setup. Both concentrate and effluent were returned to the feed tank during the test.

A thermostat of Jinghong DKB-161 was used to control the water temperature in the test.

The operating pressure is regulated by a valve, the inlet pressure is maintained at 0.4 MPa, and the recovery rate of the membrane unit is at about 1%, that is, the outlet flow rate is 1% of the influent flow rate.

6.4.1.3 Chemicals in the test

In the test carbamazepine (CBZ) was purchased from Sigma-Aldrich with 99% purity. Methanol of mobile phase in HPLC is from Sigma. Milli-Q ultrapure water and Milli-Q deionized water were used in the test. Other agents are of analytical grade.

EBSCOhost - printed on 2/14/2023 6:39 AM via . All use subject to https://www.ebsco.com/terms-of-use

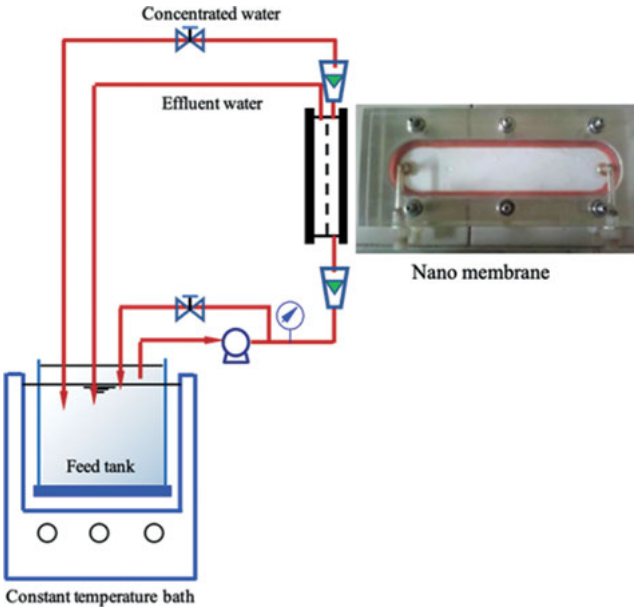

Figure 6.1: Nanofiltration membrane experimental device schematic diagram.

6.4.1.4 Methodology and preparation of sample

1 Methodology

A new membrane was used for each test. A Milli-Q deionized water filtration for about 2 h was conducted to obtain a stable flux, which was recorded as J_0. And then a 5 L of CBZ sample was filtered. The filtration duration was 5.5 h, and the sampling was performed 9 times or more, and the sampling flux J was recorded every time.

2 Preparation of CBZ stock solution and background water sample

A small amount of CBZ was first dissolved with methanol, then diluted with ultrapure water to make a high concentration stock solution. It was diluted at the required concentration when needed in the test.

a. Preparation of CBZ stock solution. 100 mg of CBZ was obtained and dissolved with a small amount of methanol, then to make a 1 L solution with ultrapure water for a 100 mg/L high concentration stock solution. It was stored in a refrigerator at 4 °C.
b. Preparation of background water samples. Since the deionized water does not contain ions, in order to make the water sample similar to that from natural water body, a 20 mmol/L NaCl and a 1 mmol/L buffer solution of $NaHCO_3$ was added in the sample. Since the water body is usually weakly alkaline, a pH of 8 was maintained in all the experiments except those specifically noted.

EBSCOhost - printed on 2/14/2023 6:39 AM via . All use subject to https://www.ebsco.com/terms-of-use

i pH: 1 mmol/L $NaHCO_3$ and 20 mmol/L NaCl solution was added to Milli-Q deionized water, and the pH of the solution was adjusted to the required value with 1 mol/L NaOH or 1 mol/L HCl.
ii Ionic strength: 1 mmol/L $NaHCO_3$ and 20 mmol/L NaCl solution was added to Milli-Q deionized water, and the pH of the solution was adjusted to be 8. Different mass of $CaCl_2$ were obtained to dissolve in the above solution to make water samples with $CaCl_2$ concentrations of 5 mmol/L, 10 mmol/L, and 20 mmol/L, respectively.
iii Humic acid (HA): A certain amount of powdered humic acid was obtained and dissolved in 5 mol/L NaOH to make a 1 L solution with ultrapure water. The pH was then adjusted to be 7 with 3 mol/L HCl. After that, the solution was filtrated with 0.45 μm microfiltration membrane. And the DOC of the solution was measured with Shimadzu TOC-V_{CPH}. The HA solution was stored in a brown bottle at 4 °C and diluted to the desired DOC concentration in the test.
iv Sodium alginate (SA): A certain amount of powdered sodium alginate was obtained to make a 1 L solution with ultrapure water. It was stirred with a magnetic stirrer at 40 °C for more than 24 h to make the SA completely dissolved. After that, the solution was filtrated with 0.45 μm microfiltration membrane. And the DOC of the SA solution was measured with Shimadzu TOC-V_{CPH}. It was diluted to the desired DOC concentration in the test.
v Tannic acid (TA): A certain amount of powdered tannic acid was obtained to make a 1 L solution with ultrapure water. It was stirred with a magnetic stirrer for more than 24 h to make the TA completely dissolved. After that, the solution was filtrated with 0.45 μm microfiltration membrane. And the DOC of the TA solution was measured with Shimadzu TOC-V_{CPH}. It was diluted to the desired DOC concentration in the test.

6.4.2 Methods

6.4.2.1 Detection method of carbamazepine (CBZ)

The CBZ was detected in this study through a high performance liquid chromatograph (Agilent 1200 Series HPLC). In the test, the external standard working curve method is adopted, that is, a series of different concentrations of CBZ standard solutions are first prepared by using the pure component of the sample, then the accurate injection is performed, after that the peak area is measured, thus the working curve is drawn, and the regression equation is obtained. The CBZ content in the sample solution using the working curve or the regression equation is calculated. The regression equation is expressed as, component concentration = b × peak area of the component + a, where, a and b are parameters to be determined.

Since the concentration of CBZ in the water sample is at trace level, the method for separating this trace component should require the sample to be injected directly, to avoid baseline fluctuations and changes in retention values, thus isocratic sepa-

EBSCOhost - printed on 2/14/2023 6:39 AM via . All use subject to https://www.ebsco.com/terms-of-use

ration methods are usually used. The sensitivity of isocratic separation methods is generally higher, due to the better detection baseline, simple equipment requirement, and shorter analysis time.

Firstly, the full-wavelength scanning of 10 mg/L CBZ solution was carried out by ultraviolet spectrophotometer. It was found that CBZ had strong absorption at wavelengths of 210 nm and 285 nm. Considering that the measurement near 210 nm is easily interfered by the peak of the solvent of methanol, 285 nm was chosen as the detection wavelength.

The chromatographic conditions for CBZ determination are listed below.

- Liquid phase chromatograph column: Zorbax Eclipse Plus C18 (Agilent);
- Detector: UV detector (VWD) at 285 nm;
- Mobile phase: methanol and ultrapure water (55:45);
- Flow rate: 1.0 mL/min;
- Analysis time: 8 min;
- Column temperature: 35 °C;
- Injection volume: 50 μL;
- The chromatographic analysis of CBZ is shown in Figure 6.2.

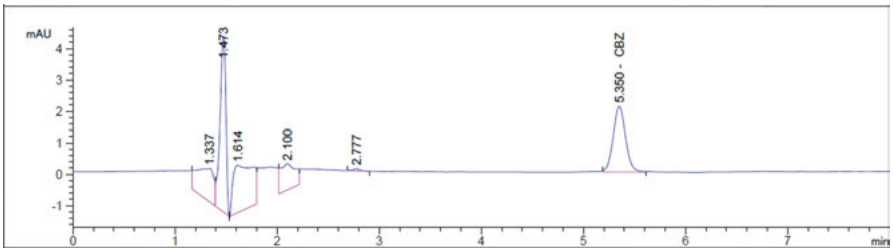

Figure 6.2: High performance liquid chromatogram of CBZ.

According to the external standard method, the concentration regression equation and detection limit of CBZ are shown in Table 6.2.

Table 6.2: Concentration regression equation and detection limit of CBZ.

Linear range/ ($\mu g \cdot L^{-1}$)	Regression equation	Correlation coefficient	Limit of detection (LOD) (S/N = 3)/ ($\mu g \cdot L^{-1}$)	Limit of quantity (LOQ) (S/N = 10)/ ($\mu g \cdot L^{-1}$)
1–100	$y = 1.45272 \times 10^{-1}x$	0.9996	1	3
100–500	$y = 1.45389 \times 10^{-1}x$	1.0000		

Taking tap water as the test object, the determination of the spiked recovery rate and the precision (based on the relative standard deviation RSD) are calculated. The test results are shown in Table 6.3.

EBSCOhost - printed on 2/14/2023 6:39 AM via . All use subject to https://www.ebsco.com/terms-of-use

Table 6.3: Recovery and precision (n = 3).

Level	Recovery (%)	RSD (%)
10	98.30	1.82
50	97.92	1.43
100	99.23	0.66

It can be seen from Table 6.3 that the recoveries are higher than 97.92% and the relative standard deviations are less than 1.82% (generally less than 2%).

Three samples of CBZ standard solutions with three mass concentration levels were taken and stored at 4 °C. The stability investigation was carried out on the day of preparation, 7th day and 15th day respectively. The results are shown in Table 6.4.

Table 6.4: Stability (n = 3).

Mass concentration level ($\mu g \cdot L^{-1}$)	Average mass concentration ($\mu g \cdot L^{-1}$)	RSD (%)
10	9.73	1.37
50	48.99	1.24
100	99.97	1.01

It can be seen from Table 6.4 that the relative standard deviation of the three measurements of each sample is less than 1.37%, indicating that this preservation method is feasible for the sample to be stored for 15 days.

6.4.2.2 Determination of ozone mass concentration

The principle to determine the concentration of ozone in the liquid phase was based on the determination of ozone in the ambient, which was the determination of liquid phase ozone concentration according to the sodium indigo disulphonate spectrophotometry method (GB/T 15437–1995), and it was then simplified according to the specific experimental conditions.

1 Calibration of standard solutions and preparation of experiment solutions

Due to the significant difference in the purity of commercial ruthenium potassium, calibration is required.

Preparation of erythro-potassium stock solution

0.50 g of eosin potassium is obtained, dissolved in 20 mL of H_3PO_4 (20 mmol/L), diluted to 1 L with H_3PO_4 (20 mmol/L), and stored in the dark with low temperature. The solution can generally be stored for 3 months. After the absorbance of the solu-

EBSCOhost - printed on 2/14/2023 6:39 AM via . All use subject to https://www.ebsco.com/terms-of-use

tion drops to 80% of the original value, the buffer solution should be reconstituted. The reconstitution of the buffer solution is to dissolve 28 g of NaH_2PO4 and 35 g of H_3PO_4 in distilled water to make 1 L solution.

2 Drawing of the standard curve

According to the calibration result, the potassium sulphate solution is diluted into a standard solution equivalent to 1.00 μg of ozone per mL, and such solution is stable in the dark at room temperature for one week.

The solutions with certain concentration gradient were prepared by using the standard solution, and the relationship between the absorbance of the water samples at a wavelength of 610 nm and the ozone concentration was measured and plotted as a standard curve to obtain the relationship between the absorbance x (cm^{-1}) and the ozone mass concentration y (mg/L). The linear relationship is y = 0.0038/x.

3 Determination of ozone mass concentration

Two 100 mL of flasks were obtained and 10 mL of buffer solution and 15 mL of blush potassium standard solution were added. One of them is used as a blank control with ultrapure water, and the other is added with 1 mL of water sample. Both flasks were diluted to the specified volume with ultrapure water. The absorbance of the two solutions was measured at a wavelength of 610 nm, and then the mass concentration of ozone in the water sample was determined based on the difference in absorbance.

4 Materials and experimental setup

The ozone generator is produced by CONT with the model No. KT-OZ-3 G. The oxygen flow rate was adjusted with a gas flow meter and was fixed at 0.6 mL/min. A three-way glass tube and a 1.5 L milled conical flask are used as an ozone reaction device, and an aeration head is disposed in the conical flask for the purpose to uniformly dissolve the ozone. The exhaust gas was absorbed by KI solution. The concentration of ozone in the solution is measured, and the nitrogen is removed by high-purity nitrogen to terminate the ozone reaction immediately after the end of ozone injection.

6.5 Effect of different operating conditions on removal of CBZ by nanofiltration

Nanofiltration (NF) has been developed rapidly in the past decade due to its smaller pore size than ultrafiltration, higher transmission than reverse osmosis and relatively low operating pressure. The molecular mass of most micro-pollutants, including PPCPs, is between 200 and 300 Da, while the nanofiltration membrane has a molecular weight cut-off comparable to this range. Therefore, the nanofiltration is considered as a viable process to remove these organic micro-contaminants. At present, many

EBSCOhost - printed on 2/14/2023 6:39 AM via . All use subject to https://www.ebsco.com/terms-of-use

studies have been carried out on the removal of PPCPs by nanofiltration and it can be found that the properties of nanofiltration membranes (relative molecular weight, porosity, hydrophilicity/hydrophobicity, charge, surface morphology, etc.) and the nature of PPCPs (relative molecular weight, molecular size and structure, polarity, acid dissociation constant, hydrophilicity/hydrophobicity, diffusion coefficient, etc.), as well as the chemical characteristics and composition of the solution are important factors affecting the removal rate of PPCPs by nanofiltration [45–48]. In this section, the removal of CBZ by two nanofiltration membranes, one with a larger pore size and the other with a smaller pore size, was first studied. The mechanism of the removal was then obtained based on the experimental results. The effects of the operating conditions on the removal of CBZ by nanofiltration, such as pH, ionic strength, initial concentration of liquid, and temperature were also investigated, which provide useful information for the subsequent study of the effect of dissolved organic matter (DOM) on the removal of CBZ by nanofiltration.

6.5.1 Test parameters

In this test the change of removal rate R (%) and membrane permeate flux J (L/($m^2 \cdot h$)) on CBZ by nanofiltration under different conditions were investigated. The above parameters can be calculated from Eqs. (6.3) and (6.4), respectively. To describe the trend of the flux, the ratio of flux J over the pure water flux J_0 was used in the experiments.

$$\mathrm{R}\,(\%) = \frac{C_f - C_p}{C_f} \times 100\% \tag{6.3}$$

$$\mathrm{J} = \frac{Q}{TS} \tag{6.4}$$

where
C_p – mass concentration of CBZ in permeate, μg/L;
C_f – mass concentration of CBZ in the feed solution, μg/L;
Q – volume of permeate, L;
A – effective membrane area, m^2;
T – time, h.

6.5.2 Effect of pore sizes of nanofiltration on the removal of CBZ

In this test, a CBZ solution with an initial mass concentration of about 100 μg/L was prepared in a background electrolyte (20 mmol/L NaCl and 1 mmol/L $NaHCO_3$, with similar methods adopted in the following sections. The pH is adjusted to about 8.0

EBSCOhost - printed on 2/14/2023 6:39 AM via . All use subject to https://www.ebsco.com/terms-of-use

and the temperature is controlled at 25 ± 1 °C. The test was carried out with both "loose" NF270 (with larger pore size) and "tight" NF90 (with smaller pore size) membrane. The test results are shown in Figures 6.3 and 6.4.

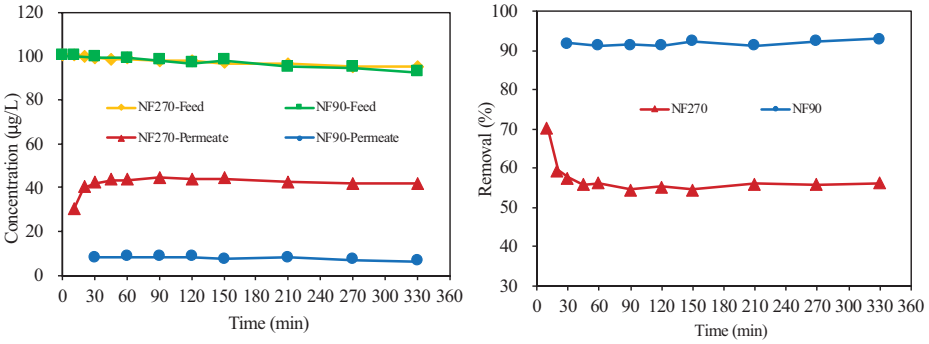

Figure 6.3: Removal of CBZ by NF270 and NF90 membranes.

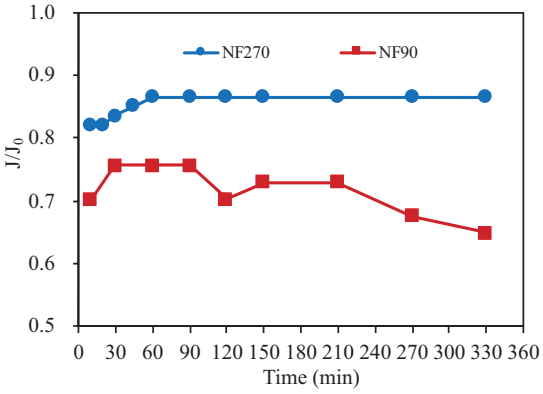

Figure 6.4: Flux changes by NF270 and NF90 membranes.

It can be seen from Figure 6.3 that as the filtration proceeds, the concentration of CBZ in the influent decreases gradually, which indicates that the two nanofiltration membranes can retain some CBZ. The octanol/water partition coefficient of CBZ is 2.45 (less than 2.7), thus CBZ is a weakly hydrophobic substance. Although both NF270 and NF90 are hydrophilic membranes, the latter has a larger contact angle than the former, so NF90 is slightly less hydrophilic than NF270. The influent mass concentration of NF270 decreased by 5.5% and NF90 by 7.4%, thus the adsorption of CBZ by NF90 is greater than that by NF270. Previous literature also pointed out that the hydrophobic NF membrane is more favorable for the adsorption of hydrophobic organic matter [49–51], which is consistent with the results from this study. When the filtration is stable, the removal rate of CBZ by NF270 and NF90 is about 56% and 92%,

EBSCOhost - printed on 2/14/2023 6:39 AM via . All use subject to https://www.ebsco.com/terms-of-use

respectively, and the latter is superior than the former in the removal of CBZ, which can be explained by the smaller pore diameter of NF90 than NF270. It can be also seen that, the removal mechanism of CBZ by NF membrane is mainly physical sieving.

As can be seen from Figure 6.4, the flux of NF90 is significantly lower than that of NF270. Since the membrane pore size of NF90 is smaller than NF270, a larger filtration resistance of NF270 is generated, resulting in lower flux. Since the removal rate of CBZ by NF90 has reached more than 90%, the improvement for the removal is limited. Thus, in order to better characterize the change of removal rate, NF270 is used in subsequent experiments.

6.5.3 Effect of initial pH on removal of CBZ by nanofiltration

A CBZ solution with an initial mass concentration of about 100 μg/L was prepared in the background electrolyte, with the temperature at 25 ± 1 °C, and the pH at 3.5, 5.0, 7.0, 8.0, and 9.5. The filtration results are shown in Figure 6.5.

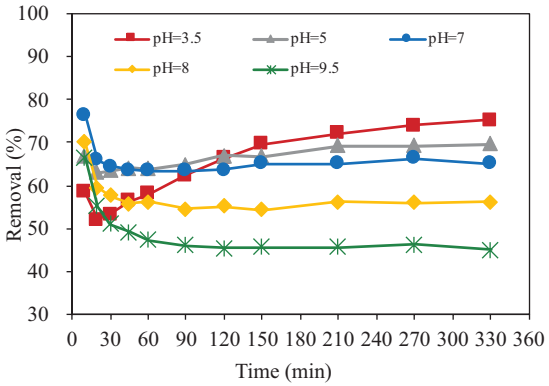

Figure 6.5: The influence of pH on flux and CBZ removal.

It can be seen from Figure 6.5 that the membrane flux shows different trends under different pH conditions. Under acidic conditions, the flux decreased significantly; at neutral conditions, the flux did not change; the flux increased under alkaline conditions.

At lower pH, the polar functional groups of the membrane are sheltered, resulting in a weakening repulsive interaction between the functional groups, and shrinkage of the pores of the membrane, which increases filtration resistance and leads to a decrease in flux; at higher pH, the repulsive interaction between the functional groups is enhanced, resulting in expansion of the pores of the membrane, reducing membrane resistance, thereby promoting an increase in flux [52]. As the pH decreases,

EBSCOhost - printed on 2/14/2023 6:39 AM via . All use subject to https://www.ebsco.com/terms-of-use

the removal rate of CBZ increases significantly. This is due to that the decrease in pH causes the pores of the membrane to shrink, the sieving effect is enhanced, and the removal rate is increased.

6.5.4 Effect of initial mass concentration on removal of CBZ from nanofiltration membrane

Different volumes of CBZ stock solution were added to the background electrolyte to make the mass concentrations of 50, 100, 300, 500 μg/L. The solutions were stored at the temperature of 25 ± 1 °C, and the pH was adjusted to 8.0. The filtration results are shown in Figure 6.6.

It can be seen from Figure 6.6 that when the initial mass concentration of CBZ is 50–500 μg/L, the flux remains nearly constant, which indicates that the trace amount of CBZ in the feed has little effect on the flux of the nanofiltration membrane. When the initial mass concentration of CBZ was 50–500 μg/L, the removal rate of CBZ was 55–62%, and there was no significant change. This is consistent with the results of Schafer et al. [53] and Zhang et al. [54] using membrane filtration to remove endocrine disruptors (EDCs). This phenomenon can be due to that the partition coefficient of the target contaminant between the bulk solution and the membrane is constant, so the initial mass concentration has no significant effect on the removal of target contaminants.

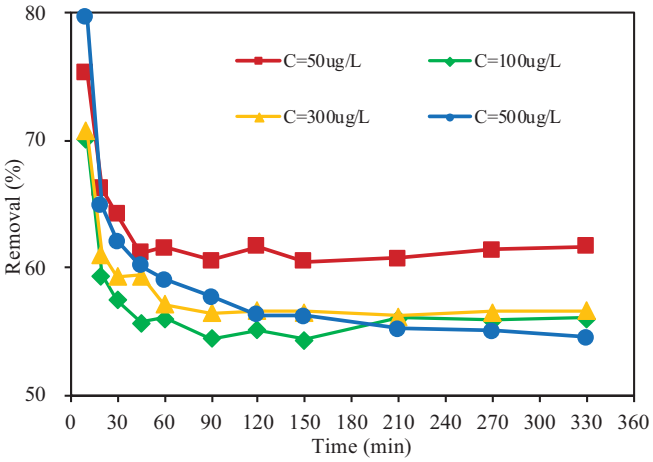

Figure 6.6: Effect of initial mass concentrations on membrane flux and CBZ removal.

EBSCOhost - printed on 2/14/2023 6:39 AM via . All use subject to https://www.ebsco.com/terms-of-use

6.5.5 Effect of ionic strength on removal of CBZ by nanofiltration

The effect of different ionic strengths on the removal of CBZ by nanofiltration was investigated through adding calcium chloride to produce hardness of water. Three water samples with calcium ion concentrations of 5, 10 and 15 mmol/L were prepared. The initial mass concentration of CBZ is about 100 μg/L, the temperature is at 25 ± 1 °C, and the pH is adjusted to 8.0. The result is shown in Figure 6.7.

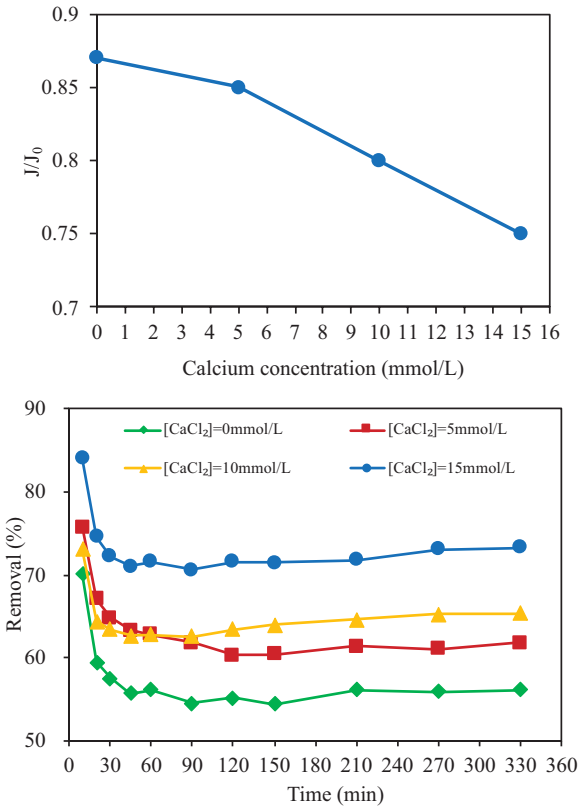

Figure 6.7: Effect of ionic strength on membrane flux and CBZ removal.

It can be seen from Figure 6.7 that as the concentration of calcium ions increases, the flux decreases significantly. This is due to the fact that divalent cations such as calcium ions can compress the thickness of the electric double layer, and then neutralize or weaken the negative charge on the surface of the membrane, thus the mutual repulsion on the functional groups on the surface of the membrane is weakened, and the permeate flux is reduced. The removal rate of CBZ increased significantly with the increase of calcium ion concentration. This is consistent with the results from Bous-

EBSCOhost - printed on 2/14/2023 6:39 AM via . All use subject to https://www.ebsco.com/terms-of-use

sahel et al. [35] and Koyuncu et al. [55]. The pore size of the membrane is reduced, the retention effect of the nanofiltration membrane on CBZ is enhanced, and the removal rate is improved. Many studies indicate that changes in ionic strength have a greater impact on membranes with larger pore sizes [23, 56].

6.5.6 Effect of temperature on removal of CBZ by nanofiltration

The influent temperatures were adjusted to 12, 17, 25, and 35 °C, respectively, to investigate the effect of temperature on the removal of CBZ by nanofiltration. The initial mass concentration of CBZ was about 100 μg/L in the background electrolyte, and the pH was adjusted to 8.0. The test results are shown in Figure 6.8.

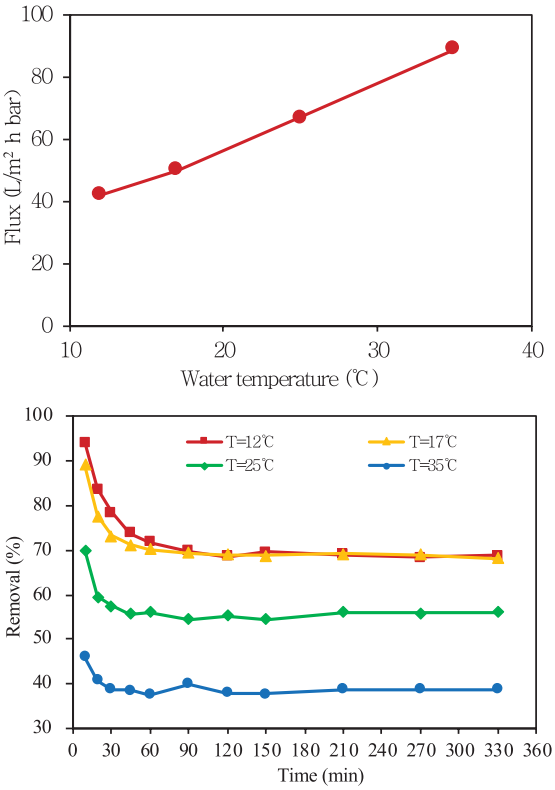

Figure 6.8: Effect of temperature on membrane flux and CBZ removal.

It can be clearly seen from Figure 6.8 that the higher the influent temperature, the larger the membrane flux. This is due to the difference in viscosity at different temperatures. At higher temperature, the viscosity of water is smaller, thus the filtration

EBSCOhost - printed on 2/14/2023 6:39 AM via . All use subject to https://www.ebsco.com/terms-of-use

resistance reduces and the flux increases. The change in temperature also significantly affects the removal of CBZ. When the water temperature is 35 °C, the removal rate is only 38%; when the water temperature is lowered to 25 °C, the removal rate is increased to 56%; when the water temperature is lowered to 17 °C, the removal rate is further increased to 68%; however, when the temperature is further reduced, the removal rate doesn't change any more. The reason for the change is due to thermal expansion and contraction that the pores of the membrane change slightly with changes in water temperature. Since the membrane pore size of NF270 is about 0.84 nm, the retained relative molecular weight is 385 ± 13 Da, which is close to the particle size of CBZ. Therefore, a slight variation in the pores of the membrane causes a significant change in the removal of CBZ. The decrease in water temperature causes the pore size of the membrane to shrink, resulting in an increase in the sieving effect, thereby improving the removal of CBZ.

6.6 Effect of dissolved organic matter on removal of CBZ from nanofiltration membrane

CBZ has been widely detected in groundwater, surface water and drinking water source. The water body contains many different kinds of organic matter. Therefore, it is necessary to study the effect of organic matter on the removal of CBZ by nanofiltration.

Natural organic matter (NOM) is an intermediate product produced during the natural circulation of plants and animals. Their molecular weight distribution is very wide, as small as 1,000 Da or up to several hundred thousand Da. The dissolved organic matter (DOM) refers to organic matter that can be dissolved in water, acid or alkali solution. It is an important organic component with active physicochemical properties and is the main object for advanced water treatment process. A large number of studies have shown that NOM has a certain influence on the removal of micro-polluted organic matter such as PPCPs in membrane filtration [57, 58]. In this section, humic acid (HA), sodium alginate (SA) and tannic acid (TA) were used as representatives of DOM to investigate the effect of NOM on CBZ removal by nanofiltration.

6.6.1 Effect of humic acid on removal of CBZ by nanofiltration

Humic acid is formed by the biological, abiotic degradation and polymerization of animal and plant residues. It is widely found in nature, especially in soil, seawater and terrestrial surface water and shallow groundwater. It is the main component of natural organic matter, accounting for 50–90% of the total organic matter in NOM.

EBSCOhost - printed on 2/14/2023 6:39 AM via . All use subject to https://www.ebsco.com/terms-of-use

HA is mainly composed of C, H, O, N, a small amount of S, P and other elements. It is an aromatic polymer with a polyvalent hydrazine and a polyphenol. In HA, the aromatic core has carboxyl, phenolic, hydroxyl, sugar, peptide and other components, and the cores are connected by various bridge bonds (-O-, -CH2-, = CH-, -NH-, -S-) [59]. In addition to a large number of benzene rings, there are a large number of functional groups, such as -OH, -COOH, ≥ O, $-PO_3H_2$, $-NH_2$, $-CH_3$, $-SO_3H$, $-OCH_3$, etc. The relative molecular weight distribution of HA ranges from several hundred to several tens of thousand. The molecular structure is different dependent on its location and other environmental conditions. HA has unique physical and chemical properties, mainly in [59]: (1) colloidal properties, i.e. the hydrogen in its main functional groups, such as – COOH, -OH can be released to be negatively charged. HA has a large surface area, high viscosity and strong adsorption capacity. (2) It is obviously acidic. Its acidity depends on the concentration of hydrogen ions that can be released, which is determined by the hydroxyl and phenol in humic acid. HA is hardly soluble in water under neutral or acidic conditions, it is a hydrophobic substance, and exhibits a soft linear macromolecular structure; under alkaline conditions, HA is soluble in water and exhibits a rigid crimped structure; when the solution is adjusted to neutral, the dissolved HA would not precipitate. (3) It can be oxidized and decomposed by oxidants.

The HA stock solution was diluted with deionized water to produce water samples with DOC mass concentrations of 1.77, 4.25, and 9.68 mg/L (based on TOC measurement). The initial mass concentration of CBZ was about 100 μg/L, with the background electrolyte containing 20 mmol/L NaCl and 1 mmol/L $NaHCO_3$, the pH is adjusted to about 8.0, and the temperature is controlled at 25 ± 1 °C. The prepared water sample was placed on a magnetic stirrer for a while to thoroughly mix the CBZ with the HA.

The effect of HA solution with different DOC concentrations on the removal of CBZ by nanofiltration with the flux (J/J_0) and removal rate (%) is shown in Figure 6.9. The control test in the figure indicates no HA dosage. The other test conditions are consistent with the test with HA, and the test conditions of SA and TA are the same, and thus it is not described later.

As can be seen from Figure 6.9, the addition of HA did not have a significant effect on the filtration flux compared to the control test without HA addition, and the tests with different DOC mass concentrations did not exhibit significant differences. Similar to the flux results, the removal rate of CBZ did not change regularly with the addition of HA or the concentration of DOC added. The lowest removal rate was about 52% and the highest about 56%, in a similar range.

EBSCOhost - printed on 2/14/2023 6:39 AM via . All use subject to https://www.ebsco.com/terms-of-use

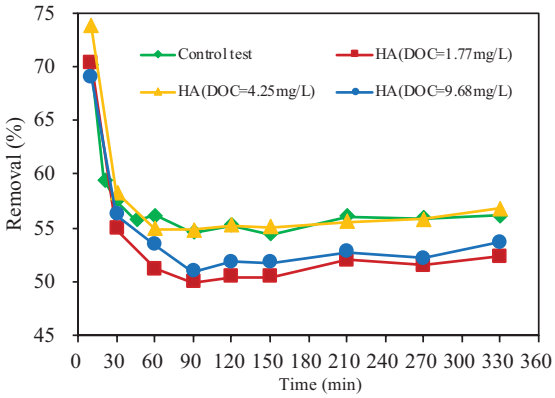

Figure 6.9: Effect of HA on membrane flux and CBZ removal.

6.6.2 Effect of sodium alginate on removal of CBZ by nanofiltration

Sodium alginate is a hydrophilic anionic polysaccharide material produced by seaweed and bacteria. It is widely used in food, medicine, textile, printing and dyeing, papermaking, daily chemicals and other products, as a thickener, emulsifier, stabilizer, carrier, sizing agent, etc. SA[$(NaC_6H_7O_6)_n$] consists mainly of sodium salt of alginic acid, and is based on a-L-mannuronic acid (M unit) and b-D-guluronic acid (G unit), connected with 1,4-glycosidic bond and composed of different GGGMMM fragments.

SA is slightly soluble in water and insoluble in most organic solvents. It is soluble in alkaline solutions to make the solutions viscous. The sodium alginate powder becomes wet with water, and the hydration of the particles makes the surface sticky. The particles can be then quickly bonded together to form a mass which is slowly fully hydrated and dissolved.

The prepared SA stock solution was diluted with deionized water to make a water sample with a DOC concentration of 1.75, 4.40, 10.64 mg/L (measured by TOC analyzer), and the initial mass concentration of CBZ is about 100 μg/L. The background electrolytes are 20 mmol/L NaCl and 1 mmol/L $NaHCO_3$ with the pH of about 8.0 and the temperature of 25 ± 1 °C. The prepared water sample was placed on a magnetic stirrer for a while to thoroughly mix the CBZ with the SA.

The effect of different concentrations of SA solutions on the removal of CBZ by nanofiltration with the flux (J/J_0) and removal rate (%) is shown in Figure 6.10.

It can be seen from Figure 6.10 that the flux decreases significantly with the increase of the concentration of SA. When the mass concentration of DOC is 10.64 mg/L, the flux decreased 33% relative to the solution without SA. In addition, the flux decreased slightly during the filtration, indicating that the membrane fouling was caused by SA when the test continued. The removal rate of CBZ after SA addition was

EBSCOhost - printed on 2/14/2023 6:39 AM via . All use subject to https://www.ebsco.com/terms-of-use

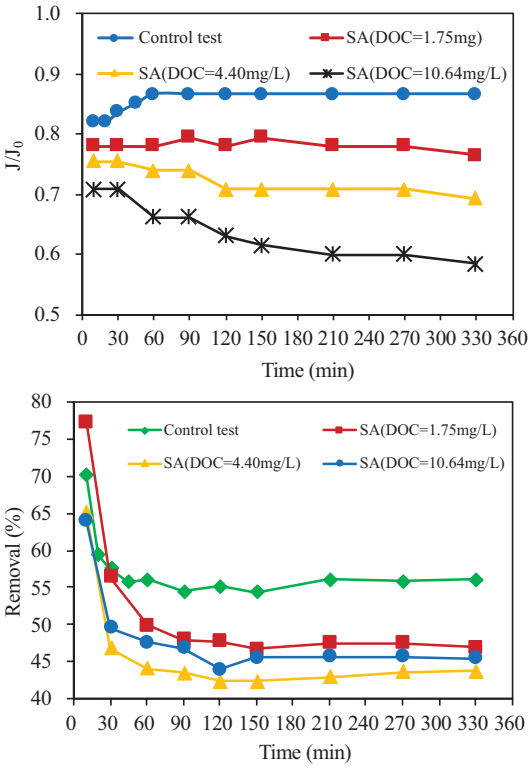

Figure 6.10: Effect of SA on membrane flux and CBZ removal.

significantly lower than that without SA, from 56% to 45%; however, when the mass concentration of DOC varied from 1.75 to 10.64 mg/L, there was no direct impact on the removal rate of CBZ.

6.6.3 Effect of tannic acid on removal of CBZ by nanofiltration

Tannic acid (TA), also known as citric acid in the pharmacopoeia, is a hydrolyzed tannin, which is hydrolyzed to be orange acid and glucose. It is one of the earliest tannins studied. TA are throughout the nature and commonly in Chinese herbal medicines (such as gallnuts, pomegranate peels, and cranes) and plant foods (such as barley, sorghum, mung beans, fruits and vegetables such as onions, grapes, and tea etc.).

TA is a yellow or light brown light non-crystalline powder or scales; it has a special slightly odor and tastes extremely sturdy. It can be soluble in water and ethanol, severely soluble in glycerin, and almost insoluble in ether, chloroform or benzene. Its polyphenol light-based structure makes it a series of unique chemical and physiolog-

EBSCOhost - printed on 2/14/2023 6:39 AM via . All use subject to https://www.ebsco.com/terms-of-use

ical activities, such as binding to proteins, alkaloids, and polysaccharides, which can change its physicochemical properties and make complexation and electrostatically interact with various metal ions. It is oxidative and has the ability to seize the free radical, and also the activities for an amphiphilic structure and derivatizations [60].

The prepared TA stock solution was diluted with deionized water to make water samples with DOC mass concentrations of 1.75, 4.15, and 7.73 mg/L (measured by TOC analyzer). The initial mass concentration of CBZ is about 100 μg/L, and the background electrolytes are 20 mmol/L NaCl and 1 mmol/L $NaHCO_3$ wtih the pH of about 8.0, and the temperature of 25 ± 1 °C. The prepared water sample is placed on a magnetic stirrer and stirred until CBZ and TA are fully mixed.

The effect of different concentrations of TA solutions on the removal of CBZ by nanofiltration with flux (J/J_0) and removal rate (%) is shown in Figure 6.11.

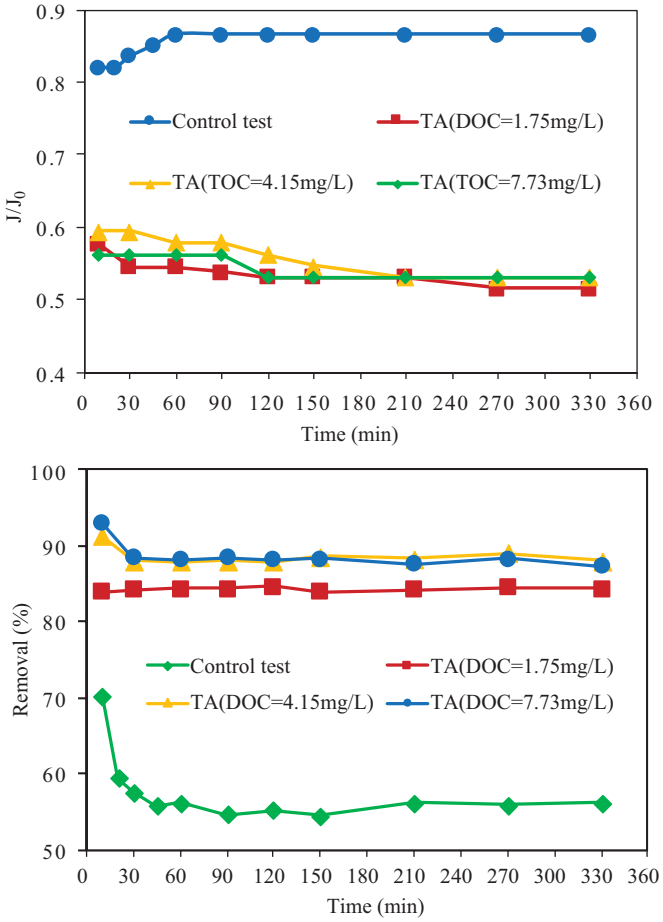

Figure 6.11: Effect of TA on membrane flux and CBZ removal rate.

EBSCOhost - printed on 2/14/2023 6:39 AM via . All use subject to https://www.ebsco.com/terms-of-use

From Figure 6.11, the flux is at a lower level from the beginning of the test, which is 39% lower than the control test without TA, and decreases slightly as the filtration continues, which shows that TA contaminates the membrane very quickly. The test results also show that the TA concentration does not have a regular effect on the flux. After the filtration is carried out for 2.5 h, the flux of the three conditions is almost the same. With the addition of TA, the removal rate of CBZ was greatly improved compared with the test without TA addition, rising from 56% to about 89%. As the concentration of TA increased, the removal rates of CBZ were slightly increased, which were 84%, 87%, and 89%, respectively.

In order to analyze the test results obtained in the above three groups of experiments, the comparison was conducted with the similar DOC concentrations of the three organic compounds of HA, SA and TA (4.25, 4.4, 4.15 mg/L) with results summarized in Table 6.5.

Table 6.5: Performance comparison with HA, SA and TA.

Parameters	CBZ	CBZ + HA	CBZ + SA	CBZ + TA
Removal rate (%)	56.1	56.8	43.8	88.1
Flux (J/J_0)	0.87	0.86	0.69	0.53

From Table 6.5, we can see that in terms of removal rate, SA < HA < TA, and in terms of flux reduction, HA < SA < TA. In order to get the reason for these phenomena, the relative molecular weight distribution and hydrophilicity of the three organic matters were analyzed with the results shown in Figures 6.12 and 6.13, respectively.

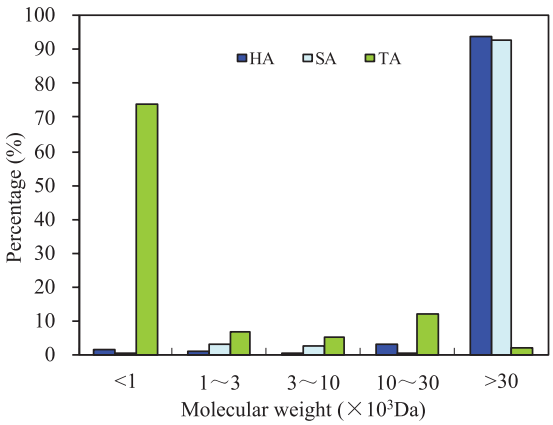

Figure 6.12: Relative molecular weight of HA/SA/TA.

EBSCOhost - printed on 2/14/2023 6:39 AM via . All use subject to https://www.ebsco.com/terms-of-use

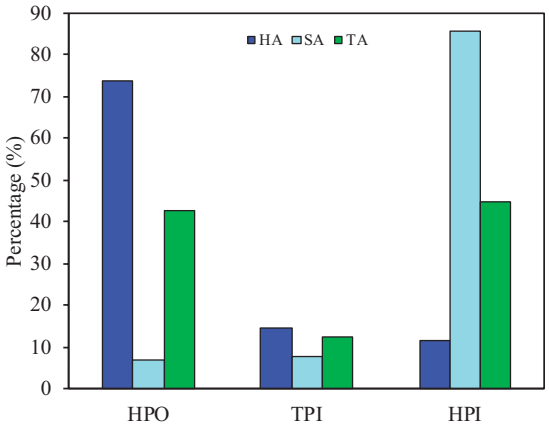

Figure 6.13: Hydrophilicity of HA/SA/TA.

It can be seen from Figure 6.12 that the organic matter with molecular weight greater than 30×10^3 Da in HA and SA accounts for more than 90% of the total DOC, indicating that both HA and SA used in this test consist of macromolecular organic matter. The molecular weight of TA less than 1 kDa is accounting for 73.7%, so the small organic matter in TA accounts for the majority. From this, it is speculated that with the addition of TA, for the NF270 membrane used in the test, the phenomenon that the flux decreased sharply from the beginning of the test and the removal rate increased significantly was due to the small molecule organic matter. The nanofiltration membrane has a smaller pore size than the ultrafiltration membrane or the microfiltration membrane, and the molecular weight of the retained molecules is generally 200–1,000 Da, so the small molecular organic matter has a greater chance of entering the pore of the membrane, adsorbing or clogging in the pore of the membrane, reducing the effective number of membrane pores or pore size, resulting in the increase in the resistance and decrease in the permeate flux. The study from Crozes et al. also shows that small molecule organic matters, especially those with particle size much smaller than membrane pore size, are major membrane fouling contributors [61]. Comerton et al. used the effluent from a membrane bioreactor, Lake Ontario water and laboratory water to investigate the sieving effect of NF270 membrane before and after contamination with organic matter [56]. It was found that MWCO of NF270 membrane after MBR effluent and Lake Ontario water was from 385 ± 13 Da to 222 ± 46 Da and 348 ± 28 Da, respectively, thus the screening effect could increase significantly with the decrease of MWCO. For CBZ, the removal mechanism of NF270 membrane is mainly sieving. Therefore, after the NF270 membrane is contaminated by TA, its MWCO becomes smaller, and the membrane has an enhanced retention effect on CBZ, so the removal rate of CBZ is greatly improved. This is consistent with the results from Plakas and Karabelas, who found that the removal rate of atrazine by NF270 membrane increased by 20% to 29% after the addition of TA [62].

EBSCOhost - printed on 2/14/2023 6:39 AM via . All use subject to https://www.ebsco.com/terms-of-use

From Figure 6.13, the strong hydrophobic substances in HA account for the majority, up to 70%, the weakly hydrophobic materials account for 14.6%, and the hydrophilic materials only account for 11.6%; in contrast, the neutral hydrophilic substances in SA account as high as 85.3%, while the strong hydrophobic substances and weakly hydrophobic substances are only about 7%; the proportion of hydrophilic organic matter and hydrophobic organic matter in TA is not much different.

Therefore, it is believed that SA and TA cause a stronger decrease in membrane flux than HA, which also has a great relationship with the hydrophilic and hydrophobic composition of the organic matter in the influent. The membrane contact angle of NF270 is 23.4°, which indicates that NF270 is a very hydrophilic nanofiltration membrane, so it is not easy to cause organic pollution in general [63]. Compared with hydrophobic organic matter, hydrophilic organic matter is more likely to be adsorbed and deposit on the surface of the hydrophilic membrane to form a cake layer, resulting in an increase in membrane resistance and a decrease in permeate flux. Moreover, it was observed after the test that the cake layer induced by SA was more difficult to be washed away by water, and the cake layer induced by HA was easily washed away by water, confirming the above explanation. Carroll et al. [64] and Fan et al. [65] separated the natural water into fractions of strong hydrophobic, weakly hydrophobic, neutral hydrophilic and charged hydrophilic components for membrane filtration test. It was found that the main organic component causing the strongest decrease in flux was the neutral hydrophilic part. Park et al. found that the hydrophilic organic substances such as proteins and polysaccharides tend to precipitate on the surface of the membrane, which is the main reason to induce the decrease in permeate flux in membrane filtration [66].

In the filtration of the SA and CBZ mixed solution, the significant decrease in CBZ removal rate may be caused by concentration polarization [67]. The contaminated layer induced by SA hinders the diffusion of CBZ into the bulk solution and increases the concentration of CBZ in the contaminated layer and on the surface of the membrane. Therefore, the CBZ has a higher transmembrane concentration gradient, thereby increasing the permeate concentration and reducing the removal rate. Jermann et al. also found that the removal rate of ibuprofen by the membrane fouled with SA was decreased, and they attributed to the concentration polarization caused by SA [68].

The cake layer induced by HA is loose, thus the increased filtration resistance is small. At the same time, the macromolecules of HA do not block the pores of the membrane, and the number of membrane pores bonded with water molecules is not reduced, thus water molecules can still permeate through the membrane pores, and the membrane permeate flux still remains. Regarding the CBZ removal rate, there was no significant difference in the control experiment or with the different DOC concentration conditions, indicating that the concentration polarization caused by HA was not as severe as in SA. Nghiem and Hawkes also found that the new NF270 membrane and fouled NF270 membrane by HA had no significant effect on CBZ removal [69].

Currently, HA has been used as a representative DOM in a large number of tests and its effect on the removal of PPCPs by nanofiltration has been investigated. It has

EBSCOhost - printed on 2/14/2023 6:39 AM via . All use subject to https://www.ebsco.com/terms-of-use

been reported that increase or decrease of removing DOM had no significant effect on removing PPCPs [70]. This is due to that, the properties of HA used in different experiments are not the same, and the relative molecular weight distribution plays a very important role in sieving [45]. In addition, the nature of each type of PPCPs varies greatly, as HA has a negative charge, so it can affect the electrostatic repulsion between charged PPCPs and membrane surface functional groups. This can have two diametrically opposite effects, either promoting or reducing the retention of micro-contaminants. On one hand, if membrane fouling enhances the electronegativity of the functional groups on the surface of the membrane, the negative contaminants can pass through the membrane, resulting in the higher rejection due to the enhancement of electrical repulsion; on the other hand, due to the negative charge of the membrane functional group is enhanced, the negative effect on the membrane itself is that the MWCO of the membrane also rises at the same time. This phenomenon is called the membrane expansion/swelling; moreover, the composition of the feed, such as ionic strength, especially the chelation of divalent cation and HA, also affects the relationship among the membrane, DOM and PPCPs. Finally, the nature of the membrane (such as zeta potential, membrane contact angle, etc.) determines the degree of membrane fouling. Therefore, further study is needed.

6.7 Effect of dissolved organic matter with ozonation pretreatment on the removal of CBZ by nanofiltration

From the above results, with the addition of tannic acid (TA), the removal rate of CBZ has been greatly improved, while the addition of humic acid (HA) basically doesn't have any effect on CBZ removal rate; on the contrary, the addition of sodium alginate (SA) even reduces CBZ removal rate. Therefore, some common pretreatment methods are used to investigate the change of properties of HA and SA after pretreatment on CBZ removal by nanofiltration.

6.7.1 Pretreatment method selection

6.7.1.1 Activated carbon adsorption

When using powdered activated carbon as a pretreatment method to remove humic acid by microfiltration, it was found that powdered activated carbon can remove many HA with low molecular weight, but has little effect on the removal of large molecular weight of HA. Wang et al. analyzed the relative molecular weight (MW) of DOM from

EBSCOhost - printed on 2/14/2023 6:39 AM via . All use subject to https://www.ebsco.com/terms-of-use

Huangpu River after ozone activated carbon process, and found that biological activated carbon can effectively remove organic pollutants with relative molecular weight of 1 to 3 kDa and also small molecule organic matter with MW < 1 kDa [71].

In summary, activated carbon can selectively adsorb organic matter. According to the previous test results, HA and SA are mostly macromolecular organics above 30 kDa, while HA is mostly hydrophobic, so activated carbon adsorption is not suitable as a pretreatment method in this test.

6.7.1.2 Coagulation

Carroll et al. conducted the membrane filtration test with the effluent with aluminum coagulation and 0.2 μm membrane filtration, and compared the membrane permeate flux with the same feed without coagulation or 0.2 μm membrane filtration [64]. They found that the decrease of membrane permeate flux without coagulation or 0.2 μm membrane filtration was caused mainly by the colloids; coagulation increases the removal effect of the organic matter and reduces the flux drop, but the reduction of the membrane permeate flux with coagulation was similar as that with 0.2 μm membrane filtration. They suggest that coagulation mainly removes colloids larger than 0.2 μm and cannot remove dissolved organic matter.

Four water samples with different hydrophilicity or hydrophobicity were filtrated to investigate the hydrophilic or hydrophobic organic removal by coagulation and also the subsequent ultrafiltration permeate flux improvement. The test results show that coagulation can effectively remove the hydrophobic component, but has little effect on the removal of hydrophilic components [72].

Although the effect of coagulation pretreatment on the reduction of organic matter is worthy of recognition, it is selective as the same as activated carbon. HA and SA are hydrophobic and hydrophilic substances, respectively, and both are macromolecular organics (MW > 30 kDa), so coagulation does not apply to these two organics.

6.7.1.3 Ozone pre-oxidation

As an excellent oxidant and disinfectant, ozone can oxidize and remove most organic and inorganic contaminants and bacteria in water treatment.

Through ozonation, the physicochemical properties and biodegradability of DOM can change significantly. The experimental results of Rodríguez et al. show that the structural properties of the organic matter have been changed significantly during ozonation [73]. The macromolecular organic matters are oxidized into small molecular organic substances, and some organic substances having an unsaturated structure are converted into a saturated structure.

EBSCOhost - printed on 2/14/2023 6:39 AM via . All use subject to https://www.ebsco.com/terms-of-use

The purpose of this experiment is to investigate the effect of different organic substances on the removal of CBZ by nanofiltration. Since ozone can change the nature of organic matter, it can meet this purpose. Therefore, this experiment uses ozone oxidation as a pretreatment method to examine the effect of HA and SA on the removal of CBZ by nanofiltration after ozonation.

6.7.2 Method

In this test, the time of ozonation was used to express different ozone dosages to compare different working conditions. The ozonation duration was selected according to the ozone concentration. When the ozone exposure time increases and the ozone concentration tends to be gentle, it is regarded to be saturated.

In each test, the HA and SA stock solutions were diluted to make a solution with a DOC concentration of about 30 mg/L. After ozonation with different duration, the solution was diluted with deionized water to a background water sample with a volume of 5 L, the DOC mass concentration of approximately 4.5 mg/L (prepared according to the DOC measured value after ozonation), initial concentration of CBZ of about 100 μg/L, background electrolyte of 20 mmol/L NaCl and 1 mmol/L $NaHCO_3$, pH of around 8.0 and the temperature at 25 ± 1 °C.

6.7.3 Effect of humic acid with ozonation pretreatment on the removal of CBZ by nanofiltration

6.7.3.1 The effect of humic acid before and after ozonation on the removal of CBZ by nanofiltration

After the HA solution with a DOC concentration of 30 mg/L was oxidized by ozone for 30 min, the ozone concentration was 3.42 mg/L, and then the ozone concentration changed slowly. It can be regarded that the ozone in the HA solution has basically reached saturation. Figure 6.14 shows the effect of HA on the CBZ removal and membrane permeate flux before and after ozonation for 30 min.

It can be seen from Figure 6.14 that the flux of ozone-oxidized HA and CBZ mixed solution is significantly lower than that of the control test and the HA filtration without ozonation, from 87% to 80%. With the concentration of DOC almost the same, when the ozonated HA mixed with CBZ is filtered, the removal rate of CBZ by nanofiltration is increased from 56% to about 63%.

From the filtration experiments with the three soluble organic compounds of HA, SA and TA, the following conclusions can be obtained that hydrophilic organic matter is more likely to cause membrane flux decrease than hydrophobic organic matter and small molecular organic matter is more likely to cause membrane flux decrease than macromo-

EBSCOhost - printed on 2/14/2023 6:39 AM via . All use subject to https://www.ebsco.com/terms-of-use

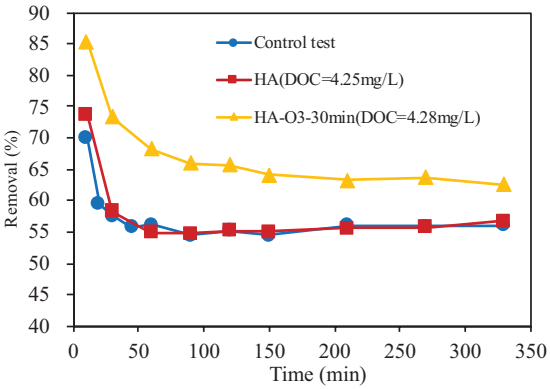

Figure 6.14: Effect of HA on membrane permeate flux and CBZ removal before and after ozonation for 30 min.

lecular organic matter. Therefore, the ozonated HA induced a severer membrane fouling and a lower permeate flux. In addition, the reason for the increase in CBZ removal rate is most likely due to the change in the physicochemical properties of HA after ozonation.

Therefore, the hydrophilic-hydrophobic fraction and relative molecular weight distribution of HA before and after ozonation were measured in this study. The results of hydrophilic-hydrophobic fraction of HA before and after ozonation (30 min, 3.42 mg/L) are shown in Figure 6.15, and the relative molecular weight distribution before and after ozonation is shown in Figure 6.16.

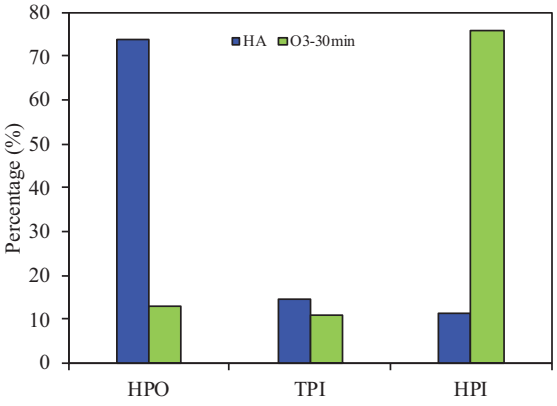

Figure 6.15: Hydrophilic hydrophobic fraction of HA before and after ozonation.

In Figure 6.15, after ozonation, the strong hydrophobic fraction in HA decreased from 73.8% to 14.3%, while the hydrophilic fraction increased from 11.5% to 74.4%, thus the hydrophilicity of HA increased significantly. The hydrophilic organic matter could induce more significant membrane fouling, stronger filtration resistance and lower

EBSCOhost - printed on 2/14/2023 6:39 AM via . All use subject to https://www.ebsco.com/terms-of-use

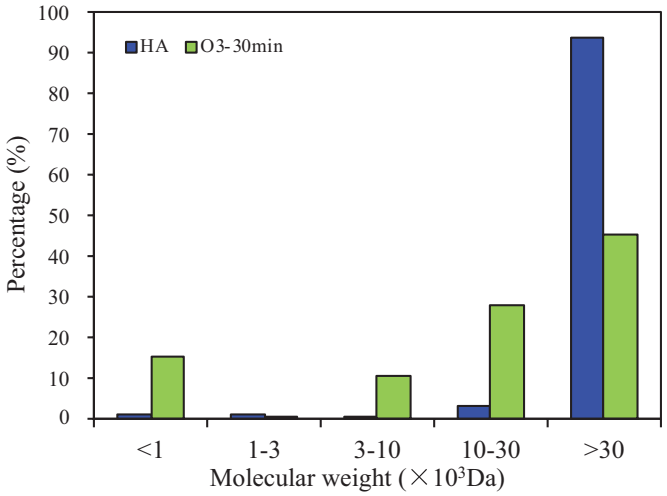

Figure 6.16: Relative molecular weight distribution of HA before and after ozonation.

permeate flux, so this could be the reason that HA induced severer membrane fouling after ozonation.

In Figure 6.16, after ozonation, the fraction of macro molecules with MWCO larger than 30 kDa in HA reduces significantly, from 93.9% to 45.2%, the fraction with MWCO between 1 kDa and 3 kDa doesn't have any obvious change, while the rest fraction increases significantly. Studies have shown that ozone can easily react with -C = C- or C = O groups, thereby destroying the benzene ring or carbon-oxygen double bond, so that the aromatic organic matter can be well removed. From the perspective structural properties, humic acid is easily oxidized by ozone, and macromolecular organic matter is converted into small molecular organic matter, increasing the composition ratio of organic matter with small relative molecular weight in water. However, the increase of organic matter with a relatively small molecular weight can easily block the membrane pores, increase the membrane filtration resistance and decreases the permeate flux, resulting in the increase of the MWCO of the membrane.

From the above two aspects, the change of both hydrophilicity and hydrophobicity and relative molecular weight distribution after ozonation can lead to the decrease of permeate flux. As the increase of MWCO is more dominant than the concentration polarization, the removal rate of CBZ is increased.

6.7.3.2 Effect of humic acid with different ozonation on the removal of CBZ by nanofiltration

In the study of ozonation, the dosage of ozonation on the removal of organic matter has attracted great attention.

EBSCOhost - printed on 2/14/2023 6:39 AM via . All use subject to https://www.ebsco.com/terms-of-use

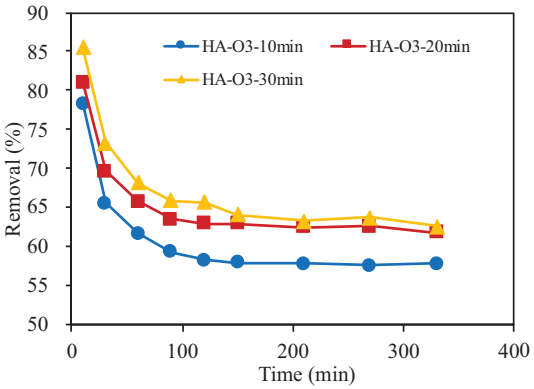

Figure 6.17: Membrane flux and CBZ removal with HA oxidized with different ozonation by nanofiltration.

Since the HA solution was exposed to ozone for 30 min and the ozone concentration did not change significantly, the ozone dissolution in the solution was basically saturated. Therefore, the time for ozonation was 10, 20 and 30 min, respectively, and the ozone concentration was 0.79, 1.05 and 3.42 mg/L, respectively. The results for membrane flux and CBZ removal rate are shown in Figure 6.17.

It can be seen from Figure 6.17 that the membrane flux of HA with 10 min oxidation (0.79 mg/L) is the highest, while it is slightly lower with the ozonation time of 20 min (1.05 mg/L) or 30 min (3.42 mg/L). The CBZ removal rate gradually increased with the increase of ozone concentrations, which were 57%, 62% and 63%, respectively. Among them, the increase of CBZ removal rate was more obvious when the oxidation time was increased from 10 min to 20 min, but the removal rate did not change much after 20 min of oxidation. This may be due to the blockage of the membrane pores by small molecular organic matter resulting in a decrease in the MWCO of the membrane. With the increase of the duration of ozonation, although the macromolecular organic matter is continuously converted into small molecular organic matter, the small molecular organic matter is also partially mineralized. So in each test the HA solution has the same initial DOC concentration. When ozonation goes to a certain level, the proportion of small molecule organic matter does not increase significantly, which induces the above change of flux and removal rate.

6.7.4 Effect of sodium alginate with ozonation pretreatment on the removal of CBZ by nanofiltration

6.7.4.1 Effect of sodium alginate on the removal of CBZ before and after ozonation

After the SA solution with DOC concentration of 30 mg/L was oxidized by ozone for 10 min, the ozone concentration was 4.47 mg/L. After that, the ozone concentration

EBSCOhost - printed on 2/14/2023 6:39 AM via . All use subject to https://www.ebsco.com/terms-of-use

changed slowly. So it can be regarded that the ozone in the SA solution has reached saturation. Figure 6.18 is the membrane flux and CBZ removal with SA before and after 10 min ozonation by nanofiltration.

It can be seen from Figure 6.18 that although the flux of SA solution after 10 min ozonation is still smaller than the control test without any organic matter, it is greatly improved than the SA solution without ozonation with the same DOC mass concentration. The CBZ removal rates are quite different before and after SA ozonation, increasing from about 42% to about 62%. After SA oxidation, the membrane flux increases, membrane fouling reduces, and CBZ removal rate also increases.

The change in the hydrophilic and hydrophobic fraction of SA before and after ozonation (10 min, 4.47 mg/L) is shown in Figure 6.19, and the relative molecular weight distribution before and after ozonation is shown in Figure 6.20.

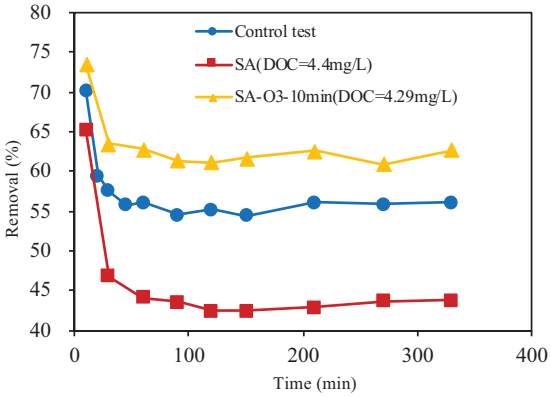

Figure 6.18: Membrane flux and CBZ removal with SA before and after 10 min ozonation by nanofiltration.

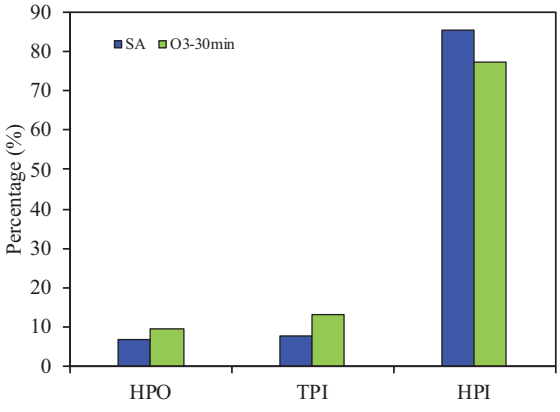

Figure 6.19: The hydrophilic and hydrophobic fraction of SA before and after ozonation.

EBSCOhost - printed on 2/14/2023 6:39 AM via . All use subject to https://www.ebsco.com/terms-of-use

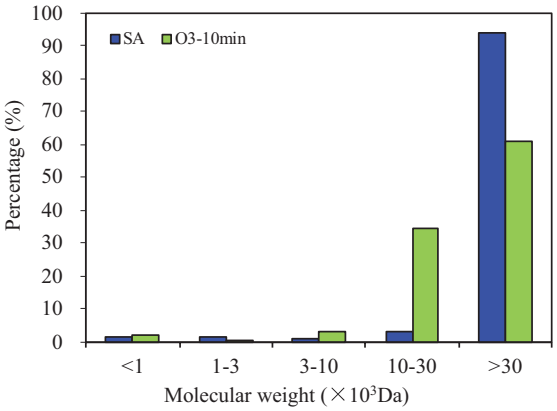

Figure 6.20: The relative molecular weight distribution of SA before and after ozonation.

It can be seen from Figure 6.19 that the hydrophilicity and hydrophobicity of the SA solution after ozonation did not change significantly. From Figure 6.20, in the SA solution, the macromolecules above 30 kDa are obviously reduced, while the fractions of 10 kDa–30 kDa are increased, and the other parts are basically unchanged.

In summary, the SA solution can easily form a fouling layer on the membrane surface to induce the increase of filtration resistance and concentration polarization, which may be due to that after ozonation, the structure of SA is changed, and the macromolecule is oxidized to smaller molecules. The interaction with the membrane is changed, the membrane fouling is reduced, the flux is improved, and the concentration polarization is alleviated thus the CBZ removal rate is increased.

6.7.4.2 Effect of sodium alginate oxidized by different concentrations of ozone on the removal of CBZ by nanofiltration

Since the ozone was introduced into the prepared SA solution for 10 min, the mass concentration of the residual ozone did not change much and basically reached saturation. Therefore, the time for introducing ozone was 2, 5 and 10 min, respectively, with the ozone concentration of 2.10, 3.42 and 4.47 mg/L, respectively. The test results are shown in Figure 6.21.

As can be seen from Figure 6.21, no matter how much ozone is injected, the membrane permeate flux or CBZ removal rates doesn't change greatly. However, the flux and CBZ removal rates are increased in the control experiments without organics or in the SA solution without ozonation. Compared with the ozonated HA solution, the mass concentration of ozonation of SA for 5 min (3.42 mg/L) was equivalent to that of HA for 30 min (3.42 mg/L). The DOC mass concentration did not change much under different ozone concentrations, and the results are shown in Table 6.6. The above test

EBSCOhost - printed on 2/14/2023 6:39 AM via . All use subject to https://www.ebsco.com/terms-of-use

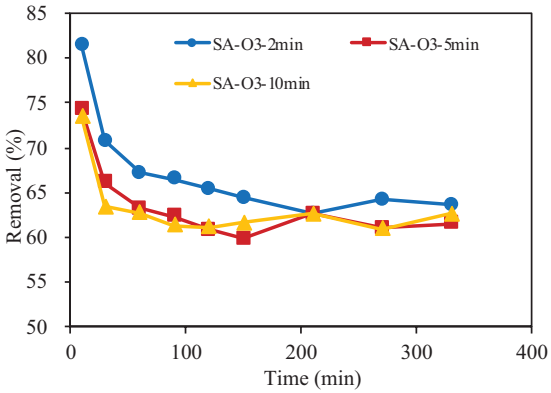

Figure 6.21: Membrane flux and CBZ removal rate with SA oxidized by different mass concentrations of ozone by nanofiltration.

results may be due to the fact that SA is not oxidizable. Ozone can only oxidize the macromolecular organics to a certain extent. Different ozonation have little effect on the organics oxidation.

Table 6.6: DOC values of SA solutions with different ozonation time.

Ozonation time	2 min	5 min	10 min
DOC removal/%	3.22	8.62	5.33

6.8 Effect of natural organic matter on removal of CBZ by nanofiltration

In earlier experiments the CBZ removal experiments with the conventional conditions (initial pH, initial mass concentration, ionic strength and water temperature, etc.), dissolved organic matter (HA, SA and TA, etc.) and HA/SA ozonation by nanofiltration were conducted with synthetic feed. To evaluate the ozonation and nanofiltration for practical application, the real feed from Taihu Lake, Yangshupu water plant and Huangpu River were collected and ozonated to investigate the complex components in natural organic matter on CBZ removal by nanofiltration.

EBSCOhost - printed on 2/14/2023 6:39 AM via . All use subject to https://www.ebsco.com/terms-of-use

6.8.1 Effect of natural organic matter in Taihu Lake on CBZ removal by nanofiltration

6.8.1.1 Experimental method

The collected Taihu Lake raw water was filtered through a 0.45 μm membrane, and then added directly to CBZ to make the CBZ initial mass concentration around 100 μg/L, and the temperature was controlled at 25 ± 1 °C.

Considering that the ionic strength in the raw water may affect the surface properties of the nanofiltration membrane and also the removal rate, the control experiment is re-conducted. In the new control experiment, the background electrolyte solution of 1 mmol/L $NaHCO_3$ remains the same, while NaCl is added until the total conductivity is the same as before to reduce the test error.

6.8.1.2 Results and discussion

The water characteristics of Taihu Lake during the test period are shown in Table 6.7.

Table 6.7: Water characteristics of Taihu Lake.

DOC ($mg \cdot L^{-1}$)	UV_{254} (cm^{-1})	SUVA (L/mg•cm)	Conductivity (μm/cm)	pH
3.55	0.077	0.022	572	7.2

Figure 6.22 shows the results of the hydrophilicity and hydrophobicity fraction of the natural organic matter in Taihu Lake. Figure 6.23 shows the relative molecular weight distribution of the natural organic matter in Taihu Lake.

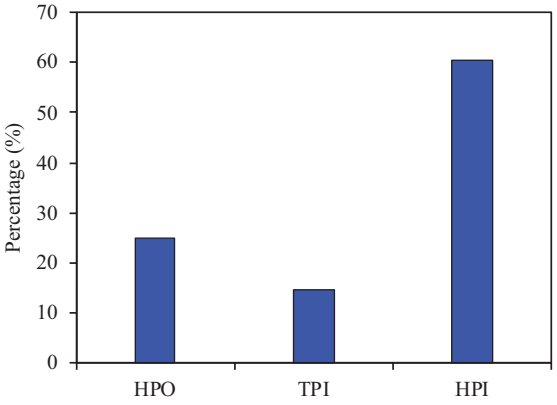

Figure 6.22: Hydrophilicity and hydrophobicity fraction of natural organic matter in Taihu Lake.

EBSCOhost - printed on 2/14/2023 6:39 AM via . All use subject to https://www.ebsco.com/terms-of-use

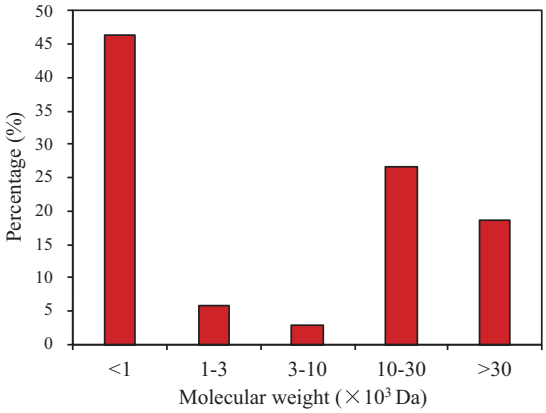

Figure 6.23: Relative molecular weight distribution of natural organic matter in Taihu Lake.

In Table 6.7, it can be seen that the DOC is very low which may be directly related to the collection point. In the hydrophilicity and hydrophobicity fraction in Figure 6.22, there are more hydrophilic organic matters than hydrophobic organic matters in Taihu Lake water, with the former accounting over 60%. In the relative molecular weight distribution in Figure 6.23, the organic matters with MWCO less than 1 kDa are 45%, and there are 25% of organic matters with MWCO of 10–30 kDa, while the macromolecules with MWCO larger than 30 kDa are accounting 18%. Thus, the micro molecules are dominant in Taihu Lake water.

Coble studied the relationship between soluble organic matters and their respective excitation/emission wavelengths, and established the parallel factor analysis of the three dimensional florescence model (PARAFAC) [74] in Table 6.8. This model has been widely used in the three dimensional florescence analysis and also in environmental detection of soluble organic matter. The florescence excitation emission map of the Taihu Lake water is shown in Figure 6.24, with the horizontal axis of emission wavelength, and vertical axis of excitation wavelength. The three values in the bracket represent excitation wavelength, emission wavelength, and absorption peak value. Such expressions are also in the later studies and thus not reported.

Table 6.8: Organics type and respective wavelengths of three dimensional florescence absorption peaks (PARAFAC model).

Name of EEM peak	Florence group	Excitation wavelength (Ex) (nm)	Emission wavelength (Em) (nm)
A	Ultraviolet humus	220–260	380–480
B	Tyrosine, protein-like substances	270–280	300–320
C	Visible area humus	300–380	400–480

EBSCOhost - printed on 2/14/2023 6:39 AM via . All use subject to https://www.ebsco.com/terms-of-use

Table 6.8 (continued)

Name of EEM peak	Florence group	Excitation wavelength (Ex) (nm)	Emission wavelength (Em) (nm)
D	Soil fulvic acid	390	509
E	Soil fulvic acid	455	521
M	Marine humus	290–320	370–420
N	Phytoplankton degradation products	280	370
T	Tryptophan, protein-like substances, or phenol	270–280 (220–230)	320–350

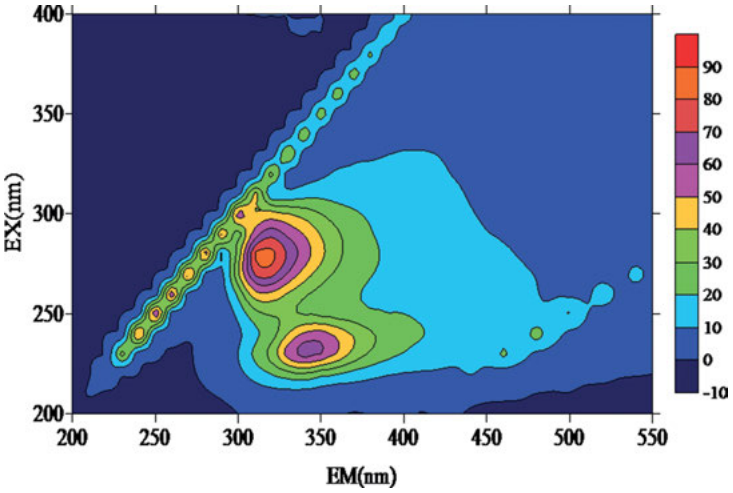

Figure 6.24: Fluorescence spectrum of Taihu Lake water.

Three fluorescence groups were detected in the Taihu Lake water. According to Table 6.8, they are a Class B fluorescence peak representing tyrosine or protein-like substances, a T-type fluorescence peak representing tryptophan, protein-like substances or phenol, and a class A fluorescence peak representing the ultraviolet humus. It can be seen from the fluorescence absorption peak values of the Taihu Lake water that the organic matter content is not high, which is similar as the measured DOC value. The absorption peak values of B and T fluorescence peaks is higher than that of Class A fluorescence peaks, indicating that the content of amino acids and protein-like substance is more than humus. The organic matter such as protein-like substance is hydrophilic, and the humus is hydrophobic, and such results are consistent with those shown in Figure 6.22.

EBSCOhost - printed on 2/14/2023 6:39 AM via . All use subject to https://www.ebsco.com/terms-of-use

The membrane filtration test with the mixture of Taihu Lake water and CBZ was conducted and the results of flux (J/J_0) and CBZ removal rate (%) are shown in Figure 6.25.

It can be seen from Figure 6.25 that the flux for the filtration of Taihu Lake water is slightly lower than that in the control test, indicating that the Taihu Lake water induces some fouling to the nanofiltration membrane. With the Taihu Lake water, the CBZ removal rate was basically higher than the control test at the end of the filtration test, from 57% to 60%, indicating that the components in Taihu Lake water can promote the removal of CBZ.

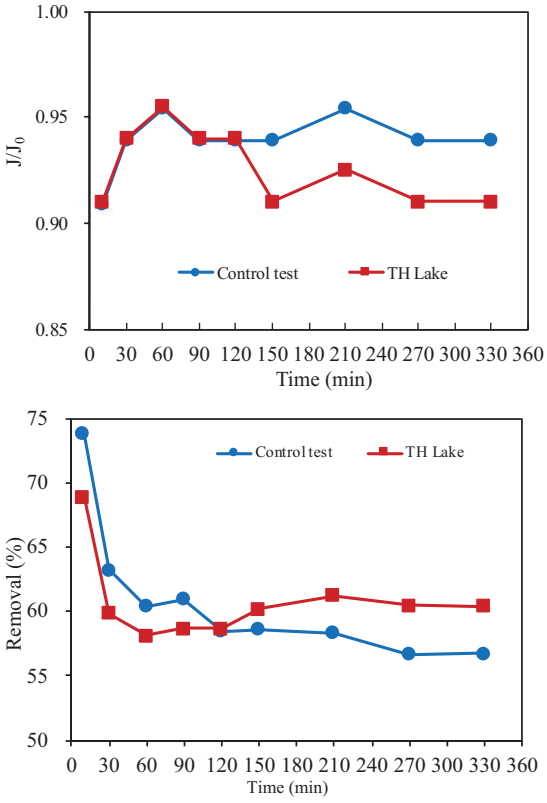

Figure 6.25: Effect of Taihu Lake water on membrane permeate flux and CBZ removal rate.

As analyzed before, there are many hydrophilic components in Taihu Lake water, and the small molecular organic matters account for a large proportion. The small molecular organic matter is more likely to block the membrane pores used in the test, causing the increase of filtration resistance and decrease of the flux. In addition, the hydrophilic organic compounds such as proteins are also easily deposited on the

EBSCOhost - printed on 2/14/2023 6:39 AM via . All use subject to https://www.ebsco.com/terms-of-use

membrane surface to induce a decrease in the flux. As the pores of the membrane are clogged and the MWCO rises, the CBZ removal rate also increases. However, due to the low content of organic matter in Taihu Lake water, the membrane fouling is not severe and the change of the flux and removal rate is not obvious.

6.8.2 Effect of effluent from various processes in Yangshupu Water Plant on CBZ removal by nanofiltration

6.8.2.1 Test method

The raw water, the effluent from the sedimentation tank, the effluent from the V-shaped filter and the effluent from the advanced treatment of ozone activated carbon in Yangshupu Water Plant were taken as the CBZ environment. The water samples from different units are used to investigate the effect of organic compositions in different processes in Yangshupu Water Plant on CBZ removal by nanofiltration.

The four water samples taken were first filtrated through a 0.45 μm membrane, and CBZ was then added for the nanofiltration test.

The initial mass concentration of CBZ is about 100 μg/L and the temperature is controlled at 25 ± 1 °C. Since the conductivities of the effluent in each process of Yangshupu Water Plant are not much different from that in Taihu Lake water, the control test results used in the previous section are adopted here.

6.8.2.2 Results and discussion

The test results are shown in Table 6.9, Figures 6.26 and 6.27.

Table 6.9: Physical and chemical properties of effluent from various processes of Yangshupu Water Plant.

Type of water sample	DOC (mg/L)	UV_{254} (cm^{-1})	SUVA (L/mg•cm)	Conductivity (μm/cm^{-1})	pH
Raw water	5.43	0.113	0.021	526	7.46
Effluent from sedimentation tank	4.65	0.073	0.016	572	7.25
Effluent from V-shaped filter	5	0.086	0.017	574	7.08
Effluent from ozone activated carbon	1.99	0.034	0.017	603	7.63

It can be obtained from Table 6.9 that the organic matter in the raw water of Yangshupu Water Plant cannot be effectively removed after the conventional process (i.e. coagulation + precipitation + filtration), and even the content of organic matter in the effluent of filter is slightly higher than that from sedimentation tank. After the advanced treatment of ozone activated carbon, the DOC value was significantly reduced.

EBSCOhost - printed on 2/14/2023 6:39 AM via . All use subject to https://www.ebsco.com/terms-of-use

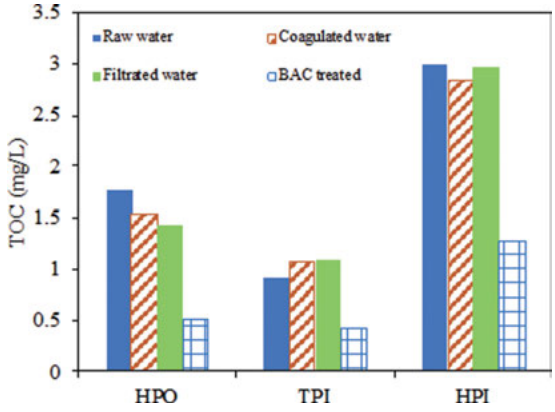

Figure 6.26: Hydrophilicity and hydrophobicity fraction of organic matters in the effluent of each process of Yangshupu Water Plant (DOC recovery rate around 80–120%).

From the hydrophilic-hydrophobic fraction of the organic matter in Figure 6.26, the hydrophilic and hydrophobic components of the organic matter in the effluent of each process are accounting almost half, and the content of the strong hydrophobic component is slightly higher than the weakly hydrophobic component. The content of each component of the raw water, effluent from sedimentation tank, effluent from the V-shaped filter is almost the same, while the DOC value of the effluent from the advanced treatment of ozone activated carbon is greatly reduced, so the content of each component is also significantly reduced as compared to the first three water samples.

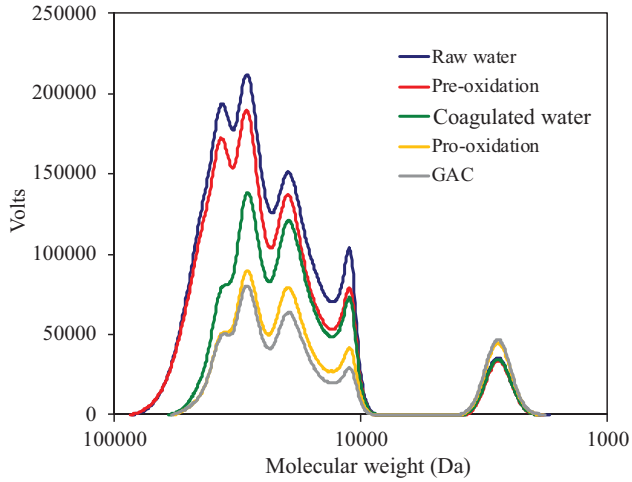

Figure 6.27: Relative molecular weight distribution of organic matters in the effluent of each process of Yangshupu Water Plant.

EBSCOhost - printed on 2/14/2023 6:39 AM via . All use subject to https://www.ebsco.com/terms-of-use

Due to the limitations of gel permeation chromatograph and the column, macromolecular organics cannot be accurately detected. As shown in Figure 6.27, the four water samples are generally composed of two parts. The first part is in 1–3 kDa, but the absorption values are, raw water > effluent from sedimentation tank ≈ effluent from the V-shaped filter > effluent from the advanced treatment of ozone activated carbon, indicating that the proportion of organic matter in this part is reduced gradually as the water plant process progresses. During the actual operation of the water plant, after coagulation and precipitation, the content of organic matter with a relatively large molecular weight can decrease. The other part is the small molecule organic matter with molecular weight below 1 kDa. As the process progressed, the proportion of small molecule organic matter increases. The properties of the effluent from sedimentation tank and V-shaped filter are almost the same as shown in Table 6.9. The TOC response of the molecules with molecular weight of 1–3 kDa almost overlaps, but the effluent from V-shaped filter has a high TOC response at the molecular weight of less than 100 Da.

The three-dimensional fluorescence spectrums of each process effluent from Yangshupu Water Plant are shown in Figure 6.28.

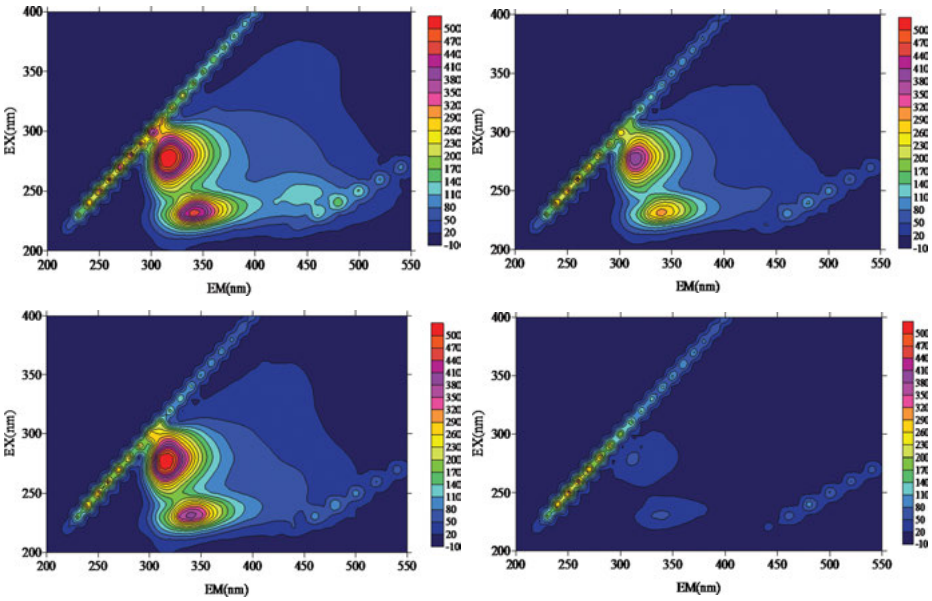

Figure 6.28: Three-dimensional fluorescence spectrums of the effluent of each process of Yangshupu Water Plant.

From the fluorescence spectrum in Figure 6.28, the four water samples contain three types of fluorescence absorption peaks, which are (1) B-type fluorescence peaks, representing tyrosine and protein-like substances; (2) T-type fluorescence peaks, representing tryptophan, protein-like or phenolic substances; (3) A class of fluorescence

EBSCOhost - printed on 2/14/2023 6:39 AM via . All use subject to https://www.ebsco.com/terms-of-use

peaks, representing the ultraviolet humus. Among them, the B and T type fluorescence peaks both represent hydrophilic substances, and the A type represents hydrophobic substances. From the content of the organic matter reflected by the response intensity, it is consistent with the DOC measurement, that is, raw water > effluent from the V-shaped filter > effluent from sedimentation tank > effluent from the advanced treatment of ozone activated carbon. With the progress of the process, the response of humus has been decreasing, but the change is not significant, and the response intensity of organic substances such as amino acids and protein-like substances is obviously reduced, especially in the effluent from the advanced treatment of ozone activated carbon.

The effect of the effluent of each process from Yangshupu Water Plant on membrane flux and CBZ removal rate is shown in Figure 6.29.

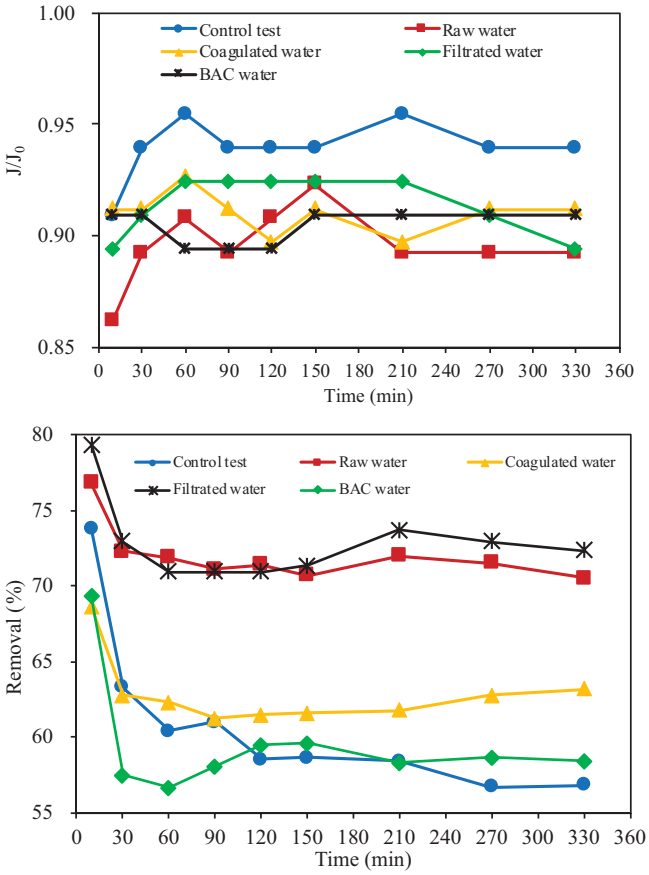

Figure 6.29: Effect of the effluent of each process from Yangshupu Water Plant on membrane flux and CBZ removal rate by nanofiltration.

EBSCOhost - printed on 2/14/2023 6:39 AM via . All use subject to https://www.ebsco.com/terms-of-use

As can be seen from Figure 6.29, the flux of natural water is relatively small as compared to the control test; the flux variation of the four water samples during the filtration process has no regular tendency, and the flux of raw water is slightly lower than other three kinds of water samples. It is worth noting that the flux of effluent from the V-shaped filter begins to decrease after filtration for 210 min and reaches the same value as the raw water at the end of filtration; however, the fluxes of the effluent from sedimentation tank and advanced treatment are close, which may be due to the complex properties of natural water bodies.

The CBZ removal rates in different water samples are quite different. The removal rate result has the order of raw water ≈ effluent from the V-shaped filter > effluent from sedimentation tank > effluent from the advanced treatment of ozone activated carbon. The removal rates of CBZ in raw water and effluent from the V-shaped filter are higher than 70%, in the effluent from the sedimentation tank 62%, and in the effluent from advanced treatment only 58%, which was similar from 56% in the control test. On the whole, the change of CBZ removal rate by nanofiltration is generally consistent with the change of DOC, indicating that more organic matter induces the higher removal of CBZ. More specifically, the DOC of the effluent from the V-shaped filter is slightly smaller than the raw water, but the CBZ removal rates are the same. Regarding the relative molecular weight distribution as analyzed before, there is a significant response peak in the filtered water below the molecular weight of 100 Da. It may be due to that this part of the small molecule substance blocks the nanofiltration membrane resulting in the increase of the resistance, the decrease of the flux and the membrane retention molecular weight, and also the increase of the removal rate. Considering the fluorescence spectrum, the contents of humus in the effluent from the sedimentation tank and the V-shaped filter are nearly the same, but the hydrophilic organic matter, protein and amino acids are higher in the effluent from the V-shaped filter than that in the effluent from the sedimentation tank. So these substances can be deposited on the surface of the membrane, to cause the resistance to rise and the flux to decrease. In addition, the contents of humic hydrophobic substances in the effluent from the sedimentation tank and the V-shaped filter are not much different, which shows that such substances have little effect on the removal of CBZ.

6.8.3 Effect of ozonation pretreatment of Huangpu River water on removal of CBZ by nanofiltration

6.8.3.1 Test method

The purpose of the test in this section is to investigate the effect of compositions in Huangpu River water on the removal of CBZ. Since the total amount of organic matter in the water after ozonation shall decrease, in order to maintain a similar DOC as in Huangpu River water, the raw water is first concentrated to achieve a DOC mass con-

EBSCOhost - printed on 2/14/2023 6:39 AM via . All use subject to https://www.ebsco.com/terms-of-use

centration of about 30 mg/L by using a nanofiltration device. Then ozone is injected, and the amount of ozone dosage is adjusted based on the experiments, with the results shown in Figure 6.30.

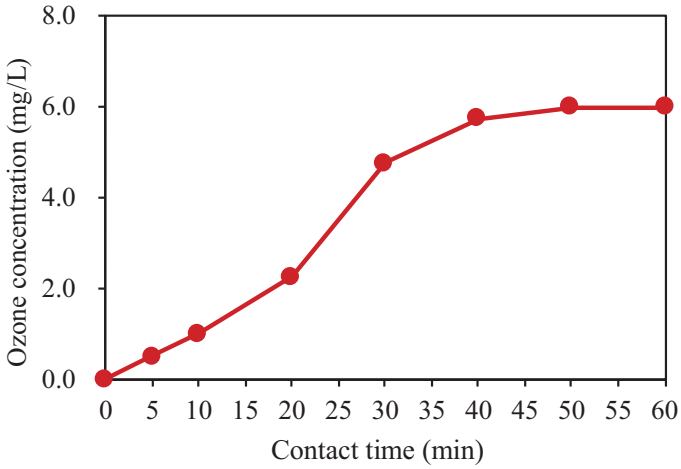

Figure 6.30: Relationship between ozone concentration and ozone contact time.

It can be seen from Figure 6.30 that after 60 min, there is basically no change of the concentration of ozone in the concentrated water of Huangpu River with a DOC concentration of 30 mg/L, so the time for ozone dosage is 10, 30 and 60 min, with the ozone mass concentrations of 1, 4.75 and 6 mg/L, respectively.

The concentrated Huangpu River water and its ozonated water are both diluted to 5 L with a DOC concentration of 4.5 mg/L. Since some ions are in the raw water, NaCl is not added, and only 1 mmol/L $NaHCO_3$ was added as a buffer solution to adjust the pH to about 8.0. The initial mass concentration of CBZ was about 100 μg/L, and the temperature was controlled at 25 ± 1 °C. The control test in the previous section was also adopted here.

6.8.3.2 Test results and discussion

The effect of Huangpu River water before and after ozone oxidation on membrane flux and CBZ removal rate is shown in Figure 6.31.

It can be seen from Figure 6.31 that the fluxes of Huangpu River before and after ozonation are smaller than the control test; the fluxes before and after ozonation do not differ much, no matter how much ozone is injected.

EBSCOhost - printed on 2/14/2023 6:39 AM via . All use subject to https://www.ebsco.com/terms-of-use

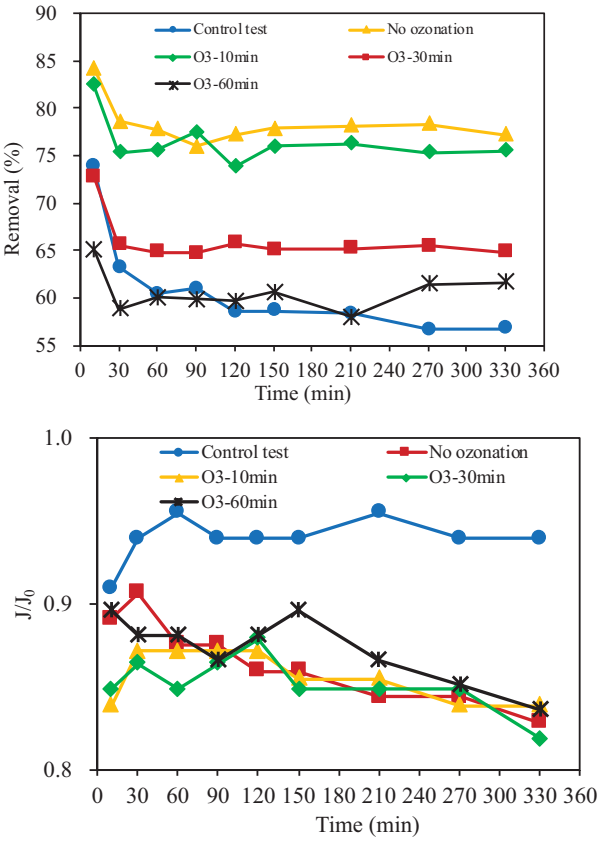

Figure 6.31: Effect of Huangpu River water before and after ozonation on membrane flux and CBZ removal rate.

When CBZ is added in the Huangpu River water, its removal rate is greater than 75%, which is significantly higher than the 56% in the control experiment. Therefore, the complex environment of the natural water body of the Huangpu River is conducive to the removal of CBZ, which is consistent with the result of Taihu Lake water. In addition, the removal rate of CBZ decreased significantly with the increase of ozone dosage. When the ozone exposure time was 60 min and the ozone concentration was 6.0 mg/L, the CBZ removal rate decreased to 60%. Since the initial DOC values of the influent water in each group are the same, the different filtration performances are not affected by the total concentrations of organic matters.

In the following, the relative molecular weight distribution, hydrophilicity and hydrophobicity, and organic composition of organic matter are analyzed to reveal the underlying mechanism of above results.

As shown in Figure 6.32, the hydrophilic substances in Huangpu River water are more than the hydrophobic substances. After ozonation, the proportion of hydro-

EBSCOhost - printed on 2/14/2023 6:39 AM via . All use subject to https://www.ebsco.com/terms-of-use

philic organic matter increased significantly (from 60% to 79%), and the amount of hydrophobic substances, especially strong hydrophobic substances, decreased from 23.6% to 11.6%.

According to the analysis above, macromolecular organic matter is easily oxidized by ozone into small molecular organic matter. As shown in Figure 6.33, in the Huangpu River water after ozonation, the amounts of macromolecular substances over 30 kDa and in the range of 10–30 kDa are reduced, and the other portions of fractions are increased. However, there is only a slightly increase of the portion of the organic matter with molecular weight less than 1 kDa.

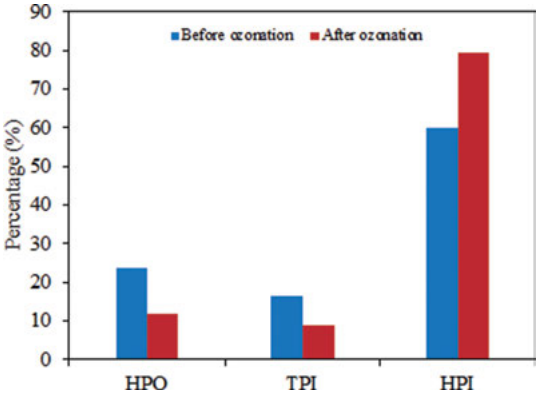

Figure 6.32: Hydrophilicity and hydrophobicity distribution of Huangpu River before and after ozonation.

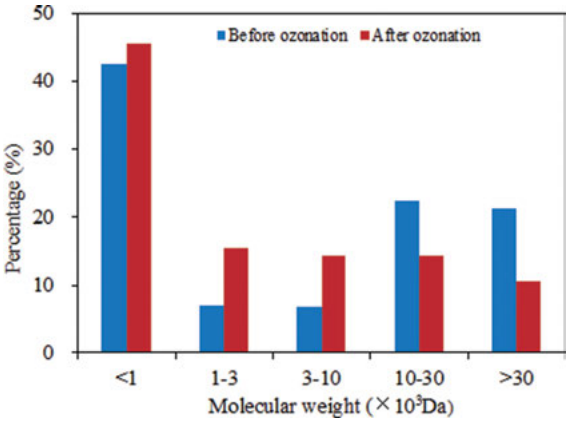

Figure 6.33: Relative molecular weight distribution of Huangpu River before and after ozonation.

Figure 6.34 shows the three-dimensional fluorescence spectrum of Huangpu River water. Two fluorescence absorption peaks exist (Figure 6.34(a)), which are Peak B

EBSCOhost - printed on 2/14/2023 6:39 AM via . All use subject to https://www.ebsco.com/terms-of-use

representing tyrosine or protein-like substance, and Peak T representing tryptophan, protein-like or phenolic substances, while the humus content in the ultraviolet region is not high. The three-dimensional fluorescence spectrum of Huangpu River water after ozonation is shown in Figure 6.34. As can be observed, most of the organic matter is oxidized, and only the hydrophilic substances such as proteins are slightly higher. Therefore, when the concentrations of DOC of the influent water in each group are the same, the proportions of the hydrophilic substance rise with the increase of the ozone dosage.

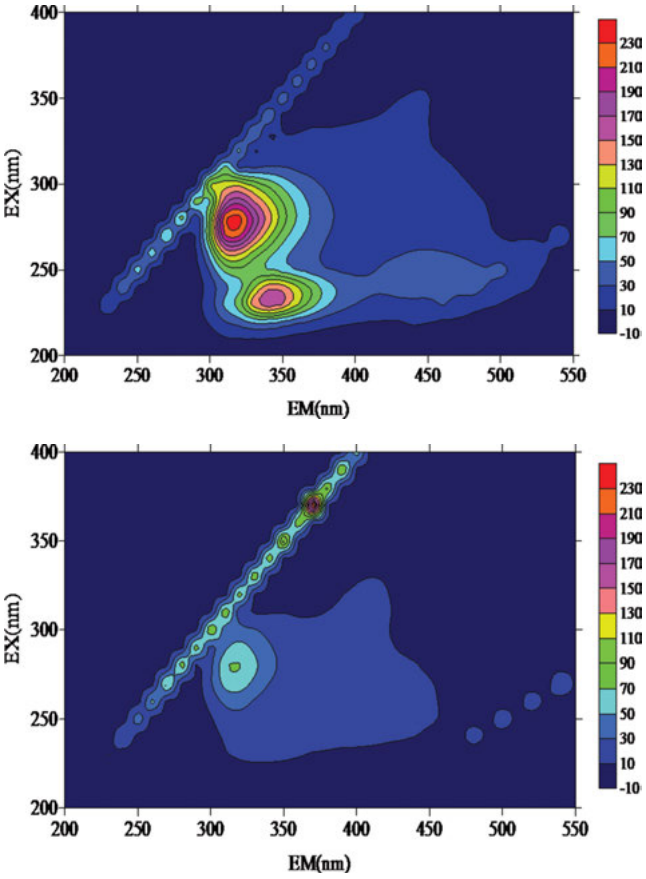

Figure 6.34: Comparison of three-dimensional fluorescence spectrum of Huangpu River before and after ozonation.

Regarding the properties of organic matter in Huangpu River water before and after ozonation, the reason for the significant decrease in CBZ removal rate caused is probably due to the increase of the hydrophilic component and severity of the concentration polarization. In addition, after ozonation, the content of small molecules below

EBSCOhost - printed on 2/14/2023 6:39 AM via . All use subject to https://www.ebsco.com/terms-of-use

1 kDa did not increase significantly, so the pore blocking of the membrane was not serious, and thus the ozonaton of Huangpu River water did not make a positive influence on CBZ removal by nanofiltration.

Based on above analysis, the similar flux before and after ozonation need further investigation. Zhang et al. examined the removal of two pesticides of atrazine and simazine from tap water and lake water environment [75]. It was found that although the removal rates of the two organic substances differed, the flux was similar. Bessiere et al. studied the effect of hydrophilic and hydrophobic organic matter in natural water on membrane fouling, and found that the hydrophilic organic matter induced the most drop of permeate flux [76]. However, when the hydrophilic organic matter was mixed with other types of organic matter, the membrane flux was increased [76]. Since the characteristics of the raw water are quite complicated, the effects of various organic substances on the membrane and the target pollutant of CBZ could either promote or compromise each other. After ozonation, the characteristics of the feed water become even more complicated. In addition to organic matter, other characteristics of the raw water, such as ionic strength, especially the amount of divalent cations in the water, affect the charge characteristics between the membrane and the organic matter and therefore play a key role on membrane performance and organic removal [77]. The effects of other properties of natural raw water and their interactions on the removal of PPCPs need further study.

6.9 Summary

In this chapter, the influence of conventional operations, dissolved natural organic matter (DOM), natural water environment and ozonation pretreatment on the removal of typical PPCP, i.e. carbamazepine (CBZ) by nanofiltration were studied. The permeate flux during nanofiltration was also examined. The conclusions are as follows.

(1) The removal of CBZ by nanofiltration depends greatly on the pore size of the nanofiltration membrane. The CBZ removal rate by the NF90 membrane with a smaller pore size (tight) is above 90%, while the removal by the NF270 membrane with a larger pore size (loose) is smaller.

(2) Factors such as pH, calcium ion concentration, and water temperature all affect the apparent pore size of the nanofiltration membrane, resulting in the change of membrane permeate flux and organic removal. When the pH is decreased or the calcium ion concentration is increased, the CBZ removal rate arises. The CBZ removal rate at low temperatures is significantly higher than at high temperatures. There is no significant effect on membrane permeate flux and CBZ removal when the initial CBZ mass concentration varies from 50–500 μg/L.

(3) Sieving is the main mechanism for nanofiltration to remove the uncharged CBZ.

EBSCOhost - printed on 2/14/2023 6:39 AM via . All use subject to https://www.ebsco.com/terms-of-use

(4) The order of the drop of the membrane flux caused by the addition of three typical dissolved organic substances such as humic acid (HA), sodium alginate (SA) and tannic acid (TA) is, HA < SA < TA; and the order of CBZ removal rate is: SA < HA < TA. In the SA solution, the membrane flux decreases with the increase of DOC concentration, while in the solution of the other two organic matters, the membrane flux or the CBZ removal does not differ significantly with the change of DOM dosage.

(5) The relative molecular weight distribution and the hydrophilicity and hydrophobicity fraction of the three dissolved organic matters show that the small molecular organic matter below 1 kDa is more likely to cause the decrease of membrane flux than the macromolecular organic matter; while the hydrophilic organic matter is easier to cause the decrease of membrane flux than the hydrophobic organic matter.

(6) Membrane fouling and concentration polarization are not severe with addition of HA, so the effect on flux drop is not serious, and the CBZ removal rate doesn't differ significantly. The addition of SA forms a strong adhesion layer, which increases the filtration resistance and concentration polarization, resulting in the decline of membrane flux and CBZ removal. With the addition of TA, the membrane pore size is blocked, the filtration resistance increases, thus the flux decreases, and the membrane MWCO decreases, resulting in the increase of CBZ removal due to the sieving effect.

(7) In the filtration of the HA solution after ozonation mixed with CBZ, the CBZ removal is higher and the membrane flux is lower as compared with the mixed solutions of HA-CBZ without ozonation, which may be due to that more micro molecules are produced after ozonation resulting in the blockage of membrane pores, rising of the filtration resistance and decreasing of the membrane MWCO. After the oxidation of HA by different concentrations of ozone, the removal rate of CBZ is increased, but when the concentration of ozone increases to certain level, the flux or CBZ removal doesn't change any more.

(8) In the filtration of the SA solution after ozonation mixed with CBZ, both the membrane flux and the CBZ removal are higher as compared with the mixed solutions of SA-CBZ without ozonation, which may be due to that the structure of SA is changed after ozonation, resulting in the alleviation of membrane fouling and concentration polarization. The membrane permeate flux or CBZ removal doesn't differ significantly when the concentrations of ozone are changed.

(9) Compared with the control test, the CBZ removal is increased and the flux is decreased when CBZ is mixed with the Taihu Lake water for the nanofiltration.

(10) The CBZ removals are all increased when CBZ is mixed with the effluent from each process of Yangshupu Water Plant (raw water, effluent from sedimentation tank, effluent from V-shape filter, effluent from advanced treatment of ozone activated carbon), with the order of raw water > effluent from V-shape

EBSCOhost - printed on 2/14/2023 6:39 AM via . All use subject to https://www.ebsco.com/terms-of-use

filter > effluent from sedimentation tank > effluent from advanced treatment of ozone activated carbon. Overall, the higher the DOC of the feed, the higher removal of CBZ; the difference among the membrane fluxes of the four effluents is not obvious.

(11) The CBZ removal is enhanced when CBZ is mixed with the Huangpu River water. After the Huangpu River water is ozonated, the CBZ removal is reduced with the increase of ozonation. However, the membrane permeate fluxes are similar with different dosages of ozone.

(12) In the filtration of CBZ mixed with natural water, there is no obvious trend of CBZ removal or the permeate flux. The reason is due to the complexities of the components and their complicated interactions in natural water.

References

[1] Bindoff, A., et al., The nanofiltration and reuse of effluent from the caustic extraction stage of wood pulping. Desalination, 1987. 67: p. 455–465.

[2] Cadotte, J., et al., Nanofiltration membranes broaden the use of membrane separation technology. Desalination, 1988. 70(1–3): p. 77–88.

[3] Eriksson, P., Nanofiltration extends the range of membrane filtration. Environmental Progress, 1988. 7(1): p. 58–62.

[4] Simpson, A.E., Kerr, C.A., and Buckley, C.A., The effect of Ph on the nanofiltration of the carbonate system in solution. Desalination, 1987. 64: p. 305–319.

[5] Al-Amoudi, A.S., Factors affecting natural organic matter (NOM) and scaling fouling in NF membranes: A review. Desalination, 2010. 259(1–3): p. 1–10.

[6] Song, J.F., et al., A critical review on membrane extraction with improved stability: Potential application for recycling metals from city mine. Desalination, 2018. 440: p. 18–38.

[7] Luo, J.Q. and Wan, Y.H., Effects of pH and salt on nanofiltration-a critical review. Journal of Membrane Science, 2013. 438: p. 18–28.

[8] Mohammad, A.W., et al., Nanofiltration membranes review: Recent advances and future prospects. Desalination, 2015. 356: p. 226–254.

[9] Bassyouni, M., et al., A review of polymeric nanocomposite membranes for water purification. Journal of Industrial and Engineering Chemistry, 2019. 73: p. 19–46.

[10] Gross, R.J. and Osterle, J.F., Membrane transport characteristics of ultrafine capillaries. The Journal of chemical physics, 1968. 49(1): p. 228–34.

[11] Meyer, K.H. and Bernfeld, P., The potentiometric analysis of membrane structure and its application to living animal membranes. The Journal of general physiology, 1946. 29(6): p. 353–78.

[12] Sievers, J.F., Considerations on the problem of detergents in waste water. Boletin de la Oficina Sanitaria Panamericana. Pan American Sanitary Bureau, 1963. 55: p. 524–34.

[13] Teorell, T., Studies on the “Diffusion Effect” upon ionic distribution. some theoretical considerations. Proceedings of the National Academy of Sciences of the United States of America, 1935. 21(3): p. 152–61.

[14] Wang, X.L., et al., The electrostatic and steric-hindrance model for the transport of charged solutes through nanofiltration membranes. Journal of Membrane Science, 1997. 135(1): p. 19–32.

EBSCOhost - printed on 2/14/2023 6:39 AM via . All use subject to https://www.ebsco.com/terms-of-use

[15] Boussouga, Y.A., Frey, H., and Schafer, A.I., Removal of arsenic(V) by nanofiltration: Impact of water salinity, pH and organic matter. Journal of Membrane Science, 2021. 618.
[16] Peng, W. and Escobar, I.C., Rejection efficiency of water quality parameters by reverse osmosis and nanofiltration membranes. Environmental Science & Technology, 2003. 37(19): p. 4435–4441.
[17] Saitua, H., Giannini, F., and Padilla, A.P., Drinking water obtaining by nanofiltration from waters contaminated with glyphosate formulations: Process evaluation by means of toxicity tests and studies on operating parameters. Journal of Hazardous Materials, 2012. 227: p. 204–210.
[18] Fang, C., et al., Effects of feed solution characteristics and membrane fouling on the removal of THMs by UF/NF/RO membranes. Chemosphere, 2020. 260.
[19] Yoon, Y., et al., Nanofiltration and ultrafiltration of endocrine disrupting compounds, pharmaceuticals and personal care products. Journal of Membrane Science, 2006. 270(1–2): p. 88–100.
[20] Ghermandi, A. and Messalem, R., The advantages of NF desalination of brackish water for sustainable irrigation: The case of the Arava Valley in Israel. Desalination and Water Treatment, 2009. 10(1–3): p. 101–107.
[21] Li, T., et al., Application of coagulation-ultrafiltration-nanofiltration in a pilot study for Tai Lake water treatment. Water Environment Research, 2020. 92(4): p. 579–587.
[22] Kang, E., et al., Effects of hydrodynamic conditions (diffusion vs. convection) and solution chemistry on effective molecular weight cut-off of negatively charged nanofiltration membranes. Desalination, 2014. 352: p. 136–141.
[23] Verliefde, A.R.D., et al., The role of electrostatic interactions on the rejection of organic solutes in aqueous solutions with nanofiltration. Journal of Membrane Science, 2008. 322(1): p. 52–66.
[24] Van der Bruggen, B. and Vandecasteele, C., Modelling of the retention of uncharged molecules with nanofiltration. Water Research, 2002. 36(5): p. 1360–1368.
[25] Schutte, C.F., The rejection of specific organic compounds by reverse osmosis membranes. Desalination, 2003. 158(1–3): p. 285–294.
[26] Kiso, Y., et al., Rejection properties of alkyl phthalates with nanofiltration membranes. Journal of Membrane Science, 2001. 182(1–2): p. 205–214.
[27] Berg, P., Hagmeyer, G., and Gimbel, R., Removal of pesticides and other micropollutants by nanofiltration. Desalination, 1997. 113(2–3): p. 205–208.
[28] Childress, A.E. and Elimelech, M., Relating nanofiltration membrane performance to membrane charge (electrokinetic) characteristics. Environmental Science & Technology, 2000. 34(17): p. 3710–3716.
[29] Lee, S., et al., Determination of membrane pore size distribution using the fractional rejection of nonionic and charged macromolecules. Journal of Membrane Science, 2002. 201(1–2): p. 191–201.
[30] Tsuru, T., et al., Reverse-osmosis of single and mixed electrolytes with charged membranes – experiment and analysis. Journal of Chemical Engineering of Japan, 1991. 24(4): p. 518–524.
[31] Wang, X.L., Wang, W.N., and Wang, D.X., Experimental investigation on separation performance of nanofiltration membranes for inorganic electrolyte solutions. Desalination, 2002. 145(1–3): p. 115–122.
[32] Ariza, M.J., et al., Effect of pH on electrokinetic and electrochemical parameters of both sub-layers of composite polyamide/polysulfone membranes. Desalination, 2002. 148(1–3): p. 377–382.
[33] Nghiem, L.D., Schafer, A.I., and Elimelech, M., Role of electrostatic interactions in the retention of pharmaceutically active contaminants by a loose nanofiltration membrane. Journal of Membrane Science, 2006. 286(1–2): p. 52–59.

EBSCOhost - printed on 2/14/2023 6:39 AM via . All use subject to https://www.ebsco.com/terms-of-use

[34] Ozaki, H. and Li, H.F., Rejection of organic compounds by ultra-low pressure reverse osmosis membrane. Water Research, 2002. 36(1): p. 123–130.
[35] Boussahel, R., Montiel, A., and Baudu, M., Effects of organic and inorganic matter on pesticide rejection by nanofiltration. Desalination, 2002. 145(1–3): p. 109–114.
[36] Kimura, K., et al., Adsorption of hydrophobic compounds onto NF/RO membranes: An artifact leading to overestimation of rejection. Journal of Membrane Science, 2003. 221(1–2): p. 89–101.
[37] Van der Bruggen, B., Braeken, L., and Vandecasteele, C., Evaluation of parameters describing flux decline in nanofiltration of aqueous solutions containing organic compounds. Desalination, 2002. 147(1–3): p. 281–288.
[38] Kiso, Y., Factors affecting adsorption of organic solutes on cellulose-acetate in an aqueous-solution system. Chromatographia, 1986. 22(1–6): p. 55–58.
[39] Huang, Z.H., et al., Removal Mechanisms for Pharmaceuticals and Personal Care Products (PPCPs) in water by NF/RO membranes. Advances in Environmental Technologies, Pts 1–6, 2013. 726–731: p. 2502–2505.
[40] Lin, Y.L., Effects of organic, biological and colloidal fouling on the removal of pharmaceuticals and personal care products by nanofiltration and reverse osmosis membranes. Journal of Membrane Science, 2017. 542: p. 342–351.
[41] Liu, T.J., Chang, E.E., and Chiang, P.C., Effects of concentrations and types of natural organic matters on rejection of compounds of emerging concern by nanofiltration. Desalination and Water Treatment, 2013. 51(37–39): p. 6929–6939.
[42] Wang, Y.F., et al., Competitive adsorption of PPCP and humic substances by carbon nanotube membranes: Effects of coagulation and PPCP properties. Science of the Total Environment, 2018. 619: p. 352–359.
[43] Nghiem, L.D. and Schafer, A.I., Adsorption and transport of trace contaminant estrone in NF/RO membranes. Environmental Engineering Science, 2002. 19(6): p. 441–451.
[44] Wang, Y.F., Huang, H.O., and Wei, X.M., Influence of wastewater precoagulation on adsorptive filtration of pharmaceutical and personal care products by carbon nanotube membranes. Chemical Engineering Journal, 2018. 333: p. 66–75.
[45] Devitt, E.C., et al., Effects of natural organic matter and the raw water matrix on the rejection of atrazine by pressure-driven membranes. Water Research, 1998. 32(9): p. 2563–2568.
[46] Kimura, K., et al., Rejection of organic micropollutants (disinfection by-products, endocrine disrupting compounds, and pharmaceutically active compounds) by NF/RO membranes. Journal of Membrane Science, 2003. 227(1–2): p. 113–121.
[47] Nghiem, L.D., Schafer, A.I., and Waite, T.D., Adsorption of estrone on nanofiltration and reverse osmosis membranes in water and wastewater treatment. Water Science and Technology, 2002. 46(4–5): p. 265–272.
[48] Van der Bruggen, B., et al., Nanofiltration as a treatment method for the removal of pesticides from ground waters. Desalination, 1998. 117(1–3): p. 139–147.
[49] Bellona, C., et al., Factors affecting the rejection of organic solutes during NF/RO treatment – a literature review. Water Research, 2004. 38(12): p. 2795–2809.
[50] Nghiem, L.D., Schafer, A.I., and Elimelech, M., Pharmaceutical retention mechanisms by nanofiltration membranes. Environmental Science & Technology, 2005. 39(19): p. 7698–7705.
[51] Nghiem, L.D., Vogel, D., and Khan, S., Characterising humic acid fouling of nanofiltration membranes using bisphenol A as a molecular indicator. Water Research, 2008. 42(15): p. 4049–4058.
[52] Braghetta, A., DiGiano, F.A., and Ball, W.P., Nanofiltration of natural organic matter: pH and ionic strength effects. Journal of Environmental Engineering-Asce, 1997. 123(7): p. 628–641.

EBSCOhost - printed on 2/14/2023 6:39 AM via . All use subject to https://www.ebsco.com/terms-of-use

[53] Schafer, A.I., Nghiem, L.D., and Waite, T.D., Removal of the natural hormone estrone from aqueous solutions using nanofiltration and reverse osmosis. Environmental Science & Technology, 2003. 37(1): p. 182–188.
[54] Zhang, Y., et al., Removal of bisphenol A by a nanofiltration membrane in view of drinking water production. Water Research, 2006. 40(20): p. 3793–3799.
[55] Koyuncu, I., et al., Removal of hormones and antibiotics by nanofiltration membranes. Journal of Membrane Science, 2008. 309(1–2): p. 94–101.
[56] Comerton, A.M., Andrews, R.C., and Bagley, D.M., The influence of natural organic matter and cations on fouled nanofiltration membrane effective molecular weight cut-off. Journal of Membrane Science, 2009. 327(1–2): p. 155–163.
[57] Lee, N., et al., Morphological analyses of natural organic matter (NOM) fouling of low-pressure membranes (MF/UF). Journal of Membrane Science, 2005. 261(1–2): p. 7–16.
[58] Narbaitz, R.M., et al., Pharmaceutical and personal care products removal from drinking water by modified cellulose acetate membrane: Field testing. Chemical Engineering Journal, 2013. 225: p. 848–856.
[59] Guo, X.X., Liu, H.T., and Wu, S.B., Humic substances developed during organic waste composting: Formation mechanisms, structural properties, and agronomic functions. Science of the Total Environment, 2019. 662: p. 501–510.
[60] Yamamoto, H., et al., Effects of physical-chemical characteristics on the sorption of selected endocrine disrnptors by dissolved organic matter surrogates. Environmental Science & Technology, 2003. 37(12): p. 2646–2657.
[61] Crozes, G., Anselme, C., and Mallevialle, J., Effect of adsorption of organic-matter on fouling of ultrafiltration membranes. Journal of Membrane Science, 1993. 84(1–2): p. 61–77.
[62] Plakas, K.V. and Karabelas, A.J., Triazine retention by nanofiltration in the presence of organic matter: The role of humic substance characteristics. Journal of Membrane Science, 2009. 336(1–2): p. 86–100.
[63] Manttari, M., Pekuri, T., and Nystrom, M., NF270, a new membrane having promising characteristics and being suitable for treatment of dilute effluents from the paper industry. Journal of Membrane Science, 2004. 242(1–2): p. 107–116.
[64] Carroll, T., et al., The fouling of microfiltration membranes by NOM after coagulation treatment. Water Research, 2000. 34(11): p. 2861–2868.
[65] Fan, L.H., et al., Influence of the characteristics of natural organic matter on the fouling of microfiltration membranes. Water Research, 2001. 35(18): p. 4455–4463.
[66] Park, N., et al., Characterizations of the colloidal and microbial organic matters with respect to membrane foulants. Journal of Membrane Science, 2006. 275(1–2): p. 29–36.
[67] Li, Q.L., Xu, Z.H., and Pinnau, I., Fouling of reverse osmosis membranes by biopolymers in wastewater secondary effluent: Role of membrane surface properties and initial permeate flux. Journal of Membrane Science, 2007. 290(1–2): p. 173–181.
[68] Jermann, D., et al., The role of NOM fouling for the retention of estradiol and ibuprofen during ultrafiltration. Journal of Membrane Science, 2009. 329(1–2): p. 75–84.
[69] Nghiem, L.D. and Hawkes, S., Effects of membrane fouling on the nanofiltration of pharmaceutically active compounds (PhACs): Mechanisms and role of membrane pore size. Separation and Purification Technology, 2007. 57(1): p. 176–184.
[70] Yuan, W. and Zydney, A.L., Humic acid fouling during microfiltration. Journal of Membrane Science, 1999. 157(1): p. 1–12.
[71] Wang, L., et al., Analysis for the removal effect of dissolved organic matters of O-3/BAC process from the view of molecular weight distribution. Proceedings of the World Engineers' Convention 2004: Vol D, Environment Protection and Disaster Mitigation, 2004: p. 241–245.

EBSCOhost - printed on 2/14/2023 6:39 AM via . All use subject to https://www.ebsco.com/terms-of-use

[72] Chen, Y., et al., Effect of coagulation pretreatment on fouling of an ultrafiltration membrane. Desalination, 2007. 204(1–3): p. 181–188.
[73] Rodriguez, F.J., Schlenger, P., and Garcia-Valverde, M., Monitoring changes in the structure and properties of humic substances following ozonation using UV-Vis, FTIR and H-1 NMR techniques. Science of the Total Environment, 2016. 541: p. 623–637.
[74] Coble, P.G., Characterization of marine and terrestrial DOM in seawater using excitation emission matrix spectroscopy. Marine Chemistry, 1996. 51(4): p. 325–346.
[75] Zhang, Y., et al., Removal of pesticides by nanofiltration: Effect of the water matrix. Separation and Purification Technology, 2004. 38(2): p. 163–172.
[76] Bessiere, Y., et al., Effect of hydrophilic/hydrophobic fractions of natural organic matter on irreversible fouling of membranes. Desalination, 2009. 249(1): p. 182–187.
[77] Cheng, W., et al., Selective removal of divalent cations by polyelectrolyte multilayer nanofiltration membrane: Role of polyelectrolyte charge, ion size, and ionic strength. Journal of Membrane Science, 2018. 559: p. 98–106.

EBSCOhost - printed on 2/14/2023 6:39 AM via . All use subject to https://www.ebsco.com/terms-of-use

EBSCOhost - printed on 2/14/2023 6:39 AM via . All use subject to https://www.ebsco.com/terms-of-use

Lin Wang, Wanzhu Zhang, Bingzhi Dong

Chapter 7
Forward Osmosis Membrane Separation Technology

7.1 Fundamentals of forward osmosis membrane separation technology

7.1.1 Principles of forward osmosis

Osmosis is a physical phenomenon that has been known to mankind since the early days of human civilization [1]. Forward osmosis (FO) is the spontaneous net movement of water across a selectively semipermeable membrane from a region of higher water chemical potential (i.e. lower osmotic pressure) to a region of lower water chemical potential (i.e. higher osmotic pressure). The principles of FO and interrelation of FO, reverse osmosis (RO) and pressure-retarded osmosis (PRO) are illustrated in Figure 7.1 [1]. As shown in Figure 7.1, when a semipermeable membrane is used to separate two solutions of different osmotic pressures (e.g. salt water and pure water), the water molecules pass through the semipermeable membrane from the side of pure water (feed solution) with low osmotic pressure to salt water (draw solution) with high osmotic pressure. Due to the additional water molecules, the salt water level continues to rise until the differential of water pressure equals that of osmotic pressure across the semipermeable membrane. This process is referred to as FO. PRO can be defined as a process similar to FO, where the hydraulic pressure (ΔP) lower than the osmotic pressure difference ($\Delta\pi$) is applied in the the hypertonic draw solution (DS) side. However, the net water flux is still in the direction of the concentrated draw solution. When RO occurs, where the hydraulic pressure (ΔP) higher than the osmotic pressure difference ($\Delta\pi$) is applied in the DS side, the water molecules reversely move from the hypertonic DS side to the hypotonic feed solution (FS) side. As shown in Figure 7.2, the relationships of the FO and RO processes are illustrated in the form of coordinate diagram by Lee et al. [2].

Lin Wang, School of Municipal and Environmental Engineering, Shandong Jianzhu University, Jinan, Shandong, P. R. China
Wanzhu Zhang, Beijing General Municipal Engineering Design & Research Institute Co., Ltd., Beijing, P. R. China
Bingzhi Dong, College of Environmental Science and Engineering, Tongji University, Shanghai, P. R. China

https://doi.org/10.1515/9783110596847-007

EBSCOhost - printed on 2/14/2023 6:39 AM via . All use subject to https://www.ebsco.com/terms-of-use

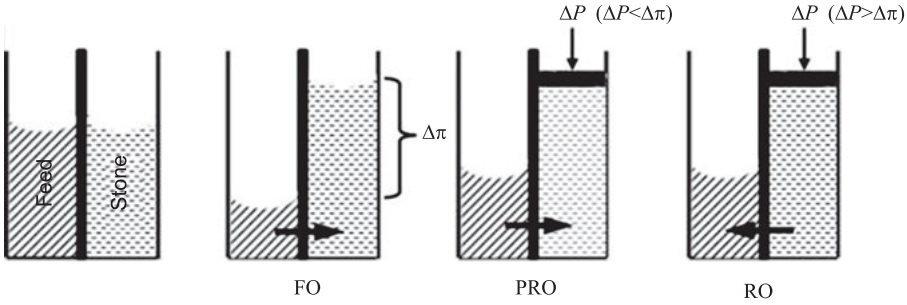

Figure 7.1: Schematic diagram of working principles for FO, PRO and RO.

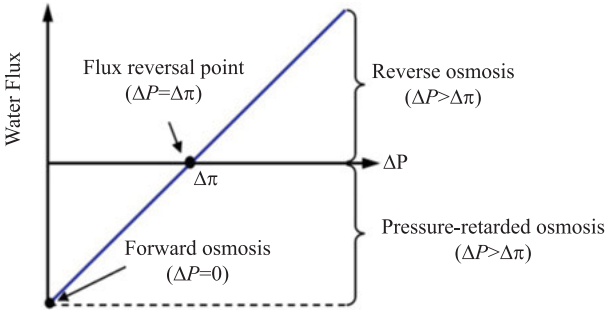

Figure 7.2: Direction and magnitude of water flux as a function of applied pressure in FO, PRO and RO.

7.1.2 Main factors affecting forward osmosis

Utilizing the natural osmotic pressure difference between a concentrated draw solution and a feed solution across a semipermeable membrane, FO does not require hydraulic pressure for its operation. In FO, pure product water is produced spontaneously when the diluted draw solution is re-concentrated to recycle the draw solute. Compared to pressure-driven membrane processes, the major advantage of the standalone FO process lies in its operation at low (mainly due to the flow resistance in the membrane module) or no hydraulic pressures. The selectively permeable membrane and hypertonic draw solution are the two key components for successful development of FO technologies. In addition, the concentration polarization (CP) occurring in FO process also plays a dominant role in the performance of FO flux.

7.1.2.1 Membranes for forward osmosis

Generally, any dense, non-porous, selectively permeable material can be used as a membrane for FO. The desired characteristics of membranes for FO would be [1]: (1)

EBSCOhost - printed on 2/14/2023 6:39 AM via . All use subject to https://www.ebsco.com/terms-of-use

high density of the active layer for high solute rejection; (2) hydrophilicity of the active layer for enhanced flux, improved recovery and reduced membrane fouling; (3) a thin membrane with minimum porosity of the support layer for low internal CP, and therefore, higher water flux; (4) high mechanical strength to sustain hydraulic pressure when used for PRO; and (5) good resistance to the acid, base and salt corrosion for the normal operation of FO under the wide range of pH and various solution conditions.

The cellulose triacetate (CTA) FO membrane, obtained from Hydration Technology, Inc. (HTI, USA), was widely used as the commercial FO membrane. The SEM image of HTI FO membrane was shown in Figure 7.3 [3]. As shown in Figure 7.3, the membrane has an asymmetric structure and its active layer is mechanically supported by embedded polyester mesh. According to Figure 7.3(c), the thickness of the membrane varied from 30 to 50 μm depending on the relative location to the polyester mesh fibers. This unique structure that a thinner embedded support layer reduces ICP and thus favors the FO membrane a better osmosis performance compared to standard RO membranes. Based on the FTIR studies on HTI membrane by Parida and Ng [4], the groups detected on dense and porous sides of the FO membrane were almost similar as the model functional groups of CTA, asserting that both sides of the FO membrane were made of similar material. The contact angles of the active layer and the support layer were 72°and 71°, respectively. AFM measurement in dry tapping mode showed that the mean roughness of the active layer and support layer was ~37 nm and ~61 nm, respectively. The results suggested that the smoother dense active layer may have low fouling propensity than the alternative membrane layer.

7.1.2.2 Draw solution

Draw solution is a key feature in FO process and is the source of the osmotic driving force for FO. The main criterion when selecting an optimal draw solution is that the draw solution has a higher osmotic pressure than the feed solution to produce high osmotic pressure difference. An effective draw solution solute must have very specific characteristics [1, 5, 6]: (1) It must have a high osmotic efficiency, meaning that it has to be highly soluble in water and have a high diffusivity, low reverse solute diffusion, low viscosity, low molecular weight, in order to reduce the internal concentration polarization (ICP). Lower ICP leads to higher water flux and favorable water recovery; (2) It must also be non-toxic, in order to ensure the quality of the produced water by FO; (3) It should have the chemical compatibility of the FO membrane, meaning that the draw solution can not react or degrade the membrane; (4) The draw solute must easily and economically be separated and recycled in the production of potable water.

EBSCOhost - printed on 2/14/2023 6:39 AM via . All use subject to https://www.ebsco.com/terms-of-use

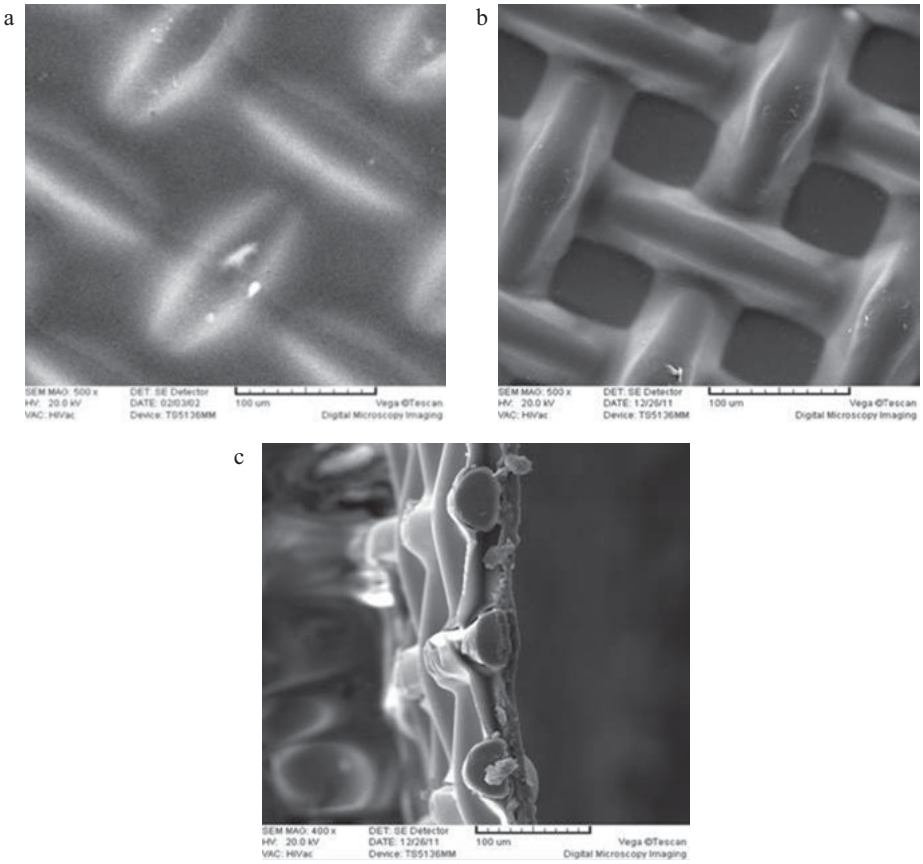

Figure 7.3: SEM images of the clean FO membrane.

7.1.2.3 Concentration polarization in FO processes

Based on the theory of osmosis, FO can use the draw solution with very high osmotic pressure to generate higher water flux compared to RO [1]. However, it is found in these FO studies that permeate water fluxes were far lower than anticipated based on the osmotic pressure difference across the membrane. The lower-than-expected water flux is mainly attributed to the specific CP phenomena in FO. A diagram depicting this phenomenon for different membrane orientations in FO process is given in Figure 7.4. c_1 and c_5 are the concentrations of the bulk feed and draw solution, respectively; c_2 and c_4 are the concentrations of the feed-membrane and draw solution-membrane interfaces, respectively; and c_3 is the concentration at the active layer-support layer interface.

In FO, two types of CP are applicable-external CP (ECP) and ICP [1]. ECP in FO is similar to CP in pressure-driven membrane processes. When the feed solution flows

EBSCOhost - printed on 2/14/2023 6:39 AM via . All use subject to https://www.ebsco.com/terms-of-use

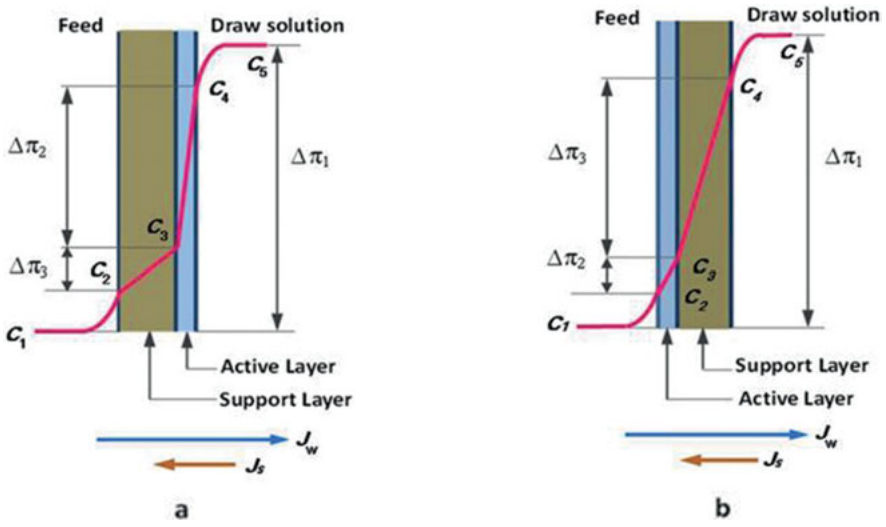

Figure 7.4: (a) Concentrative internal CP, and (b) dilutive internal CP across an asymmetric membrane in FO.

on the active layer of the membrane (shown in Figure 7.4(b)), solutes build up at the active layer, causing that the concentration of the solution at the membrane surface is higher than that of the bulk solution. This may be called concentrative ECP ($c_2 > c_1$). Simultaneously, the draw solution in contact with the porous support layer side of the membrane is being diluted at the permeate-membrane interface by the permeating water. This is called dilutive ECP ($c_4 < c_5$). Both concentrative and dilutive ECP occur near two sides of membrane surfaces due to the availability of two membrane orientations (i.e. the active layer facing the feed or draw solution) in FO. ECP reduces the effective osmotic pressure difference across the active layer of membrane. This adverse effect of ECP on the FO process can be minimized by increasing flow velocity and turbulence at the membrane surface [1].

ICP is a unique phenomenon occurring in the FO process. This CP phenomenon normally can take place within the porous support layer of the asymmetric membrane, while not existing in the dense symmetric membrane [1, 7]. If the porous support layer of the FO membrane faces the feed solution, the solutes in the feed diffuse and accumulate into the support layer, consequently resulting in a concentrative polarized layer established along the interface between the inside of the dense active layer and the support layer ($c_3 > c_2$). This is called concentrative ICP, which is similar to concentrative ECP [1, 8]. If the porous support layer of the FO membrane faces the draw solution, the draw solution within the porous support layer becomes diluted due to the water permeating the active layer, and therefore a dilutive polarized layer builds up within the porous support layer ($c_3 < c_4$). This is referred to as dilutive ICP. Due to the ICP phenomenon occurring within the porous support layer, it cannot

EBSCOhost - printed on 2/14/2023 6:39 AM via . All use subject to https://www.ebsco.com/terms-of-use

be alleviated by cross-flow. It is found that the CP occurring across the asymmetric FO membrane causes the loss of driving force due to ICP, and therefore, the effective osmotic pressure driving force across the active layer is lower than the osmotic pressure difference across the membrane (shown in Figure 7.4). As a result, the reduced effective osmotic pressure driving force aggravates the reduction of the FO water flux and the decrease of the FO recovery [9]. According to the commercial FO membrane being the asymmetric membrane, ICP plays a significant role in the loss of the water flux of FO [1].

7.1.3 Modeling of internal concentration polarization

In the practical operation of FO technology, a small quantity of salt can permeate through the membrane due to the incomplete semipermeability of FO membrane. In addition, the effective osmotic pressure driving force across the active layer is far lower than the osmotic pressure difference of the bulk solutions ascribed to the ECP and ICP. Therefore, the practical water flux is much lower than the expected water flux [1]. Many researchers have investigated on the establishment of the mass transfer model for FO and the further illumination of the mechenism of FO process.

The results show that the water permeation through the membrane can be affected by the coupled influence of hydraulic resistance caused by membrane structure and ICP in the support layer. The relationship of water flux and ICP in a FO process can be modeled by the classical solution-diffusion model, based on the theory of thin-film mass transfer, and the diffusion-convection transport of solute in the porous support layer [2, 8, 10].

Considering the active layer facing the draw solution (AL-facing-DS) configuration (shown in Figure 7.4(a)), and applying the solution-diffusion model to the nonporous active layer, the water flux J_w and solute flux J_s can be presented as follows:

$$J_w = A\,(\pi_4 - \pi_3) \tag{7.1}$$

$$J_s = B\,(c_4 - c_3) \tag{7.2}$$

where A and B are the transport coefficients for water and solute, respectively; c_4 and π_4 are the solute concentration and osmotic pressure of the draw solution; and c_3 and π_3 are the solute concentration and osmotic pressure at the interface of FO support layer and rejection layer.

Until the solute transport in the support layer has achieved an equilibrium after some time, the transport of solute into the support by convection (J_wC) and that due to the solute back-transport through the rejection layer (J_s) have to be balanced by the solute diffusion away from the support:

EBSCOhost - printed on 2/14/2023 6:39 AM via . All use subject to https://www.ebsco.com/terms-of-use

$$J_w C + J_s = D_{eff} \frac{dc}{dx} \tag{7.3}$$

where C is the solute concentration in the porous support layer at a distance x away from the interface between the active layer and the support layer, and D_{eff} is the effective diffusion coefficient of solute in the porous support layer, being the product of the solute diffusion coefficient D_s and porosity ε of the porous support layer.

The boundary conditions for Eq. (7.3) are:

when $$x = 0,\ c = c_3 \tag{7.4}$$

and

when $$x = l_{eff} = \tau l,\ c = c_2 \tag{7.5}$$

where l_{eff} is the effective thickness of the support layer, l is the actual thickness of the support layer, and τ is the tortuosity of the porous support layer.

Solving Eqs. (7.1)–(7.5) it can be obtained:

$$J_w = \frac{1}{K} \ln \left(\frac{c_3 + B\left(c_4 - c_3\right)/A\left(\pi_4 - \pi_3\right)}{c_2 + B\left(c_4 - c_3\right)/A\left(\pi_4 - \pi_3\right)} \right) \tag{7.6}$$

where K is the solute resistivity within the membrane porous layer, given by

$$K = \frac{l\tau}{\varepsilon D_s} = \frac{S}{D_s} \tag{7.7}$$

In Eq. (7.7), S is a structural parameter, analogous to the boundary layer thickness for external concentration polarization in a typical reverse osmosis process, is given by $l\tau/\varepsilon$.

If we assume that the effect of concentrative ECP is negligible (i.e., $c_2 = c_1$) and the osmotic pressure of a solution is proportional to its concentration, Eq. (7.6) can be simplified to:

$$J_w = \frac{1}{K} \ln \left(\frac{\pi_3 + \frac{B}{A}}{\pi_2 + \frac{B}{A}} \right) \tag{7.8}$$

where the osmotic pressure π_3 at the interface of FO support layer and rejection layer can be determined from Eq. (7.1) (i.e., $\pi_3 = \pi_4 - J_w/A$). Thus,

$$J_w = \frac{1}{K} \ln \left(\frac{B + A\pi_4 - J_w}{B + A\pi_2} \right) \tag{7.9}$$

EBSCOhost - printed on 2/14/2023 6:39 AM via . All use subject to https://www.ebsco.com/terms-of-use

If we assume that the effect of dilutive ECP is negligible (i.e., $c_4 = c_5$) and the osmotic pressure of a solution is proportional to its concentration, the water flux equation for the active layer facing the feed water (AL-facing-FW) mode can be similarly derived as:

$$J_w = \frac{1}{K}\ln\left(\frac{B+A\pi_4}{B+J_w+A\pi_2}\right) \tag{7.10}$$

In Eq. (7.7), K is used to measure the solute's ability to diffuse into or out of the membrane support layer, and can quantify the severity of ICP within the membrane porous layer; larger values of K are associated with more severe ICP [1, 8, 10]. The effective reduction of the solute resistivity K is a main way to improve the FO performance. The diffusion coefficient D_s of the solute can be increased by changing the types of solutes in draw solutions or increasing the temperature of the solutions, which could partly alleviate the ICP due to the easier diffusion of solute in the porous support layer. However, the change of the types of the draw solutions may aggravate the difficulty of the recovery of draw solutions, and therefore, the theoretically decreased ICP could be possibly counteracted by other unfavorable factors and the methods mentioned above are not the optimal [9]. On the other hand, the solute resistivity K can be reduced by decreasing the structural parameter S. The thinner porous support layer, the lower tortuosity and the higher porosity of the membrane porous layer are more beneficial to reduce the structural parameter S. Thus, the methods of decreasing the structural parameter S has become one of the focus studies in the field of FO membrane fabrication [1, 11].

7.2 The practical significance of the forward osmosis technology for water purification

Water is the source of life, and safe drinking water is basic to human survival. Water resources have become strategic economic resources that affect the development of various countries in the world. In China, water scarcity is one of the important restriction factors for the economic development and social progress, being characterized by the quantity-oriented and quality-oriented shortage. Due to the uneven distribution of water resources in time and space, the shortage of water amount exists in most areas in the north and parts of the south of China. The drinking water sources in urban areas are suffering from considerable pollutions, especially in areas of the Taihu Lake, the Dian Lake and the Chao Lake and basins of Huai River, Hai River and Liao River. The water shortage caused by the degrading water quality in these areas is becoming more and more serious, mainly being caused by the organic pollution. In addition, due to the geological features, the problems of high salinity and hardness in groundwater ubiquitously exist in the northwest and other regions of China.

EBSCOhost - printed on 2/14/2023 6:39 AM via . All use subject to https://www.ebsco.com/terms-of-use

Currently, the exploration and utilization of non-traditional sources is an important way to solve the subsistence crisis caused by water problems and alleviate the harm from the water shortage. The non-traditional sources usually include reclaimed water (treated sewage and wastewater) that is different from conventional water resources, and contaminated water which is not suitable for drinking water resource before the purification treatments, such as the polluted surface water, groundwater, sea water, brackish water, mine water, rain and flood water. However, the existing conventional water treatment processes cannot afford the effective purification of the non-traditional sources. The organic pollutants with "three genicity effects" (carcinogenicity, teratogenicity and mutagenicity) are not efficiently removed by the conventional processes (the removal is only about 20%–30%), and can easily produce a quantity of disinfection by-products in the chlorination process. The practice shows that the pressure-driven membrane processes, such as RO, NF, UF and MF, have great advantages and application prospects of the treatment of the non-traditional sources. The hybrid (double) membrane processes (i.e. RO/NF coupled with UF/MF) have been used successfully for removing the micropollutants and natural organic matter (NOM) from the non-traditional water. However, the performance of the pressure-driven membrane processes can be significantly affected by irreversible membrane fouling [12–14] which is mainly caused by the deposition and adsorption of the dissolved organic matter on or within the membrane [15]. The wide application of the pressure-driven membrane technologies has been hampered by the membrane fouling which cause the reduction of the quantity and quality of produced water by membrane processes and aggravation of the additional energy consumption. On the other hand, the NF and RO processes produce high quality potable water from impaired water, while simultaneously concentrating the impurities in the feed. It is inevitable that the direct discharge of the concentrated water without any appropriate disposal would bring the secondary pollution to the environment. Therefore, there is an urgent need for investigation on the novel water treatment method for the efficient removal of the dissolved organic matter and proper selection of the economical and efficient treatment method of the concentrated water. These promising technologies not only can effectively relieve the membrane fouling and thus improve the treatment efficiency of non-traditional water by membrane processes, but also have significant social effects on ensuring the safety of the drinking water quality and safeguarding the level of people's health.

As an emerging membrane technology, FO has the great potential for the treatment of non-traditional water. During the FO treatment process, the unconventional water is usually used as the feed and the electrolytes of high concentration (e.g. NaCl) are applied for the draw solutes. Most dissolved organic pollutants are rejected by the FO membrane and consequently do not permeate into the draw solution. For the regeneration of the produced water from the draw solution, it is usually necessary to combine the FO process with other pressure-driven membrane processes, such as the hybrid FO-RO process. Also, the FO can be employed as the post-treatment process for

EBSCOhost - printed on 2/14/2023 6:39 AM via . All use subject to https://www.ebsco.com/terms-of-use

the recovery of the concentrated water of NF, in which the concentrated water is used as the feed solution.

Compared to the conventional hydraulic pressure-driven membrane processes, the hybrid FO and pressure-driven membrane system offers several potential advantages on the treatment of non-traditional water including following aspects: 1) the multi-barrier protection of the quality of the produced water due to the effective removal of the organic pollutants; 2) low energy consumption of the hybrid FO and pressure-driven membrane process due to the operation of FO without energy loss; 3) the decrease of volumes of backwashing water and quantities of chemicals and the consequently extension of operation cycle of the membrane system ascribed to the loose and easy-removed fouling layer formed during the FO process that does not require the applied hydraulic pressure; 4) the significantly increase of volumes of produced water and decrease of amounts of discharged concentrated water attributed to the high water recovery (that sometimes reaches 90% or above) of the hybrid FO and pressure-driven membrane system based on the higher recovery of the individual FO process.

Besides the application of the non-traditional water treatment, the FO process can also be used for the emergency life support in extreme cases. In China, many areas are severely affected by natural disasters, such as earthquakes, floods and so on. These frequently occurring large natural disasters can cause long term scale of water cut, power off and other problems in the disaster areas, which endangers the life and health of the people in the local areas. The high-performance FO membrane can be developed for the production of the "emergency life bags". The draw solution filled in the "emergency life bag" is the high concentration solution of sucrose and electrolytes that can replenish the needed nutrients of the human body and must have a high osmotic pressure. When the impaired water is filled into the "emergency life bag", the water molecules can spontaneously permeate to the side of the high concentration solution under the action of osmotic pressure, and meanwhile, the microorganisms, viruses and other toxic and harmful substances in the impaired water are effectively rejected by the FO membrane. At the end of osmosis, the draw solution filled in the "emergency life bag" can be drunk directly as beverage and supplies water and energy to the users.

7.3 Applications of forward osmosis in water purification

Forward osmosis has currently become one of the promising issues among the separation research using membranes in terms of high performance membrane production [16–21], selection and development of draw solutes [5, 22–26], combination of membrane processes [1, 27] and so on, because of its huge potential in water purification. FO has been applied in desalination, wastewater treatment and reusing, water

EBSCOhost - printed on 2/14/2023 6:39 AM via . All use subject to https://www.ebsco.com/terms-of-use

purification, etc., combined with other technologies becoming a new, creative technology. Research abroad on FO has been converted from lab to pilot scale, while still in the startup stage in China today.

7.3.1 Seawater desalination

In 1970s, researchers came up with an idea of desalination using FO technology. However, the unsettled problems, such as membrane fabrication and draw solution selection, blocked the transition from research to actual production. The conception that desalination of seawater and brine by FO has been realized due to the development of the commercial FO membrane.

Generally, two types of desalination using FO are in practice, according to the method of fresh water production from diluted draw solution [28], i.e. one is the FO system with thermal decomposable draw solute, that the volatile gases (CO_2, SO_2, etc.) volatilize from the diluted draw solution by heating leaving the fresh water behind. The volatile gases could be recycled in the system. McGinnis [28] described a new FO system using a combined draw solute (KNO_3 and SO_2) for desalination in a patent. KNO_3 has the advantage of a temperature sensitive solubility that could be easily separated out from the cooling diluted draw solution when reaching the saturation point. The rest of KNO_3 solution flows into another FO system as feed solution. The second system uses SO_2 as draw solute that could be separated out of the diluted draw solution by heating. McCutcheon et al. [5, 22] posed another type of draw solution (NH_4HCO_3 and NH_4OH) in desalination process. This process could achieve a higher water flux and recovery ratio, with a rejection rate up to 95–99%. Also, a higher water flux leads to a more effective desalination result. However, the applicability and safety of this conception remained unconfirmed or required improvement.

In the other types of desalination process, water-soluble salt or particulates are used as draw solutes and the fresh water is produced from the diluted draw solution by other methods. FO process is regarded as a pre-treatment of any other desalination systems. Ling and Chung [29] used hydrophilic nano particles as draw solutes in desalination and recycled the particles through ultrafiltration process. Magnetic particles in nanoscale are also used as draw solutes in the research for their easy separation from draw solution in a magnetic field. But the problems of the cost and the aggregation among the particles are still required to solve. Tan and Ng [30] have studied seven solutes (NaCl, KCl, $CaCl_2$, $MgCl_2$, $MgSO_4$, Na_2SO_4 and $C_6H_{12}O_6$) in an FO-NF desalination system. Zhao et al. [27] used salts with divalent ion as draw solute for desalination of brine and produced freshwater using an NF application. Cath et al. [31] had studied the water purification with an FO-RO system using seawater as draw solution. The application of FO in desalination has now arrived to a pilot stage.

Additionally, FO has been applied for the concentration and reuse of concentrates in RO and NF processes. Tang et al. [32] used two types of RO membranes without

EBSCOhost - printed on 2/14/2023 6:39 AM via . All use subject to https://www.ebsco.com/terms-of-use

support layer in FO desalination of concentrates to explore the effect of membrane structure on the treatment and gained a higher rejection rate, over 99.7%, than the normal FO membranes. Also, the recovery rate could be up to 76% with the draw solution of a constant higher concentration. Martinetti et al. [33] achieved a higher system recovery rate (up to 90%) during concentrating the concentrates in RO by FO.

7.3.2 Wastewater treatment

Domestic sewage has a lower osmotic pressure than sea water but a higher fouling tendency in membrane fouling. FO has a great practical prospect in wastewater treatment because of its difficulty in membrane fouling. Early in 1980s, FO had been studied as a possible treatment in industrial wastewater purification. In recent years, Cath et al. [31] had studied on the potable water production from polluted raw water using FO system. Cartinella et al. [34] had studied the removal of endocrine disrupting chemicals (EDCs) in domestic sewage by FO and found that the removal efficiency of natural estrogens and estradiol by FO was about 77–99%, according to the filtration period and characteristics of feed water. Holloway et al. [35] combined FO with RO process to concentrate sewage sludge due to the advantage of low fouling tendency of FO membranes. HTI Co. Ltd., the manufacturer of commercial FO membranes, pointed out the suitability of FO in the water treatment fields of oil- and gas-containing wastewater, industrial and domestic sewage, nuclear waste and landfill leachate.

FO membrane could also be applied in membrane bioreactor (MBR) replacing the conventional MF/UF membrane for wastewater treatment. Then the diluted draw solution of FO was used for fresh water production by RO. Cornelissen et al. [36] reported that the membrane fouling in osmosis membrane bioreactor (OsMBR) alleviated greatly compared to that in MBR, as well as the energy cost. Xiao and co-workers [37] built a model of salt accumulation to analyze the FO performance in OsMBR. They found that the ratio of water- to salt-permeability coefficient of FO membrane and the ratio of sludge age to hydraulic retention time were two key factors to improve the reactor performance, with the lowest values leading to the least water flux decrease caused by salt accumulation.

7.3.3 Emergency life bags

HTI Co. Ltd. has developed a hydration bag for water purification in a war or other emergency situations (Figure 7.5). It is one of a few commercial products using FO in the market. One product, called X-Pack, has a double-pack structure with a selective permeable membrane as inner bag and a layer of waterproof material wrapping the inner membrane for holding water. The potable draw solution (sugar or concentrated

EBSCOhost - printed on 2/14/2023 6:39 AM via . All use subject to https://www.ebsco.com/terms-of-use

beverage) and some penetration agent are put in the inner bag, while the emergency raw water is positioned in the space between the two bags, then the freshwater can be produced and dilute the potable draw solution for drinking. This type of hydration bag has the advantages of light weight, and it is potable and cheap. The emergency life pack can be applied in the case when encountering major natural disasters.

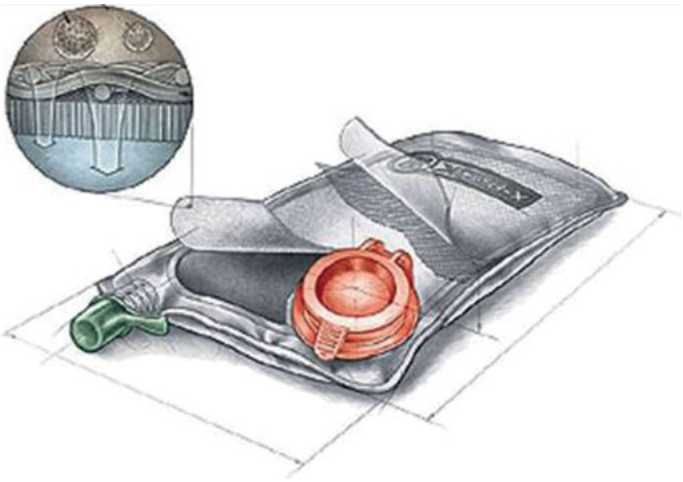

Figure 7.5: Illustration of water purification hydration bag.

7.3.4 Water purification

It is important to study the performance of FO on the removal of various pollutants and the membrane fouling during purification process for unconventional water treatment, considering kinds of organics and inorganics in the water sources.

Zou et al. [38] investigated the effects of initial water flux, membrane orientation, cross-flow velocity and characteristics of feed water and draw solution on the FO membrane fouling by algae solution. It was reported that the Mg^{2+} in feed water would aggravate the FO membrane fouling by algae and a high initial water flux level would accelerate the membrane fouling rate in the FO process. Tang et al. [10] used humic acid as a model foulant to explore the influence of ICP and membrane fouling on water flux. It was found that a better flux stability occurred in the AL-facing-FW orientation due to the alleviated impact of draw solution dilution and membrane fouling, and the deposition of humic acid on the membrane was minor. Thelin et al. [39] studied the FO membrane fouling behavior by natural organic matters (NOM) in groundwater in the AL-facing-DS orientation. It was reported that the water flux decreased with the foulants deposition on the membrane. The concentration of NOM had a minor effect on the FO fouling tendency and the increased ionic strength in porous supporting

EBSCOhost - printed on 2/14/2023 6:39 AM via . All use subject to https://www.ebsco.com/terms-of-use

layer exacerbated the membrane fouling. Different membrane materials and structures significantly influenced the membrane fouling behaviors. Mi and Elimelech et al. [40–42] analyzed various FO membrane fouling behaviors and drew the conclusions as follows.1) membrane fouling by organic matters was closely related to intermolecular interactions; 2) membrane fouling by organic matters was affected by the combination of chemical (calcium bonding) and hydraulic (osmotic drag and shear force by crossflow) factors; 3) membrane material significantly affected the membrane fouling by organic matters proved by AFM; 4) organic matters deposited on the membrane and formed a loose pollutant layer that was easily flushed with mechanical methods and without any external driving force during FO process.

Xie et al. [43] compared the performance of FO and RO in three hydrophobic trace contaminants removal (bisphenol A (BPA), triclosan (TCS) and diclofenac). It was reported that the removal efficiency of BPA was higher in FO than RO process, while no obvious difference of TCS between these two membrane purifications. NaCl in draw solution blocked the effects of filtration through pores and membrane adsorption of trace contaminants due to its obvious reverse diffusion, while $MgSO_4$ and glucose with weaker reverse diffusion had no obvious effect on that. Valladares Linares et al. [44] reported that the organic foulants deposition on the active layer could strength the negative charge and the hydrophilicity of membrane surface, and the fouling layer could also increase the adsorption of hydrophilic foulants on the membrane surface. Changes of the membrane surface properties could increase the performance of removal of hydrophilic ionic and hydrophobic neutral trace foulants. Jin et al. [45] found that the organic matters obviously affected the removal efficiency of inorganic foulants such as B and Sb at different membrane orientations. Organic foulants deposition in the active layer increased the mechanically trapping of Sb, while the foulants in supporting layer decreased the removal efficiency of B in FO.

Generally, forward osmosis system has the potential for the unconventional water source treatment but still need to improve and develop systematically to solve the unsettled problems of purification performance of various dissolved organic matters affected by kinds of factors.

7.4 Study on the purification efficiency of the concentrated natural surface water by FO technology

Despite its effective removal of micro-foulants and natural organic matter (NOM) in raw surface water, the nanofiltration (NF), often combined with ultrafiltration (UF), is limited by regenerative treatment of concentrated water. Forward osmosis (FO), which is characterized by effective rejection and low energy dissipation, has been regarded as an ideal solution. The tannic acid was used as the substitute for natural DOM in

EBSCOhost - printed on 2/14/2023 6:39 AM via . All use subject to https://www.ebsco.com/terms-of-use

surface water to investigate effects of physical (e.g., concentration of draw solution – initial flux level, membrane orientation) and chemical (e.g., initial concentration of foulants, ionic strength, pH) factors on flux and retention efficiency of tannic acid by the FO membrane. In addition, the practical FO performance of purification of concentrated raw surface water in which DOM was enriched by MF/NF processes was investigated under the effects of the membrane orientation and concentration of organic compounds in raw water.

7.4.1 Materials and methods

7.4.1.1 FO membrane

A tri-cellulose acetate (CTA), forward-osmosis plate membrane by Hydration Technology, Inc. (HTI, USA), was used in this study. Its features are discussed in Section 7.1.2.

7.4.1.2 Draw and feed solutions

Unless otherwise specified, all chemicals and reagents used in this study were of analytical grade. Milli Q water with a resistivity of 18.2 MΩ · cm was used to prepare all working solutions.

NaCl (Sinopharm Chemical Reagent Co. Ltd., China) and tannic acid were used as the draw solution solute and the substituent foulant, respectively. As a polyphenol, tannic acid can be representative of hydrophilic organic compounds (representing micro-molecules). According to the technical description by the supplier, the average molecular weight of tannic acid is 1,701 g/mol and its empirical formula is $C_{76}H_{52}O_{46}$. However, tannic acid is, practically, a mixture of relevant hydrolysates such as five gallic acid units, ester-linked to a pentagalloylglucose core.

The surface water was collected from Taihu Lake, which is characterized by severe eutrophication. Raw water with different initial concentrations (10 and 20 mg/L) were generated by a bench-scale hybrid MF/NF system, and the concentrated raw water was filtered using a 0.45 μm membrane. Table 7.1 shows the qualities of the surface water.

7.4.1.3 Forward osmosis setup

Figure 7.6 illustrates the bench-scale setup for crossflow FO. Symmetric channels ($180 \times 46 \times 1.25$ mm^3) were established on the two sides of the forward osmosis membrane. Plastic mesh spacers were placed on the forward osmosis membrane to support the membrane and enhance effects of disturbance and mass transfer by water flow. Two variable-speed peristaltic pumps were used for parallel recycling cross flows of

EBSCOhost - printed on 2/14/2023 6:39 AM via . All use subject to https://www.ebsco.com/terms-of-use

Table 7.1: The qualities of the surface water.

	TOC = 10 mg/L		TOC = 20 mg/L	
Composition	**Concentration**		**Concentration**	
	mg/L	**mM**	**mg/L**	**mM**
TOC	10.29		20.32	
UV_{254} (cm^{-1})	0.162		0.320	
SUVA (L/mg · m)	1.57		1.57	
pH	8.32 ± 0.2		8.40 ± 0.2	
Total dissolved solids	366		584	
Calcium, Ca^{2+}	80	2.0	164	4.1
Magnesium, Mg^{2+}	23.3	0.97	48	2.0
Sodium, Na^{+}	42.6	1.85	69	3.0
Potassium, K^{+}	5.85	0.15	12.1	0.31
Boron, B	0.7	0.07	1.4	0.14

feed and draw solutions on different sides of the membrane. The rates of cross flows were maintained at 600 mL/min. During the test, the temperatures of feed and draw solutions were kept constant in a water bath, through controlling the heat transfer by submerged plastic heat exchanger coils within the water bath.

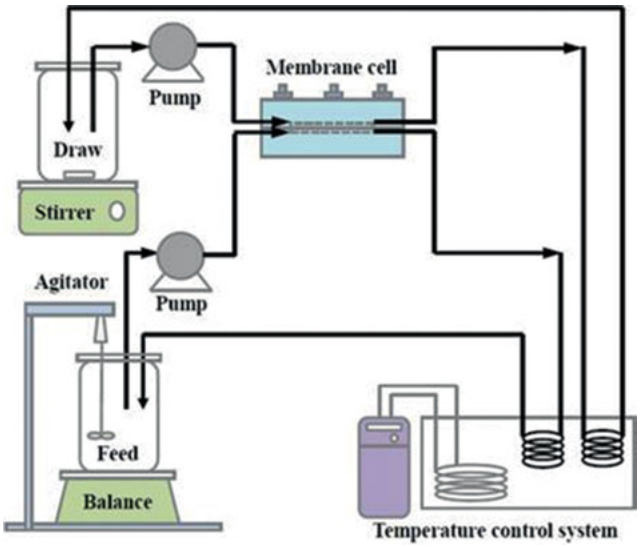

Figure 7.6: Schematic diagram of the bench-scale forward osmosis (FO) setup.

A 5 L concentrated NaCl solution (0.3–4 M) was used as the draw solution. The feed solution was placed on a digital balance connected to a computer data logging system.

EBSCOhost - printed on 2/14/2023 6:39 AM via . All use subject to https://www.ebsco.com/terms-of-use

This digital balance uploaded mass variations of the feed solution in designated time intervals. In this way, the permeate flux of the membrane could be determined. Additionally, the reverse diffusion flux of salt solutes was calculated based on the conductivity of the feed solution, which was recorded with the conductivity meter.

7.4.1.4 FO Experimental procedure

Before each forward osmosis test, the membrane was equilibrated using NaCl solution as the draw solution, and a background solution with no foulants as the feed solution (pH, ionic strength, and Ca^{2+} concentration was kept consistent with those of working solutions) for at least 30 min until the water flux stabilized. Then, the foulant-containing feed solution was injected into the feed container for an 8-hour fouling test. The pH value of the raw solution was maintained constant (using HCl and/or NaOH). To guarantee the reliability of flux data, each test was repeated twice or more, depending on the criticality of the data. Unless specified otherwise, the conditions of the purification test were as follows:

Feed solution: 10 mg/L tannic acid at 10 mM ionic strength (adjusted by NaCl) and pH of 5.8 ± 0.1 in the removal of tannic acid tests; the water samples were collected from Taihu Lake (see Table 7.1) in purification of natural water tests;

Draw solution: concentrated NaCl solution (0.5 to 4.0 M in the removal of tannic acid tests and 2.0 M for purification of natural water tests);

Crossflow rate of feed and draw solutions: 17.4 cm/s;

Temperature: 22 ± 1 °C.

Since the osmotic driving force for forward osmosis flux degraded due to the diluting draw solution and the internal concentration polarization effect, the water flux declines in purification tests can be attributed to both membrane fouling and reduction of apparent osmotic driving force between two sides of the membrane. Hence, baseline tests were included to eliminate effects of osmotic driving force drop on the flux. In baseline tests, a background solution with no foulants was used as the feed solution and the conditions were aligned with those of fouling tests. The baseline flux obtained was then used for normalization of fouling fluxes. The normalization flux is the ratio of fouling flux ($J_{fouling}$) and baseline flux ($J_{Baseline}$), and it solely reflects the degree of membrane fouling. In all fouling tests, fluxes obtained were expressed as real fouling and normalized fluxes.

7.4.1.5 Analytical methods

1. Molecular weight fractionation

The relative molecular weight distributions of organic compounds in tannic acid and natural water samples were measured with a combination of high-performance liquid

EBSCOhost - printed on 2/14/2023 6:39 AM via . All use subject to https://www.ebsco.com/terms-of-use

chromatograph (HPLC, Waters e2695, USA), a ultraviolet absorbance (UVA) detector (Waters 2489, USA), and total organic carbon (TOC) online detector (Modified Sievers 900 Turbo, USA), as described elsewhere [46].

The TOC detector can virtually measure all organic carbon of the samples, whereas the UVA detector can detect organic compounds with aromatic or double bonds only. Hence, the combination of these two detectors can reveal both relative molecular weight distributions of different compounds and contents of macromolecule organic compounds with low UV responses, thus qualitatively determining contents of aromatic and aliphatic organic compounds.

2. Hydrophobic/hydrophilic fractionation

Component separation was executed for tannic acid and natural water from Taihu Lake using Amberlite XAD-8 and XAD-4 resin. Strong hydrophobic fraction (HPO), transphilic fraction (TPI) and hydrophilic fraction (HPI) were obtained in TOC analysis [47].

3. Removal, retention, and adsorption of foulants

The removal rate, retention rate, and adsorption of organic compounds in tannic acid and raw water from Taihu Lake by the forward osmosis membrane were determined by the following TOC method. During the test, a 20 mL sample was collected regularly and alternatively from raw solutions and draw solutions for TOC measurement. The quantification limit of the TOC detector used for high salt content samples was 0.1 mg/L.

Unlike conventional pressure-driven membranes, the permeate concentration of forward osmosis membrane is diluted by the draw solution. Hence, the actual permeate concentration $C_{p(t)}$ and removal rate of foulant can be obtained by:

$$C_{p(t)} = \frac{C_{d(t)}V_{d(t)} - C_{d(t-1)}V_{d(t-1)}}{V_{p(t)}} \tag{7.11}$$

$$Removal = \left(1 - \frac{C_{p(t)}}{C_{f(t)}}\right) \times 100\% \tag{7.12}$$

where $V_{p\,(t)}$ is the volume of water penetrated from feed solution to draw solution at time t. $V_{d\,(t)}$ and $V_{d\,(t-1)}$ are the volume of draw solution at time t and (t–1), respectively. $C_{d\,(t)}$ and $C_{d\,(t-1)}$ are the foulant concentration in the draw solution at time t and (t–1), respectively. $C_{f\,(t)}$ is the foulant concentration in the feed solution at time t.

The retention rate of foulant by forward osmosis membrane can be calculated by:

$$Retention = \frac{C_{f(t)}V_{f(t)}}{C_{f(0)}V_{f(0)}} \times 100\% \tag{7.13}$$

EBSCOhost - printed on 2/14/2023 6:39 AM via . All use subject to https://www.ebsco.com/terms-of-use

where $C_{f(0)}$ is the initial concentration of foulant in the feed solution at $t = 0$. $V_{f(0)}$ and $V_{f(t)}$ are the volume of feed solution at times t and $t = 0$, respectively.

According to the mass balance, foulant adsorption on forward osmosis membrane can be calculated by:

$$Adsorption = \frac{C_{f(0)}V_{f(0)} - C_{f(t)}V_{f(t)} - \left(C_{d(t)}V_{d(t)} - C_{d(t-1)}V_{d(t-1)}\right)}{M} \tag{7.14}$$

where M is the effective membrane area of the forward osmosis membrane.

To guarantee that foulant adsorption on forward osmosis setups (i.e., tubes and spacers) was negligible, a blank test was conducted using membrane components without the membrane. The mass loss demonstrated that the additional adsorption of foulants on the forward osmosis recycling system is negligible.

To verify accuracy of the proposed method, the forward osmosis membrane, after fouling, was eluted to determine actual foulant adsorption. The fouled membrane was immersed in NaOH solution (pH = 10.5) and sonicated at 25 °C for 15 min to guarantee desorption equilibrium of foulants. Finally, the quantity of the foulant was measured by the TOC analyzer. As shown in Table 7.2, the calculated adsorption was consistent with the practically measured elution, demonstrating accuracy of the proposed method.

Table 7.2: Mass adsorption of tannic acid and natural DOM in FO.

Operating condition	Adsorption (μg/cm^2)	
	Mass balance calculation	Direct extraction measurement
Orientation: AL-DS FW: 10 mg/L tannic acid (pH = 8) DS: 2 M NaCl	48.60	49.57
Orientation: AL-DS FW: 10 mg/L tannic acid (1 mM Ca^{2+}) DS: 2 M NaCl	53.78	55.20
Orientation: AL-FW FW: 10 mg/L tannic acid DS: 2 M NaCl	4.63	5.80
Orientation: AL-DS FW: 20 mg/L natural DOM DS: 2 M NaCl	19.97	22.14

EBSCOhost - printed on 2/14/2023 6:39 AM via . All use subject to https://www.ebsco.com/terms-of-use

7.4.2 Results and discussion

7.4.2.1 Fraction characteristics of tannic acid and natural DOM

Figure 7.7 shows ratios of hydrophobic/hydrophilic components of tannic acid and natural organic compounds in raw water from Taihu Lake. As observed, in the natural DOM, the percentage of hydrophilic components was approximately 50.4%, relatively predominated over the hydrophobic fraction, which is consistent with other studies on the natural surface water treatment [47, 48]. Additionally, hydrophobic/hydrophilic components of tannic acid were approximatively consistent with those of natural organic compounds, indicating that tannic acid can be a representative of natural DOM in respect of organic hydrophilicity/hydrophobicity.

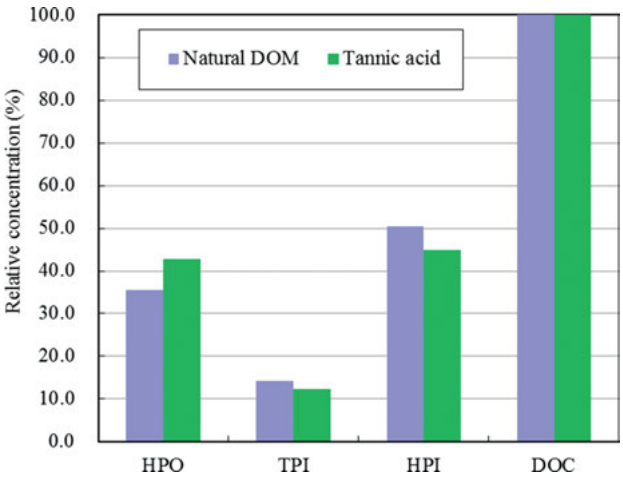

Figure 7.7: Organic fractionations of natural DOM and tannic acid.

Figure 7.8 shows molecular weight distributions of tannic acid and natural organic compounds (10 mg C/L as DOC concentration for each sample) measured by HPLC-UVA/TOC. Two peaks are present for UVA (Figure 7.8(c)) and TOC (Figure 7.8(d)) of tannic acid. The apparent molecular weights (AMW_{UVA}) of UVA at the peak top was estimated to 1,399 Da and 618 Da. For the TOC detection, the peak area in the 1,399 Da is a dominant component of overall TOC peak area, suggesting that the component with apparent molecular weight of 1,399 Da is the major component of tannic acid (the component with apparent molecular weight of 618 Da may be a hydrolysate of tannic acid).

The TOC of natural DOM had three peaks (Figure 7.8(b)), which correspond to the AMW_{TOC} of 1,004,680, 4,633, and 1,082 Da. Both UVA and TOC detectors exhibited high peak intensity responses to components with AMW at 4,633 and 1,082 Da. It can be

EBSCOhost - printed on 2/14/2023 6:39 AM via . All use subject to https://www.ebsco.com/terms-of-use

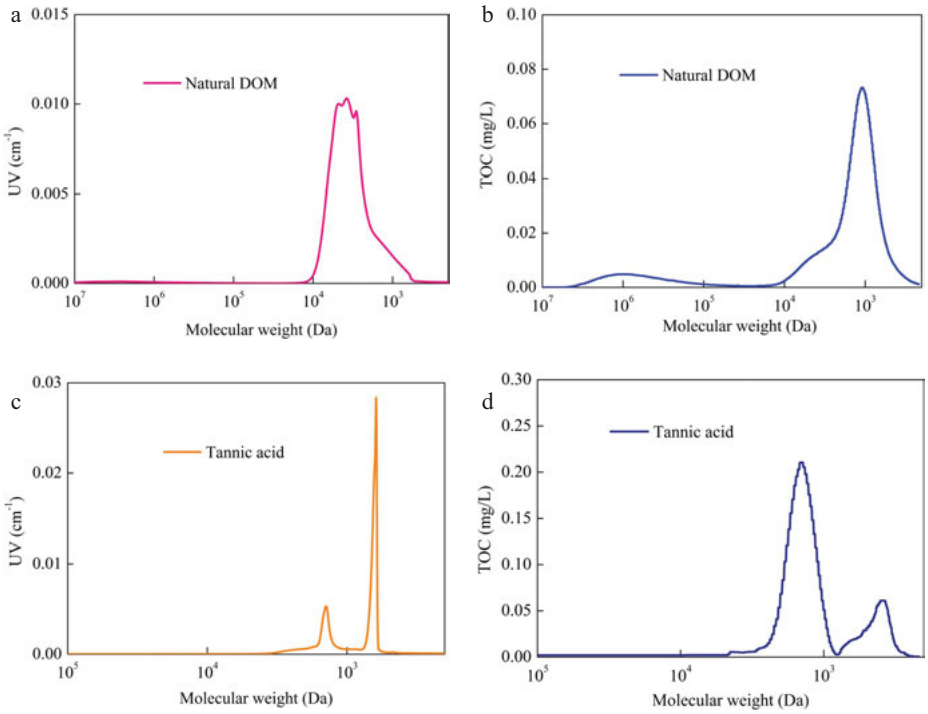

Figure 7.8: (a) UVA and (b) DOC peaks versus MW distribution of natural DOM (10 mg C/L). (c) UVA and (d) DOC peaks versus MW distribution of tannic acid (10 mg C/L).

deduced that natural DOM with relative molecular weight distributions between 4,633 and 1,082 Da consist of humic substances with high UVA (i.e., high aromatic features) and low molecular weight. Although it gave a lower response for UVA than the 4,633 Da fraction, the 1,082 Da fraction appeared to be the predominant fraction in natural DOM according to the higher area percentage of TOC. In summary, this test should focus on the distribution of the component with apparent molecular weight of 1,082 Da to investigate treatment potential of forward osmosis process, which is also one of the critical reasons for choosing tannic acid as the substitute for natural DOM due to its notable similar dominant molecular weight distribution compared with natural DOM.

7.4.2.2 Effects on purification of tannic acid

1. Performance of FO membrane

To monitor the mass transfer during forward osmosis under different membrane orientations, baseline tests were conducted at different initial concentrations of draw solution (i.e., osmotic pressure). Table 7.3 summarizes water flux (J_w), solute flux (J_s), and reverse solute flux (J_s/J_w) under different membrane orientations.

EBSCOhost - printed on 2/14/2023 6:39 AM via . All use subject to https://www.ebsco.com/terms-of-use

Table 7.3: FO water flux (J_w) and solute flux (J_s) in baseline tests for tannic acid purification.

Draw Solution	Membrane Orientation	C_s (M)	Osmotic Pressure (bar)	J_w L/(m^2 · h)	J_s M/(m^2 · h)	J_s/J_w (M)	Average J_s/J_w (M)	K (s/m)
NaCl	AL-DS	0.3	12.8	4.5	0.14	0.032	0.035	4.05×10^5
		0.5	21.9	7.9	0.27	0.034		
		1	47.0	16.2	0.49	0.031		
		2	106.6	24.9	0.80	0.032		
		4	263.6	35.7	1.54	0.043		
	AL-FW	0.3	12.8	3.9	0.16	0.041	0.044	2.69×10^5
		0.5	21.9	7.2	0.26	0.037		
		1	47.0	10.1	0.53	0.053		
		2	106.6	15.0	0.66	0.044		
		4	263.6	19.0	0.82	0.043		

For both orientations, water flux and solute flux clearly increased nonlinearly with the concentration C_s of the draw solution. This may be attributed to the internal concentration polarization (ICP) in the supporting layer of the forward osmosis membrane [8–10, 38]. However, water flux and solute flux in AL-facing-DS mode were significantly higher than those in AL-facing-FW mode, especially at higher concentrations of draw solution. According to the similar reported observations, this may be attributed to the fact that the dilution ICP, when the active layer faces the feed solution, had a more significant effect on reduction of effective osmotic pressure difference between two sides of the active layer of membrane (compared with the concentrative ICP when the active layer faces the draw solution) [1, 8–10, 38]. Meanwhile, the ICP can affect solute flux by reducing its driving force – effective concentration difference between two sides of the active layer of the membrane [10].

The reverse solute flux (J_s/J_w), which is the ratio of solute flux and water flux, can also characterize the performance of the forward osmosis membrane. In this study, the average J_s/J_w are 0.035 M (2.05 g/L) and 0.044 M (2.57 g/L) when the active layer of the membrane faces the draw and feed solutions, respectively. This is consistent with the results of Zou *et al.* [38]. Although J_s/J_w in the two orientations were consistent, low J_s/J_w (i.e., low solute flux J_s and high water flux) is preferred for the selection of draw solution [38] and membrane orientation [49], as low J_s/J_w leads to low solute flux and high water flux, which represents better selectivity and higher efficiency of the FO membrane. Since the water flux was high when the active layer of the membrane faces the draw solution, the active layer of the membrane was set in this mode for this study.

As shown in Table 7.3, the solute resistivity (K) of the porous supporting layer was 4.05×10^5 s/m and 2.69×10^5 s/m when the active layer of membrane faces the draw

EBSCOhost - printed on 2/14/2023 6:39 AM via . All use subject to https://www.ebsco.com/terms-of-use

solution and the feed solution, respectively. This is consistent with studies of Tang *et al.* [10] and Gray *et al.* [8]. Based on Eqs. (7.9) and (7.10), the forward osmosis water flux can be effectively improved by reducing K.

According to results of baseline tests, both concentration of draw solution and membrane orientation had significant effects on water flux during forward osmosis, thus affecting purification performances. Therefore, concentration of draw solution and membrane orientation were regarded as primary physical factors affecting removal of tannic acid by forward osmosis. Additionally, components in the feed solution was continuously concentrated during treatment of concentrated water of nanofiltration by forward osmosis, and it is necessary to understand effects of chemical factors, such as conditions of the feed solution on removal of tannic acid by forward osmosis, in terms of initial concentration of tannic acid, pH, and ionic strength of Ca^{2+}.

2. Effect of initial flux level (concentration of draw solution)

To study the effect of initial flux level on tannic acid purification by FO membrane, four different initial flux levels (7.9, 16.2, 24.9 and 35.7 L/($m^2 \cdot h$)) were investigated for the AL-facing-DS mode. The results are shown in Figure 7.9.

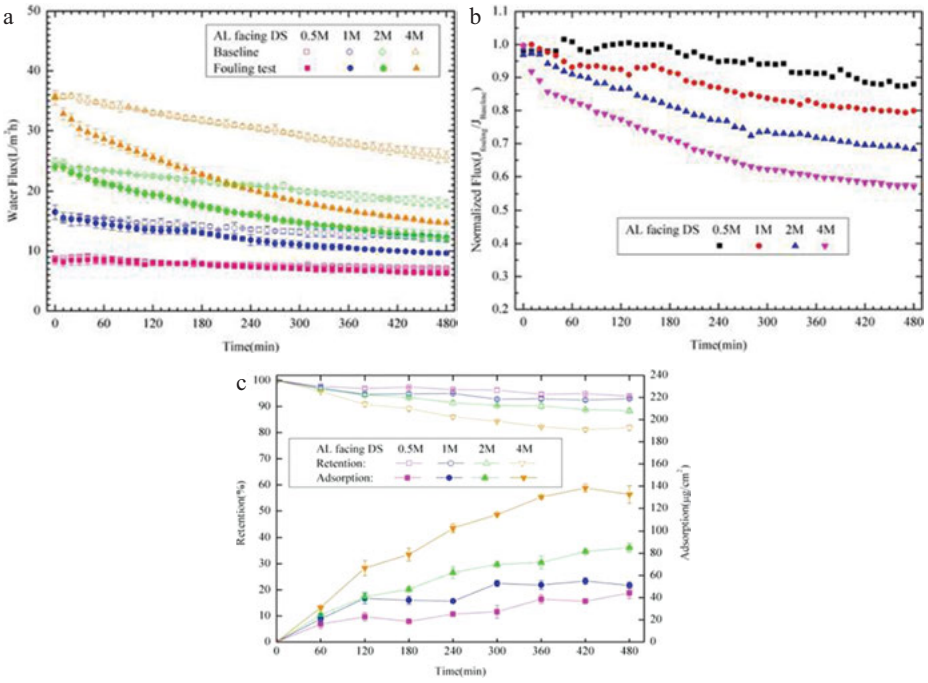

Figure 7.9: Effect of initial flux level on purification of tannic acid.

EBSCOhost - printed on 2/14/2023 6:39 AM via . All use subject to https://www.ebsco.com/terms-of-use

Figure 7.9(a) shows baseline and fouling fluxes of a FO membrane as a function of time at different initial flux levels (i.e., concentrations of draw solution). The initial baseline flux increased significantly with the concentration of draw solution. This may be attributed to the fact that increasing concentration of draw solution leads to a greater concentration difference of solutions on the two sides of the forward osmosis membrane, which then results in a greater effective osmotic pressure difference. Additionally, the decreasing rates of baseline flux at higher initial fluxes (e.g., for 2 M and 4 M DS) were higher than those of lower initial fluxes. This may be attributed to the fact that high initial fluxes lead to increased water penetration volumes, and thus increased dilution of draw solution and concentration of feed solution. At a specific initial flux, comparison of baseline and fouling fluxes of the FO membrane reveals that the tannic acid solution results in exacerbated flux loss [10, 42], further demonstrated as the normalized fluxes in Figure 7.9(b). When the initial flux increased from 8 to 36 L/($m^2 \cdot h$), fouling of the FO membrane by the tannic acid solution was more severe. This is consistent with studies related to pressure driven membranes (e.g., RO and NF) [50, 51] and osmotically driven membranes (e.g., FO) [10, 38, 42]. As shown in Figure 7.9(b), at relatively high initial flux level (e.g., for 4 M), the normalized flux drop at initial stages ($t \leq 1$ h) of tannic acid filtration by FO was significantly noticed. However, the decreasing rate of the normalized flux at 4 M DS concentration was reduced after 40 min. Additionally, the declined rates of normalized fluxes at relatively higher initial fluxes (e.g., for 4 M and 2 M) were slower after 5 h, indicating that fouling of the FO membrane by tannic acid at higher initial flux levels in AL-facing-DS mode would be relieved by filtration. This is favorable to water flux stability after longer filtration period.

Tang et al. [10] proposed the presence of a critical flux in osmotically driven FO membranes. A critical flux was observed in this study as well: if the initial flux ≤ 18 L/($m^2 \cdot h$) (i.e., $C_s \leq 1$ M), FO membrane fouling was minor; if the initial flux > 18 L/($m^2 \cdot h$), FO membrane fouling was significant. The presence of a critical flux in FO membranes by organic fouling is consistent with other studies as well [38, 49, 52].

The experimental results demonstrated that removal rate of tannic acid by FO membrane when the active layer faces the draw solution was at or above 99.0% for all the DS concentrations tested during the entire filtration period. Hence, forward osmosis can effectively remove tannic acid in the AL-facing-DS orientation, regardless of the concentration of draw solution. Because tannic acid can barely penetrate the forward osmosis membrane and the loss of tannic acid in the experimental system was negligible, it can be concluded that the decrease of tannic acid in feed solution is mainly attributed to the adsorption of tannic acid on the FO membrane. For this reason, low adsorption of tannic acid and thus high retention rate by the membrane can serve as indicators that forward osmosis can effectively remove tannic acid. Figure 7.9(c) shows the trends of adsorption of tannic acid on the FO membrane and its retention rate for each DS concentration in the AL-facing-DS mode.

According to Figure 7.9(c), the retention rate of tannic acid decreased significantly as the initial flux level increased. This can be attributed to the increased adsorption

EBSCOhost - printed on 2/14/2023 6:39 AM via . All use subject to https://www.ebsco.com/terms-of-use

of tannic acid on the membrane, caused by increasing initial flux level. The effect of initial flux level on tannic acid fouling of the FO membrane can be generally attributed to two categories of hydrodynamic interactions: (1) permeation drag, induced by convection flow toward the membrane, and (2) shear force, induced by cross flow parallel to the membrane [42]. For the AL-facing-DS mode, the porous supporting layer faces the tannic acid solution, and shear force degrade drastically due to the vanished cross flow in the supporting layer. As a result, shear force cannot effectively remove tannic acid molecules from the membrane. Hence, permeation drag plays a key role in adsorption of tannic acid. At low initial flux levels (i.e., for 0.5 M and 1 M DS), the weaker permeation drag force led to fewer adsorption amount of tannic acid molecules in the porous supporting layer. The amount of tannic acid adsorbed on the membrane increased slowly and the adsorption reached 70% of the total adsorption amount at 4 h, and retention rate of tannic acid dropped gradually to ~93% over the residual filtration time. As shown in Figure 7.9(b), weaker adsorption of tannic acid eventually led to minor reduction of fouling flux at 0.5 M and 1 M DS concentrations. At higher initial flux levels (e.g., for 2 M and 4 M DS), increased permeation drag promoted the adsorption of tannic acid, resulting in significantly reduced retention rates of tannic acid by forward osmosis. At the end of filtration, retention rates of tannic acid at the two DS concentrations were approximately 89% and 83%, respectively.

The greater adsorption of tannic acid at higher initial flux levels led to more severe internal clogging within the porous supporting layer. As a result, the porosity of the supporting layer was probably reduced, causing an increased structural parameter S, and thus a greater solute resistivity K (Eq. (7.7)). As discussed in Section 7.1.3, the reduced porosity of the supporting layer has a negative effect on the ICP in the FO membrane, and thus on the flux loss. Tang *et al.* proposed a similar mechanism for humic acid fouling of concentration-driven forward osmosis membranes [10]. Additionally, the increasing rate of tannic acid adsorption as a function of time decelerated after 5 h at higher initial flux levels, resulting in slower decrease of normalized flux (see Figure 7.9(b)). Under these conditions, more severe flux drop at the initial stage of forward osmosis led to a weaker effect of permeation drag on adsorption of tannic acid. For this reason, the quantity of tannic acid molecules carried to the membrane surface decreased, and thus the adsorption rate of tannic acid became lower. The decreased tannic acid adsorption rate therefore lowered the rate of internal clogging and thus the reduction rate of support layer porosity, which caused solute resistivity K to increase more slowly and the normalized flux to decrease more slowly. Although the adsorption of tannic acid at 40 min was not calculated, the explanation above may also be suitable for the earlier change in the decrease rate of normalized flux at the 4 M DS concentration.

3. Effect of membrane orientation

Figure 7.10 illustrates the effect of membrane orientation on the purification of tannic acid by forward osmosis. To align a similar initial flux level (~20 L/($m^2 \cdot h$)), the con-

EBSCOhost - printed on 2/14/2023 6:39 AM via . All use subject to https://www.ebsco.com/terms-of-use

centration of draw solution was set to be 4 M and 2 M, when the active layer of membrane faces the feed solution and draw solution, respectively.

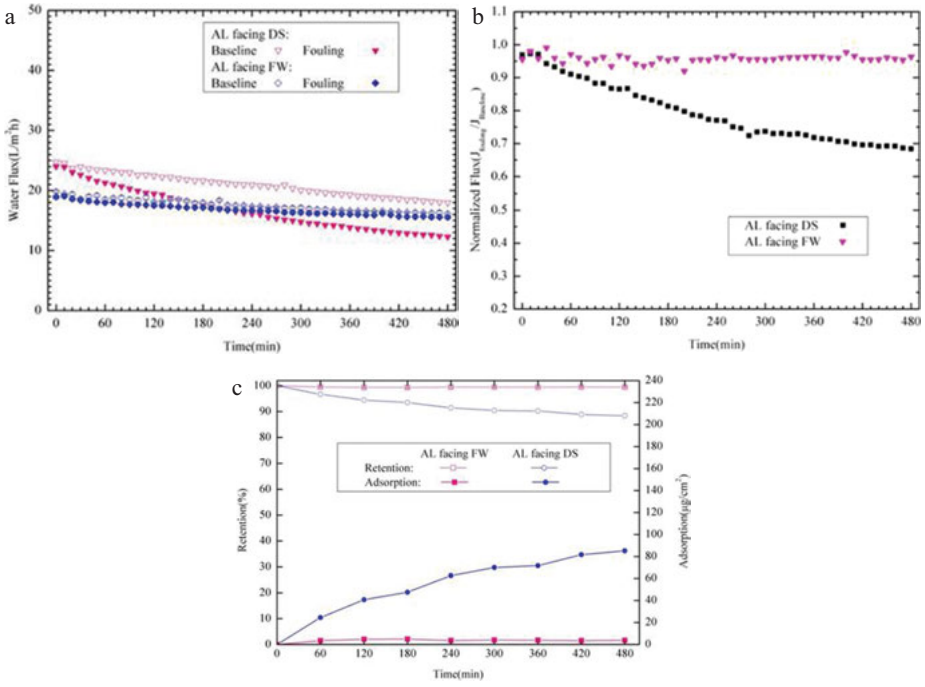

Figure 7.10: Effect of membrane orientation on purification of tannic acid.

As shown in Figure 7.10(a), the baseline and fouling flux in the AL-facing-FW mode was compared with the alternative membrane orientation. As shown in Figure 7.10(b), the normalized flux loss for the AL-facing-DS orientation was 30%, whereas that for the AL-facing-FW orientation was negligible. Hence, the fouling resistance of the FO membrane in the AL-facing-FW mode is superior, consistent with previous studies [10, 38]. This may be attributed to the exacerbated initial ICP in this orientation. Tang *et al.* [10, 38] proposed a self-compensation effect of ICP. Specifically, the decreased flux induced by the dilution of the DS concentration and membrane fouling would lead to severe degradation of ICP in FO membranes, which results in significantly enhanced effective driving force on two sides of the membrane, thus partially compensating for flux loss [10, 38].

Our results suggested negligible differences in the removal rate of tannic acid under different membrane orientations. However, the retention rate of tannic acid by FO membrane in the AL-facing-FW orientation during the entire period was approximately 100%, which is significantly higher than in the AL-facing-DS configuration (see Figure 7.10(c)). This is mainly attributed to the fact that tannic acid prefers not

EBSCOhost - printed on 2/14/2023 6:39 AM via . All use subject to https://www.ebsco.com/terms-of-use

to be adsorbed on the dense skin layer of the membrane, consistent with previous studies of FO membrane fouling [10, 52]. Additionally, this adsorption behavior of tannic acid may be a reason behind the high stability of fouling flux in the AL-facing-FW orientation.

In the AL-facing-FW mode, the adsorption of tannic acid on the active layer of the membrane was affected by both permeations drag and shear force induced by cross flow on the bulk feed solution side. Since the initial flux was aligned, the initial permeation drag in the two cases can be regarded as similar. When the active layer of membrane faces the feed solution, shear forces can hinder the adsorption of tannic acid molecules on the active layer of the membrane, and the smoother active layer prevents tannic acid molecules from entering the porous supporting layer, resulting in reduced tannic acid adsorption.

In summary, the stabilization of water flux and high tannic acid retention (i.e., low fouling tendency) was favored during the purification of tannic acid by forward osmosis in the AL-facing-FW orientation at the expense of more severe ICP and flux inefficiency compared to the alternative orientation.

4. Effect of initial concentration of tannic acid

Figure 7.11 illustrates the effect of initial concentration of tannic acid on filtration flux and retention performance of the forward osmosis membrane. As observed, the FO membrane flux significantly declined at an increasing rate as the initial concentration of tannic acid increased. This is consistent with studies of RO/NF [53]. With an initial concentration of tannic acid of 45 mg/L, the FO membrane flux fell 50% during the first 3 h. This may be attributed to severe internal clogging in the supporting layer. As shown in Figure 7.11(c), the adsorption of tannic acid per square centimeter of supporting layer increased significantly at higher initial concentration of tannic acid. This result supported the above explanation. Tang *et al.* [53] claimed that the collision frequency of NOM molecules onto the membrane surfaces increased with the high initial concentration of feed solution. Hence, high initial concentration of feed solution promotes the adsorption of NOM molecules onto the membrane. Additionally, the results revealed that the retention of tannic acid by FO membrane became slightly higher with the increased initial feed concentrations. Nevertheless, the initial tannic acid concentration had negligible effects on removal rate of tannic acid by the FO membrane. These results demonstrated that the FO membrane can treat the NOM in high concentrations in the NF concentrated water and brackish water.

5. Effect of pH

Figure 7.12 illustrates effects of pH (3.6, 5.8, and 7.8) on the purification of tannic acid by the FO membrane. Baseline flux was independent from pH, although the baseline flux at pH 3.6 slightly increased within 180 min initial filtration. This may be attributed to the fact that this pH value is close to the isoelectric point of the CTA membrane. In this case,

EBSCOhost - printed on 2/14/2023 6:39 AM via . All use subject to https://www.ebsco.com/terms-of-use

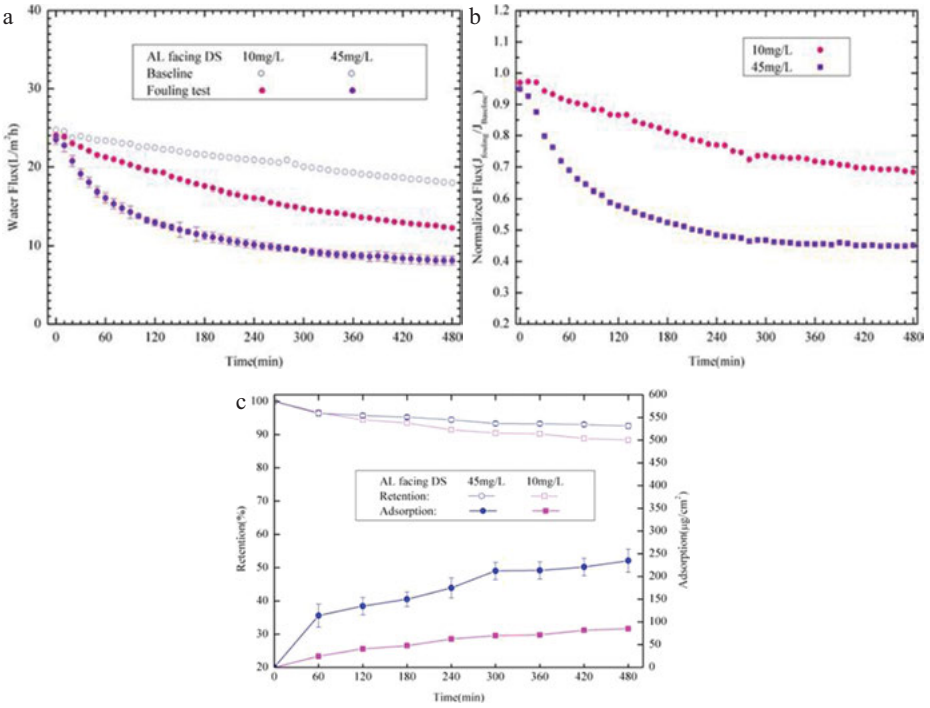

Figure 7.11: Effect of initial organic concentration on purification of tannic acid.

effective negative charges on the membrane surface were less, which may affect the flow channel structure in the supporting layer [54]. As shown in Figure 7.12(a), fouling fluxes induced by the tannic acid solution on the FO membrane at pH 3.6 and 7.8 were similar. As shown in Figure 7.12(b), the reduction of fouling fluxes at pH 3.6 and 7.8 were approximately 10% compared to that at pH 5.8 from 2 h to the end of the fouling test. In summary, the effect of the pH value of feed solution on fouling flux in forward osmosis was minor in this study, which is consistent with the study of Zou *et al.* [38].

Results revealed that the pH value of feed water had negligible effects on the removal rate of tannic acid. Indeed, removal rates of tannic acid exceeded 99.0% at all pH values, although the adsorption was extremely variable (see Figure 7.12(c)). After the initial filtration (≥3 h), the adsorption of tannic acid on the FO membrane decreased as the pH value increased, resulting in the high retention rate of tannic acid. Adsorption rate of tannic acid increased slowly for the high pH, which can be attributed to the increasing effective negative charges on the membrane surface and tannic acid at this high pH level. Previous studies have demonstrated that negative charges on the CTA membrane surface increased with the increasing pH [54]. Additionally, tannic acid molecules may be neutral with a pH < 4.5 and negatively charged with pH value > 4.5 (i.e., the isoelectric point of tannic acid was approximately 4.5). Thus, the dissociated tannic acid molecules can be exposed to electrostatic repulsion

EBSCOhost - printed on 2/14/2023 6:39 AM via . All use subject to https://www.ebsco.com/terms-of-use

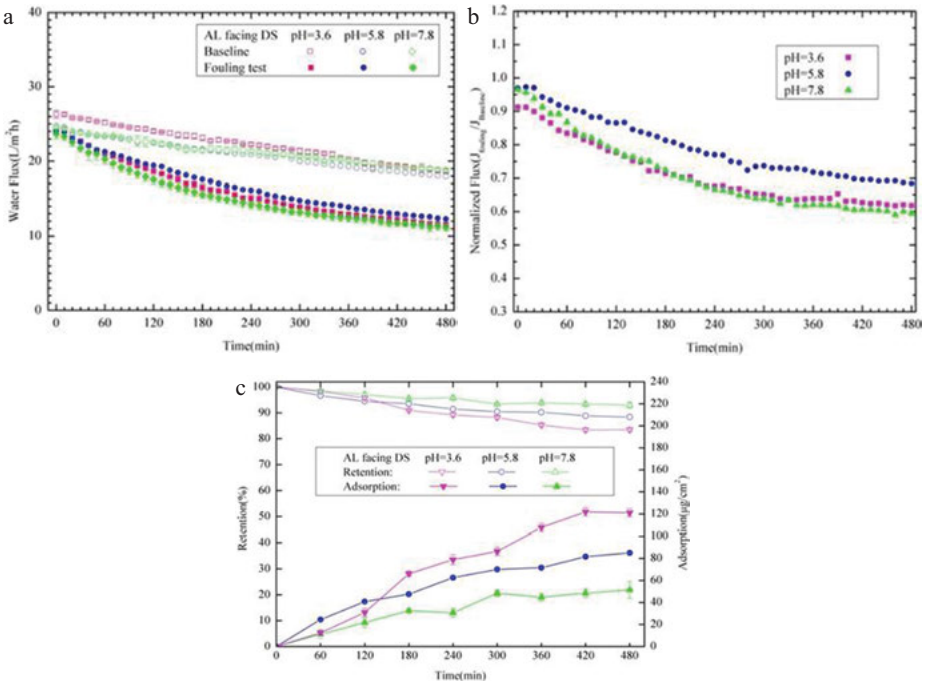

Figure 7.12: Effect of pH on purification of tannic acid.

with the negatively charged FO membrane and the tannic acid molecules adsorbed on the membrane surface, resulting in reduced adsorption at high pH [55]. At high pH value, the adjacent functional groups in the molecules were exposed to strong electrostatic repulsion and the tannic acid presented a large linear molecular structure, resulting in a loose fouling layer in the supporting layer [50]. Studies of NF and RO have also revealed that the adsorption of DOM on membrane surfaces increases as the pH decreases [50, 54]. Unlike NF and RO, however, the reduced adsorption of tannic acid did not significantly enhance the flux of the FO membrane. The reduced adsorption of tannic acid at high pH may be due to that the fouling layer of FO membrane was looser and the FO process was free from hydraulic pressure (as compared with pressure-driven processes). Hence, the reduced adsorption of tannic acid and a looser fouling layer can significantly change the compact and dense fouling layer during NF and RO, but not the original loose fouling layer and the corresponding fouling flux in FO.

6. Effect of ionic strength

Figure 7.13 illustrates the effect of ionic strength (calcium ions) of the feed solution on the purification of tannic acid by FO. Ca^{2+} concentration in the feed solution had a negligible effect on the baseline flux. However, the FO flux decreased signif-

EBSCOhost - printed on 2/14/2023 6:39 AM via . All use subject to https://www.ebsco.com/terms-of-use

icantly as the Ca^{2+} concentration increased in presence of tannic acid. As shown in Figure 7.13(b), the membrane fouling at a 1 mM Ca^{2+} was severe, and the normalized flux of FO decreased from 80% to 52%.

The results revealed that Ca^{2+} concentration in the feed solution had a minor effect on the removal of tannic acid by FO. However, the adsorption of tannic acid onto the membrane surface decreased as the Ca^{2+} concentration increased (see Figure 7.13(c)), resulting in enhanced retention rate of tannic acid by the FO membrane in feed solution containing Ca^{2+}.

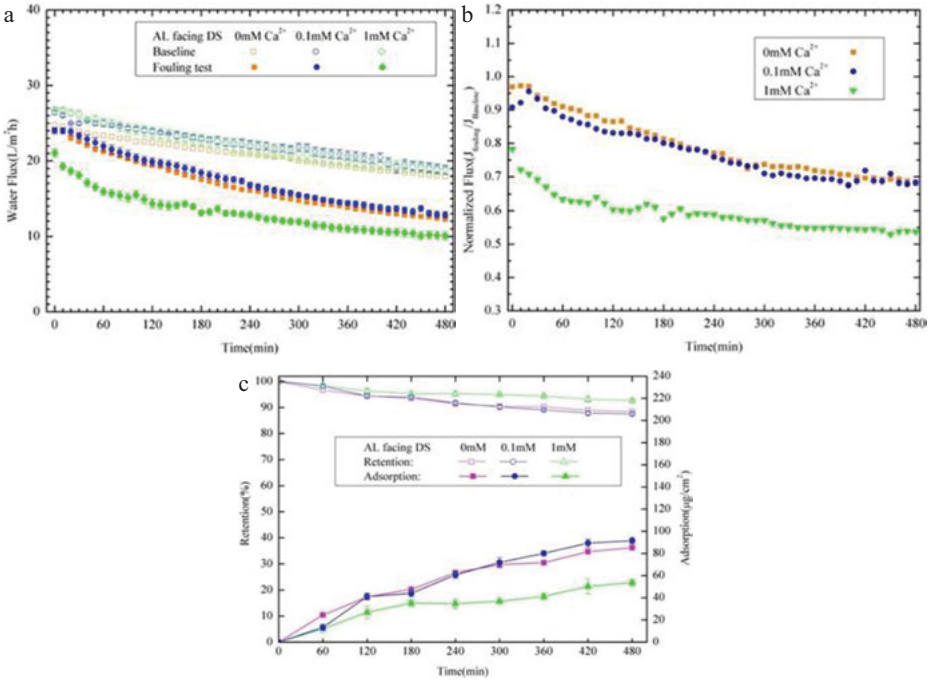

Figure 7.13: Effect of Ca^{2+} concentration on purification of tannic acid.

The effect of calcium ions on the fouling of pressure-driven membranes (i.e., NF and RO membranes) have been thoroughly investigated. It has been pointed out that Ca^{2+} may reduce the foulant charges by binding with carboxyl-based acidic functional groups through complex formation, thus increasing foulant adsorption onto the membrane surfaces [50]. However, in our study, Ca^{2+} in the feed solution had a negative effect on adsorption of tannic acid onto the membrane surface (see Figure 7.13(c)). Although charge neutralization and the intermolecular binding of tannic acid molecules by calcium ions were beneficial to the adsorption of tannic acid on the membrane surface, lower permeation drag caused by the significantly reduced initial flux of forward osmosis may hinder the adsorption of tannic acid on the membrane surface.

EBSCOhost - printed on 2/14/2023 6:39 AM via . All use subject to https://www.ebsco.com/terms-of-use

Additionally, severe flux drop at high Ca^{2+} concentration can be partially attributed to the small coiled molecular morphology of tannic acid [50], which may result in a more dense fouling layer of tannic acid in the supporting layer and thus more severe internal clogging (i.e., more severe ICP) compared to the absence of calcium ions.

7.4.2.3 Purification of natural DOM by forward osmosis

Figure 7.14 shows the purification of natural DOM by forward osmosis. During the FO filtration, the membrane fouling flux in the AL-facing-DS mode dropped drastically, whereas the fouling flux remained stable in the AL-facing-FW mode, as the initial TOC concentration of feed water increased. Like the tannic acid fouling tests in Section 7.4.2.2, the FO membrane exhibited low fouling tendency and water flux stability in the AL-facing-FW mode, regardless of the initial TOC concentration of natural DOM. However, the AL-facing-DS mode is prone to more severe water flux loss with increased initial TOC concentration of natural DOM.

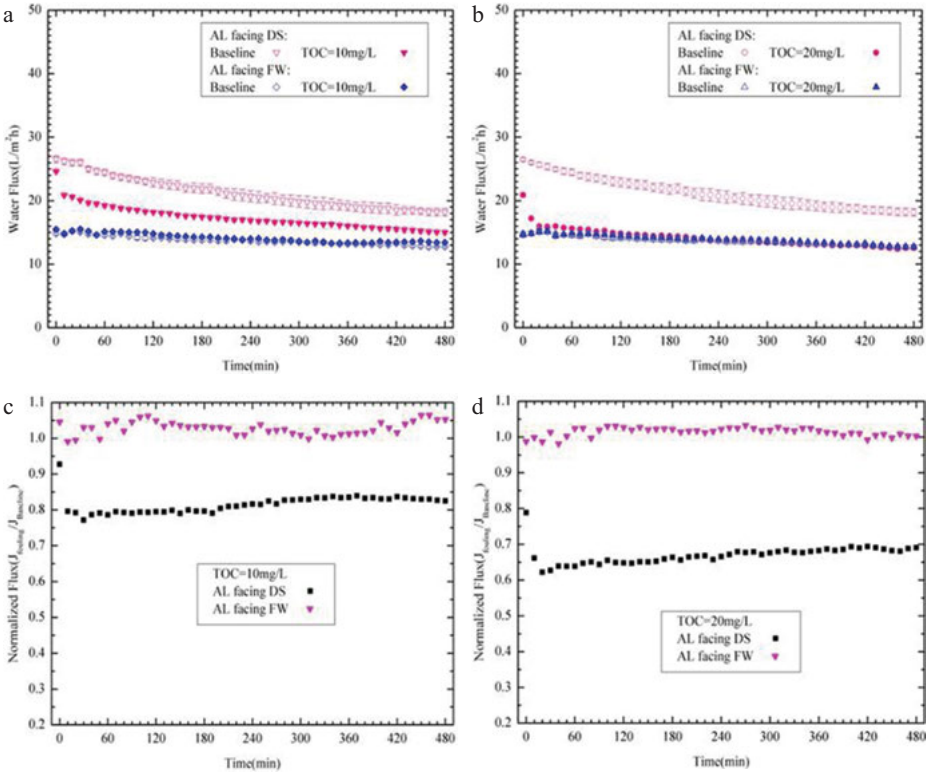

Figure 7.14: Natural DOM purification tests with FO membrane in two membrane orientations.

EBSCOhost - printed on 2/14/2023 6:39 AM via . All use subject to https://www.ebsco.com/terms-of-use

Zhao *et al.* [49] reported the iso-flux point in forward osmosis, i.e., the point where water fluxes under different membrane orientations were equal. At initial TOC concentration of 10 mg/L, the fouling flux in the AL-facing-DS mode was higher than that in the AL-facing-FW mode during the entire experiment period (Figure 7.14(a)). At initial TOC concentration of 20 mg/L, the fouling fluxes under different membrane orientations were equal at 6 h (see Figure 7.14(b)). In other words, the iso-flux point was only observed at this initial TOC concentration. At initial TOC concentrations of 10 and 20 mg/L, normalized fluxes in the AL-facing-DS mode dropped by 20% and 35%, respectively, within the very start ($t \leq 30$ min) and then stabilized at the corresponding normalized flux level until the end of the FO filtration (see Figure 7.14(c, d)). This demonstrates that the fouling tendency of raw water, with initial TOC concentrations of 10 and 20 mg/L, was high at initial stages of FO filtration, but lower in subsequent stages. According to the concept of the iso-flux point in this study, its presence at initial TOC concentration of 10 mg/L was later, and thus FO flux was favored in the AL-facing-DS mode; its presence at initial TOC concentration of 20 mg/L was earlier, and thus FO flux was favored in the AL-facing-FW mode.

Experimental results revealed that removal rates of natural DOM by FO, with different initial TOC concentrations, exceeded 99.0% under both membrane orientations during the 8 h filtration period. This is consistent with results of previous studies on the removal of tannic acid by FO. As shown in Figure 7.15, the adsorption of natural NOM at the initial stage of the test was negligible under both membrane orientations at different initial TOC concentrations. As a result, the retention rates of natural DOM by FO exceeded 98.0%.

Based on the relatively low adsorption of tannic acid on the FO membrane at high Ca^{2+} concentration (1 mM) and pH value (pH = 7.8), the negligible adsorption of natural DOM in the AL-facing-DS mode may be partially attributed to the conditions of the concentrated raw water, e.g., higher Ca^{2+} concentration (~4.1 mM) and pH value (~8.5).

In addition, as shown in Figure 7.8(a), the first peak of natural DOM at 1,004,680 Da exhibited relatively low UVA response. Hence, the DOM of 1004.68 kDa may consist of macromolecules with low-UVA responses, such as hydrophilic polysaccharides and proteinaceous substances [56]. As water from Taihu Lake was characterized with severe eutrophication, these low-UVA macromolecules may originate from microbial biopolymers and exopolymers generated by phytoplankton and algae in the Taihu Lake water. Although these macromolecules with low UVA responses only account for a small part of the total natural DOM (about 2% of the total peak area of TOC, as shown in Figure 7.8(b)), these macromolecules may affect the adsorption of natural DOM by the FO membrane in the AL-facing-DS mode.

At the initial filtration stage, the natural DOM molecules were brought to the rough porous supporting layer of the FO membrane by permeation drag induced by initial flux. Due to the surface resistance resulting from the rough supporting layer, these molecules migrated more slowly, as compared with those in the bulk feed solution. These macromolecules, with slower movement, had large sizes that can be regarded

EBSCOhost - printed on 2/14/2023 6:39 AM via . All use subject to https://www.ebsco.com/terms-of-use

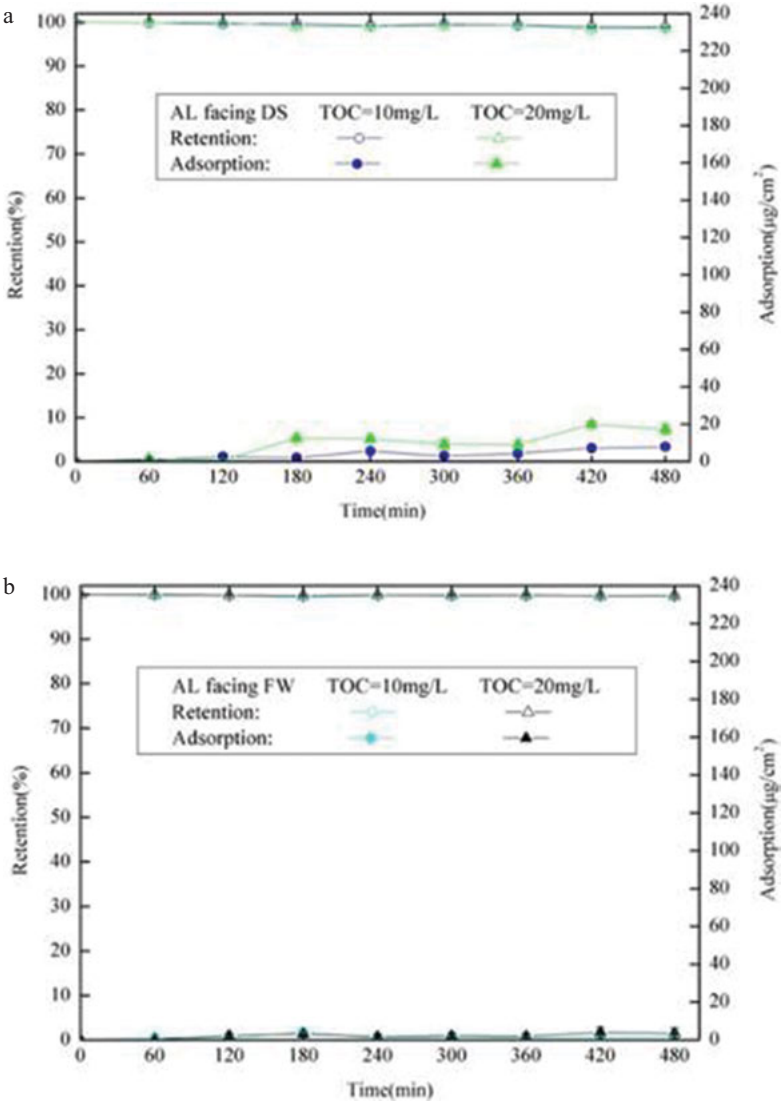

Figure 7.15: The natural DOM retention and adsorption by FO membrane at initial TOC concentration of 10 mg/L and 20 mg/L.

as a moving "cake layer", which may lead to increased thickness of the supporting layer. Owing to the negligible adsorption of DOM in the supporting layer, few DOM molecules were entrapped within the supporting layer and these organic compounds caused no significant changes to the porosity of the FO membrane. Assuming that all other parameters in Eq. (7.7) were constant during membrane fouling, the increasing membrane thickness led to increasing solute resistivity K and exacerbated ICP, in turn, resulting in drastic flux drop at the initial FO filtration stage ($t \leq 40$ min). Due to

EBSCOhost - printed on 2/14/2023 6:39 AM via . All use subject to https://www.ebsco.com/terms-of-use

decreased flux and the correspondingly reduced permeation drag, the quantity of DOM brought to the FO membrane surface was reduced. Hence, the effect of macromolecules on the membrane thickness was lessened. In this way, the growth of membrane thickness was decelerated, such that the drastic flux decline decelerated after the initial stage (t > 40 min). Additionally, the macromolecules partially hindered natural DOMs with low molecular weight (e.g., 1,082 Da) from entering the supporting layer.

In summary, the adsorption of natural DOM on the FO membrane, as well as the fouling flux trend in the AL-facing-DS mode, was different from that of tannic acid. The mechanism of membrane fouling by DOM in FO purification of natural surface water warrants further study.

7.4.3 Summary

This study focused on the purification of DOM in concentrated natural surface water by an FO membrane. Physical and chemical factors affecting water flux and retention by the FO membrane were investigated with tannic acid as the surrogate for natural DOM. The following conclusions can be drawn:

(1) For both AL-facing-DS and AL-facing-FW orientations, the FO membrane can effectively remove the tannic acid and natural DOM.
(2) In the AL-facing-DS orientation, the permeation drag induced by water flux may play a dominant role in the adsorption of tannic acid and natural DOM into the porous supporting layer of FO membrane.
(3) Higher concentrations of foulants (i.e., tannic acid and natural DOM) and Ca^{2+} in the feed solution led to more significantly decreased fouling flux, but increased retention of foulants.
(4) The membrane orientation had negligible effect on the removal of natural DOM by the FO membrane.

As a new separation technology, the results of this study could provide a framework for the future research on the treatment of natural surface water by forward osmosis.

7.5 Study on the purification efficiency of mixed organic foulants by FO technology

Although forward osmosis (FO) exhibits low fouling tendency and high fouling reversibility compared to nanofiltration (NF) and reverse osmosis (RO), the practical water treatment by FO is mainly limited by membrane fouling, especially organic fouling by dissolved organic matter (DOM). As compared with a single foulant, molecular weight distribution and hydrophobicity of mixed organic foulants are more complicated, leading

EBSCOhost - printed on 2/14/2023 6:39 AM via . All use subject to https://www.ebsco.com/terms-of-use

to even more complicated, distinguishing purification behavior by FO membrane. This study proposes systematic investigation of FO membrane fouling by mixed organic foulants and investigates key factors influencing it, including hydrodynamic factors (water flux level and cross-flow velocity) and conditions of the feed solution. Tannic acid and alginate were selected as the model organic foulants, and the mass adsorption of individual foulants in mixed fouling layers and the correlation with flux decline under different conditions was quantified to investigate mechanisms of mixed organic fouling.

7.5.1 Materials and methods

7.5.1.1 FO membrane

The flat sheet cellulose triacetate (CTA) FO membranes were purchased from Hydration Technology, Inc. (HTI, USA) and more detailed characteristics are described in Section 7.4.1.1 and Section 7.4.2.2.

7.5.1.2 Feed and draw solution

Unless otherwise specified, all chemical reagents used in this study were of analytical grade. All solutions were prepared using Milli-Q water (resistivity = 18.2 MΩ•cm). The draw solute used was sodium chloride (NaCl, purchased from Sinopharm Chemical Reagent Co. Ltd., China).

Sodium alginate ($(NaC_6H_7O_6)n$, SA) and tannic acid (TA) were used as model organic foulants. SA and TA represent polysaccharides and humic substances, respectively, which are commonly observed in natural water. TA is a hydrophilic substance with low molecular weight and a polyphenol structure [57]. SA is a negatively charged (in water) hydrophilic polysaccharide originating from algae and bacteria [56]. SA has high molecular weight and consists of two typical monomers, repeating mannuronic and guluronic acid residues [56, 58].

7.5.1.3 FO experiments

The primary FO tests were conducted using a bench-scale cross-flow FO membrane module. Section 7.4.1.3 presents a detailed description of this FO membrane system. A new membrane coupon was used for each test. A FO test consisted of both preparation and fouling tests. In the preparation test, the membrane was loaded in the module for equilibration. The draw solution was aligned with that in the fouling test, whereas the feed solution had a similar background electrolyte but contained no foulants. Equilibration was conducted for at least 30 min until the stabilization of water

EBSCOhost - printed on 2/14/2023 6:39 AM via . All use subject to https://www.ebsco.com/terms-of-use

flux. In fouling tests, foulants were added to the feed solution and each fouling test had a period of 8 h. The initial pH value of feed solution was adjusted using a HCl and/or NaOH solution, and the pH value of the solutions could be kept constant. To ensure the reliability of flux data, the test under each working condition was repeated at least once depending on the criticality of the data. In each test, only one parameter (e.g., foulant concentration, initial flux, cross-flow velocity, pH value, and concentration of Ca^{2+}) was selected to be variable, while others remained constant. Unless otherwise stated, conditions adopted for the fouling tests were as follows:

Feed solution: 10 mg/L mixed foulants concentration (5 mg/L TA concentration and 5 mg/L SA concentration), 10 mM ionic strength (adjusted by NaCl), pH = 6.5 ± 0.1;
- Draw solution: concentrated NaCl solution (0.5–4.0 M);
- Membrane orientation: AL-facing-DS orientation;
- Cross-flow velocity on both sides of membrane: 17.4 cm/s;
- Temperature: 22 ± 1 °C.

As the fouling test progressed, the osmotic driving force for FO flux kept decreasing due to the dilution of the draw solution and ICP. As a result, the continuous decline of water flux during the fouling test was induced by both membranes fouling and the reduction of apparent osmotic driving force. Therefore, baseline tests were conducted to eliminate the water flux loss attributed to the reduction of osmotic driving force. A baseline test was conducted for each condition. In baseline tests, all operation parameters were aligned with the corresponding fouling test, except that no foulants were present in the feed solution. Results of baseline test were used to calculate the normalized flux in the fouling test. Normalized flux is the ratio of practical fouling flux ($J_{Fouling}$) in the fouling test and baseline flux ($J_{Baseline}$) at a corresponding moment in the baseline test. It solely reflects the degree of membrane fouling. The membrane flux under specific conditions was described by both practical fouling flux and normalized flux.

7.5.1.4 Analysis method

1 Analysis of molecular weight and hydrophobicity of organic substances

The molecular weight distributions of foulants were investigated using a high-performance liquid chromatograph (HPLC, Waters e2695, USA) with an ultraviolet absorbance (UVA) detector (Waters 2489, USA) and a total organic carbon (TOC)-specific detector (Modified Sievers 900 Turbo, USA). Analysis methods of the above listed instruments are described in Section 7.4.1.5.

Through solid-phase extraction, foulants can be divided into strong hydrophobic components (HPO), transphilic components (TPI) and hydrophilic components (HPI) using Amberlite XAD-8 and XAD-4 resins [47]. The concentration of each component was measured using the TOC analyzer.

EBSCOhost - printed on 2/14/2023 6:39 AM via . All use subject to https://www.ebsco.com/terms-of-use

2 Removal rate, retention rate, and adsorption of foulant

In purification tests of mixed foulants, the concentration of single or mixed components were examined using the TOC measurements [57] to calculate removal rate and retention rate, as well as foulant adsorption on the membrane. The detection limit of the TOC analyzer for high-salt samples was approximately 0.1 mg/L.

For the analysis of the adsorption of foulants in the fouling layer on the FO membrane, the TA concentration were calculated using the standard curve method. A more detailed calculation method for the adsorption of TA and SA is shown in our previous study [59].

Blank tests were involved to eliminate deposition of foulants on other apparatus of the FO system (e.g., tubes and membrane module spacers). In blank tests, no membrane was loaded in the membrane module, whereas other parameters were aligned with those in fouling tests. The mass of foulant was measured before and after tests, and results suggested that the additional adsorption of single and mixed foulants on other apparatus of the FO system were negligible.

To verify the validity of equations for removal rate, retention rate, and adsorption of foulants by the FO membrane, foulants were extracted from the FO membrane to determine the actual amount of foulants adsorbed onto the membrane. After fouling tests, membranes were sonicated in dilute NaOH solution (pH = 10.5) at 25 °C for 15 min, until the desorption equilibrium of foulants. Then, the quantity and composition of foulants were determined and compared with mass balance calculation results (see Table 7.4). The results obtained by the mass balance calculation, and results obtained using the extraction measurement, were statistically similar under the given operating conditions, demonstrating good validity of the equations used.

Table 7.4: Mass adsorption of mixed and single foulants in FO.

Operating condition	Total adsorption (μg/cm²)		Tannic acid adsorption (μg/cm²)		Alginate adsorption (μg/cm²)	
	Mass balance calculation	Direct extraction measurement	Mass balance calculation	Direct extraction measurement	Mass balance calculation	Direct extraction measurement
FW: 2 mg/L tannic acid and 8 mg/L alginate DS: 2 M NaCl	36.60	37.18	30.37	30.67	6.23	6.51
FW: 5 mg/L tannic acid and 5 mg/L alginate DS: 4 M NaCl	97.94	98.26	93.59	94.37	4.35	3.89

EBSCOhost - printed on 2/14/2023 6:39 AM via . All use subject to https://www.ebsco.com/terms-of-use

Table 7.4 (continued)

Operating condition	Total adsorption (μg/cm²)		Tannic acid adsorption (μg/cm²)		Alginate adsorption (μg/cm²)	
	Mass balance calculation	Direct extraction measurement	Mass balance calculation	Direct extraction measurement	Mass balance calculation	Direct extraction measurement
FW: 5 mg/L tannic acid and 5 mg/L alginate (cross-flow velocity: 1.7 cm/s) DS: 2 M NaCl	32.80	33.65	29.82	31.82	2.98	1.83
FW: 5 mg/L tannic acid and 5 mg/L alginate (pH = 7.8 + 1 mM Ca) DS: 2 M NaCl	36.63	37.30	29.17	29.33	7.46	7.97

3 Measurement of resistance by the FO membrane

In mixed foulant tests, the fouling characteristics of single or mixed foulants by the FO membrane were investigated using the serial resistance model. The membrane flux, J_w, can be calculated by:

$$J_w = \frac{\Delta P}{\mu R_t} = \frac{\Delta P}{\mu(R_m + R_s + R_p)} \tag{7.15}$$

where J_w is the membrane flux; ΔP is the transmembrane pressure difference (Pa); μ is the viscosity of the permeate (Pa · s); R_t is the overall resistance (m^{-1}); R_m is the intrinsic resistance induced by membrane structure and the concentration polarization of feed water (m^{-1}); R_s is the surface resistance induced by the fouling layer deposited on the supporting layer (m^{-1}); and R_p is the internal resistance induced by pore plugging within the supporting layer (m^{-1}). These resistances were measured using methods reported elsewhere [60, 61] and as follows: (i) 2 M NaCl and DI water were used as draw solution and feed water, respectively, and the average membrane flux of the clean membrane within the first hour was measured to determine the R_m; (ii) After each 8 h filtration cycle, draw solution and feed solution were replaced with fresh 2 M NaCl solution and DI water. The average membrane flux of the used FO membrane within the first 30 min was measured to determine the R_t; and (iii) the fouled membrane was extracted and flushed using DI water to remove the surface fouling layer. Then, the pure water flux of the rinsed membrane within the first 30 min was measured with 2 M NaCl as draw

EBSCOhost - printed on 2/14/2023 6:39 AM via . All use subject to https://www.ebsco.com/terms-of-use

solution to obtain the sum of $R_m + R_p$. The fouling resistance, R_s, was determined by subtracting $R_m + R_p$ from R_t. Finally, the fouling resistance of pore plugging R_p was then obtained by subtracting R_s and R_m from R_t.

7.5.2 Results and discussion

7.5.2.1 Composition characteristics of tannic acid and alginate

Figure 7.16 shows hydrophobic/hydrophilic components of tannic acid and alginate as measured experimentally. As reported in our previous study, the hydrophobic/hydrophilic components of tannic acid were similar to those of DOM in natural surface water [57]. Hence, tannic acid can be used as a model foulant for natural DOM. Compared with tannic acid, alginate was characterized by larger content of hydrophilic components and higher hydrophilicity. Therefore, alginate is an ideal model foulant for hydrophilic organics in natural surface water.

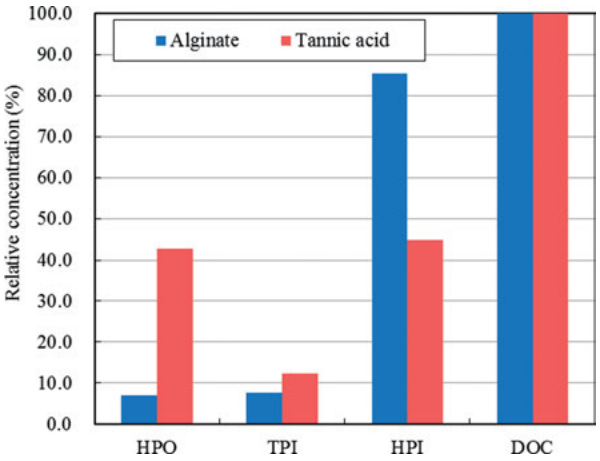

Figure 7.16: Organic fractionations of tannic acid and alginate.

Figure 7.17 illustrates distributions of the molecular weights of tannic acid and alginate. For UVA (Figure 7.17(a)) and TOC (Figure 7.17(b)) of tannic acid, two peaks were observed. The apparent molecular weight (AMW_{UVA}) at the two top peaks was 1,394 Da and 699 Da, respectively. According to the higher proportion of the TOC area of the peak in the total TOC, the 1,394 Da component was dominant in tannic acid. Notably, the dominant molecular weight distribution of tannic acid was similar to that of DOM in natural surface water [57].

EBSCOhost - printed on 2/14/2023 6:39 AM via . All use subject to https://www.ebsco.com/terms-of-use

For TOC of alginate (see Figure 7.17(b)), two peaks were observed and the AMW_{TOC} of the top peak was estimated to be 407,210 and 1,993 Da. Despite the UVA detector exhibited a low peak response for AMW at 407,210 Da (see Figure 7.17(a)), the area of the TOC at the peak of 407,210 Da was approximately 89.2% of the overall TOC peak area, indicating that alginate is dominated by macromolecules with low UVA responses. In addition, the component with AMW_{TOC} of 1,993 Da may be attributed to the salt boundary peak. The

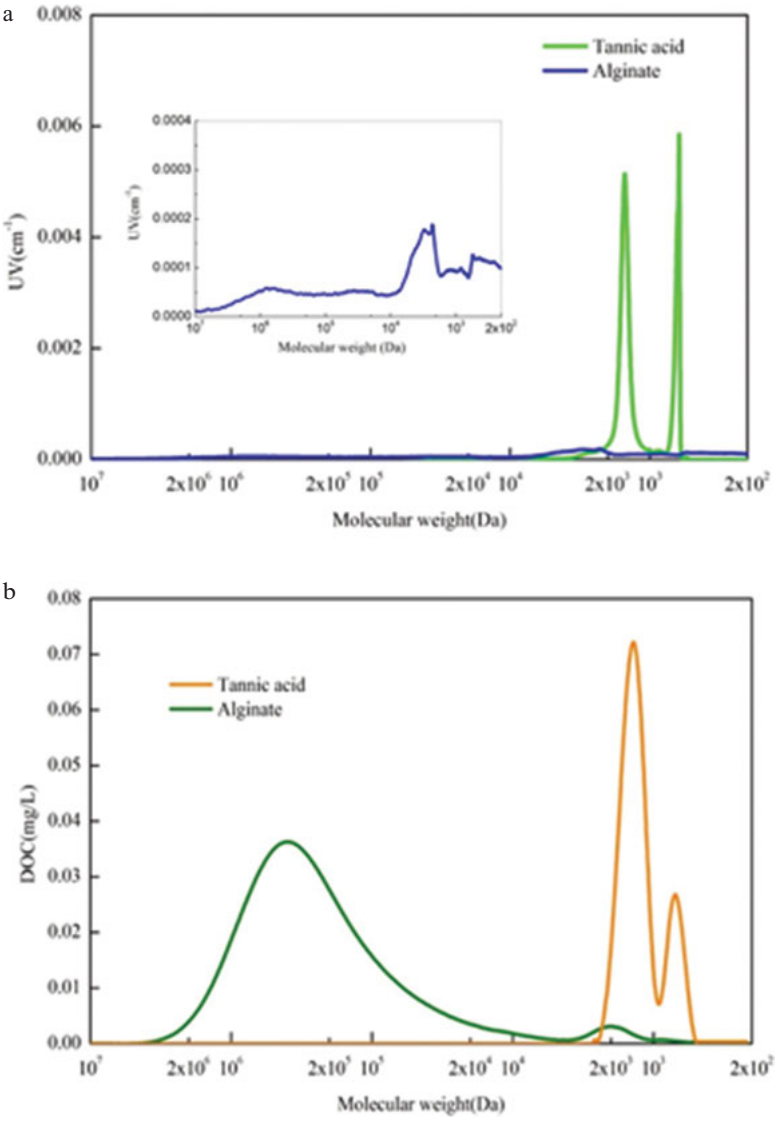

Figure 7.17: (a) UVA peaks versus MW distribution of tannic acid and alginate (10 mg C/L), and (b) DOC peaks versus MW distribution of tannic acid and alginate (10 mg C/L).

EBSCOhost - printed on 2/14/2023 6:39 AM via . All use subject to https://www.ebsco.com/terms-of-use

magnitude of the molecular weight of alginate (~10^5) seemed to be consistent with that of macromolecule organics with low UVA responses in natural surface water (10^5–10^6) [57]. This is one of the key reasons that alginate was selected as a surrogate for low-UVA macromolecules. Additionally, the macromolecules with low UVA may possibly affect the adsorption characteristics of natural DOM by FO membranes.

7.5.2.2 Effect of feed organic foulant composition

The effect of concentration ratios of tannic acid to alginate in feed water on the purification of mixed organic foulants by FO were investigated. The overall foulant DOC concentration in feed water was set to 10 mg/L. Figure 7.18(a, b) shows the baseline and fouling fluxes of the FO membrane, respectively, with initial flux of 25 L/($m^2 \cdot h$) (i.e., 2 M NaCl as the draw solution).

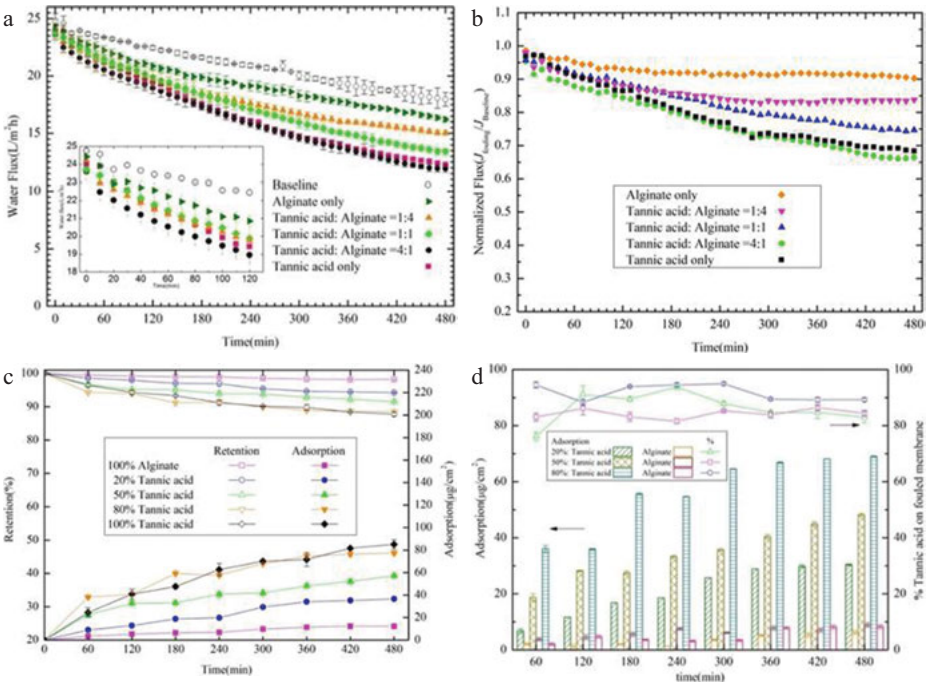

Figure 7.18: Effect of feed organic foulant composition on mixed foulants purification.

During the entire filtration period, the flux decline of feed water containing alginate alone was minimal (~10% flux loss). This may be attributed to the fact that the initial flux was lower than the critical flux for the alginate fouling [62]. As the relative concentration of tannic acid in feed water increased from 20% to 80%, FO fouling flux dropped more drastically. When the relative concentrations of tannic acid were 80% and 100%,

EBSCOhost - printed on 2/14/2023 6:39 AM via . All use subject to https://www.ebsco.com/terms-of-use

the most severe fouling occurred and the reduction of fouling flux was up to ~30%. Although the reductions of normalized initial flux at different foulant concentration ratios during the early 2 h of FO filtration were similar, the reduction of normalized flux decelerated and approached the quasi-steady state after 2 h filtration when the feed water contained a minor amount of tannic acid (e.g., 20% tannic acid), as seen in Figure 7.18(b). This demonstrated that the concentration ratio of foulants in feed water had a negligible effect on the reduction of initial fouling flux, whereas the presence of tannic acid may have facilitated the fouling of the FO membrane compared to alginate.

For the AL-facing-DS orientation, the removal rate of alginate and mixed foulants was at or above 99.0%, which is consistent with that of tannic acid in the earlier studies [57]. The stable complete removal rates suggested that FO membranes can effectively remove medium molecules (e.g., tannic acid) and macromolecules (e.g., alginate), regardless of the concentration ratio of mixed foulants. As discussed in our previous studies, low adsorption and thus high retention rates indicated good performance of FO in purification of DOM. Figure 7.18(c) illustrates the total adsorption of mixed foulants on the membrane surface and the retention rates by the FO membrane.

As shown in Figure 7.18(c), the retention rate by the FO membrane degraded drastically with the concentration ratio of tannic acid in feed water increased from 0 to 100%. This may be attributed to increased foulant adsorption on the membrane due to the higher relative concentration of tannic acid. When the concentration ratio of tannic acid was 20%, the overall adsorption of foulants at the end of FO filtration was ~40 μg/cm^2, whereas in absence of tannic acid it was ~10 μg/cm^2. When the concentration ratio of tannic acid was 50~100%, the overall adsorption of foulants increased further, resulting in the drastic flux drop under those conditions.

To fully understand the adsorption of foulants in the mixed fouling system, the adsorption of tannic acid and alginate on the membrane and the ratio of tannic acid in adsorbed foulants during the entire filtration period was shown in Figure 7.18(d). Figure 7.19 shows the membrane resistances measured experimentally in order to elucidate the fouling behavior of single or mixed foulants.

As shown in Figure 7.18(d), at a specific concentration ratio of tannic acid to alginate, the adsorption of tannic acid increased significantly as filtration progressed and stabilized gradually after the initial filtration stage of 4 h. However, the adsorption of alginate increased slightly with time, and approached a constant value (~10 μg/cm^2) at the end of filtration. This is consistent with results of feed water containing alginate only (Figure 7.18(c)). Additionally, the adsorption of tannic acid per square centimeter of support layer at a specific point increased significantly with the increase of the concentration of tannic acid in feed water. This may be attributed to the fact that the collision frequency of these organics onto the membrane surface increased with the higher initial concentration of tannic acid. The adsorption of alginate was not significantly affected by the concentration ratio of foulants in feed water. Notably, the ratio of tannic acid in all adsorbed foulants was nearly at or above 80% over the duration of filtration in all mixed fouling cases, including the case where the concentration of tannic acid in feed water

EBSCOhost - printed on 2/14/2023 6:39 AM via . All use subject to https://www.ebsco.com/terms-of-use

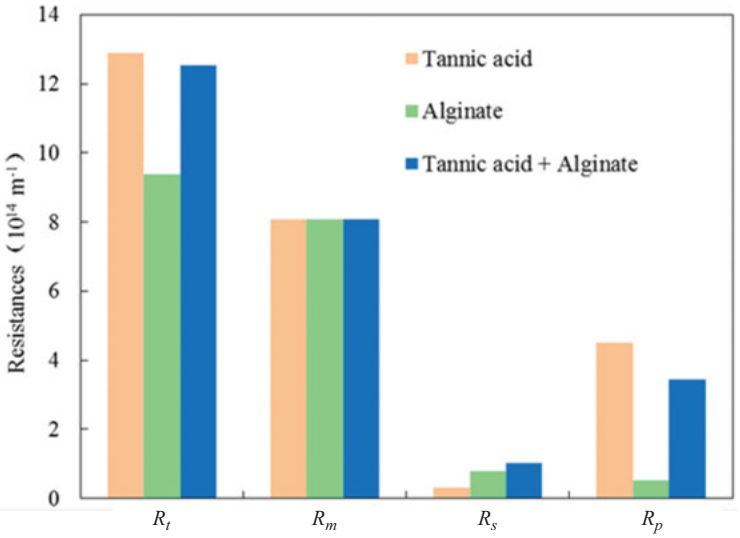

Figure 7.19: Membrane resistances of FO filtration of single or mixed tannic acid and alginate.

was 20%, demonstrating that the effect of tannic acid on FO membrane fouling were more significant than that of alginate in the mixed fouling system.

Figure 7.19 illustrates the effect of mixed fouling on the resistance of FO membrane. The overall membrane resistance R_t induced by tannic acid was larger than that induced by alginate, demonstrating that more severe membrane fouling occurs when a single tannic acid is in the feed. Among membrane resistances induced by tannic acid, the internal resistance R_p was approximately 35% of overall resistance, which was significantly larger than the surface resistance R_s. These results suggest that more tannic acid molecules prefer to be entrapped within the porous support layer, instead of its surface. Nevertheless, the surface resistance R_s was slightly larger than the internal resistance R_p for membrane fouling induced by alginate, indicating that alginate prefers to adsorb on the surface of the supporting layer. The membrane resistances with mixed fouling was similar to that of fouling by tannic acid, although the overall resistance R_t and the internal resistance R_p with mixed fouling was slightly lower than by tannic acid. This is consistent with the results of membrane flux shown in Figure 7.18(a, b), and further demonstrated the dominant role of tannic acid in mixed fouling of the FO membrane. Additionally, surface resistance R_s with mixed fouling was slightly higher than that by either organic. This may be attributed to the fact that some tannic acid molecules in the mixed fouling system were deposited on the membrane surface, instead of within the inner support layer. Experiments also revealed that intrinsic resistance R_m was the dominant component of overall resistance of the FO membrane in all cases, indicating the filtration performance by FO membranes could be effectively enhanced by reducing the intrinsic resistance and relieving the concentrated concentration polarization in the supporting layer.

EBSCOhost - printed on 2/14/2023 6:39 AM via . All use subject to https://www.ebsco.com/terms-of-use

Figure 7.20 shows the SEM images of the supporting layer of the FO membrane that was exposed to the fouling after filtration of feed water containing tannic acid, alginate, or mixed foulants. As shown in Figure 7.20(a), only minor NaCl salts deposited on the support layer of the FO membrane after fouling by tannic acid, and no visible tannic acid molecules were observed. This is consistent with the assumption that more tannic acid molecules adsorbed in the porous supporting layer. Nevertheless, an obvious organic fouling layer packed with NaCl crystal was observed on the surface of the supporting layer of the FO membrane after fouling by alginate (see Figure 7.20(b)). The alginate fouling layer had a sparse and loose structure, which may be attributed to the slight adsorption of alginate on the membrane surface and the absence of hydraulic pressure in FO. According to the fouling patterns of tannic acid and alginate on the membrane surface, the mixed fouling layer observed in Figure 7.20(c) is mainly attributed to alginate molecules accumulated on the surface of the support layer.

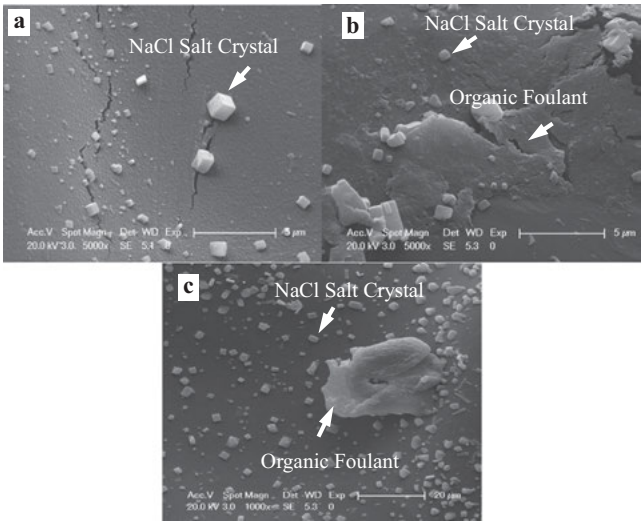

Figure 7.20: SEM image of fouled FO membranes sampled after (a) the tannic acid, (b) the alginate and (c) the mixed tannic acid and alginate fouling experiment with 10 mg/L of organics in the feed solution.

Based on the analysis of the mass adsorption and membrane resistances, as well as SEM images, the mechanism of single and mixed fouling can be deduced. First, for the AL-facing-DS orientation, more tannic acid molecules entered and adsorbed in the porous supporting layer because of the initial permeation drag caused by the convective permeate flow toward the membrane when the feed water contained greater tannic acid molecules, resulting in more severe internal clogging within the porous layer and thus reduced the porosity of the supporting layer. Eventually, the ICP effect was exacerbated and the flux decline was greater.

EBSCOhost - printed on 2/14/2023 6:39 AM via . All use subject to https://www.ebsco.com/terms-of-use

Previous studies have claimed that alginate molecules tend to form gel structures due to their greater intermolecular adhesion, resulting in a thicker fouling layer on the membrane surface and severe membrane fouling [42, 58]. However, this study showed that alginate did not induce severe FO membrane fouling with either single or mixed fouling. The results may be attributed to the different experimental conditions (e.g., the initial flux). In this study, a minority of alginate molecules entered the porous supporting layer under the effect of permeation drag induced by the initial flux, whereas the majority moved with the bulk solution in a direction parallel to the membrane surface under the effect of shear force induced by the cross flow. In the boundary layer that was close to the rough surface of supporting layer, the greater resistance hindered the migration of alginate molecules and a few alginate molecules eventually accumulated on the membrane surface. Instead of significantly altering the porosity of the supporting layer, the alginate molecules accumulated on the membrane surface can likely increase the thickness of the support layer and form a fluid-like, sparse, loose "cake layer" due to their large molecular sizes [63]. In this way, the thickness of the membrane increased, resulting in the enhanced hydraulic resistance to permeate flow through the membrane, and thus the flux decline.

For mixed fouling, the similar flux declines at the early stage suggested the minor effects of the ratio of the two foulants in the feed water on the initial FO fouling. As filtration progressed, the pore-clogging enhanced ICP [10] caused by the tannic acid might play a more significant role in exacerbating the FO flux decline than the fluid-like "cake layer" improved hydraulic resistance induced by the alginate. In summary, it implies that the FO membrane may favor the purification of alginate macromolecules with the stabilized filtration flux and high retention rate in mixed fouling of the FO membrane, as compared with tannic acid.

7.5.2.3 Effect of initial flux

The effect of the initial flux level (i.e., the initial concentration of NaCl in draw solution) on the purification of mixed foulants by FO membrane are shown in Figure 7.21. The initial flux was 8–36 L/($m^2 \cdot h$) (i.e., 0.5–4.0 M NaCl as draw solution).

Figure 7.21(a) shows the baseline and fouling fluxes of the FO membrane as a function of time under different initial flux levels. The initial flux can be increased with the increasing DS concentration. However, the higher initial flux at greater DS concentration (i.e., 2 M and 4 M) leads to severe fouling flux decline. This result is consistent with the single fouling test of tannic acid [57], as well as other studies of osmotically driven membranes (e.g., FO) [10, 38, 42, 64] and pressure driven membranes (e.g., RO and NF) [50, 51, 65]. As shown in Figure 7.21(b), the normalized flux reduced by approximately 10–15% during the first 20 min, which accounted for 40–50% of the overall flux drop during filtration, demonstrating that normalized flux

EBSCOhost - printed on 2/14/2023 6:39 AM via . All use subject to https://www.ebsco.com/terms-of-use

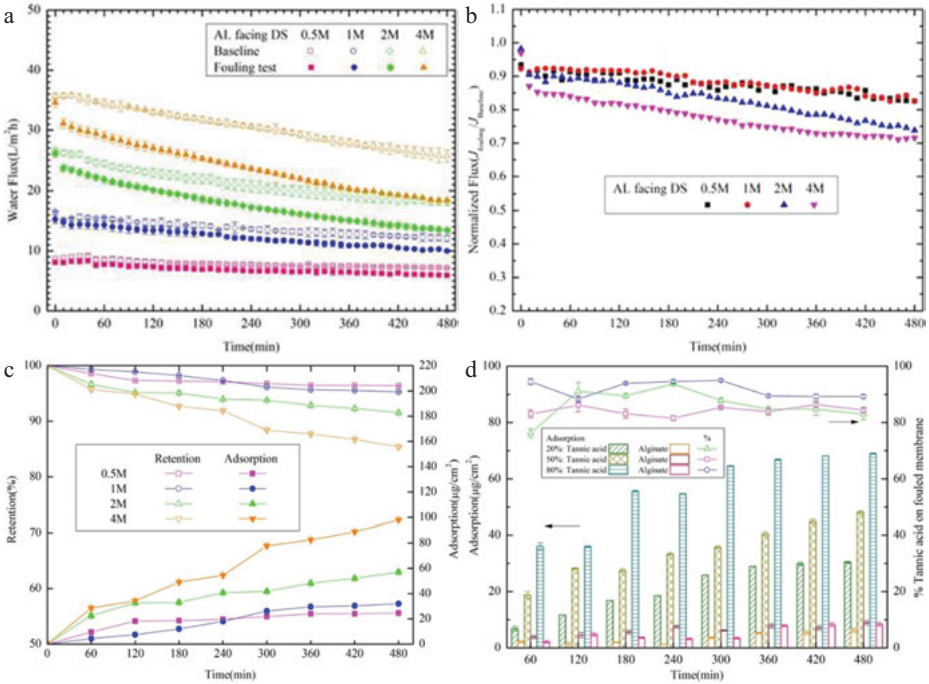

Figure 7.21: Effect of initial flux level on mixed foulants purification.

in mixed fouling reduced slowly after the initial drop at the early stage under the different initial flux levels. For this reason, the FO membrane flux tended to be stable during a longer filtration period. Additionally, the initial normalized flux dropped slightly during the first 3 h when the initial flux was ≤ 26 L/(m^2 · h) (i.e., DS concentration ≤ 2 M), however, the normalized flux at higher initial flux levels dropped drastically after the early 3 h of filtration (e.g., for 2 M), or from the beginning of filtration (e.g., for 4 M). A significant drop of mixed fouling flux of the FO membrane was only observed when the initial flux exceeded 16 L/(m^2 · h) (i.e., 1 M DS concentration). It is suggested that the concept of critical flux (defined as a flux below which the minor membrane fouling occurs, whereas above it significant membrane fouling is observed), coined by Tang et al. for the osmotically driven FO membrane [10, 38, 49, 52], is also applicable in the filtration of mixed foulants by the FO membrane in AL-facing-DS orientation.

Experiments revealed that the initial flux had the negligible effect on the removal of mixed foulants by the FO membrane. Indeed, the removal rates of mixed foulants by the FO membrane were above 99.0% under all the initial flux values. Nevertheless, as shown in Figure 7.21(c), the adsorption of mixed foulants increased and thus the retention rates decreased as the initial flux increased. This conclusion is consistent with that of single fouling by tannic acid [57]. However, the retention rate of mixed foulants was slightly higher (~5%) than that of tannic acid in single fouling

EBSCOhost - printed on 2/14/2023 6:39 AM via . All use subject to https://www.ebsco.com/terms-of-use

at various initial flux levels, demonstrating the advantage of FO membranes in the treatment of mixed organic foulants in natural water. Notably, tannic acid and alginate exhibited distinguished fouling behaviors at initial fluxes tested. As shown in Figure 7.21(d), more adsorption of tannic acid molecules onto the membrane surface occurred when the initial flux level (i.e., DS concentration) increased, whereas the minimal adsorption of alginate molecules onto the membrane surface was independent from the initial flux. It is suggested that the increasing initial flux may have a more pronounced effect on the adsorption of tannic acid than that of alginate on the FO membrane. Since the tannic acid adsorption was significantly affected by the FO flux, the absorbed mass percentage of tannic acid accounted for nearly 80.0–98.0% of the fouling layer over the duration of FO filtration regardless of the initial flux levels. This result once again suggests that tannic acid may be the dominant foulant in mixed fouling of the FO membrane under the initial flux tested.

According to the mechanism discussed in Section 7.5.2.2, the greater initial permeation drag was caused by higher initial flux. As a result, more tannic acid molecules were entrapped into the porous supporting layer and the pore-clogging enhanced ICP caused by the tannic acid aggravated, resulting in more severe membrane flux decline at elevated initial flux levels. However, greater permeation drag induced by higher initial flux seems to have a minor effect on improving the migration of alginate toward the supporting layer. As a result, higher initial flux did not lead to changes of alginate adsorption on the membrane surface. Mi and Elimelech [42] proposed that the effect of permeation drag on FO fouling induced by alginate were limited. She *et al.* [64] demonstrated that a thicker and denser fouling layer of alginate was observed on FO membrane surface under the higher initial flux, resulting in greater hydraulic resistances, which was not in accordance with conclusions in this study. This may be attributed to the high initial concentration of alginate (100 mg/L) and additional applied pressures on the side of feed water (i.e., PRO mode) in their research. Assuming similar fluid-like "cake layers" induced by some alginate developed on membrane surfaces under different initial fluxes, identical hydraulic resistance were generated. As a result, trends of initial fouling flux loss were similar (~15%).

Nevertheless, the continuous slow reduction of fouling flux after the initial drop may be mostly attributed to the adsorption of tannic acid in the supporting layer. The trends of the fouling flux decline (Figure 7.21(a, b)) were similar during the entire filtration period at low initial fluxes (0.5 M and 1 M DS concentration) and at the early stage (3 h) when initial flux was 26 L/($m^2 \cdot h$) (2 M DS concentration). This may be attributed to similar minor adsorption of tannic acid (~40 μg/cm^2 in Figure 7.21(d)) under these conditions. Compared with single fouling by tannic acid [57], the decelerated flux drop in mixed fouling may be related to the limited adsorption of tannic acid on the FO membrane due to the lower initial concentration of tannic acid (5 mg/L) in the mixed fouling treatment.

EBSCOhost - printed on 2/14/2023 6:39 AM via . All use subject to https://www.ebsco.com/terms-of-use

7.5.2.4 Effect of cross-flow velocity

Figure 7.22 illustrates the effect of cross-flow velocity on the purification of mixed foulants by FO. As shown in Figure 7.22(a), the initial baseline flux at low cross-flow velocity (1.7 cm/s) was 24% lower than that at high cross-flow velocity (17.4 cm/s). This may be attributed to the more severe external concentration polarization (ECP) caused by the lower cross flow velocity [38]. Additionally, it was demonstrated that the baseline flux was relatively stabilized at low cross-flow velocity compared to that at the higher cross-flow velocity. This may be attributed to the reduced dilution of the draw solution and concentration of feed water caused by less water passing through the FO membrane. Zou *et al.* [38] proposed that the dramatically reduced and stable baseline flux at low cross-flow velocity may result in a reduced tendency for FO membrane fouling. In this experiment, fouling fluxes at different cross-flow velocity were aligned at the end of filtration with mixed fouling, despite different initial fluxes (Figure 7.22(a)). As shown in Figure 7.22(b), the normalized flux at low cross-flow velocity exhibited a lower decline rate after the initial drop (~12%) at the early stage. Therefore, the normalized flux at low cross-flow velocity gradually exceeded that at high cross-flow velocity after 5 h of filtration, demonstrating the tendency of membrane fouling can be relieved by reducing the cross-flow velocity in the longer FO purification of mixed foulants. In contrast, previous studies have found that organic fouling of pressure driven membranes is exacerbated by reducing cross-flow velocity [66].

The present experiment revealed that the effect of cross-flow velocity on the removal rate of mixed foulants by FO membrane were negligible. Indeed, the removal rate of mixed foulants by the FO membrane at both cross-flow velocity was at or above 99.0%. As shown in Figure 7.22(c), the adsorption of mixed foulants at low cross-flow velocity was significantly lower, resulting in the enhanced retention rate. As shown in Figure 7.22(d), tannic acid was the dominant foulant on the fouled membrane compared to the alginate at both cross-flow velocities.

As mentioned above, the adsorption of tannic acid is mainly affected by the permeation drag. Due to the more severe reduced initial fouling flux at low cross-flow velocity, the permeation drag in this case was lower, resulting in the limited adsorption of tannic acid. Mi *et al.* reported that [42] the crossflow velocity in the supporting layer vanished, and the shear force induced by the crossflow velocity had a negligible effect on the organic foulant molecules in the porous supporting layer. This is consistent with the effect of cross-flow velocity on single fouling by tannic acid [59]. Nevertheless, the alginate macromolecules moved more slowly near the rough surface of the supporting layer at low cross-flow velocity in mixed fouling. As a result, the thickness of the boundary layer may increase, resulting in the increased hydraulic resistance caused by ECP. This phenomenon may be the cause of the notable flux decline at the early stage of FO filtration of mixed foulants at low cross-flow velocity, which is consistent with findings of single fouling by alginate at the same condition of

EBSCOhost - printed on 2/14/2023 6:39 AM via . All use subject to https://www.ebsco.com/terms-of-use

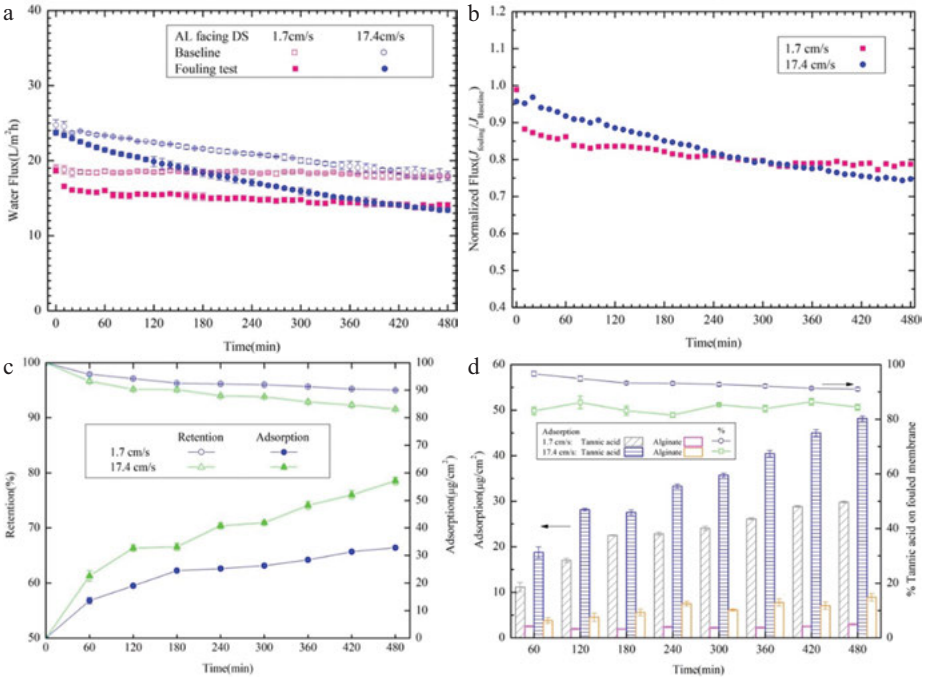

Figure 7.22: Effect of cross flow velocity on mixed foulants purification.

cross-flow velocity [59]. Due to the reduction of initial fouling flux and thus degraded permeation drag at low cross-flow velocity, the quantity of alginate molecules that migrated toward the membrane surface decreased, resulting in slightly reduced adsorption of alginate.

In summary, this suggests that the low cross-flow velocity has an influence on increasing the hydraulic resistance related to alginate-induced ECP, as well as aggravating the initial flux decline in mixed fouling. The reduction of initial fouling flux had an adverse effect on the adsorption of tannic acid. As a result, the pore-clogging enhanced ICP caused by the adsorption of tannic acid was relieved, thus partly compensating for the detrimental effect of low cross-flow velocity on mixed fouling flux at the early stage. Further research is needed into the optimization of cross-flow conditions for the improvement of FO efficiency.

7.5.2.5 Effect of feed solution chemistry

The effect of pH and concentration of calcium of feed water on the purification of mixed foulants by the FO membrane were also investigated in Figure 7.23. The feed water contained 5 mg/L tannic acid and 5 mg/L alginate. In fouling tests focusing on the effect of pH without calcium, the flux at filtration of feed water with pH 7.8 was

EBSCOhost - printed on 2/14/2023 6:39 AM via . All use subject to https://www.ebsco.com/terms-of-use

defined as baseline flux. In fouling tests focusing on the effect of calcium, the flux at filtration of feed water with pH 6.5 and 1 mM Ca^{2+} was defined as the baseline flux. As shown in Figure 7.23(a), the mixed fouling flux decline at pH 6.5 and 7.8 was nearly consistent, demonstrating that the effect of pH of feed water on mixed fouling were negligible. This is consistent with other studies on single organic fouling by Wang et al. [57] and Zou et al. [38], as well as the observation of single alginate fouling shown in Wang et al. [59].

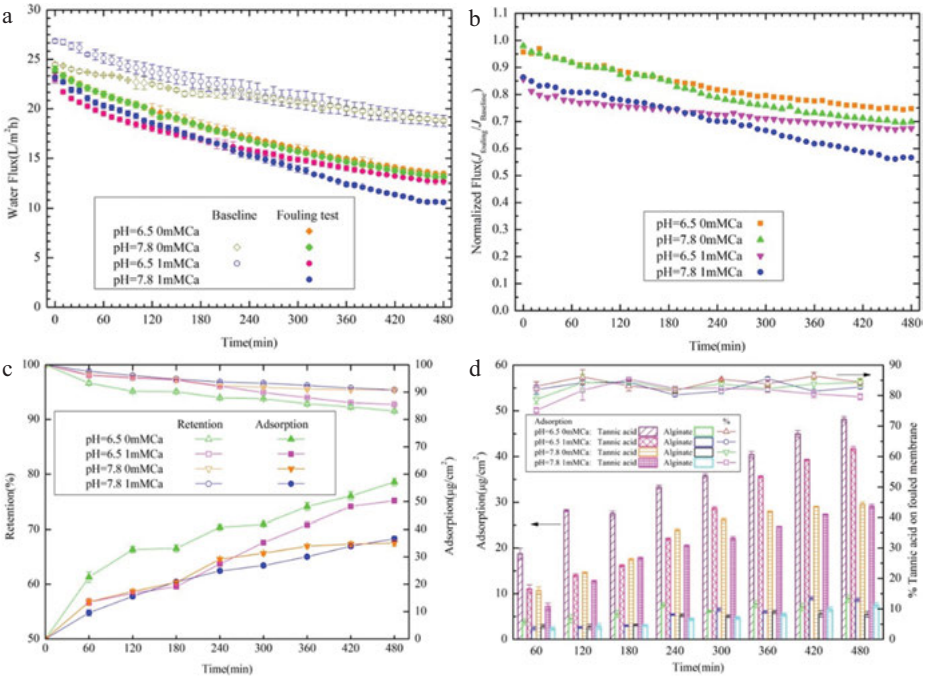

Figure 7.23: Effect of solution chemistry on mixed foulants purification.

As mentioned above, the effect of feed water pH on the removal rates of mixed foulants was negligible. Indeed, removal rates of mixed foulants were above 99.0%, regardless of pH. As shown in Figure 7.23(c), the adsorption of mixed foulant on the FO membrane decreased drastically as the pH increased, although fluxes at different pH values were consistent. As a result, the retention rates by the FO membrane enhanced as the pH increased. Additionally, the increasing rate of mixed foulant adsorption was much lower at higher pH value. Figure 7.23(d) shows the composition of the foulant layer. As observed, the adsorption of tannic acid at higher pH was significantly lower than that at lower pH. At higher pH, the effective negative charge carried by tannic acid [55] and the FO membrane surface [54] increased, resulting in the enhanced electrostatic repulsion and thus reduced adsorption of tannic acid. However, as demonstrated by tests of single fouling by tannic acid [57], the reduction

EBSCOhost - printed on 2/14/2023 6:39 AM via . All use subject to https://www.ebsco.com/terms-of-use

of tannic acid adsorption and looser structure of the fouling layer seemed to have a negligible effect on the fouling flux. In addition, the content of alginate in the fouling layer exhibited negligible change within the pH range tested. Previous studies [65] have demonstrated that alginate had a negative zeta potential and nearly constant above pH 6, suggesting that alginate was completely deprotonated and has similar negative charge at the pH evaluated in this study. Based on this, it can be concluded that the electrostatic repulsion between dissociated alginate molecules and the negatively-charged membrane surface and between the alginate in solution and the adsorbed alginate was similar at different pH values, possibly resulting in subtle differences between the adsorption behavior of alginate. On the other hand, the relative amount of tannic acid in the fouling layer was independent from the increased pH, remaining at nearly or above 80.0%, suggesting that the adsorption of tannic acid was the dominant factor in mixed fouling at pH tested.

At pH of 6.5 and 7.8, the FO flux more significantly reduced in the presence of Ca^{2+} in feed water compared to that in the absence of Ca^{2+}. In single fouling by tannic acid [57] or alginate [59], Ca^{2+} also exhibited the adverse effect on the fouling flux. According to the normalized flux shown in Figure 7.23(b), the initial flux decline (~15%) at different pH values was similar in the presence of Ca^{2+}; however, the normalized flux at pH 7.8 declined more noticeably than that at pH 6.5 after the early stage ($t \geq 3$ h), demonstrating the significant effect of solution containing Ca^{2+} at pH 7.8 on the flux decline of mixed fouling of the FO membrane.

As mentioned above, the presence of Ca^{2+} in feed water had a minor effect on the removal of mixed foulants by the FO membrane. However, Ca^{2+} had the remarkable different effect on the adsorption and retention of mixed foulants in feed water at both pH 6.5 and pH 7.8 (see Figure 7.23(c)). At pH 6.5, the presence of Ca^{2+} led to the reduced adsorption of mixed foulants on the membrane surface and thus slightly higher enhanced retention of mixed foulants compared to the absence of Ca^{2+}. However, the presence of Ca^{2+} had minimal effect on the adsorption and retention of mixed foulants at pH 7.8, probably attributed to the original, obviously decreased, adsorption of tannic acid at pH 7.8 without Ca^{2+} in the feed. Additionally, the adsorption of mixed foulants at high pH was lower than that at low pH, and the retention rate of mixed foulants was consequently higher after the early 3 h of the FO filtration in presence of Ca^{2+}. From the results observed in absence of Ca^{2+} in the feed, Figure 7.23(d) shows that tannic acid plays a dominant role in mixed fouling of the FO membrane at both pH values in the presence of Ca^{2+}. For this reason, the adsorption of tannic acid had a similar trend with the mixture adsorption at the corresponding pH value. According to the minimal adsorption amount, the adsorption of alginate on the membrane surface was not obviously affected by pH value in the presence of Ca^{2+}. This result is consistent with that of single fouling by alginate under the identical conditions of pH and Ca^{2+} [59].

It has been well-recognized that the presence of Ca^{2+} can reduce the charge of organic foulants and thus enhance their adsorption on membrane surfaces, as Ca^{2+}

EBSCOhost - printed on 2/14/2023 6:39 AM via . All use subject to https://www.ebsco.com/terms-of-use

can bind with acidic functional groups (predominantly carboxylic) of foulants through complex formation [50]. However, this study revealed that the presence of Ca^{2+} led to the reduced adsorption of tannic acid in the mixed fouling system on the membrane surface (Figure 7.23(d)). In the presence of Ca^{2+} in feed water, the initial fouling flux at the early stage declined drastically, resulting in significantly reduced permeation drag and eventually prohibited the adsorption of tannic acid, especially at pH 6.5, although the Ca^{2+} facilitated tannic acid adsorption on the membrane surface due to its effect on charge neutralization and intermolecular binding of tannic acid macromolecules. On the other hand, some researchers have described the bridging effect of Ca^{2+} on neighboring alginate molecules, resulting in development of a dense gel layer of alginate on membrane surfaces, and thus severe flux declines [42, 62, 67]. In contrast, the marked effect of Ca^{2+} on fouling flux and alginate adsorption was not observed in this study, whether or not the tannic acid was present in the feed. This may be attributed to the fact that the applied initial flux in this study was below the critical value for alginate fouling, which may hinder the deposition and accumulation of alginate on membrane surfaces and reduce the effect of Ca^{2+} on fouling by alginate.

In addition, the severe reduced mixed fouling flux with feed water containing 1 mM Ca^{2+} may be partially attributed to different configurations of tannic acid and alginate molecules. The complexation of Ca^{2+} led to reduced interchain electrostatic repulsion of mixed foulant molecules and a small coiled foulant macromolecules configuration. As a result, a more compact mixed fouling layer formed [50]. For tannic acid, the small coiled molecules in the presence of Ca^{2+} can result in a more compact fouling layer in the porous structure and thus more severe pore-clogging enhanced ICP compared to the absence of calcium ions. Meanwhile, alginate molecules in the presence of Ca^{2+} can also readily migrate from the surface of the supporting layer into its porous structure, partially aggravating the pore-clogging enhanced ICP.

Because of the condition of 1 mM Ca^{2+} in base solution close to the characteristic of the solution chemistry in natural surface water [57], this study focused on the analysis of mixed fouling flux of feed water with pH 7.8 and 1 mM Ca^{2+}. In presence of Ca^{2+} in base solution, the electrostatic repulsion of adjacent functional groups in foulant-calcium complexation enhanced, resulting in reduced compactness of the mixed fouling layer, which possibly relieved pore-clogging enhanced ICP and thus reduced initial flux drop within the early stage of FO filtration compared to pH 6.5. On the other hand, the fouling flux at low pH exhibited superior stability than that at high pH. This may be partially attributed to the reduced ICP caused by initial drastic flux decline at low pH. Eventually, the effective driving force (i.e., concentration difference on the two sides of the active layer) increased and it compensated for the subsequent membrane fouling. Tang et al. proposed the "compensating ICP" effect and believed that it was the reason for stabilized flux when the active layer of an FO membrane was oriented toward the feed solution [10]. It implied that the "compensating ICP" effect may also cause less severe flux decline and thus potentially favor a

EBSCOhost - printed on 2/14/2023 6:39 AM via . All use subject to https://www.ebsco.com/terms-of-use

more stable water flux after longer fouling filtration under the condition of 1 mM Ca^{2+} at pH 7.8 in the feed.

7.5.2.6 Effect of hydrodynamic and chemical conditions

Figure 7.24 conceptually illustrates the effect of hydrodynamic conditions (e.g., initial flux, cross-flow velocity) and chemical properties of feed water (e.g., pH, concentration of calcium ions) on the purification of mixed foulants by the FO membrane, as well as the relevant fouling mechanism. The grey shaded area in Figure 7.24 denotes the hydrodynamic and chemical conditions that may induce a more severe ICP effect.

As shown in Figure 7.24(a), according to the greater permeation drag, the higher initial flux and cross-flow velocity can reduce the FO retention by inducing more foulant molecules, mainly tannic acid, entrapped within the porous supporting layer. Meanwhile, the foulants adsorbed in the porous structure led to the more severe internal clogging enhanced ICP effect, eventually resulting in severe flux drop (Figures 7.21(a) and 7.22(a)) under the high initial flux and cross flow velocity.

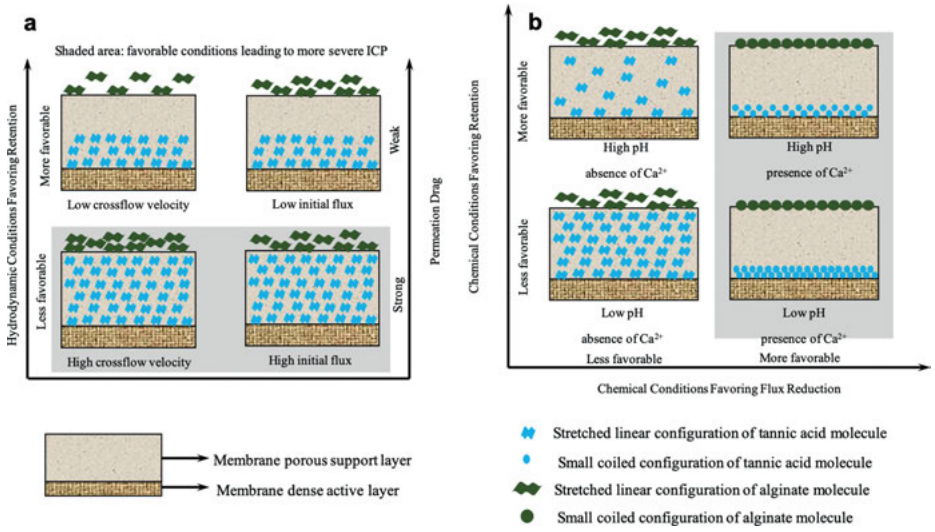

Figure 7.24: Schematic description of the effect of (a) hydrodynamic conditions, and (b) solution chemistry on the FO purification performance of mixed organic foulants.

As shown in Figure 7.24(b), chemical properties of feed water affected both the adsorption quantities and configuration of tannic acid and alginate, thus affecting performance of the FO membrane. Regardless of Ca^{2+}, the electrostatic repulsion enhanced with the higher pH of feed water. Hence, the adsorption of mixed foulants decreased, and thus the retention increased. On the other hand, the presence of Ca^{2+} led to a

EBSCOhost - printed on 2/14/2023 6:39 AM via . All use subject to https://www.ebsco.com/terms-of-use

greater drop in the FO membrane flux by mixed foulants. As shown in Figure 7.24(b), a compact mixed fouling layer developed with the small coiled complexation of calcium and tannic acid and alginate molecules on the FO membrane. The shaded area shows the dense fouling layer of tannic acid in the supporting layer in the presence of calcium ions. This resulted in more severe pore clogging enhanced ICP.

7.5.3 Summary

The physical and chemical factors influencing water flux and retention of the FO membrane was investigated in this study. The AL-facing-DS orientation was used for the FO purification of mixed foulants. Tannic acid and alginate were used as model organic foulants for polysaccharides and humic dissolved organic matters.

For the AL-facing-DS orientation, the FO membrane can effectively remove the mixed and single tannic acid and alginate foulants. The higher the ratio of tannic acid in the mixed foulants in the feed, the more severe the fouling flux decline with lower mixed foulants' retention were observed, suggesting that tannic acid might be the dominant foulant in the purification of mixed foulants by FO membranes compared with alginate. The mixed fouling flux decline increased with increasing initial flux level and Ca^{2+} concentrations in feed water. Tannic acid was also found to be the main component of the mixed fouling layer. The permeation drag induced by water flux level and chemical interactions related to Ca^{2+} concentration and pH in the feed solution, may have the significant effect on both the adsorption of tannic acid in the supporting layer of the FO membrane and thus the retention of mixed foulants.

These results of the purification of mixed foulants by the FO membrane may contribute to a further understanding of fouling mechanisms and its application of FO in natural surface water treatment where fouling by polysaccharide/humic acid mixture may possibly occur.

References

[1] Cath, T.Y., Childress, A.E., and Elimelech, M., Forward osmosis: Principles, applications, and recent developments. Journal of Membrane Science, 2006. 281(1–2): p. 70–87.
[2] Lee, K.L., Baker, R.W., and Lonsdale, H.K., Membranes for power-generation by pressure-retarded osmosis. Journal of Membrane Science, 1981. 8(2): p. 141–171.
[3] Wang, L., Chu, H., and Dong, B., Effects on the purification of tannic acid and natural dissolved organic matter by forward osmosis membrane. Journal of Membrane Science, 2014. 455(0): p. 31–43.
[4] Parida, V. and Ng, H.Y., Forward osmosis organic fouling: Effects of organic loading, calcium and membrane orientation. Desalination, 2013. 312: p. 88–98.
[5] McCutcheon, J.R., McGinnis, R.L., and Elimelech, M., A novel ammonia-carbon dioxide forward (direct) osmosis desalination process. Desalination, 2005. 174(1): p. 1–11.

EBSCOhost - printed on 2/14/2023 6:39 AM via . All use subject to https://www.ebsco.com/terms-of-use

[6] Zhao, S.A.F. and Zou, L.D., Relating solution physicochemical properties to internal concentration polarization in forward osmosis. Journal of Membrane Science, 2011. 379(1–2): p. 459–467.
[7] Tan, C.H. and Ng, H.Y., Modified models to predict flux behavior in forward osmosis in consideration of external and internal concentration polarizations. Journal of Membrane Science, 2008. 324(1–2): p. 209–219.
[8] Gray, G.T., McCutcheon, J.R., and Elimelech, M., Internal concentration polarization in forward osmosis: Role of membrane orientation. Desalination, 2006. 197(1–3): p. 1–8.
[9] McCutcheon, J.R. and Elimelech, M., Influence of concentrative and dilutive internal concentration polarization on flux behavior in forward osmosis. Journal of Membrane Science, 2006. 284(1–2): p. 237–247.
[10] Tang, C.Y.Y., et al., Coupled effects of internal concentration polarization and fouling on flux behavior of forward osmosis membranes during humic acid filtration. Journal of Membrane Science, 2010. 354(1–2): p. 123–133.
[11] Gerstandt, K., et al., Membrane processes in energy supply for an osmotic power plant. Desalination, 2008. 224(1–3): p. 64–70.
[12] Jean-Michel Laîné, J.P.H., Clark, M.M., Mallevialle, J., Effects of ultrafiltration membrane composition. Journal American Water Works Association, 1989. 81(11): p. 61–67.
[13] Schäfer, A.I., Fane, A.G., and Waite, T.D., Fouling effects on rejection in the membrane filtration of natural waters. Desalination, 2000. 131(1–3): p. 215–224.
[14] Mänttäri, M., et al., Fouling effects of polysaccharides and humic acid in nanofiltration. Journal of Membrane Science, 2000. 165(1): p. 1–17.
[15] Yuan, W. and Zydney, A.L., Humic acid fouling during ultrafiltration. Environmental Science & Technology, 2000. 34(23): p. 5043–5050.
[16] Yip, N.Y., et al., High performance thin-film composite forward osmosis membrane. Environmental Science & Technology, 2010. 44(10): p. 3812–3818.
[17] Yang, Q., Wang, K.Y., and Chung, T.S., Dual-layer hollow fibers with enhanced flux as novel forward osmosis membranes for water production. Environmental Science & Technology, 2009. 43(8): p. 2800–2805.
[18] Wang, R., et al., Characterization of novel forward osmosis hollow fiber membranes. Journal of Membrane Science, 2010. 355(1–2): p. 158–167.
[19] Zhang, S., et al., Well-constructed cellulose acetate membranes for forward osmosis: Minimized internal concentration polarization with an ultra-thin selective layer. Journal of Membrane Science, 2010. 360(1–2): p. 522–535.
[20] Tiraferri, A., et al., Relating performance of thin-film composite forward osmosis membranes to support layer formation and structure. Journal of Membrane Science, 2011. 367(1–2): p. 340–352.
[21] Qiu, C., et al., High performance flat sheet forward osmosis membrane with an NF-like selective layer on a woven fabric embedded substrate. Desalination, 2012. 287: p. 266–270.
[22] McCutcheon, J.R., McGinnis, R.L., and Elimelech, M., Desalination by ammonia-carbon dioxide forward osmosis: Influence of draw and feed solution concentrations on process performance. Journal of Membrane Science, 2006. 278(1–2): p. 114–123.
[23] Achilli, A., Cath, T.Y., and Childress, A.E., Selection of inorganic-based draw solutions for forward osmosis applications. Journal of Membrane Science, 2010. 364(1–2): p. 233–241.
[24] Ge, Q.C., et al., Hydrophilic superparamagnetic nanoparticles: Synthesis, characterization, and performance in forward osmosis processes. Industrial & Engineering Chemistry Research, 2011. 50(1): p. 382–388.
[25] Liu, Z.Y., et al., A low-energy forward osmosis process to produce drinking water. Energy & Environmental Science, 2011. 4(7): p. 2582–2585.
[26] Yen, S.K., et al., Study of draw solutes using 2-methylimidazole-based compounds in forward osmosis. Journal of Membrane Science, 2010. 364(1–2): p. 242–252.

EBSCOhost - printed on 2/14/2023 6:39 AM via . All use subject to https://www.ebsco.com/terms-of-use

[27] Zhao, S.F. and Zou, L.D., Effects of working temperature on separation performance, membrane scaling and cleaning in forward osmosis desalination. Desalination, 2011. 278(1–3): p. 157–164.
[28] Zhao, S.F., et al., Recent developments in forward osmosis: Opportunities and challenges. Journal of Membrane Science, 2012. 396: p. 1–21.
[29] Ling, M.M. and Chung, T.S., Desalination process using super hydrophilic nanoparticles via forward osmosis integrated with ultrafiltration regeneration. Desalination, 2011. 278(1–3): p. 194–202.
[30] Tan, C.H. and Ng, H.Y., A novel hybrid forward osmosis – nanofiltration (FO-NF) process for seawater desalination: Draw solution selection and system configuration. Desalination and Water Treatment, 2010. 13(1–3): p. 356–361.
[31] Cath, T.Y., et al., A multi-barrier osmotic dilution process for simultaneous desalination and purification of impaired water. Journal of Membrane Science, 2010. 362(1–2): p. 417–426.
[32] Tang, W.L. and Ng, H.Y., Concentration of brine by forward osmosis: Performance and influence of membrane structure. Desalination, 2008. 224(1–3): p. 143–153.
[33] Martinetti, C.R., Childress, A.E., and Cath, T.Y., High recovery of concentrated RO brines using forward osmosis and membrane distillation. Journal of Membrane Science, 2009. 331(1–2): p. 31–39.
[34] Cartinella, J.L., et al., Removal of natural steroid hormones from wastewater using membrane contactor processes. Environmental Science & Technology, 2006. 40(23): p. 7381–7386.
[35] Holloway, R.W., et al., Forward osmosis for concentration of anaerobic digester centrate. Water Research, 2007. 41(17): p. 4005–4014.
[36] Cornelissen, E.R., et al., Membrane fouling and process performance of forward osmosis membranes on activated sludge. Journal of Membrane Science, 2008. 319(1–2): p. 158–168.
[37] Xiao, D.Z., et al., Modeling salt accumulation in osmotic membrane bioreactors: Implications for FO membrane selection and system operation. Journal of Membrane Science, 2011. 366(1–2): p. 314–324.
[38] Zou, S., et al., The role of physical and chemical parameters on forward osmosis membrane fouling during algae separation. Journal of Membrane Science, 2011. 366(1–2): p. 356–362.
[39] Thelin, W.R., et al., Natural organic matter fouling in pressure retarded osmosis. Journal of Membrane Science, 2013. 438: p. 46–56.
[40] Mi, B.X. and Elimelech, M., Organic fouling of forward osmosis membranes: Fouling reversibility and cleaning without chemical reagents. Journal of Membrane Science, 2010. 348(1–2): p. 337–345.
[41] Mi, B.X. and Elimelech, M., Gypsum scaling and cleaning in forward osmosis: measurements and mechanisms. Environmental Science & Technology, 2010. 44(6): p. 2022–2028.
[42] Mi, B. and Elimelech, M., Chemical and physical aspects of organic fouling of forward osmosis membranes. Journal of Membrane Science, 2008. 320(1–2): p. 292–302.
[43] Xie, M., et al., Comparison of the removal of hydrophobic trace organic contaminants by forward osmosis and reverse osmosis. Water Research, 2012. 46(8): p. 2683–2692.
[44] Linares, R.V., et al., Rejection of micropollutants by clean and fouled forward osmosis membrane. Water Research, 2011. 45(20): p. 6737–6744.
[45] Jin, X., et al., Removal of boron and arsenic by forward osmosis membrane: Influence of membrane orientation and organic fouling. Journal of Membrane Science, 2012. 389: p. 182–187.
[46] Kawasaki, N., et al., Fast and precise method for HPLC-size exclusion chromatography with UV and TOC (NDIR) detection: Importance of multiple detectors to evaluate the characteristics of dissolved organic matter. Water Research, 2011. 45(18): p. 6240–6248.
[47] Song, Y.L., et al., Huangpu River water treatment by microfiltration with ozone pretreatment. Desalination, 2010. 250(1): p. 71–75.
[48] Xu, B., et al., Characteristics of organic material in Huangpu River and treatability with the O-3-BAC process. Separation and Purification Technology, 2007. 57(2): p. 348–355.

EBSCOhost - printed on 2/14/2023 6:39 AM via . All use subject to https://www.ebsco.com/terms-of-use

[49] Zhao, S.F., Zou, L.D., and Mulcahy, D., Effects of membrane orientation on process performance in forward osmosis applications. Journal of Membrane Science, 2011. 382(1–2): p. 308–315.
[50] Hong, S.K. and Elimelech, M., Chemical and physical aspects of natural organic matter (NOM) fouling of nanofiltration membranes. Journal of Membrane Science, 1997. 132(2): p. 159–181.
[51] Tang, C.Y. and Leckie, J.O., Membrane independent limiting flux for RO and NF membranes fouled by humic acid. Environmental Science & Technology, 2007. 41(13): p. 4767–4773.
[52] Wang, Y.N., et al., Direct microscopic observation of forward osmosis membrane fouling. Environmental Science & Technology, 2010. 44(18): p. 7102–7109.
[53] Tang, C.Y., Kwon, Y.N., and Leckie, J.O., Fouling of reverse osmosis and nanofiltration membranes by humic acid – Effects of solution composition and hydrodynamic conditions. Journal of Membrane Science, 2007. 290(1–2): p. 86–94.
[54] Xu, P., et al., Effect of membrane fouling on transport of organic contaminants in NF/RO membrane applications. Journal of Membrane Science, 2006. 279(1–2): p. 165–175.
[55] Wang, J.H., et al., Behaviors and mechanisms of tannic acid adsorption on an amino-functionalized magnetic nanoadsorbent. Desalination, 2011. 273(2–3): p. 285–291.
[56] Yangali-Quintanilla, V., et al., Rejection of pharmaceutically active compounds and endocrine disrupting compounds by clean and fouled nanofiltration membranes. Water Research, 2009. 43(9): p. 2349–2362.
[57] Wang, L., Chu, H.Q., and Dong, B.Z., Effects on the purification of tannic acid and natural dissolved organic matter by forward osmosis membrane. Journal of Membrane Science, 2014. 455: p. 31–43.
[58] Zazouli, M.A., Nasseri, S., and Ulbricht, M., Fouling effects of humic and alginic acids in nanofiltration and influence of solution composition. Desalination, 2010. 250(2): p. 688–692.
[59] Wang, L., et al., Forward osmosis filtration for removal of organic foulants: Effects of combined tannic and alginic acids. Water Research, 2016. 91: p. 251–263.
[60] Lutchmiah, K., et al., Forward osmosis for application in wastewater treatment: A review. Water Research, 2014. 58: p. 179–197.
[61] Tang, C.Y.Y., et al., Modeling double-skinned FO membranes. Desalination, 2011. 283: p. 178–186.
[62] Liu, Y.L. and Mi, B.X., Combined fouling of forward osmosis membranes: Synergistic foulant interaction and direct observation of fouling layer formation. Journal of Membrane Science, 2012. 407: p. 136–144.
[63] Xie, M., et al., Impact of organic and colloidal fouling on trace organic contaminant rejection by forward osmosis: Role of initial permeate flux. Desalination, 2014. 336: p. 146–152.
[64] She, Q.H., et al., Organic fouling in pressure retarded osmosis: Experiments, mechanisms and implications. Journal of Membrane Science, 2013. 428: p. 181–189.
[65] Wang, Y.N. and Tang, C.Y., Nanofiltration membrane fouling by oppositely charged macromolecules: Investigation on flux behavior, foulant mass deposition, and solute rejection. Environmental Science & Technology, 2011. 45(20): p. 8941–8947.
[66] Seidel, A. and Elimelech, M., Coupling between chemical and physical interactions in natural organic matter (NOM) fouling of nanofiltration membranes: Implications for fouling control. Journal of Membrane Science, 2002. 203(1–2): p. 245–255.
[67] Lee, S. and Elimelech, M., Salt cleaning of organic-fouled reverse osmosis membranes. Water Research, 2007. 41(5): p. 1134–1142.

EBSCOhost - printed on 2/14/2023 6:39 AM via . All use subject to https://www.ebsco.com/terms-of-use

EBSCOhost - printed on 2/14/2023 6:39 AM via . All use subject to https://www.ebsco.com/terms-of-use

Huaqiang Chu, Zhenxun Yu, Wen Sun

Chapter 8
Dynamic Membrane Reactor for Micro-polluted Surface Water/Municipal Wastewater Treatment

Membrane technology has been rapidly developed in water treatment, which is considered as a substitute to conventional clarification and filtration processes [1, 2]. Membrane bioreactor (MBR) has gained great attention in water and wastewater treatment in recent years. However, the MBR application is limited by factors such as the high membrane modules cost, membrane fouling and high energy consumption [3, 4]. In order to overcome the drawbacks of the traditional MBR, a new dynamic membrane technology has been developed.

The dynamic membrane can be formed on the underlying support mesh when filtering a solution containing fine particles, thus it is also named secondary membrane [5], which was first utilized in reverse osmosis by the Oak Ridge National Laboratory in 1965 [6]. The dynamic membrane formed on MF and UF membrane surface exhibited high anti-fouling characteristics. Meanwhile, the membrane retention capacity of the big pore mesh could be increased by the formed dynamic membrane. The dynamic membrane induced a high solid-liquor separation efficiency and a high filtration flux [7]. The cleaning of dynamic membrane for membrane fouling control can be reached by tap water backwash, air backwash, or brushing without using chemical reagents.

Diatomite particles have been used as carriers for microorganisms as its characteristics of high porosity, good hydrophilicity and high chemical stability [8], and the zoogloeae formed on the diatomite are identified as bio-diatomite. Such related technology with the combination of the bio-diatomite reactor and the anoxic/aerobic processes had been proposed [9, 10], which contained high concentrations of microorganisms and species diversities for wastewater treatment with high and stable treatment efficiency and good effluent quality.

Bio-diatomite dynamic membrane (BDDM) was developed by the deposition of bio-diatomite particles on the big-pore stainless steel support mesh, which exhibited a high solid-liquid separation efficiency and a high filtration flux [11]. Combined with traditional water/wastewater treatment process, the bio-diatomite dynamic membrane reactor (BDDMR) can be figured out, which can be used for municipal wastewa-

Huaqiang Chu, College of Environmental Science and Engineering, Tongji University, Shanghai, P. R. China
Zhenxun Yu, School of Civil and Environmental Engineering, Ningbo University, Ningbo, Zhejiang, P. R. China
Wen Sun, College of Environmental Science and Engineering, Suzhou University of Science and Technology, Suzhou, Jiangsu, P. R. China

https://doi.org/10.1515/9783110596847-008

EBSCOhost - printed on 2/14/2023 6:39 AM via . All use subject to https://www.ebsco.com/terms-of-use

ter treatment [12] and micro-polluted surface water treatment [13]. The characteristics of the BDDM operation was presented in the following section.

8.1 The bio-diatomite dynamic membrane bioreactor for municipal wastewater treatment

8.1.1 Experimental materials

8.1.1.1 Experimental set up

The BDDM reactor contained an anoxic tank, an aerobic tank and a dynamic membrane filter (DMF) in sequence, whose total effective volume was 0.035 m^3 (Figure 8.1). The BDDM support module was fixed in submerged mode with a double-sided effective filtration area of 0.084 m^2 (28 cm × 15 cm) (Figure 8.2). Four stainless steel meshes with different equivalent apertures (74 μm, 80 μm, 106 μm and 120 μm) were used as the support layer (Figure 8.3). The two stainless steel meshes (106 μm and 120 μm) were both made using the plain weave mode with homogeneous apertures, while the other two stainless steel meshes (74 μm and 80 μm) were made using the twill weave mode with non-uniform apertures (Chinese GB/T 19628.2-2005).

8.1.1.2 Experimental operation mode

The inoculation activated sludge (about 5,400 mg/L MLSS) for the bio-diatomite cultivation and raw municipal wastewater were obtained from a municipal wastewater treatment plant in Shanghai, China. The parameters of the raw municipal wastewater were present in Table 8.1. During the inoculation period, the diatomite was added continuously into the bioreactor to reach a concentration of about 7,000 mg/L. Then, the bioreactor was continuously operated through two peristaltic pumps for feeding raw municipal wastewater and withdrawing the effluent. The MLSS and MLVSS of the matured bio-diatomite mixed liquor were maintained at about 11,000 mg/L and 4,500–5,000 mg/L, respectively. The recycle rate of mixed liquor in the DMF to the anoxic tank was two times the influent flow.

The operation pressure measured by a high-precision vacuum pressure gauge was used to calculate the transmembrane pressure (TMP). The operation period of BDDM clarified into three stages, i.e., precoating, filtration and backwash (Figure 8.1). In the precoating stage, the bio-diatomite mixed liquor was recirculated and the effluent was withdrawn for SS analysis at fixed time intervals. Then, in the filtration stage a constant flux was adapted combined with a continuous increase of the BDDM thickness, which also resulted in the rising of filtration resistance. The filtration was ter-

EBSCOhost - printed on 2/14/2023 6:39 AM via . All use subject to https://www.ebsco.com/terms-of-use

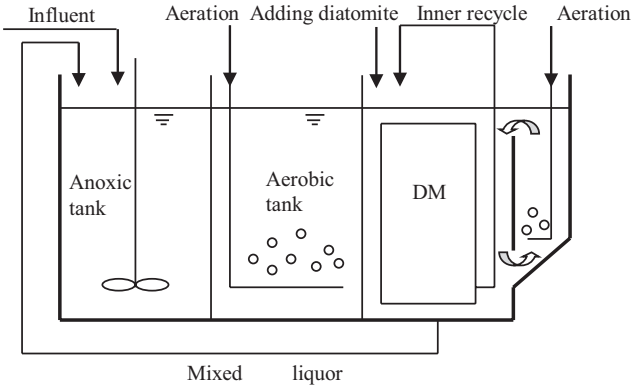

(a) Precoating stage

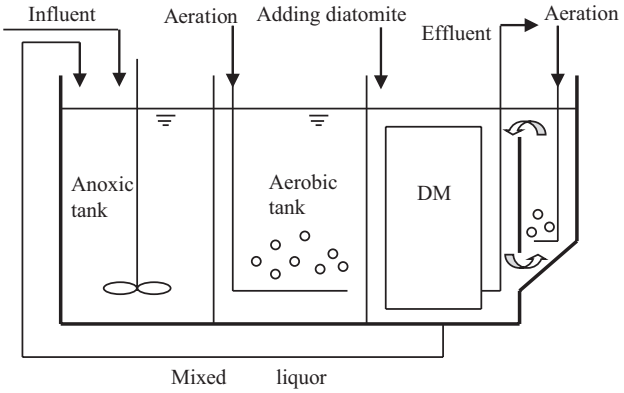

(b) Filtration stage

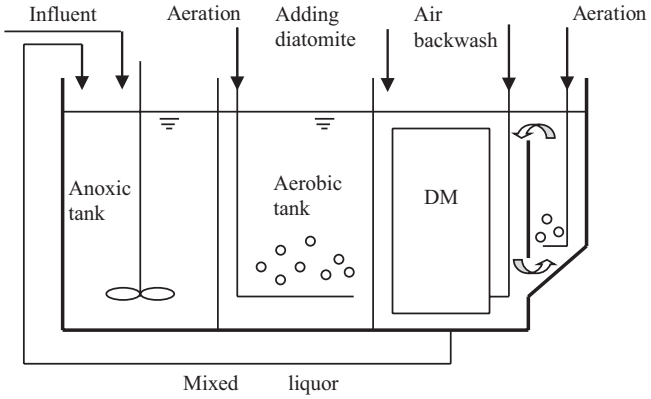

(c) Backwash stage

Figure 8.1: Three operation stages of the BDDM reactor.

EBSCOhost - printed on 2/14/2023 6:39 AM via . All use subject to https://www.ebsco.com/terms-of-use

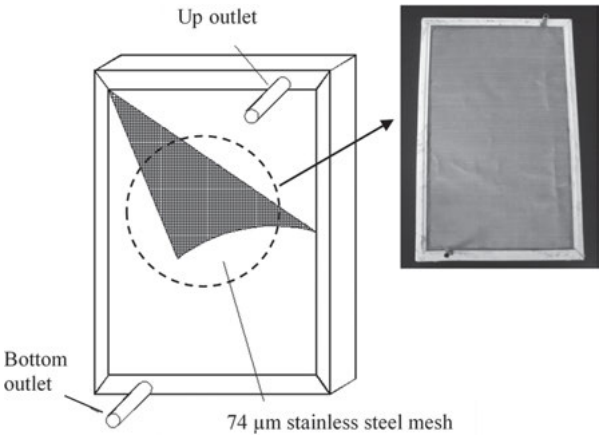

Figure 8.2: Picture of BDDM support module.

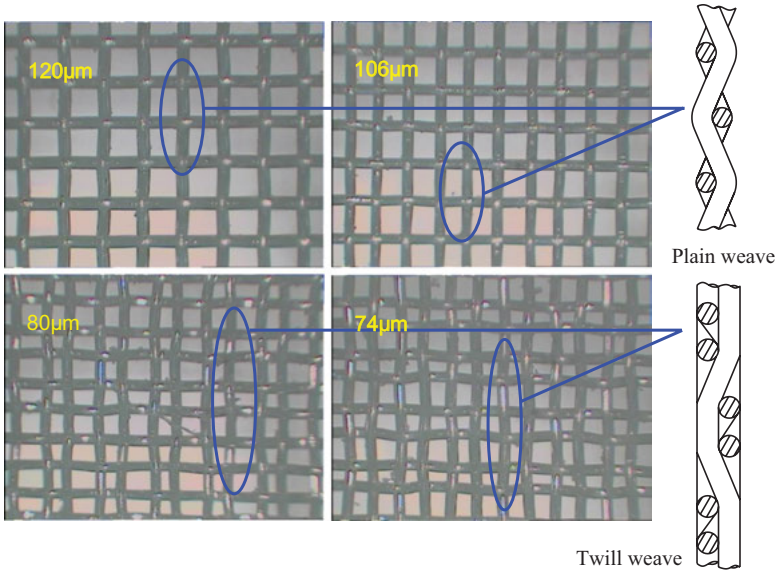

Figure 8.3: 40-time pictures of the stainless steel meshes.

Table 8.1: Parameters of raw municipal wastewater.

Water quality parameters	Concentration
COD (mg/L)	113.4–582.7
NH_4-N (mg/L)	5.6–15.3
SS (mg/L)	20.5–360.5
Water temperature (°C)	15.0–33.5
pH	6.5–7.4

EBSCOhost - printed on 2/14/2023 6:39 AM via . All use subject to https://www.ebsco.com/terms-of-use

minated once the operation pressure reached 40 kPa and then backwash was started. The on-line air backwash was adapted by an electromagnetic air pump through the bottom outlet of the BDDM module. The operation parameters of the BDDM reactor are shown in Table 8.2.

Table 8.2: Operation parameters of the BDDM reactor.

Operation parameters	Value
MLSS (mg/L)	11,000
Design flux (L/(m^2 · h))	8.6–130.0
SRT (d)	40–87
HRT (h)	7[a]
Water temperature (°C)	16–33
DO in aerobic tank (mg/L)	3–4
DO in anoxic tank (mg/L)	<0.15

[a]. HRT was calculated under the flux of 60 L/(m^2 · h) that lasted 2 months to test pollutants removal efficiency in the BDDM reactor.

8.1.2 Pollutants removal by the BDDM reactor

Compared with the pollutants in the raw feed water, it can be seen from Table 8.3 that the BDDM reactor exhibits effective capacity for pollutants removal of COD, NH_4-N, TN and SS. The dynamic membrane shows good solid-liquid separation efficiency [14]. During the experiment, the whole dynamic membrane module was carefully taken out from the bioreactor, and then put into a tank filled with the raw municipal wastewater to examine the removal efficiency of soluble COD and NH_4-N by BDDM independently. Results show that BDDM alone could achieve little NH_4-N removal, and the COD removal rate was below 40%, which was primarily due to the suspended COD retention. Therefore, it can be concluded that the removal of soluble COD and NH_4-N was mainly ascribed to the microbial degradation in the bio-diatomite reactor. The efficiency of biodegradation for pollutants could be enhanced by the high concentration of MLSS in the reactor. Both nitrification in the aerobic tank and denitrification in the anoxic tank occurred at a high level, reaching 6.09 mg NH_4-N/g VSS · h and 5.05 mg NO_3-N/g VSS · h, respectively. Hence, a high removal efficiency of NH_4-N and TN was achieved, which was consistent with the previous results [10, 15]. The long sludge age in the bioreactor was beneficial for the reproduction of nitrifying bacteria, and a DO concentration of 3–4 mg/L was also adequate for their growth [16, 17]. Meanwhile, denitrification could effectively proceed at a low DO concentration of < 0.15 mg/L in the anoxic tank. All these factors exerted positive effects on pollutant removal.

EBSCOhost - printed on 2/14/2023 6:39 AM via . All use subject to https://www.ebsco.com/terms-of-use

Table 8.3: Parameters of treated municipal wastewater.

Water quality parameters	Concentration
COD (mg/L)	8.1–28.1
NH_4-N (mg/L)	0.08–0.53
TN (mg/L)	6.18–14.90
SS (mg/L)	0
Turbidity (NTU)	0.392–0.726

8.1.3 Effect of the pore size of the support mesh on the bio-diatomite dynamic membrane filtration

8.1.3.1 Precoating process of the BDDM

The BDDM contains three operation stages, and the first stage is the precoating stage with bio-diatomite cake layer deposited on the support mesh, which was monitored in real-time as the support module was placed into the bio-diatomite reactor under a constant water head of 0.6 m. The result from six operation periods measured at the same time interval were shown in Figure 8.4.

At the beginning, the effluent SS concentrations decreased sharply and then declined slowly for all four stainless steel meshes, with the inflection points at 2 min, 5 min, 5 min and 5 min for the 74 μm, 80 μm, 106 and 120 μm stainless steel meshes, respectively. The time of the inflection point indicates the formation of the dynamic membrane, but the mixed liquor permeating into the membrane module had not been completely discharged yet [12]. As the precoating time was extended to 15 min, 30 min, 40 min or 50 min, the effluent SS concentration was below 10 mg/L slowly under the stainless steel meshes of the 74 μm, 80 μm, 106 μm and 120 μm, respectively, which complies with the First Class, Type A of the Chinese Discharge Standard of Pollutants for Municipal Wastewater Treatment Plant (GB 18918-2002). Therefore, the stainless steel mesh with a small equivalent aperture can shorten the precoating time and exhibit better solid-liquor separation capacity of the BDDM.

8.1.3.2 Operation pressure and SS of the BDDM

A constant flux of 50 L/($m^2 \cdot h$) was selected to test the pore size effect of the support mesh on the BDDM filtration process till the operation pressure reached 40 kPa. The parameter of the effluent SS was used to reflect the BDDM retention capacity under different stainless steel support meshes, as shown in Figure 8.5. It can be seen that the relationships between the operation pressure and the filtration time can all be fixed with an exponential equation, and their whole filtration length were all about 6 h

EBSCOhost - printed on 2/14/2023 6:39 AM via . All use subject to https://www.ebsco.com/terms-of-use

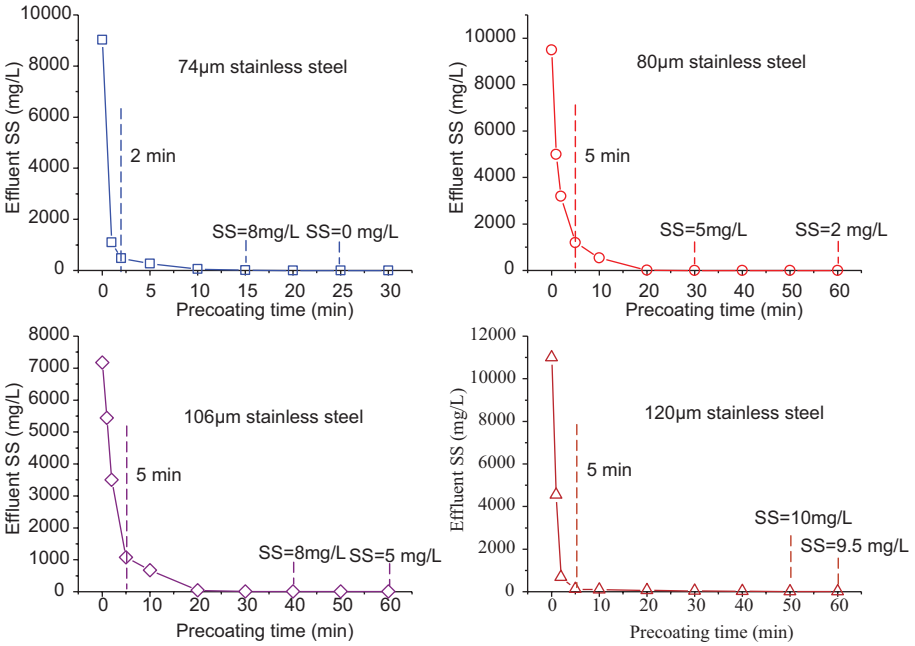

Figure 8.4: The changes of effluent SS with time in the precoating stage.

under the fixed operation pressure of 40 kPa. The effluent SS was stable in the range of 0–0.20 mg/L during the whole filtration process with the 74 μm stainless steel support mesh. Whereas, the variations of the effluent SS concentrations could be divided into two stages. In the first stage, the effluent SS concentrations below 10 mg/L with stainless steel support meshes of 80 μm, 106 μm, and 120 μm were about 3.5 h, 4.5 h and 2 h, respectively, with the values also elevated as the equivalent aperture increased. Then, the effluent SS exhibited big fluctuation ranges beyond 10 mg/L of the three different stainless steel support meshes, with value being the biggest produced by the support mesh of 120 μm. Therefore, the pore size of the stainless-steel support mesh exerted a strong influence on the SS retention capacity of the BDDM as the filtration process extended. The smaller equivalent aperture of the stainless-steel support mesh is helpful for the better SS retention capacity of the BDDM, which is consistent with the results of an activated sludge dynamic membrane formed on nylon meshes reported by Kiso et al. [18]. Though the rigidity and intensity of the stainless-steel mesh were much stronger than the textile meshes, the effect of the pore size of different materials support meshes on dynamic membrane filtration performance is equivalent.

Based on the above research results, the stainless-steel mesh of the equivalent aperture 74 μm was selected for the further study of the BDDM.

EBSCOhost - printed on 2/14/2023 6:39 AM via . All use subject to https://www.ebsco.com/terms-of-use

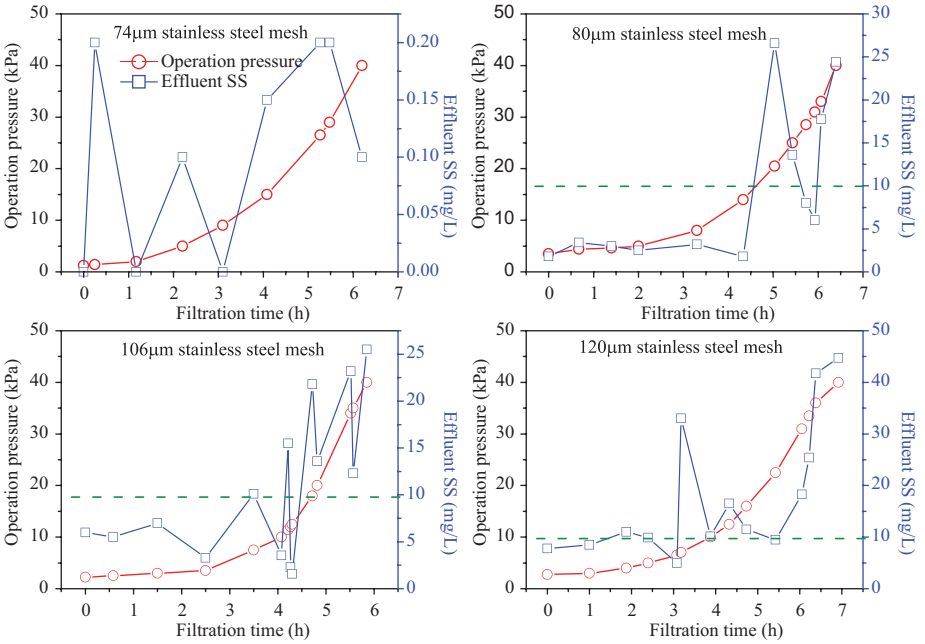

Figure 8.5: Variations of effluent SS with filtration time.

8.1.4 The operation characteristics of the BDDM

8.1.4.1 The relation between filtration flux and filtration time

The filtration time is defined between the time interval from the BDDM formation to the operation pressure of 40 kPa. The experimental results of the filtration flux and the filtration time are present in Table 8.4. The following exponential equation ($R^2 = 0.972$) can be induced from the above data:

$$J = 114.23 t_f^{-0.4169} \tag{8.1}$$

where J and t_f represent the filtration flux ($L/(m^2 \cdot h)$) and the filtration time (h), respectively.

Figure 8.6 presents the relationship between the operation pressure, also called the transmembrane pressure, and the filtration time at different filtration fluxes. The Darcy's law of Eq. (8.2) was used to figure out the filtration resistance in this study:

$$R = \frac{\Delta P}{\mu J} \tag{8.2}$$

EBSCOhost - printed on 2/14/2023 6:39 AM via . All use subject to https://www.ebsco.com/terms-of-use

Table 8.4: Different filtration flux versus filtration time.

Filtration flux, J (L/(m^2 · h))	8.6	17	22	30	35	40	45	50
Filtration time, t_f (h)	248.00	79.83	48.00	35.50	23.73	17.00	10.60	7.45
Filtration flux, J (L/(m^2 · h))	60	70	80	90	100	110	120	130
Filtration time, t_f (h)	4.92	3.55	3.05	2.17	1.55	1.05	0.62	0.43

where R is the filtration resistance (m^{-1}), ΔP is the transmembrane pressure (Pa), J is the filtration flux (m/s), and μ is the filtrate viscosity (Pa · s).

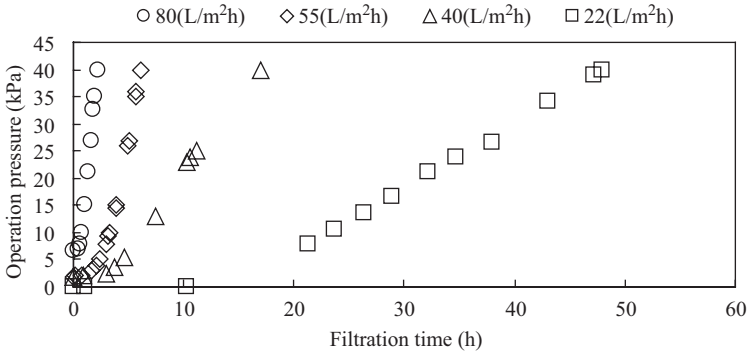

Figure 8.6: Changes of the operation pressure at different filtration fluxes.

The calculated filtration resistances with the filtration time are shown in Figure 8.7, and the filtration resistance of the stainless steel mesh was ignored here.

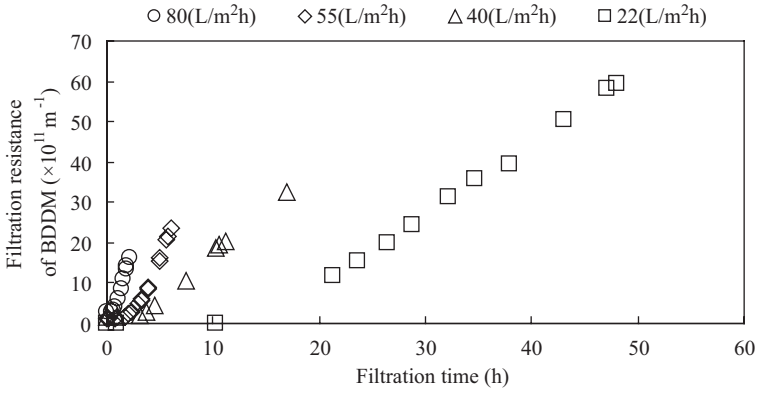

Figure 8.7: The filtration resistance versus the filtration time.

EBSCOhost - printed on 2/14/2023 6:39 AM via . All use subject to https://www.ebsco.com/terms-of-use

In the filtration process, the concentration of bio-diatomite mixed liquor was high and the cross-flow effect on the BDDM was weak. The resistance of BDDM could increase as the thickness of BDDM became thicker with the extended operation time, which is called the thickness-increase resistance in this study. Although the diatomite is almost incompressible, it is inevitable that the BDDM cake layer can be compressed partially for the existed space and the compressible attached microorganisms [19, 20], whose permeation space is gradually reduced with the increase of thickness-increase resistance. The resistance caused by the compaction of the BDDM is called the compaction resistance in this study. It can be concluded that both the thickness-increase resistance and the compaction resistance provide contribution to the filtration resistance of BDDM. Figure 8.7 shows that the filtration resistance of BDDM increased rapidly at a high filtration flux combined with shorten filtration time. With a low filtration flux, a low filtration resistance of BDDM was present during the early filtration stage by the slow growth of the BDDM thickness. However, the compaction resistance of the BDDM started to rise quickly as the thickness resistance increased during the intermediate and final stages. The above conclusion can be reflected clearly by the fact that the filtration resistance increased with the increasing slopes as a function of the filtration time.

8.1.4.2 Fluxes of different operation stages

Regarding the BDDM operation process, the total amount of wastewater produced was equal to the amount discharged during the filtration stage, because there was no effluent from the precoating and backwash stages. The average design flux discharged by a unit filtration area of BDDM during a complete operation process can be calculated using Eq. (8.3):

$$J_t = \frac{t_f . J}{T_t} = \frac{t_f . J}{t_p + t_f + t_b} \tag{8.3}$$

where J_t is the average design flux ($L/(m^2 \cdot h)$), J is the design flux ($L/(m^2 \cdot h)$), T_t is the operation period (h), t_p is the precoating time (h), t_f is the filtration time (h), and t_b is the backwash time (h).

Combined with the data in Table 8.4 and the selected precoating time of 25 min and backwash time of 2 min, the average design flux as a function of operation period is plotted in Figure 8.8. A maximal average design flux of 77.5 $L/(m^2 \cdot h)$ at 2 h can be found in Figure 8.8 corresponding to the design flux of 100 $L(m^2 \cdot h)$. The experimental data in the close region of the maximal point (77.5 $L/(m^2 \cdot h)$, 2 h) could be fitted by Eq. (8.4) ($R^2 = 0.973$):

$$J_t = -11.76 T_t^2 + 46.804 T_t + 32.237 \tag{8.4}$$

EBSCOhost - printed on 2/14/2023 6:39 AM via . All use subject to https://www.ebsco.com/terms-of-use

where J_t = average design flux ($L/(m^2 \cdot h)$) and T_t = operation period (h). The definition of the average design flux can be adapted to select the suitable design flux for the effective operation of BDDM.

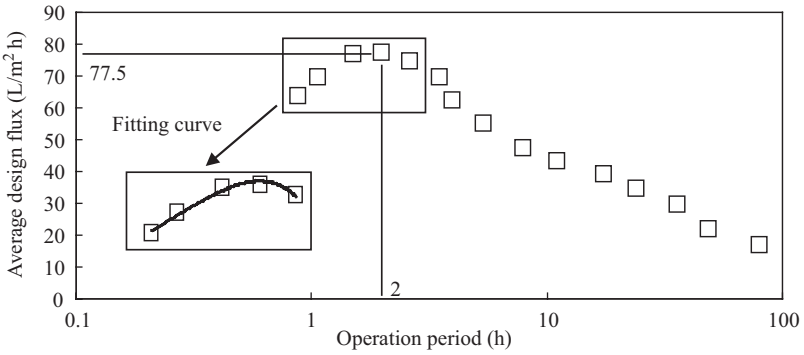

Figure 8.8: Average design flux versus operation period.

8.1.4.3 BDDM morphology

The SEM pictures of different section of the BDDM are shown in Figure 8.9. The surface of cake layer was flat (Figure 8.9(a, b)) with fine and homogeneous deposits on its surface, as well as high porosity and a little roughness of the cake layer. All the above properties are fine, and homogeneous, which are beneficial for improving filtration flux and SS retention capability of BDDM.

There were deeply impressions left on the back surface of the BDDM by the embedded stainless steel mesh lines (Figure 8.9(d)). At the beginning of the formation of BDDM, the bio-diatomite particles were intercepted by the support mesh lines. Though the size of the diatomite particles is much smaller than the mesh aperture, microorganisms and extracellular polymer substances adhered to the surface of diatomite make the bio-diatomite particles bind tightly through bridging action. Once the BDDM is formed, the support meshes mainly exert the function of supporting the cake layer and improving the strength of the dynamic membrane.

8.1.4.4 BDDM backwash

The on-line air backwash was used to clean the BDDM, and the clean results were shown in Table 8.5 and Figure 8.10.

Under the same backwash pressure and flux, Case B of high design flux and short filtration time was much more effective than Case A of low design flux and long filtration time. The residual bio-diatomite covered more than 30% of the

EBSCOhost - printed on 2/14/2023 6:39 AM via . All use subject to https://www.ebsco.com/terms-of-use

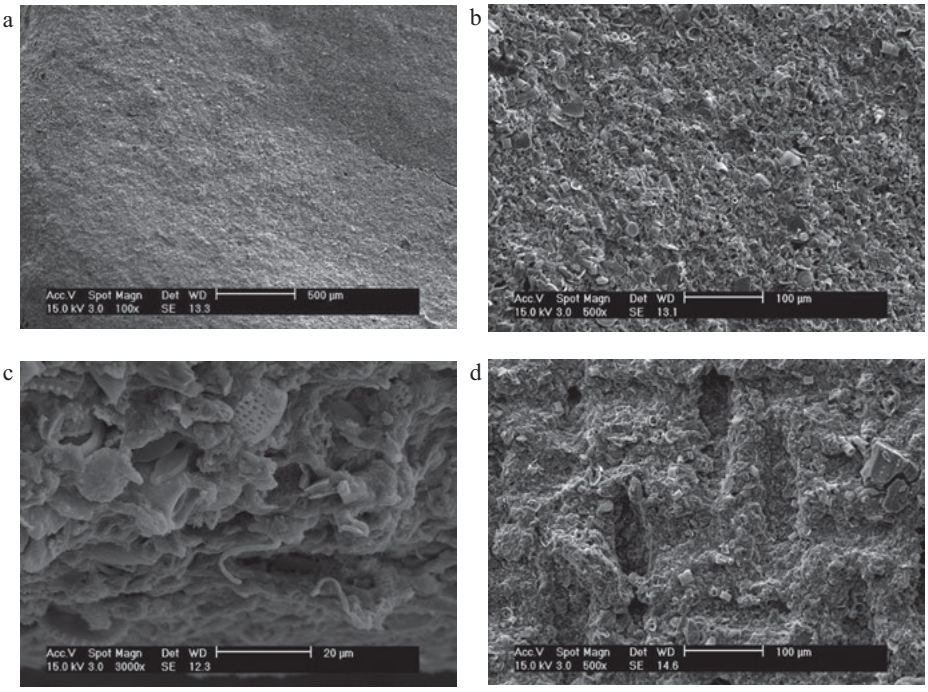

Figure 8.9: SEM pictures of different sections of the BDDM: a and b, the surface facing the mixed liquor; c, the back surface to the support mesh; d, the side of the cross section near the support mesh.

module surface in Case A with a relatively longer backwash time of 3 min. whereas, the cleaning efficiency of Case B was much higher with only 2 min backwash. Microorganisms adhesion between the support mesh and the BDDM cake layer might be the reason for the clean difference. At a high design flux, microorganisms had a short time to reproduce and form membrane-mesh adhesion with a short backwash interval. While the effect of microorganisms' adhesion at a low design flux was opposite. It can be concluded that a reasonable high design flux is facilitated for stable operation of BDDM.

Table 8.5: Backwash parameters of two typical work conditions.

Case	Design flux ($L/(m^2 \cdot h)$)	Filtration time (h)	Operation pressure (kPa)	Backwash flux ($m^3/(m^2 \cdot h)$)	Backwash pressure (kPa)	Backwash time (min)
A	22	48	40	18.58	10	3
B	40	9.3	20	18.58	10	2

EBSCOhost - printed on 2/14/2023 6:39 AM via . All use subject to https://www.ebsco.com/terms-of-use

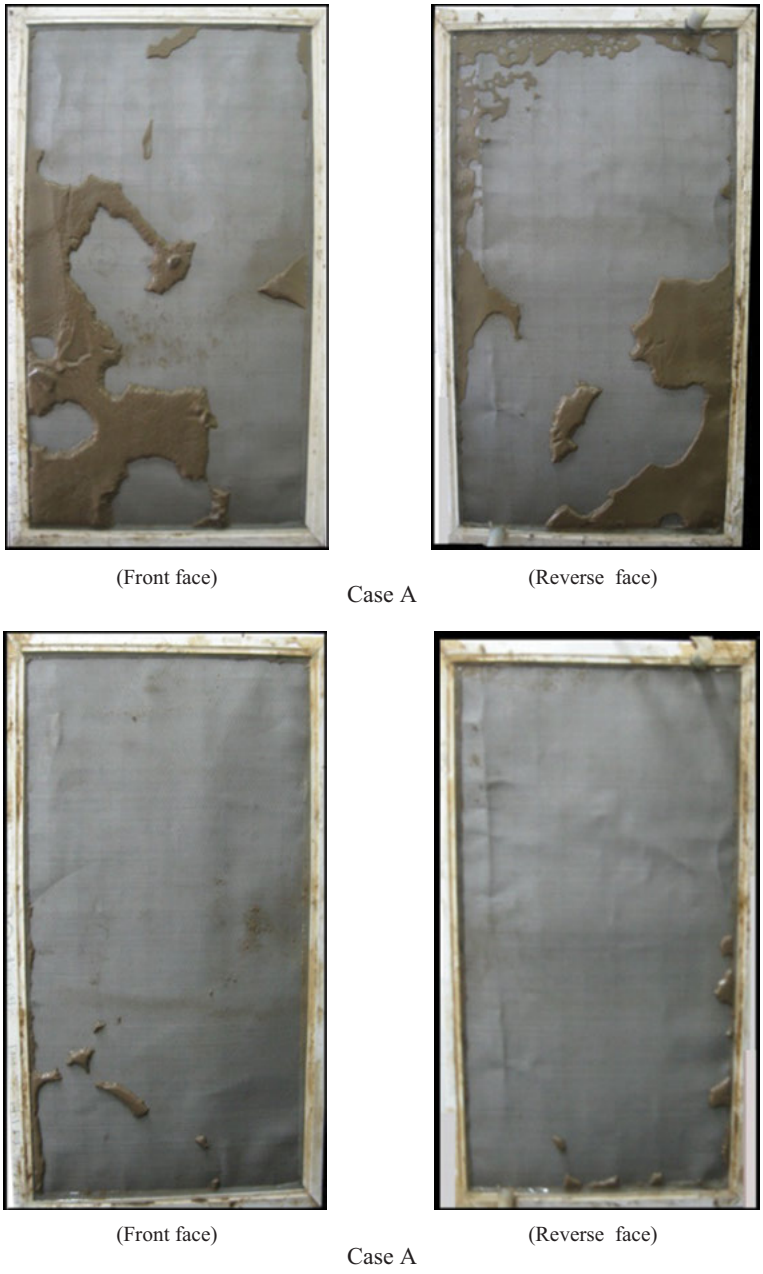

Figure 8.10: Residual layer on support mesh surface after backwash.

EBSCOhost - printed on 2/14/2023 6:39 AM via . All use subject to https://www.ebsco.com/terms-of-use

8.2 The BDDMR for micro-polluted surface water treatment with laboratory scale

8.2.1 Materials and methods

The aerobic BDDMR with total effective volume of 8.1 L was shown in Figure 8.11. Stainless steel mesh with an equivalent aperture of 74 μm was used for the BDDM support module with a double-sided effective filtration area of 0.046 m^2 (20 cm × 11.5 cm). The raw surface water was obtained from Sanhaowu river on Tongji campus (Table 8.6). Diatomite particles with an equivalent diameter of 5–20 μm were continuously added to the bioreactor. The concentrations of MLSS and MLVSS in the BDDMR were maintained at about 12,000 mg/L and 3,500–4,000 mg/L, respectively. The average sludge age was set at 40 d.

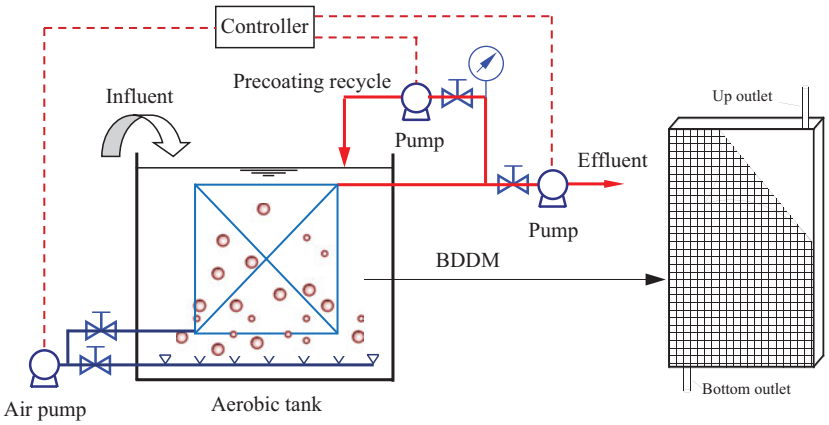

Figure 8.11: Diagram of the BDDMR process.

Table 8.6: Characteristics of raw water.

Water quality parameters	Range
Temperature (°C)	18.6–29.6
pH	6.92–7.83
Turbidity (NTU)	2.5–4.7
COD_{Mn} (mg/L)	4.4–6.1
TOC (mg/L)	2.3–3.2
UV_{254} (cm^{-1})	0.061–0.084
NH_4-N (mg/L)	0.41–2.52

The BDDM filtration flux of 50 L/(m^2 · h) was fixed corresponding to an HRT of 3.5 h. A high-precision vacuum pressure gauge was installed on the effluent pipe for the

EBSCOhost - printed on 2/14/2023 6:39 AM via . All use subject to https://www.ebsco.com/terms-of-use

operation pressure measurement. The filtration was stopped once the operation pressure reached 40 kPa and then on-line air backwash was started.

8.2.2 Results and discussion

8.2.2.1 Operation properties of the BDDM

In the precoating process, the effluent SS decreased swiftly in the first 2 min, and then declined slowly to below the detection limit at about 15 min (Figure 8.12(a)). Meanwhile, the filtration flux showed a similar variation trend. The TMP increased rapidly with the increasing flux, and the operation flux is correlated with the filtration time (Figure 8.12(b)). A long filtration time can worsen the backwash efficiency because the residual bio-diatomite particles are over-compacted on the surface of the support mesh. Therefore, 50 L/($m^2 \cdot h$) was selected as the operation flux in the next study.

8.2.2.2 Pollutant removal

The pollutant removal efficiencies by the BDDMR were shown in Figure 8.13 when the bioreactor kept stable operation status. The parameters of effluent quality should comply with the regulation of Chinese National Standards for Drinking Water Quality (CNSDWQ, GB5749-2006).

The BDDMR exhibited excellent solid-liquid separation capacity with a stable effluent turbidity concentration of 0.26–0.43 NTU (Figure 8.13(a)), whose value was much lower than the regulation below 1.0 NTU of the CNSDWQ (GB5749-2006). Figure 8.13(b) shows that the COD_{Mn} of the influent varied from 4.4 to 6.1 mg/L, but a quite stable effluent concentration (i.e., 2.37 mg/L on average) was achieved by the BDDMR. The CNSDWQ (GB5749-2006) regulates a maximum contamination level (MCL) of 3.0 mg/L for COD_{Mn}. If the micro-polluted raw water with COD_{Mn} concentration of 6.0 mg/L or even higher, a water treatment plant with the conventional process of coagulation/sedimentation/sand filtration can hardly reduce COD_{Mn} to below 3.0 mg/L (CNSDWQ, GB5749-2006)). Therefore, the BDDMR may be a promising technology to face this big challenge. The BDDMR has a good removal efficiency for DOC and UV_{254} of 47.6% and 53.7% on average, respectively (Figure 8.13(c, d)). Meanwhile, the NH_4-N effluent was below 0.35 mg/L with high removal efficiency of 75.5–89.8% (Figure 8.13(e)). It can be seen from Figure 8.13(f) that the three detected trihalomethanes of $CHCl_3$, $CHCl_2Br$ and $CHClBr_2$ with an effluent concentration of 53, 49 and 8 μg/L, respectively, corresponding to a removal efficiency of 67%, 48% and 55%, which indicate that THMFP could be removed effectively by the BDDMR.

EBSCOhost - printed on 2/14/2023 6:39 AM via . All use subject to https://www.ebsco.com/terms-of-use

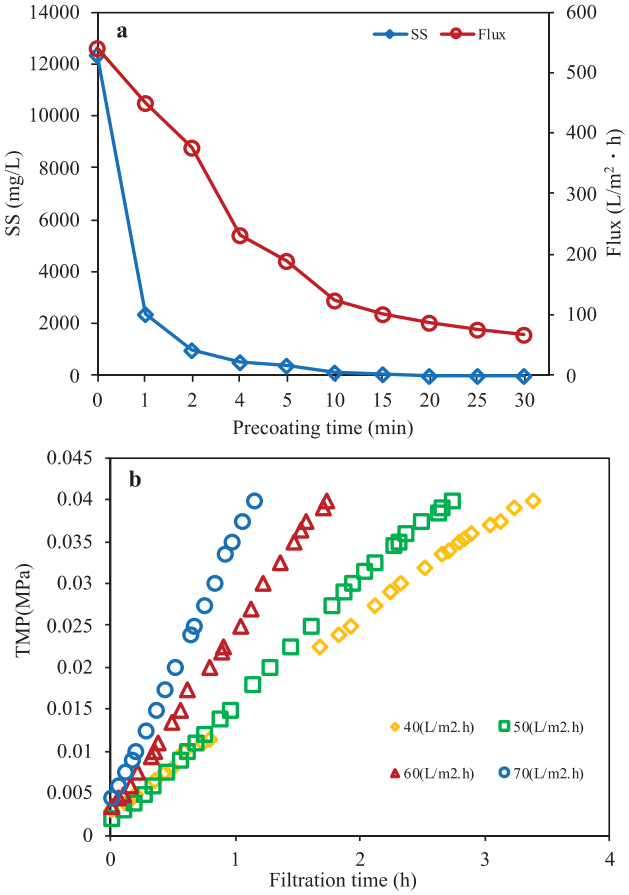

Figure 8.12: (a) Variations of flux and effluent SS in the precoating stage; and (b) variations of operation pressure under different design fluxes.

The mechanisms contributing to the pollutant removal in the BDDMR may be ascribed to the microbial degradation, membrane interception and bio-diatomite adsorption. The removal efficiencies of COD_{Mn}, NH_4-N, DOC and UV_{254} by the BDDM alone were only 8.7%, 5.4%, 8.9% and 10.3%, respectively, as shown in Figure 8.14. Therefore, the major capacity of BDDM was for SS retention. In this experiment, a high concentration of MLSS (ca. 12,000 mg/L) and MLVSS (3,500–4,000 mg/L) were obtained in the BDDMR, thus the biodegradation of dissolved organic materials and ammonia was enhanced. Therefore, the removal of COD_{Mn}, NH_4-N, DOC and UV_{254} was mainly achieved by the microbial degradation of the bio-diatomite mixed liquor.

EBSCOhost - printed on 2/14/2023 6:39 AM via . All use subject to https://www.ebsco.com/terms-of-use

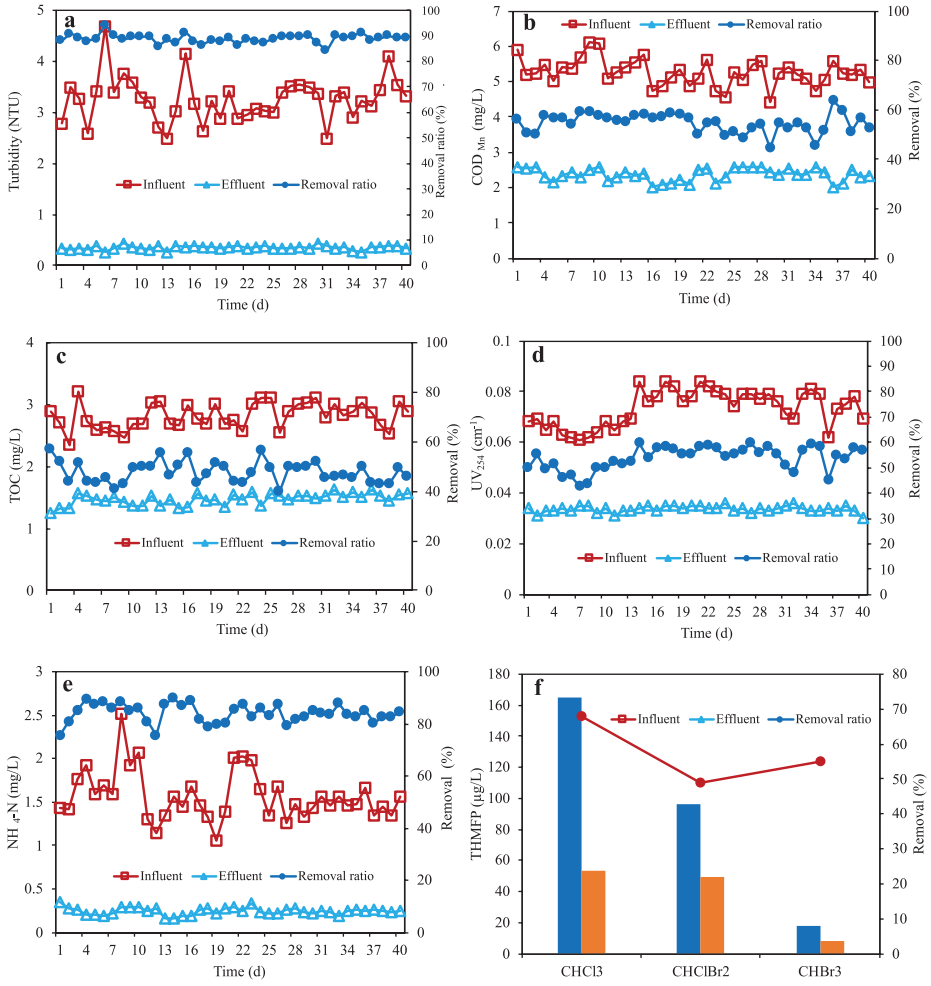

Figure 8.13: Pollutants removal by BDDMR.

8.2.2.3 Backwash of BDDM

The backwash stage started when the TMP increased to 40 kPa. The online air backwash was also adopted in this study [12]. The air backwash parameters were set at air pressure of 20 kPa and air flux of 7.2 L/($m^2 \cdot s$) under the blackwash time of 2 s. As expected, it can be seen from Figure 8.15(a, b) that the cake layer could be removed completely from the membrane surface after air backwash, with clean surface restored. The BDDM cut from the support module had a smooth surface and about 23 mm thickness (Figure 8.15(c, d). The bio-diatomite particles was combined by microorganisms

EBSCOhost - printed on 2/14/2023 6:39 AM via . All use subject to https://www.ebsco.com/terms-of-use

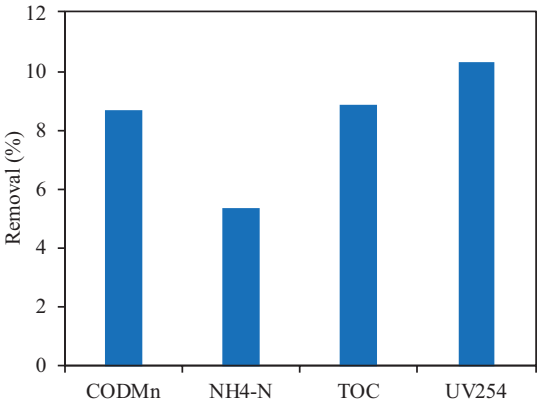

Figure 8.14: Removal of pollutants by BDDM alone. Data represents the average values of triplicate experiments.

and extracellular polymer substances (Figure 8.15(e)), which was similar to the BDDM formed in the aforementioned municipal wastewater treatment process.

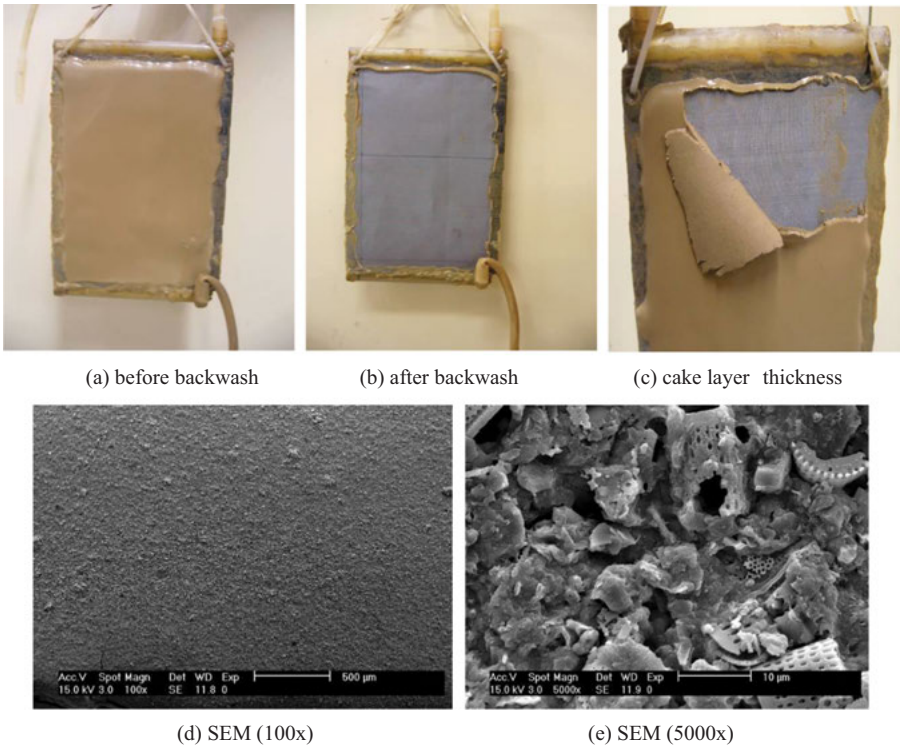

Figure 8.15: Pictures of BDDM under different circumstances.

EBSCOhost - printed on 2/14/2023 6:39 AM via . All use subject to https://www.ebsco.com/terms-of-use

8.3 Pilot-scale hybrid BDDMR for slightly polluted water purification

8.3.1 Materials and methods

8.3.1.1 Experimental materials

The effective volume of the pilot-scale BDDMR was 0.768 m^3 (1.2 m × 0.8 m × 0.8 m) (Figure 8.16), in which five flat-sheet dynamic membrane modules were fixed with a double-sided effective filtration area of 0.4 m^2 per module (Figure 8.17). Characteristics of raw water collected from Taihu Lake are shown in Table 8.7.

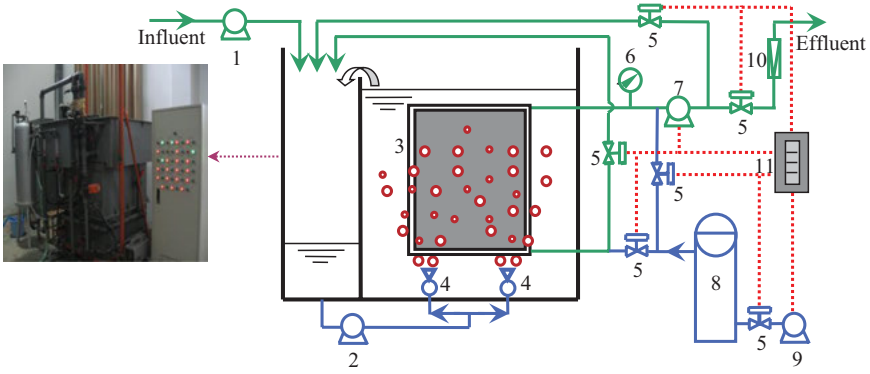

Figure 8.16: Diagram of the BDDMR: (1) feed pump; (2) circumfluence pump; (3) dynamic membrane support module; (4) water air-diffuser; (5) solenoid valves; (6) manometer; (7) suction pump; (8) pressure vessel; (9) air pump; (10) flowmeter; (11) controller.

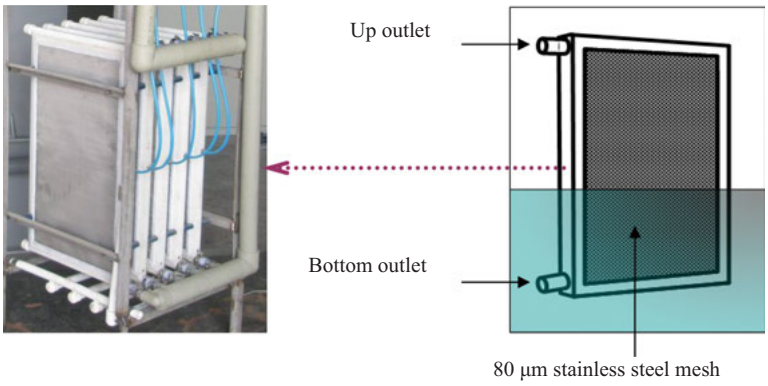

Figure 8.17: Pictures of the BDDMR support module.

EBSCOhost - printed on 2/14/2023 6:39 AM via . All use subject to https://www.ebsco.com/terms-of-use

Table 8.7: Characteristics of raw water.

Parameters	Range
Turbidity (NTU)	6.28–17.6
COD_{Mn} (mg/L)	3.28–5.44
UV_{254} (cm^{-1})	0.083–0.121
NH_4-N (mg/L)	0.04–0.28
Br^- (μg/L)	<10–30
Temperature (°C)	15.8–36.7
pH	7.47–8.80

8.3.1.2 Experimental protocol

It can be seen from Table 8.7 that the raw water with slightly pollution was dystrophic for microbial growth due to the lack of nitrogen and organic carbon. Thus, the following methods were adapted to provide sufficient nutrients for microbial growth. In the first 5 days, glucose and ammonium sulfate were added to the influent to increase COD_{Mn} and NH_4-N to around 10 mg/L and 1.0–3.0 mg/L, respectively. Then, the biodiatomite was matured after 30 days of under the continuously operation mode of feeding the raw water.

A constant water head (0.8 m) was set to drive the precoating process in the first 10 min, and then a suction pump was started for 10 min to enhance BDDM formation, whose effluent was fed back to the mixing area through the precoating pipe. Once the precoating process was finished, the solenoid valve on the effluent pipe was simultaneously opened while the one on the precoating pipe was turned off. The SRT of the BDDMR was set at 50 d by discharging 2% of the mixed liquor in the reactor and adding the corresponding diatomite daily.

The following experiment was carried out to figure out the specific mechanism for pollutant removal in the BDDMR. The diatomite adsorption was defined alone in a fully mixed reactor with MLSS of 10 g/L and HRT of 8.0 h. The BDDM module covered with cake layer was carefully taken out of the pilot-scale bioreactor and submerged into another tank only with the same raw water from the Miao-jing River, which was used to test the pollutant removal effect by the BDDM alone.

8.3.2 Results and discussion

8.3.2.1 BDDM precoating process

The operation process of the BDDM was referred from the above studies. Under the constant water head (0.8 m) for the precoating process driving in the first 10 min, the

EBSCOhost - printed on 2/14/2023 6:39 AM via . All use subject to https://www.ebsco.com/terms-of-use

effluent turbidity declined swiftly from 975 NTU to 58.5 NTU. And then a suction pump was started for 10 min to enhance the BDDM formation (Figure 8.18), resulting in a fluctuation peak of effluent turbidity at 637 NTU. After 40 min, the effluent turbidity was less than 1 NTU. The precoating time in the above laboratory experiment was 25 min under the constant water head of 60 cm without pump suction. The added pump suction here was in order to connect with the filtration process automatically.

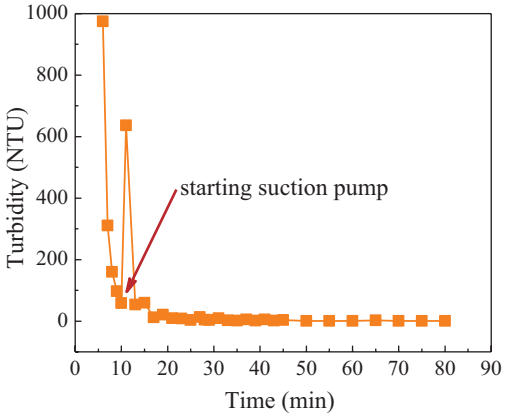

Figure 8.18: Effluent turbidity versus pre-coating time.

8.3.2.2 Pollutant removal by the BDDMR

Pollutant removal by the BDDMR is shown in Figure 8.19 during an 80 d steady-state operation period. The effluent turbidity was less than 1.0 NTU under the influent fluctuation from 8.22 to 17.6 NTU. From the particle counting results shown in Figure 8.19(b), the total particles number in the influent was 69,624 per mL, and reduced sharply to 296 per mL in the effluent with a removal efficiency of 99.57%. The particle number with the diameter from 2 μm to 10 μm accounted 98.77% of the total particle number in the influent. Therefore, the BDDM exhibited high retention capacity of small particles.

The average removal efficiency of COD_{Mn}, UV_{254} and NH_4-N by the BDDMR was 52.9%, 50.58% and 80.2%, respectively, which were much higher than those capacities of the traditional coagulation-sedimentation-sand filtration process, ultrafiltration and microfiltration membrane separation, as well as even higher than those in a membrane bioreactor (MBR) for drinking water treatment [21, 22].

The removal efficiencies of the three types of THMs were shown in Figure 8.20. It can be seen that the concentrations of $CHCl_3$, $CHCl_2Br$, and $CHClBr_2$ in the effluent was 35.6, 19.7, and 9.9 μg/L, respectively, corresponding to the removal efficiencies of 51.7%, 49.6%, and 47.1%, respectively. All of the THMs concentrations comply with the requirements of the CNSDWQ (GB5749-2006).

EBSCOhost - printed on 2/14/2023 6:39 AM via . All use subject to https://www.ebsco.com/terms-of-use

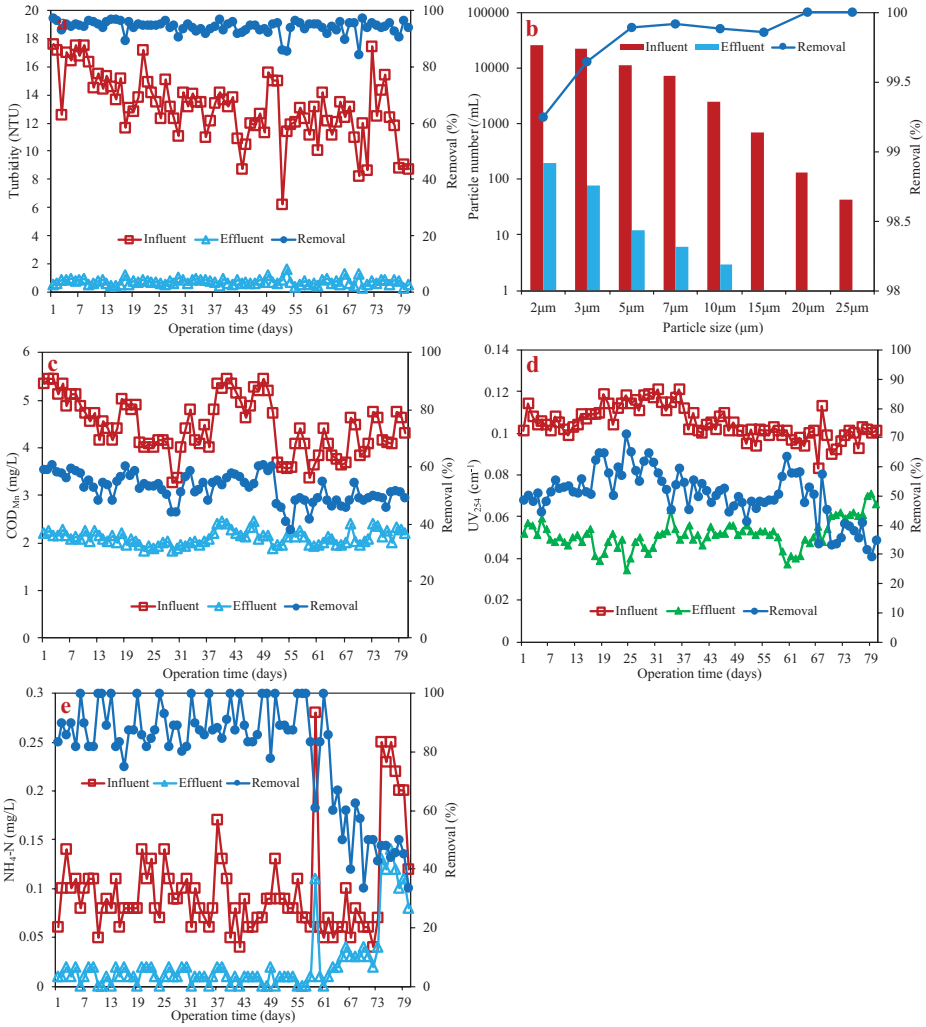

Figure 8.19: Pollutant removal by BDDMR.

8.3.2.3 Backwash of BDDM

Figure 8.21 shows the TMP changes as a function of operation time at four different dynamic membrane fluxes. In the early filtration stage, the TMP kept invariant of all the four filtration conditions, and the stage was shortened as the filtration flux increased. Then, the TMP rose quickly to 4.5 kPa of each of the selected fluxes, and the TMP curve had greater slope with the larger flux. As the operation process proceeded, air bubbles and rapidly augmented turbidity appeared in the effluent. Therefore, an

EBSCOhost - printed on 2/14/2023 6:39 AM via . All use subject to https://www.ebsco.com/terms-of-use

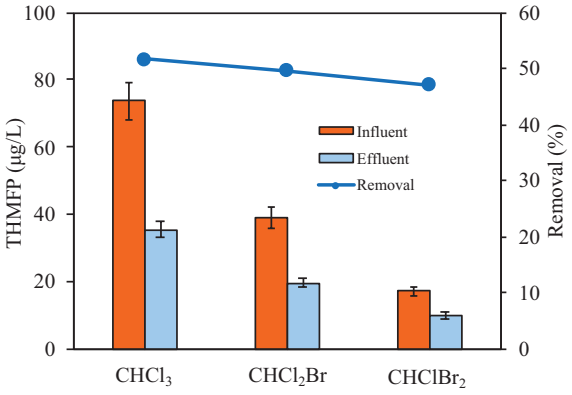

Figure 8.20: Removal of THMFP by the BDDMR.

on-line air pressure vessel backwash with an air pressure of 3.5 kgf/cm^2 was used to slough off the dynamic membrane cake layer from the support mesh.

The picture and SEM of the module support mesh and cake layer after backwash were presented in Figure 8.22. It can be seen that there was still some cake layer residual on the support mesh after backwash, and some substances like microorganisms and extra-cellular polymer substances tightly attached to the module support mesh. The backwash process of BDDM still need optimization to improve the backwash efficiency in the large-scale utilization.

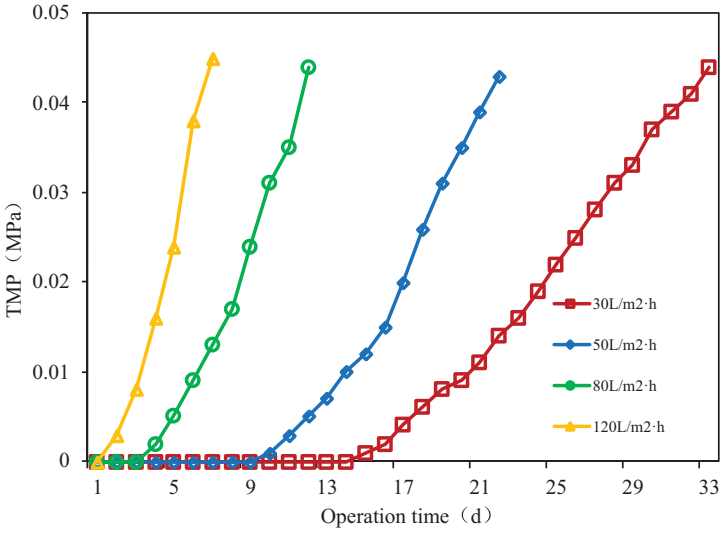

Figure 8.21: TMP versus operation time at different fluxes.

EBSCOhost - printed on 2/14/2023 6:39 AM via . All use subject to https://www.ebsco.com/terms-of-use

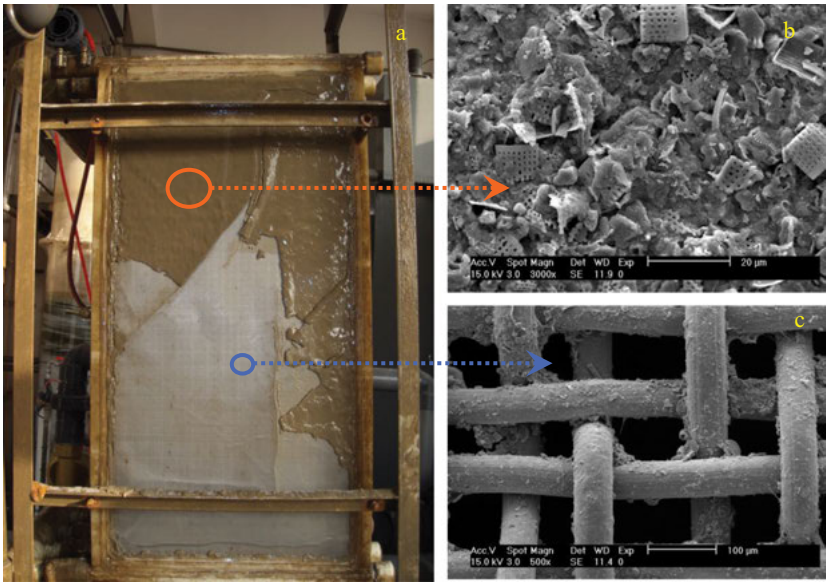

Figure 8.22: Real picture of the backwashed module (a); SEM observations of cake layer (b) and backwashed stainless steel mesh (c).

8.3.2.4 Pollutant removal mechanisms of BDDMR

Three mechanisms, such as microbial biodegradation, bio-diatomite adsorption, and bio- diatomite dynamic membrane rejection, are employed to explain the removal of pollutants by the BDDMR.

1 Specific individual effect for pollutant removal

The dynamic membrane alone could reduce COD_{Mn}, UV_{254}, TOC and NH_4-N of the influent by 9.9%, 10.2%, 9.7% and 6.5%, respectively (Figure 8.23). Meanwhile, diatomite static adsorption with the same raw surface water and diatomite concentration of three hours was carried out to examine the removal efficiency of pollutants through diatomite adsorption alone, which showed that 15.4%, 5.0%, 20.0% and 12.5% of COD_{Mn}, UV_{254}, TOC, and NH_4-N was removed, respectively. Once the diatomite was covered by the microorganisms, the diatomite adsorption capacity was basically stopped. The pollutants removal was mainly ascribed to microbial degradation when the bio-diatomite was matured, while the diatomite addition was provided as the carrier material for attaching microorganisms in the system.

EBSCOhost - printed on 2/14/2023 6:39 AM via . All use subject to https://www.ebsco.com/terms-of-use

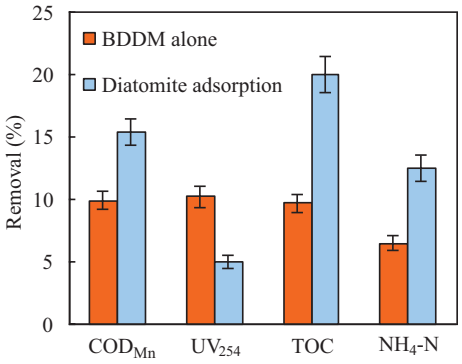

Figure 8.23: Pollutants removal by BDDM alone and diatomite adsorption alone.

2 DOM fractions and MW distributions analysis

Here, DOM of the water sample was separated into four fractions, i.e. HPO, TPI, N-HPI, and C-HPI, as shown in Figure 8.24. In the mixed liquor, the removals of HPO, TPI, N-HPI and C-HPI were approximately 54.6%, 52.2%, 17.0% and 7.3%, respectively. The cake layer alone achieved little removal effect for the four fractions with the rejection efficiencies of HPO, TPI, N-HPI and C-HPI being only 8.3%, 6.2%, 3.1% and 1.5%, respectively. The BDDMR was able to effectively eliminate the fractions of HPO and TPI.

From Figure 8.24(b), the apparent molecular weight distribution (MWD) of organic matters in the influent were mainly in the range from 3,200 to 1,000 Da with four obvious peaks, which declined by approximately 15% after BDDMR treatment. It also can be concluded that the dynamic membrane alone could partially remove the peak cluster of MWD of 1,000–3,200 Da, and the organic matter with a MWD less than 1,000 Da could penetrate the membrane.

3 Bacterial community analysis in BDDMR

The variations of microbial communities of the bio-diatomite in the BDDMR was analyzed by the PCR-DGGE with the operation time changes, as shown in Figure 8.25. There is obvious difference of the bacterial community structures between the operation beginning and the matured stage of the bio-diatomite. At the beginning of the operation, no obvious degradation of pollutants occurred by the uncultured freshwater bacterium (Band 2) and uncultured acidobacteria bacterium (Band 3) microbes. The microbes of uncultured bacteroidetes (Band 4), uncultured acidobacteria bacterium (Band 5) and uncultured candidate division OD1 bacterium (Band 6) became dominant after 30 days of cultivation. The uncultured bacteroidetes bacterium could induce carbon conversion and may play a critical role in carbonaceous organic material degradation [23]. Acidobacterial bacterium was a diverse and widely distributed

EBSCOhost - printed on 2/14/2023 6:39 AM via . All use subject to https://www.ebsco.com/terms-of-use

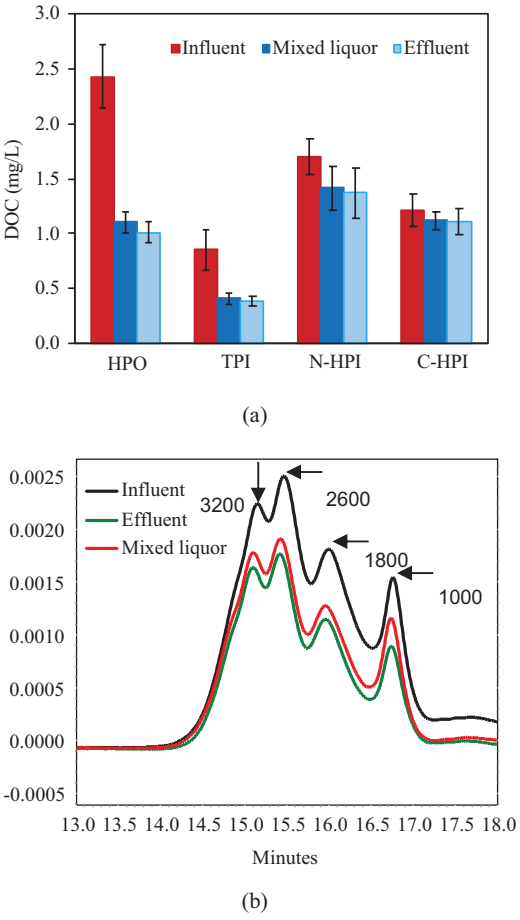

Figure 8.24: Fractions and MW distribution analysis.

group of microorganisms that has few cultivated representatives [24]. Candidate division OD1 was globally distributed in freshwater settings and dominant in the environmental libraries of plankton.

EBSCOhost - printed on 2/14/2023 6:39 AM via . All use subject to https://www.ebsco.com/terms-of-use

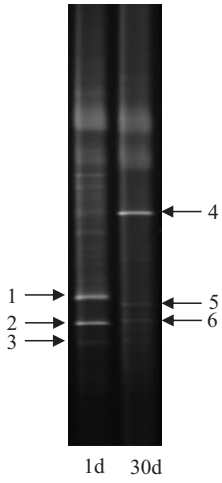

Figure 8.25: Variations of microbial communities of the bio-diatomite in different operation time.

8.4 Summary

A novel bio-diatomite dynamic membrane reactor was developed, which can be used in municipal wastewater treatment and micro-polluted surface water treatment. The BDDMR could effectively remove organic matters and ammonium nitrogen, which was mainly ascribed to microbial degradation of the bio-diatomite mixed liquor with high concentrations of MLSS (12,000 mg/L) and MLVSS (3,500–4,000 mg/L) and the BDDM alone and diatomite absorption was much less effective in removing pollutants.

The BDDM formed on the stain-steel support mesh showed a smooth surface and a thickness of 2–3 mm, with the operation process including the precoating stage, filtration stage and backwash stage. The BDDM exhibited excellent capacity of solid-liquid separation with high filtration flux. Air backwash with low pressure could slough off the BDDM effectively.

References

[1] Choi, K.Y.-J. and Dempsey, B.A., In-line coagulation with low-pressure membrane filtration. Water Research, 2004. 38(19): p. 4271–4281.

[2] Howell, J.A., Chua, H.C., and Arnot, T.C., In situ manipulation of critical flux in a submerged membrane bioreactor using variable aeration rates, and effects of membrane history. Journal of Membrane Science, 2004. 242: p. 13–19.

[3] Gander, M., Jefferson, B., and Judd, S., Aerobic MBRs for domestic wastewater treatment: A review with cost considerations. Separation and Purification Technology, 2000. 18(2): p. 119–130.

EBSCOhost - printed on 2/14/2023 6:39 AM via . All use subject to https://www.ebsco.com/terms-of-use

[4] Xie, R.J., Gomez, M.J., and Xing, Y.J., Permeate flux optimization of a pilot microfiltration plant for cost-effectiveness of water reclamation for reuse. Journal of Environmental Science and Health, Part A, 2006. 41(7): p. 1169–1181.
[5] Kuberkar, V.T. and Davis, R.H., Modeling of fouling reduction by secondary membrane. Journal of Membrane Science, 2000. 268(1): p. 243–258.
[6] Marcinkowsky, A.E., et al., Hyperfiltration studies Salt rejection by dynamically formed hydrous oxide membranes. Journal of the American Chemical Society, 1966. 88(24): p. 5744–5750.
[7] Fuchs, W., et al., Influence of operational conditions on the performance of a mesh filter activated sludge process. Water Research, 2004. 39(5): p. 803–810.
[8] Khraisheh, M.A.M., Al-degs, Y.S., and Mcminn, W.A.M., Remediation of wastewater containing heavy metals using raw and modified diatomite. Chemical Engineering Journal, 2003. 99(2): p. 177–184.
[9] Zhao, Y., et al., Municipal wastewater water treatment by moving-bed-biofilm reactor with diatomaceous earth as carriers. Water environment research, 2006. 78(4): p. 392–396.
[10] Jin, W., et al., Treatment of municipal wastewater using combined bio-diatomaceous earth. Journal of Tongji University, 2005. 33(12): p. 1626–1629.
[11] Al-Malack, M.H. and Anderson, G.K., Cleaning techniques of dynamic membranes. Separation and Purification Technology, 1997. 12(1): p. 25–33.
[12] Chu, H., et al., Characteristics of bio-diatomite dynamic membrane process for municipal wastewater treatment. Journal of Membrane Science, 2008. 325(1): p. 271–276.
[13] Chu, H., et al., Bio-diatomite dynamic membrane reactor for micro-polluted surface water treatment. Water Research, 2009. 44(5): p. 1573–1579.
[14] Fan, B., et al., A submerged dynamic membrane bioreactor for domestic wastewater treatment. Chinese Journal of Enviromental Science, 2002. 23(6): p. 51–56.
[15] Xu, J., et al., Continuous-flow test for treatment of municipal wastewater using raw diatomaceous earth. China Water & Wastewater, 2007.
[16] Tchobanoglous, G., Burton, F.L., and Stensel, H.D., Wastewater engineering: Treatment and reuse. 2003, McGraw-Hill, NewYork.
[17] Rittmann, B.E. and McCarty, P.L., Environmental Biotechnology: Principles and Applications. 2001, McGraw-Hill, NewYork.
[18] Kiso, Y., et al., Wastewater treatment performance of a filtration bio-reactor equipped with a mesh as a filter material. Water Research, 2000. 34(17): p. 4143–4150.
[19] Lu, W., et al., Compression of deformable gel particles. Powder Technology, 2001. 116(1): p. 1–12.
[20] Hwang, K.J., Yu, Y.H., and Lu, W.M., Cross-flow microfiltration of submicron microbial suspension. Journal of Membrane Science, 2001. 194(2): p. 229–243.
[21] Sagbo, O., et al., Effect of PAC addition on MBR process for drinking water treatment. Separation and Purification Technology, 2007. 58(3): p. 320–327.
[22] Tian, J., et al., Membrane coagulation bioreactor (sMBR) for drinking water treatment. Water Research, 2008. 42(14): p. 3910–3920.
[23] Blümel, M., Süling, J., and Imhoff, J.F., Depth-specific distribution of Bacteroidetes in the oligotrophic Eastern Mediterranean Sea. Microbiology Ecology, 2007. 46: p. 209–224.
[24] Radajewski, S., McDonald, I.R., and Murrell, J.C., Stable-isotope probing of nucleic acids: A window to the function of uncultured microorganisms. Current Opinion in Biotechnology, 2003. 14(3): p. 296–302.

EBSCOhost - printed on 2/14/2023 6:39 AM via . All use subject to https://www.ebsco.com/terms-of-use

Qingqing Zhao, Yong Wei, Kuo Gao

Chapter 9
Pollution Removal by TiO_2/UV Photocatalysis Coupled with Membrane Filtration

9.1 Humic acid removal TiO_2/UV photocatalysis coupled with membrane filtration

Humic acid (HA), is an important components of natural organic matter (NOM). It mainly comes from the decomposition products of plant/animal metabolism and exists in both surface and ground water. HA in water would affect the taste and the impressions, and contend for adsorption sites during coagulation and activated carbon treatment. Besides, during chlorination, HA could be transformed into disinfection by-products, such as trihalomethane (THM), haloacetic acid and haloacetonitrile. Therefore, it is important to control the concentration of HA in surface water treatment. Previous work has demonstrated that it is different to remove NOM (including HA) in conventional treatment. Generally speaking, TOC removal rate is about 10–50% during conventional purification [1].

Although micro-filtration (MF) and ultra-filtration (UF) could remove some macromolecule efficiently, such as turbidity and pathogen, their removal performance for NOM is poor. It is believed that MF/UF removal rates for NOM are less than 10% [2, 3].

Photocatalytic oxidation is an efficient method to remove HA. The study about photocatalytic oxidation started to raise, since Japanese scholars Fujishima and Honda published a paper on Nature in 1972 [4], saying that optical radiation on TiO_2 monocrystal electrode can decompose water and produce hydrogen. In 1977, Frank and Bard achieved great progress in oxidation of pollutants with semiconductor [5]. They studied the photodecomposition of p-dihydroxybenzene, I^-, Br^-, Cl^-, Fe^{2+}, Ce^{3+} and Cr^{3+} with ultraviolet ray radiating TiO_2 polycrystal electrode, and found TiO_2 powder performed well in pollutant photodecomposition. In 1984, Ollis et al. made great progress in photocatalytic decomposition of organic pollutant, and published the first paper on the application of photocatalysis for wastewater disposal [6], followed by a large number of studies [7]. Due to the high photocatalytic performance and stability, less environmental pollution and low cost, TiO_2 became the commonly used photocatalyst and this technique became a hot spot research [8]. TiO_2 could

Qingqing Zhao, Kuo Gao, College of Environmental Science and Engineering, Tongji University, Shanghai, P. R. China
Yong Wei, School of Environmental and Safety Engineering & School of Urban Construction, Changzhou University, Changzhou, Jiangsu, P. R. China

https://doi.org/10.1515/9783110596847-009

EBSCOhost - printed on 2/14/2023 6:39 AM via . All use subject to https://www.ebsco.com/terms-of-use

be applied as suspended powder, and it could be fixed on some materials, such as glass, quartz, stainless steel, etc. [9, 10]. On the one hand, the surface area and photocatalytic activity of TiO_2 decrease significantly if fixed [11], on the other hand, if TiO_2 disperses in water, although photodecomposition performance enhances, it is difficult to reclaim this catalysis.

Photocatalysis coupled with membrane separation could handle these problems [12]. Membrane could not only separate photocatalysis, but also selectively separate some photo-decomposed molecule. Compared to common photocatalytic reactor, submerged membrane-photocatalysis reactor (SMPR) has some characteristics [13–16], i.e. on one hand, membrane can limit the reaction environment of photocatalysis, thus solving the dilemma of reaction and separation in the reactor; on the other hand, hydraulic retention time (HRT) could be easily controlled by adjusting the outflow. This system has two advantages, i.e. it could enhance organic matter removal, and reduce the membrane pollution in the meantime. Therefore, these two parts could complement each other, prolonging the lifespan of membrane and improving the performance [17].

Most membrane used in SMPR is hollow fiber membrane, and the performance of air cleaning is important to that of SMPR separation: effective air cleaning benefits for the reduction of fouling resistance, prolonging the cleaning cycle and lifespan of membrane. As for plate membrane module [18], the up-flow gas-liquid fluid could enhance the contact area, and the upward shear force benefits washing membrane, thus relieving the deposit and clogging of photocatalyst on the membrane surface. Comparing to the hollow fiber membrane, the pollution rate of plate membrane is much slower, since the powerful water-gas cross flow significantly improves cleaning performance [19].

This study presents a new submerged flat membrane photocatalysis reactor (FSMPR), which uses commercial TiO_2 as catalyst to decompose HA. The effects of ultraviolet illumination intensity, TiO_2 dosage, initial HA concentration, pH value and H_2O_2 dosage to HA removal rate were systematically investigated.

Besides, plenty of studies only focused on some general parameters, such as TOC analysis and ultraviolet spectroscopy, for evaluating performance and impact on membrane pollution [20–24]. Although these parameters could reflect the overall evaluation of reactor performance, they cannot be used to analyze the reaction mechanism and its impact to the whole system. Therefore, experiments under intermittent model were performed as well (using commercial TiO_2 and FSMPR to decompose HA with initial pH of 7). During the reaction, the concentration of DOC, the variation of UV_{254} and the ultraviolet/visible spectrum, UV adsorption index (UVAI), THMFPs were monitored, and the other characteristics of organic matter, such as relative molecular mass (MW), three-dimensional fluorescence spectrum (EEMs) and TMP, were analyzed. Several different methods were used to demonstrate the chemical reaction process and the impacts of intermediate products to membrane separation performance.

EBSCOhost - printed on 2/14/2023 6:39 AM via . All use subject to https://www.ebsco.com/terms-of-use

9.1.1 Materials and methods

9.1.1.1 Materials

The photocatalyst used in this study is nanoscale TiO_2 powder (Degussa, P25, average diameter = 25 nm, SSA = 50 m^2/g). A small amount of TiO_2 was accurately weighed and mixed in ultrapure water prior to use. The flat membrane is made of polyvinylidene fluoride (PVDF, provided by Jiangsu blue sky membrane), and its mean pore size is 0.08 μm, with effective membrane area of 0.02 m^2 (single surface for outflow). Water used in this study was produced by Milli-Q, with the electrical resistivity larger than 18 MΩ · cm. The raw water was prepared by resolving HA (Shanghai Jufeng Chemical Technique Co. Ltd) in ultrapure water and dilute to some extent, with assistance of NaOH (pH = 12). 1 g HA was resolved in 100 mL NaOH (0.1 M) and diluted to 1,000 mL. The mixture was filtered by cellulose acetate membrane (mean pore size = 0.45 μm, Shanghai Xingya Purification Material Co. Ltd) to remove the insoluble powder, and stored in refrigerator. Before use, the mixture pH was adjusted to 7 by 0.1 M HCl and 0.01 M NaOH, and diluted to the desired concentration (presented by DOC). Other chemical agents used were all analytical grade. The membrane sank in ethyl (3%, V/V) for 24 h, and then washed by ultrapure water to remove the organic matter prior to use. All the membrane samples were stored in ultrapure water (4 °C).

HA used in this study is a kind of macromolecular condensation compound, combined with phenolic hydroxyl group, carboxyl group, alcoholic hydroxyl group matters. HA has no unified construction. Generally speaking, HA has one or some aromatic nucleus as core, surrounded by plenty of linear chain and branched chain connecting to each other with ether bond, ester bond and other kinds of covalent bonds. The Fourier transform infrared spectrum (FTIR) is presented in Figure 9.1 that 3401.4 cm^{-1} may represent OH, NH or the stretching vibration peak of hydrogen bond association, arene and carboxylic acid; 1597.5 cm^{-1} may represent symmetric stretching vibration peak of benzene ring; and 1114.7 cm^{-1} may represent stretching vibration peak of -C-O. Other peaks are listed in Table 9.1.

9.1.1.2 Experimental setup

In this study a new photocatalysis membrane separation reactor, named submerged flat membrane photocatalysis reactor (FSMPR), is designed. The body of the reactor is made of food-grade stainless steel plate, with effective volume of 8 L (L × B × H, 18 cm × 12 cm × 40 cm). Stainless steel cover plate (B × H × δ, 18 cm × 12 cm × 40 cm), whose bottom is 5 cm far away from the bottom of the reactor, separates the reactor into two parts, i.e. photocatalysis reaction zone and membrane separation zone, whose volume ratio is 1:1 and connected with each up-down flow path. There are three ultraviolet sources (16 W, 253.7 nm, Philip), which have their own on-off systems,

EBSCOhost - printed on 2/14/2023 6:39 AM via . All use subject to https://www.ebsco.com/terms-of-use

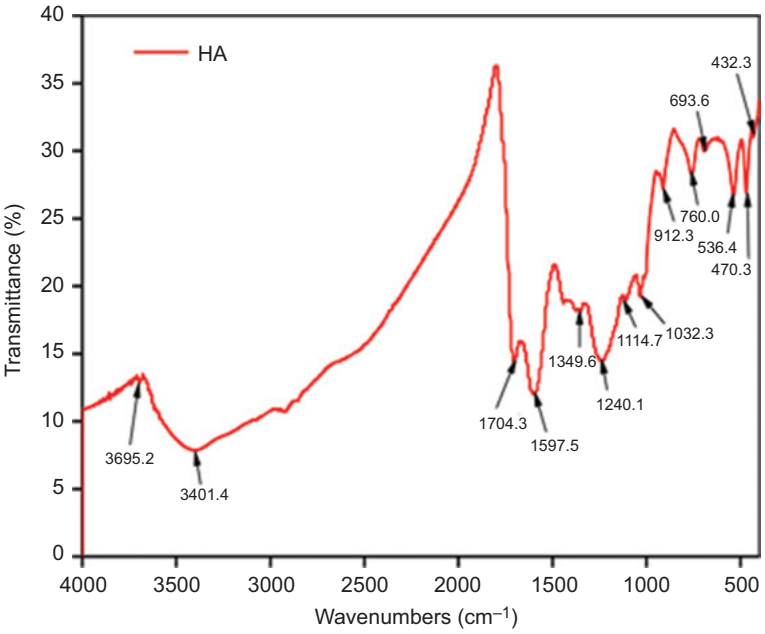

Figure 9.1: The FTIR Spectrum of HA.

Table 9.1: The FTIR spectrum of HA

Peak Position (cm^{-1})	Function Group
3401.4	OH or NH, Hydrogen Bond Association, Arene, Carboxylic Acid
1704.3	COOH and C = O
1597.5	Symmetric Stretching Vibration Peak of Benzene Ring
1349.6	δ_{CH2}
1240.1	Stretching/Bending Vibration Peak of -COOH
1114.7	Stretching Vibration Peak of -C-O
1032.3	C-N
912.3	Surface Bending Vibration Peak of CH_2
760.0	Symmetric Surface Bending Vibration Peak of C-H on the Aromatic Ring
693.6	Substituted Benzene

vertically fixed in the middle of the quartz cover. With a rectangular micropore air diffusion equipment (titanium plate, air throughput: 0–4 L/min), on the one hand, the air could enhance the exchange between reaction zone and separation zone; on the other hand, the up-flow water could wash the membrane and reduce the membrane pollution. In addition, in order to promote the material exchange between two zones, the reactor equips a recycle pump (1 min/L). Samples were drawn periodical

EBSCOhost - printed on 2/14/2023 6:39 AM via . All use subject to https://www.ebsco.com/terms-of-use

under steady experimental condition. After experiment, the membrane was washed by water and chemical agent, and then sank in ultrapure water until next experiment.

The reaction mechanism and influence factors, such as ultraviolet illumination intensity, TiO_2 dosage, initial HA concentration, pH value and H_2O_2 dosage were studied under intermittent condition. Methods including DOC, UV, THMFP, AWM and EEMs were applied to detect the reaction intermittent products for the investigation of reaction mechanism and their membrane separation characteristics.

The schematic diagram of the reactor applied in intermittent condition is presented in Figure 9.2. Before turning on the aeration pump and the ultraviolet light, the reactor was filled with HA solution and TiO_2. The reactor operation adapts the intermittent pattern (the outflow was recycled to the reactor), maintaining constant effective volume of 8 L. During the experiment, the membrane flux was controlled by the rotating speed of peristaltic pump and the operation of pump by time relay (rest 1 min after work for 10 min), and the reactor temperature was maintained at 25 °C by circulating cooling water. The transmembrane pressure (TMP) was measured by precious pressure gauge fixed on outflow pipe.

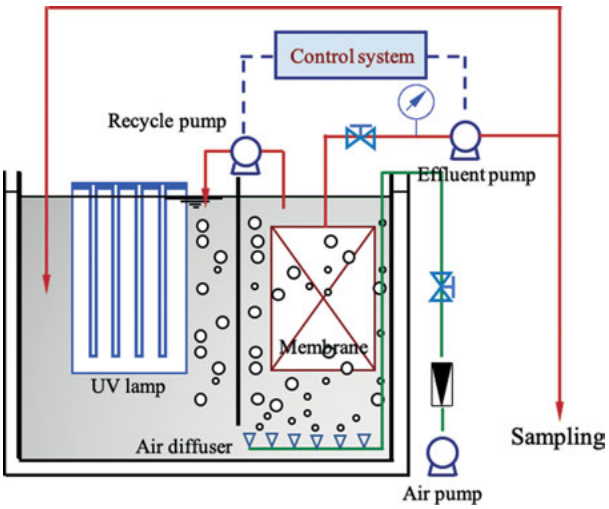

Figure 9.2: The schematic diagram of the reactor.

9.1.2 Results and discussions of influence factors

9.1.2.1 The influence of ultraviolet intensity

The intensity of ultraviolet light is an important factor to HA removal. In this study, it was adjusted by the number of lights that are turned on. Figures 9.3 and 9.4 present the HA removal rate and decomposition rate as the function of light intensity, respectively

EBSCOhost - printed on 2/14/2023 6:39 AM via . All use subject to https://www.ebsco.com/terms-of-use

(TiO_2 = 0.5 g/L, DOC_0 = 10 mg/L). After ultraviolet radiated for 240 min, compared to one-light group, the removal rate of three-light and two-light improves 25% and 15%, respectively; on the other hand, if we ignore the adsorption of TiO_2, in three-light group, DOC decomposition rate constant is 0.0080 min^{-1}, which is 1.95 times to that of one-light group (0.0041 min^{-1}) and 1.67 times to two-light group (0.0048 min^{-1}). We could conclude that ultraviolet intensity greatly influences the HA removal, i.e. when the number of lights reduces, the light intensity reduces as well, and as consequence, part of TiO_2 lacks of light and the electrons remain stable, resulting in less electron hole pair and •OH and finally reducing HA catalytic oxidation capacity. Thus, increasing ultraviolet intensity in a proper range could enhance the organic matter decomposition rate of the reactor.

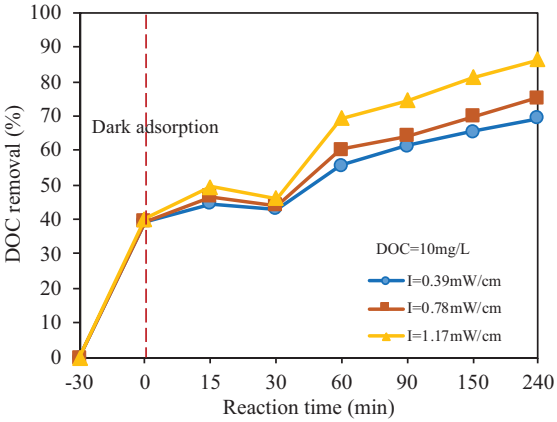

Figure 9.3: The HA removal rate as the function of light intensity.

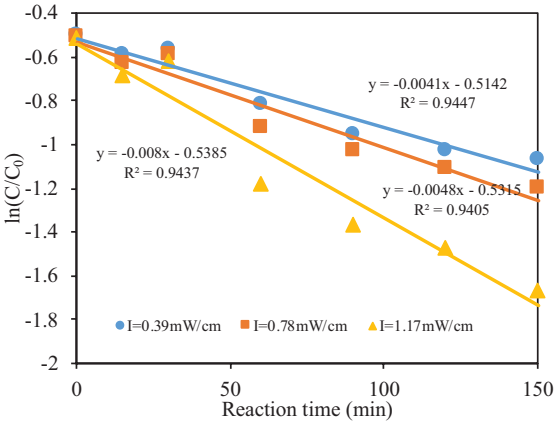

Figure 9.4: The HA decomposition rate as the function of light intensity.

EBSCOhost - printed on 2/14/2023 6:39 AM via . All use subject to https://www.ebsco.com/terms-of-use

9.1.2.2 The influence of TiO_2 concentration

Previous studies have suggested that photocatalysis efficiency has a strong relationship with TiO_2 concentration. As the increasing of TiO_2 concentration, the photocatalysis reaction activity and catalysis oxidation rate increases. However, in the meantime, too much TiO_2 would increase the turbidity and thus weaken the ultraviolet adsorption and prohibit the promotion of reaction rate. In this study, three different TiO_2 concentrations, 0.1 g/L, 0.5 g/L and 1.0 g/L were investigated. Figure 9.5 presents the results of DOC removal rate with different TiO_2 concentration as a function of reaction time. The initial HA concentration is 10 mg/L, and after ultraviolet radiation for 150 min, DOC removal rate is up to 80% when TiO_2 concentrations are 0.5 and 1.0 g/L, while when TiO_2 concentration is 0.1 g/L, DOC removal rate is only 67%.

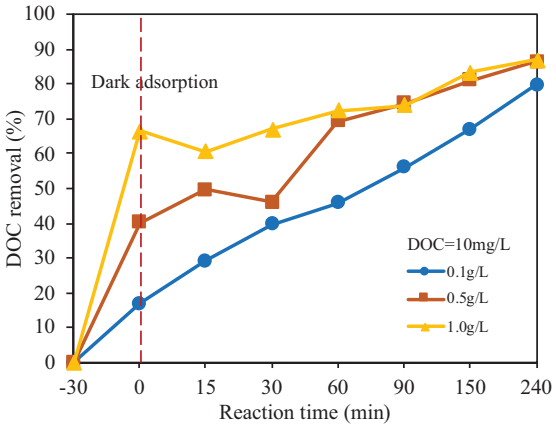

Figure 9.5: The influence of TiO_2 mass concentration on removal of HA.

In order to minimize the influence of TiO_2 adsorption, 30 min dark adsorption was performed before turning on the light. Thus, DOC removal during this time is attributed to the TiO_2 physical adsorption, and DOC removal rate are 17% (0.1 g/L), 40% (0.5 g/L) and 60% (1.0 g/L), respectively. Thus, prior to ultraviolet radiation, the DOC removal is ascribed to TiO_2 adsorption. When TiO_2 concentration are 0.5 and 1.0 g/L, DOC slightly increases at 30 and 15 min, respectively, which might be explained by the release of intermittent products. And these intermittent products often exhibit better hydrophilia. After that, the DOC decline is mainly attributed to the mineralization of organic matters by photocatalytic oxidation. After radiation for 240 min, there is 13% DOC residual (0.5 and 1.0 g/L), which indicates that part of HA and intermittent products are refractory with TiO_2/UV treatment. The results of fitting suggest that adsorption follows first order reaction (Eq. (9.1)), and the adsorption balance equation fits

EBSCOhost - printed on 2/14/2023 6:39 AM via . All use subject to https://www.ebsco.com/terms-of-use

Langmuir model (Eq. (9.2)); besides, the multiphase photocatalysis reaction complies with Langmuir-Hinshelwood dynamic model [25–27]:

$$r = -kq \tag{9.1}$$

$$q = \frac{q_{\max} bc}{1 + bc} \tag{9.2}$$

where r represents reaction rate; k is the first order reaction constant; c is the substrate concentration in solution; q_{max} is maximal adsorption capacity; and b is the adsorption balance constant of Langmuir. When c is small enough, the equation could be simplified as first order reaction Eq. (9.3), in which k_a represents the constant of first order reaction and C_0 initial substance concentration:

$$\ln\left(\frac{C}{C_0}\right) = -k_a t \tag{9.3}$$

If the initial adsorption could be ignored, the photocatalytic oxidation process follows the first order reaction, as shown in Figure 9.4, which suggests that L-H model could describe the HA decomposition by TiO_2/UV. The reaction rate constants are 0.0061, 0.0080, 0.0051 min^{-1} when TiO_2 concentrations are 0.1, 0.5 and 1.0 g/L, respectively. As shown in Figure 9.5, the DOC decomposition rate first raises and then declines as the concentration of TiO_2 increases. This is because that proper increase of TiO_2 could increase the reaction surface, while too much could increase the solution turbidity and thus weaken ultraviolet adsorption. In Figure 9.6, when TiO_2 concentration increases to 1.0 g/L, the decomposition rate is smaller than that of 0.5 g/L, even smaller than that of 0.1 g/L, which suggests that ultraviolet adsorption is a limiting factor. Therefore, in a certain range, reaction rate is not in a positive correlation with TiO_2, and too much could constrain the reaction process.

9.1.2.3 The influence of initial HA concentration

Langmuir-Hinshelwood (L-H) model is generally used to describe the influence of initial substance concentration to organic photocatalytic decomposition rate. It is assumed in L-H model that once reaching the adsorption saturation point, there is no more adsorption. Numerous studies demonstrated that the reaction rate constant of TiO_2/UV photocatalysis increases as initial substance concentration increases [27, 28], while some get the opposite conclusion [17]. In this study, two initial HA concentrations, 5 and 10 mg/L (DOC), similar to other work, were adopted (Figure 9.7). Ignoring the initial dark adsorption, it is interesting to notice that the reaction rate constant of these two groups are very close (0.0079 and 0.0080 min^{-1}). Thus, this phenomenon

EBSCOhost - printed on 2/14/2023 6:39 AM via . All use subject to https://www.ebsco.com/terms-of-use

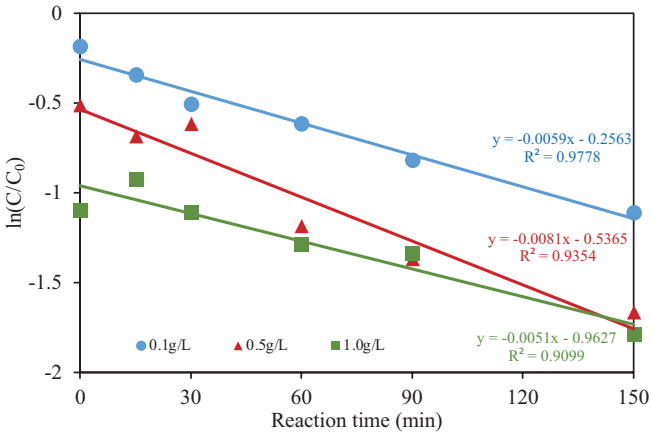

Figure 9.6: The influence of TiO_2 mass concentration on HA degradation rate.

cannot be due to lacking ultraviolet photon with higher initial HA concentration. This should be attributed to that larger part of HA is adsorbed by TiO_2 with lower initial HA concentration. As shown in Figure 9.8, in the dark adsorption period, the HA removal rate reaches 53% when initial HA concentration is 5 mg/L, while that is only 40% when initial HA concentration is 10 mg/L. This suggests that the adsorption capacity of certain amount of TiO_2 is limited, i.e. when adsorption process reaches balance, no more adsorption occurs. Therefore, lower initial HA concentration with higher removal rate is mainly attributed to adsorption, but the photocatalysis reaction constant does not increase significantly.

9.1.2.4 The influence of initial pH

In photocatalysis system, pH is an important factor to determine the characteristics of the solid catalyst and the solute molecules. Therefore, pH value could influence the reaction rate of photocatalysis system and TiO_2 adsorption rate. In this study, initial pH was adjusted to 4.5, 7.0 and 9.4 by NaOH and HCl, and the initial HA concentration is 10 mg/L (DOC) with TiO_2 of 0.5 g/L. As shown in Figure 9.9, when the initial pHs are 4.5 and 7.0, the DOC removal rates are 67% and 40%, respectively. However, when initial pH is adjusted to 9.4, DOC removal rate is only 17%. These results demonstrate that HA is more inclined to attach to TiO_2 under acidic condition, which agrees with previous work [29].

Figure 9.10 shows the results of dynamic fitting. It presents that pH value influences HA decomposition significantly and lower pH promotes photocatalysis rate and the whole removal rate. The photocatalysis process could be described by Eqs. (9.4)–(9.6):

EBSCOhost - printed on 2/14/2023 6:39 AM via . All use subject to https://www.ebsco.com/terms-of-use

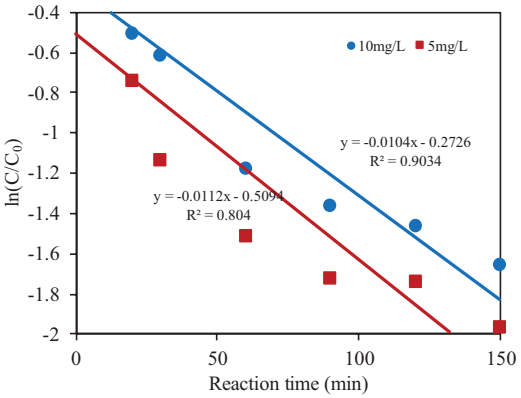

Figure 9.7: The influence of initial HA concentration on DOC degradation rate.

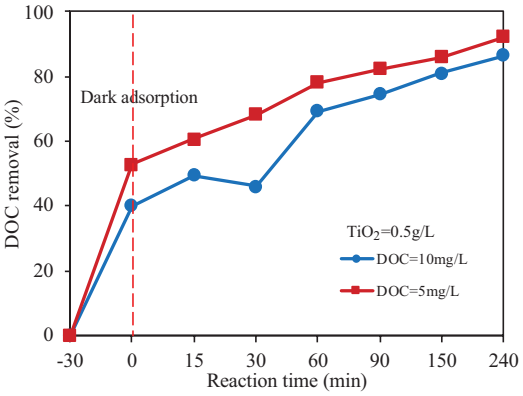

Figure 9.8: The influence of initial HA concentration on DOC removal.

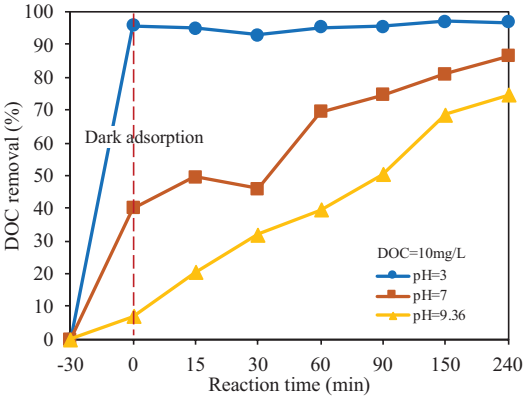

Figure 9.9: The influence of initial pH on removal of DOC.

EBSCOhost - printed on 2/14/2023 6:39 AM via . All use subject to https://www.ebsco.com/terms-of-use

$$TiO_2 + OH^{-1} + 2H^+ + \bullet O_2^- \rightarrow 3 \bullet OH + TiO_2 \tag{9.4}$$

Equilibrium rate constant K_e is often calculated by Eq. (9.5):

$$K_e = \left[\bullet OH\right]^3 / \left(\left[OH^-\right]\left[H+\right]^2\left[\bullet O_2^-\right]\right) \tag{9.5}$$

Since $[OH^-][H^+] = K_w = 10^{-14}$, Eq. (9.5) could be adopted to Eq. (9.6):

$$\left[\bullet OH\right]^3 = K_e K_w \left[H^+\right]\left[\bullet O_2^-\right] \tag{9.6}$$

[•OH] increases as $[H^+]$ increases. As shown in Figure 9.10, the constant of photocatalysis decomposition decreases as pH increases: $K_{pH4.5}$(0.0110 min^{-1}) > $K_{pH7.0}$(0.0080 min^{-1}) > $K_{pH9.4}$(0.0071 min^{-1}). Therefore, photocatalysis decomposition with initial pH of 4.5 is faster than that with 9.4, and the lower pH is in favor of photocatalysis reaction.

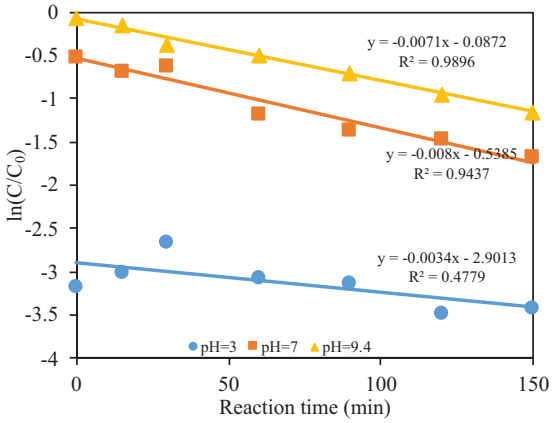

Figure 9.10: The influence of initial pH on DOC degradation rate.

9.1.2.5 The influence of H_2O_2

Figures 9.11 and 9.12 demonstrate that the addition of a little H_2O_2 could promote the removal and decomposition rate in photocatalysis-membrane system. After the addition of H_2O_2, the constant of apparent reaction rate increases 71%, from 0.008 to 0.013 min^{-1}, for which the synergistic effect between ultraviolet and H_2O_2 greatly promotes the reaction rate. The synergistic effect could be described as equations from (9.7) to (9.11):

EBSCOhost - printed on 2/14/2023 6:39 AM via . All use subject to https://www.ebsco.com/terms-of-use

$$TiO_2 + h\nu \rightarrow h^+ + e^- \tag{9.7}$$

$$h^+ + H_2O \rightarrow \bullet OH + e^- \tag{9.8}$$

$$h^+ + OH^- \rightarrow \bullet OH \tag{9.9}$$

$$H_2O_2 + h\nu \rightarrow 2\bullet OH \tag{9.10}$$

$$H_2O_2 + e^- \rightarrow \bullet OH + OH^- \tag{9.11}$$

Eqs. (9.7) to (9.9) describe the process of TiO_2 photocatalysis and •OH production; Eq. (9.10) represents the process that H_2O_2 is radiated by ultraviolet and produces •OH; while Eq. (9.11) describes the process that H_2O_2 captures the electron and then produce •OH. The reaction between H_2O_2 and conduction electron enhance the concentration of •OH; besides, H_2O_2 could suppress the electron hole recombination, which can be used to evaluate the oxidation efficiency of electron hole, thus to enhance the number of •OH production. The synergistic effect among UV, H_2O_2 and TiO_2 produces more •OH, thus promoting the photocatalytic decomposition of HA.

As shown in Figures 9.11 and 9.12, the addition amount of H_2O_2 could influence photocatalytic oxidation efficiency of HA. After adding 1 M H_2O_2, the DOC removal rate improves from 86.3% to 92.7%, and the decomposition rate from 0.0080 to 0.014 min^{-1}. However, when H_2O_2 dosage increases to 10 M, the removal rate and decomposition rate decreases to 86.2% and 0.0075 min^{-1}, respectively. This phenomenon could be explained by Eqs. (9.12) and (9.13):

$$H_2O_2 + \bullet OH \rightarrow H_2O\bullet + H_2O \tag{9.12}$$

$$H_2O\bullet + \bullet OH \rightarrow H_2O + O_2 \tag{9.13}$$

Too much H_2O_2 would react with •OH and lead to •OH loss, prohibiting the improvement of reaction rate. Therefore, a proper amount of H_2O_2 could enhance photocatalytic decomposition performance.

9.1.3 Results and discussion of photocatalysis enhanced membrane separation

Based on the results above, in this part, experiments were conducted under the conditions of: 1) three ultraviolet light (intensity = 1.17 mW/cm^2); 2) TiO_2 concentration = 0.5 g/L; 3) initial HA concentration = 10 mg/L (DOC); 4) initial pH = 7.0. In order to investigate the reaction mechanisms, no H_2O_2 was added.

EBSCOhost - printed on 2/14/2023 6:39 AM via . All use subject to https://www.ebsco.com/terms-of-use

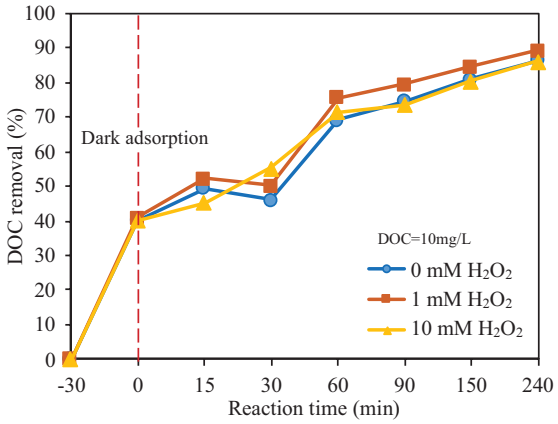

Figure 9.11: The effect of H_2O_2 addition on removal of DOC.

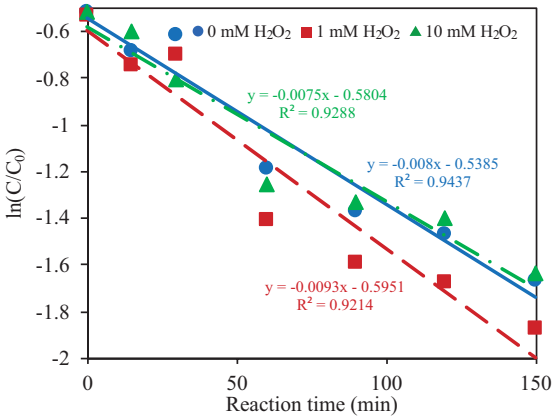

Figure 9.12: The effect of H_2O_2 addition on DOC degradation rate.

9.1.3.1 The removal of HA

Figure 9.13 presents the DOC and UV_{254} removal rate as a function of time in FSMPR. A large amount of DOC and UV_{254} removal prior to ultraviolet radiation is due to the TiO_2 adsorption. After radiation for 30 min, DOC has a slight increase but the UV_{254} goes through a successive descent, which indicates that the desorbed intermittent products have better hydrophilicity than HA, and cannot adsorb ultraviolet at 254 nm. Figure 9.14 presents the variation of adsorption of FSMPR in the range of 190–600 nm. As the reaction processes, the adsorption intensity gradually decreases and finally disappears. Prior to ultraviolet radiation, a rapid decrease occurs, which could be due to TiO_2 adsorption. After that, the gradual descent is owning to the photocatalytic

EBSCOhost - printed on 2/14/2023 6:39 AM via . All use subject to https://www.ebsco.com/terms-of-use

effect of TiO_2, which exhibits excellent performance for HA catalytic oxidation under ultraviolet radiation. Besides, the spectrum provides solid evidence that the intermittent products have no adsorption of light, especially at 254 nm.

Besides, the removal rate of UV_{254} is apparently higher than that of DOC. After radiation for 150 min, the removal rate of UV_{254} is close to 100%, while that of DOC is only 86%. Since the removal of UV_{254} can only present the decomposition of HA [30] but that of DOC could reflect the mineralization extent of organic matters, this result indicates that the HA mineralization is apparently slower than HA photocatalytic decomposition. As shown in Figure 9.15, the removal processes of UV_{254} and DOC both follow first order reaction dynamic model, and their decomposition rate constants are 0.021 and 0.010 min^{-1}, respectively. The former is 2.1 times as much as the latter, which demonstrates that TiO_2 photocatalytic decomposition for HA is much faster than that of DOC. After 150 min radiation, there is still 1.5 mg/L DOC residual in the solution, indicating that this part of organic matter is not mineralized, which may come from the raw water or intermittent products. In order to get higher mineralization rate, the reaction must be prolonged.

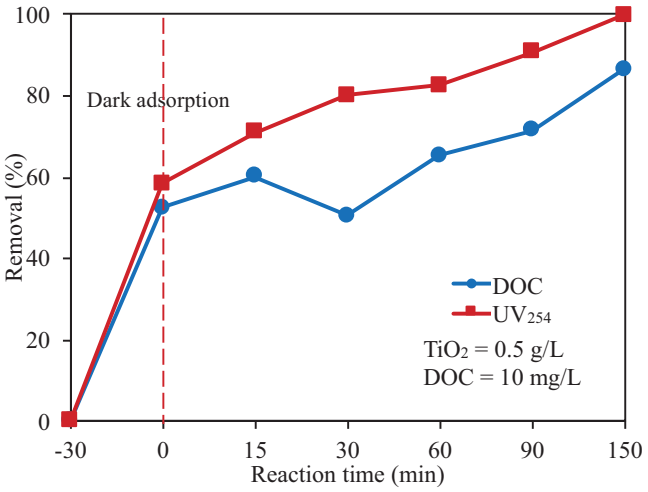

Figure 9.13: The removal of DOC and UV_{254} in FSMPR system.

Specific ultraviolet adsorption (SUVA) is defined as the ratio of UV_{254} and DOC. Water with high SUVA often has a large amount of NOM, such as HA. Previous study has found that SUVA has a relationship with the relative molecular mass and the structure of aromatic compounds [31]. Thus, SUVA could be used to describe the structure of aromatic compounds, and to evaluate the characteristics of DOC. Figure 9.16 presents the variation of SUVA: the first drop is due to the hydrophobic matter adsorption by TiO_2; the fast decrease after radiation for 30 min is due to the production of

EBSCOhost - printed on 2/14/2023 6:39 AM via . All use subject to https://www.ebsco.com/terms-of-use

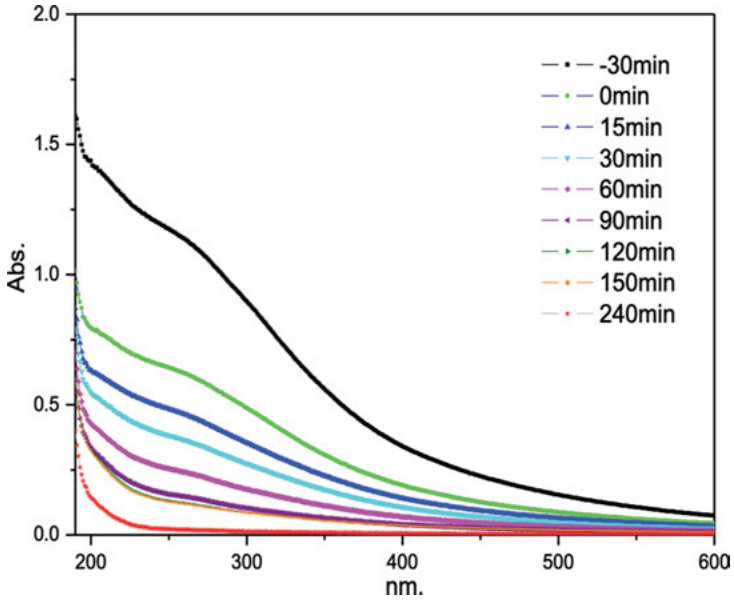

Figure 9.14: The variation of absorbance at different time in FSMPR system.

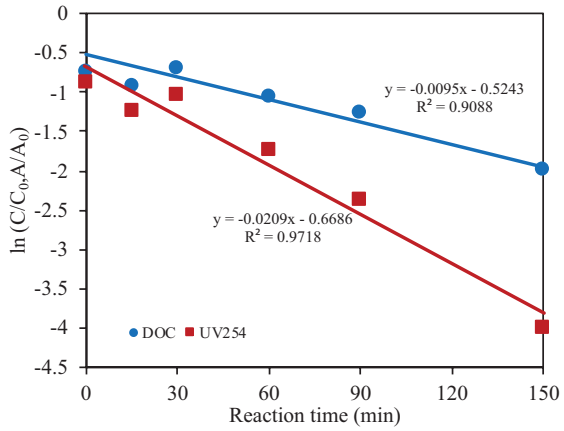

Figure 9.15: DOC and UV_{254} degradation rate in FSMPR system.

intermittent products with no adsorption at 254 nm; after that, the SUVA goes through a gentle decrease. It is documented that membrane pollution and DBP production are all related to SUVA [32–34]. Thus, after treatment by FSMPR, the lower SUVA promises less DBP production and membrane pollution.

EBSCOhost - printed on 2/14/2023 6:39 AM via . All use subject to https://www.ebsco.com/terms-of-use

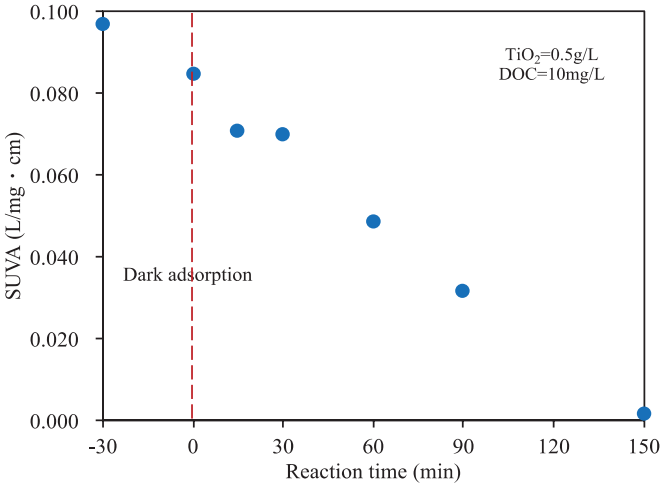

Figure 9.16: SUVA degradation in FSMPR system.

9.1.3.2 THMFP Analysis

THMFP is often used to evaluate the chlorination by-products. Figure 9.17 presents the trihalomethane value of the chlorinated water after different reaction time. The total THMFP only has one type, trichloromethane, which is because of the low bromide concentration. The raw water has 570 μg/L THMFP, which could be due to that chlorine is inclined to react with electron-rich organic matters, such as aromatic substances and 1, 3-dicarbonyl adipose groups [35]. Thus, the structure of organic matters greatly influences the chlorine consumption and trichloromethane production. After 150 min treatment, THMFP reduces to 19 μg/L. And the effluent after 90 min disposal could meet the national sanitary standard for drinking water (GB 5749-2006, $CHCl_3 < 60$ μg/L), which demonstrates that the system could efficiently remove the precursor of trihalomethane. Besides, it is interesting to notice that the variation of THMFP is similar to that of UV_{254} and DOC, but the removal of THMFP is a little bit faster than that of DOC. The specific TTHMFP (THMFP/DOC) analysis found that the initial value of 57 μg/mg reduces to 14 μg/mg, suggesting that trichloromethane precursor is easily photocatalytic decomposed by TiO_2. Although 150 min radiation is not enough for mineralization, it is long enough to change the structure of trichloromethane precursor and reduce the reaction activity of residual organic matters with chlorine [36].

9.1.3.3 Membrane separation efficiency analysis

The transmembrane pressure (TMP) is applied to evaluate the membrane pollution. Under a certain condition, when the membrane flux is fixed, TMP should be as low as

EBSCOhost - printed on 2/14/2023 6:39 AM via . All use subject to https://www.ebsco.com/terms-of-use

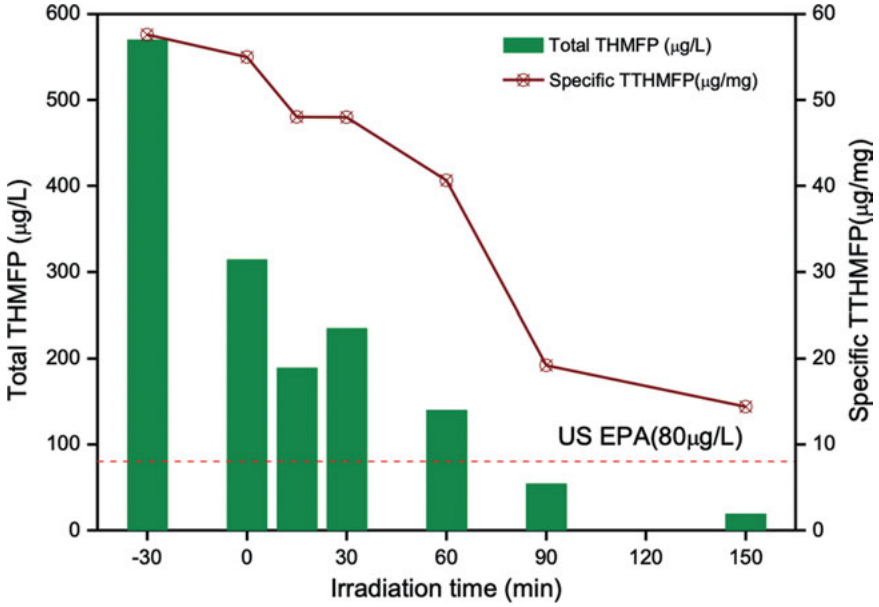

Figure 9.17: The variation of total THMFP and specific TTHMFP before and after FSMFR treatment.

possible; otherwise, it would accelerate the membrane pollution, shorten the wash cycle and finally the lifespan [37]. Membrane pollution, such as the formation of cake layer and membrane pore blocking, always occurs after it separates different kinds of solution, resulting in the increase of TMP. This resistance model is also suitable for evaluation of 240 min membrane pollution characteristics. Table 9.2 lists the proper resistance, the cake layer resistance and the pore blocking resistance. The proper resistance is determined by the physical and chemical characteristics of the membrane itself, such as the thickness and the form of pores; the cake layer resistance is determined by the porosity, thickness and compressibility of cake layer; and the pore blocking resistance is determined by the catalyst or organic pollution which come into the pore. According to this model, the membrane flux (J) could be calculated by Eq. (9.14) [38–42]:

$$J = \frac{\Delta P}{\mu(R_m + R_c + R_p)} \tag{9.14}$$

where J represents membrane flux ($L/(m^2 \cdot h)$); m solution viscosity coefficient ($Pa \cdot s$); R_m, R_c and R_p membrane proper resistance, cake layer resistance and pore blocking resistance, respectively.

From Figure 9.18 and Table 9.2, we could obtain:

(1) when membrane just filters TiO_2 suspension (0.5 g/L), TMP increases at first and then remains stable. This could be due to that TiO_2 could result in slight pore

EBSCOhost - printed on 2/14/2023 6:39 AM via . All use subject to https://www.ebsco.com/terms-of-use

blocking (0.2×10^{11} m^{-1}) and little cake layer resistance (0.3×10^{11} m^{-1}); the aeration under membrane module could provide gas-liquid flow and constrain the TiO_2 sedimentation on membrane and the increase of TMP;

(2) HA in natural underground and surface water is the main reason for the membrane pollution [43, 44]. When membrane filters the solution only having HA ($DOC_0 = 10$ mg/L), TMP increasing rate equals to 15 Pa/min, which is mainly caused by pore blocking resistance (3.3×10^{11} m^{-1}) and little cake layer resistance (0.2×10^{11} m^{-1});

(3) when membrane filters the mixture of HA solution ($DOC_0 = 10$ mg/L) and TiO_2 (0.5 g/L) with no radiation, TMP increasing rate is 23 Pa/min, 1.54 times as much as that of HA solution filtration, which is mainly caused by pore blocking resistance (2.9×10^{11} m^{-1}) and cake layer resistance (2.7×10^{11} m^{-1}); Lee et al. have investigated the mechanism of membrane pollution when filtering the mixture of HA and TiO_2, and they believed that linear HA molecular would occupy the interspace of TiO_2 particles, greatly increasing the cake layer resistance [22]. The cake layer resistance of the mixture (2.7×10^{11} m^{-1}) is 9 times as much as that of TiO_2 suspension (0.3×10^{11} m^{-1}), and 13 times of HA solution (0.2×10^{11} m^{-1});

(4) thus, in order to decrease the TMP, it is necessary to decompose the HA in solution and on the surface of TiO_2. When the ultraviolet lights are turned on, TMP just increases a little at first and then remains stable, which is caused by slight pore blocking resistance (0.4×10^{11} m^{-1}) and little cake layer resistance (0.6×10^{11} m^{-1}). This demonstrates that no obvious membrane pollution occurs and TiO_2/UV is an effective method to control membrane pollution.

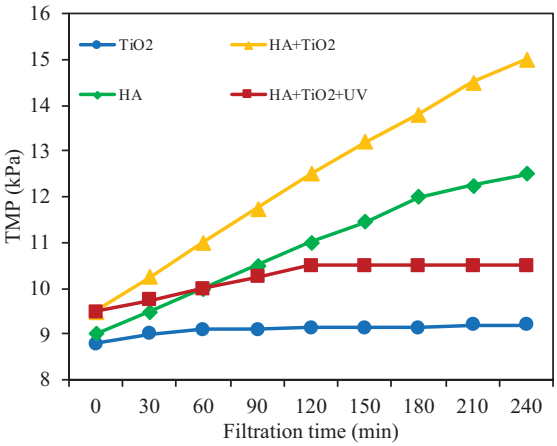

Figure 9.18: TMP variation in filtration of different types of solutions.

EBSCOhost - printed on 2/14/2023 6:39 AM via . All use subject to https://www.ebsco.com/terms-of-use

Table 9.2: The composition of membrane resistance after filtering different solutions for 240 min

Resistance/Proportion	TiO_2	HA	HA + TiO_2	HA + TiO_2+UV
$R_m/10^{11}m^{-1}/(\%)$	8.8/94.6	9.0/71.4	9.5/62.9	9.6/90.5
$R_c/10^{11}m^{-1}/(\%)$	0.3/3.2	0.2/1.6	2.7/17.9	0.6/5.7
$R_p/10^{11}m^{-1}/(\%)$	0.2/2.2	3.3/26.2	2.9/19.2	0.4/3.8
$R_t/10^{11}m^{-1}/(\%)$	9.3/100	12.6/100.0	15.1/100.0	10.6/100.0

Note: R_t represents the total membrane resistance

9.1.3.4 The analysis of relative molecular mass distribution

As shown in Figure 9.19, gel chromatogram analysis presents relatively wide distribution of molecular mass and composition (1×10^3–10×10^4 Da) with strong relative intensity (coordinating with high concentration) for initial sample at –30 min, which are typical characteristics of hydrophobic aromatics and long-chain aliphatic molecules. There are two major peaks with molecule weight at 931 Da and 2,485 Da.

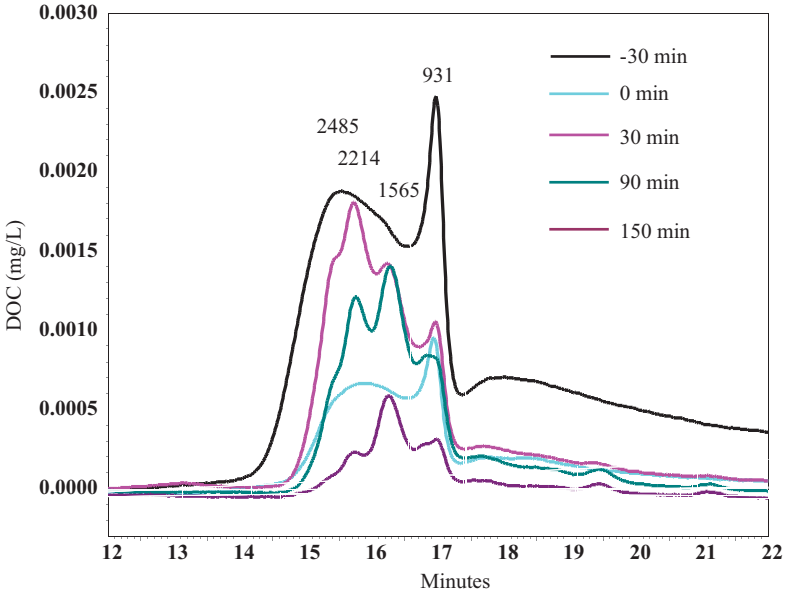

Figure 9.19: The variation of distribution of molecular weight in FSMPR system.

Figure 9.19 also shows the variation of HA molecule weight after dark adsorption and other treatment with FSMPR when pH is set as 7.0 and TiO_2 dosage is 0.5 g/L. After 30 min dark adsorption, the intensity of two major molecule peaks decrease

EBSCOhost - printed on 2/14/2023 6:39 AM via . All use subject to https://www.ebsco.com/terms-of-use

significantly, but the outline of molecule weight distribution doesn't change with no new peak, which indicating there is no new organic matter. This is because that TiO_2 could adsorb part of HA molecules (including small and big molecules). In contrast, after 30 min photocatalytic oxidation, two new peaks, at 2,214 Da and 1,565 Da arise, and the peak at 2,484 Da, representing big molecule, decreases significantly. It is interesting to notice that the intensity after 30 min photocatalytic oxidation is larger than that of 0 min, which could be explained by the production of hydrophilic organics. In the meantime, the organics coordinating to two new peaks at 2,214 Da and 1,565 Da have smaller molecule weight than that of 2,485 Da. Besides, after 150 min treatment, the peak intensity at 1,565 Da is much stronger than others, which indicates that those part of organics are difficult to degrade in FSMPR. These results demonstrate that UV/TiO_2 could degrade hydrophobic macromolecular organics and produce hydrophilic micromolecular organics with no significant membrane pollution, although these micromolecular organics are resistant to mineralize. Table 9.3 lists the weight average molecule weight (M_w), number average molecule weight (M_n) and coordinating molecule weight distribution ratio (M_w/M_n). The three values of initial sample are 2,403 Da, 198 Da and 12.1, respectively, but those of the sample after 150 min treatment are 1,246 Da, 296 Da and 4.2, respectively, indicating that the organics after treatment have narrow molecule weight distribution and simple organic composition.

Table 9.3: The variation of M_w, M_n and M_w/M_n after FSMPR treatment

Time/min	M_w/Da	M_n/Da	M_w/M_n
−30	2,403	198	12.1
0	1,682	328	5.1
30	1,736	282	6.2
90	1,393	239	5.8
150	1,246	296	4.2

9.1.3.5 Three-dimensional fluorescence spectroscopy EEM analysis

Three-dimensional fluorescence spectroscopy EEMs is a powerful method to identify the types of organics. The peak intensity and position induced by HA photocatalytic oxidation vary along treatment duration. As shown in Figure 9.20, remarkable changes of EEMs fluorescence peak intensity and position occur. As shown in Table 9.4, initial HA has two major peaks, peak A and peak T, respectively (Figure 9.20(a)). Peak A coordinates to typical ultraviolet-zone humic fluorescence matter [45–47],

EBSCOhost - printed on 2/14/2023 6:39 AM via . All use subject to https://www.ebsco.com/terms-of-use

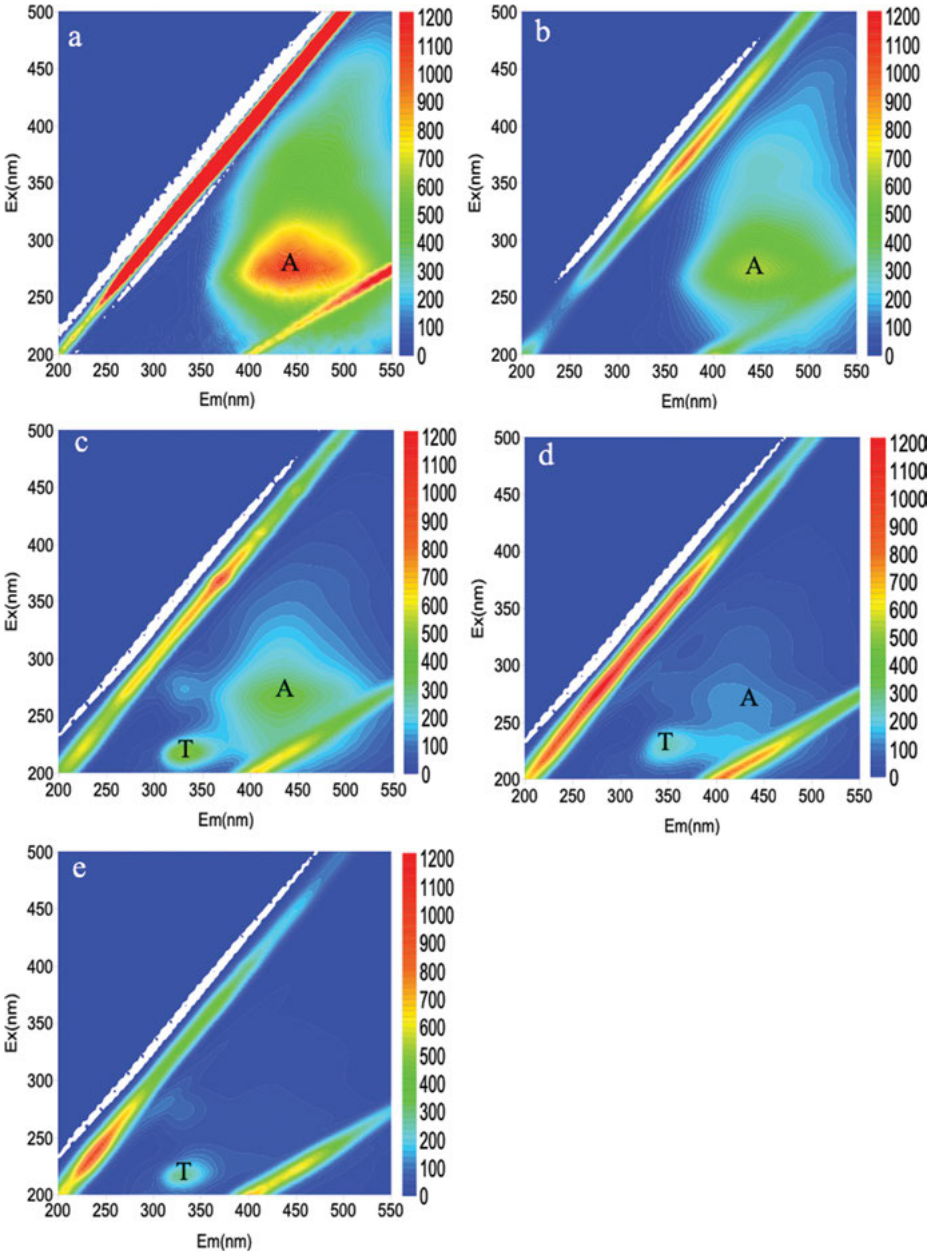

Figure 9.20: Three-dimensional fluorescence spectroscopy in FSMPR system.

EBSCOhost - printed on 2/14/2023 6:39 AM via . All use subject to https://www.ebsco.com/terms-of-use

possessing major excitation and emission wavelength (Ex/Em = 275/445 nm, intensity of 970.5). After 30 min dark adsorption (Figure 9.20(b)), although the peak intensity decreases from 970.5 to 639.1, peak A position doesn't change (E_x 275 nm/ E_m 445 nm), indicating that TiO_2 adsorption is a pure physical process and doesn't transform the structure of HA to produce new organics. As shown in Figure 9.20(c), after 30 min photocatalytic oxidation, the intensity of peak A (E_x 265 nm/ E_m 435 nm, intensity of 354.1) decreases and a new peak, namely peak T (E_x 215 nm/ E_m 330 nm, intensity of 491.7) arises, coordinating to protein fluorescence peak [48, 49]. Red shift and blue shift occur on excitation axis and emission axis, respectively. The red shift is related to the presence of carbonyl, hydroxyl, alkoxy, amino and carboxyl groups, and the blue shift to aromatic degradation and microorganic transformation to microorganic, such as the rupture of aromatic ring, the decrease of aromatic ring number and conjugate chain structure bond, transformation of linear structure to nonlinear structure, and the elimination of carbonyl, hydroxyl and amino groups [50–52]. After 90 min treatment (Figure 9.20(d)), the intensity of peak A (E_x 260 nm/ E_m 420 nm, intensity of 139.7) and T (E_x 230 nm/ E_m 350 nm, intensity of 247.7) both decreases. Finally, peak A nearly disappears after 150 min treatment, but peak T (E_x 215 nm/ E_m 330 nm, intensity 296.3) increases a little, indicating that protein is a mid-product of photocatalytic oxidation. Although HA was not removed totally, the residual organics with molecule weight of 1,565 Da wouldn't induce the membrane fouling, as analyzed by the gel chromatography.

Table 9.4: The variation of three-dimensional fluorescence spectroscopy after FSMPR treatment

Time/min	E_x (nm)/E_m (nm)	Intensity	Peak	Type
−30	275/445	970.5	A	HA
0	275/445	639.1	A	HA
30	265/435	354.1	A	HA
	215/330	491.7	T	Protein
90	260/420	139.7	A	HA
	230/350	247.7	T	Protein
150	215/330	296.3	T	Protein

9.1.4 Summary

In this section the effect of ultraviolet intensity, TiO_2 and HA concentration, pH value and H_2O_2 dosage upon HA removal with FSMPR is studied. Despite of TiO_2 adsorption, relatively strong UV intensity, low pH and proper H_2O_2 dosage are favored for HA removal. DOC removal rate and photocatalytic oxidation rate constant are calculated

EBSCOhost - printed on 2/14/2023 6:39 AM via . All use subject to https://www.ebsco.com/terms-of-use

under different conditions, and the reaction mechanism of photocatalytic coupling membrane separation is analyzed. The major conclusions are:

(1) After 150 min treatment with FSMPR, more than 86% DOC and almost 100% UV_{254} could be removed, and the THMFP could be reduced to less than 19 μg/L;
(2) TiO_2/UV pretreatment is effective to control membrane pollution, and as long as the photocatalytic reaction proceeds, TMP could not increase significantly when filtering TiO_2 and HA mixture;
(3) The decrease of membrane pollution is mainly due to that photocatalytic oxidation could transform those hydrophobic UV-zone HA microorganic into hydrophilic micromolecular protein; although these mid-products could not be mineralized within 150 min treatment, they could not lead to membrane pollution.

9.2 Surface water purification with TiO_2/ UV-membrane

The purpose of this section is to investigate the performance of FSMPR system for NOM degradation of Taihu Lake and membrane pollution control, and to analyze the NOM degradation path and variation and the mechanism for membrane pollution control.

9.2.1 Materials and methods

9.2.1.1 NOM source

The water is derived from Taihu Lake and filtered with 0.45 mm membrane to separate colloidal. The main features of water sample are: pH = 8.0, UV_{254}=0.08 cm^{-1}, DOC=3.5 mg/L, SUVA=2.29 L/(mg · m), turbidity = 1.65 NTU and chroma = 2.5 HU.

9.2.1.2 Photocatalysis and membrane module

All the chemical agents are of analytical grade, and water used is made by Millipore Super-Q plus. TiO_2 powder (P25, SSA = 50 m^2/g, average diameter = 25 nm) was purchased from Degussa (Germany). Before usage, a certain amount of TiO_2 was mixed with little ultrapure water to prepare TiO_2 sludge. The flat membrane is made of polyvinylidene fluoride (PVDF, provided by Jiangsu blue sky membrane), and its mean pore size is 0.08 μm, with effective membrane area of 0.02 m^2 (single surface for outflow). Before first use, the new membrane module was sank in ethylate (3/97, V/V) for 24 h and then purified with water to remove soluble organics. All the pretreated membrane module was stored in 4 °C water, which was frequently changed.

EBSCOhost - printed on 2/14/2023 6:39 AM via . All use subject to https://www.ebsco.com/terms-of-use

9.2.1.3 Experimental device

A self-made submerged flat membrane photocatalysis reactor (FSMPR) was used in this section, and the schematic diagram is presented in Figure 9.21. After filling the reactor and water tank with water sample, TiO_2 was dosed, and then the aeration pump and the ultraviolet light were turned on. The system was equipped with water level gauge to maintain the constant water volume in a reactor of 8 L. Membrane flux could be adjusted by the peristaltic pump, the operating condition was controlled by the time relay, and the system temperature was controlled at 25 °C with the aid of cooling circulating water. During the experiment, the range of membrane flux is from 30 to 90 L/($m^2 \cdot h$), and the TMP was measured by accurate pressure meter fixed on water outlet.

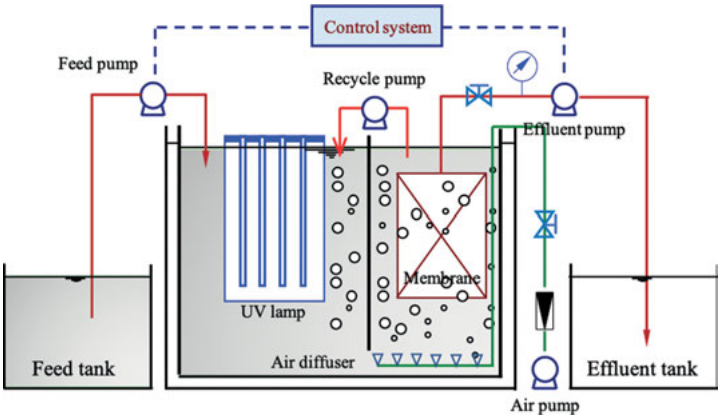

Figure 9.21: The schematic diagram of FSMPR.

9.2.2 The loss of catalyst and the control of suspension mass concentration

Previous work had found that TiO_2 would deposit on membrane surface or in the pore after long term operation, which leads to membrane pollution, TiO_2 suspension concentration reduction and catalyst loss [16]. It is well-known that the reaction rate of organic photocatalytic oxidation is related to the TiO_2 concentration [2, 12]. To some extent, TiO_2 concentration decrease leads to reaction rate reduction, which is not expected. Thus, it is important to maintain TiO_2 suspension mass concentration. Previous work proves that bubbling from bottom of membrane module could effectively mitigate catalyst deposit on membrane surface [16], and the char-

EBSCOhost - printed on 2/14/2023 6:39 AM via . All use subject to https://www.ebsco.com/terms-of-use

acteristic of bubble and gas flow would influence the shear force on membrane surface [53]. In this study, the influence of bubbling from the bottom of membrane module on TiO_2 deposition on membrane surface is studied, and TiO_2 concentration is measured to evaluate the performance when big bubble aeration with a certain gas flux is adopted. Under this condition, if TiO_2 concentration doesn't decrease significantly, it demonstrates that flat membrane with bubbling from bottom could successfully maintain catalyst concentration and avoid deposition on membrane surface.

Catalyst concentration in reactor is evaluated by measuring mixture turbidity. Figure 9.22 presents the relationship between TiO_2 concentration (0, 0.2 g/L, 0.4 g/L, 0.6 g/L, 0.8 g/L) and turbidity of mixture, which is mixed with deionized water. Results demonstrate that turbidity is in a linear correlation with TiO_2 concentration ($R^2 = 0.99$). When the initial TiO_2 concentration is set at 0.5 g/L and membrane flux is 50 L/($m^2 \cdot h$), the suspended TiO_2 concentration and membrane suction pressure are measured under aeration and non-aeration. Results prove that bubbling from membrane bottom could maintain TiO_2 concentration without significant increase of TMP, thus reducing TiO_2 deposition and mitigating membrane pollution (Figure 9.23). In contrast, without aeration, TiO_2 concentration decreases significantly with TMP increase, indicating TiO_2 deposition on membrane surface. Figure 9.24 presents TiO_2 deposition on membrane surface under these two operation models for 48 h, and it provides direct evidence that aeration from membrane bottom could effectively maintain TiO_2 concentration and mitigate its deposition. Thus, the following experiments are performed with aeration (gas flux = 4 L/min).

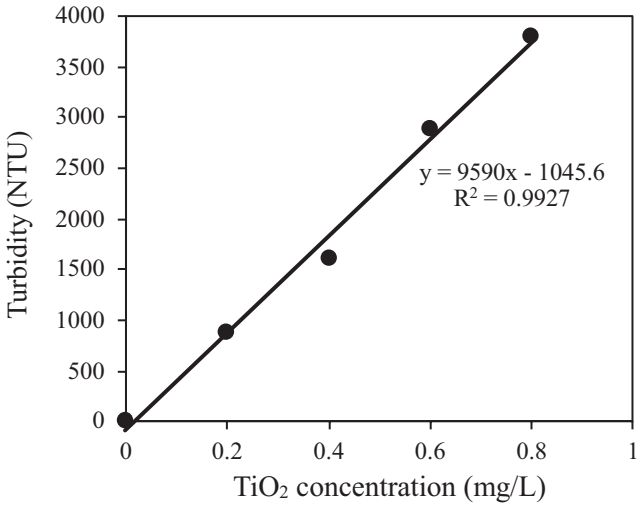

Figure 9.22: The relationship between TiO_2 concentration and turbidity.

EBSCOhost - printed on 2/14/2023 6:39 AM via . All use subject to https://www.ebsco.com/terms-of-use

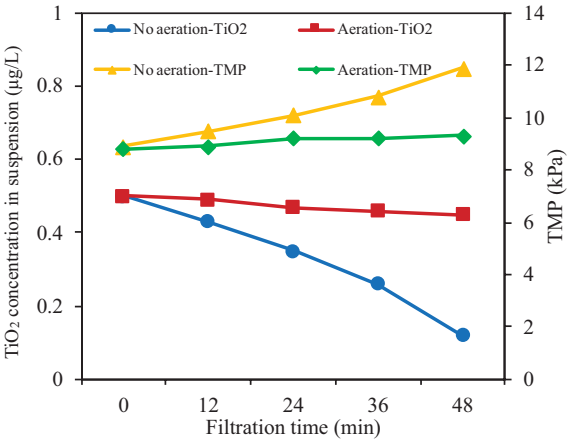

Figure 9.23: The relationship between TiO_2 concentration and TMP in suspension with and without aeration (TiO_2 0.5 g/L, 50 L/($m^2 \cdot h$)).

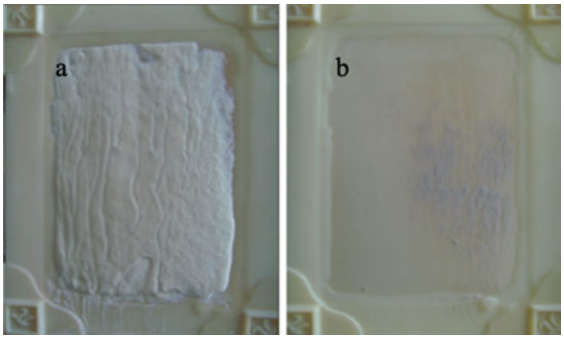

Figure 9.24: TiO_2 deposit on membrane surface.

9.2.3 The optimization of hydraulic retention time

This study is performed under continuous model (CSTR). Since organic photocatalytic oxidation is related to reaction time, it is necessary to determine the optimized HRT.

Under CSTR model, if organics could totally pass through the membrane, its HRT could be determined by the membrane flux. Hence, controlling organic HRT in reactor could get good removal performance. As shown in Figure 9.25, longer HRT with smaller membrane flux is favored for high DOC removal rate. When J = 30 L/($m^2 \cdot h$), after 420 min reaction, DOC removal rate achieves 70% and maintains stable. This is because that longer HRT endows organics abundant reaction time for photocatalytic oxidation, and favors more thorough degradation. In contrast, shorter HRT leads to

EBSCOhost - printed on 2/14/2023 6:39 AM via . All use subject to https://www.ebsco.com/terms-of-use

poorer performance, i.e. when J = 60 and 90 L/(m^2 · h), DOC removal rate decreases to 61% and 53%, respectively.

The variation of membrane suction pressure is presented in Figure 9.26. When J = 30 and 60 L/(m^2 · h), after 480 min operation, little membrane suction pressure increase is observed; when J = 90 L/(m^2 · h), membrane suction pressure increases slightly at the beginning, and then remains stable after 180 min. It is obvious that pollutant removal has some relationship with membrane suction pressure, i.e. when J = 30 and 60 L/(m^2 · h), high pollutant removal rate is achieved, thus there is no remarkable membrane suction pressure increase; however, when J = 90 L/(m^2 · h), organic removal rate is relatively low and part of pollutant is not catalytically oxidized and thus contaminates the membrane and results in the increase of membrane suction pressure; as the operation proceeds, those organics on membrane are degraded, which leads to the relative stable membrane suction pressure after 180 min. In order to better illustrate the relationship between organic removal and membrane suction pressure, following section is investigated via comparing membrane suction pressure values under different conditions.

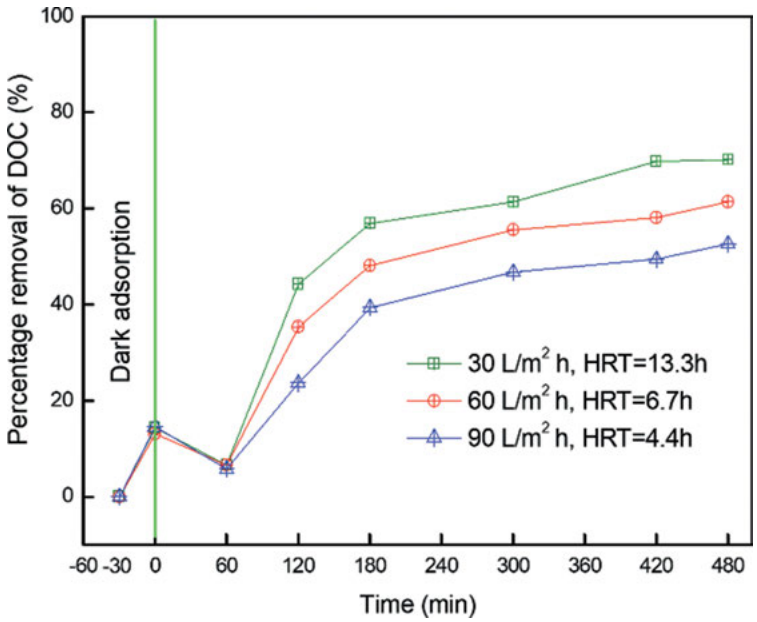

Figure 9.25: The variation of DOC removal at different flux (TiO_2 = 0.5 g/L, pH = 8, aeration 4 L/min).

EBSCOhost - printed on 2/14/2023 6:39 AM via . All use subject to https://www.ebsco.com/terms-of-use

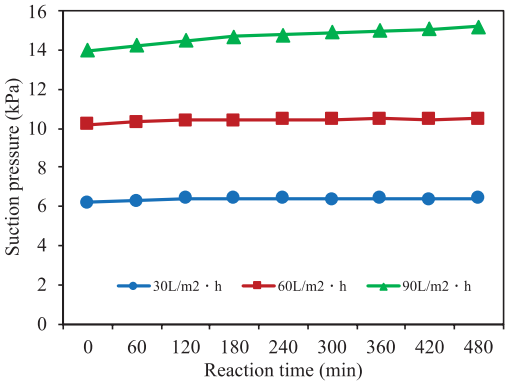

Figure 9.26: TMP variation at different flux (TiO_2 = 0.5 g/L, pH = 8, aeration 30 L/(m^2 · h)).

9.2.4 The variation of membrane suction pressure with different working conditions

The Darcy's law indicates that the variation of membrane suction pressure reflects membrane pollution resistance with certain membrane flux. Figure 9.27 presents membrane suction pressure variation under three different conditions with membrane flux of 30 L/(m^2 · h). As excepted, for raw water and raw water mixed with TiO_2 without UV, membrane suction pressure linearly increases with reaction time, with the slope of 1.7 and 3.2 Pa/min, respectively. The latter is 1.9 times larger than the former, which could be due to that flexible linear macromolecules could twine TiO_2 and fill in the blank of TiO_2, increasing membrane cake layer construction resistance and membrane resistance [22]. Although membrane suction pressure increases slowly when just filtering raw water, photocatalytic oxidation is applied to reduce the membrane fouling caused by organics. Membrane suction pressure remains stable when UV radiation is applied since it promotes organic photocatalytic oxidation and reduce membrane pollution, demonstrating that photocatalysis helps mitigate membrane pollution [2, 21, 22, 54].

9.2.5 Organic removal performance and mechanism analysis

In order to better understand the organic degradation performance of photocatalytic membrane separation and the membrane pollution mechanism of Taihu lake water, DOC, UV_{254}, SUVA, UV-vis adsorption, THMFP, apparent molecule weight (AMW) and hydrophilic/hydrophobic separation are applied to evaluate the removal performance of the reactor, organic characteristic variation and membrane filtration characteristic. The operation condition is the same as that in the former section (TiO_2 concentration = 0.5 g/L, membrane flux = 30 L/(m^2 · h), gas flow = 4 L/min).

EBSCOhost - printed on 2/14/2023 6:39 AM via . All use subject to https://www.ebsco.com/terms-of-use

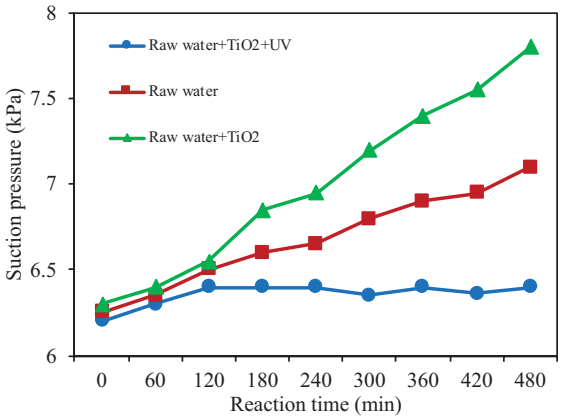

Figure 9.27: TMP variation at different working conditions.

9.2.5.1 Photocatalytic removal of DOC and UV_{254}

As presented in Figure 9.28, poor removal performance of DOC and UV_{254} (14.3% and 11.3%, respectively) are observed within the initial 30 min dark adsorption. This is because that the solution pH is slight basic (pH = 8) and the TiO_2 surface is negatively charged, thus repelling negatively charged hydrophobic organics [55]. DOC and UV_{254} decrease simultaneously in the following 420 min operation, and the removal rates reach 70% and 86%, respectively. UV_{254} removal rate is always larger than that of DOC, which is determined by the characteristic of photocatalysis. Photocatalysis firstly dissociates the macromolecular organics (especially the aromatic macromolecule with larger UV adsorption) into micromolecular, and then mineralizes them to CO_2 and H_2O [56]. It is interesting to notice that organic adsorption-desorption is observed during DOC degradation, namely, DOC at 60 min in effluent is higher than that at 30 min. This is because that part of micromolecular organics, which is derived from macromolecular organic degradation, flows out before being mineralized, resulting in DOC increase for a short time. In contrast, similar phenomenon is not observed for UV_{254} degradation, indicating that these hydrophilic organics cannot adsorb UV. Figure 9.29 presents UV-vis adsorption spectrum in the range of 230–400 nm. It can be observed that UV_{254} decreases in the initial 30 min which is due to TiO_2 adsorption, while the following decline is due to photocatalytic oxidation. And the decline trend of UV adsorption curve without increment suggests that mid-products of photocatalytic oxidation don't have UV adsorption ability.

The degradation rate constants of these two indicators could be well described by the L-H model. In order to better describe the degradation rate, the initial dark adsorption process is excluded. As shown in Figure 9.30, the initial DOC degradation rate is 0.0027 cm^{-1}/min, while that of UV_{254} is 0.0041 cm^{-1}/min, 1.5 times larger as the former.

EBSCOhost - printed on 2/14/2023 6:39 AM via . All use subject to https://www.ebsco.com/terms-of-use

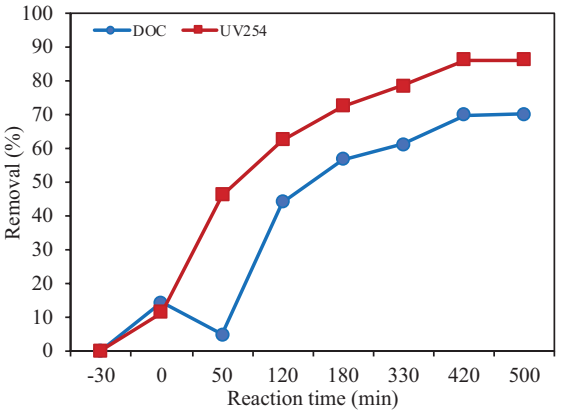

Figure 9.28: Removal of DOC and UV_{254} in Taihu Lake water by FSMPR system.

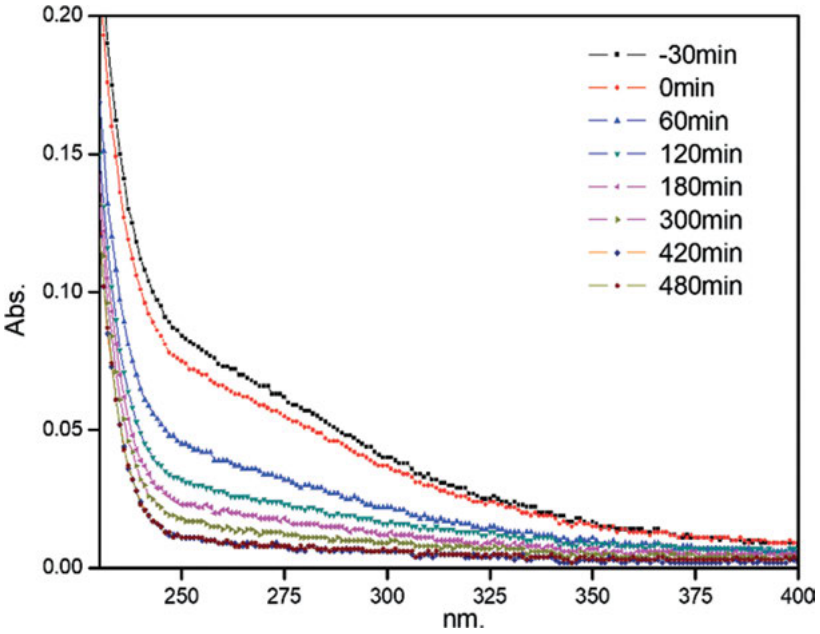

Figure 9.29: UV-vis adsorption spectrum in Taihu Lake water by FSMPR system.

This suggests that mineralization is faster than macromolecular organic dissociation. The value of SUVA is referred to the ratio of UV_{254} and DOC. As shown in Figure 9.31, SUVA decreases dramatically in the initial 60 min, and then tends to be stable. Previous work documents that membrane pollution and the formation of DBP are both related to SUVA. It is obvious that the decrease of SUVA is favored for membrane pollu-

EBSCOhost - printed on 2/14/2023 6:39 AM via . All use subject to https://www.ebsco.com/terms-of-use

tion mitigation and DBP formation. The effect of SUVA upon membrane pollution can be seen in Figures 9.25 and 9.26. Although DOC removal performance is relatively poor, the membrane pollution is effectively controlled, since photocatalytic oxidation firstly remove macromolecular organics, which contribute a lot to membrane pollution [2].

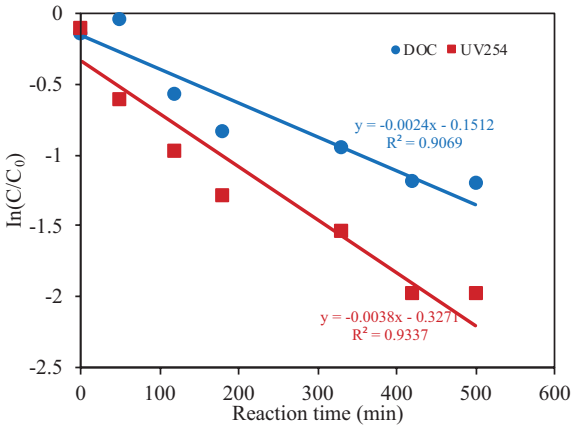

Figure 9.30: The DOC and UV_{254} degradation rate in FSMPR system.

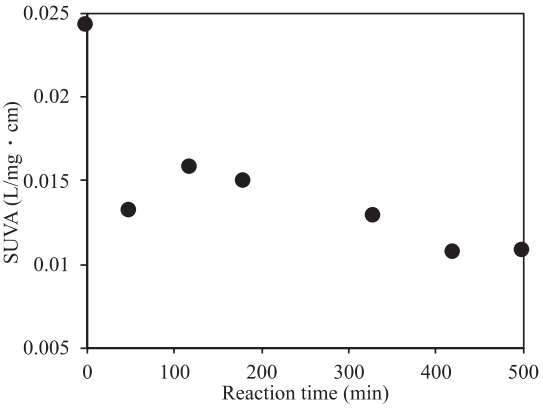

Figure 9.31: The removal of SUVA by FSMPR system.

9.2.5.2 Photocatalytic removal of THMFP

The removal of trihalomethane formation potential is presented in Figure 9.32. After operation under CSTR model for 180 min (membrane flux = 30 L/(m^2 · h), HRT = 13.4 h), THMFPs decreases from 169 μg/L to 49 μg/L, and the removal rate is up to 71%. The quality of effluent meets the limitation of USEPA (<80 μg/L) and that of CHNSDWQ (GB

EBSCOhost - printed on 2/14/2023 6:39 AM via . All use subject to https://www.ebsco.com/terms-of-use

5749-2006) (the sum of ratio between real concentration of FMs and limitation is less than 1). In this study, the sum is 0.97, and the four FMs are all less than their limitation ($CHCl_3 = 10 < 60$ μg/L, removal rate = 89%, $CHCl_2Br = 18 < 60$ μg/L, removal rate = 50%, $CHClBr_2 = 15 < 100$ μg/L, removal rate = 42%, $CHBr_3 = 6 < 100$ μg/L, removal rate = 40%). After 420 min operation, the THMFP in effluent remains stable and decreases to 18.9 μg/L, and the removal rate is 89%. In the meantime, THMFP generating index (THMFP/DOC) decreases from the initial 49.5 to 18.5, and the sum of ratio is 0.40. as shown in Figure 9.33, formation potential of these four THM is less than their limitation ($CHCl_3 = 6 < 60$ μg/L, removal rate = 94%, $CHCl_2Br = 6 < 60$ μg/L, removal rate = 84%, $CHClBr_2 = 4 < 100$ μg/L, removal rate = 85%, $CHBr_3 = 2.9 < 100$ μg/L, removal rate = 71%). Although part of DOC still remains in effluent, the THMFP removal performance is higher than that of DOC, indicating photocatalytic oxidation could preferentially remove the THMFP precursor and transform their structure, reducing the production of THMs [57].

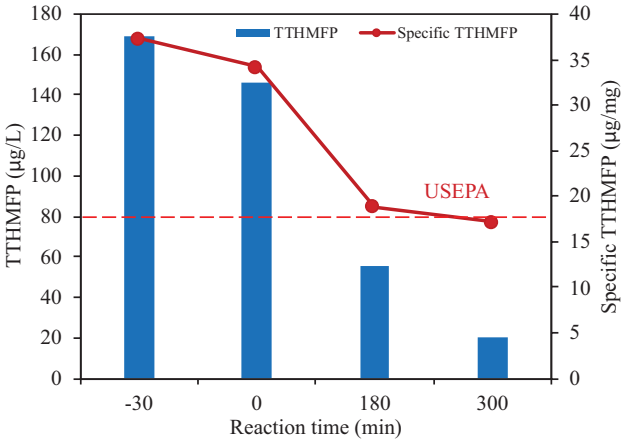

Figure 9.32: The variation of TTHMFP and specific TTHMFP.

9.2.5.3 The influence of photocatalysis on AMW

The distribution of apparent molecule weight (AMW) in sample is measured by gel chromatogram. Figure 9.34 presents the AMW distribution of Taihu lake after different time reaction. For the raw water, AMW majorly distributes in the range of 800–5,000 Da, the peak positions are 2,789 Da, 2,345 Da, 1,565 Da, 931 Da, respectively, and a micromolecular peak is at 261 Da. As the treatment proceeds, intensity of AMW peaks decrease significantly. The initial 30 min dark adsorption process mainly removes organics of AMW in the range of 2,000–5,000 Da. The intensity of peak at 2,789 Da, which is referred to hydrophobic HA and rich acid, decreases 38%, while that at 2,000 Da, which is referred to hydrophilic micromolecular organics, only decreases around 10%. As reaction time pro-

EBSCOhost - printed on 2/14/2023 6:39 AM via . All use subject to https://www.ebsco.com/terms-of-use

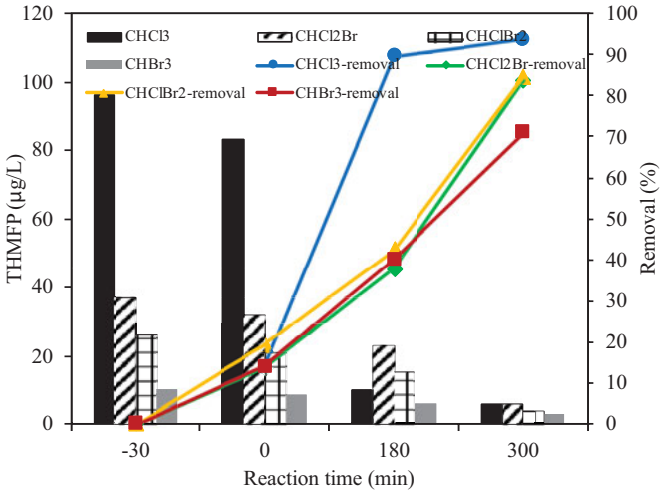

Figure 9.33: The removal of four types of THMFP in Taihu Lake.

longs, intensity of all the peaks descents gradually, especially for the peak at 2,000 Da. After 180 min, intensity of peaks at 2,789 Da, 2,345 Da and 1,565 Da decrease more than 90%, and that at 931 Da decrease 80%, indicating that remarkable degradation occurs on micromolecular organics coupling with significant decrease of DOC. At the end of reaction, decrease rate of peaks at 2,789 Da, 2,345 Da and 1,565 Da are more than 95%, almost disappear. The intensity at 931 Da doesn't change significantly and a new peak with low intensity appears at 1,173 Da, suggesting that the process of macromolecular matter dissociation and micromolecular organic mineralization come to the end. The intensity of 261 Da peak remains stable in the whole process, which indicates that organics in this molecular mass range is hard to be photocatalytic oxidized.

9.2.5.4 Hydrophilic/hydrophobic separation

Figures 9.35 and 9.36 present the variation of DOC about four kinds of constituents (HPO, TPI, C-HPI N-HPI) in Taihu lake water after treatment. In raw water, HPO accounts for 32.9% and the coordinating DOC is 1.122 mg/L. Generally, the majority of HPO is HA, coming from soil filtration and sedimentation release. The MW of HPO is mainly in the range of 2,000–5,000 Da, and the intensity of 2,789 Da is the highest, most derived from domestic sewage. The DOC of TPI is 0.553 mg/L, accounting for 16.2%. The MW of this part of organics concentrates in the range of 800–2,000 Da, with the majority of fulvic acid derived from sediment release. The DOC value of C-HPI is 0.384 mg/L, accounting for 11.2%, and the majority is protein and amino acid. The DOC of N-HPI is 1.355 mg/L, accounting for 39.7%. This part of organics contains macromolecular amylose and micromolecular aldehyde, ketone and alcohol [56]. The

EBSCOhost - printed on 2/14/2023 6:39 AM via . All use subject to https://www.ebsco.com/terms-of-use

majority of molecular distribution is lower than $1{,}000 \times 10^3$ Da, derived from algae secretion and playing the role of food for heterotrophic bacteria.

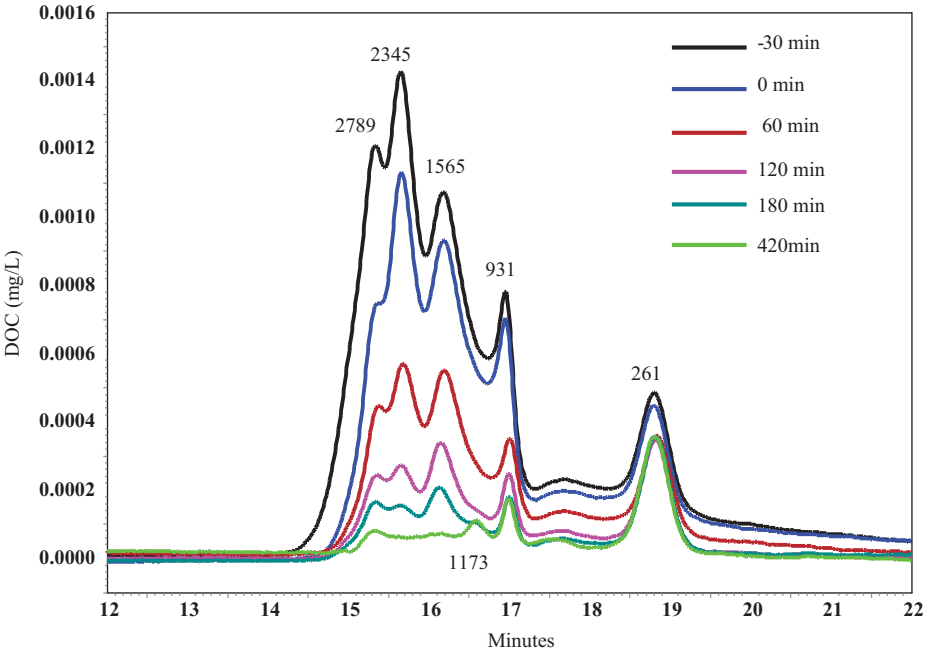

Figure 9.34: The variation of AMW distribution in FSMPR system.

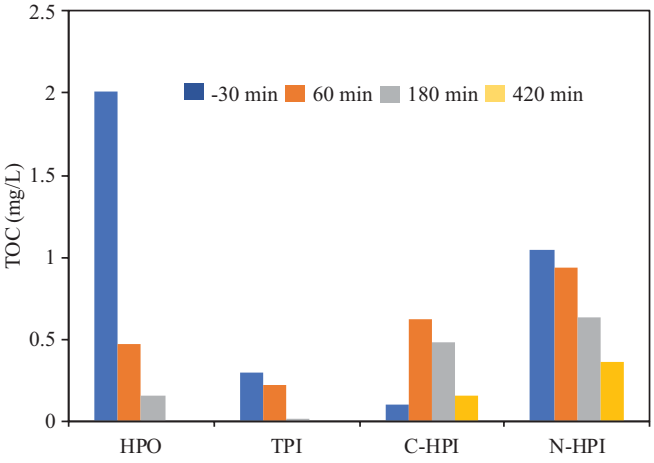

Figure 9.35: The variation of DOC of four fractions in Taihu Lake by treatment of FSMPR system.

EBSCOhost - printed on 2/14/2023 6:39 AM via . All use subject to https://www.ebsco.com/terms-of-use

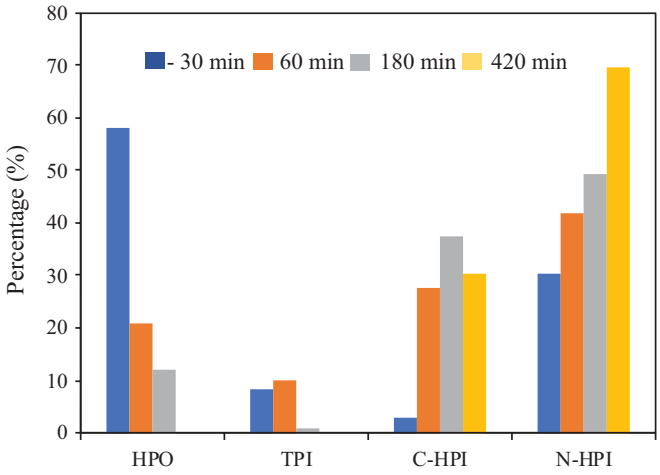

Figure 9.36: The variation of DOC percentage of four fractions in Taihu Lake by treatment of FSMPR system.

Hydrophilic and hydrophobic organics take about half of organics in raw water, respectively. FEMPR treatment could remove most hydrophobic organics, while its performance for hydrophilic organics is relatively poor. Generally speaking, hydrophobic organics have aromatic rings, which are easy to be oxidized by photocatalysis, thus this part of organics, referred to UV_{254}, could be easily destroyed. After 60 min treatment, HPO and TPI are significantly decreased, and the content of C-HPI increases, indicating these macromolecular organics are photocatalytic oxidized into hydrophilic micromolecular organics, with most being carboxylic acid, and finally mineralized into CO_2 and H_2O. For N-HPI, this part of organics is resistant to photocatalytic oxidation. At the end of operation, the effluent quality remains stable, most HPO and TPI disappear, but part of C-HPI and N-HPI still remain in solution. Although little descent is observed, part of C-HPI and N-HPI are difficult to degrade, especially N-HPI at 261 Da of MW. N-HPI contains macromolecular amylose and micromolecular aldehyde, ketone and alcohol, and are resistant to photocatalytic oxidation [36, 58].

9.2.6 Summary

Photocatalysis coupling flat membrane ultra-filtration not only maintains the TiO_2 concentration in the reactor and settles the problem for fine TiO_2 separation, but also reduces organics on membrane surface and mitigates membrane pollution. This study applies CSTR model to treat Taihu lake water, and conclusions are listed in the following:

EBSCOhost - printed on 2/14/2023 6:39 AM via . All use subject to https://www.ebsco.com/terms-of-use

(1) A novel FSMPR technique is applied for surface water treatment. Bubbling from the bottom of membrane module could effectively avoid TiO_2 deposition on membrane surface and maintain its concentration in the reactor.
(2) When the HRT = 13.4 h and membrane flux is 30 L/($m^2 \cdot$ h), after 420 min operation, the quality of effluent tends stable, i.e. the removal rates of UV_{254} and DOC achieve 86% and 70%, respectively, and THMFP meets the limitation of CHNSDWQ (GB 5749-2006).
(3) The distribution of AMW and results of hydrophilic/hydrophobic separation suggest that FSMPR could remove almost hydrophobic organics with molecular weight in the range of 2,000–5,000 Da and part of hydrophilic organics. Photocatalytic oxidation firstly dissociates hydrophobic macromolecular organics into hydrophilic micromolecular organics, and then mineralizes them into CO_2 and H_2O. There is still part of hydrophilic organics remaining in the solution, of which the molecular mass is smaller than 1,000 Da. Especially the part with molecular mass of 261 Da, whose removal rate is only 25%.

References

[1] Jacangelo, J.G., et al., Selected processes for removing nom – an overview. Journal American Water Works Association, 1995. 87(1): p. 64–77.
[2] Huang, X.H., Leal, M., and Li, Q.L., Degradation of natural organic matter by TiO2 photocatalytic oxidation and its effect on fouling of low-pressure membranes. Water Research, 2008. 42(4–5): p. 1142–1150.
[3] Vickers, J.C., Thompson, M.A., and Kelkar, U.G., The use of membrane filtration in conjunction with coagulation processes for improved nom removal. Desalination, 1995. 102(1–3): p. 57–61.
[4] Fujishima, A. and Honda, K., Electrochemical photolysis of water at a semiconductor electrode. Nature, 1972. 238(5358): p. 37–8.
[5] Frank, S.N. and Bard, A.J., Heterogeneous photocatalytic oxidation of cyanide and sulfite in aqueous-solutions at semiconductor powders. Journal of Physical Chemistry, 1977. 81(15): p. 1484–1488.
[6] Ollis, D.F., et al., Heterogeneous photoassisted catalysis – conversions of perchloroethylene, dichloroethane, chloroacetic acids, and chlorobenzenes. Journal of Catalysis, 1984. 88(1): p. 89. 96.
[7] Malati, M.A., The photocatalysed removal of pollutants from water. Environmental Technology, 1995. 16(11): p. 1093–1099.
[8] Xi, W.M. and Geissen, S.U., Separation of titanium dioxide from photocatalytically treated water by cross-flow microfiltration. Water Research, 2001. 35(5): p. 1256–1262.
[9] Dijkstra, M.F.J., et al., Experimental comparison of three reactor designs for photocatalytic water purification. Chemical Engineering Science, 2001. 56(2): p. 547–555.
[10] Dijkstra, M.F.J., et al., Comparison of the efficiency of immobilized and suspended systems in photocatalytic degradation. Catalysis Today, 2001. 66(2–4): p. 487–494.
[11] Sopyan, I., et al., A film-type photocatalyst incorporating highly active TiO2 powder and fluororesin binder: Photocatalytic activity and long-term stability. Journal of Electroanalytical Chemistry, 1996. 415(1–2): p. 183–186.

EBSCOhost - printed on 2/14/2023 6:39 AM via . All use subject to https://www.ebsco.com/terms-of-use

[12] Fu, J.F., et al., A new submerged membrane photocatalysis reactor (SMPR) for fulvic acid removal using a nano-structured photocatalyst. Journal of Hazardous Materials, 2006. 131(1–3): p. 238–242.
[13] Chin, S.S., et al., Hybrid low-pressure submerged membrane photoreactor for the removal of bisphenol A. Desalination, 2007. 202(1–3): p. 253–261.
[14] Chin, S.S., et al., Factors affecting the performance of a low-pressure submerged membrane photocatalytic reactor. Chemical Engineering Journal, 2007. 130(1): p. 53–63.
[15] Choo, K.H., et al., Use of an integrated photocatalysis/hollow fiber microfiltration system for the removal of trichloroethylene in water. Journal of Hazardous Materials, 2008. 152(1): p. 183–190.
[16] Huang, X., et al., Operational conditions of a membrane filtration reactor coupled with photocatalytic oxidation. Separation and Purification Technology, 2007. 55(2): p. 165–172.
[17] Huang, H., Schwab, K., and Jacangelo, J.G., Pretreatment for low pressure membranes in water treatment: A review. Environmental Science & Technology, 2009. 43(9): p. 3011–3019.
[18] Shim, J.K., Yoo, I.K., and Lee, Y.M., Design and operation considerations for wastewater treatment using a flat submerged membrane bioreactor. Process Biochemistry, 2002. 38(2): p. 279–285.
[19] Judd, S., Submerged membrane bioreactors: Flat plate or hollow fibre? Filtration & Separation, 2002. 39(5): p. 30–31.
[20] Bai, H.W. and Sun, D.D., Hybrid TiO2 photocatalytic oxidation and ultrafiltration for humic acid removal and membrane fouling control. Water Science and Technology-Water Supply, 2011. 11(3): p. 324–332.
[21] Choo, K.H., Tao, R., and Kim, M.J., Use of a photocatalytic membrane reactor for the removal of natural organic matter in water: Effect of photoinduced desorption and ferrihydrite adsorption. Journal of Membrane Science, 2008. 322(2): p. 368–374.
[22] Lee, S.A., et al., Use of ultrafiltration membranes for the separation of TiO2 photocatalysts in drinking water treatment. Industrial & Engineering Chemistry Research, 2001. 40(7): p. 1712–1719.
[23] Li, F., et al., A concentrate-and-destroy technique for degradation of perfluorooctanoic acid in water using a new adsorptive photocatalyst. Water Research, 2020. 185.
[24] Zhao, H.X., et al., CNTs-TiO2/Al2O3 composite membrane with a photocatalytic function: Fabrication and energetic performance in water treatment. Separation and Purification Technology, 2013. 116: p. 360–365.
[25] Hoffmann, M.R., et al., Environmental applications of semiconductor photocatalysis. Chemical Reviews, 1995. 95(1): p. 69. 96.
[26] Sopajaree, K., et al., An integrated flow reactor-membrane filtration system for heterogeneous photocatalysis. Part II: Experiments on the ultrafiltration unit and combined operation. Journal of Applied Electrochemistry, 1999. 29(9): p. 1111–1118.
[27] Valente, J.P.S., Padilha, P.M., and Florentino, A.O., Studies on the adsorption and kinetics of photodegradation of a model compound for heterogeneous photocatalysis onto TiO2. Chemosphere, 2006. 64(7): p. 1128–1133.
[28] Parra, S., et al., Photocatalytic degradation of atrazine using suspended and supported TiO2. Applied Catalysis B-Environmental, 2004. 51(2): p. 107–116.
[29] Bekbolet, M., Suphandag, A.S., and Uyguner, C.S., An investigation of the photocatalytic efficiencies of TiO2 powders on the decolourisation of humic acids. Journal of Photochemistry and Photobiology a-Chemistry, 2002. 148(1–3): p. 121–128.
[30] Wiszniowski, J., et al., Photocatalytic decomposition of humic acids on TiO2 Part I: Discussion of adsorption and mechanism. Journal of Photochemistry and Photobiology a-Chemistry, 2002. 152(1–3): p. 267–273.

EBSCOhost - printed on 2/14/2023 6:39 AM via . All use subject to https://www.ebsco.com/terms-of-use

[31] Leenheer, J.A. and Croue, J.P., Characterizing aquatic dissolved organic matter. Environmental Science & Technology, 2003. 37(1): p. 18a–26a.
[32] Drikas, M., Chow, C.W.K., and Cook, D., The impact of recalcitrant organic character on disinfection stability, trihalomethane formation and bacterial regrowth: An evaluation of magnetic ion exchange resin (MIEX (R)) and alum coagulation. Journal of Water Supply Research and Technology-Aqua, 2003. 52(7): p. 475–487.
[33] Kim, H.C. and Yu, M.J., Characterization of natural organic matter in conventional water treatment processes for selection of treatment processes focused on DBPs control. Water Research, 2005. 39(19): p. 4779. 4789.
[34] Zhao, Y., Taylor, J., and Hong, S.K., Combined influence of membrane surface properties and feed water qualities on RO/NF mass transfer, a pilot study. Water Research, 2005. 39(7): p. 1233–1244.
[35] Harrington, G.W., et al., Characterization of natural organic matter and its reactivity with chlorine. Water Disinfection and Natural Organic Matter, 1996. 649: p. 138–158.
[36] Liu, S., et al., TiO(2) photocatalysis of natural organic matter in surface water: Impact on trihalomethane and haloacetic acid formation potential. Environmental Science & Technology, 2008. 42(16): p. 6218–6223.
[37] Xiao, Y.T., et al., Progress of applied research on TiO2 photocatalysis-membrane separation coupling technology in water and wastewater treatments. Chinese Science Bulletin, 2010. 55(14): p. 1345–1353.
[38] Belfort, G., Davis, R.H., and Zydney, A.L., The behavior of suspensions and macromolecular solutions in cross-flow microfiltration. Journal of Membrane Science, 1994. 96(1–2): p. 1–58.
[39] Ho, C.C. and Zydney, A.L., A combined pore blockage and cake filtration model for protein fouling during microfiltration. Journal of Colloid and Interface Science, 2000. 232(2): p. 389–399.
[40] Kim, J.S., Lee, C.H., and Chang, I.S., Effect of pump smear on the performance of a crossflow membrane bioreactor. Water Research, 2001. 35(9): p. 2137–2144.
[41] Li, H., et al., Direct observation of particle deposition on the membrane surface during crossflow microfiltration. Journal of Membrane Science, 1998. 149(1): p. 83–97.
[42] Zhang, X.W., et al., Combination of one-dimensional TiO2 nanowire photocatalytic oxidation with microfiltration for water treatment. Water Research, 2009. 43(5): p. 1179. 1186.
[43] Howe, K.J. and Clark, M.M., Fouling of microfiltration and ultrafiltration membranes by natural waters. Environmental Science & Technology, 2002. 36(16): p. 3571–3576.
[44] Yuan, W. and Zydney, A.L., Humic acid fouling during microfiltration. Journal of Membrane Science, 1999. 157(1): p. 1–12.
[45] Coble, P.G., Del Castillo, C.E., and Avril, B., Distribution and optical properties of CDOM in the Arabian Sea during the 1995 Southwest Monsoon. Deep-Sea Research Part Ii-Topical Studies in Oceanography, 1998. 45(10–11): p. 2195–2223.
[46] Stedmon, C.A. and Markager, S., Resolving the variability in dissolved organic matter fluorescence in a temperate estuary and its catchment using PARAFAC analysis. Limnology and Oceanography, 2005. 50(2): p. 686–697.
[47] Stedmon, C.A. and Markager, S., Tracing the production and degradation of autochthonous fractions of dissolved organic matter by fluorescence analysis. Limnology and Oceanography, 2005. 50(5): p. 1415–1426.
[48] Baker, A. and Inverarity, R., Protein-like fluorescence intensity as a possible tool for determining river water quality. Hydrological Processes, 2004. 18(15): p. 2927–2945.
[49] Mayer, L.M., Schick, L.L., and Loder, T.C., Dissolved protein fluorescence in two Maine estuaries. Marine Chemistry, 1999. 64(3): p. 171–179.
[50] Coble, P.G., Characterization of marine and terrestrial DOM in seawater using excitation emission matrix spectroscopy. Marine Chemistry, 1996. 51(4): p. 325–346.

EBSCOhost - printed on 2/14/2023 6:39 AM via . All use subject to https://www.ebsco.com/terms-of-use

[51] Korshin, G.V., et al., Influence of chlorination on chromophores and fluorophores in humic substances. Environmental Science & Technology, 1999. 33(8): p. 1207–1212.
[52] Swietlik, J., et al., Reactivity of natural organic matter fractions with chlorine dioxide and ozone. Water Research, 2004. 38(3): p. 547–558.
[53] Yamanoi, I. and Kageyama, K., Evaluation of bubble flow properties between flat sheet membranes in membrane bioreactor. Journal of Membrane Science, 2010. 360(1–2): p. 102–108.
[54] Pidou, M., et al., Fouling control of a membrane coupled photocatalytic process treating greywater. Water Research, 2009. 43(16): p. 3932–3939.
[55] Liu, S., et al., Removal of humic acid using TiO2 photocatalytic process – Fractionation and molecular weight characterisation studies. Chemosphere, 2008. 72(2): p. 263–271.
[56] Liu, S., et al., Comparison of photocatalytic degradation of natural organic matter in two Australian surface waters using multiple analytical techniques. Organic Geochemistry, 2010. 41(2): p. 124–129.
[57] Zhang, H., et al., Characterization of dissolved organic matter fractions and its relationship with the disinfection by-product formation. Journal of Environmental Sciences, 2009. 21(1): p. 54–61.
[58] Tran, H., et al., Clarifying the role of silver deposits on titania for the photocatalytic mineralisation of organic compounds. Journal of Photochemistry and Photobiology a-Chemistry, 2006. 183(1–2): p. 41–52.

EBSCOhost - printed on 2/14/2023 6:39 AM via . All use subject to https://www.ebsco.com/terms-of-use

EBSCOhost - printed on 2/14/2023 6:39 AM via . All use subject to https://www.ebsco.com/terms-of-use

Index

acid cleaning 161, 162, 165
activated carbon adsorption 145, 238
aeruginosa 36, 48, 50, 51, 55, 82
air cleaning 354
AL-facing-DS 272, 279, 288, 289, 290, 291, 292, 297, 298, 300, 302, 308, 310, 312, 320
algal organic matter 16, 17, 18, 24, 25, 36, 37, 39
alkaline cleaning 161, 162, 165
amphiphilic copolymer 110, 111, 124, 125
Anabaena 36, 48, 50, 51, 55, 82
Aphanizomenon 36, 48, 50, 51, 55, 82
applicable-external CP 270
aromatic protein 46, 165
assimilable organic carbon 11
axial vibratory membrane 62

backwash 168, 180, 276, 325, 326, 334, 335, 337, 339, 341, 347, 348, 351
bacterial community 349
bio-diatomite dynamic membrane reactor 325, 351
blending modification 110, 124
bovine serum albumin 111, 136

cake layer 73, 75, 80, 82, 97, 104, 106, 143, 145, 167, 190, 236, 299, 311, 313, 330, 334, 335, 336, 341, 344, 347, 348, 349, 369, 370, 380
carbamazepine 215, 217, 219
charged hydrophilic 21, 22, 23, 35, 38, 39, 40, 41, 44, 46, 49, 58, 75, 143, 236
Chlorella 36, 50, 51, 55, 61, 94
coagulation 109, 145, 147, 149, 150, 153, 154, 158, 159, 160, 161, 162, 163, 165, 166, 167, 182, 188, 189, 190, 191, 192, 198, 199, 200, 201, 202, 203, 204, 205, 206, 238, 250, 252, 339, 345, 353
COD_{Mn} 157, 158, 182, 183, 193, 338, 339, 340, 344, 345, 348
colloid 8, 13, 50, 73, 74, 75, 85, 143, 144, 147, 169, 213, 215, 230, 238, 375
concentration polarization 94, 143, 236, 241, 244, 258, 260, 268, 269, 272, 273, 283, 288, 304, 309, 314
cross-flow velocity 279, 301, 302, 304, 314, 315, 319
Cyclotella 36, 50, 51, 55, 82

DAX-8 20, 75
desalination 147, 276, 277, 278
Dextran 111, 122, 136
diatomite 325, 326, 329, 330, 334, 335, 339, 340, 341, 344, 348, 349, 351
disinfection by-product 20, 275, 353
DOC 3, 7, 27, 28, 80, 83, 93, 99, 145, 147, 148, 149, 151, 152, 153, 154, 157, 172, 181, 182, 183, 184, 185, 193, 195, 198, 219, 230, 231, 233, 234, 235, 236, 239, 242, 243, 244, 245, 246, 247, 248, 250, 251, 253, 254, 255, 256, 258, 260, 261, 286, 287, 306, 339, 340, 354, 355, 357, 358, 359, 360, 361, 362, 363, 364, 365, 366, 367, 368, 370, 374, 375, 378, 379, 380, 381, 382, 383, 384, 385, 386, 387, 388
dynamic contact angle 122, 123, 134
dynamic membrane 325, 326, 329, 330, 331, 335, 343, 346, 348, 349, 351

electrostatic steric hindrance model 213
emergency life bag 278
endocrine disrupting chemical 278
EOM 61, 62, 64, 65, 66, 68, 69, 70, 82
equilibrium contact angle 123
extracellular polymeric substances 147

$f_{450/500}$ 33, 91
FESEM 113, 132, 133, 134
fixed-charge model 213
flos-aquae 82
fluorescence spectrum 1, 25, 26, 27, 28, 29, 106, 176, 252, 254, 257, 258, 354
forward osmosis 267, 268, 274, 276, 280, 281, 282, 283, 284, 285, 287, 288, 289, 290, 291, 293, 294, 296, 297, 298, 300
FRR 132
fulvic acid fluorescence 28, 51

Gaoyou 5, 7, 8, 9, 22, 31, 33, 35, 38, 40, 42, 43, 44, 45, 46, 51, 54, 56, 78, 90
Ge Lake 37, 41, 46, 75
Gel Permeation Chromatography 1

hollow fiber membrane 148, 198, 354
HPLC-UV-TOC 3

https://doi.org/10.1515/9783110596847-010

EBSCOhost - printed on 2/14/2023 6:39 AM via . All use subject to https://www.ebsco.com/terms-of-use

HPSEC-UV-TOC 12, 85, 161
Huangpu River 4, 5, 7, 8, 9, 10, 15, 22, 31, 33, 34, 35, 38, 40, 42, 43, 44, 45, 54, 78, 90, 192, 193, 194, 195, 196, 198, 202, 238, 245, 254, 255, 256, 257, 258, 261
humic acid 4, 9, 11, 14, 18, 20, 21, 23, 26, 27, 28, 35, 36, 37, 39, 56, 57, 58, 73, 84, 85, 97, 104, 143, 165, 178, 216, 219, 229, 230, 237, 239, 241, 260, 279, 291, 320
hydraulic retention time 278, 354, 378
hydrophilicity 1, 9, 20, 23, 24, 37, 43, 110, 111, 112, 115, 116, 118, 134, 136, 143, 196, 198, 216, 223, 234, 238, 240, 241, 244, 246, 247, 256, 260, 269, 280, 286, 305, 325, 365
hydrophobicity 1, 20, 22, 26, 37, 43, 73, 75, 81, 83, 100, 106, 109, 143, 144, 216, 223, 238, 241, 244, 246, 247, 251, 256, 257, 260, 286, 300, 302

ICP 269, 270, 271, 272, 274, 279, 288, 291, 292, 293, 297, 299, 302, 310, 311, 313, 315, 318, 319, 320
IFRP 126, 127, 128, 129, 130, 131, 132, 133, 134, 135, 136
initial contact angle 122
initial flux 76, 77, 83, 94, 146, 188, 281, 289, 290, 291, 293, 296, 298, 302, 307, 311, 312, 313, 314, 315, 317, 318, 319, 320
ionic strength 2, 27, 73, 93, 215, 223, 227, 228, 237, 245, 246, 259, 279, 281, 283, 289, 295, 302
IRA-958 20, 75
irreversible fouling rate 63
irreversible membrane fouling 61, 62

Kunshan 4, 5, 7, 8, 9, 22, 25, 31, 33, 35, 38, 40, 42, 43, 44, 45, 54, 78

liquid chromatograph 168, 219, 284, 302

macromolecule 8, 9, 11, 13, 14, 15, 34, 36, 43, 45, 47, 48, 58, 84, 87, 91, 144, 145, 185, 189, 190, 194, 196, 216, 236, 244, 247, 284, 298, 306, 308, 311, 314, 318, 353, 380, 381
mass adsorption 301, 310
medium molecule 11, 15, 46, 48, 58, 308
membrane bioreactor 146, 235, 278, 326, 345
membrane fouling 26, 61, 62, 63, 65, 66, 68, 70, 73, 74, 75, 76, 77, 78, 80, 81, 82, 85, 86, 87, 90, 91, 92, 93, 94, 95, 98, 99, 100, 101, 102, 103, 104, 106, 143, 144, 145, 146, 147, 148, 151, 157, 159, 160, 162, 165, 166, 167, 168, 169, 172, 173, 174, 176, 180, 182, 184, 187, 188, 192, 198, 199, 203, 206, 237, 240, 243, 244, 250, 259, 260, 269, 275, 278, 279, 283, 290, 292, 293, 296, 297, 299, 300, 302, 309, 311, 312, 314, 318, 325, 374, 380
membrane pore size 93, 144, 153, 225, 229, 260
membrane resistance 225, 236, 308, 309, 310, 371, 380
mesoporous carbon 173
microalgae 61, 62
Microcystis 17, 36, 48, 50, 51, 55, 82, 94
microfiltration 75, 77, 94, 97, 99, 143, 146, 154, 192, 193, 212, 219, 235, 237, 345
microorganism 73, 276, 325, 334, 335, 336, 341, 347, 348, 350
microporous carbon 173
MIEX 147, 184
molecular weight 1, 2, 3, 4, 5, 7, 8, 9, 10, 11, 12, 13, 15, 16, 17, 19, 26, 31, 34, 35, 43, 46, 48, 50, 51, 53, 54, 56, 57, 58, 75, 81, 83, 91, 92, 102, 106, 144, 145, 146, 153, 154, 155, 168, 184, 195, 196, 197, 198, 211, 212, 214, 229, 230, 234, 235, 237, 240, 241, 243, 244, 246, 247, 251, 252, 254, 256, 257, 260, 269, 281, 283, 284, 286, 287, 300, 301, 302, 305, 307, 349, 371, 388

nanofiltration 94, 211, 212, 213, 214, 215, 216, 217, 222, 223, 224, 225, 226, 227, 228, 229, 230, 231, 232, 233, 235, 236, 237, 239, 241, 242, 243, 244, 245, 246, 249, 250, 253, 254, 255, 259, 260, 280, 289, 300
neutral hydrophilic 20, 21, 22, 23, 24, 25, 35, 39, 40, 41, 43, 44, 45, 46, 48, 49, 51, 75, 76, 83, 143, 144, 161, 162, 236
NF90 217, 224, 225, 259
NF270 217, 224, 225, 229, 235, 236, 259
NH4-N 328, 329, 330, 340
NOM 73, 74, 75, 76, 78, 80, 82, 90, 91, 94, 95, 98, 100, 102, 143, 144, 145, 147, 160, 161, 169, 172, 182, 187, 206, 216, 229, 275, 279, 280, 293, 298, 353, 366, 375

EBSCOhost - printed on 2/14/2023 6:39 AM via . All use subject to https://www.ebsco.com/terms-of-use

OCD method 10, 11, 19
online coagulation 145
organic matter 1, 2, 3, 4, 5, 7, 8, 9, 10, 11, 12, 13, 14, 18, 19, 20, 21, 22, 23, 25, 26, 30, 31, 33, 34, 35, 37, 39, 41, 42, 43, 44, 45, 46, 50, 51, 54, 55, 56, 57, 58, 59, 73, 75, 81, 82, 83, 85, 90, 91, 92, 93, 94, 95, 96, 97, 103, 104, 109, 143, 144, 145, 146, 147, 161, 182, 194, 195, 196, 198, 203, 214, 215, 216, 223, 224, 229, 234, 235, 236, 237, 238, 239, 240, 241, 242, 243, 245, 246, 247, 248, 249, 250, 251, 252, 253, 254, 256, 257, 258, 259, 260, 275, 279, 280, 300, 320, 349, 351, 353, 354, 355, 358, 359, 366, 368, 372
ozonation 145, 146, 192, 193, 194, 196, 198, 200, 201, 202, 203, 205, 237, 238, 239, 240, 241, 242, 243, 244, 245, 254, 255, 256, 257, 258, 259, 260, 261

parallel factor analysis 247
PEG 110, 111, 125, 126, 130
PEGMA-r-MMA 111, 125, 126
permeate ?ux 76
photocatalysis 353, 354, 355, 359, 360, 361, 363, 364, 376, 380, 381, 384, 387
polysaccharide 8, 9, 13, 17, 21, 36, 37, 44, 45, 54, 61, 68, 73, 82, 84, 85, 98, 102, 103, 104, 106, 143, 144, 145, 169, 172, 178, 189, 231, 233, 236, 298, 301, 320
powdered activated carbon 145, 237
PPCP 214, 215, 216, 222, 229, 236, 259
precoating 326, 330, 331, 334, 339, 340, 344, 351
pressure-retarded osmosis 267
Principal component analysis 172
protein 8, 9, 13, 17, 21, 26, 27, 28, 31, 33, 34, 35, 36, 37, 38, 44, 45, 46, 54, 56, 58, 61, 68, 73, 74, 84, 85, 90, 91, 92, 95, 98, 102, 104, 127, 132, 143, 145, 165, 169, 172, 176, 178, 187, 189, 233, 236, 247, 248, 249, 252, 254, 258, 298, 374, 375, 385
PVDF 62, 76, 77, 99, 100, 102, 109, 110, 111, 112, 114, 115, 116, 117, 118, 119, 120, 121, 122, 123, 124, 125, 126, 127, 128, 129, 130, 131, 132, 133, 134, 135, 136, 148, 194, 198, 355, 375
PVDF-TiO_2 112, 115, 116
PVP 110

Qingcaosha 13, 15, 23, 24, 36, 37, 41, 46, 75, 77, 79

r(a, c) 33, 34, 35, 90, 91
r(t, b) 33, 34, 35, 90, 91, 92
reverse osmosis 79, 94, 147, 157, 211, 212, 216, 222, 267, 273, 300, 325
reversible foulant 63, 64, 66, 162
reversible fouling rate 63
reversible membrane fouling 61, 62, 65, 66, 70, 146, 147, 167

scanning electron microscopy 62, 102
Scenedesmus 36, 49, 50, 51, 55, 82
small molecular organic 9, 13, 15, 21, 235, 238, 239, 241, 242, 249, 257, 260
small molecule 4, 7, 11, 13, 15, 26, 37, 47, 49, 50, 56, 58, 59, 80, 146, 147, 153, 162, 169, 176, 194, 196, 235, 238, 242, 252, 254, 258
sodium alginate 3, 11, 21, 219, 229, 231, 237, 242, 244, 260
space charge model 213
SS 326, 328, 329, 330, 331, 332, 335, 338, 339, 340, 344, 351, 355, 375
standard coagulation 145
strong hydrophobic 20, 21, 22, 23, 35, 37, 38, 39, 40, 41, 42, 44, 47, 48, 49, 58, 143, 161, 236, 240, 251, 257, 284, 302
submerged flat membrane photocatalysis reactor 354, 355, 376
submerged membrane-photocatalysis reactor 354
surface modification 110, 111, 112, 124
suspended solid 20, 73
SUVA 7, 9, 10, 22, 23, 28, 80, 83, 157, 246, 250, 282, 366, 368, 375, 380, 382, 383

Taihu 12, 13, 14, 15, 17, 19, 23, 24, 25, 33, 36, 37, 40, 46, 54, 56, 57, 58, 75, 76, 78, 79, 87, 89, 90, 93, 95, 99, 148, 151, 153, 154, 155, 158, 159, 160, 165, 166, 176, 177, 178, 179, 182, 245, 246, 247, 248, 249, 250, 256, 260, 274, 281, 283, 284, 286, 298, 343, 375, 380, 382, 384, 385, 386, 387
tannic acid 3, 11, 21, 144, 219, 229, 232, 237, 260, 280, 281, 283, 284, 285, 286, 287, 288, 289, 290, 291, 292, 293, 294, 295, 296, 297, 298, 300, 301, 303, 304, 305,

EBSCOhost - printed on 2/14/2023 6:39 AM via . All use subject to https://www.ebsco.com/terms-of-use

306, 307, 308, 309, 310, 311, 312, 313, 314, 315, 316, 317, 318, 319, 320
temperature 2, 27, 76, 101, 109, 111, 115, 118, 120, 122, 123, 136, 181, 198, 217, 220, 221, 222, 223, 224, 225, 226, 227, 228, 230, 231, 233, 239, 245, 246, 250, 255, 259, 274, 277, 282, 328, 329, 357, 376
THMFP 339, 347, 354, 357, 368, 375, 380, 383, 384, 385, 388
three-dimensional AFM 116, 117
three-dimensional fluorescence spectroscopy 25, 26, 27, 51, 374
TiO_2 110, 111, 112, 114, 115, 116, 117, 135, 353, 354, 355, 357, 358, 359, 360, 361, 364, 365, 366, 368, 369, 370, 371, 374, 375, 376, 377, 378, 379, 380, 381, 387, 388
TMP 63, 64, 66, 67, 70, 76, 148, 150, 151, 152, 153, 158, 161, 168, 169, 199, 200, 203, 206, 326, 339, 341, 346, 347, 354, 357, 368, 369, 370, 375, 376, 377, 378, 380, 381
TN 329, 330
total fouling rate 63
total organic carbon concentration 3
transphilic 22, 23, 24, 75, 284, 302
tryptophan fluorescence 28, 31, 38
tyrosine fluorescence 28
ultrafiltration membrane filtration 2, 4, 5, 7, 10, 19
UV absorbance 3, 185, 192
UV_{254} 7, 8, 13, 18, 83, 95, 98, 145, 148, 149, 151, 152, 153, 155, 157, 158, 172, 175, 176, 182, 183, 184, 185, 188, 189, 193, 195, 196, 198, 200, 246, 250, 282, 338, 339, 340, 344, 345, 348, 354, 365, 366, 367, 368, 375, 380, 381, 382, 383, 387, 388

vibration membrane 61, 64
visible region humic acid fluorescence 28

weakly hydrophobic 20, 21, 22, 35, 37, 40, 41, 44, 47, 49, 58, 59, 75, 143, 224, 236, 251
Wuhu 13, 15, 23, 24

XAD-4 20, 75, 284, 302
Xiangjiang 12, 13, 14, 23, 24, 36, 37, 40, 75, 76, 78, 79, 87, 88, 89, 90
X-ray photoelectron spectroscopy 118
XRD 112, 113, 115, 123, 131, 134, 135

Yangcheng 75, 76, 77, 102, 103, 104
Yellow River 5, 7, 9, 10, 15, 22, 25, 31, 33, 35, 38, 40, 42, 43, 44, 45, 80, 105, 106

zeta potential 144, 237, 317

EBSCOhost - printed on 2/14/2023 6:39 AM via . All use subject to https://www.ebsco.com/terms-of-use